Vol. 47, No. 3 / 2015

e: ISSN 2068 – 2239
p: ISSN 2068 – 4215

# INMATEH – AGRICULTURAL ENGINEERING

SEPTEMBER - DECEMBER

***Nu ne asumăm responsabilitatea pentru conținutul lucrarilor ştiințifice şi pentrru opiniile publicate in acest volum. Ele reprezintă punctul de vedere al autorului.***

***No liability is assumed by the editorial staff for the content of scientific papers and opinions published in this volume. They represent the author's point of views.***

# Editorial

The National Institute of Research-Development for Machines and Installations designed to Agriculture and Food Industry - INMA Bucharest has the oldest and most prestigious research activity in the field of agricultural machinery and mechanizing technologies in Romania.

**Short History**

- In 1927, the first research **Center for Agricultural Machinery** in Agricultural Research Institute of Romania - ICAR (Establishing Law was published in O.D. no. 97/05.05.1927) was established;
- In 1930, was founded **The Testing Department of Agricultural Machinery and Tools** by transforming Agricultural Research Centre of ICAR - that founded the science of methodologies and experimental techniques in the field (Decision no. 2000/1930 of ICAR Manager - GHEORGHE IONESCU ŞIŞEŞTI);
- In 1952, was established the Research Institute for Mechanization and Electrification of Agriculture - ICMA Băneasa, by transforming the Department of Agricultural Machines and Tools Testing;
- In 1979, the Research Institute of Scientific and Technological Engineering for Agricultural Machinery and Tools – ICSITMUA was founded - subordinated to Ministry of Machine Building Industry - MICM, by unifying ICMA subordinated to MAA with ICPMA subordinated to MICM;
- In 1996 the National Institute of Research-Development for Machines and Installations designed to Agriculture and Food Industry – INMA was founded – according to G.D. no.1308/25.11.1996, by reorganizing ICSITMUA, G.D no. 1308/1996 coordinated by the Ministry of Education and Research G.D. no. 823/2004;
- In 2008 INMA has been accredited to carry out research and developing activities financed from public funds under G.D. no. 551/2007, Decision of the National Authority for Scientific Research - ANCS no. 9634/2008.

As a result of widening the spectrum of communication, dissemination and implementation of scientific research results, in 2000 was founded the institute magazine, issued under the name of SCIENTIFIC PAPERS **(INMATEH)**, ISSN 1583 – 1019.

Starting with volume 30, no. 1/2010, the magazine changed its name to **INMATEH - Agricultural Engineering**, appearing both in print format (ISSN 2068 - 4215), and online (ISSN online: 2068 - 2239). The magazine is bilingual, being published in Romanian and English, with a rhythm of three issues / year: January-April, May-August, September-December and is recognized by CNCSIS – with $B^+$ category. Published articles are from the field of AGRICULTURAL ENGINEERING: technologies and technical equipment for agriculture and food industry, ecological agriculture, renewable energy, machinery testing, environment, transport in agriculture etc. and are evaluated by specialists inside the country and abroad, in mentioned domains.

Technical level and performance processes, technology and machinery for agriculture and food industry increasing, according to national requirements and European and international regulations , as well as exploitation of renewable resources in terms of efficiency, life, health and environment protection represent referential elements for the magazine „**INMATEH - Agricultural Engineering**".

We are thankful to all readers, publishers and assessors.

Editor in chief,
Ph. D. Eng. Pirnă Ion

# Managing Editorial Board - INMA Bucharest


**Editor in Chief**
**Pirnă Ion,** General Manager, Prof.Hon.Ph.D.Eng, SR I, Corresponding member of ASAS, pirna@inma.ro

**Executive Editor**
**Vlăduț Valentin,** Ph.D.Eng, SR II;
valentin_vladut@yahoo.com
**Popa Lucreția,** PhD.Eng, SR II;
lucretia_popa@yahoo.com

**Assistant Editor**
**Drâmbei Petronela,** Ph.D.Eng, SR I;
petronela_drambei@yahoo.com
**Cioica Nicolae,** Ph.D. Eng, IDT II;
ncioica@yahoo.com

**Logistic support, database**
**Muraru Virgil,** Ph.D.Eng, SR I;
vmuraru@inma.ro
**ȚicuTania,** techn;
tanya_manu@yahoo.com

**Scientific Secretary**
**Cârdei Petre,** math.,
petru_cardei@yahoo.com

**Official translators**
**Barbu Mihaela,** Prof. English, French
**Nedelcu Mihail**, Ph.D. Eng., SR III

## Editorial Board

- Acad. HERA Cristian - Romania, Honorary President of ASAS - Academy of Agricultural and Forestry Sciences "Gheorghe Ionescu Şişeşti", member of Romanian Academy;
- Acad. Prof. Ph.D. SIN Gheorghe - Romania, President of ASAS - Academy of Agricultural and Forestry Sciences "Gheorghe Ionescu Şişeşti";
- Prof. Ph.D. NICOLESCU I. Mihai - Romania, Vicepresident of ASAS - Academy of Agricultural and Forestry Sciences "Gheorghe Ionescu Şişeşti";
- Hon.Prof. Ph.D.Eng. GÂNGU Vergil - Romania, President of the Department of Agricultural Mechanization of ASAS - Academy of Agricultural and Forestry Sciences "Gheorghe Ionescu Şişeşti";
- Ph.D. Eng. NICOLESCU C. Mihai - Romania, Scientific General Secretary of the ASAS - Academy of Agricultural and Forestry Sciences "Gheorghe Ionescu Şişeşti";
- Assoc.Prof. Ph.D. Eng. BELC Nastasia - Romania, IBA Bucharest;
- Ph.D. Eng. BUȚU Alina - Romania, INSB Bucharest;
- Prof. Ph.D. Eng. PARASCHIV Gigel - Romania, P.U. Bucharest;
- Prof. Ph.D. Eng. BIRIŞ Sorin - Romania, P.U. Bucharest;
- Prof. Ph.D. Eng. NICULIȚĂ Petru - Romania, USAMV Bucharest;
- Prof. Ph.D. Eng. VLASE Sorin - Romania, "Transilvania" University Braşov;
- Prof. Ph.D. Eng. ROŞ Victor - Romania, Technical University Cluj Napoca;
- Prof. Ph.D. Eng. FILIP Nicolae - Romania, Technical University Cluj Napoca;
- Prof. PhD. Eng. VOICU Gheorghe - Romania, P.U. Bucharest;
- Prof. PhD. Eng. GERGEN Iosif - Romania, USAMVB Timişoara;
- Prof. Ph.D. Eng. ȚENU Ioan - Romania, USAMV Iaşi;
- Assoc.Prof. Ph.D.Eng. BUNGESCU Sorin - Romania, USAMVB Timişoara;
- Prof. Ph.D.Eng. FENYVESI László - Hungary, Hungarian Institute of Agricultural Engineering Godolo;
- Prof. Ph.D.Eng. KOSUTIC Silvio - Croatia, University of Zagreb;
- Ph.D. BIOCCA Marcello - Italy Agricultural Research Council, Agricultural Engineering Research Unit;
- Prof. Ph.D.Eng. MIHAILOV Nikolay - Bulgaria, University of Rousse;
- Assoc.Prof. Ph.D.Eng. ATANASOV At. - Bulgaria, University of Rousse;
- Assoc.Prof. Ph.D. ERTEKIN Can - Turkey, Akdeniz University Antalia;
- Prof. Ph.D.Sc. Eng. VARTUKAPTEINIS Kaspars - Latvia, Latvia University of Agriculture, Institute of Agricultural Machinery;
- ir. HUYGHEBAERT Bruno - Belgium, Walloon Agricultural Research Center CRA-W;
- Prof. Ph.D. Eng. FABBRO Dal Inacio Maria - Brazil, Campinas State University;
- Prof. PhD. Eng. DE WRACHIEN Daniele - Italy, State University of Milan;
- Prof. PhD. Guanxin YAO - P.R. China, Along Agriculture R&D Technology and Management Consulting Co., Ltd;
- Prof. PhD. Eng. GONZÁLEZ Omar - Republic of Cuba, Central University "Marta Abreu" de las Villas.



**In the present, *INMATEH - Agricultural Engineering* journal is indexed in the next international databases:**
**ULRICHSWeb: Global Serials Directory, CABI, SCIPIO, ELSEVIER /SciVerse SCOPUS, Index COPERNICUS International, EBSCO Publishing, Elektronische Zeitschriftenbibliothek**

**INMATEH - Agricultural Engineering**
vol. 47, no.3 / 2015
NATIONAL INSTITUTE OF RESEARCH-DEVELOPMENT FOR MACHINES AND INSTALLATIONS DESIGNED TO AGRICULTURE AND FOOD INDUSTRY - INMA Bucharest
6 Ion Ionescu de la Brad Blvd., sector 1, Bucharest
Three issues per year,
e ISSN: 2068 – 2239
p ISSN: 2068 – 4215
Edited by: INMA Bucharest

**Copyright: INMA Bucharest / Romania**

# CUPRINS / *CONTENT*


| | | Pag. |
|---|---|---|
| 1. | **EXPERIMENTAL COMPARATIVE STUDY BETWEEN TWO TYPES OF MECHANISM USED IN GRASSLAND DRILLS TRANSMISSION /**<br>***STUDIU COMPARATIV EXPERIMENTAL ÎNTRE DOUĂ TIPURI DE MECANSIME UTILIZATE ÎN TRANSMISIA MAŞINILOR DE REGENERAT PAJIŞTI***<br>**Ph.D.Eng. Manea D.[1)], Prof. Ph.D.Eng. Voicu Gh.[1)], Prof.Ph.D.Eng. Paraschiv G.[1)], Ph.D.Eng. Marin E.[2)]**<br>[1)]University Politehnica of Bucharest, Faculty of Biotechnical Systems Engineering / Romania<br>[2)]National Institute of Research - Development for Machines and Installations designed to Agriculture and Food Industry – INMA, Bucharest / Romania | 5 |
| 2. | **SOIL-CUTTING PERFORMANCE ANALYSIS OF A HANDHELD TILLER'S ROTAVATOR BY FINITE ELEMENT METHOD (FEM) /**<br>***基于有限元法的微耕机旋耕刀辊土壤切削性能分析***<br>**Prof. Ph.D. Mingjin Yang[1, 2)], Ms. Student Po Niu[1)], Ms. Bin Peng[1)], Ph.D. Ling Yang[1)], Ph.D. Yunwu Li[1)], Prof. Xiaobing Chen[2)], Prof. Zhuomin Peng[*2)]**<br>[1)]College of Engineering & Technology, Southwest University, Chongqing / P. R. China<br>[2)]Agricultural Machinery Quality Control and Inspection Technology Centre, Nanjing Research Institute for Agricultural Mechanization Ministry of Agriculture, Nanjing / P. R. China | 13 |
| 3. | **FLOW FIELD SIMULATION AND ANALYSIS OF BAG FILTER FOR AGRICULTURE SEWAGE /**<br>***农业污水袋式过滤器内流场特性仿真分析***<br>**Prof. Ph.D. Feng Zi-ming, Fang Xin, Gao Qiming, Ding Huanhuan**<br>School of Mechanical Science and Engineering, Northeast Petroleum University, Daqing/ China | 21 |
| 4. | **MATHEMATICAL MODELLING AND COMPARATIVE SIMULATION OF THE VIBRATIONS OF VIBRO-CULTIVATORS AND AGRICULTURAL CULTIVATORS /**<br>***MODELARE MATEMATICA SI SIMULAREA COMPARATIVA A VIBRAȚIILOR COMBINATOARELOR SI CULTIVATOARELOR AGRICOLE***<br>**Math. Cardei P[1,2)]., Ph.D. Eng. Muraru V[1,2)]., Ph.D. Eng. Constantin N.[2)], Ph.D. Eng. Muraru C.[1,2)] , Ph.D. Cilan T.[2)], Eng. Hodre C. D.[2)],PhD.Stud. Eng. Matache Mihai[1)]**<br>[1)]INMA Bucharest/ Romania; [2)]SVILUPPO-INSIEME SI VICE Chisineu-Cris, Arad county/ Romania | 31 |
| 5. | **EFFECTS OF LIQUID FILM MULCHING ON SOIL EVAPORATION AND COTTON PLANT GROWTH BY DRIP IRRIGATION /**<br>***液体地膜覆盖对滴灌棉花土壤蒸发和作物生长的影响***<br>**M.E.Yunguang Li [1), 2)], Ph.D.Jinzhu Zhang [1), 2)], Ph.D.Zhenhua Wang [1), 2)] , M.E.Wenhao Li [1), 2)], Ph.D.Haoliang Yu [3)],**<br>[1)]College of Water Resources and Architectural Engineering, Shihezi University, Shihezi / China;<br>[2)]Corps Key Laboratory of Modern Water-saving Irrigation, Shihezi University, Shihezi / China;<br>[3)]Massey University, Palmerston North University / New Zealand | 36 |
| 6. | **EXPERIMENTAL RESEARCH OF AGRICULTURAL EQUIPMENT TYRES DESIGNED TO THEIR RATIONAL USE /**<br>***CERCETAREA EXPERIMENTALĂ A PNEURILOR DE PE ECHIPAMENTELE AGRICOLE, ÎN VEDEREA UTILIZĂRII RAȚIONALE A ACESTORA***<br>**Ph.D. Stud. Eng. Lazăr G., Ph.D. Eng. Ciupercă R., Ph.D. Eng. Nedelcu A., Ph.D. Stud. Eng. Zaica A., Ph.D. Eng. Popa L., Ph.D. Stud. Eng. Ştefan V., Ph.D. Stud. Eng. Petcu A.**<br>National Institute of Research - Development for Machines and Installations designed to Agriculture and Food Industry – INMA, Bucharest / Romania | 49 |
| 7. | **ANALYSIS OF THE UNSTEADY FLOW OF CENTRIFUGAL AGRICULTURAL AUTO WATER PUMPS WITH VARIABLE CURVATURES /**<br>***变曲率离心式农用汽车水泵的非定常流动分析***<br>**Lect. Ph.D. Xue Dangqin [1)], Lect. Ph.D. Ma Shibang [2)], Lect. Ph.D. Eng. Shi Huojie [3,4)], Prof. Ph.D.Hou Shulin[4)]**<br>[1)] School of Mechanical ＆Automotive Engineering, Nanyang Institute of Technology, Henan / China; [2)] Nangyang Normal University, Henan / China; [3)]Department of Biological Systems Engineering, Washington State University, Pullman/USA; [4)] College of Engineering ,China Agricultural University, Beijing / China | 55 |
| 8. | **ENERGY ANALYSIS OF MANUFACTURING PROCESS OF BIODEGRADABLE AGRICULTURAL FILMS /**<br>***ANALIZA ENERGETICĂ A PROCESULUI DE FABRICAȚIE A FOLIILOR AGRICOLE BIODEGRADABILE***<br>**Ph.D. Eng. Deac T.[1)]., Ph.D Stud. Eng. Nagy E. M.[2)]., Eng. Coța C.[2)], Ph.D. Eng. Cioica N.[2)], Eng. Gyorgy Z.[2)]**<br>[1)]Technical University of Cluj-Napoca, Faculty of Mechanics / Romania;<br>[2)]INMA Bucharest Branch of Cluj Napoca | 67 |
| 9. | **DETERMINATION OF THE RELAXATION TIME AT STATIC COMPRESSION OF IDARED APPLES VARIETY /**<br>***DETERMINAREA DURATEI DE RELAXARE LA SOLICITARI STATICE DE COMPRESIUNE A MERELOR DIN SOIUL IDARED***<br>**Ph.D.Eng. Veringă D.[1)], Ph.D.Eng. Vintilă M.[1)], Ph.D.Eng. Popa L.[2)], Ph.D.Stud.Eng.Ştefan V[2)], Ph.D.Stud.Eng.Petcu A.S. [2)]**<br>[1)] I.C.D.I.M.P.H. – HORTING Bucharest / Romania; [2)] INMA Bucharest / Romania | 75 |

10. **OPTIMIZATION DESIGN OF FRUIT PICKING END-EFFECTOR BASED ON ITS GRASPING MODEL /** 81
*基于抓取模型的水果采摘末端执行器优化设计*
**Assoc. Prof. Ms. Lin Hanhui[1)], Assoc. Prof. Ph.D. Cai Ken *[2)] ,**
**Assoc. Prof. Ph.D. Chen Huazhou[3)], Eng. Zeng Zhaofeng[4)]**
[1)] Center for Educational Technology, Guangdong University of Finance and Economics, Guangzhou / China;
[2)] School of Information Science and Technology, Zhongkai University of Agriculture and Engineering, Guangzhou / China; [3)] College of Science, Guilin University of Technology, Guilin / China;
[4)] Department of Mathematics and Computer Science, California State University, East Bay/ U.S.A

11. **EXPERIMENTAL RESEARCH OF SOYBEAN DRYING PROCESS INTENSIFICATION /** 91
***ЕКСПЕРИМЕНТАЛЬНЕ ДОСЛІДЖЕННЯ ІНТЕНСИФІКАЦІЇ ПРОЦЕСУ СУШІННЯ СОЇ***
**Ph.D.Eng. Kirchuk R., Ph.D.Eng. Tsiz I., Ph.D. Stud. Tsiz K.**
Lutsk National Technical University (Ukraine)

12. ***THE INFLUENCE OF SUSPENDING RODS ELASTICITY ON CIRCULAR MOTION OF A PLANSIFTER FOR SIFTING MILL PRODUCTS /*** 99
***INFLUENȚA ELASTICITĂȚII TIJELOR DE SUSPENDARE ASUPRA MIŞCĂRII CIRCULARE A SITEI PLANE PENTRU CERNEREA PRODUSELOR DE MĂCINIŞ***
**Ph.D. Stud. Eng. Ivancu B., Prof. Ph.D. Eng. Voicu Gh., Prof. Ph.D. Eng. Filip I.,**
*Polytechnic University of Bucharest, Faculty of Biotechnical Systems Engineering / Romania*

13. **MATHEMATICAL MODELLING OF THE KNEADING PROCESS FOR A HORIZONTAL MIXER /** 105
***MODELAREA MATEMATICĂ A PROCESULUI DE FRĂMÂNTARE LA UN MALAXOR ORIZONTAL***
**Prof. Ph.D.Eng. Voicu Gh.[1)], Eng. Muscalu Gh. [1)], Ph.D.Eng. Stefan E.M.[1)],**
**Ph.D.Eng. Tudor P. [1)], Ph.D.Eng. Nedelcu A.[2)]**
[1)]University Polytechnic Bucharest, Faculty of Biotechnical Systems Engineering / Romania;
[2)]INMA Bucharest / Romania

14. **STUDY ON THE SHAPE DETECTION METHOD FOR THE PRECIOUS SEAFOODS BASED ON COMPUTER VISION /** 113
*基于计算机视觉的海珍品体形检测方法研究*
**Assoc. Prof. Huihui Wang[1,2)], Master.stud. Shiyuan Xing[1,2)], Master.stud. YuansongZheng[1,2)],**
**Master.stud. Weiwei Gu[1,2)], Lect. Master. Yan Lv[1,2)], Prof. Ph.D. Jixin Yang[1,2)]**
[1)]School of Mechanical Engineering and Automation, Dalian Polytechnic University, Dalian Liaoning 116034;
[2)]National Engineering Research Center of Seafood, Dalian Liaoning 116034

15. **STUDY OF THE VIBRATIONS OF A PLOW BLADE /** 121
***STUDIUL VIBRAȚIILOR UNEI LAME DE PLUG***
**Lecturer PhD. Eng. Orăşanu N., Assoc. Professor PhD. Eng. Dragomirescu C.**
University "Politehnica" of Bucharest, Department of Mechanics

16. **NUMERICAL AND EXPERIMENTAL VIBRATION ANALYSIS OF THE SUSPENSION SYSTEM OF AN AGRICULTURAL MACHINERY /** 127
***ANALIZĂ NUMERICĂ ŞI EXPERIMENTALĂ A VIBRAȚIILOR SISTEMULUI DE SUSPENSIE AL UNEI MAŞINI AGRICOLE***
**Assoc. Prof. PhD. Eng. Craifaleanu A., Assoc. Prof. PhD. Dragomirescu C.**
University "Politehnica" of Bucharest, Department of Mechanics / Romania

17. **STUDY ON FIELD WATER-SALT BALANCE SIMULATION USING SWAP MODEL: A CASE STUDY OF FARMLAND IN THE CENTRAL SHAANXI PLAIN /** 135
*基于 SWAP 的田间水盐平衡模拟研究——以关中农田为例*
**M.S. Liang Dong[1)], Ph.D. Quan Quan*[1)], Prof. Ph.D. Bing Shen[1)], Prof. Ph.D. Wan Luo [2)], Ph.D. Qinger Jung [3)]**
[1)] State Key Laboratory Base of Eco-hydraulic Engineering in Arid Area, Xi'an University of Technology, Xi'an / China; [2)] Yangzhou University, Yangzhou / China

18. ***STABILITY ANALYSIS OF THE AGRICULTURAL ARTICULATED VEHICLE BASED ON INTERVAL METHOD /*** 145
*基于区间数学法的农业铰接车的稳定性分析*
**Ph.D. Wei Kou [1, 2)], Prof. Xinhui Liu [1, 2)], Ph.D. Wei Chen [1, 2)]**
[1)] College of Mechanical Science and Engineering, Jilin University, Jilin/China;
[2)] China State Key Laboratory of Automobile Simulation and Control, Jilin University, Jilin/China

19. **THE STUDY OF BULK MATERIAL KINEMATICS IN A SCREW CONVEYOR-MIXER /** 155
***ДОСЛІДЖЕННЯ КІНЕМАТИКИ СИПКОГО МАТЕРІАЛУ В ГВИНТОВОМУ КОНВЕЄРІ-ЗМІШУВАЧІ***
**Hewko B.M., Popovich P.V., Diachun A.Y., Lyashuk O.L., Liubachivskyi R.O.**
Ternopil Ivan Pul'uj National Technical University, Ruska str., 56, Ternopil, Ukraine

20. **STUDY ON RESISTANCE AND STRUCTURE OPTIMIZATION OF TREE TRUNK INJECTOR'S NEEDLE HEAD /** 163
*注干机针头的进针阻力和结构优化研究*
**Assoc. Prof. Shang Qingqing[1)]，Stud. Jiang Tiantian[1)], Prof. Ph.D. Yin Tongming[2)]**
[1)]College of Electronic and Mechanical Engineering, Nanjing Forestry University
[2)] College of Forestry, Nanjing Forestry University

# EXPERIMENTAL COMPARATIVE STUDY BETWEEN TWO TYPES OF MECHANISM USED IN GRASSLAND DRILLS TRANSMISSION
# /
# *STUDIU COMPARATIV EXPERIMENTAL ÎNTRE DOUĂ TIPURI DE MECANSIME UTILIZATE ÎN TRANSMISIA MAŞINILOR DE REGENERAT PAJIŞTI*

**Ph.D.Eng. Manea D.[1)], Prof. Ph.D.Eng. Voicu Gh.[1)], Prof.Ph.D.Eng. Paraschiv G.[1)], Ph.D.Eng. Marin E.[2)]**
[1)]University Politehnica of Bucharest, Faculty of Biotechnical Systems Engineering / Romania
[2)]National Institute of Research - Development for Machines and Installations designed to Agriculture and Food Industry – INMA, Bucharest / Romania
*Tel: 0724350567; E-mail: manea_dragos_05@yahoo.com*

***Abstract:*** *This paper presents the laboratory tests of the two types of mechanism for seed rate adjustment of grassland drills, in the same working conditions. Tests were conducted on an automated installation, which simulates the working speed of the drill, collects, measures and displays seed quantities. The main quality work indices as: the deviation in relation to the average of samples, the unevenness degree of seeds distribution on the grassland drill working width and seeding rate, were determined and compared.*

***Keywords:*** *quality work indices, cam-rocker, gear drive, drill, grasslands*

## INTRODUCTION

Grassland is an important land use type in Europe, comprising approximately 35% of the agricultural land area. There is large spatial variability in both grassland systems and productivity between European regions. Observed relations between grassland and crop variability suggest that similar factors explaining variability in crop productivity (i.e. climate and management) also affect grasslands [11].

Because a long period of time were not applied even the most basic grasslands maintenance measures, considering that on can get efficient production without technological inputs, now modern EU policies are formulated to solve problem of biodiversity decline and destruction of grassland landscapes and sensitive habitats in Europe [4].

The interaction between seed rate and nitrogen levels was only significant for dry matter for Sorghum fodder sown with seed rate of 120 kg/ha and 180 kg N/ha resulted in significantly higher dry matter than all other combinations [1]. Seed rates did not affect the straw yield of forage oats significantly [6].

Authors of [5] compared four kinds of seeders, a seed broadcaster with roller, a seed broadcaster with harrow, a drill seeder and a seeder with rotary band cultivator, to assess the influence of the seeding method on the success of overseeding. The seeder with rotary band cultivator gave slightly better results. Following their studies, authors concluded that the seeding method only slightly influences the success of overseeding.

In practice there are two main types of transmissions for driving the metering devices of the grassland drills. The first type is represented by the gear drive (Northon gearboxes), that deliver 24 ... 128 transmission ratios, for each transmission ratio value being achieved a certain seeding rate [2]. Disadvantages of using the Northon type gear mechanism in the transmission system are: large constructive dimension; high weight; complicated

***Rezumat:*** *În această lucrare sunt prezentate rezultatele obținute la testarea în laborator a două tipuri de mecanisme pentru reglarea normei de însămânțare a maşinilor de regenerat pajişti, în aceleaşi condiții de lucru. Cercetările experimentale s-au desfăşurat pe o instalație automatizată, care simulează viteza de lucru a maşinii, colectează, măsoară şi afişează cantitățile de semințe. Au fost determinați şi comparați următorii indici calitativi de lucru: abaterea în raport cu media probelor, gradul de neuniformitate a distribuției pe lățimea de lucru şi normele de însămânțare.*

***Cuvinte cheie:*** *indici calitativi de lucru, camă-balansier, roți dințate, semănătoare, pajişti*

## INTRODUCERE

Pajiştile ocupă o suprafață importantă în Europa, reprezentând aproximativ 35% din terenul agricol. Există o variabilitate spațială mare între regiunile Europei, atât în sistemele de pajişti cât şi în cele productive. Relațiile observate între pajişti şi variabilitatea culturilor sugerează faptul că factori similari care influențează productivitatea culturilor (ex. climatul şi managementul) afectează de asemenea şi pajiştile [11].

Deoarece o lungă perioadă de timp nu s-au aplicat chiar şi cele mai elementare măsuri de întreținere a pajiştilor, considerându-se că se pot obține producții eficiente fără inputuri tehnologice, în prezent politicile moderne ale UE sunt formulate pentru a rezolva problema declinului biodiversității şi distrugerea pajiştilor şi a habitatelor sensibile din Europa [4].

Interacțiunea dintre norma de însămânțare şi nivelele de azot a fost semnificativă doar pentru furajul de Sorg semănat cu o normă de 120 kg/ha şi fertilizat cu 180 kg N/ha, rezultând o cantitate semnificativ mai mare de materie uscată decât orice altă combinație [1]. Normele de însămânțare nu au afectat semnificativ cantitatea de paie a ovăzului furajer [6].

Pentru a evalua influența metodei de semănat asupra succesului supraînsămânțării, autorii lucrării [5] au comparat patru tipuri de semănători, o semănătoare cu tăvălug, o semănătoare cu grapă, o semănătoare universală şi un agregat de pregătit solul cu cuțite rotative şi supraînsămânțat. Agregat de pregătit solul şi supraînsămânțat a avut rezultate puțin mai bune. În urma studiilor, autorii au concluzionat că metoda de semănat influențează doar în mică măsură succesul supraînsămânțatului.

În practică sunt două tipuri principale de transmisii pentru antrenarea aparatelor de dozare ale maşinilor de regenerat pajişti. Primul tip este reprezentat de transmisia cu roți dințate (cutia de viteze Northon), care poate realiza 24 ... 128 rapoarte de transmitere, pentru fiecare raport realizându-se o anume normă de însămânțare [2]. Dezavantajele utilizării mecanismului de

adjustments; require lubrication after few hours of operation; they have components subject to erosion. The second type is transmission with cam-rocker mechanisms, which provide the driving of seed metering devices through an intermittent motion.

Worldwide, famous manufacturers of agricultural machinery (ex. Pottinger, Gaspardo, Morris, Amazone, Hassia, Sulky) used cam mechanisms in the transmission of seed drills, due to the multiple benefits they offer, namely: simplified construction and operations of distribution control, reduced manufacturing costs and improved machine design. Also, it ensures the very precise distribution of seeds and the possibility of easy adjustment of the seed rate.

Precise distribution of the amount of seed needed per hectare, prescribed by the agro-technical conditions for each crop, has positive implications for saving seeding material and thus saving additional expenses to transport seed at sown parcels [10].

Since 1999, National Institute of Research-Development for Machines and Installations Designed to Agriculture and Food Industry - INMA Bucharest was researched and introduced into series manufacturing a mechanism having two cams mounted parallel and out of phase, that can adapt on all machines for sowing cereals in operation [3].

In [9] was carried out a comparative study on quality working indices performed by cam mechanisms compared to the gear drive mechanisms used in the transmission of metering devices as spurs cylinders type of the wheat drills.

In the paper [7], author studied the distribution uniformity of wheat and peas seeds, if using a pulse gearbox and a Norton gearbox. Comparing the data obtained for the two types of transmissions and for the two categories of seeds, it found that for low values of transmission ratios were obtained similar values of the coefficient of variation of seeds frequency for both gearboxes, hence the unevenness motion degree passed through the cam - rocker mechanism does not influence the uniformity of seeds distribution.

From the analysis of the research conducted so far, we found the weak effort to conduct applied research regarding the quality work indices of the cam - rocker mechanism from the grassland drills transmission.

This paper aimed mainly to perform comparative experimental researches between the quality work indices of a gearbox with two cam-rocker mechanisms and a Northon type gearbox, in order to optimize the distribution process of small and very small herb seeds.

## MATERIAL AND METHOD

In this comparative study of quality work indices, were performed laboratory tests with an experimental model of drill for grassland regeneration equipped with a gearbox Pottinger type, manufactured by INMA Bucharest [8] and the results were compared with those obtained with a grasslands regeneration machine in operation, equipped with a Northon gearbox adjusted for the same working conditions.

Tests were conducted on the automated installation presented in Figure 1, which mainly consist of: an electric gear motor with variable speed continuously adjustable by a frequency converter, to simulate the working speed of the drill; band provided with seed collection boxes,

tip Northon sunt: dimensiuni constructive mari; masă ridicată; reglaje complicate; necesită ungere după cîteva ore de funcționare; are componente supuse eroziunii. Cel de al doilea tip este reprezentat de transmisiile cu mecanisme camă-balansier, care realizează antrenarea aparatelor de dozare printr-o mişcare intermitentă.

Pe plan mondial, producători renumiți de maşini agricole (ex. Pottinger, Gaspardo, Morris, Amazone, Hassia, Sulky) au utilizat mecanisme cu camă în transmisia semănătorilor, datorită multiplelor avantaje pe care acestea le oferă: construcție şi reglaje simplificate, costuri de producție reduse şi îmbunătățirea design-ului maşinii. De asemenea, asigură distribuția foarte precisă a semințelor şi posibilitatea de reglare uşoară a normelor de însămânțare.

Distribuția precisă a cantității de semințe necesară la hectar, impusă de condițiile agrotehnice pentru fiecare cultură în parte, are implicații pozitive în economisirea materialului semincer, conducând astfel la reducerea cheltuielilor cu transportul la parcelele semănate [10].

Începând cu anul 1999, Institutul Național de Cercetare-Dezvoltare pentru Maşini şi Instalații destinate Agriculturii şi Industriei Alimentare - INMA Bucureşti a cercetat şi introdus în fabricația de serie un mecanism având două came montate în paralel şi defazat, care poate fi adaptat pe toate maşinile de semănat aflate în exploatare [3].

În lucrarea [9] a fost realizat un studiu comparativ privind indicii calitativi de lucru realizați de mecanismul cu camă şi mecanismul cu roți dințate utilizat în transmisia aparatelor de dozare a semințelor de tip cilindri cu pinteni de la semănătorile de păioase.

În lucrarea [7], autorul a studiat uniformitatea de distribuție a semințelor de grâu şi mazăre, utilizând o cutie de viteze cu impulsuri şi o cutie Northon. Prin compararea datele obținute pentru cele două tipuri de transmisii şi cele două categorii de semințe, pentru valori mici ale rapoartelor de transmitere s-au obținut valori similare ale coeficientului de variație şi prin urmare gradul de neuniformitate al mişcării mecanismului camă-balansier nu influențează uniformitatea de distribuție a semințelor.

Din analiza cercetărilor desfăşurate până în prezent, am descoperit slaba preocupare pentru realizarea unor cercetări aplicative privind indicii calitativi de lucru ai mecanismului camă-balansier din transmisia maşinilor de regenerat pajişti.

Lucrarea de față are ca scop principal realizarea unor cercetări experimentale comparative între indicii calitativi de lucru ai unei cutii de viteze având două mecanisme camă-balansier şi ai unei cutii de viteze Northon, în scopul optimizării procesului de distribuție a semințelor mici şi foarte mici de ierburi.

## MATERIAL ŞI METODĂ

În cadrul acestui studiu comparativ, au fost realizate teste în laborator cu un model experimental de maşină pentru regenerat pajişti echipată cu cutie de viteze Pottinger, model realizat la INMA Bucureşti [8], iar rezultatele au fost comparate cu cele obținute cu o maşină de regenerat pajişti aflată în exploatare şi echipată cu cutie de viteze Northon, reglată pentru aceleaşi condiții de lucru.

Testele s-au desfăşurat pe o instalație automatizată prezentată în figura 1, care este compusă în principal din: un motoreductor electric cu turație variabilă reglabilă continuu cu un convertizor de frecvență, pentru simularea viteze de lucru a maşinii; o bandă prevăzută cu cutii de colectare a semințelor, acționată de alt motoreductor electric; o balanță electronică pentru cântărirea cantității de

powered by another electric gear motor; an electronic scale for measuring quantity of seeds collected from each individual metering device and finally the whole amount of seeds; an automated control and monitoring panel, having an PLC (programmable logic computer). The selected parameters were: active length of fluted cylinders (minimum, medium and maximum), working speed (three speeds), lever position of the gearboxes output shaft speed control (seven positions). For each sequence of performing the experimental researches, one of these parameters were kept constant, others successively changed in certain ranges of values, then the parameter maintained constant assigned a new value and again all parameters have changed sequentially.

The combined action of seed dosage adjustment, working speed and gearbox output shaft speed, leads to quality work indices (deviation in relation to the average of samples, coefficient of variation and the seed rates).

The experimental research methodology developed in this paper is based on the national standard provisions [12]. The tests were carried out by actuating the metering devices, collecting seeds distributed by each metering device and weighing them with an accuracy of ± 0.2 g.

Each sample was carried out in five repetitions. The duration of each sample was browsing corresponding to an area of 100 $m^2$.

semințe colectată de la fiecare aparat de dozare şi a cantității totale; un panou automatizat de control şi monitorizare, având un PLC (programmable logic computer).

Parametrii selectați au fost: lungimea activă a cilindrilor cu caneluri (minimă, medie, maximă), viteza de lucru (trei viteze), poziția manetei de reglare a turației arborelui de ieşire al cutiei de viteze pe sectorul gradat (şapte poziții). Pentru fiecare secvență de desfăşurare a cercetărilor experimentale, unul dintre aceşti parametrii a fost menținut constant, ceilalți schimbându-se succesiv în anumite game de valori, apoi parametrului menținut constant i s-a atribuit o nouă valoare şi din nou ceilalți parametrii s-au schimbat secvențial.

Acțiunea combinată a reglajului dozării semințelor, vitezei de lucru şi turației arborelui de ieşire din cutia de viteze, a condus la obținerea indicilor calitativi de lucru (abaterea în raport cu media probelor, coeficientul de variație şi normele de însămânțare).

Metodologia de cercetare experimentală dezvoltată în această lucrare are la bază prevederile standardului național [12]. Probele s-au efectuat prin acționarea aparatelor de dozare, colectarea şi cântărirea semințelor distribuite de fiecare aparat cu o precizie de ± 0.2 g.

Fiecare probă s-a efectuat în cinci repetiții. Timpul necesar fiecărei probe a fost corespunzător parcurgerii unei suprafețe de 100 $m^2$.

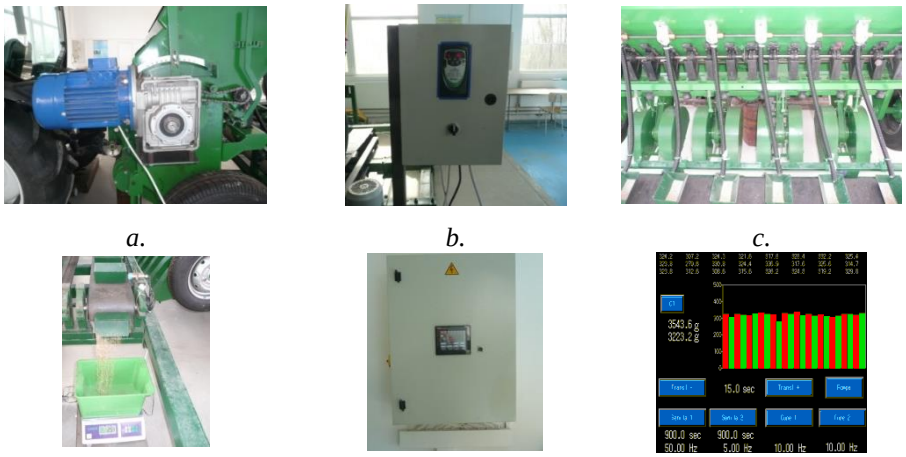


**Fig. 1 -** Details of the experimental installation:
*a - fitting the electric gear motor on the input shaft of cam - rocker device; b- frequency converter; c - band with seed collection boxes; d - collecting and weighing the seeds with the electronic scale; e - control and monitoring panel; f - data record and display with specialized software*

The conditions under which the experiments have been performed: the charge of the seed hopper - 80%; the number of metering devices used concomitantly - 8; the active lengths of fluted cylinders - minimum ($l_1$=7 mm), medium ($l_2$=14 mm), maximum ($l_3$=28 mm); simulated working speeds - $v_1$=0.83 m/s, $v_2$=1.38 m/s, $v_3$=1.94 m/s; rotation speeds of the electric gear motor shaft, corresponding to the three working speeds - 29 rot/min, 48 rot/min, 67 rot/min; positions of the adjustment lever of the Pottinger gearbox - L-40, L-50, L-60, L-70, L-80, L-90, L-100; positions of the adjustment lever of the Northon gearbox - C-2, C-5, C-8, C-10, C-13, C-15, C-17; duration of a sample, corresponding to the three working speeds - 68 s, 41 s, 29 s; seed used - *Trifolium repens,* which had following physical characteristics: purity 98.5%; mass of 1000 seeds 2.1 g; specific mass 1.06 g/ $cm^3$.

Seed flow uniformity was highlighted by the *deviation in relation to the average of samples (D*), calculated with the relation (1):

Condițiile în care s-au desfăşurat cercetările experimentale: încărcarea buncărului de semințe - 80%; numărul aparatelor de dozare utilizate concomitent - 8; lungimea activă a cilindrilor cu caneluri - minimă ($l_1$=7 mm), medie ($l_2$=14 mm), maximă ($l_3$=28 mm); vitezele de lucru simulate - $v_1$=0.83 m/s, $v_2$=1.38 m/s, $v_3$=1.94 m/s; turația arborelui motoreductorului, corespunzătoare celor trei viteze de lucru - 29 rot/min, 48 rot/min, 67 rot/min; pozițiile manetei de reglaj a cutiei de viteze Pottinger - L-40, L-50, L-60, L-70, L-80, L-90, L-100; pozițiile manetei de reglaj a cutiei de viteze Northon- C-2, C-5, C-8, C-10, C-13, C-15, C-17; durata unei probe, corespunzătoare vitezelor de lucru - 68 s, 41 s, 29 s; sămânța utilizată *Trifolium repens*, cu următoarele caracteristici fizice: puritatea 98.5%; masa a 1000 semințe 2.1 g; greutatea specifică 1.06 g/ $cm^3$.

Uniformitatea debitului a fost pusă în evidență de *abaterea în raport cu media probelor (D*), calculată cu relația (1):

$$D = \frac{q_{max}^{5} - q_{min}^{5}}{q_{med}^{5}}, \% \quad (1)$$

where: $q_{max}^{5}$, $q_{min}^{5}$, $q_{med}^{5}$ are the maximum, minimum and average quantity of seeds at five repetitions;

The unevenness degree of seeds distribution on the grassland drill working width was highlighted by the *coefficient of variation* ($C_v$), calculated with the relation (2):

unde $q_{max}^{5}$, $q_{min}^{5}$, $q_{med}^{5}$ sunt cantitățile maxime, minime şi medii de semințe colectate la cinci repetiții.

Gradul de neuniformitate a distribuției semințelor pe lățimea de lucru a maşinii de regenerat pajişti a fost evidențiat de *coeficientul de variație* ($C_v$), calculat cu relația (2):

$$C_v = \frac{S}{\bar{x}} \times 100, \% \quad (2)$$

where: $S$ is the standard deviation and was calculated with the relation (3):

unde: $S$ este abaterea standard, care a fost calculată cu relația (3):

$$S = \sqrt{\frac{1}{n-1}\sum_{i=1}^{n}(x_i - \bar{x})^2}, \text{ g} \quad (3)$$

where: $n$ is the number of metering devices; $x_i$ – the average of seed amount from each metering device; $\bar{x}$ – the absolute average calculated with the relation (4):

unde: n este numărul aparatelor de dozare; $x_i$ - media cantităților de semințe de la fiecare aparate de dozare; $\bar{x}$ - media absolută, calculată cu relația (4):

$$\bar{x} = \frac{1}{n}\sum_{i=1}^{n} x_i, \text{ g} \quad (4)$$

*The seed rate* (*Q)* was calculated with the relation (5):

Normele de însămânțare (*Q)* au fost calculate cu relația (5):

$$Q = q \cdot 100, \text{ kg/ha} \quad (5)$$

Where:
*q* este the average amount of seed in kg, distributed on the area of 100 $m^2$.

Unde:
*q* reprezintă cantitatea medie de sămânță în kg, distribuită pe o suprafață de 100 $m^2$.

**RESULTS AND DISCUSSION**

The data from the purchase operations for three working speeds (0.83 m/s, 1.38 m/s, 1.94 m/s), three active lengths of fluted cylinders (minimum, medium and maximum) and seven positions of the gearboxes adjustment lever (Pottinger: L-40, L-50, L-60, L-70, L-80, L-90, L-100; Northon: C-2, C-5, C-8, C-10, C-13, C-15, C-17), were processed with Excel.

Using the equations (3) and (4) were calculated the values of the following parameters: average quantity of seed at five repetitions ($q_{med}^{5}$), absolute average ($\bar{x}$) and standard deviation ($S$).

The values obtained for the deviation in relation to the average of samples *(D*), by applying equation (1) are graphically compared in Figure 2.

Analyzing the comparative graphs in Figure 2, have emerged the following observations:

- for the working speeds of 0.83 m/s and 1.38 m/s, the values of deviation in relation to the average of samples of the cam - rocker mechanism are higher than those obtained with the gear drive mechanism in 95.23% of compared cases;
- the remaining cases (4.77%) include following situations: the maximum active length of fluted cylinders and working speed of 0.83 m/s, at lever positions of L-80 (*D:0.09%)* and C-13 (*D:0.52%*); the maximum active length of fluted cylinders and working speed of 1.38 m/s, at lever positions of L-90 (*D:0.08%*) and C-15 (*D:0.16%*);
- for the working speed of 1.94 m/s, the values of deviation in relation to the average of samples of the cam - rocker mechanism are higher than those obtained with the gear drive mechanism in 100% of compared cases.

The values obtained for the coefficient of variation ($C_v$), by applying equation (2), are graphically compared in Figure 3.

**REZULTATE ŞI DISCUȚII**

Datele achiziționate pentru cele trei viteze de lucru (0,83 m/s; 1,38 m/s; 1,94 m/s), trei lungimi active ale cilindrilor cu caneluri (minimă, medie şi maximă) şi şapte poziții ale manetelor de reglaj ale cutiilor de viteze (camă-balansier: L-40, L-50, L-60, L-70, L-80, L-90, L-100; roți dințate: C-2, C-5, C-8, C-10, C-13, C-15, C-17), au fost prelucrate cu programul Excel.

Utilizând ecuațiile (3) şi (4) au fost calculate valorile următorilor parametrii: cantitatea medie de semințe la cinci repetiții ($q_{med}^{5}$), media absolută ($\bar{x}$) şi abaterea standard ($S$).

Valorile obținute pentru abaterea în raport cu media probelor *(D*), prin aplicarea ecuației (1) sunt comparate grafic în figura 2.

Din analiza graficelor comparative din figura 2 se desprind următoarele observații:

- pentru vitezele de lucru de 0,83 m/s şi 1,38 m/s, valorile abaterii în raport cu media probelor ale mecanismului camă-balansier sunt mai mari decât cele obținute cu mecanismul cu roți dințate, în 95,23% dintre cazurile comparate;
- în restul cazurilor (4,77%) sunt incluse următoarele situații: lungimea activă maximă a cilindrilor cu caneluri şi viteza de lucru de 0,84 m/s, la pozițiile manetei de reglaj M-80 (*D:0,09%)* şi respectiv C-13 (*D:0,52%*); lungimea activă maximă a cilindrilor cu caneluri şi viteza de lucru de 1,38 m/s, la pozițiile manetei de reglaj M-90 (*D:0,08%)* şi respectiv C-15 (*D:0,16%*);
- pentru viteza de lucru de 1,95 m/s, valorile abaterii în raport cu media probelor a dispozitivului camă-balansier sunt mai mari decât cele obținute cu dispozitivul cu roți dințate în 100% din cazurile comparate.

Valorile obținute pentru coeficientul de variație *(*$C_v$), prin aplicarea ecuației (2), sunt prezentate grafic comparativ în figura 3.

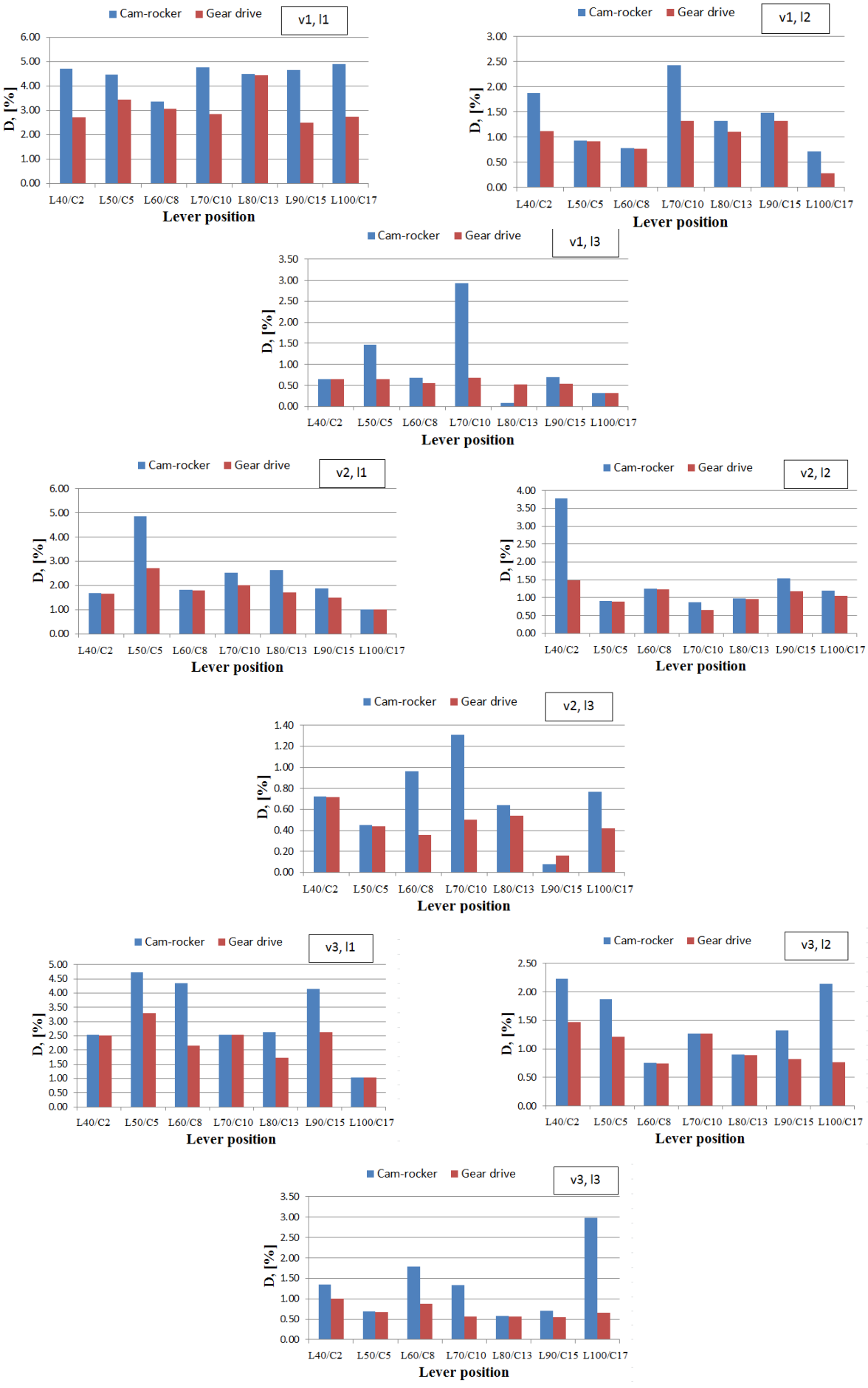


**Fig. 2 -** Comparative graphs of the deviation in relation to the average of samples *(D)*

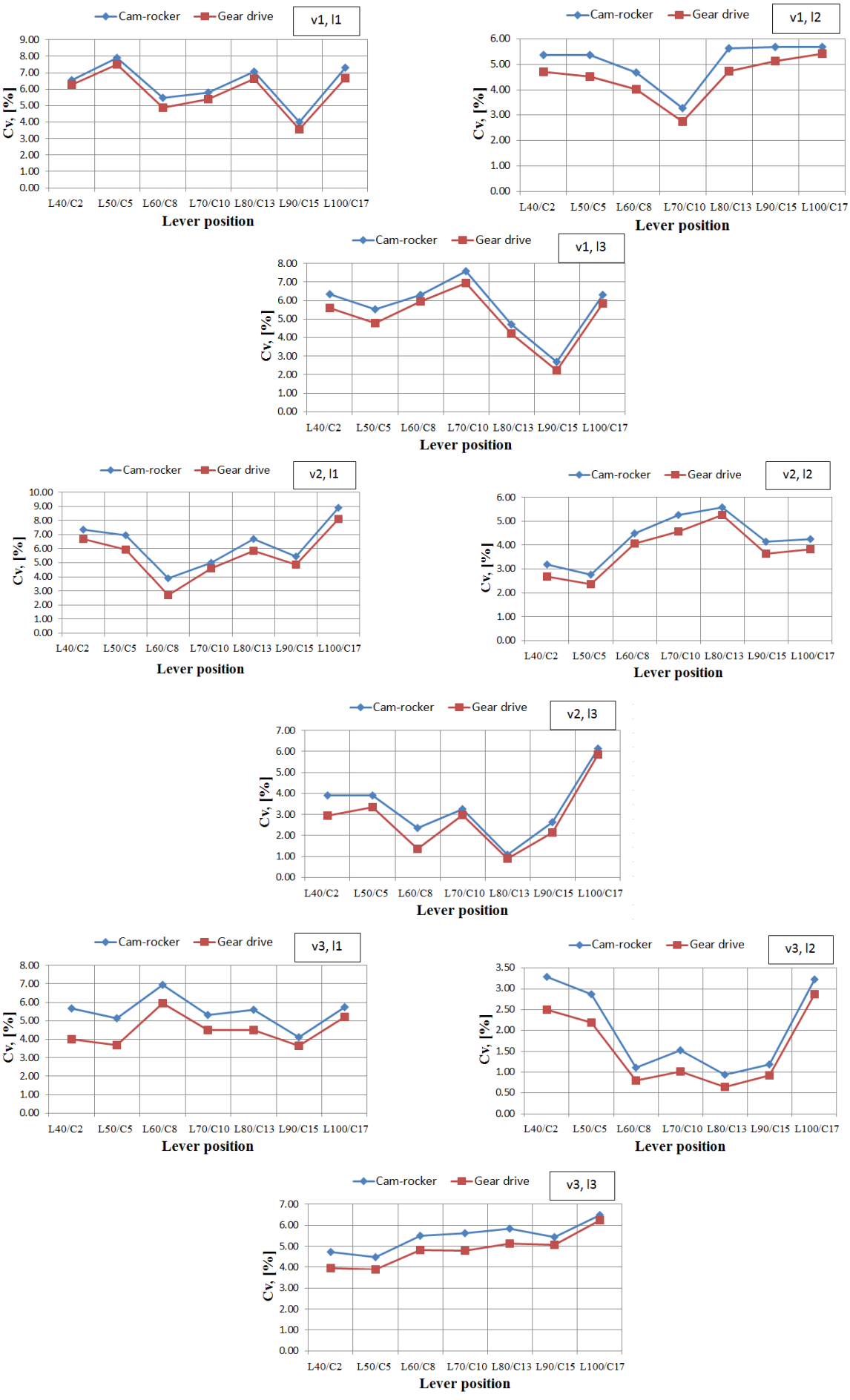


**Fig. 3 -** Comparative graphs of the coefficient of variation ($C_v$)

Analyzing the comparative graphs in Figure 3, have emerged the following observations:
- the coefficient of variation values of the cam - rocker mechanism are higher than those obtained with the gear drive mechanism in 100% of compared cases;
- values of coefficient of variation close to the maximum limit of 8% were observed for the working speed of 0.83 m/s, lever position L-50 of the cam - rocker mechanism, respectively C-5 in the case of gear drive mechanism, at the minimum active length of the fluted cylinders;
- values of coefficient of variation that exceed the maximum limit of 8% were observed for the working speed of 1.38 m/s, lever position L-100 of the cam - rocker mechanism, respectively C-17 in the case of gear drive mechanism, at the medium active length of the fluted cylinders.

Therefore, it is better to avoid the last two operating modes.

The seed rates values, resulted from the experiments with the two types of mechanisms are presented in Table 1.

Din analiza graficelor comparative din figura 3 se desprind următoarele observaţii:
- valorile coeficientului de variaţie al dispozitivului camă-balansier sunt mai mari decât cele obţinute cu dispozitivul cu roţi dinţate în 100% dintre cazurile comparate;
- valori ale coeficientului de variaţie apropiate de limita superioară de 8% au fost observate pentru viteza de lucru de 0,83 m/s, poziţia manetei M-50 pentru dispozitivul camă-balansier, respectiv C-5 în cazul dispozitivului cu roţi dinţate, la lungimea activă minimă a cilindrilor cu caneluri;
- valori ale coeficientului de variaţie care depăşesc limita superioară de 8% au fost observate pentru viteza de lucru de 1,38 m/s, poziţia manetei M-100 pentru dispozitivul camă-balansier, respectiv C-17 în cazul dispozitivului cu roţi dinţate, la lungimea activă medie a cilindrilor cu caneluri.

De aceea este bine să se evite aceste ultime două moduri de lucru.

Valorile normelor de însămânţare rezultate în urma experimentărilor cu cele două tipuri de mecanisme sunt prezentate în tabelul 1.

**Table 1**

**Values of the seed rates (*Q*)**

| Working speed, [m/s] | Lever position | Active length of the fluted cylinders | | |
|---|---|---|---|---|
| | | minimum | medium | maximum |
| | | *Q* [kg/ha] | | |
| 0.83 / 1.38 /1.94 | L-40 | 2.54/2.36/2.36 | 5.32/5.30/5.38 | 12.24/11.06/11.82 |
| | C-2 | 2.57/2.39/2.39 | 5.39/5.37/5.45 | 12.41/11.21/11.98 |
| | L-50 | 3.12/2.88/2.96 | 6.42/6.61/6.42 | 15.04/13.36/14.48 |
| | C-5 | 3.192.95/3.03 | 6.58/6.78/6.58 | 15.42/13.69/14.84 |
| | L-60 | 3.55/3.31/3.68 | 7.70/8.03/7.96 | 17.76/16.68/17.88 |
| | C-8 | 3.59/3.34/3.72 | 7.79/8.12/8.05 | 17.96/16.87/18.09 |
| | L-70 | 4.19/3.96/3.94 | 9.06/9.15/9.42 | 20.51/19.89/20.97 |
| | C-10 | 4.20/3.98/3.95 | 9.09/9.18/9.46 | 20.58/19.97/21.05 |
| | L-80 | 4.87/4.56/4.57 | 10.62/10.18/11.05 | 22.74/21.88/24.13 |
| | C-13 | 4.95/4.64/4.65 | 10.81/10.36/11.25 | 23.14/22.27/24.56 |
| | L-90 | 5.56/5.30/5.31 | 12.10/11.74/12.04 | 25.98/25.21/25.71 |
| | C-15 | 5.58/5.33/5.34 | 12.16/11.80/12.10 | 26.11/25.34/25.83 |
| | L-100 | 6.50/5.91/5.81 | 14.06/13.35/13.09 | 19.01/28.65/27.49 |
| | C-17 | 6.52/5.92/5.82 | 14.10/13.39/13.13 | 19.06/28.73/27.57 |

Analyzing the data in Table 1 it was observed that the values of seed rates calculated for the three working speeds, three active lengths of fluted cylinders and seven positions of the adjustment lever, are lower in 100% of compared cases for the cam - rocker mechanism than those obtained with the gear drive mechanism. This is an advantage because it leads to a significant saving of seed.

Meanwhile, it was observed that the range of seed rates is between 2.54 ÷ 27.49 kg/ha for the cam - rocker mechanism and between 2.57 ÷ 27.57 kg/ha for the gear drive mechanism, completely covering the agro requirements, which for the clover seed are contained in the range of 1.5 ÷ 16.5 kg / ha.

Analizând datele din tabelul 1, s-a observat că valorile normelor de însămânţare calculate pentru cele trei viteze de lucru, trei lungimi active ale cilindrilor cu caneluri şi şapte poziţii ale manetelor de reglaj, sunt mai mici, în 100% din cazurile comparate, pentru dispozitivul camă-balansier decât cele obţinute cu dispozitivul cu roţi dinţate. Acesta este un avantaj, deoarece conduce la o economie importantă de sămânţă.

În acelaşi timp, s-a observat că gama normelor de însămânţare este cuprinsă între 2,54÷27,49 kg/ha pentru dispozitivul camă-balansier şi între 2,57÷27,57 kg/ha pentru mecanismul cu roţi dinţate, acoperind complet cerinţele agrotehnice, care pentru seminţele de trifoi sunt cuprinse între 1,5÷16,5 kg/ha.

## CONCLUSIONS

The higher values of the working quality indices performed by the cam - rocker mechanism compared with the gear drive mechanism, but which qualifies agrotechnical requests, are compensated by the higher net benefits when use it on the grasslands drills transmission.

The values of seed rates obtained with the cam-rocker mechanism were slightly lower compared to those performed by the gear drive mechanism. In other words, the cam-rocker mechanism allows the precise adjustment of the seed rates, leading to a significant saving of seed.

## ACKNOWLEDGEMENTS

The work has been funded by the Sectoral Operational Programme Human Resources Development 2007-2013 of the Ministry of European Funds through the Financial Agreement POSDRU/159/1.5/S/134398.

## REFERENCES

[1]. Ayub M., Tanveerz A., Ali S., Athernadeem M., (2002) - *Effect of different nitrogen levels and seed rates on growth, yield and quality of sorghum (Sorghum bicolor)* fodder, Indian Journal of Agricultural Sciences 72 (11): 648-50;
[2]. Căproiu St., (1982) - *Agricultural Machinery for Soil Tillage, Sowing and Crop Maintenance*, Didactic and Pedagogical Publisher;
[3]. Cojocaru I., Gângu V., Neacşu M., Marin E., (2000) - *Gearbox with pulse intended for sowing cereals*, Patent no. 115668B1;
[4]. Dragomir N., Pet I., Dragomir C., Frățilă I., Cristea C., Rechițean D., Sauer M., Tapalagă I., (2010) - *Multifunctional structure of permanent pastures in Romania*. Scientific Papers Animal Science and Biotechnologies, Banat´s University of Agricultural Sciences and Veterinary Medicine. Agroprint Timisoara, Romania;
[5]. Huguenin-Elie O., Stutz C. J., Luescher A., (2006) - *Grassland improvement by overseeding,* Revue Suisse d Agriculture 39 (1): 25-29**;**
[6]. Kumar D., Seth R., Gangaiah B., (2006) - *Influence of seed size and seed rate on seed yield of forage oats (Avena sativa),* Indian Journal of Agricultural Sciences 76 (3): 154-6;
[7]. Loghin F., (2010) - *Contributions regarding the kynematics and the dynamics of transmissions with intermitent motion of universal seed drills*, PhD Thesis, University Transilvania from Brasov;
[8]. Manea D., Marin E., Paraschiv G., Voicu Gh., (2014) - *Testing experimental model of drill for grasslands regeneration***.** In: Proceedings of the 43rd International Symposium Actual Tasks on Agricultural Engineering, pp. 331-341;
[9]. Marin E., (2004) - *Contributions to improving functional parameters of transmissions from cereals sowing machines, by using cam mechanisms,* PhD Thesis, University Transilvania from Brasov;
[10]. Marin E., (2007) - *Cam mechanisms for transmission of distribution of cereals sowing machines*, Terra Nostra Publisher, Iaşi;
[11]. Smit H. J., Metzger M. J., Ewert F., (2008) - *Spatial distribution of grassland productivity and land use in Europe*, Agricultural Systems 98: 208–219;
[12]. *** SR ISO 7256/2:1992 - *Seeding and planting machinery. Test methods. Part 2: drills*, ASRO.

## CONCLUZII

Valorile mai mari ale indicilor calitativi de lucru realizați de mecanismul camă-balansier în comparație cu mecanismul cu roți dințate, dar care se încadrează în cerințele agrotehnice, sunt compensate de avantajele net superioare atunci când sunt utilizate în transmisia maşinilor de regenerat pajişti.

Valorile normelor de însămânțare obținute cu mecanismul camă-balansier sunt cu puțin mai mici în comparație cu cele realizate de mecanismul cu roți dințate. Cu alte cuvinte, mecanismul camă-balansier permite reglarea cu precizie a normelor de însămânțare, conducând la o importantă economie de sămânță.

## MULȚUMIRI

Rezultatele prezentate în această lucrare au fost obținute cu sprijinul Ministerului Fondurilor Europene prin Programul Operațional Sectorial Dezvoltarea Resurselor Umane 2007-2013, Contract nr. POSDRU/159/1.5/S/ 134398**.**

## BIBLIOGRAFIE

[1]. Ayub M., Tanveerz A., Ali S., Athernadeem M., (2002) - *Efectul diferitelor cantități de azot şi al normelor de însămânțare asupra creşterii, recoltei şi calității furajului de sorrg (Sorghum bicolor),* Jurnalul Indian al Ştiințelor Agricole 72 (11): 648-50;
[2]. Căproiu St., (1982) - *Maşini agricole pentru prelucrarea solului, semănatul şi întreținerea culturilor*, Editura Didactică şi Pedagogică;
[3]. Cojocaru I., Gângu V., Neacşu M., Marin E., (2000) - *Cutie de viteze cu impulsuri pentru semănatul cerealelor*, Brevet nr. 115668B1;
[4]. Dragomir N., Pet I., Dragomir C., Frățilă I., Cristea C., Rechițean D., Sauer M., Tapalagă I., (2010) - *Structura multifuncțională a pajiștilor permanente din România*, Lucrări ştiințifice de Zootehnie şi Biotehnologii, Universitatea de Ştiințe Agricole şi Medicină Veterinară a Banatului, Editura Agroprint Timişoara, România;
[5]. Huguenin-Elie O., Stutz C. J., Luescher A., (2006) - *Regenerarea pajiştilor prin supraînsămânțare,* Revue Suisse d'Agriculture 39 (1): 25-29;
[6]. Kumar D., Seth R., Gangaiah B. (2006) - *Influența dimensiunilor semințelor şi a normelor de sămânță asupra recoltei furajului de ovăz (Avena sativa),* Jurnalul Indian al Ştiințelor Agricole 76 (3): 154-6;
[7]. Loghin F., (2010) - *Contribuții privind cinematica şi dinamica transmisiilor cu mişcare intermitentă a semănătorilor universale*, Teză de doctorat, Universitatea Transilvania din Brasov;
[8]. Manea D., Marin E., Paraschiv G., Voicu Gh., (2014) - *Testarea modelului experimental de maşină pentru regenerarea pajiştilor*. În: Proceedings, Cel de al 43-lea Simpozion Internațional Aspecte actuale ale Ingineriei Agricole, pag. 331-341;
[9]. Marin E., (2004) - *Contribuții la optimizarea parametrilor funcționali a transmisiilor maşinilor de semănat cereale, prin utilizarea mecanismelor cu camă,* Teză de doctorat, Universitatea Transilvania din Brasov.
[10]. Marin E., (2007) - *Mecanisme cu camă din transmisia maşinilor de semănat cereale*, EdituraTerra Nostra, Iaşi;
[11]. Smit H. J., Metzger M. J., Ewert F., (2008) - *Distribuția spațială a productivității pajiştilor şi utilizarea terenului în Europa*, Sisteme Agricole 98: 208–219;
[12]. *** SR ISO 7256/2:1992 - *Maşini pentru semănat şi plantat. Metode de testare. Partea a 2-a: semănători*, ASRO.

# SOIL-CUTTING PERFORMANCE ANALYSIS OF A HANDHELD TILLER'S ROTAVATOR BY FINITE ELEMENT METHOD (FEM)
/
# 基于有限元法的微耕机旋耕刀辊土壤切削性能分析

**Prof. Ph.D. Mingjin Yang[1, 2)], Ms. Student Po Niu[1)], Ms. Bin Peng[1)], Ph.D. Ling Yang[1)], Ph.D. Yunwu Li[1)], Prof. Xiaobing Chen[2)], Prof. Zhuomin Peng[*2)]**

[1)]College of Engineering & Technology, Southwest University, Chongqing / P. R. China
[2)]Agricultural Machinery Quality Control and Inspection Technology Centre, Nanjing Research Institute for Agricultural Mechanization Ministry of Agriculture, Nanjing / P. R. China
*Tel: +8615366093016; Email: zhuominp@sina.com*

***Abstract:*** *Handheld tillers are the main tilling machinery in hilly areas, with rotavators as the main tilling parts of the machines. The soil move, soil-cutting force and power consumption, accompanying the tilling process, are crucial to the performance of a handheld tiller. In this study, rotavators were chosen as a case study, and soil-cutting model of the rotavators was built and solved, by Finite Element Method (FEM), for the soil-cutting performance analysis, and the effectiveness of the analysis was validated as well, which will benefit and provide reference for design, optimization, and performance match of the handheld tillers. The results showed that: 1) during tilling process, particles of the top layer soil get the highest velocity and acceleration, and velocity and acceleration of middle layer and bottom layer particles decrease sequentially; 2) soil-cutting force of the rotavators increases to a maximum, and it gradually decreases to reach a relatively stable status with a certain fluctuation; 3) power consumption, combination of kinetic power and internal power, is mainly consumed by means of internal energy, and the ratio of kinetic power and internal power is 1: 9.5.*

***Keywords:*** *soil-cutting, handheld tiller, rotavator, power consumption, FEM*

## INTRODUCTION

Handheld tillers are the main tilling machinery in hilly areas, and the tilling land includes upland field, paddy field, blocks in greenhouse, orchards, etc. Different from traditional power tiller with power take-off from tractor to drive the machine, a handheld tiller is often driven forward by the resultant force from soil-cutting [7, 9,13]. Rotavator, as a combination of rotary blades and wheel axle, is the main tilling part of a handheld tiller. The wheel axle of the rotavator bears resultant force from rotary blade soil-cutting and driven torque from transmission, which results in complex deformations, such as bending, torsion and shearing, and strong vibration to the tiller. Therefore, structure and parameters of a rotavator directly affect the performance of a handheld tiller and have a great impact on soil-cutting quality, power consumption and balancing characteristics of the machine [6].

Since the 1990s, growing concerns about tilling issues of handheld tillers have been shown, and the implementation of Finite Element Method (FEM) and optimization has been applied more and more to the soil-cutting study. In such applications, Abo-Elnor (2003) studied the soil-tool interaction to investigate the effect of cutting speed and angle on cutting forces over large blade displacements based on predefined failure surfaces [1]. Zhou (2009) studied the stress distribution

***摘要：****微耕机是丘陵山区主要的耕作机械，旋耕刀辊是微耕机的主要耕作部件。土壤切削过程中的土壤运动、切削力和消耗功率对微耕机的性能有着至关重要的影响。为了获得微耕机旋耕刀棍的土壤切削性能，本研究以旋耕刀辊为主要研究对象，通过有限元的方法，建立旋耕刀辊土壤切削模型并求解，并验证了土壤切削性能分析的有效性，为旋耕弯刀的设计、优化及微耕机的性能匹配提供参考。结果表明：1）在工作过程中，表层粒子获得的速度和加速度最大，中层粒子次之，深层粒子最小；2）旋耕刀棍土壤切削力增大到最大值后逐渐减小并在一定范围内波动；3）微耕机的功率消耗由动能和内能两部分组成，主要由内能决定，且动能、内能消耗功率比为 1：9.5*

***关键词：****土壤切削；微耕机；旋耕刀辊；功率消耗；有限元*

## 引言

微耕机是丘陵山区的主要耕作机械，主要用于旱田、水田及温室大棚和果园等小面积作业。与传统耕耘机械动力来自拖拉机机械不同的是，微耕机前进的动力主要来自土壤的切削反力 [7，9，13]。旋耕刀辊由刀轴和旋耕弯刀组成，是微耕机的主要耕作部件。在微耕机的耕作过程中，刀轴受旋耕弯刀土壤切削过程的土壤反力和发动机驱动力矩的共同作用会发生弯曲、扭转或者剪切等复杂变形，给微耕机带来强烈振动。因而，旋耕刀辊的结构和参数直接影响微耕机的性能，对土壤切削质量、微耕机的功率消耗和平衡性等指标有较大影响 [6]。

自 20 世纪 90 年代以来，微耕机耕作问题得到了越来越多的关注。有限元法和优化越来越广泛地应用于土壤切削的研究。Abo-Elnor 研究了土壤和刀具之间的相互作用，以获悉刀具预定义疲劳表面上在大位移条件下切削速度和切削角对切削力的影响 [1]。周明等运用有有限元分析方法对土壤剪切力的分布和螺旋型旋耕刀辊横刀工作机理进行了

of soil and transverse knife on helical rotavator of a tiller by FEM method, and found that increased cutting speed and angle could make larger cutting resistance, between which the relationship were non-linear [12]. Xia (2013) analyzed the effects of soil-cutting parameters on tilling performance of the helical rotavator, and located the maximum equivalent stress point on the transverse knife [8]. Asl (2010) determined the mathematical model of power requirement of the rotary blades and the equations of surface area per unit volume of soil tilled, checked the validity of the model for prediction of power requirement via experiments conducted in indoor soil bin, and obtained optimized rotary blade [2]. Yang (2014) simulated and evaluated the power consumption of a handheld tiller's rotary blade at different levels of control factors of soil-cutting parameters by method of Smoothed Particle Hydrodynamics (SPH) [10]. But, the studies mentioned above were mostly focused on the soil-blade interaction, and literatures regarding to soil-cutting performance of the rotavators of a handheld tiller can scarcely be found. Then, references for design, optimization, and performance match of the handheld tillers are not enough to rely upon.

In this study, rotavators of a handheld tiller were chosen as a case study, and the soil-cutting model of the rotavators was built and solved by FEM Method within ANSYS for the soil-cutting performance analysis, and the effectiveness of the analysis was validated as well.

## MATERIAL AND METHOD

### *Material*

Considering the climate, geological conditions and soil characteristics in Chongqing, China, soil model MAT147 by LS-DYNA was adopted in this study [3,16]. Parameters of soil were defined for FEM analysis, as shown in Table 1.

Rotary blades (rotary radius 185mm) of type III suitable for shallow tillage were employed. The blades were qualified for Chinese national standard GB/T 5669-2008 [14]. Parameters of the blades were defined, as shown in Table 2.

研究，指出直线型横刀切削阻力随着切削速度和切削角度的增大而增大并呈非线性关系 [12]。夏俊芳研究了土壤切削参数对螺旋刀辊的耕作性能的影响，确定了螺旋横刀最大等效应力发生部位 [8]。Asl 确定了旋耕弯刀功率消耗的数学模型和单位面积切土量的方程，校验了通过数学模型预测的功率消耗和室内土槽实验结果，并得到优化的旋耕弯刀 [2]。杨玲基于光滑粒子流体动力学方法 SPH 的方法模拟和评价了不同土壤切削参数和因子水平条件下的微耕机旋耕弯刀的功率消耗[10]。但是上述研究大多集中在旋耕弯刀和土壤的相互作用，关于微耕机旋耕刀辊土壤切削性能相关的研究文献很难发现，因而不足以为微耕机设计、优化和性能匹配提供足够的参考和支撑。

本研究以微耕机旋耕刀辊为主要研究对象，通过 ANSYS 建立微耕机旋耕刀辊土壤切削有限元模型并求解，分析了旋耕刀辊土壤切削性能，同时对分析的有效性进行了校验。

## 材料和方法

### *材料*

结合中国重庆地区气候、地质条件以及土壤特性，本研究采用 LS-DYNA 中提供的 MAT147 土壤模型 [3，16]。确定用于有限元分析的土壤的具体参数，见表 1。

采用 III 型旋耕弯刀，该型弯刀适于浅耕作业，回转半径 185mm。旋耕弯刀符合中国国家标准 GB/T 5669-2008 相关规定 [14]。旋耕弯刀的参数见表 2。

**Table 1**

**Parameters of soil**

| Parameters | Value |
|---|---|
| Bulk density, kg/mm$^3$ | 2.35e-6 |
| Porosity, % | 39.2 |
| Specific gravity | 2.68 |
| Bulk modulus, Pa | 3.5e+07 |
| Moisture, % | 21 |
| Shear modulus, Pa | 2.0e+07 |
| Within friction angle, radian | 0.436 |
| Cohesion, Pa | 2.2e+04 |

**Table 2**

**Parameters of rotary blade**

| Parameters | Value |
|---|---|
| Rotary radius, mm | 185 |
| Material | 65Mn |
| Density, kg/mm$^3$ | 7.83e+3 |
| Elastics modulus, Pa | 2.07e+11 |
| Poisson's ratio | 0.35 |

### *Method*

**a) FEM model of soil-cutting**

Main links to set up a FEM model of soil-cutting of a rotavator are as follows:

1) FEM model of rotavator

Build the 3-D solid model of the rotavator by Pro/E, as

### *方法*

**a）旋耕刀辊土壤切削有限元模型**

建立旋耕刀辊土壤切削有限元模型的主要步骤为：

1）旋耕刀辊有限元模型的建立

通过 Pro/E 建立旋耕刀辊的 3-D 实体模型，如图 1 所示。

shown in Figure 1, and save it as format .igs or .*x-t. Import the model to HyperMesh to mesh grids with grid size 6mm, and refine them according to requirement of surface complexity of the rotavator, then the FEM model of the rotavator was obtained, as shown in Figure 2.

将建立好的实体模型以.igs 或.*x-t 格式保存，导入 HyperMesh 中，定义网格尺寸为 6mm 并进行网格划分，由于旋耕刀辊曲面复杂，根据要求对网格进行细化，网格细化后得到旋耕刀辊的有限元模型，如图 2 所示。

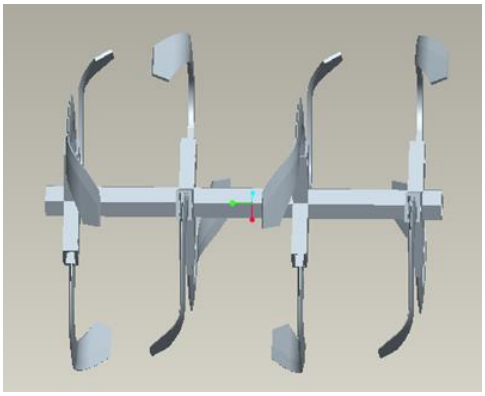

**Fig.1 -** The 3-D solid model of rotavator

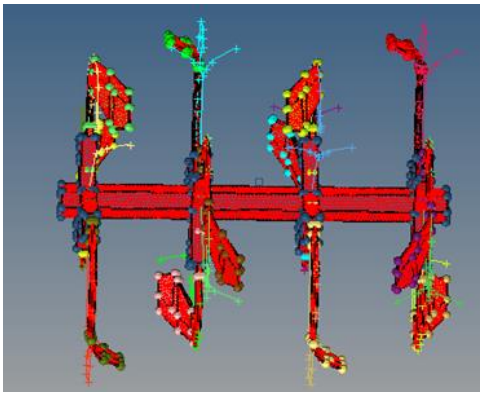

**Fig.2 –** The FEM model of rotavator

2) FEM model of soil
According to soil model MAT147 provided by ANSYS, build the 3-D solid model of soil with dimensions as required. Transform the solid model to SPH model in LS-PREPOST, and define element types and parameters of the soil. Set Lagrange single-point integration algorithm, and mesh grids with grid size of 10mm, then the FEM model of soil (soil SPH model) was obtained, as shown in Figure 3.

2）土壤有限元模型
根据 ANSYS 提供的 MAT147 土壤模型和实际土壤尺寸，建立土壤 3-D 实体模型。在 LS-PREPOST 内将土壤实体模型转化为 SPH 模型，定义单元类型和土壤材料，采用 Lagrange 型单点积分算法，定义网格尺寸为 10mm，并对模型进行进行划分，建立土壤有限元模型（土壤 SPH 模型），如图 3 所示。

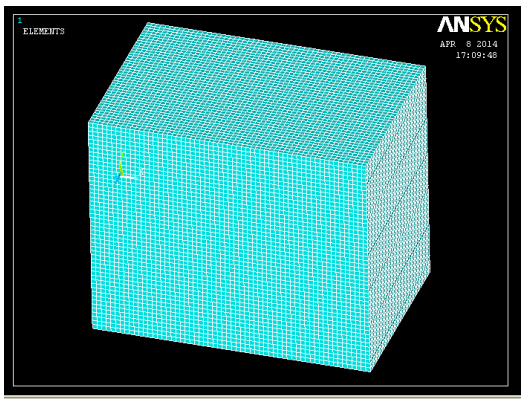


**Fig.3 -** The FEM model of soil

3) Boundary condition and contact
Define rotary blades of the rotavator as rigid bodies with stable forward speed and rotation speed, and add symmetry constraint SPH_SYMMETRY_PLANE for the soil SPH model on both sides and bottom surfaces of the soil. Define rotary blades as contact PART and soil as target PART, and add the contact between rotary blades and the soil as AUTOMATIC_NODES_TO_SURFACE. Set sliding interface penalties 0.2, and dynamic and static coefficient friction 0.20, 0.18, respectively [9].

3）边界条件及接触
定义旋耕刀辊的旋耕弯刀为刚体，旋耕弯刀前进速度和回转速度稳定。对土壤 SPH 模型添加对称约束 SPH_SYMMETRY_PLANE，约束土壤两侧面和底面。定义旋耕弯刀为接触 PART，土壤为目标 PART。添加旋耕弯刀与土壤之间的接触为自动点面接触 AUTOMATIC_NODES_TO_ SURFACE。设定滑动界面惩罚因子为 0.2，动、静摩擦因子分别为 0.18 和 0.20 [9]。

4) FEM model of soil-cutting
Import the FEM model of rotavator to LS-PREPOST, generate SPH (soil SPH model) for the rotavator, and load parameters of the rotavator and soil-cutting on Keyword Manager panel in LS-PREPOST, then the FEM model of soil-cutting was available for process, as shown in Figure 4.

4）旋耕刀辊土壤切削有限元模型的建立
将旋耕刀辊有限元模型导入 LS-PREPOST 中，为旋耕刀辊生成土壤 SPH 模型，在 LS-PREPOST 的 Keyword 管理界面添加旋耕刀辊和土壤切削参数，从而得到旋耕刀辊土壤切削有限元模型，如图 4 所示。

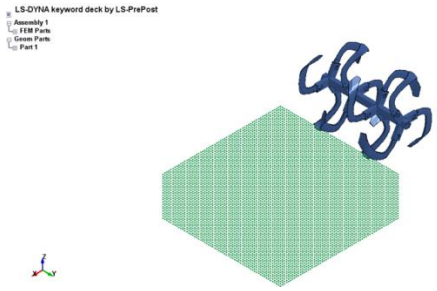


**Fig.4 -** The FEM model of soil-cutting

**b) Power consumption of soil-cutting**

The power consumption of soil-cutting of a rotavator consists of 2 parts, and one is for the machine moving forward, and the other is for the soil-cutting and soil-throwing. Define the former as kinetic power, and the latter as internal power, and the power consumption can be calculated by empirical method as follows:

1) Kinetic power

The kinetic power for the handheld tiller moving forward can be expressed as [4]:

$$P = Fv_m \quad (1)$$

Where, $P$ is kinetic power kW; $F$ is the resultant force along the forward move of the tiller, N; $v_m$ is the forward speed of the tiller, m/s.

2) Internal power

The internal power can be expressed as follow [15]:

$$N = 0.1K_\lambda dv_m B \quad (2)$$

where $N$ is internal power, kW; $K_\lambda$ is tillage resistance of rotary tilling, N/cm$^2$, and $K_\lambda = K_1K_2K_3K_4K_\alpha$; $K_\alpha$ is soil resistance, and $K_\alpha = 12$ for common clay soil, with stubble, of moisture content 20% and tilling depth 13cm. $K_1$ is correction coefficient for tilling depth, $K_2$ is correction coefficient for moisture content of the soil, $K_3$ is correction coefficient for vegetation conditions of the soil, and $K_4$ is the correction coefficient for operation mode of the tilling operation. Set $K_1 = 0.93$, $K_2 = 1.0$, $K_3 = 1.1$, and $K_4 = 0.71$ in this study. $d$ is tilling depth, cm; $B$ is tilling width, m.

**RESULTS**

By solving the FEM model of soil-cutting of the rotavator, the information of soil move with animation effect, soil-cutting force, and power consumption can be obtained for the corresponding analysis.

***Soil move***

From the animation information of soil move while soil-cutting of the rotavator, the following findings were observed: during the soil-cutting, there is no soil move before rotary blades contact the soil. With rotavator travelling forward, the lengthwise edges of two blades on the rotavator firstly contact the soil concurrently, and the soil is cut apart by the blades along forward direction. With the rotavator travelling further, the contact areas and contact points between soil and blades increase, and the soil particles, surrounding the blades, are driven apart along surfaces of the rotary blades under the co-act of shearing and squeezing, which results in the soil deformation and move. Then, the particles move with parabolic mode after they leave the surface of rotary blades to obtain effects of soil-throwing and pulverization. For quantitatively studying the soil move of different tillage layers, 3 SPH soil particles, representing surface layer, middle layer, and deep layer of tillage soil, were chosen for soil move analysis, and they were numbered as 28885 (A), 30000 (B), and 29992 (C), in Fig.5.

**b）微耕机刀辊土壤切削功率消耗**

旋耕刀辊土壤切削的功率消耗由用于旋耕刀辊前进的动能功率消耗和用于土壤变形和运动的内能功率消耗两部分组成，其功率计算公式分别如下。

1）动能功率

旋耕刀辊前进消耗的动能功率可由下式计算 [4]：

$$P = Fv_m \quad (1)$$

式中，$P$ 为旋耕刀辊前进的动能功率，kW；F 为微耕机沿前进方向的土壤反力，N；$v_m$为微耕机的前进速度，m/s。

2）内能功率

用于土壤变形和运动的内能功率可由下式计算[15]：

$$N = 0.1K_\lambda dv_m B \quad (2)$$

式中，$N$ 为刀辊土壤切削和抛土功耗，kW；$K_\lambda$ 为旋耕比阻，N/cm$^2$，$K_\lambda = K_1K_2K_3K_4K_g$；$K_g$ 为土壤阻力系数，对于一般粘土、麦茬，耕深 13cm，土壤含水率为 20%，土壤阻力系数一般取 13；$K_1$ 为耕深修正系数，取 1.0；$K_2$ 为土壤含水率修正系数，取 0.93；$K_3$ 为植被修正系数，取 1.1；$K_4$ 为作业方式修正系数，取 0.71；$d$ 为耕深，cm；$B$ 为耕作幅宽，m。

**结果与分析**

通过求解旋耕刀辊土壤切削有限元模型，可以获悉带动画效果的土壤运动情况、土壤切削力和土壤切削功率消耗等信息，并进行相关分析。

***土壤运动***

通过对旋耕刀辊土壤切削过程土壤运动动画分析可知：在土壤切削过程中，在旋耕弯刀接触土壤表层之前，土壤粒子没有运动变化，随着旋耕刀辊的旋转前进，两把旋耕弯刀的侧切刃同时首先接触土壤，在旋耕弯刀的作用下，土壤沿弯刀前进方向被切割分开，随着刀辊的继续前进，弯刀与土壤的接触面积增大，接触点增多，刀片周围的土壤粒子在弯刀剪切和挤压的作用下沿刀片表面散开，使土壤发生变形和运动。土壤粒子以抛物线的模式运动离开旋耕弯刀表面，从而获得抛土和碎土的效果。

为了定量研究不同耕层土壤的运动情况，在 SPH 粒子中选取 3 个粒子分别代表土壤表层粒子 28885（A）、中层粒子 30000（B）和深层粒子 29992（C）以进行土壤运动分析，土壤粒子标记如图 5 所示。

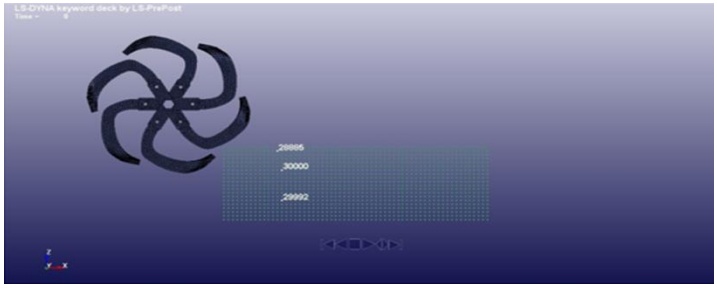

**Fig.5 -** Marked SPH soil particles

By solving the FEM model of soil-cutting of the rotavator, the velocity, acceleration and displacement curves of the particles were obtained by means of simulation, as shown in Figure 6. Of which, the red curves were of particle A, green curves were of particle B, and blue curves were of particle C. From curves of velocity and acceleration of the marked SPH soil particles as shown in Figures 6 a) and 6 b), there are 3 stages of the particles' move: 1) during 0-0.3s, the rotary blades of the rotavator does not contact the 3 marked soil particles, and the particles does not show any obvious move with small values of velocity and acceleration; 2) during 0.3-0.8s, the rotary blades start to contact the marked particles, and the particles of different layers, subjected to forces from rotary blades and the surrounding soil, obtain different velocity and acceleration as: particles of the top layer particles get the highest velocity and acceleration, and velocity and acceleration of middle layer and bottom layer particles decrease sequentially; 3) after 0.8s, the rotary blades leave the marked particles, and the forces acting on the particles decrease, then the velocity and acceleration decrease as well. Furthermore, from curves of displacement of the marked SPH soil particles as shown in Figure 6 c), after the contact of soil and blades, the top layer particles get the highest displacement, which reflects that the top layer soil is deformed and destroyed seriously because of shearing force provided by the rotary blades of the rotavator. This soil move observation has a similar pattern as Xia's study [8]

通过求解旋耕刀辊土壤切削有限元模型和仿真分析，可以获悉不同深度粒子速度曲线、加速度曲线和位移曲线，如图 6 所示。其中，粒子 A 用红色线条表示，粒子 B 用绿色线条表示，粒子 C 用蓝色线条表示。通过对图 6 a）、6 b）的速度曲线和加速度曲线分析可得，粒子的运动有 3 个过程：1）在 0-0.3s 阶段，刀辊的旋耕弯刀没有切削到标记的 SPH 粒子时，3 个粒子几乎都没有运动变化，其速度和加速度值很小；2）0.3-0.8s 阶段，旋耕弯刀开始接触到标记粒子，不同耕层土壤粒子受到旋耕弯刀和周围土壤的力的作用，获得不同的速度和加速度：表层粒子的速度和加速度最大，中层粒子次之，深层粒子的速度和加速度最小；3）在 0.8s 之后，旋耕弯刀离开标记粒子，土壤粒子受力减小，速度和加速度也同时减小。而且，通过对图 6 c）中标记 SPH 土壤粒子的位移曲线可知：经历旋耕弯刀和土壤的接触以后，表层土壤粒子的位移量最大，这表明表层土壤粒子由于旋耕刀辊弯刀提供的剪切力而产生的变形和破坏严重。这种土壤运动现象与夏俊芳研究得到的土壤运动方式相似 [8]。

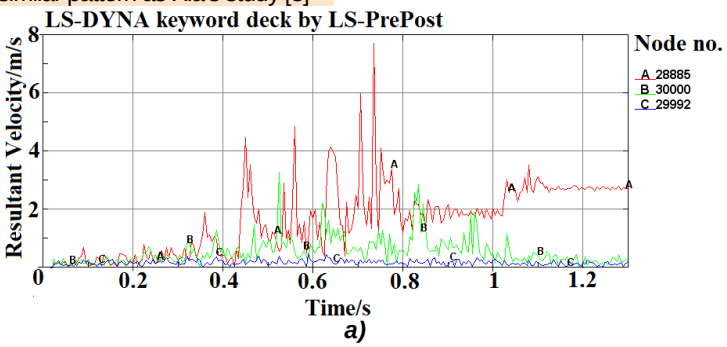


*a)*

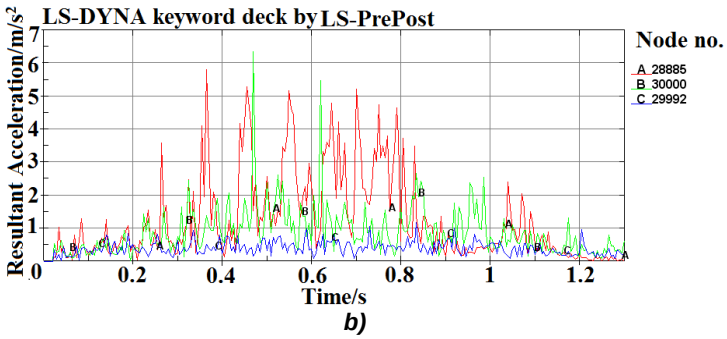


*b)*

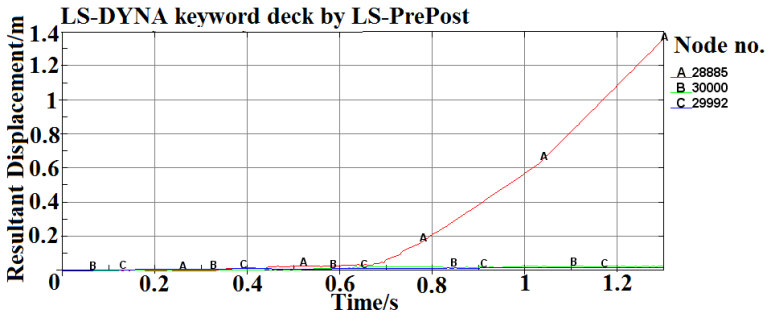


*c)*

**Fig.6 -** Soil move of different layers
a) Speed curve; b) Acceleration curve; c) Displacement curve

***Soil-cutting force***

The curve of soil-cutting force by FEM method was obtained, as shown in Figure 7. In the initial stage of soil-cutting, the soil-cutting force is relatively small with low fluctuations, and with the processing of soil-cutting, the soil-cutting force increases gradually, and it reaches a certain status with a relatively high fluctuations. The reason for the observed curve pattern of soil-cutting force is as follows: in the initial stage of soil-cutting, there are only two rotary blades on the rotavator contact the soil, and after that more and more blades take part in the soil-cutting operation to stabilize the soil-cutting force. This soil-cutting force observation coincides with Lin's study on that of rotary blade [5].

In fact, when the rotary blades start to contact the soil, with the forward travel of the blades, the contact areas of soil-blade increase, the soil deforms elastically, and the force acting on the soil increases gradually. With the increases of deformation and force acting on the soil, the soil deforms plastically, and it follows the soil hardening, then the soil-cutting force reaches maximum value, and the soil structure breaks down and is destroyed accordingly. After that, there is soil softening effect which results in decrease of soil-cutting force. Therefore the soil-cutting process is stabilized at a status with a certain fluctuations [12].

***土壤切削力***

通过有限元法得到土壤切削力曲线，如图 7 所示。在土壤切削的初始阶段，土壤切削力很小，并且在一个较小范围内波动。随着切削过程的进行，切削力逐渐增大并达到一定水平，其波动也相对较大。这种土壤切削力曲线变化主要原因在于：在土壤切削的初始阶段，旋耕刀辊只有两把旋耕弯刀接触并切削土壤，随着时间增加，均匀布置的多把旋耕弯刀依次切削土壤，使切削力变得均匀稳定。这种土壤切削力的现象与林昌华对旋耕弯刀的研究结论吻合[5]。

事实上，当旋耕弯刀开始接触土壤，随着旋耕弯刀不断前行，刀具和土壤的接触面积增大，土壤产生弹性变形，作用在土壤上的切削力逐渐增加。随着土壤变形和土壤切削力的增加，土壤产生塑性变形，随之产生土壤硬化，此时土壤切削力达到最大值，土壤结构遭到破坏，发生初始失效，土壤切削力逐渐减小。因而土壤切削过程进入稳定切削状态，但土壤切削力在一定范围内波动 [12]。

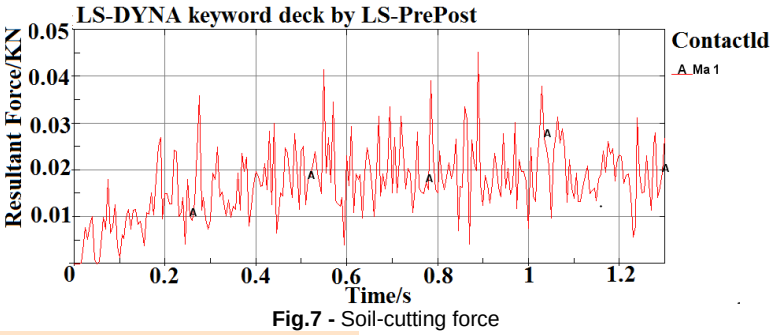


**Fig.7 -** Soil-cutting force

***Power consumption***

The curves of energy of soil-cutting by FEM method were obtained, as shown in Figure 8. Of which, Figure 8 (a) is curve of kinetic energy, Figure 8 (b) is curve of internal energy, and Figure 8 (c) is curve of total energy of soil-cutting, and the energy information can be employed to calculated the corresponding power consumption. The total energy of soil-cutting is the addition of kinetic energy and internal energy. The total energy of soil-cutting of rotavator increases linearly after the initial soil-cutting stage. The internal energy constitutes a high proportion of total energy of soil-cutting, namely, the power consumption of soil-cutting is mainly consumed by means of internal energy. According to power consumption Equations (1) and (2) in section 2,

***功率消耗***

通过有限元法得到土壤切削能量曲线，如图 8 所示。其中，土壤切削过程的动能消耗如图 8 a）所示，内能消耗如图 8 b）所示，总能量消耗如图 8 c）所示。土壤切削能量信息可以用于计算相应的土壤切削功率消耗。土壤切削总能量消耗是内能消耗和动能消耗之和。在经历了土壤切削初始阶段以后，旋耕刀辊土壤切削力线性增加。内能组成了土壤切削总能量的大部分，也就是说，土壤切削功率主要通过内能的方式消耗。根据公式（1）和（2），以重

taking a handheld tiller SR1Z-80 with mass 80kg and rated power 4kW (manufactured by Chongqing Shineray Agricultural Machinery Co., Ltd.) as an example, the power consumption by means of kinetic energy and internal energy was 0.15kW and 1.42kW for one rotavator of the tiller (the handheld tiller brings 2 rotavators for the tillage), and the ratio of kinetic energy and internal energy is 1:9.5, and it is consistent with the relationship between curves of kinetic energy and internal energy of soil-cutting as shown in Figure 8, which validates effectiveness of the FEM analysis of soil-cutting.

庆鑫源农机股份有限公司生产的 SR1Z-80 微耕机（80kg，4kW）为例。微耕机一个旋耕刀辊通过动能和内能消耗的功率分别为 0.15kW 和 1.42kW（一台微耕机带左右 2 个旋耕刀辊），动能和内能消耗的功率之比为 1：9.5，这与图 8 中土壤切削动能和内能曲线关系相符合，验证了旋耕刀辊土壤切削有限元分析的有效性.

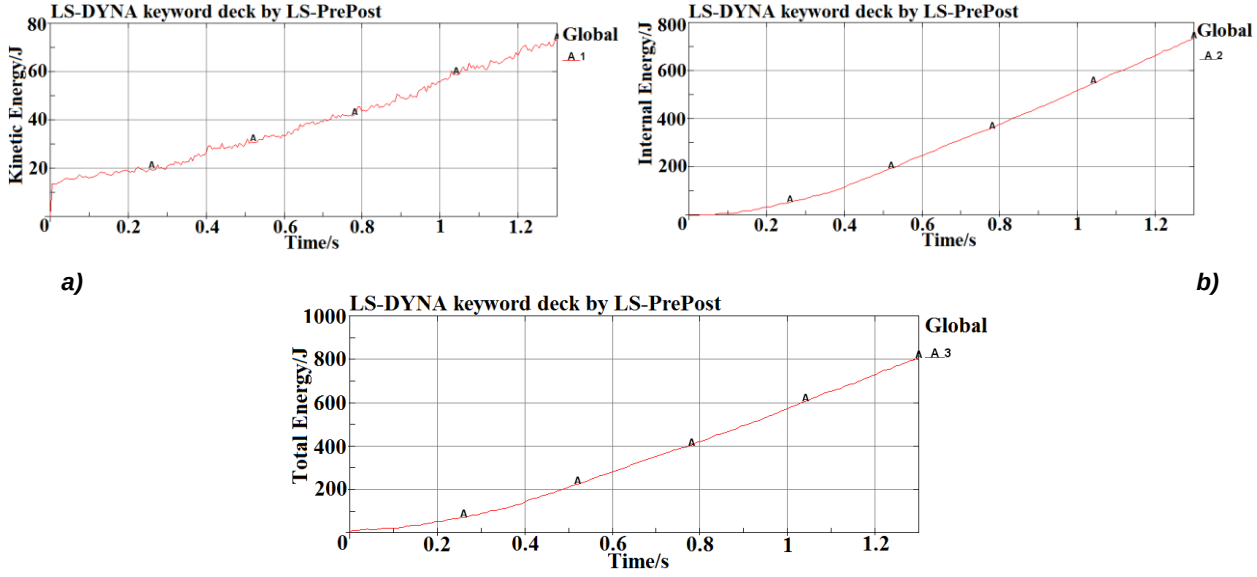


*a)* *b)* *c)*

**Fig.8 -** Total energy of soil-cutting
a) Kinetic energy; b) Internal energy; c) Total energy

## CONCLUSIONS

The soil-cutting performance analysis of a handheld tiller's rotavator by FEM method was conducted, and the effectiveness of the analysis was validated in this study. During soil-cutting of the rotavator, soil of different layers gets different velocity and acceleration, and the top layer soil gets the highest velocity and acceleration. The soil-cutting force increases to a maximum, and follows a gradual decrease to reach a relatively stable status with some fluctuation. Power consumption, combination of kinetic power and internal power, is mainly consumed by means of internal energy, with ratio of kinetic power and internal power 1: 9.5.

## 结论

通过有限元法分析了微耕机旋耕刀辊的土壤切削性能，验证了土壤切削性能分析的有效性。在旋耕刀辊土壤切削过程，不同深度的粒子获得不同的速度和加速度，表层粒子获得的速度和加速度最大。土壤切削力先增加到最大值，之后逐渐减小从而进入稳定切削状态，并在一定范围内波动。功率消耗，主要包括动能功率消耗和内能功率消耗，且主要由内能功率消耗决定，动能功率消耗和内能功率消耗之比为 1：9.5。

## ACKNOWLEDGEMENT

The study was supported by the National Natural Science Foundation of China (No. 51475385), the Scientific Research Foundation for the Returned Overseas Chinese Scholars, Ministry of Education of China (No. 2013-1792), Fundamental Research Funds for the Central Universities of China (No. XDJK2014C033), and Funds from Nanjing Research Institute for Agricultural Mechanization, Ministry of Agriculture (2014-1053).

## 致谢

本研究得到中国国家自然科学基金项目（51475382）、中国教育部留学回国人员科研启动基金（2013-1792）、中国中央高校基本科研业务费专项资金资助项目（XDJK2014C033）和中国农业部南京农机化研究所资助项目（2014-1053）的资助。

## REFERENCES

[1]. Abo-Elnor M., Hamilton R., Boyle J.T., (2003) - *3D dynamic analysis of soil-tool interaction using the finite element method.* Journal of Terramechanics, vol. 40, no. 1/2003, ISSN 0022-4898, pg. 51-62;
[2]. Asl J.H., Surendra S., (2009) - *Optimization and*

## 参考文献

[1] Abo-Elnor M., Hamilton R., Boyle J. T. (2003) - *3D dynamic analysis of soil-tool interaction using the finite element method*. Journal of Terramechanics, 第 40 卷, 第 1 期/2003, ISSN 0022-4898, 51-62;

*evaluation of rotary tiller blades: computer solution of mathematical relations.* Soil and Tillage Research, vol.106, no. 1/ 2009, ISSN 0167-1987, pg. 1-7;
[3]. Lewis B.A., (2004) - *Manual for LS-DYNA soil material model 147.* Report of Turner-Fairbank Highway Research Center, Georgetown, USA;
[4]. Li B., (2008) - *Agricultural machines,* China Agriculture Press, ISBN 978-7-109-08403-2, Beijing, P. R. China;
[5]. Lin C., Kang S., Qin F., et al., (2015) - *Simulation analysis and optimization of rotary blade on FEM.* Agricultural Development & Equipments, no. 1/2015, ISSN 1673-9205, pg. 55-57;
[6]. Peng B., (2014) - *Modeling and simulation of soil-cutting dynamics of rotary roller of mini-tiller.* M.S. thesis, Southwest University, P. R. China;
[7]. Shi L., Zhang H., Zhai Z., et al, (2004) - *Present situation and development of two-wheel tractor*. Journal of Agricultural Mechanization Research, no. 5/2004, ISSN 1003-188X, pg. 1-3;
[8]. Xia J., He X., Yu S., et al., (2013) - *Finite element simulation of soil cutting with rotary knife roller based on ANSYS/LS-DYNA software.* Transactions of the Chinese Society of Agricultural Engineering, vol. 29, no. 10/2013, ISSN 1002-6819, pg. 34-41;
[9]. Xue Z., Lv X., Tang W., (2011) - *The simulation of soil cutting with screw cutter based on ANSYS/LS-DYNA971.* Journal of Agricultural Mechanization Research, vol. 33, no. 4/2011, ISSN 1003-188X, pg. 13-16;
[10]. Yang L., Zhu L.-X., Chen J., et al, (2014) - *Simulation and evaluation of soil-cutting power parameter of a handheld tillers rotary blade.* International Agricultural Engineering Journal, vol. 23, no. 4/2014, ISSN 0858-2114, pg. 21-27;
[11]. Zeng D., (1995) - *Machinery-soil dynamics*, Beijing Science and Technology Press, ISBN 7-5304-1602-2, Beijing, P. R. China;
[12]. Zhou M., (2009) - *Research on FEM-based working mechanism of transverse knife on helical rotary roller.* M.S. thesis, Huazhong Agricultural University, P. R. China;
[13]. Zhu L., Yang L., Yang M., et al, (2011) - *Technical status and development trend of the mini-tiller in China.* Journal of Agricultural Mechanization Research, vol. 33, no. 7/ 2011, ISSN 1003-188X, pg. 236-239;
[14]. *** Chinese Standard Committee, (2008) - *Rotary tiller-rotary blades and blade holders*, *GB/T 5669-2008*. Chinese Standard Press, P. R. China;
[15]. *** Chinese Academy of Agricultural Mechanization Sciences, (2007) - *Design manual of agricultural machinery,* Chinese Agricultural Science and Technology Press, ISBN 978-7-80233-335-2, Beijing, P. R. China;
[16]. *** U.S. Department of Transportation Federal Highway Administration, (2004) - *Evaluation of LS-DYNA soil material model 147.* Report of Turner-Fairbank Highway Research Center, Georgetown, USA.

[2]. Asl J.H., Surendra S. (2009) - *Optimization and evaluation of rotary tiller blade: computer solution of mathematical relations*. Soil & Tillage Research. 第 106 卷, 第 1 期/2009, ISSN 0167-1987, 1-7;
[3]. Lewis B.A., (2004) - *Manual for LS-DYNA soil material model 147*. Report of Turner-Fairbank Highway Research Center, Georgetown, USA;
[4]. 李宝筏. (2008) - *农业机械学.* 中国农业出版社，ISBN 978-7-109-08403-2, 北京, 中国;
[5]. 林昌华, 康松林, 秦飞龙, 等. (2015) - *旋耕刀有限元仿真分析及优化*. 农业开发与装备, 第 1 期, ISSN 1673-9205, 55-57;
[6]. 彭彬. (2014) - *微耕机刀辊切土动力学建模及仿真*. 硕士论文, 中国: 西南大学;
[7]. 时玲, 张海东, 翟兆斌, 等. (2004) - *我国微耕机技术现状与发展方向*. 农机化研究, 第 5 期/2004, ISSN 1003-188X, 1-3;
[8]. 夏俊芳, 贺小伟, 余水生, 等. (2013) - *基于 ANSYS/LS-DYNA 的螺旋刀辊土壤切削有限元模拟*. 农业工程学报, 第 29 卷, 第 10 期/2013, ISSN 1002-6819, 34-41;
[9]. 薛子萱, 吕新民, 唐卫卫. (2011) - *螺旋刀具土壤切削过程模拟分析 - 基于 ANSYS/LS-DYNA971*. 农机化研究, 第 33 卷, 第 4 期/2011, ISSN 1003-188X,13–16;
[10]. Yang L, Zhu L-X, Chen J, et al. (2014) - *Simulation and evaluation of soil-cutting power parameter of a handheld tillers rotary blade*. International Agricultural Engineering Journal, 第 23 卷, 第 4 期/2014, ISSN 0858-2114, 21-27;
[11]. 曾德超. (1995) - *机械土壤动力学*. 北京科学技术出版社, ISBN 7-5304-1602-2, 北京, 中国.
[12]. 周明. (2009) - *基于有限元法的螺旋型旋耕刀辊横刀工作机理研究*. 中国: 华中农业大学;
[13]. 朱留宪, 杨玲, 杨明金, 等. (2011) - *我国微型耕耘机的技术现状及发展*. 农机化研究, 第 33 卷, 第 7 期/2011, ISSN 1003-188X, 236-239;
[14]. 中国国家标准化管理委员会, (2008) - *旋耕机械刀和刀座, GB/T 5669-2008*. 中国标准出版社, 中国;
[15]. 中国农业机械化科学研究院. (2007) - *农业机械设计手册*. 中国农业科学技术出版社, ISBN 978-7-80233-335-2, 北京, 中国;
[16]. U.S. Department of Transportation Federal Highway Administration, (2004) - *Evaluation of LS-DYNA soil material model 147*. Report of Turner-Fairbank Highway Research Center, Georgetown, USA.

# FLOW FIELD SIMULATION AND ANALYSIS OF BAG FILTER FOR AGRICULTURE SEWAGE
# /
# 农业污水袋式过滤器内流场特性仿真分析

**Prof. Ph.D. Feng Zi-ming, Fang Xin, Gao Qiming, Ding Huanhuan**
School of Mechanical Science and Engineering, Northeast Petroleum University, Daqing/ China
*Tel: 008604596503121; E-mail: xueyuanfzm@163.com*

***Abstract:*** *According to the agriculture sewage in the process of filtering impurity, medium pressure drop is not allowed to exceed 0.02MPa requirements. Using computational fluid dynamics (CFD) technology to study the porosity of bag filter, the inlet velocity of filter and the agriculture sewage viscosity change, which influence the pressure drop. The calculation results show that the higher the porosity, the higher outlet back-pressure and the agriculture sewage viscosity is higher，so when it flows through the filter, its pressure drop is higher. CFD technology can replace a part experimental study and it can provide guidance for the filter bag selection and replacement.*

***Keywords:*** *agriculture sewage, bag filter, flow field, pressure drop, porosity, numerical simulation*

## INTRODUCTION

At present, in view of global water shortages, urban sewage and rainwater recycling problem has aroused people's wide concern. Urban sewage and rainwater recycling are reused for non-potable water, such as agricultural irrigation, watering road, supplement waterscape, building water [2,3,7]. But the wastewater usually needs to filter. To meet the requirements of water quality, some pollutants must be removed, such as suspended solids, pathogenic bacteria/viruses, turbidity, organic matter, including nitrogen, phosphorus and other plant nutrients [6].

Qi et al [8] analyzed the reason which made the air current distribution uneven and proposed the improvement of which modifies the structure of inlet and adds guide plate in the lower-case. They obtained the flow field, the streamline and granule path which were around improvement with the software of CFD. The conclusion may provide the reference to performance, improve and design of fabric filters. Rocha [5] used CFD techniques to review the distribution of volumetric outflows in the bags and pressure drop for a more efficient and economic filtering operation, and provided an inferior operational pressure drop and a better distribution of fluids between the bags. A numerical simulation of CFD for bag filter was conducted to replace the experimental study by Fu et al [1], the numerical results shown that the main reasons of flow field non-uniformity are the higher inlet velocity and unreasonable bag chamber structure and the computer results are basically consistent with experimental ones, which indicated that CFD technology can replaces some test studies. Li et al [4] used CFD method to compute the velocity field between the bag filter, they analyzed the influence of different distances between the air nozzle and the filtering bag and different injecting times on the dust-cleaning effect, and supplied theoretical basis to design the optimal pulse bag filter.

***摘要：****针对农业污水在过滤杂质流程中，介质压降不许超过 0.02MPa 的要求，利用 CFD 技术研究过滤袋孔隙率、过滤器出口被压、过滤器进口流速和农业污水粘度的变化对压降的影响，计算结果表明：孔隙率越大，出口被压越大，进口流速越大，农业污水粘度越大，农业污水流经过滤器后的压降越大。CFD 技术可以替代部分的试验研究，并对过滤袋的选择和替换提供指导。*

***关键词：****农业污水，过滤袋，流场，压降，数值仿真*

## 前言

目前，针对全球性水资源短缺问题, 城市污水与雨水的再利用问题已引起人们的广泛关注。城市污水与雨水的再利用目标为非饮用水，诸如农业灌溉、浇洒道路、补充水景、建筑用水等场合[2,3,7]。但污水和雨水一般需要过滤。为满足水质要求而被去除的污染物通常为悬浮物、浊度、有机物、病原菌/ 病毒, 甚至还包括氮、磷等植物性营养元素[6]。

齐银等人[8]分析了过滤袋内气流分布不均匀的原因，并提出在了改进入口结构和增加导流板的方法。并通过 CFD 软件的计算获得了流场、极限流线和颗粒的运动轨迹，获得成果为提高过滤袋的性能提供了参考。Rocha, S.M.S[5]等人运用 CFD 技术回顾了过滤袋经济操作时的内流流场的分布和压力降，并给出不利操作和合理操作时的过滤袋内压力分布。付海明[1]等人使用数值计算 CFD 软件取代实验，进行过滤袋的仿真计算，计算结果表明；流场分布不均匀的主要原因是较高的进口速度和不合理的过滤袋角部结构，并且计算结果与实验结果吻合较好，说明 CFD 技术可以取代一些实验研究。李志华等人[4]使用 CFD 方法计算了袋式过滤器的内流场，并分析了不同距离在气嘴和滤袋及不同射流时间内对灰尘清理效果的影响，并提供了用于优化设计过滤袋的理论基础。

According to several papers from the specialty literature [1,7], sifting of intermediate products is affected by several factors, the most important being: size and shape of the grist particles, character of the relative motion of the particles on the sieve surface, characteristics of sifting sieve fabric, revolution of plansifter, and the amount of material that reaches on the sieve.

Before agriculture sewage irrigating into farmland, impurity needed to be filtered by using bag filter (as shown in Fig.1). The permeability of bag filter will change, so this paper uses CFD technology to do numerical simulation about filter internal flow field, according to the filter bag porosity, outlet pressure, inlet velocity, agriculture sewage viscosity, so as to provid references for replacement cycle of the filter bag and for prediction of pressure drop loss.

根据专业论文文献[1]和[7]的论述，中间产品的筛选是受几个因素的影响，最重要的是；谷物颗粒的大小和形状，粒子在筛面的相对运动特性，筛布的特性，平面筛的旋转，筛上材料的数量等。

农业用污水在灌溉农田前需要用过滤袋（如图 1）滤掉杂质，使用过程中，过滤袋的渗透性会发生变化，因此本文使用 CFD 技术对过滤袋空隙度、出口压力、进口流速、农业污水粘度对过滤器内流场进行了数值仿真，从而为过滤袋的更换周期和压降损失的预估提供了参考。

**Fig. 1** - Bag Filter

## MATERIAL AND METHOD

Table 1 shows the basic characteristic parameters of flowing medium (agriculture sewage). Fig.2 is a three-dimensional geometric model of the filter, inlet diameter and outlet diameter are 160mm, the diameter of the container is 610mm, the height of the container is 1260mm. The length of the filter bag is 820mm and its diameter is 160mm, thickness is 2.8mm.

As shown in Fig. 2, geometry model of the filter is a single container and a single filter bag. The cylindrical structure which in the middle of figure is filter bag, when we do the numerical simulation, we assume it as porous materials.

The following statistics is part of the grid information of inlet liquid: inlet liquid grid of filter is 223600, outlet liquid grid of filter is 139500, and the total number of bag filter grid is 139700. The grids are divided by using ANSYS-ICEM software, self-adaption tetrahedral mesh as a main part and making grid of filter bag's part flow region becomes dense. All the wall surface of filter are divided in boundary layer. The quality of grid as shown in Fig.3-d, the minimum quality coefficient is 0.4, which fully meets the computational fluid dynamics software CFX to mesh quality requirements.

The boundary conditions are as follows；Reference pressure is 0.1 MPa. Fluid temperature is 40. Heat transfer option is isothermal. Turbulence model is k-epsilon. Wall function is scalable. Area porosity is isotropic. Loss model is isotropic loss. Loss velocity type is superficial. Inlet normal speed is 0.421 m/s. Inlet turbulence intensity is 5%. Outlet average static pressure is 3.5 MPa.

## 材料与方法

表 1 为流动介质（农业污水）的基本特性参数。图 1 为过滤的三维几何模型，进口直径和出口直径为 160mm，容器直径 610mm，容器高度 1260mm，过滤袋长 820mm，直径 160mm，厚度 2.8mm。

如图 2 所示，本过滤器的几何建模为单容器、单过滤袋。图中中间的圆筒结构为过滤袋，数值仿真是假设为多空介质材料。

过滤器的进液结构部分网格信息统计如下：过滤器进液网格 22.36 万，过滤器出液网格 13.95 万，过滤袋部分网格总数 13.97 万。网格采用 ANSYS-ICEM 软件进行网格划分，自适应四面体网格为主体，过滤袋部分流域进行网格加密，过滤器所有壁面进行了边界层划分。网格质量如图 3-d 所示，最小质量系数为 0.4，完全满足流体计算动力学软件 CFX 对网格质量的要求。

边界条件如下；参考压力为 0.1 MPa. 流体温度为 40℃. 热传导方式为等温过程。 湍流模型为 k-epsilon. 壁面函数为可扩展。多孔介质为各向同性 。损失模型为各向同向损失模型。 损失速度形式为表面型。进口法向速度为 0.421 m/s. 进口湍流强度为 5%. 出口平均静压力为 3.5 MPa.

Table 1

**Basic Characteristic Parameters of Flow Medium**

| Category | Data | Category | Data |
|---|---|---|---|
| Medium | Agriculture Sewage | Medium density | 1010 kg/m$^3$ |
| concentration | 15000PPM | Dynamic viscosity | 494 mPa.s |
| viscosity | 494mPa.s | Specific pressure heat capacity | 4178 J/kg.k |
| Operation temperature | 40℃ | Coefficient of thermal expansion | 5.405×10-4k$^{-1}$ |
| inlet pressure | 3.5MPa | Heat conductivity coefficient | 66.35×10-2W/mk |
| Maximum flow | 150m3/h | Porosity of filter bag | 0.45 |

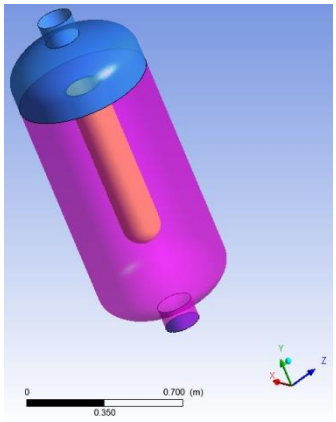

**Fig. 2** - 3D Perspective of Filter

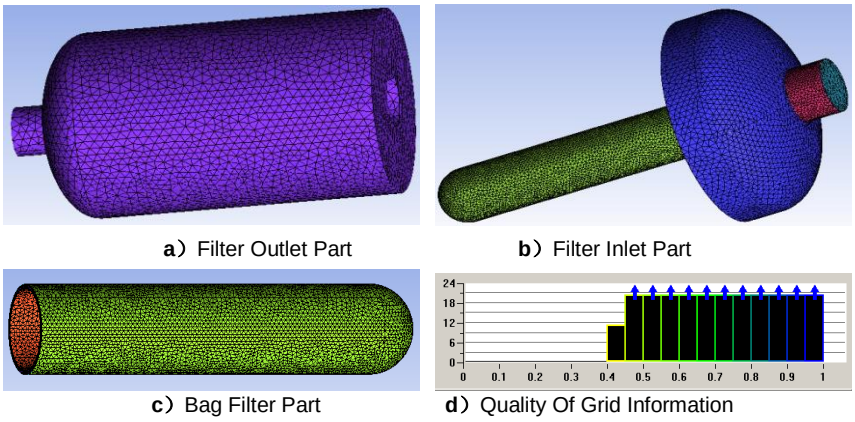


**Fig. 3** - Three-Dimensional Mesh of Filter

## 1. Theoretical Basis

- **Navier-Stokes Equations**

The general Navier-Stokes equations written in a Cartesian frame can be expressed as:

$$\frac{\partial}{\partial t}\int_{\Omega} U d\Omega + \int_{S} \vec{F}_I \cdot d\vec{S} + \int_{S} \vec{F}_V \cdot d\vec{S} = \int_{\Omega} S_T d\Omega \quad (1)$$

Where $\Omega$ is the volume and $S$ is the surface, $U$ is the vector of the conservative variables. $\vec{F}_I$ and $\vec{F}_V$ are respectively the inviscid fluid and viscous flux vectors. $E$ and $q_i$ the total energy and the heat flux components. $\kappa$ and $S_T$ are respectively the laminar thermal conductivity and the source terms.

- **Standard $k-\omega$ Model**

The turbulence kinetic energy $k$, and its rate of dissipation, $\omega$, are obtained from the following transport equations:

$$\frac{\partial}{\partial t}(\rho k) + \frac{\partial}{\partial x_i}(\rho k u_i) = \frac{\partial}{\partial x_j}\left[\left(\mu + \frac{\mu_t}{\sigma_k}\right)\frac{\partial k}{\partial x_j}\right] + G_k + G_b - \rho\varepsilon - Y_M + S_k \quad (2)$$

$$\frac{\partial}{\partial t}(\rho \varepsilon) + \frac{\partial}{\partial x_i}(\rho \varepsilon u_i) = \frac{\partial}{\partial x_j}\left[\left(\mu + \frac{\mu_t}{\sigma_\varepsilon}\right)\frac{\partial \varepsilon}{\partial x_j}\right] + G_{1\varepsilon}\frac{\varepsilon}{k}(G_k + C_{3\varepsilon}G_b) - C_{2\varepsilon}\rho\frac{\varepsilon^2}{k} + S_\varepsilon \quad (3)$$

In these equations, $G_K$ represents the generation of turbulence kinetic energy due to the mean velocity gradients, $G_b$ is the generation of turbulence kinetic energy due to buoyancy. $Y_M$ indicates the contribution of the fluctuating dilatation in compressible turbulence to the

## 1. 基本理论

- **纳维-斯托克斯方程**

一般纳维斯托克斯方程用笛卡尔坐标进行书写如下；

其中$\Omega$代表体积，$S$代表面积，$U$代表保守变量的矢量。$\vec{F}_I$和$\vec{F}_V$分别代表非粘性和粘性流动矢量。$E$和$q_i$分别代表总能和热流量元素。$\kappa$和$S_T$分别代表层流带热系数和源项。

- **标准$k-\omega$模型**

湍流动能为$k$，它的耗散率为$\omega$，两个变量可以通过下面输运方程获得：

式中，$G_K$是指由层流速度梯度而产生的湍流动能，$G_b$表示由于浮力引起的湍动能的产生项，对于不可压缩流体，$Y_M$可压湍流中脉动扩张值，对于不可压流体，

overall dissipation rate. $C_{1\varepsilon'}$ $C_{2\varepsilon'}$ and $C_{3\varepsilon}$ are constants. $\sigma_k$ and $\sigma_\varepsilon$ are the turbulent Prandtl numbers for $k$ and $\varepsilon$, respectively. $S_k$ and $S_\varepsilon$ are user-defined source terms.

The turbulent (or eddy) viscosity, $\mu_t$ is computed by combining $k$ and $\varepsilon$ as follows: $\mu_t = \rho C_\mu \frac{k^2}{\varepsilon}$

Where $C_\mu$ is a constant.

The model constants $C_{1\varepsilon}, C_{2\varepsilon}, C_\mu, \sigma_k$ and $\sigma_\varepsilon$ have the following default values: $C_{1\varepsilon} = 1.44, C_{2\varepsilon} = 1.92,$ $C_\mu = 0.09,$ $\sigma_k = 1.0,$. $\sigma_\varepsilon = 1.3$.

## 2. Numerical Simulation Results and Discussion

The simulation calculation cases include change of porosity, outlet pressure, inlet velocity and viscosity of fluid. Porosities are respectively 0.2、0.3、0.45、0.6、0.8, outlet pressures are respectively 0.5 MPa, 1.5 MPa, 2.5 MPa, 3.5 MPa, inlet velocities are respectively 0.168m/s, 0.421 m/s, 0.841 m/s, 1.682 m/s, 2.522 m/s, viscosities are respectively 0.001 mPa.s, 0.05 mPa.s, 0.1 mPa.s, 0.25 mPa.s, 1.5mPa.s.

### Influence of Porosity on Pressure Drop

- **Porosity VS Velocity Vector Distribution**

Porosity directly affects the flow velocity distribution of the filter, as is shown in figure 4, Imports around have whirlpool, have obvious local pressure loss. Inlet velocity is larger, after entering the filter, the space increases suddenly, the liquid will be slow down. After the liquid medium enters into the filter bag, due to narrow the space of flows, speed suddenly increases, now the liquid medium enters into the tapering bore channel and flow, and there is no small loss. The speed at the outlet increased with the increase of porosity, and in this case the loss is smaller than the import losses.

$C_{1\varepsilon'}$ $C_{2\varepsilon'}$ 和 $C_{3\varepsilon}$ 为经验常数项。$\sigma_k$ 和 $\sigma_\varepsilon$ 分别为与耗散率 $\varepsilon$ 和湍动能 $k$ 对应的 Prandtl 数。$S_k$ 和 $S_\varepsilon$ 是用户自定义源项。

湍流粘性（涡粘性）$\mu_t$ 是通过 $k$ 和 $\varepsilon$ 的合并计算得出，如式：$\mu_t = \rho C_\mu \frac{k^2}{\varepsilon}$

其中 $C_\mu$ 是常数。. 模型常量 $C_{1\varepsilon}, C_{2\varepsilon}, C_\mu, \sigma_k$ 和 $\sigma_\varepsilon$ 的默认缺省值分别为：$C_{1\varepsilon} = 1.44, C_{2\varepsilon} = 1.92,$ $C_\mu = 0.09,$ $\sigma_k = 1.0,$. $\sigma_\varepsilon = 1.3$。

## 2. 数值模拟结果和讨论

仿真计算案例包括改变孔隙度、出口压力、进口流速和流体粘性。孔隙度分别为 0.2、0.3、0.45、0.6、0.8 取值，出口压力分别为 0.5MPa、1.5 MPa、2.5 MPa、3.5 MPa，进口流速分别为 0.168m/s、0.421 m/s、0.841 m/s、1.682 m/s、2.522 m/s，粘性分别为 0.001 mPa.s、0.05 mPa.s、0.1 mPa.s、0.25 mPa.s、1.5mPa.s。

### 孔隙度对压降的影响

- **孔隙度——速度矢量分布图**

孔隙度直接影响过滤器流动速度分布，由图 4 可知，进口四周有漩涡产生，有明显的局部压力损失。进口速度较大，进入过滤器后，空间突然增大，液体减速。液体介质进入过滤袋后，由于流动空间的缩小，速度由突然加速，此时输入渐缩孔道流动，也有不小的损失。出口处速度随着孔隙度的增加而增加，此时损失相对进口为小。

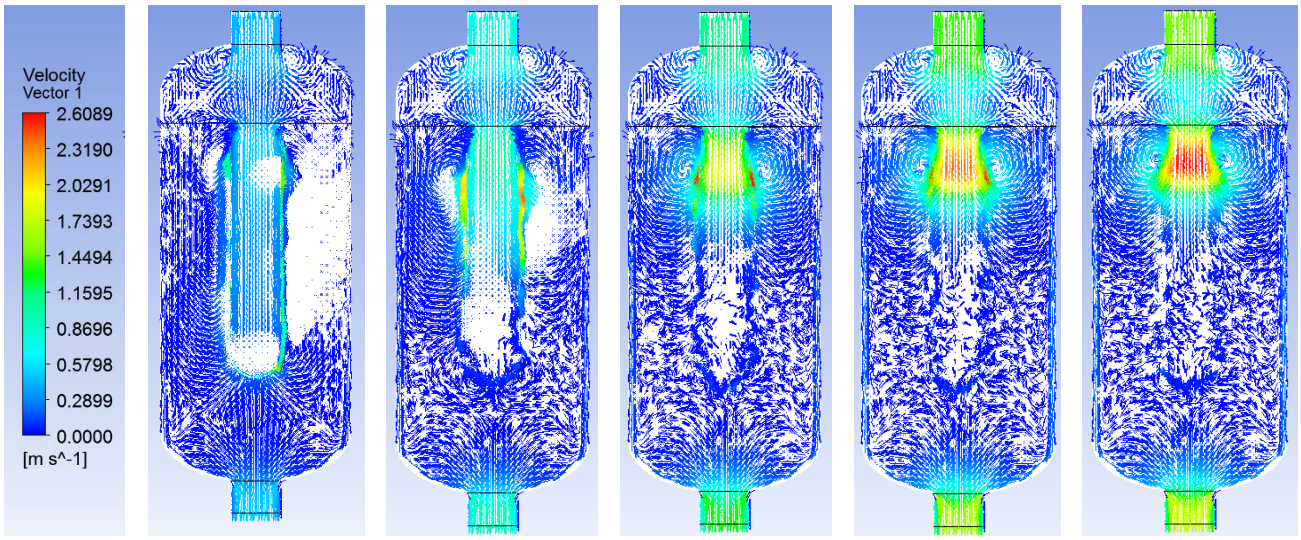


**Fig.4** - Effect of filter bag porosity on flow field velocity vector distribution

- **Porosity in comparison with total pressure distribution diagram**

The total pressure of filter inlet has obvious gradient change, after the liquid moves through the inlet into the cylinder, which space increases suddenly, so liquid becomes expansion and deceleration, pressure increases and velocity decreases. The orifice around has whirlpool, there is the greater pressure loss. Another place of the greater pressure loss is the inlet part of the filter bag, because of the whirlpool around inlet. As the porosity increases, the variation of the inlet pressure is not obvious (expect the porosity is 0.2). But the total pressure loss at the inlet of the filter bag gradually retreats to the outlet of filter bag.

Along with the porosity increasing, the pressure loss is increased slightly. But overall, the total pressure loss doesn't change much, remaining at around 360Pa. The total pressure loss is calculated using the CFD technology and can reflect the change of pressure drop in the filter bag.

- **孔隙度——总压分布图**

过滤器进口有明显的总压力梯度变化，液体由进口进入筒体后，空间突然增大，液体膨胀减速，压力增加，速度减小。在孔口四周有漩涡产生，此处压力损失较大。另一处损失较大的地方为过滤袋进口部分，近袋口处有漩涡产生。随着孔隙率的增加，进口压力变化并不明显（孔隙度为 0.2 除外）。但是过滤袋进口处的总压损失渐渐退至滤袋口部。

随着空隙度的增加压力损失略有增加，但是总体来说，总压损失变化并不大，保持在 360Pa 左右。说明利用 CFD 技术计算的总压力损失能够反映压降在过滤袋内的变化规律。

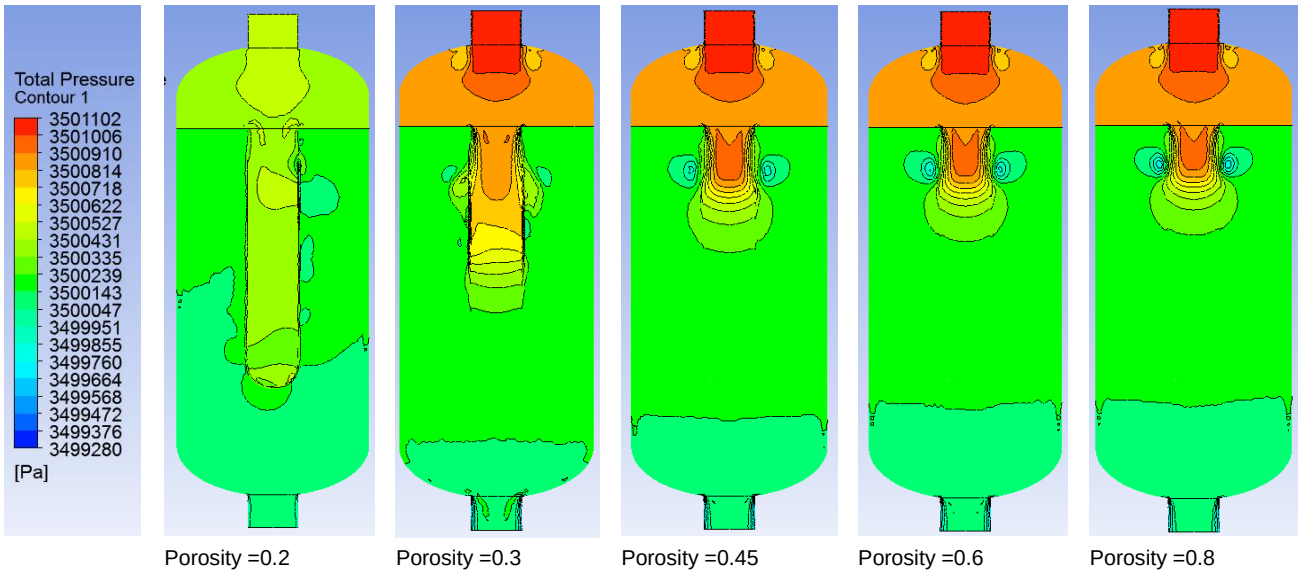


**Fig.5** - Effect of filter bag porosity on flow field total pressure distribution

**3. Influence of Outlet Pressure on Pressure Drop**

- **Outlet Pressure VS Velocity Vector Distribution**

The outlet pressure is refers to setting back pressure in the liquid orifice of filter, which is respectively calculated according to 0.5MPa, 1.5MPa, 2.5MPa, 3.5MPa. As is shown in Fig.6, with the increasing of the back pressure, the whirlpool scale at the bag mouth around becomes smaller. This is caused by the downstream pressure that is relatively large. The velocity vector distribution in inlet and outlet of the filter are similar.

**3 出口压力对压降的影响**

- **出口压力——速度矢量分布图**

出口压力是指在过滤器出液孔口处，设置的背压，分别按 0.5MPa、1.5MPa、2.5MPa、3.5MPa 进行分别计算。由图 6 可知，随着背压的增加，滤袋口部四周的漩涡尺度变小，这是因为下游压力较大所致。过滤器进口与出口处的速度矢量分布规律比较相似。

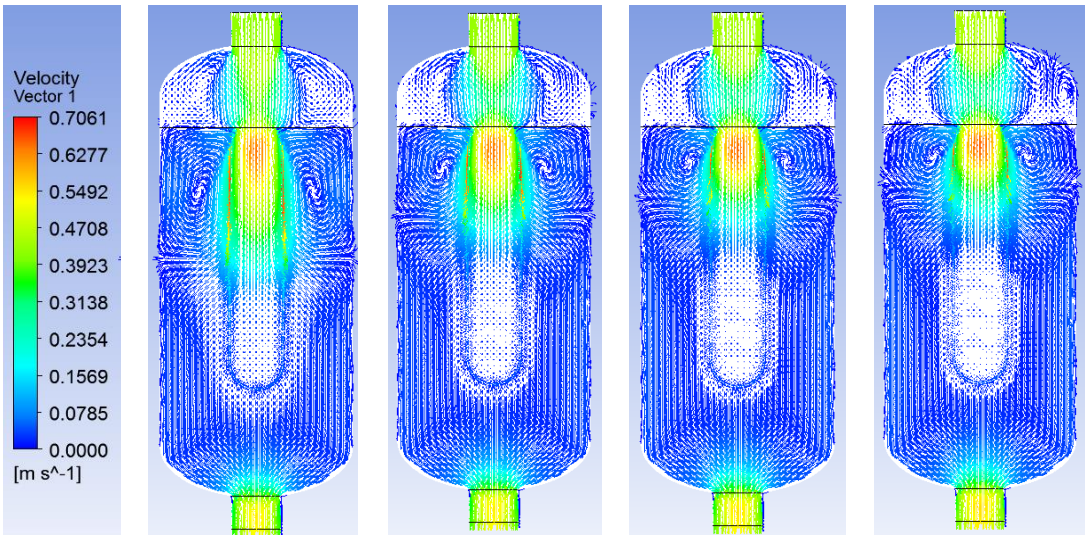


**Fig.6** - Effect of outlet pressure on the velocity vector distribution

- **Outlet Pressure Vs Total Pressure Distribution**

Fig.7 is the contour map of total pressure on the cross section of the filter in different back pressure. With the outlet pressure increasing, the total pressure drop increases. Especially the filter bag near the inlet has apparent change and the higher back pressure is, the earlier pressure is reduced. The outlet pressure is from 0.5MPa to 1.5MPa, the pressure loss increases rapidly, pressure loss increases in processes which are from 100Pa to 550Pa and from 1.5MPa to 3.5MPa, the pressure tends to be stable, which is basically maintained at around 580Pa.

- **出口压力——总压分布图**

图 7 为不同被压下，过滤器中截面上的总压力等值线图。随着出口被压得增加，总压力下降幅度增加，特别是滤袋进口附近有明显的变化，背压越大，压力降低的越早。出口压力在 0.5MPa 到 1.5MPa 时，压力损失增加较快，压力损失从 100Pa 增加到 550Pa，从 1.5MPa 到 3.5MPa 的过程中，压力趋于稳定，基本保持在 580Pa 左右。

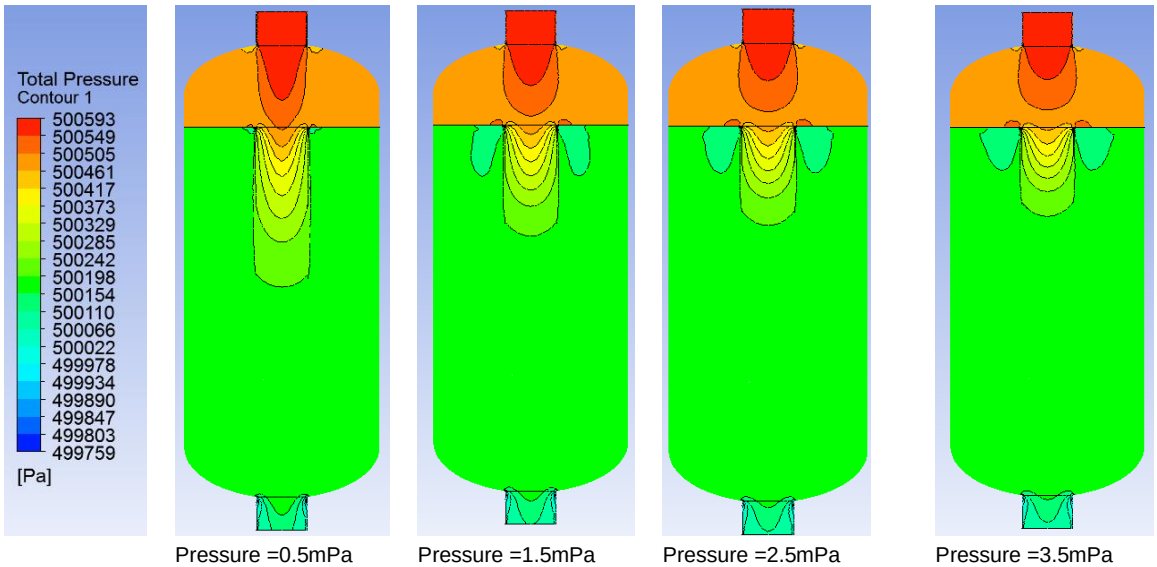


**Fig.7** - Effect of outlet pressure on flow field total pressure distribution

**4. Effect of outlet Velocity on the Pressure Drop**

- **Outlet Velocity Vs Velocity Vector Distribution**

This paper carries out simulation calculation on different inlet velocity 0.168m/s, 0.421 m/s, 0.841 m/s,

**4. 出口流速对压降的影响**

- **出口流速——速度矢量分布图**

分别进行了 0.168m/s、0.421 m/s、0.841 m/s、1.682

1.682 m/s and 2.522 m/s by using CFD. It can be seen from figure 8 that velocities vector changes along with the increase of speed. The greater inlet velocity is, the greater high speed area which in filter bag is. When the speed reaches 2.522m/s, there is great velocity in the filter bag. The greater inlet velocity is, the greater whirlpool which in the vicinity of Bag of entrance is. When the velocity is maximum, most of the cylinder space have full of turbulence.

m/s 和 2.522 m/s 进口流速的 CFD 仿真计算。由图 8 可以看出速度矢量随速度增加后的变化规律。进口流速越大，滤袋内的高速区越大，当速度达到 2.522m/s 时，整个滤袋内都保持较高的速度。进口速度越大，袋口附件的漩涡越大，最大速度时，漩涡充满大部分的筒体空间。

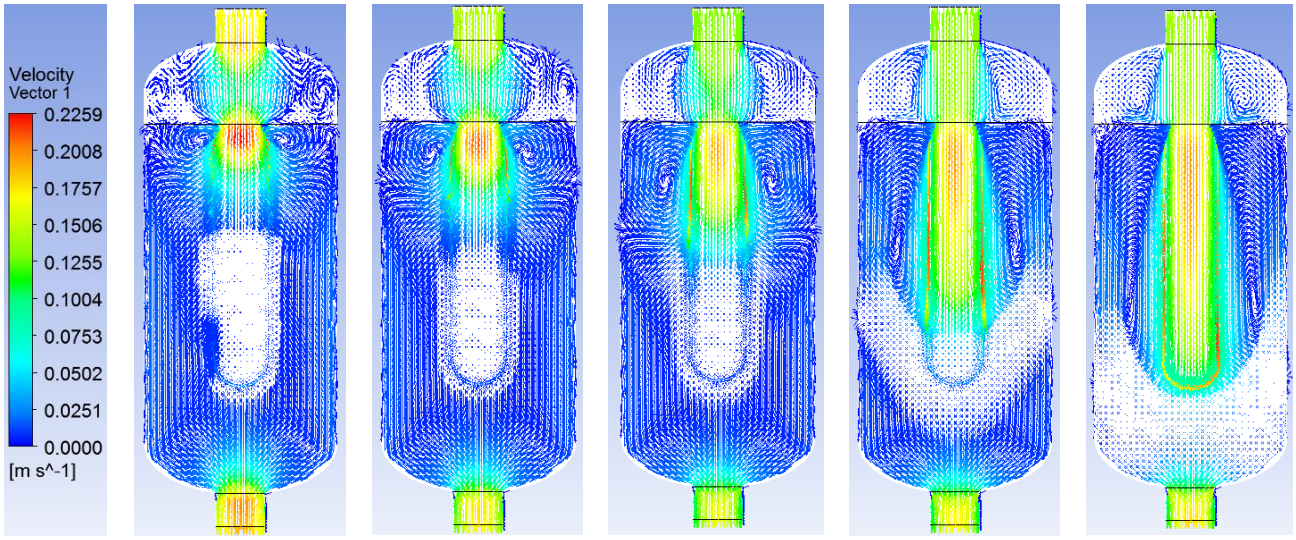


0.168m/s 0.421m/s 0.841m/s 1.682m/s 2.522m/s

**Fig.8** - Effect of outlet velocity on flow field velocity vector distribution

- **Inlet Velocity Vs the Total Pressure Distribution**

Fig.9 is the total pressure contour map under different inlet velocities. With the increase of the inlet velocity, total pressure areas are also larger. The total pressure gradient is larger, so that the total pressure loss is bigger. With the increase of inlet velocity, which increases from 0.1m/s to 2.6m/s, the pressure drop is increased rapidly and they is non-linear positive correlation. Changes in growth amplitude are large, which range from 170Pa to near 10000Pa and across 2 orders of magnitude.

- **进口流速——总压分布图**

图 9 是不同进口流速下的总压力等值线图，随着进口速度的增加，总压值较大的区域也大，总压力梯度较大，说明总的压力损失较大。随着进口流速的增加，从 0.1m/s 增加到 2.6m/s，压降也急剧增加，二者相关性为非线性正相关。而且增长幅值变化很大，从 170Pa 到近 10000Pa，跨越了 2 个数量级。

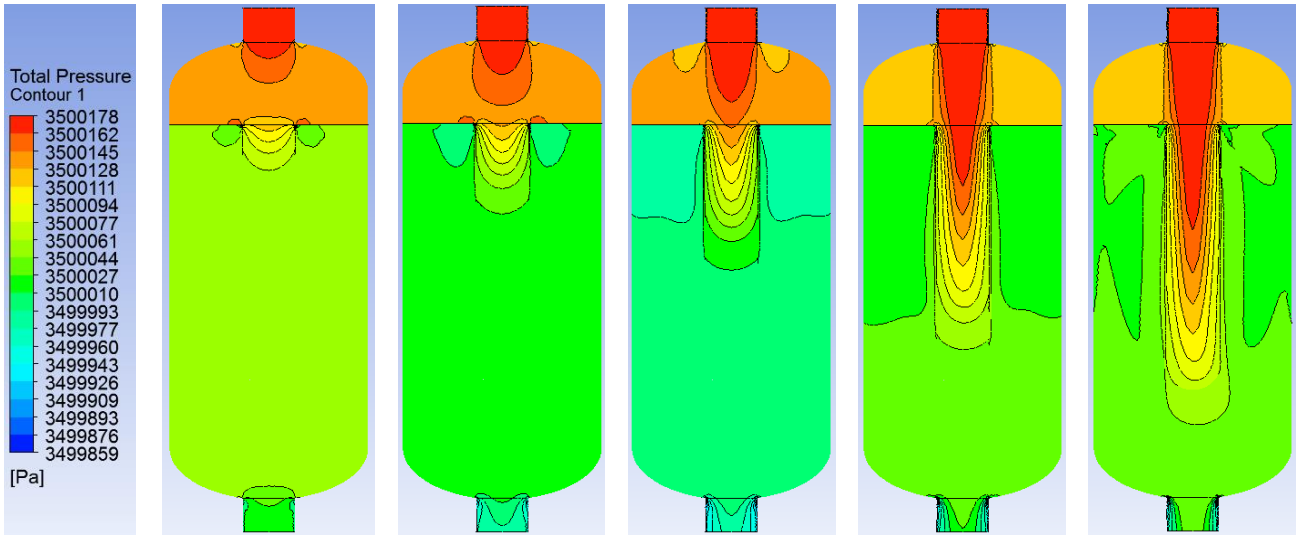


0.168m/s 0.421m/s 0.841m/s 1.682m/s 2.522m/s

**Fig.9** - Effect of inlet velocity on flow field total pressure distribution

**5. Effect of Viscosity on Pressure Drop**

- **Viscosity Vs the Velocity Vector Distribution**

Viscosity represents the macroscopic properties of fluid which is linked by a stress applied to the fluid and the resulting deformation rate in a certain relationships; it shows the internal friction of fluid. As for numerical viscosity, it is equal to the fluid shear stress which is under the unit of velocity gradient. The velocity gradient is also called fluid motion angle deformation rate, so it also shows the relationship between shear ratio and angular distortion rate.

Fig.10 shows the two-dimensional vector flow chart of filter cross section under different viscosity.

When the viscosity is small, the whole flow field has strong turbulence and at this moment the flow loss is smaller.

As the viscosity increases, there are more and more rules of flow pattern. Most of the region is the laminar region, but the inlet of cylinder and filter bag have an obvious vortex.

**5 粘性对压降的影响**

- **粘性——速度矢量分布图**

粘性是施加于流体的应力和由此产生的变形速率以一定的关系联系起来的流体的一种宏观属性，表现为流体的内摩擦。黏度数值上等于单位速度梯度下流体所受的剪应力。速度梯度也表示流体运动中的角变形率，故黏度也表示剪应力与角变形率之间比值关系。

图 10 为不同粘度下的过滤器中截面二维矢量流动图，小粘度时整个流场紊流较强，此时损失较小。随着粘性的增加，流谱越来越规则，大部分区域为层流区，但是在筒体进口和滤袋进口处均有较明显的漩涡。

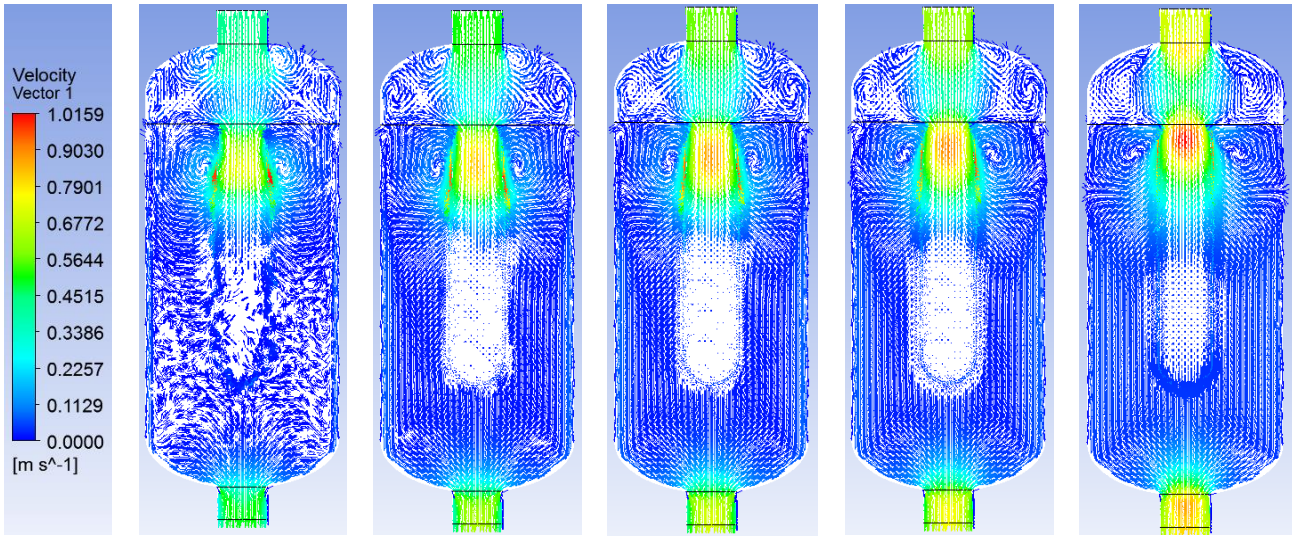


**Fig.10** - Effect of viscosity on flow field velocity vector distribution

- **Viscosity Vs the Total Pressure Distribution**

Fig.11 shows the total pressure contour map of different viscosities. In the vicinity of the inlet filter bag, the viscosity is smaller so that the pressure gradient is greater, and the flow pattern has a greater mess.

With the increase of fluid viscosity, flow spectrum was shifted to the laminar flow pattern, but if the viscosity is greater, so the pressure loss is also greater.

As the viscosity increases, and the pressure drop is also increased, and the whole curve is approximately direct proportion with linear increasing.

Filter viscosity is respectively 50cP, 495cP, 1500cP, pressure losses are respectively 370Pa, 600Pa, 920Pa.

- **粘性——总压分布图**

图 11 表示不同粘度下的总压等值线图，在滤袋进口附近，粘度越小，压力梯度越大，流谱越紊乱，随着粘度的增加，流谱渐渐转向层流流谱，但是粘度越大压力损失越大。

随着粘性的增加，压力降增加，整体曲线近似线性地正比例增加。过滤器粘度为 50cP，495cP，1500cP 时，压力损失分别为 370Pa，600Pa，920Pa。

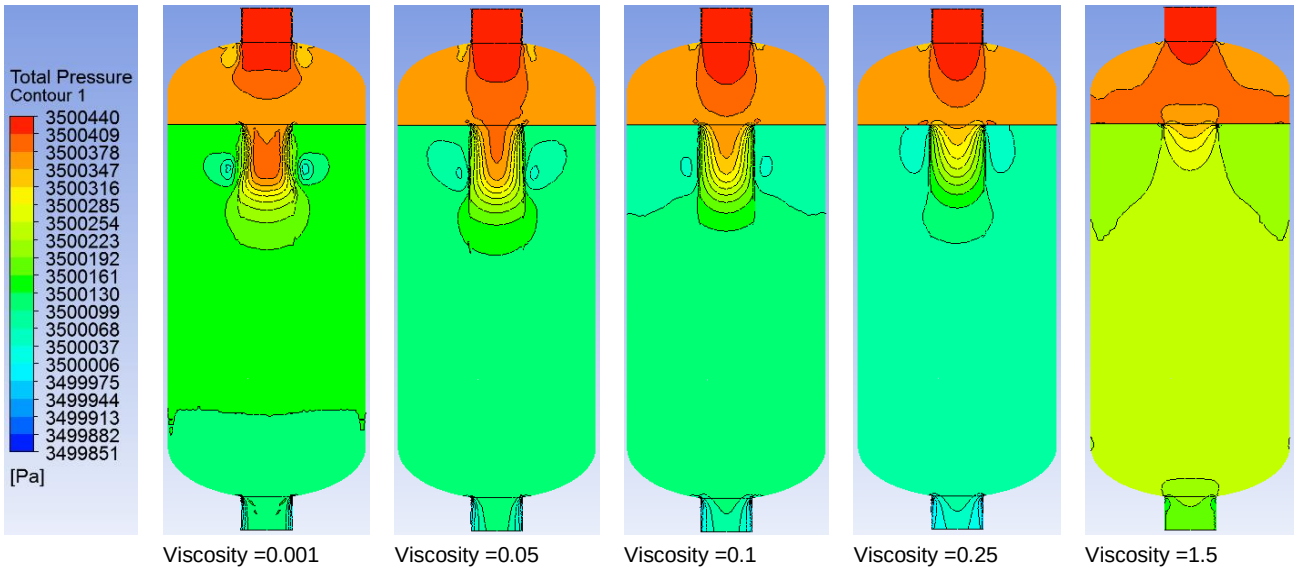


**Fig.11 -** Effect of viscosity on flow field total pressure distribution

## CONCLUSION

In this paper, the filter bag is simplified as a porous medium material. Filter bag is established into CFD numerical simulation model, and numerical calculations are performed about the effects of porosity, outlet back-pressure, inlet velocity and viscosity on the pressure. The calculation results show that;

The total pressure loss which is calculated by using the CFD technology can reflect the change regulation of pressure drop in the filter bag.

With the increase of porosity, pressure loss increased slightly, but overall, the change of total pressure loss is not large, remaining at around 360Pa.

The outlet pressure is from 0.5MPa to 1.5 MPa and the pressure loss increases rapidly, it increases from 100Pa to 550Pa. In the process from 1.5MPa to 3.5MPa, the pressure tends to be stable, it basically maintained at around 580Pa. With the increase of inlet velocity, which increases from 0.1m/s to 2.6m/s, the pressure drop is increased rapidly and there is non-linear positive correlation. Changes in growth amplitude are large, which range from 170Pa to near 10000Pa and across 2 orders of magnitude. As the viscosity increases, and the pressure drop is also increased, and the whole curve is approximately the direct proportion of linear increasing.

## REFERENCES

[1]. Fu H.M., Zhao Y.J., (2010) - *Dynamic test and optimization of flow field in bag filter*. Journal of Central South University. Volume 41, Issue 2, pp.799-806;

[2]. Hao X.D., Vander J.H.J.M., (2003) - *New Way of Wastewater Resourced*. Water & Wastewater Engineering, Volume 29, Issue 6, pp.27-29;

[3]. Luo y., (2003) - *Introduction to membrane filtration sewage directly used for agricultural irrigation technical measures*. Gansu science and technology, Volume 19, Issue 11, pp.14-15;

[4]. Li Z.H., Liu J.F., Jiao L., (2011) - *The numerical simulating research about the pulse cleaning process of*

## 结论

通过将过滤袋简化为多空介质材料，建立对应袋式过滤器的 CFD 数值仿真模型，进行孔隙率、出口被压、进口流速和粘性对压降影响的数值计算，计算结果表明；

利用 CFD 技术计算的总压力损失能够反映压降在过滤袋内的变化规律。随着空隙度的增加压力损失略有增加，但是总体来说，总压损失变化并不大，保持在 360Pa 左右。出口压力在 0.5MPa 到 1.5MPa 时，压力损失增加较快，从 100Pa 增加到 550Pa，从 1.5MPa 到 3.5MPa 的过程中，压力趋于稳定，基本保持在 580Pa 左右。随着进口流速的增加，从 0.1m/s 增加到 2.6m/s，压降也急剧增加，二者相关性为非线性。而且增长幅值变化很大，从 170Pa 到近 10000Pa，跨越了 2 个数量级。随着粘性的增加，压力降增加，整体曲线近似线性地正比例增加。

## 参考文献

[1]. Fu H.M., Zhao Y.J., (2010) -*袋式除尘器流场动态测试及优化*. 中南大学学报， 卷.41, 期.2, p. 799-806；

[2]. 郝晓地,Vander J.H.J.M., (2003) -*污水资源化新途径—直接膜过滤用于农业灌溉*. 给水排水, 第 29 卷，第 6 期，27-29;

[3]. 罗瑛, (2003) -*浅谈直接膜过滤污水用于农业灌溉的技术措施*,甘肃科技, 第 19 卷，第 11 期，39-15;

[4]. Li Z.H., Liu J.F., Jiao L.,(2011) -*脉冲式清洗过滤袋的*

*bag filter*. Asian Workshop on Polymer Processing 2011, Qingdao, China, pp.509-514

[5]. Rocha S.M.S., Vieira L.G.M., Aguiar M.L., Damasceno J.J.R., (2010) - *Fluid dynamics study of the influence of direction of the gas flow in fabric filter*. Materials Science Forum, 7th International Latin-American Conference on Powder Technology, Brazil, pp.520-524;

[6]. Ueda T., (1996) - *Treatment of domestic sewage from rural settlements by a membrane bioreactor*. Water Science and Technology, Volume 34, Issue 9, pp.189-196;

[7]. Xing W., (2013) - *Adsorbent modified filter bag in the application of the irrigation and drainage*. Technology of Soil and Water Conservation, Volume 32, Issue 2, pp.13-15;

[8]. Yin Q., Hu M.Y., Zhang J., Hou W.L., (2009) - *Computer simulation of air flow distribution characteristics in inner filtering fabric filters*. 2009 WRI World Congress on Computer Science and Information Engineering, United States, pp.419-423.

*数值仿真研究*，亚洲聚合物加工研讨会议2011，青岛，中国, 509-514.

[5]. Rocha S.M.S., Vieira L.G.M., Aguiar M.L., Damasceno J.J.R., (2010) -*影响织物过滤器气流方向流体动力学研究*， 第七届拉丁美洲粉体力学技术国际会议，巴西，520-524;

[6]. Ueda T., (1996) -*Treatment of domestic sewage from rural settlements by a membrane bioreactor*. Water Science and Technology, Vol.34, No.9, 189-196;

[7]. 邢伟, (2013) -*吸附剂改良过滤袋在农田排水渠中的应用,* 水土保持应用技术, 第 32 卷，第 2 期，13-15;

[8]. Yin Q., Hu M.Y., Zhang J., Hou W.L., (2009) - *计算机过滤织物过滤器内部气流分布特征的模拟*，2009年计算机科学和信息工程WRI世界大会, 美国, 419-423.

# MATHEMATICAL MODELLING AND COMPARATIVE SIMULATION OF THE VIBRATIONS OF VIBRO-CULTIVATORS AND AGRICULTURAL CULTIVATORS
# /
# *MODELARE MATEMATICA SI SIMULAREA COMPARATIVA A VIBRAȚIILOR COMBINATOARELOR SI CULTIVATOARELOR AGRICOLE*

**Math. Cârdei P[1,2)]., Ph.D. Eng. Muraru V[1,2)]., Ph.D. Eng. Constantin N.[2)], Ph.D. Eng. Muraru C.[1,2)] , Ph.D. Cilan T.[2)], Eng. Hodre C. D.[2)], PhD.Stud. Eng. Matache M.[1)]**
[1)]INMA Bucharest/ Romania; [2)]SVILUPPO-INSIEME SI VICE Chisineu-Cris, Arad county/ Romania
*Tel: 0726142837; E-mail: petru_cardei@yahoo.com*

***Abstract:*** *Inspiration for investigations described in this article was to explain the differences between a cultivator and a vibro-cultivator. Starting from the basic model of linear of damped oscillator, the authors complicate the equations and specify or enrich some terms meanings entering the specific terms of agricultural machinery for soil works. First, these models attempt to explain the oscillating behaviour of working bodies in different operating modes of agricultural machinery. Subsequently, the practical application will consist in the control of these vibrations, using adjustable parameters of working processes. Furthermore, this simulator is useful for theoretical study of the behaviour of an active part in presence of friction and nonlinear damping, and also of complex phenomena including the equation of motion of the unit.*

***Keywords:*** *mathematical model, simulation, vibrations, vibro-cultivator, cultivator*

## INTRODUCTION

The mathematical model described in this article tries to describe the behaviour of the whole working body - working part support (AOLSOL) in soil, subassembly appropriate to vibro-cultivator or cultivator [1].

This model aims:

- to describe the difference between the functioning of the cultivator and the vibro-cultivator AOLSOL, partially to motivate the construction of the latter;
- to emphasize geometric material constants or the most important geometrical parameters that would make the difference between the working processes of the two machines, in terms of AOLSOL;
- to investigate possible ways of optimizing the operating mode in case of vibro - cultivator.

We do not know similar attempts in the area, especially related to the consideration of nonlinear mixed friction (viscous and dry).

Attempts to describe the mechanics of such vehicles are found, for example in [6], but not at the level of theoretical modelling.

## MATERIAL AND METHOD

The mathematical model considered for a first approach is relatively simple, classic in literature, for example [2]: linear damped oscillator described by second order differential equation:

***Rezumat:*** *Sursa de inspirație pentru realizarea investigațiilor descrise în acest articol a fost explicitarea deosebirilor dintre un cultivator şi un vibro-cultivator. Pornind de la modelul elementar al oscilatorului liniar cu amortizare, autorii complică ecuațiile şi particularizează sau îmbogățesc semnificația unor termeni introducând în ecuații termeni specifici maşinilor agricole de lucrat solul. Pentru început, aceste modele încearcă să explice comportamentul oscilator al organelor de lucru în diverse regimuri de funcționare ale maşinilor agricole. Ulterior aplicația practică va consta în controlul acestor vibrații folosind parametrii de regim reglabili. Mai mult, acest simulator este utilizabil pentru studiul teoretic al comportamentului unui organ activ în prezenta unor frecări şi amortizări neliniare, de asemenea şi a unor fenomene complexe care includ ecuația de mişcare a agregatului.*

***Cuvinte cheie:*** *model matematic, simulare, vibrații, combinator, cultivator*

## INTRODUCERE

Modelul matematic descris în acest articol încearcă să descrie comportamentul ansamblului organ de lucru - suport organ de lucru (AOLSOL) în sol, subansamblu caracteristic al unui cultivator sau vibro-cultivator, [1].

Acest model are următoarele scopuri:

- să descrie diferența dintre modul de funcționare al AOLSOL al cultivatorului şi cel vibro-cultivatorului, în parte pentru a motiva construcția acestuia din urmă;
- să evidențieze constantele de material sau parametrii geometrici cei mai importanți care ar face diferența între procesele de lucru ale celor doua maşini, în ceea ce priveşte AOLSOL;
- să investigheze eventuale posibilități de optimizare a regimului de lucru în cazul vibro-cultivatorului.

Nu cunoaştem încercări similare în domeniu, mai ales legate şi de considerarea unor frecări neliniare mixte (vâscoase si uscate).

Încercări de descriere a mecanicii unor astfel de maşini se găsesc, de exemplu în [6], dar nu la nivel de modelare teoretică.

## MATERIAL ŞI METODĂ

Modelul matematic considerat pentru o primă abordare este unul relativ simplu, clasic în literatura de specialitate, de exemplu [2]: oscilatorul liniar cu amortizare, descris de ecuația diferențială de ordinul al doilea:

$$m\ddot{x} + c\dot{x} + kx = \psi \,, \tag{1}$$

where $x$ is the relative displacement of the mass centre of AOLSOL, $m$ is the mass AOLSOL, $c$ is damping coefficient of AOLSOL, $k$ is the stiffness coefficient of AOLSOL and $\psi$ is excitation force. The structure of each parameter will be subject to further clarifications. Obviously, $\dot{x}$, and $\ddot{x}$ are derivatives of the first order and second order of relative displacement, $x$.

The relative displacement is a function of time t, which is subject to initial conditions:

în care: $x$ este deplasarea relativă a centrului de masă al AOLSOL, $m$ este masa AOLSOL, $c$ este coeficientul de amortizare al AOLSOL, $k$ este coeficientul de rigiditate al AOLSOL, iar $\psi$ este forța excitatoare. Structura fiecărui parametru va constitui subiectul unor precizări ulterioare. Evident, $\dot{x}$ şi $\ddot{x}$, sunt derivatele de ordinul întâi, respectiv al doilea ale deplasării relative $x$.

Deplasarea relativă este o funcție de timp, $t$, care trebuie să respecte condițiile inițiale:

$$x(t_0) = x_0,\ \dot{x}(t_0) = \dot{x}_0 \tag{2}$$

In physical terms, damping coefficient $c$ is given by the amortization of the soil and stiffness coefficient $k$ is AOLSOL stiffness, mainly given by the support of the working body.

Note: AOLSOL is not a classic oscillator. It can be likened more to a phenomenon of hauling a very rigid linear pendulum through a viscous fluid.

The working body together with a part of the support is assimilated with pendulum mass, the amortization being given by the medium through which the part moves (soil) and the stiffness by the stiffness property of the working body support.

For damping, can be considered a more complex form obtained by combining viscous friction with the dry one, taking into account the soil moisture:

Din punct de vedere fizic, coeficientul de amortizare $c$, este dat de amortizarea produsă de sol, iar coeficientul de rigiditate $k$ este rigiditatea AOLSOL, dată în principal de suportul organului de lucru.

Observație: AOLSOL nu este un oscilator clasic. El poate fi asemănat mai mult cu un fenomen de tracțiune a unui pendul liniar foarte rigid printr-un fluid vâscos.

Organul de lucru împreună cu o parte a suportului se asimilează masei pendulului, amortizarea este dată de mediul prin care organul se mişcă (solul), iar rigiditatea de proprietatea de rigiditate a suportului organului de lucru.

Pentru amortizare poate fi considerată o forma mai complexă, obținută prin combinarea frecării vâscoase cu cea uscată, ținând seama şi de umiditatea solului:

$$c = c_v \cdot f(u) + \frac{c_u}{|\dot{x}|} \cdot g(u) \tag{3}$$

where $c_v$ is the coefficient of viscous damping, $c_u$ is the dry friction coefficient, $f$ is a function that increases with soil moisture and $g$ is a decreasing function of soil moisture, $u$. Functions $f$ and $g$ may be known in special cases only on experimental basis, depending on the texture and soil composition.

Excitation force, $\psi$ is produced by the interaction between AOLSOL and soil. To simulate a large range of phenomena, it is considered for the excitation force the next form:

în care $c_v$ este coeficientul de amortizare vâscoasă, $c_u$ coeficientul de frecare uscată, $f$ este o funcție crescătoare cu umiditatea solului iar funcția $g$ este o funcție descrescătoare cu umiditatea, $u$. Funcțiile $f$ şi $g$ se pot cunoaşte în particular numai pe baze experimentale, depinzând şi de textura şi compoziția solului.

Forța excitatoare, $\psi$ este produsă de interacțiunea dintre AOLSOL şi sol. Pentru a simula o gamă cât mai largă de fenomene, se consideră pentru funcția excitatoare forma:

$$\psi(t) = F(t) + \varphi(t) \tag{4}$$

where $F$ is the force of resistance to deformation of the soil, which can be considered as:

în care $F$ este forța de rezistența la deformare a solului, care se poate considera de forma:

$$F(t) = Ka(t)b(t) + \varepsilon abv^2(t) \tag{5}$$

where $K$ is the coefficient of resistance to deformation of the soil, it is working depth and b is working width, $v$ is the working speed and $\varepsilon$ is a coefficient that depends on soil characteristics and the shape and condition of the working surface. It is considered that the working depth and width are functions of time, primarily due to consideration of the transition phase from working idle stage in steady state, and secondly, that these two characteristics of farm soil machines can randomly vary and, especially the working depth. On the other hand, in transitive stage, the working width increases with the working depth for many types of working part. If these issues can be neglected, then $a$ and $b$ can be considered constant as the coefficient of resistance to deformation of the soil, $K$.

The function $\varphi(t) = rF(t)\sin(2\pi ft)$ is the random

în care $K$ este coeficientul de rezistența la deformare al solului, $a$ este adâncimea de lucru, iar $b$ este lățimea de lucru, $v$ este viteza de lucru, iar $\varepsilon$ este un coeficient care depinde de caracteristicile solului si forma si starea suprafeței organului de lucru. Se consideră că adâncimea şi lățimea de lucru pot fi funcții de timp, în primul rând datorită considerării etapei tranzitive de la starea de repaus la lucru în regim stabilizat, iar în al doilea rând, pentru că aceste două caracteristici ale maşinilor de lucrat solul pot varia şi aleator, mai ales adâncimea de lucru. Pe de alta parte, în etapa tranzitivă lățimea de lucru creşte cu adâncimea de lucru pentru multe tipuri de organe de lucru. Dacă aceste aspecte pot fi neglijate, atunci $a$ şi $b$ se pot considera constante ca şi $K$.

Funcția $\varphi(t) = rF(t)\sin(2\pi ft)$ este componenta

component of the force of resistance to soil deformation.

The solution of the problem (1), (2), with hypotheses (3), (4), (5), even with nonlinearity considered in (3) can be given using the techniques of operational calculus [2] (even piecewise).

The presence of more complicated nonlinearities in $x$ or $\dot{x}$ cancels the possibility of using operational calculus if linearization is not applied. But the linearization limits decisively our investigations. On the other hand, calculating the convolution product using suitable computer programs is ineffective for long time and complicated nonlinearities. For these reasons we chose to build the simulator AL SOL based on the numerical solution of the problem. This option offers the possibility of using a wide variety of nonlinearities. Convergence difficulties for long simulation times may occur also in this case. They can be partially solved by modifying the numerical schemes used.

## RESULTS

To facilitate understanding, especially in simulation example chosen, I considered a linear viscous friction (f(u)=1, g(u)=0) in (3)). In a future article it will address the full friction type (3), and other types of friction and even stiffness. Next objective is to investigate the existence of internal parameters (dry friction, dry friction and nonlinear viscous friction, possibly others) of the model, capable of producing vibration even if the excitation function is constant in time. The subject is vast and currently with little chance of experimental covering. Therefore, the investigation it is only a long-term goal. AOLSOL physical model comprises the working parts of the vibro-cultivator designed in a research project.

The total value of the working part and of its support (vibrating portion, AOLSOL) is m = 5.388 kg (chosen so that the natural frequency of the model to be equal to the experimentally determined value). The own support damping (characteristic to metal) is not considered in this model. Stiffness coefficient is calculated in accordance with [3], using the formula:

aleatoare a forței de rezistență la deformare a solului.

Soluția problemei (1), (2), cu ipotezele (3), (4), (5), chiar cu neliniaritatea considerată în (3), se poate da folosind tehnicile calculului operațional, [2] (măcar pe porțiuni).

Prezența unor neliniarități mai complicate în $x$ sau $\dot{x}$ anulează posibilitatea folosirii calculului operațional dacă nu se aplică liniarizări. Liniarizarea limitează însă decisiv investigațiile noastre. Pe de alta parte, calculul produsului de convoluție folosind programe de calcul consacrate, este ineficient pentru timpi lungi şi neliniarități complicate. Pentru aceste motive am optat pentru construcția simulatorului AOLSOL bazat pe soluția numerică a problemei. Această opțiune oferă şi posibilitatea considerării unei mari varietăți de neliniarități. Dificultăți de convergență pentru timpi lungi de simulare şi folosind neliniarități complicate, pot să apară, de asemenea şi în acest caz. Acestea se pot rezolva parțial modificând parametrii schemelor numerice folosite.

## REZULTATE

Pentru facilitarea înțelegerii, în exemplul de simulare ales, am considerat o frecare vâscoasă liniară (f(u)=1, g(u)=0 în (3)). Într-un articol viitor se va aborda frecarea integrală de tip (3), precum şi alte tipuri de frecări şi chiar rigidități. Obiectivul următor este cercetarea existenței unor parametri interni (frecarea uscata, frecarea uscata si vâscoasă neliniară, eventual altii) ai modelului, capabili sa producă vibrații chiar dacă funcția excitatoare este constantă în timp. Subiectul fiind foarte vast şi, momentan cu puține şanse de acoperire experimentală. Ca urmare investigația este numai un obiectiv pe termen lung. Modelul fizic al AOLSOL îl constituie organe de lucru ale combinatorului conceput în cadrul unui proiect de cercetare.

Masa totală a organului de lucru cu suport (porțiunea vibratoare, AOLSOL) are valoarea m=5,388 kg (aleasă astfel încât modelul să aibe frecvența proprie egală cu valoarea determinată experimental). Amortizarea proprie a suportului (proprie metalului) nu se consideră în acest model. Coeficientul de rigiditate se calculează în conformitate cu [3], după formula:

$$k = \frac{3EI}{l^3} \tag{6}$$

where $E$ is the modulus of elasticity of the support material (steel in our case, so $E$ = 2.1 • $10^{11}$ Pa), $I$ is the moment of inertia of the cross section of the rod holder:

în care $E$ este modulul de elasticitate al materialului suportului (oțel în cazul nostru, deci $E$= 2,1•$10^{11}$ Pa), $I$ este momentul de inerție al secțiunii transversale a barei suportului:

$$I = \frac{a_s^4}{12} \tag{7}$$

because it is considered as a square section with edge $a_s$. The section edge is set to $a_s$ = 0.025 m. The length of the support (the support to the point of attachment of the working element) is $l$, with the value of $l$ = 0.788 m. For the spring constant of the oscillator, value $k$ = 41 902 N / m is obtained.

The purely viscous damping is characterized by $c_v$ value according to [4] or [5], given by:

deoarece se consideră o secțiune pătrată cu latura $a_s$. Latura secțiunii are valoarea $a_s$= 0,025 m. Lungimea suportului (de la rezemare până la punctul de fixare al organului de lucru) este $l$, având valoarea $l$= 0,788 m. Se obține pentru constanta de elasticitate a oscilatorului, valoarea $k$= 41902 N/m.

Amortizarea de tip pur vâscoasă este caracterizata de valoarea $c_v$ conform [4] sau [5], dată de formula:

$$c_v = 30.924ab\sqrt{K\rho} \tag{8}$$

Considering an average soil density, $\rho$=1900 kg / m$^3$ and $K$ = 73000 N / m$^2$, the damping coefficient is obtained after [4] or [5], by calculation (8), with the value $c_v$ = 3769 kg / s.

For the above data, the oscillator shows the supercritical damping, therefore oscillations are only possible due to exciter force. The natural frequency of the purely elastic system (damped null) is 14.035 Hz. If it is considered a depth $a$ = 12 cm and the working width 8.6 cm, then the exciter force constant component has the value $F$ = 1022 N. Excitation oscillating component has an amplitude of 25% in constant force, $F$. Its frequency has different critical values around the corresponding own frequency oscillator without damping system.

If the unit moves perpendicularly on ploughing lines resulted from previous work, then a working width $B$ = 25 cm and an equal depth , it is obtained a critical speed for producing resonance with value $v_{cr}$ = 3.509 m / s (12.631 km / h) .

For the numerical solution of the problem, I used an algorithm of Runge Kutta type of fourth rank in Mathcad mathematical software. Parametric study of the working part model oscillations is based on this simulator which uses the Runge Kutta algorithm.

The simulator developed in order to study oscillations of the cultivator or vibro - cultivator support and working parts is used to:

-testing in extreme situations for which certain phenomena are known;

-investigating of the use of the model to define the difference between cultivator and vibro-cultivator;

- investigating of the existence of an optimal resonance working process for the vibro-cultivator;

-investigating of the effects of parameters non-linearity comparing to amplitude or oscillation speed of the working part of the vibro-cultivator.

The first three topics will be addressed in this article, the latter being subject to subsequent approaches.

Considerând o valoare medie a densității solului, $\rho$=1900 kg/m$^3$ şi $K$= 73000 N/m$^2$, se obține pentru coeficientul de amortizare, după [4] sau [5], prin calcul cu (8) valoarea $c_v$= 3769 kg/s.

Pentru datele de mai sus, oscilatorul are amortizare supracritică, prin urmare, oscilații sunt posibile numai datorită forței excitatoare . Frecvența proprie a sistemului pur elastic (cu amortizare nulă) este de 14,035 Hz. Dacă adâncimea de lucru se consideră $a$= 12 cm şi lățimea de lucru 8,6 cm, atunci componenta constantă a forței excitatoare are valoarea $F$= 1022 N. Componenta oscilantă a excitației are o amplitudine de 25 % din forța constantă, $F$. Frecvența acesteia ia diferite valori în jurul celei critice care corespunde frecvenței proprii a sistemului oscillator fără amortizare. Dacă agregatul se deplasează perpendicular pe liniile de arătura rezultată din lucrarea anterioara, atunci pentru o lățime de lucru $B$= 25 cm şi o adâncime egală, se obține viteza critică pentru producerea rezonanței cu valoarea $v_{cr}$= 3,509 m/s ( 12,631 km/h). Pentru rezolvarea numerică a problemei, am folosit un algoritm de tip Runge Kutta de ordinul al patrulea, în programul Mathcad. Studiul parametric al modelului oscilațiilor organului de lucru se face folosind simulatorul bazat pe acest algoritm numeric.

Simulatorul elaborat în scopul studiului oscilațiilor organelor de lucru cu suport ale combinatorului sau vibro-combinatorului, se foloseşte pentru:

-testarea în situații limită pentru care unele fenomene se cunosc;

-investigarea folosirii modelului pentru definirea diferenței între cultivator şi vibro-cultivator;

-investigarea existenței unui regim de rezonanță optimal în funcționarea de tip vibrocultivator;

-investigații privind efectele neliniarităților unor parametrii în raport cu amplitudinea sau viteza de oscilație a organului de lucru al vibrocultivatorului.

Primele trei subiecte vor fi abordate in acest articol, ultimul fiind subiectul unei abordări ulterioare.

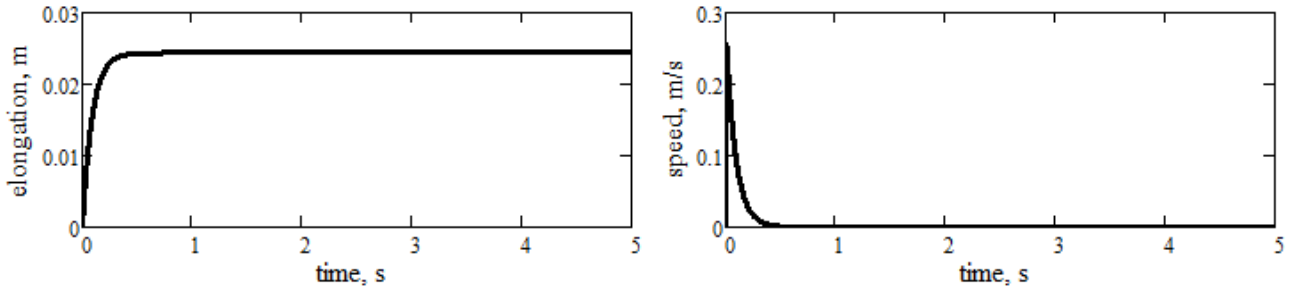


**Fig. 1 -** AOLSOL history elongation (left) and its rate of change (right) subjected to constant force excitation over time (no oscillatory component).

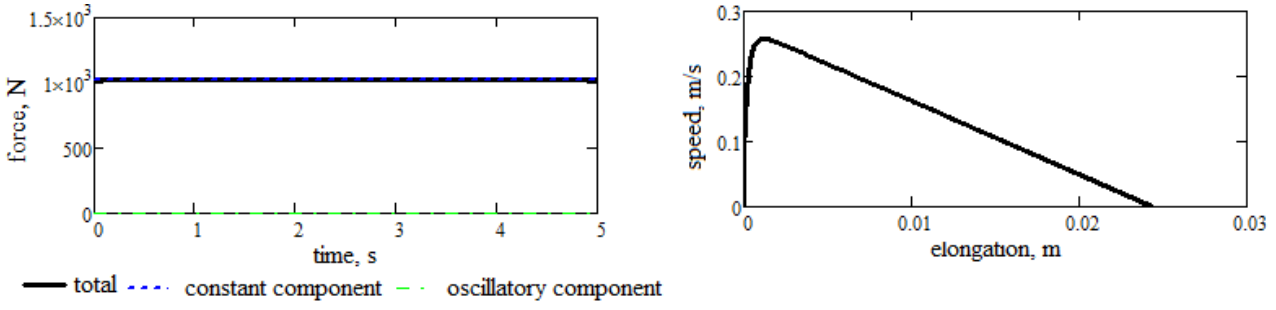


**Fig. 2 -** AOLSOL exciter force history and its components (left) and movement in the phase plane (right).

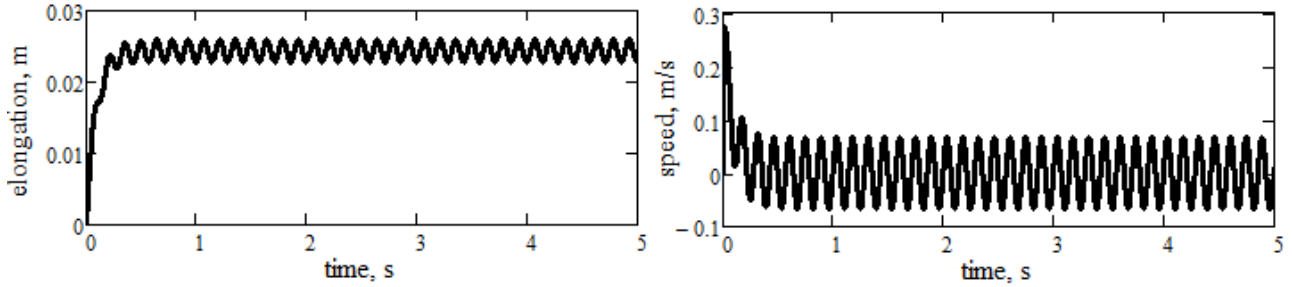


**Fig. 3 -** AOLSOL history elongation (left) and its rate of change (right) subjected to force excitation over time (with oscillatory component).

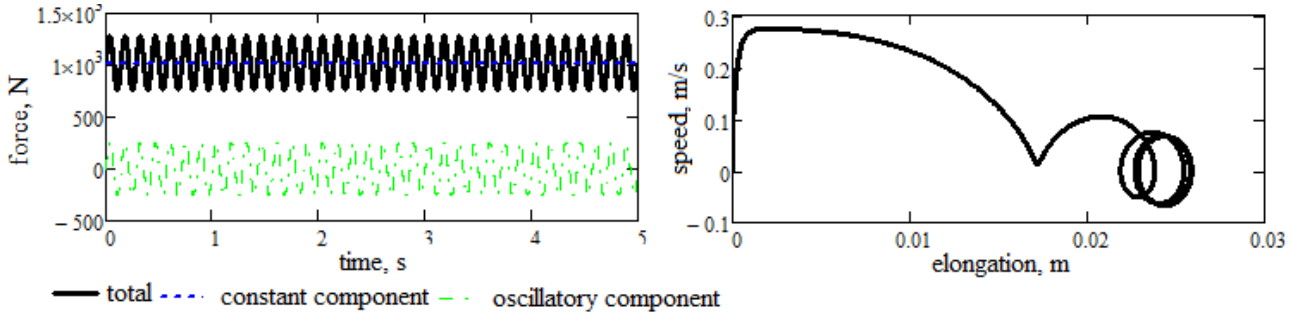


**Fig. 4 -** AOLSOL exciter force history and its components (left) and movement in the phase plane (right).

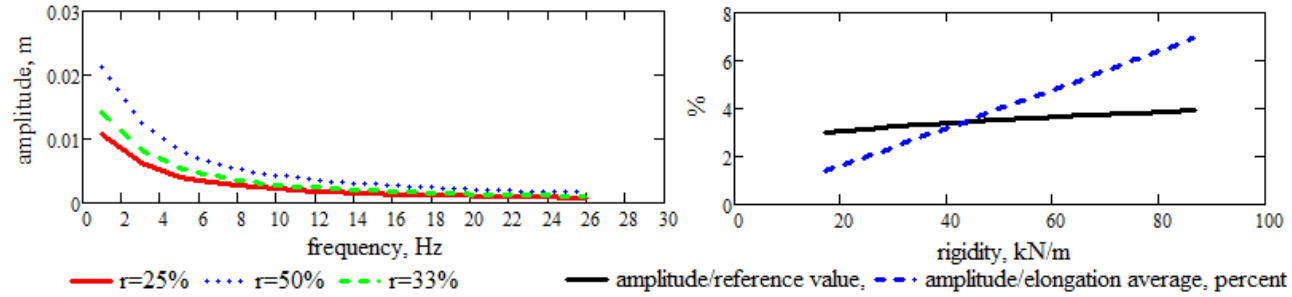


**Fig. 5 -** Variation of oscillator amplitude with the frequency of excitation force (left) and variation of the ratio of amplitude oscillator and relative displacement in case of the constant force exciter and of the ratio between the oscillator amplitude and the average value of its elongation (right).

In Fig.1-5, we plotted very few results from very many that can be obtained and plotted using the model AOLSOL oscillator.

In Fig. 1 and 2 we plotted the results that show AOLSOL behaviour when the excitation force has only non-zero constant component, oscillating component being null. The working speed is the critical speed, 12,631 km / h. In Fig. 3 and 4 we plotted the results which show- AOLSOL oscillator behaviour where force has both non-zero excitatory components, In this case working speed is equal to the critical speed, but the unit obliquely displaces on ploughing lines. In this way the force of excitation frequency is half the critical frequency.

In Fig.5 are given the qualitative results of the model (simulator). In Fig. 5 (left) is represented the variation of the centre of mass of the working part amplitude, depending on the frequency of the oscillator component of the excitation force, for three fixed values of the ratio between the amplitude of the oscillators component and constant component of the exciter force. In Fig. 5 (right) is represented the variation of the amplitude ratios of the centre of mass of the working part and the maximum elongation when the oscillation exciter force is null or average value of elongation AOLSOL if excitation force is oscillating, depending on the AOLSOL stiffness. For this case the unit works with the critical velocity, obliquely on the ploughing lines, exciter force being of frequency of 7 Hz.

În fig. 1 - 5 au fost reprezentate grafic foarte puține rezultate dintre foarte multele care se pot obține şi cerceta folosind modelul AOLSOL.

In fig. 1 si 2 au fost reprezentate grafic rezultate care arată comportamentul AOLSOL în cazul în care forța excitatoare are numai componenta constantă nenulă, componenta oscilatorie fiind nulă. Viteza de lucru este viteza critica, 12.631 km/h. În fig. 3 şi 4 am reprezentat grafic rezultate care arată comportamentul AOLSOL în cazul în care forța excitatoare are ambele componente nenule. În acest caz viteza de lucru este egala cu viteza critică, dar, agregatul se deplaseaza oblic pe liniile de arătură. In acest fel frecventa forței excitatoare este jumătate din frecventa critică.

În fig.5 sunt date rezultate calitative ale modelului (simulatorului). În fig. 5 (stânga) se reprezintă variația amplitudinii centrului de masă al organului de lucru, funcție de frecvența componentei oscilatoare a forței de excitație, pentru trei valori fixate ale raportului dintre amplitudinea componentei oscilatoare şi a celei constante ale forței excitatoare. În fig. 5 (dreapta) se reprezintă variația rapoartelor dintre amplitudinea centrului de masă al organului de lucru şi valoarea maximă a elongației în cazul forței excitatoare cu oscilație nulă, respectiv valoarea medie a elongației AOLSOL în cazul forței excitatoare oscilante, funcție de rigiditatea AOLSOL. Pentru acest caz agregatul lucrează cu viteza critică, oblic pe liniile de aratură, forța excitatoare având frecvența de 7 Hz.

## CONCLUSIONS

Although the study of this oscillator is only at its beginning, we can draw some conclusions about its usefulness and the applications in the design of vibro-cultivators.

The first conclusion is that AOLSOL can make the difference between a cultivator and a vibro-cultivator if is given a conventional limit value for the ratio of amplitude oscillatory motion and constant component elongation force produced by exciter force, for example.

It may introduce other difference criteria between cultivator and vibro-cultivator using AOLSOL oscillator model.

Another important conclusion is that the simulator AOLSOL can be used to design (depending on soil characteristics) the support with a working part at a stiffness to allow it to take part of vibro-cultivator or cultivators categories.

The mathematical model on which relies AOLSOL simulator also allows the design of an optimal mode of operation that can be produced by oscillating force exciter component.

However, one has found that at this level, the optimized mode of operation is in conflict with the principle of optimality required by geometry rectangular plots. The model may be completed in various ways, among which: the introduction of the nonlinear friction, nonlinear stiffness, developing models to include the equation of motion of the unit. Any progress in this building will require a large amount of experimental data, which is currently difficult to guess.

From the experimental point of view, the model was built on real data of working parts and supports of a vibro-cultivator in the prototype stage. The deflection caused by static exciter force constant component, with the value of 24 mm, for a value of 755 N force, was a key criterion for the start of simulator building. The value of static deflection of 24 mm for 755 N force applied to the centre of mass of the working part was set on the test. The natural frequency was also a fundamental criterion for the choice of constants model to get the value measured in the laboratory, namely 14.035 Hz. Correlation with experimental results is done in a subsequent phase, as we have this data and simulator construction progresses.

## REFERENCES

[1]. Anghel S., Babiciu P., Caproiu S. (1972) – *Dictionary of Mechanical Harvester*, CERES Printing House;

[2]. Brânzanescu V., Stănăşilă O, (1994) – *Special mathematical theory, examples, applications,* All Printing House;

[3]. Buzdugan Gh., Fetcu L., Rades M.,(1982) – *Mechanical Vubrations,* Didactic and Pedagogical Printing House, Bucharest;

[4]. Koten H. van, Hoogenboom P. C. J., (2012) - *Vibration of machine foundations and surrounding soil*, HERON Vol. 57 (2012) No. 1;

[5]. Mahajan S. P., Budhu M., (2008) - *Shear Viscosity of Clays to Compute Viscous Resistance*, The 12th International Conference of International Association for Computer Methodes and Advances in Geomechanics (IACMAG), Goa, India;

[6] Fenyvesi L., Hudoba Z., (2009) - *Vibrated Tillage Tools for Energy Saving*, Journal of Agricultural Machinery Science, 5(4), 445-449.

## CONCLUZII

Deşi studiul acestui oscilator este la început, se pot trage cateva concluzii asupra utilității acestuia şi asupra aplicațiilor lui în proiectarea vibro-cultivatoarelor.

Prima concluzie este aceea ca AOLSOL poate face diferența între un cultivator si un vibro-cultivator dacă se dă prin convenție o valoare limită pentru raportul dintre amplitudinea mişcarii oscilatorii şi elongația produsă de componenta constantă a forței excitatoare, de exemplu.

Se pot introduce şi alte criterii de diferență între cultivator şi vibro-cultivator folosind modelul oscilatorului AOLSOL.

O altă concluzie importantă este aceea ca simulatorul AOLSOL poate fi folosit pentru a proiecta (funcție şi de caracteristicile solului) un suport cu organ de lucru la o rigiditate care sa-i permită sa facă parte din categoria cultivatoarelor sau vibro-cultivatoarelor.

Modelul matematic pe care se bazează simulatorul AOLSOL, permite de asemenea proiectarea unui regim de lucru optimal care poate fi produs de componenta oscilantă a forței excitatoare.

Am constatat însa că, la acest nivel, procesul de lucru astfel optimizat intra în conflict cu principiul de optimalitate dat de geometria parcelelor dreptunghiulare.

Modelul are multe perspective de completare, printre care menționăm: introducerea frecărilor neliniare, introducerea unor rigidități neliniare, dezvoltarea până la modele care să includă ecuația de mişcare a agregatului.

Orice progres în această construcție va necesita un mare volum de date experimentale. Ori la acest capitol este, la ora actuală, greu de intuit.

Din punct de vedere experimental, modelul a fost construit pe date reale ale organelor de lucru şi suporților acestora ale unui vibro-cultivator aflat în etapa de prototip. Valoarea săgeții statice produse de componenta constantă a forței excitatoare, cu valoarea de 24 mm, pentru o valoare a forței de 755 N, a fost un criteriu de bază pentru startul construcției simulatorului. Săgeata statică de 24 mm, pentru forței de 755 N la centrul de masă al organului de lucru, a fost stabilită pe standul de încercări. Frecvența proprie fundamentală a fost de asemenea un criteriu de alegere a constantelor de model, pentru a obține valoarea măsurată în condiții de laborator, 14,035 Hz. Corelarea cu rezultatele experimentale se face în continuare pe măsura ce avem aceste date şi construcția simulatorului avansează.

## BIBLIOGRAFIE

[1]. Anghel S., Babiciu P., Caproiu S. (1972) – *Dictionar de mecanica agricola,* Editura Ceres;

[2]. Branzanescu Vasile, Octavian Stanasila,(1994) - *Matematici speciale, teorie, exemple, aplicatii*, editura All, Bucuresti;

[3]. Buzdugan Gh., Fetcu L., Rades M.,(1982) - *Vibratii mecanice*, Editura Didactica si Pedagogica, Bucuresti;

[4]. Koten H. van, Hoogenboom P. C. J.,(2012) – *Vibratia masinii si a solului din zona aferenta*, HERON Vol. 57 (2012) Nro. 1;

[5]. Mahajan S. P., Budhu M.,(2008) – *Vascozitatea la forfecare a argilei pentru a afla rezistenta vascuoasa a solului*, A 12-a Conferinta Internationala a Asociatiei pentru Metodele de calculator si Progresele Geomecanice (IACMAG), Goa, India;

[6] Fenyvesi L., Hudoba Z., (2009) – *Unelte vibratorii de lucrat solul pentru economisirea de energie*, Revista de Stiinta a Masinilor Agricole, 5(4), 445-449.

# EFFECTS OF LIQUID FILM MULCHING ON SOIL EVAPORATION AND COTTON PLANT GROWTH BY DRIP IRRIGATION

/

# *液体地膜覆盖对滴灌棉花土壤蒸发和作物生长的影响*

**M.E.Yunguang Li [1), 2)], Ph.D.Jinzhu Zhang [1), 2)], Ph.D.Zhenhua Wang [1), 2)] , M.E.Wenhao Li [1), 2)], Ph.D.Haoliang Yu [3)],**
[1)]College of Water Resources and Architectural Engineering, Shihezi University, Shihezi / China;[2)]Corps Key Laboratory of Modern Water-saving Irrigation, Shihezi University, Shihezi / China; [3)]Massey University, Palmerston North University / New Zealand
*Tel:18999335751; E-mail: xjshzzjz@sina.cn*

***Abstract:*** *The feasibility of using liquid films as substitute to plastic films and the combination of liquid film mulching technique and drip irrigation were investigated to explore a solution to the increasingly serious white pollution induced by agricultural film residues in cotton fields in arid areas. With the adoption of bucket tests, five different mulching treatments (liquid film 1900 kg/hm$^2$, LFD1; liquid film 2200 kg/hm$^2$, LFD2; liquid film 2500 kg/hm$^2$, LFD3; ordinary plastic film, PFD; in bare soil, NFD) were performed on the cotton plants, and the effects of different treatments on soil moisture and temperature, as well as the growth of cotton plants and roots, were monitored and analyzed. The results indicate that liquid film spraying can promote the growth of cotton roots and affect the growth and development of cotton plant. In particular, the squaring stage was 2–5 days earlier with liquid film than that in bare land, and the yields were increased by 7.1%–14.39%. Compared with the results on the use of plastic films, soil evaporation were increased by 1.85%–6.90%; the ground temperature at 5 cm was reduced by 1°C, with a decreasing ratio of 2.5%–7.7%; the decreasing ratios of the ground temperature at 10 cm soil depth were 3.0%–6.4%; the growth stages were 1–2 days later; the yield was only reduced by 0.11%. The amount of liquid film (not less than 2500 kg/hm$^2$) combined with the drip irrigation and plastic mulch film of cotton with drip irrigation is a water-saving and yield-increasing effect compared with the NFD, with liquid film can be degradable; hence, the proposed technique can be used in numerous applications because of these non-pollution characteristics. With the urgent need to protect the agricultural ecological environment and to conserve agricultural water, the use of liquid film can be improved on the basis of sustainable and efficient agricultural development.*

***Keywords:*** *Cotton by drip irrigation; Liquid film mulching; Soil moisture; Soil temperature; Growth and development*

## INTRODUCTION

Mulching for soil moisture conservation is an effective measure for saving water resources, increasing crop yields, and improving crop quality due to its capacity to effectively regulate and control soil moisture in farmlands and to enhance crop water production efficiency. Because of its remarkable function in increasing cotton yield and quality, plastic film mulching cultivation technology has currently been widely applied in Xinjiang, the largest cotton producing area in China. However, plastic films are usually used for many years, and it cannot be recycled timely and effectively, which results in an increasing amount of plastic film residues in most cotton producing farmlands in Xinjiang. Inevitably, these residues have caused serious pollution to soils and the surrounding environments. Improving cotton yield without any pollution is generally recognized as a challenge [6,7,13].

***摘要：****为了探寻解决干旱区棉田日益严重的“白色污染”问题的途径，本论文研究了液体地膜代替塑料薄膜与滴灌结合的可行性。试验采用桶栽方法，设置了 5 种处理（液体地膜 1900 kg/hm$^2$，LFD1；液体地膜 2200 kg/hm$^2$，LFD2；液体地膜 2500 kg/hm$^2$，LFD3；普通塑膜，PFD；裸地对照，NFD），监测和分析了不同处理对滴灌棉花土壤水分、温度及作物生长、根系的影响。结果表明，喷施液体地膜可以促进棉花根系的生长，影响棉花植株的生长和发育。特别地，喷施液体地膜后的滴灌棉花蕾期比裸地对照提前 2–5 天，产量比裸地对照增加了 7.1%–14.39%。与塑料地膜相比，土壤蒸发量增加了 1.85%–6.90%；5cm 处的地温降低了 1℃，下降 2.5% -7.7%，10cm 处的地温下降 3.0%–6.4%；生育期晚了 1–2 天；产量也只减少了 0.11%。适量液体地膜（不少于 2500 kg/hm$^2$） 与滴灌结合可以与塑料地膜膜下滴灌棉花具有相当的节水、增产效果（与 NFD 相比），液体地膜具有的可降解、无污染特点将使该技术具有较大的应用潜力。随保护农业生态环境和农业节水的迫切需要，从农业持续高效发展的角度出发，液体地膜栽培具有广阔的应用前景。*

***关键词:*** *滴灌棉花; 液体地膜; 土壤水分; 土壤温度; 生长发育*

## 引言

覆盖保墒可对农田土壤水进行有效调控，提高作物水分生产效率，是节约水资源、提高作物产量及改善作物品质的有效措施。由于塑料地膜覆盖栽培技术能大幅度提高棉花的产量与质量， 所以在中国最重要的棉花产区-新疆被广泛采用。但塑料地膜的长年使用及回收措施的不力，造成新疆大部分棉区土壤中的地膜残留量越来越多，土壤中的残膜给土壤及生活环境带来严重的污染，这已是公认的难题 [6,7,13]。

Liquid film is a kind of composite black–brown viscous liquid that is degradable, thus making it environmentally friendly. After being mixed with water and sprayed on soil, this liquid film can become a layer of black immobilizing film on soil surfaces, which can contribute significantly in enhancing soil temperature and inhibiting water evaporation [3,18].

The use of potato-dreg-based degradable liquid film can increase soil temperature and moisture content by 0.8–1.6 °C and 6.4%–17.9%, respectively [2].

Compared with the conditions on traditional bare land, the soil that is processed with liquid film mulching technology exhibits substantial improvements, particularly in the topsoil with depth of 0–25 cm, where daily mean temperature and average moisture content were increased by 2.38 °C and 2.50%, respectively, and the yield of potato tubers was increased by approximately 27.17% [4].

The soil temperature during liquid film mulching can be enhanced by 0.5–1.3 °C [5].

Liquid film mulching can increase soil temperature, especially for soil under medium-water and water-deficient treatments, where soil temperature can be increased by approximately 7.4% [8].

Both plastic film mulching and liquid film mulching exhibit favorable moisture-holding and water-promotion effects. Specifically, in topsoil with depth of 0–10 cm, plastic film mulching exhibits relatively remarkable effects, whereas in deep soil layer with depth of 30–40 cm, liquid film mulching is more preferred [12].

By using plastic films, the soil layers with depth of 0–5, 5–10, and 10–15 cm have increased their average soil temperatures by 4.92%, 3.45%, and 0.65% compared with the results using liquid films [15].

When the liquid film used is 225 kg/hm$^2$, the weed inhibition ratio of the soil is the highest, being up to 65.7%; whereas, when the liquid film used was 300 kg/hm$^2$, the ratio of yield increase of the soil was the greatest, up to 19.7% [16].

By using liquid films, the seeding emergence ratio of corn plant can be increased by 17%, i.e., the liquid film contributes to corn plant growth and development; the corn yield can also be increased with liquid film by 17.4% greater than without liquid film mulching [19].

Therefore, to date, few studies were made on the effects of liquid film mulching technique on the growth and development of cotton plant by drip irrigation, especially the studies in Xinjiang, where drip irrigation under mulching is widely applied. In this study, we conducted experiments on cotton plant by drip irrigation under liquid films to analyze the effects of liquid film mulching on soil moisture and temperature, as well as, on the growth of crop and underground root system. Thus, the analysis of these effects can provide theoretical and technical guidance for the scientific applications of liquid films. With the urgent need to protect the agricultural and ecological environment and to conserve agricultural water, the sustainable and efficient development of agriculture in China becomes increasingly extensive.

## MATERIAL AND METHODS

### *Brief introduction of the test area*

The tests were conducted during the period from April to October, 2014. The test field was located in the test site of Corps Key Laboratory of Modern Water-saving Irrigation (85° 59′ E and 44° 19′ N) with an elevation of 412 m. Its annual average sunshine duration is up to 2865 hours, and the frost-free period lasts for 170 days. The accumulated temperatures above 10 °C and above

液体地膜是一种复合环保型可降解黑褐色粘稠液体，兑水喷施后，可在土壤表层形成一层黑色固化膜，能够显著提高土壤温度、抑制土壤水分蒸发等[3,18]。

马铃薯渣基液体降解地膜可提高地温 0.8–1.6℃，提高土壤含水量 6.4%–17.9%[2]。

与传统裸地相比，液体地膜覆盖处理使土壤的性质得到改善，特别是使耕层土壤（0–25cm）日平均温度和平均含水率分别提高 2.38℃和 2.50%，可使马铃薯块茎产量增加 27.17%[4]。

使用液态地膜，可提高地温 0.5–1.3℃ [5]。

液膜覆盖的土壤增温效果明显，特别是中、低水分处理，增温 7.4%左右[8]。

塑料地膜覆盖和液体地膜覆盖均有较好的保水促水效应。具体来说，塑料地膜覆盖的保水促水效应在 0–10cm 表耕层较为突出，而液体地膜在 30–40cm 土层的保水促水效果则优于塑料地膜[12]。

塑料地膜在 0–5、5–10 和 10–15 cm 土层较液体地膜处理平均温度分别提高 4.92%、3.45%和 0.65%[15]。

液态地膜用量 225kg/hm$^2$ 的处理杂草抑制率最高，为 65.7%；用量 300kg/hm$^2$ 的处理增产率达 19.7%[16]。

液态地膜能使玉米的出苗率提高 17%，促进玉米的生长与发育，提高玉米产量，较对照高出 17.4%[19]。

因此，到目前为止，液体地膜覆盖对滴灌棉花的影响研究相对较少，特别是在膜下滴灌广泛应用的新疆。本研究通过液体地膜覆盖滴灌棉花试验，分析液体地膜覆盖对滴灌棉花土壤水分、温度及作物生长、根系的影响，从而为液体地膜的科学应用提供理论与技术指导。随保护农业生态环境和农业节水的迫切需要，从农业持续高效发展的角度出发，液体地膜栽培在中国具有广阔的应用前景。

## 材料与方法

### *研究区概况*

试验于 2014 年 4 月-10 月进行，试验地点位于现代节水灌溉兵团重点实验室试验基地（85°59′E、44°19′N、海拔 412 m），年平均日照时数 2865 h，无霜期 170 d。 >10℃积温为 3463.5℃，>15℃积温为 2960.0℃。年

15 °C were 3463.5 and 2960.0 °C, respectively. The annual average air temperature of the areas is 7.7 ± 0.90 °C. In particular, the annual highest air temperature appears in July, which averages at 25.4 ± 0.74 °C, whereas the annual lowest air temperature appears in January, which averages at −5.5 ± 2.07 °C. The annual precipitation in the area is approximately 213 ± 56.7 mm, and the annual evaporation capacity is approximately 1342 ± 413 mm [17].

平均气温（7.7±0.90）℃，一年中的最高气温出现在 7 月，平均气温（25.4±0.74）℃；最低气温出现在 1 月，平均气温（−5.5±2.07） ℃。年降水量（213±56.7） mm，年蒸发量（1342±413） mm [17]。

***Test materials***

In the tests, liquid film (Lv'ye/Greenfield; Yangling Mingrui Chemical Science & Technology Co., Ltd., Shaanxi, China) was used. These liquid films are composed of residual oils, emulators, and water, which account for 50%, 30%, and 10% of the liquid film, respectively. The early-maturing Xinlu No. 48 cotton (Huiyuan 710) was selected. Ordinary plastic films (Tianye Co., Ltd., Xinjiang) were used for comparison. These plastic films were 0.008 ± 0.0003 mm in thickness and were mainly composed of polyethylene. The adopted single-wine labyrinth drip irrigation tapes were also provided by Tianye Co., Ltd., Xinjiang, and the spacing and flow rate of drip holes were 30 cm and 2.6 L/h, respectively.

***试验材料***

供试液膜为明瑞牌绿野液态地膜，由中国陕西杨凌明瑞化工科技有限公司生产，各组分重量含量为：渣油（50%）、乳化剂（30%）、水（10%）及其它；棉花品种为新陆早 48 号（惠远 710）；普通塑料地膜由新疆天业公司生产，其主要成分为聚乙烯，厚度为（0.008 ± 0.0003）mm；单翼迷宫式滴灌带由中国新疆天业公司生产，滴孔间距 30 cm，滴孔流量 2.6 L/h。

***Test design***

The tests were performed in plastic buckets (Fig. 1), and bucket cultivation was adopted. Fifteen plastic buckets were used in the test, and the height and inner diameters at the top and bottom of the bucket were 0.52, 0.45, and 0.35 m, respectively.

***试验设计***

采用桶栽试验见图 1，试验用塑料桶规格为 0.52 m×0.45 m×0.35 m（高×顶部内径×底部内径），共 15 个试验用塑料桶。

**Fig.1** - Plastic bucket for testing

The plastic buckets were filled with medium loams with bulk density of 1.37 kg/m$^3$. In the tests, five different treatment conditions were conducted on cotton plants as follows: LFD1 (1900 kg/hm$^2$ liquid films), LFD2 (2200 kg/hm$^2$ liquid films), LFD3 (2500 kg/hm$^2$ liquid films), PFD (plastic films), and NFD (cotton cultivated without mulching films for comparison). Each treatment was repeated for three times. On April 21, the cotton plants were sown by dry sowing and wet germination. At the distances of 15–20 cm away from the center of buckets, equilateral triangles were drawn, and 3–4 cotton seeds were placed in each vertex. The buckets formed two columns, and two drip-irrigation tapes were used for water supply. A 450 m drip-irrigation tape was placed above the top openings of 7 buckets, while the other tape that was 510 cm long was placed above the top openings of the remaining 8 buckets. For each bucket, 2 drip holes, which are 7.5 cm away from the internal wall of top opening, were made. Pressure regulating valve, pressure gauge, and water meter were installed at the connection of each drip-irrigation tape to regulate and control pressure and irrigation. On April 22, the liquid films were

桶中装填土壤类型为中壤土，平均容重 1.37 kg/m$^3$。试验共设 5 个处理水平：液体地膜 1900 kg/hm$^2$，LFD1；液体地膜 2200 kg/hm$^2$，LFD2；液体地膜 2500 kg/hm$^2$，LFD3；普通塑料地膜，PFD；裸地对照，NFD；各处理 3 次重复。4 月 21 日采用“干播湿出”方式播种。在试验桶中心的 15–20cm 范围内画等边三角形，3 个顶点上各放 3–4 个棉籽，把桶排成 2 列，用 2 条滴灌带供水，1 条长 450 cm 的滴灌带贴着试验桶放置于 7 个桶的顶口上；另一条长 510cm 的滴灌带贴着试验桶放置于 8 个桶的顶口上，每个桶内有 2 个滴孔，滴孔距顶口内边壁各 7.5cm。在每条滴灌带的接口处安装有调压阀、压力表和水表，灌水时

sprayed, with the amounts of 1900, 2200, and 2500 kg/hm$^2$. The liquid films were diluted in water in the proportion of 1:2, and then evenly sprayed on the soil surfaces of the buckets by using a sprayer. For plastic films, an ordinary amount of 50 kg/hm$^2$ was used in the tests. The irrigations and fertilizer applications were identical under different treatment conditions. During the whole growth period, the irrigation frequency was 11, with irrigation quota and irrigation water quota of approximately 378 mm and 35 mm, respectively. The local deep fresh groundwater was adopted as the irrigation water source, with the mineralization degree of 1.3 g/L. The fertilizing amount was 832 kg/hm$^2$ (it should be noted that urea and potassium phosphate were applied by way of topdressing with irrigation according the ratio of 2:1). The other management measures were similar to those used in ordinary cotton fields. As stated above, drip irrigation was used in the tests. The drip holes of drip-irrigation tape were pressed closely against the soil surface, and then water was gradually permeated into the soils through capillary channels (i.e., the reserved capillary channels formed during the formation of liquid films because the evaporation of water). Therefore, drip irrigation would not cause any damage on liquid films.

***Technology Roadmap***

利用调压阀调控压力，利用水表控制灌水量。4 月 22 日喷施液体地膜，用量分别为：1900 kg/hm$^2$；2200 kg/hm$^2$；2500 kg/hm$^2$，兑水稀释 2 倍，使用喷雾器械均匀喷施于桶中土壤表面。塑料地膜用量同一般棉田用量一致，即 50 kg/hm$^2$。各处理灌水施肥一致，全生育期灌水次数共 11 次，灌溉定额 378 mm，灌水定额在 35 mm 左右，灌溉水源为当地深层地下淡水，矿化度 1.3 g/L，施肥量 832 kg/hm$^2$（尿素和磷酸钾铵按照 2:1 的比例进行滴灌随水追施），其他管理措施同一般棉田。由于采用的是滴灌方式，滴灌带的滴孔紧贴桶中土壤表面，滴孔中滴出的水经过毛细孔道（液体地膜在成膜过程中，由于水分蒸发形成并保留的毛细孔道）逐渐渗入土壤之中，所以不会对液体地膜造成破坏。

***技术路线图***

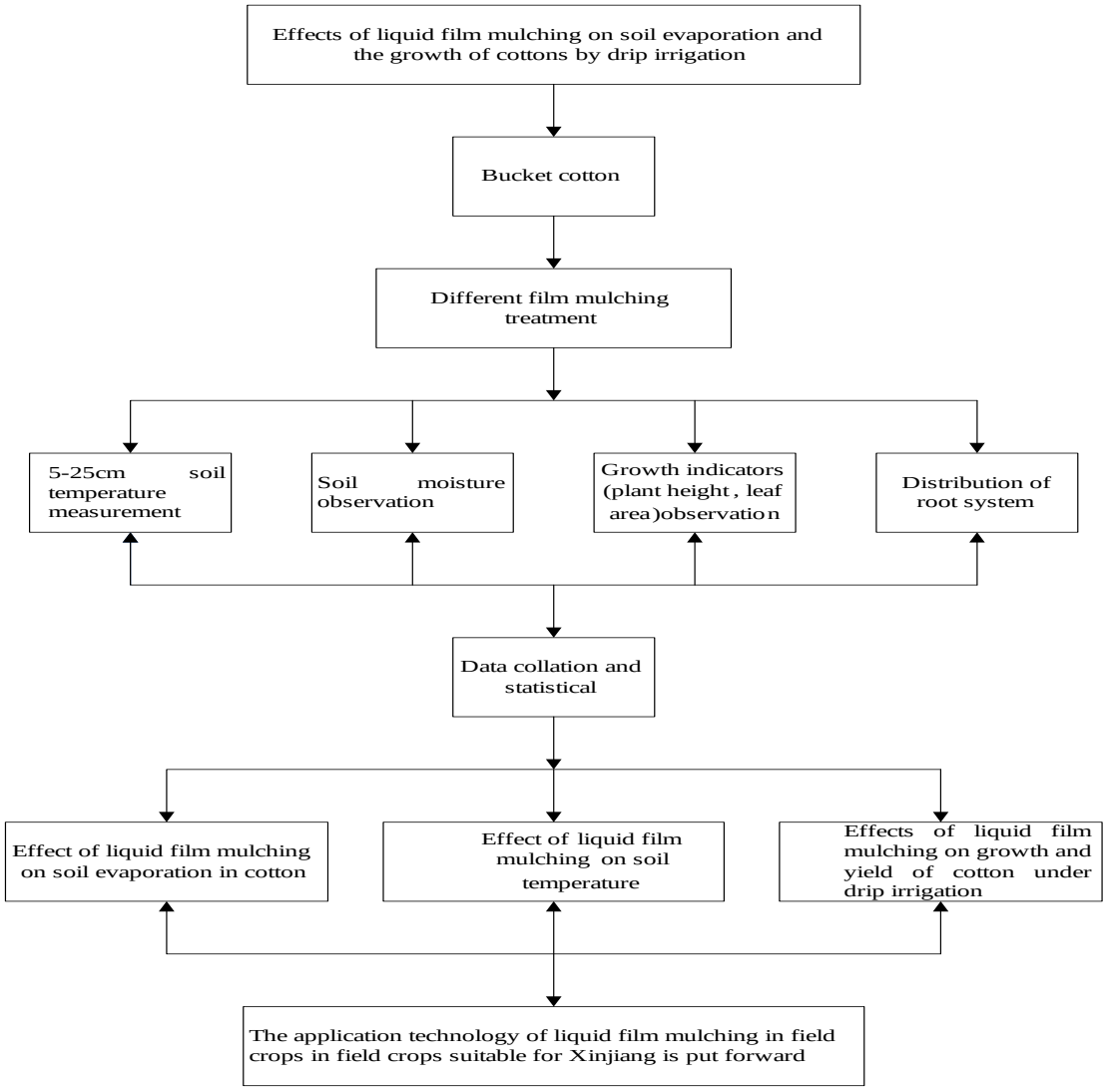


**Fig.2** - Technology Roadmap

***Measurement and calculation method***

*Measurements of soil moisture and ground temperature*

In measuring soil moisture, the masses of the plastic buckets before and after irrigation were measured by using the electronic scale (XK3150), and then the soil evaporation capacity can be determined.

In measuring ground temperature (Fig. 3), five angle-stem earth thermometers were placed in each plastic bucket, and then the soil temperatures at 5–25 cm depth were measured and averaged daily during 10:00, 16:00, and 20:00.

***测定和计算方法***

*水分和地温观测*

灌前和灌后使用 XK3150(W)型电子秤称量各桶的质量，进而测定土壤蒸发量。

使用曲管地温表见图 3，每个桶放置地温计 5 支（5–25 cm），每天 10:00、16:00 与 20:00 时记载测定 5–25 cm 土层温度，求平均值。

**Fig.3** - Bent stem earth thermometer

*Observation and measurement of cotton roots*

At the boll-opening stage, the root systems of cotton plant were used by transverse section method. Each 10 cm long root system was selected as a sampling unit. The soil samples were soaked for 24 h and then sifted by using a 0.5-mm sieve. Subsequently, all the root systems were obtained, and photographs of these were taken. Thereafter, the root length was quantified using computer-assisted image analysis technique. Finally, all these root systems were placed into the oven for 72 h at 65 °C and were weighed by using an electronic balance with precision at 0.1 mg.

The root length density (RLD) and root weight density (RWD) can be calculated by the following formulas:

*棉花根系观测*

在吐絮期内采用横向切片法取出根系，每 10cm 为一取样单元，将取出的土样浸泡 24 h 后过 0.5 mm 筛，捡出所有根系并拍照，用计算机图像分析技术量化总根长，之后放入烘箱，在 65℃下烘 72 h，采用精度为 0.1mg 的电子天平称其质量。

各项目计算公式：

$$RLD = \frac{TL}{V} \quad (1)$$

$$RWD = \frac{DM}{V} \quad (2)$$

where TL is the overall root length in soils, V is soil volume and, DM is the mass of dry matter of roots in unit soil column.

其中 *TL* 为土体内根系总长度； *V* 为土体体积；*DM* 为单元土柱土体内根系干物质质量。

**RESULTS**

***Effects of liquid film mulching on soil evaporation***

Soil evaporation volume can be obtained by weighing the buckets successively for six days in two irrigation periods after liquid film mulching treatment. Fig. 4 displays the variation of soil evaporations using different mulching treatments, which shows that after one-time irrigation, the evaporation volume decreased gradually with prolonged irrigation time. Compared with the condition on bare land, the soil evaporations using liquid film mulching decreased on all treatments, and the average decreasing amplitude and ratio were 0.25–3.21 mm and 4.27%–29.14%, respectively. Specifically, compared with bare land condition, when using LFD1, LFD2, and LFD3 treatments, the soil evaporation volumes were reduced by 0.25–1.82, 0.63–3.21, and 0.57–2.14 mm, respectively, with the decreasing ratios of

**结果与分析**

***液体地膜覆盖对土壤蒸发量的影响***

不同覆盖处理对土壤蒸发量的影响见图 4。由图 4 可以看出，在液体地膜处理后的两个灌水周期内分别选择连续的 6 天对桶进行称重。结果表明，在一次灌水后，随着时间的延长，蒸发量越来越小。液体地膜覆盖土壤蒸发量较裸地平均减少 0.25–3.21 mm，降低 4.27–29.14%。LFD1 土壤蒸发量较裸地减少 0.25–1.82 mm，降低 4.27–16.57%。LFD3 和 LFD2 土壤蒸发量较裸地分别减少

4.27%–16.57%, 15.44%–29.14%, and 13.85%–19.43%, respectively. Compared with the condition using plastic film mulching, the evaporation volumes of soils using LFD1, LFD2, and LFD3 increased by 0.31–1.89, 0.13–1.57, and 0.06–0.5 mm, respectively, with the increasing ratios of 9.26–25.86%, 3.70%–21.55%, and 1.85%–6.90%, respectively. The soil evaporation in the other irrigation periods exhibit similar tendency among these different treatment methods. The results indicate that, although liquid film mulching is inferior to plastic film mulching in terms of soil moisturizing effect, liquid film is superior in bare land conditions without any mulching. The evaporation in soils after liquid film mulching is the evaporation controlled by water flux profile at an extremely low level under the limitation imposed by organic thin-films; whereas, water is completely isolated when using plastic films. Apparently, the amount of liquid films also affects soil evaporation. With low application amount, the film properties are poor, whereas with high application amount, the film properties become desirable. However, these films were easily damaged when the cotton seedlings and weeds emerge from the ground. In addition, during the formation of films, the reserved capillary channels due to water evaporation became the channels for rainwater seepage after mulching. Therefore, compared with plastic films, liquid films are more beneficial to rainwater infiltration into soils.

0.63–3.21 mm 和 0.57–2.14 mm，降低 15.44–29.14%和 13.85–19.43%。LFD1、LFD2 和 LFD3 土壤蒸发量较塑料地膜分别增多 0.31–1.89 mm、0.13–1.57 mm 和 0.06–0.5 mm，增加 9.26–25.86%、3.70–21.55%和 1.85–6.90%。另一灌水周期也有类似的规律。分析表明，液体地膜覆盖土壤保湿效应虽低于塑料地膜，但显著高于裸地。与塑料地膜相比，液体地膜覆盖地面后的蒸发，是有机薄膜限定下的极低水平水分通量剖面控制的蒸发，不同于塑料地膜完全隔绝水分。液体地膜施用量不同，对不同处理的土壤蒸发量影响程度亦有明显差异，其原因是施用量小，成膜质量较差，施用量大，成膜质量虽较高，但棉苗、杂草等出土过程中膜面受损较大。此外，液体地膜在成膜过程中，由于水分蒸发形成并保留的毛细孔道，成为覆盖后雨水渗透的通道，所以较塑料地膜更有利于雨水下渗土壤。

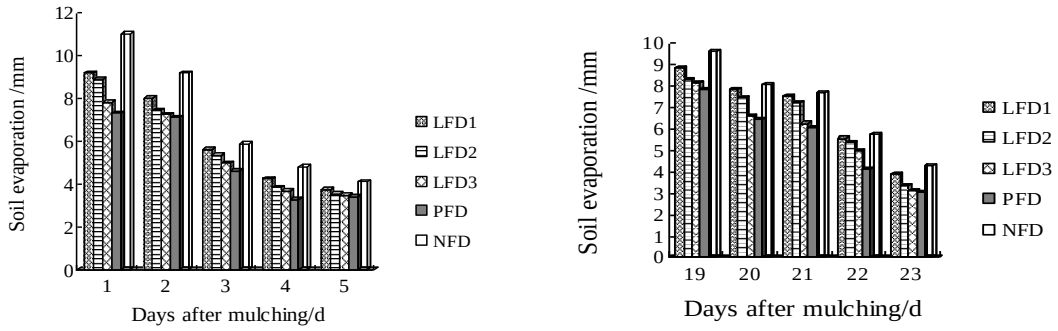


**Fig.4** - Soil evaporation using different mulching treatments

***Effects of liquid film mulching on ground temperature***

Fig. 5 displays the variation of ground temperatures with time using different mulching treatments. Fig. 6 displays the average ground temperatures at 5–25 cm depth using different mulching treatments. The ground temperatures using different processing methods differ considerably. Generally, ground temperature can be enhanced to varying degrees by applying mulching treatments, and the increasing ratio eventually decreases with soil depth and prolonged irrigation time. The ground temperatures in LFD3 treatment were the highest among all treatments. Specifically, compared with bare land conditions, the ground temperature at 5 cm depth increased by 0.5–5 °C, with the increasing ratio of 2.33%–16.67%. The ground temperature at 10 cm depth increased by 0.5–4.5 °C, with the increasing ratio of 2.50%–16.36%. Compared with the conditions when using plastic film mulching, the ground temperatures at 5 cm depth were reduced by 1–5 °C. In particular, the condition using LED3 treatment in 35 days after spraying liquid film, the ground temperature was only 1 °C below that of plastic films, with the decreasing ratio of 2.5%–7.7%. The ground temperature of soil with liquid film at 10 cm depth exhibited the decreasing ratio of 3.0%–6.4% compared with plastic films. These results suggest that liquid films exhibit a moisturizing effect, which is primarily

***液体地膜覆盖对地温的影响***

不同覆盖处理随时间变化对地温的影响见图 5。不同覆盖处理后 5-25cm 土层的平均地温变化见图 6。由图 5、6 可以看出，各处理不同土层间地温差异显著，各覆盖处理均不同程度提高土壤温度，且幅度随着土层的加深而减弱，随着时间的延长而变小。液体地膜处理中，LFD3 地温最高。具体地说，5cm 地温较裸地升高 0.5–5℃， 增温 2.33%–16.67%。10cm 地温较裸地升高 0.5–4.5℃，增温 2.50%–16.36%。与塑料地膜覆盖相比，在 5cm 处的地温减少 1–5℃。特别地，在 LED3 处理条件下，喷施 35 天后和塑料地膜覆盖相比，5cm 处地温只降低了 1℃，降低 2.5%–7.7%；10cm 处地温降低 3.0%–6.4%。结果表明，液体地膜具有一定的保温效应。其原因是液体地膜喷施

due to the layer of immobilizing films that formed on the soil surface after spraying. The immobilizing films have terminated the water exchange between soils and the surrounding environment. Meanwhile, these black immobilizing films can absorb a great deal of solar energy, which leads to increased soil heat flux. The increase of soil temperature directly affects microbial activities and nutrient variation in soils, thus affecting the growth and development of root systems and nutrient absorption.

后，于土壤表面形成一层黑色固化膜，该膜阻隔了土壤与外界的部分水分交换，黑色固化膜也能吸收较多的吸收太阳能，最终使土壤热通量增大。土壤的增温直接影响土壤微生物的活动及养分的变化，从而影响作物根系生长发育和养分吸收。

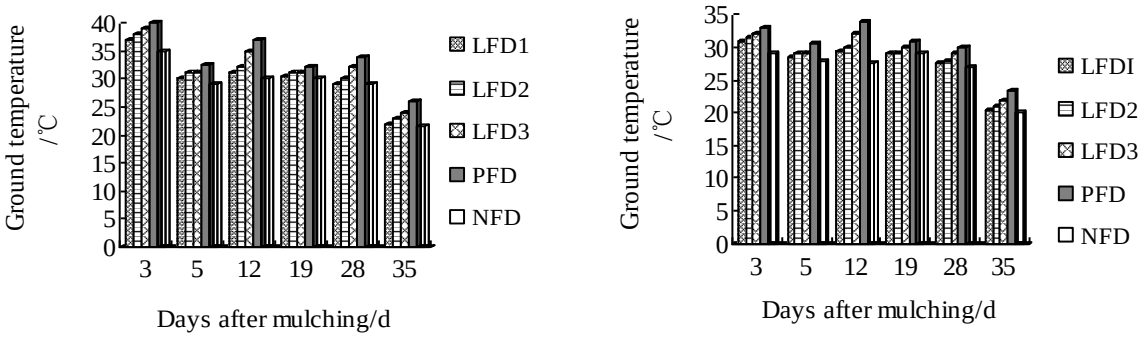


At 5 cm soil depth　　At 10 cm soil depth

**Fig.5** - Ground temperatures using different mulching treatments

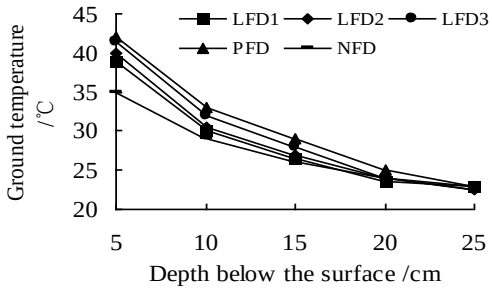


**Fig.6** - Ground temperatures at different soil depth using different mulching treatments

***Effects of liquid film mulching on the cotton's growth and development***

Table 1 illustrates the growth of cotton plants in different mulching treatments, which shows that the growth of cotton plants after mulching was faster than in bare land. For the cotton plants using LFD3 and LFD2 treatments, 10 and 11 days were required from sowing to emergence of seedlings, and the lengths were shortened by 4 and 3 days compared with that in bare land, respectively. The cotton plants in liquid films entered the squaring stage that was 2–5 days earlier than that in bare land, whereas the cotton plants in plastic films entered the initial flowering stage that was 5 days earlier than that in bare land. Apparently, the amount of liquid films affected the growth and development of cotton plants, i.e., with the increasing amount of liquid films, the early growth periods began earlier. However, with the increase of the amount of liquid film, the cotton plants were more likely to be senile at later growth periods. The primary reason is that liquid films can contribute to the preservation of soils moisture and the temperature increase. These effects are more apparent in topsoil, and thus the cotton plants have difficulty rooting, which is related to the information that the water and nutrients in deep soils cannot be fully utilized at the later growth stages of cotton plant.

***液体地膜覆盖对棉花生长发育的影响***

不同覆盖处理对棉花生长发育的影响见表 1。由表 1 可以看出，各覆盖处理棉花发育进程都快于裸地对照。LFD3 从播种到出苗需要 10d，比裸地早 4d。LFD2 从播种到出苗需要 11d，比裸地早 3d。现蕾期，喷施液体地膜比裸地对照提早 2–5d。初花期，塑料地膜覆盖仅比裸地对照提早 5d。不同覆盖处理基本在同一时间到达吐絮期。滴灌条件下液体地膜用量大小影响棉花的生育期进程，即随着液体地膜用量的加大，棉花的前期生育期随之提前。但据观察：随着液体地膜用量增大，棉花在生长后期易出现早衰现象。其原因是由于液体地膜具有保墒增温性能，这种效应在土壤表层影响较明显，从而导致棉株根系不易下扎，于生育后期不能充分利用土壤深层水肥有关。

Table 1

**Effects of different mulching treatments on the growth and development of cotton plant**

| Treatment | Sow (Month–day) | Seedling (Month–day) | Squaring stage (Month–day) | Initial flowering stage (Month–day) | Boll opening stage (Month–day) |
|---|---|---|---|---|---|
| LFD1 | 4-21 | 5-3 | 6-18 | 7-3 | 8-19 |
| LFD2 | 4-21 | 5-2 | 6-17 | 7-1 | 8-18 |
| LFD3 | 4-21 | 5-1 | 6-15 | 6-30 | 8-18 |
| PFD | 4-21 | 4-30 | 6-13 | 6-29 | 8-17 |
| NFD | 4-21 | 5-5 | 6-20 | 7-4 | 8-19 |

***Effects of liquid film mulching on the root length density of drip-irrigation cotton plants***

Significantly positive correlations exist among the biomass of leaf area per plant, the biological yield above the ground, and the number of reproductive organs [9–11,14]. Root length density is the overall length of root systems per a unit volume of soils, which reflects the number of capillary roots and directly reflects the extension and intensity of root systems to absorb water and nutrients. Fig. 7 displays the root length densities of the drip-irrigation cottons in different mulching treatments. Compared with the data using the treatment of NFD, the root length densities of the soils at 20–30 cm depth in the LFD1 and LFD2 treatments increased by 405.063 and 851.974 m/m$^3$, respectively. The root length density of the soils in LFD3 was 915.803 m/m$^3$ higher than that in NFD, but 63.823 m/m$^3$ lower than that in PFD. These results indicate that the liquid film application at an appropriate amount can contribute to the root system growth of cotton plant, which lays solid foundations for growth and development, and finally, to achieve high yield. In addition, all of the root length densities in different treatments initially increased and then decreased with increasing soil depth. The root systems beneath the plough layer, although its density is fairly small, play quite important roles in absorbing and utilizing the nutrients and water in subsoil.

***液体地膜覆盖对滴灌棉花根长密度的影响***

棉花根系生物量与单株叶面积、地上部生物学产量及生殖器官产量之间均存在显著的正相关[9-11,14]。根长密度表示单位土体内根系总长度，反映根系毛细根数量，也间接反映了根系吸收水分、养分的范围和强度。液体地膜覆盖对滴灌棉花根长密度的影响见图 7。由图 7 可以看出，在 20–30cm 土层内，LFD1 和 LFD2 的根长密度较 NFD 分别增加 405.063 m/m$^3$ 和 851.974 m/m$^3$。LFD3 的根长密度较 NFD 增加 915.803m/m$^3$，较 PFD 减少 63.823 m/m$^3$。结果表明，适量的液体地膜覆盖促进了棉花根系的生长，亦为地上部良好的生长发育及获得较高的产量奠定了良好基础。棉花根长密度在不同土层中变化趋势来看，各处理下的根长密度分布都是随土层深度的增加先增大后减小，耕层以下土层中的根系，其量虽然少，但对于吸收和利用下层土壤中的养分、水分起着重要的作用。

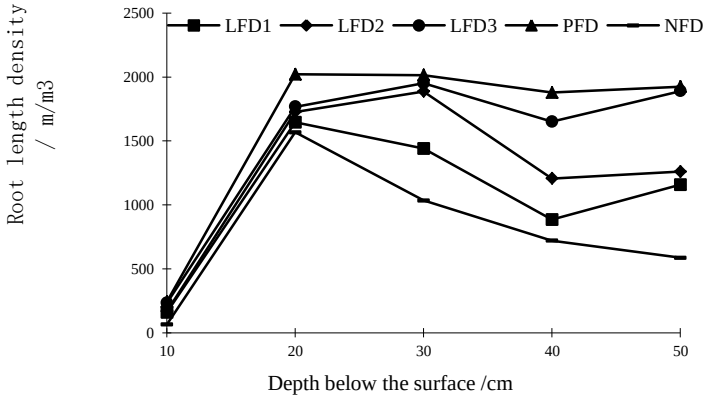


**Fig.7** - Root length densities in different mulching treatments

***Effects of liquid film mulching on the root weight density of drip-irrigation cotton plants***

Root weight density is the gross mass of the dry matters in roots, which directly reflects the mass of root systems and indirectly reflects the extension and intensity of root systems to absorb water and nutrients. Fig. 8 displays the root length densities of drip-irrigation cottons determined by using different processing methods, which shows a negative exponential function between cotton root weight density and soil depth. At 10–20 cm soil

***液体地膜覆盖对滴灌棉花根重密度的影响***

根重密度表示单位土体里面根系干物质总质量，反映根系质量，也间接反映根系吸收水分、养分的范围和强度大小。液体地膜覆盖对滴灌棉花根重密度的影响见图 8。由图 8 可以看出，棉花根重密度与土层深度呈负指数关系，以地表层的根重密度最大。在 10–20cm 土层内，LFD1 和

depth, the root densities in the LFD1 and LFD2 treatments increased by $0.1335\times10^{-4}$ g/cm$^3$ and $0.4496\times10^{-4}$g/cm$^3$, respectively, compared with that in NFD. The root weight density using LFD3 was $1.3645\times10^{-4}$ g/cm$^3$ being greater than that in NFD, but $0.4429\times10^{-4}$ g/cm$^3$ lower than that in PFD. These results indicate that liquid films, in the appropriate amount, can be comparable with plastic films in terms of root weight density. More importantly, the white pollution caused by plastic film residues can be thoroughly eliminated.

LFD2 较 NFD 分别增加 $0.1335\times10^{-4}$g/cm$^3$ 和 $0.4496\times10^{-4}$g/cm$^3$。LFD3 的根重密度较 NFD 增加 $1.3645\times10^{-4}$g/cm$^3$，较 PFD 减少 $0.4429\times10^{-4}$g/cm$^3$。结果表明，适量的液体地膜覆盖效果已接近塑料地膜，从另一方面来说，也可以彻底消除“白色污染”。

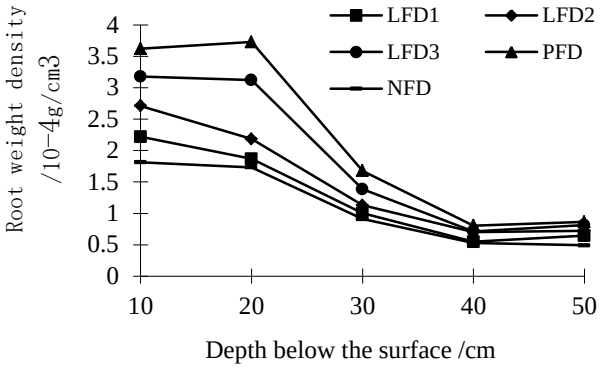


**Fig.8** - Root weight densities using different mulching treatments

***Effects of liquid film mulching on the yield of drip-irrigation cotton plants***

Table 2 presents the yield structures of cotton plants in different mulching treatments, showing that the boll number per plant was increased by 0.31–0.67 compared with that in bare land. After liquid film spraying, the yields were approximately 4980–5317 kg/hm$^2$, which were increased by 7.1%–14.39% relative to the results in bare land. However, compared with the result using plastic films, the yields were reduced by 28–365 kg/hm$^2$, with the decreasing ratio of yield of 0.11%–7.4%. Notably, the yields of the cotton plants in LFD3 treatment were considerably close to that in plastic films. Conclusively, the cotton yields by drip irrigation in liquid films, although lower than that in plastic films, were apparently higher than the yield on bare land. From the perspective of ecological sustainability, liquid film spraying is of great application value. Practices proved that premature seedling is the key for a high cotton yield, which also requires a favorable soil environment. Therefore, liquid films can contribute to the enhancement of boll numbers and the improvement of boll quality.

***液体地膜覆盖对滴灌棉花产量的影响***

不同覆盖处理对棉花产量结构的影响见表 2。由表 2 可以看出，喷施液体地膜比裸地对照单株铃数增加 0.31–0.67 个。液体地膜覆盖产量为 4980–5317kg/hm$^2$，比裸地增产 7.1%–14.39%。液体地膜覆盖相对塑料地膜减产 28–365kg/hm$^2$，减产率 0.11%–7.4%，但 LFD3 产量已接近塑料地膜。由此说明，滴灌条件下液体地膜覆盖棉花产量虽次于塑料地膜，然而适量液体地膜覆盖棉花产量明显高于裸地，从生态可持续角度也具有可应用价值。实践证明，壮苗早发是棉花获取高产的关键，而棉花早发需要一个较好的土壤环境，液体地膜覆盖有利于促进棉花增结铃数、提高铃质量。

**Table 2**

**Yield structures of cotton plants in different mulching treatments**

| Treatment | Boll number per plant | Single boll weight (g) | Seed cotton yield (kg/hm$^2$) | Growth ratio compared with the condition without mulching (%) |
|---|---|---|---|---|
| LFD1 | 4.87 | 5.09 | 4980 | 7.10 |
| LFD2 | 5.21 | 5.25 | 5196 | 11.79 |
| LFD3 | 5.23 | 5.28 | 5317 | 14.39 |
| NFD | 4.56 | 4.77 | 4648 | — |
| PFD | 5.24 | 5.31 | 5345 | 14.50 |

**Discussion**

Currently, many similar research results on the role of liquid film in preservation of soil moisture and enhancement of soil temperature were presented. However, the research regarding the combination of liquid film mulching cultivation technique and drip irrigation and their effects on soil moisture and temperature, as well as cotton growth and root systems, is still quite rare. In the present work, not only the effects of liquid film mulching on cotton growth and development, as well as the root systems, were analyzed, but also the effects on soil moisture and temperature. The results indicate that, after liquid film spraying on drip-irrigation cotton plants, the soil temperature can be remarkably enhanced, and simultaneously the soil evaporation capacity can be significantly reduced, i.e., the absorption and synthesis capacity of the root systems can be improved. The elevated root activity can also provide solid foundations for promoting the growth and development of over ground cotton plants and achieving high yields, which are characterized by premature growth of cotton plants, greater mass of cotton bolls, and significant increase in yield. Moreover, different amounts of liquid film also exhibited different degrees of mulching effects. A favorable soil ecological environment is an important prerequisite for high yield of cottons, since it firstly affect the growth and development of underground roots and then the growth of over ground cotton plants, and finally leads to a high cotton yield. Although the liquid film is inferior to plastic film in the aspects of soil moisture preservation and yield growth, it can be beneficial to the seepage of rainwater into soils, deeper rooting, the increase of the ratio of root weight beneath the soils, and the maintenance of strong absorption and synthesis capacity of the cotton root at the later growth stages. In addition, by using liquid films, the premature senility of cotton plants can be effectively prevented. After liquid film spraying, the boll numbers per cotton plant increased by 0.31–0.67 compared with the values on bare land; the average cotton seed yields were enhanced by 7.1%–14.39% compared with the values on bare land, but were reduced by 0.11%–7.4% compared with the values using plastic films. These results are slightly inconsistent with the previous research results. In further studies, we should expand the test range of liquid film mulching. In particular, we should conduct tests in farmland and probe into the effects of intensity and frequency of liquid film spraying on drip-irrigation cotton plants. Moreover, a related technical specification of liquid film mulching should be established and improved.

Liquid film, a novel cover material for cultivation in farmlands, is highly efficient, nontoxic, innocuous, and can be changed into organic fertilizers through biodegradation and light degradation [1]. Liquid films are not only applied in the cultivation of grains and cotton in fields, but also are applicable for the growth and development of fruits and vegetables in orchards. However, liquid film mulching technique should be further improved in terms of degradation characteristics and rain-wash resistance performances. As a consequence, these liquid films can be completely degraded within the mulching period, and moreover, they cannot be degraded very prematurely to lose their mulching effect. As the plastic films are commonly used for many years, the film residues causes severe contamination in cotton fields. Liquid films, owing to their low costs, strong adaptability to geographic and geomorphic conditions, favourable emergency, and ecological effects, can remarkably enhance the economic and ecologic benefits of cotton fields.

**讨论**

液体地膜覆盖的保墒增温特点与已有众多研究结果类似，但液体地膜覆盖与滴灌结合，从而改变或影响滴灌棉花土壤水分、温度及作物生长、根系，已有研究成果相对较少。本论文不仅分析了液体地膜覆盖对滴灌棉花生长发育和根系的影响，同时也分析了液体地膜覆盖对土壤水分、温度的影响。结果表明，液体地膜覆盖滴灌棉花可提高土壤温度并显著降低土壤蒸发量，从而促进棉株根系吸收与合成能力，而根系活力的增强，亦为地上部棉株生长发育及获得较高的产量奠定了良好基础。表现为棉株早发，铃质量大，增产效果显著。液体地膜不同用量覆盖效应存在一定差异。其原因是良好的土壤生态环境是棉花获得高产的重要基础，它首先影响到棉株地下部根系的发育，进而影响到地上部棉株的生长，最终才能实现棉花高产。这些效应表现虽然是液体地膜覆盖低于塑料地膜，但液体地膜更有利于雨水下渗土壤、棉花根系下扎，提高土壤下层根量比例，维持中后期棉株根系较强的吸收与合成能力，从而有效防止棉花早衰。喷施液体地膜比裸地对照单株铃数增加 0.31–0.67 个。液体地膜覆盖平均籽棉产量较裸地增长 7.1%–14.39%，较塑料地膜降低 0.11%–7.4%，这一点与前人研究结果不太一致。在以后的科研工作中，逐步扩大液体地膜的试验范围，尤其是大田试验，深入研究液体地膜喷施强度、喷施频率等对滴灌棉花的影响，形成并完善液体地膜配套应用技术规程。

液体地膜是一种新型的农田栽培覆盖材料， 高效、无毒无害，可以由生物和光降解转化为有机肥[1]，不仅适用于大田粮、棉等作物，也适用于果园、蔬菜及其它作物生长需要，但对其性能、防雨水冲刷等方面需要在工艺上进一步完善，使其在有效覆盖期内，既能被完全降解，又不致于过早降解而失去应有的覆盖效应。随塑料地膜的长年应用，残膜严重污染棉田。而液体地膜成本低廉、对地形地貌适应能力强，应急性好，也具有良好的生态效应，可显著提高棉田的经济效益和生态效益。

## CONCLUSIONS

(1) By spraying liquid films on drip-irrigation cotton plants, the soil evaporation capacity can be reduced by 4.27%–29.14%, and the soil temperatures at 5 cm depth can be enhanced by 2.33%–16.67% compared with the values on bare land. Liquid film spraying can promote the growth of cotton roots and affect the growth and development of cotton plant. In particular, the squaring stage of cotton plants in liquid films was 2–5 days earlier than that in bare land and the yields were increased by 7.1%–14.39%. The mulching effect using an appropriate amount of liquid films was comparable with the results using plastic films, that is, soil evaporation was increased by 1.85%–6.90%. The ground temperatures at 5 cm depth were 1°C lower than the values using plastic films, with the decreasing amplitude of 2.5%–7.7%. The decreasing amplitudes of the ground temperature at 10 cm depth were 3.0%–6.4%. The growth stages were 1–2 days later, and finally, the yield was only reduced by 0.11%.

(2) For the cotton cultivation by drip irrigation in arid areas, the spraying of an appropriate amount of liquid films can achieve a favorable mulching effect that is comparable with plastic films. Moreover, the liquid films can thoroughly eliminate increasing white pollution caused by film residues in farmlands, and thus contribute to the sustainable development of ecological environment in farmlands. Liquid film mulching is a feasible technique in cotton production by drip irrigation. With the urgent need to protect the agricultural ecological environment and agricultural water conservation, the sustainable and efficient development of agriculture in China is more extensive.

## ACKNOWLEDGEMENT

This work was supported by the Project of Shihezi University for High-level Talent Introduction (RCZX201322) and the National Natural Science Foundation of China (51369027).

## REFERENCES

[1]. Bai Rijun and Zhang Qiang, (2003) -*Application of functional polymer materials in land desertification controlling in Shanxi Province*, Shanxi Agricultural Sciences, vol.31, no.3, pp.87-91;
[2]. Bao Honghui, Cao Longhui, Wei Chunhong, (2014) - *Study on the field characteristics of potato-dreg-based multifunctional degradable liquid films*, Journal of Agrotechny, no.8, pp.1-3;
[3]. Chen Baolian, Wang Renhui and Cheng Guoxiang, (2001) - *Application of emulsified asphalts in agriculture*, Petroleum Asphalt, vol.15, no.2, pp.44-47;
[4]. Duan Yizhong and Kang Furen, (2014) - *Effects of different mulching materials on the soil water content and temperature and water use efficiency in dry land for potatoes* ,Bulletin of Soil and Water Conservation,vol.34, no.5, pp.55-59, 66;
[5]. Guan Enyan, (2011) - *Effects of liquid films on seedling growth*, Modern Horticulture, no.7, pp.5-7;
[6]. Haruyuki Kanehiro, (1999) -*Plastic Litter pollution in the Marine Environment*, Journal of the Mass Spectrometry Society of Japan, vol.47, no.6, pp.319-321;
[7]. Huang Zhanbin and Shan Lun, (2000) - *Discussion on the technical route and approaches for China's dryland farming construction*, Agricultural Research in the Arid Areas, vol.18, no.2, pp.1-6;
[8]. Li Caixia, Zhou Xinguo, Qiang Xiaoman, (2010) - *Soil*

## 结论

（1）液体地膜喷施在滴灌棉花上，可以使土壤蒸发量减少 4.27%–29.14%，在 5cm 处的地温较裸地对照提高 2.33%–16.67%，喷施液体地膜可以促进棉花根系的生长，影响棉花植株的生长和发育。特别地，喷施液体地膜后的滴灌棉花蕾期比裸地对照提前 2–5 天，产量比裸地对照增加了 7.1%–14.39%。与塑料地膜相比，土壤蒸发量增加了 1.85%–6.90%；5cm 处的地温降低了 1℃，下降 2.5% -7.7%，10cm 处的地温下降 3.0%–6.4%；生育期晚了 1–2 天；产量也只减少了 0.11%。

（2）在干旱区滴灌棉田，喷施适量的液体地膜，可以达到和塑料地膜相当的覆盖效果。另外，使用液体地膜可以彻底消除残留在农田的“白色污染”，从而可使农田生态环境得到可持续发展。在滴灌棉花生产中采用液体地膜覆盖是一项可行技术。随保护农业生态环境和农业节水的迫切需要，从农业持续高效发展的角度出发，在中国更具有广泛的发展潜力。

## 致谢

石河子大学高层次人才引进项目（RCZX201322），国家自然科学基金项目（51369027）

## 参考文献

[1]. 白日军,张强. (2003) -*功能高分子材料在山西省土地荒漠化防治中的应用*,山西农业科学, 第 31 卷, 第 3 期,87-91;
[2]. 包鸿慧,曹龙奎,魏春红. (2014) -*马铃薯渣基多功能可降解液体地膜田艺特性的研究*,农产品加工（学刊）, 第 8 期,1-3;
[3]. 陈保莲,王仁辉,程国香. (2001) -*乳化沥青在农业上的应用*,石油沥青, 第 15 卷, 第 2 期,44-47;
[4]. 段义忠,亢福仁. (2014) -*不同覆盖材料对旱地马铃薯土壤水热状况及其水分利用效率的影响*,水土保持通报, 第 34 卷, 第 5 期,55-59,66;
[5]. 管恩艳. (2011) -*液态地膜对苗木生长的影响*,现代园艺, 第 7 期,5-7;
[6]. Haruyuki Kanehiro. (1999) -*塑料垃圾污染海洋环境*,日本质谱学会杂志, 第 47 卷, 第 6 期,319-321;
[7]. 黄占斌,山仑. (2000) -*论我国旱地农业建设的技术路线与途径*,干旱地区农业研究, 第 18 卷, 第 2 期,1-6;
[8]. 李彩霞,周新国,强小嫚. (2010) -*不同水分处理下液体地*

*environments and production effect of corn fields using liquid film mulching under different water treatments*,Corn Science, vol.18, no.3, pp.108-112;
[9]. Li Shaokun and Wang Chongtao, (2000) - *Effects of cultivating measures on the growth of roots and overground parts of cottons in North Xinjiang*, China Cotton, vol.27, no.5, pp.12-13;
[10]. Li Yongshan, Feng Liping, Guo Meili, (1992) - *Study on the root's growth characteristics and the relationship between cultivation measures and yield---Part I Relationship between cotton root's growth characteristics and physiological activity and the overground parts*, Cotton Science, vol.4, no.1, pp.49-56;
[11]. Li Yongshan, Feng Liping, Guo Meili, (1992) -*Study on the root's growth characteristics and the relationship between cultivation measures and yield---Part II Effects on the cultivation measures on the cotton root's growth and the relationship between cultivation measures with yield*,Cotton Science, vol.4, no.2, pp. 59-66;
[12]. Lv Qiang, Xiong Ying, Chen Mingcan, (2008) - *Effects of different mulching methods on the growth of tobacco seedlings and the ecologic environment of topsoil*, Agricultural Research in the Arid Area, vol.26, no.1, pp.86-89;
[13]. Roy P, Surekha P, Rajagopal C., (2011) -*Surface oxidation of low-density polyethylene films to improve their susceptibility toward environmental degradation*, Journal of Applied Polymer Science, vol.122, no.4, pp.2765-2773;
[14]. Tang Shifang, Wang Yilu, Yu Fengqun, (1985) - *Study on the growth characteristics of cotton roots*, China Cotton, vol.12, no.1, pp.70-79;
[15]. Tao Yang and Luo Xuegang. (2009) -*Study on the applications of lignin-based liquid films*, Hubei Agricultural Sciences, vol.48, no.12, pp.3000-3003;
[16]. Wang Pingli, Li Xiaowan, Wang Xinyan, (2013) - *Effects of liquid films on corn's growth, development and yield*, Henan Agricultural Sciences, vol.42, no.4,pp.47-49;
[17]. Yang Chuangjie, Luo Yi, Sun Lin, (2012) - *Experimental study on the mineralization degree of irrigation water on the cotton's growth along Manasi river basin*, Resource Sciences, vol.34, no.4, pp.660-667;
[18]. Yang Qinghua, Han Jinfeng, He Dexian, (2004) - *Study on the water-retention effect of liquid film mulching*, Research of Soil and Water Conservation, vol.18, no.4, pp.29-32;
[19]. Zhang Chunyan and Yang Xinmi, (2008) -*Effects of liquid films on corn's growth and yield* ,Journal of Qingdao Agriculture University (natural science edition), vol.25, no.3, pp.227-230.

*膜覆盖玉米田土壤环境与产量效应*,玉米科学, 第 18 卷, 第 3 期,108-112;
[9]. 李少昆,王崇桃. (2000) -*栽培措施对北疆棉花根系及地上部生长的影响*,中国棉花, 第 27 卷, 第 5 期,12-13;
[10]. 李永山,冯利平,郭美丽. (1992) -*棉花根系的生长特性及其与栽培措施和产量关系的研究Ⅰ棉花根系的生长和生理活性与地上部分的关系*,棉花学报, 第 4 卷, 第 1 期,49-56;
[11]. 李永山,冯利平,郭美丽. (1992) -*棉花根系的生长特性及其与栽培措施和产量关系的研究Ⅱ栽培措施对棉花根系生长的影响及其与地上部和产量的关系*,棉花学报, 第 4 卷, 第 2 期,59-66;
[12]. 吕强,熊瑛,陈明灿. (2008) -*不同覆盖方式对烟苗根系生长及耕层生态环境的影响*,干旱地区农业研究, 第 26 卷, 第 1 期,86-89;
[13]. Roy P, Surekha P, Rajagopal C. (2011) -*提高低密度聚乙烯薄膜的表面氧化可以降低它们对环境的敏感性*,应用聚合物科学杂志, 第 122 卷, 第 4 期,2765-2773;
[14]. 唐仕芳,王以禄,余风群. (1985) -*棉花根生长特性研究*, 中国棉花, 第 12 卷, 第 1 期,70-79;
[15]. 陶杨,罗学刚. (2009) -*木质素液体地膜的应用研究*,湖北农业科学, 第 48 卷, 第 12 期,3000-3003;
[16]. 王萍莉,李小万,王新燕. (2013) -*液态地膜对玉米生长发育及产量的*,河南农业科学, 第 42 卷, 第 4 期,47-49;
[17]. 杨传杰,罗毅,孙林. (2012) -*灌溉水矿化度对玛纳斯流域棉花生长影响的试验研究*,资源科学, 第 34 卷, 第 4 期, 660-667;
[18]. 杨青华,韩锦峰,贺德先. (2004) -*液体地膜覆盖保水效应研究*,水土保持学报, 第 18 卷, 第 4 期,29-32;
[19]. 张春艳,杨新民. (2008) -*液态地膜对玉米生长及产量的影响*,青岛农业大学学报（自然科学版）, 第 25 卷, 第 3 期, 227-230.

# EXPERIMENTAL RESEARCH OF AGRICULTURAL EQUIPMENT TYRES DESIGNED TO THEIR RATIONAL USE
# /
# *CERCETAREA EXPERIMENTALĂ A PNEURILOR DE PE ECHIPAMENTELE AGRICOLE, ÎN VEDEREA UTILIZĂRII RAȚIONALE A ACESTORA*

**Ph.D. Stud. Eng. Lazăr G., Ph.D. Eng. Ciupercă R., Ph.D. Eng. Nedelcu A., Ph.D. Stud. Eng. Zaica A., Ph.D. Eng. Popa L., Ph.D. Stud. Eng. Ştefan V., Ph.D. Stud. Eng. Petcu A.**
National Institute of Research - Development for Machines and Installations designed to Agriculture and Food Industry – INMA, Bucharest / Romania
*Tel: 0740367860; E-mail: lazar@inma.ro*

***Abstract:*** *Soil compaction is one of the most important factors of anthropogenic influence on soil physical properties with immediate effect over the farms management and environment. The paper presents the results of experimental research carried out with a mobile stand designed and built for testing several types of tyres used on agricultural machinery in order to determine their influence on soil and energy parameters. Parameters measured, footprint, penetration resistance, tensile strength and tyres rational and efficient utilization contribute to reduce soil compaction and settlement.*

***Keywords:*** *tyres, agricultural machinery, penetration resistance, soil protection*

## INTRODUCTION

Soil artificial compaction (anthropic) is determined by aggregates passing in the field when they perform the agricultural works required by the mechanizing technologies or during transport of technological and farming products. [5,6,7]

In Romania, most of soils are compacted, being of heavy and average structure (the clay content varying between 30-50%), low drain and often they comprise an impermeable soil layer [9].

Soil compaction also affects water dynamics in the soil, erosion, nitrogen and carbon cycle in soil, the energy necessary and efficacy of farming operations, as well as, pesticides washing, soil biology and plant cultivation technologies.

Soil compaction, determined by agricultural traffic results in soil structure damaging in its surface and depth layers, modifying the pores size, pores continuity, thus, of water and air permeability. All these may have negative effects on soil biological activity, its physico-chemical balance and production.

The direct effect of soil compaction on total porosity is manifest by reducing soil ability to retain water and air in a sustainable manner.

Soil compaction and settlement determine the appearance of deeper and more compacted strips, enhancing the surface erosion risk, water slop, inappropriate use of nutrients by plants and their leaching in depth.

Intensity and extent of artificial compaction depends on a multitude of general but also local factors, such as: climate, equipment technical characteristics and methods of implementation of different components of

***Rezumat:*** *Compactarea solului este unul dintre cei mai importanți factori de influența antropică asupra proprietăților fizice ale solului cu efecte imediate asupra managementului fermelor agricole şi asupra mediului înconjurător. În lucrare sunt prezentate rezultate ale cercetărilor experimentale realizate cu un stand mobil proiectat şi realizat pentru a efectua testarea mai multor tipuri de pneuri utilizate pe echipamentele tehnice din agricultură, în vederea determinării influenței acestora asupra solului şi a parametrilor energetici. Parametrii măsurați pata de contact, rezistența la penetrare, forța de tracțiune contribuie la alegerea* si *utilizarea rațională şi eficientă a pneurilor pentru reducerea compactării şi tasării solului.*

***Cuvinte cheie:*** *pneuri, maşini agricole, compactarea şi tasarea solului, rezistenta la penetrare, protecția solului*

## INTRODUCERE

Compactarea artificială a solului (antropică) se datorează traficului efectuat de agregate pe teren pentru efectuarea diferitelor lucrări agricole impuse de tehnologiile de mecanizare sau de efectuarea unor lucrări de transport a produselor tehnologice sau agricole. [5,6,7]

În România, majoritatea solurilor sunt compactate, cu textură mijlocie şi grea (conținutul de argilă variază între 30-50%), drenaj prost şi adesea cu un strat de sol impermeabil. [9].

Compactarea solului afectează dinamica apei în sol, eroziunea, ciclul azotului şi carbonului în sol, necesarul de energie şi eficacitatea lucrărilor agricole, spălarea pesticidelor, biologia solului, precum şi tehnologiile de cultivare a plantelor.

Compactarea solului, cauzată de traficul agricol, are ca efect deteriorarea structurii solului în straturile de suprafață şi în adâncime, modificarea distribuției porilor după mărime, continuitatea porilor şi deci a permeabilității pentru apă şi aer. Acestea pot avea efecte negative asupra activității biologice din sol, asupra echilibrului fizico-chimic şi asupra producției.

Efectul direct al tasării solului asupra porozității totale se manifestă prin reducerea capacității acestuia de a reține în mod durabil apa şi aerul.

Compactarea şi tasarea solului conduc la formarea unor benzi mai adânci şi compacte, sporind astfel riscul producerii eroziunii de suprafață, al băltirii apei, al proastei utilizări a nutrienților de către plante şi a levigării lor în adâncime.

Intensitatea şi extinderea procesului de compactare artificială depinde de o multitudine de factori având caracter general, dar şi specific local, precum: clima, caracteristicile tehnice ale echipamentelor agricole şi modalitățile de implementare în practică a diferitelor

agricultural technological systems, intrinsic features of each type of soil. [8].

Load size on running systems of farming equipment during its movement or staying on soil surface represents a very important factor especially for avoiding the deep artificial compaction of soil.

Therefore, in order to avoid the appearance and development of artificial compaction, in most countries it is recommended to limit the mass on axle to 4000...6000 kg, the wheels on axle should be increased (utilization of additional axles), and working pressure in the processed agricultural field should be limited to approx.50...60 kPa and about 80 kPa in case of running system with twinned wheels [1].

Researches have been made related to wheel-soil interaction, aiming at a rational use of tyres as a general rule and especially in terms of farming equipment when running conditions are totally different from running in highroads, researches to which generally refer the studies, their majority addressing to motor cars and tractors [1, 2, 3, 4].

Experimental researches performed with a mobile stand were designed to wheel- (tyre)-soil relation in case of tyres used with farming trailers and technical equipment, where are used especially carrying tyres instead of driving tyres, starting from tests and researches made up to now on tractors tyres [1].

## MATERIAL AND METHOD

In order to study the tyre soil interaction of different types of tyres designed to agricultural machines, the *Stand for tyres testing, STP*, figure 1 was achieved as a main technical mobile equipment of uniaxial type, designed to perform different typo-dimensional tests, at different air pressure and in different types of lands; the result was to draw up a practical guide designed to be used by all the interested persons for a rational and optimum use of tyres on agricultural equipment.

componente ale sistemelor tehnologice agricole; însuşirile intrinseci specifice fiecărui tip de sol. [8].

Mărimea sarcinilor pe sistemele de rulare ale echipamentelor agricole în timpul deplasării sau staționării pe suprafața solului reprezintă un factor deosebit de importantă, îndeosebi pentru evitarea inducerii compactării artificiale a solului în adâncime.

Din acest motiv pentru evitarea apariției şi dezvoltării compactării artificiale, în majoritatea țărilor se recomandă limitarea masei pe osie la 4000...6000 kg, se încurajează creşterea numărului de roți pe osie sau a numărului de osii (utilizarea osiilor auxiliare), iar presiunea în pneuri, în timpul lucrului pe terenul agricol prelucrat, se limitează la cca.50...60 kPa şi la cca.80 kPa în cazul sistemului de rulare cu roți jumelate [1].

In domeniul abordat au fost realizate cercetări referitoare la interacțiunea roată –sol urmărind utilizarea rațională a pneurilor în general, şi pe mijloacele din agricultură în special, unde condițiile de rulare sunt cu totul diferite față de rularea pe drumurile amenajate, la care în general se referă studiile elaborate, majoritatea acestora adresându-se automobilelor şi tractoarelor [1, 2, 3, 4].

Cercetările experimentale, efectuate cu un stand mobil, au vizat relația roată (pneu) – sol în cazul pneurilor utilizate pe remorci şi pe echipamentele tehnice utilizate în agricultură, unde sunt utilizate cu precădere pneuri portante şi mai puțin motoare, plecând de la experiențele şi cercetările efectuate până în prezent pe pneurile de tractoare [1].

## MATERIAL ŞI METODĂ

Pentru studierea interacțiunii pneu-sol a diverselor tipuri de pneuri destinate maşinilor agricole, s-a realizat *Standul pentru testare pneuri, STP*, figura 1, sub forma unui echipament tehnic de bază mobil, de tip monoax şi destinat efectuării testărilor pentru mai multe tipodimensiuni de pneuri, la diferite presiuni ale aerului în pneu şi pe diverse tipuri de teren în vederea elaborării unui îndrumar practic, care să fie utilizat de către toți factorii interesați, în scopul final al utilizării raționale şi optime a pneurilor pe utilajele agricole.


**Fig. 1 – Stand for tyre testing**, STP, equipped with tyres for testing
*1. shutter; 2. assembled chassis; 3. body shell; 4. drivetrain; 5. tyre to be tested*

Tests were performed with testing stand trailed by tractor NH TD 80D New Holland, of 50HP.

Body was loaded with approx.5000kg loading material, after which the aggregate Stand of testing + tractor NH TD 80D, moved forward in the testing land: asphalt, earth road, stubble field, processed field for establishing agricultural crops.

Testările s-au efectuat cu standul de testare tractat de tractorul NH TD 80D New Holland, cu o putere de 50CP.

Bena standului s-a încărcat cu cca.5000kg material de lestare (balast), după care agregatul Stand de testare + tractorul NH TD 80D, s-a deplasat pe loturile de testare: asfalt, drum de pământ, mirişte, teren prelucrat pentru înființarea culturilor agricole.

Testing stand was alternatively equipped, for testing with 5(five) types of tyres, organized in such way that conclusions should be drawn comparatively in two variants, according to table 1.

Testing load measured on tyre has maintained steady and was of 2.63 tons.

There were made tests for five types of tyres at three air pressures, respectively: 3, 5; 3; 2.5 bar. A few aspects during the tests are shown in figure 2.

**Apparata used**

For performing the measurements during the experiments, the following specialized equipment was used:

-Tensiometric bar, 0-60 kN, with two channels for traction and compression;

-System of data acquisition;

- Laptop ;

- Romanian lever scale;

- TEKSCAN system with net and amplifying system of MG6 Plus, HBM type;

- Gauge tape 0-5 m, Series no. QK5529;

- Manometer, Series no. 3295;

- Penetrometer SOIL COMPACTION METER SC 900 – SPECTRUM;

- Penetrometer Penetrologger with GPS, Eijkelkamp, Series no. 29266403 with humidity sensor for soil Theta Probe, type ML2x; Delta-T Company, England.

Standul de testare a fost echipat alternativ, pentru testări, cu 5(cinci) tipuri de pneuri, organizate astfel încât concluziile să fie formulate comparativ, în două variante, conform tabel 1.

Sarcina de testare pe pneu măsurată, s-a menținut constantă si a fost de 2,63 tone.

S-au realizat experimentări pentru cinci tipuri de pneuri: la trei presiuni ale aerului din pneu, respectiv: 3, 5; 3; 2,5 bar. Câteva aspecte din timpul experimentărilor sunt prezentate în figura 2.

**Aparatura utilizată**

Pentru efectuarea măsurătorilor în timpul experimentelor s-au utilizat următoarele echipamente specializate:

-Bară tensiometrică, 0-60 kN, cu două canale pentru tracțiune şi compresiune;

-Sistem achiziție date;

- Laptop ;

- Basculă ROMÂNĂ;

- Sistem TEKSCAN cu plasă şi sistem de amplificare de tip MG6 Plus, HBM;

- Ruletă de măsură 0-5 m, Seria nr. QK5529;

- Manometru, Seria nr. 3295;

- Penetrometru SOIL COMPACTION METER SC 900 – SPECTRUM;

- Penetrometru Penetrologger cu GPS, Eijkelkamp, Seria nr. 29266403 cu senzor umiditate pentru sol Theta Probe, tip ML2x; Firma Delta-T Anglia.

**Table 1**

**Variants of tyres tested**

| Den.No. | Variant I | | |
|---|---|---|---|
| | Approximately equal diameters and different widths | | |
| | **Tyre Code** | **Diameter** (D) | **Width** (section B) |
| 1. | Tyre 11.5-15.3 | 845 mm | 290 mm |
| 2. | Tyre 400-15.5 | 874 mm | 404 mm |
| 3. | Tyre 19.0/45-17 | 866 mm | 491 mm |
| **Den.No.** | **Variant II** | | |
| | **Approximately equal width and different diameters** | | |
| | **Tyre Code** | **Diameter** (D) | **Width** (section B) |
| 1. | Tyre 14.9 R24 | 1237 mm | 392 mm |
| 2. | Tyre 16.0/70-20 | 1078 mm | 405 mm |
| 3. | Tyre 400-15.5 | 874 mm | 404 mm |

**Fig. 1** – Aspects during the tests (contact spot, resistance to running, settlement)

**RESULTS**

During the tests, a series of parameters that influence both tyres state and their action on soil, were determined. They were: pressure in tyre, running and static range, contact spot, resistance to running, humidity and penetration resistance and also the parameters allowing to estimate the mark left in soil by loaded tyres.

In this paper, we have referred to determinations of traction force (resistance to running) and penetration resistance, which clearly inform about the energy

**REZULTATE**

In timpul experimentărilor s-au determinat o serie de parametri care influențează atât starea pneurilor cât şi acțiunea acestora asupra solului, precum: presiunea în pneu, razele de rulare şi statice, pata de contact, rezistența la rulare, umiditatea şi rezistența la penetrare precum şi parametri care permit aprecieri asupra urmei lăsate pe sol după trecerea pneurilor sub sarcină.

În lucrarea de față s-au făcut referiri asupra determinărilor forței de tracțiune(rezistență la rulare) şi rezistenței la penetrare care dau indicii clare asupra consumului energetic şi a gradului de tasare şi a compactării.

consumption and compression and compaction level.

Values of traction force determined are shown in table 2, and those of penetration resitance in table 3.

Variations of the two parameters, for tested tyres, at different pressures of air in tyre and in different types of land, were presented as diagrams. A few representative examples are shown in diagrams from figures 3, 4.

Valorile forței de tracțiune determinate sunt prezentate în tabelul 2, iar ale rezistenței la penetrare în tabelul 3.

Variațiile celor doi parametri, pentru pneurile testate, la diferite presiuni ale aerului în pneu şi pe diferite tipuri de suprafețe, atât individual cât si comparativ pentru cele două variante testate, au fost prezentate sub forma unor diagrame. Câteva exemple reprezentative sunt prezentate în diagramele din figurile3, 4.

**Table 2**

**The values of the traction force (rolling resistance)**

| Type of tyre [code] | Pressure Bar | | | | | | | | | | | |
|---|---|---|---|---|---|---|---|---|---|---|---|---|
| | 2.5 | 3 | 3.5 | 2.5 | 3 | 3.5 | 2.5 | 3 | 3.5 | 2.5 | 3 | 3.5 |
| | Type of land | | | | | | | | | | | |
| | Asphalt road | | | Earth road | | | Stubble | | | Processed land | | |
| | Traction force | | | | | | | | | | | |
| **11,5-15,3** | 1.453 | 1.052 | 0.499 | 2.108 | 1.438 | 0.7975 | 5.261 | 4.379 | 3.446 | 10.285 | 9.110 | 8.389 |
| **400 -15,5** | 2.404 | 1.54 | 0.788 | 4.088 | 3.463 | 2.012 | 7.832 | 6.816 | 5.905 | 11.620 | 10.252 | 9.672 |
| **19.0 / 45-17** | 2.505 | 1.72 | 0.828 | 4.283 | 3.803 | 2.215 | 8.105 | 6.902 | 6.218 | 11.822 | 10.462 | 9.908 |
| **16.0 / 70-20** | 1.312 | 0.8174 | 0.625 | 5.042 | 2.302 | 1.858 | 6.788 | 4.783 | 4.503 | 9.783 | 8.886 | 8.015 |
| **14.9 R 24** | 1.211 | 0.791 | 0.583 | 4.721 | 2.089 | 1.708 | 6.223 | 4.598 | 4.102 | 9.325 | 8.325 | 7.912 |

**Table 3**

**The penetration resistance for processed land for tyre 19.0/45 R17**

| Penetration resistance before crossing of the tyres | | | | After crossing | | | | | | | | |
|---|---|---|---|---|---|---|---|---|---|---|---|---|
| | | | | Tyre 19/45 17 | | | | | | | | |
| | | | | Pressure in tyre 2,5 bar | | | Pressure in tyre 3 bar | | | Pressure in tyre 3,5 bar | | |
| **Depth (cm)** | **Point 1** | **Point 2** | **Point 3** | **Point 1** | **Point 2** | **Point 3** | **Point 1** | **Point 2** | **Point 3** | **Point 1** | **Point 2** | **Point 3** |
| **0** | 0.35 | 0.27 | 0.39 | 0.35 | 0.24 | 0.28 | 0.46 | 0.42 | 0.43 | 0.58 | 0.61 | 0.58 |
| **1** | 0.35 | 0.27 | 0.42 | 0.35 | 0.64 | 0.89 | 0.52 | 0.73 | 0.9 | 0.69 | 0.82 | 0.91 |
| **3** | 0.47 | 0.36 | 0.52 | 0.63 | 0.98 | 1.19 | 0.74 | 1.03 | 1.11 | 0.85 | 1.09 | 1.04 |
| **5** | 0.72 | 0.46 | 0.56 | 0.66 | 1.04 | 1.01 | 0.86 | 1.06 | 0.99 | 0.97 | 1.09 | 0.98 |
| **7** | 0.79 | 0.51 | 0.79 | 0.81 | 0.92 | 1.04 | 0.9 | 1.02 | 1 | 0.89 | 1.12 | 0.96 |
| **9** | 0.9 | 0.52 | 0.97 | 0.94 | 0.98 | 1.17 | 0.95 | 1.1 | 1.09 | 0.89 | 1.22 | 1.02 |
| **11** | 0.98 | 0.7 | 1.03 | 1.08 | 1.15 | 1.28 | 0.95 | 1.3 | 1.19 | 1.09 | 1.45 | 1.1 |
| **13** | 1.11 | 1.12 | 1.11 | 1.25 | 1.36 | 1.34 | 1.2 | 1.44 | 1.38 | 1.09 | 1.53 | 1.42 |
| **15** | 1.12 | 1.38 | 1.11 | 1.39 | 1.41 | 1.37 | 1.1 | 1.47 | 1.48 | 1.12 | 1.53 | 1.6 |
| **17** | 1.2 | 1.76 | 1.15 | 1.45 | 1.47 | 1.65 | 1.12 | 1.61 | 1.66 | 1.22 | 1.76 | 1.67 |
| **19** | 1.16 | 1.94 | 1.42 | 1.56 | 2.02 | 1.85 | 1.4 | | | 1.25 | | |
| **21** | 1.3 | 2.44 | 1.78 | 1.94 | 2.31 | 2.03 | 1.68 | | | 1.43 | | |

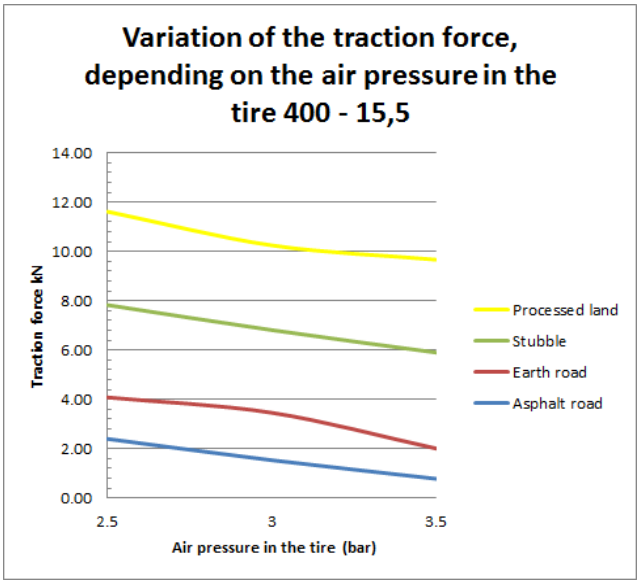


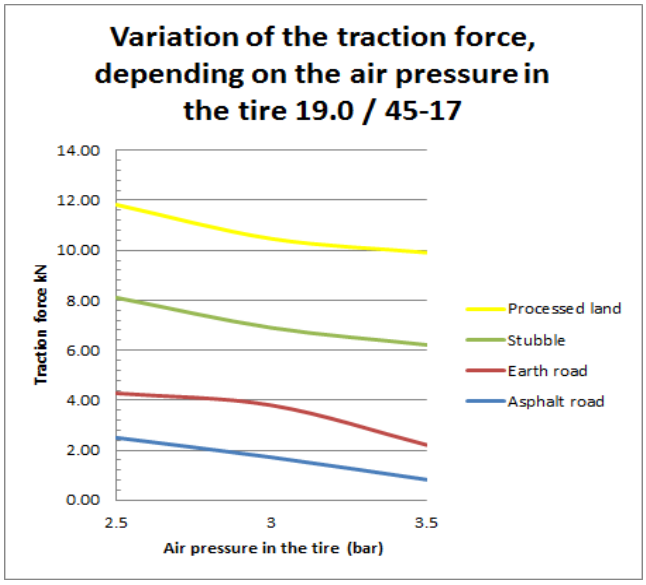

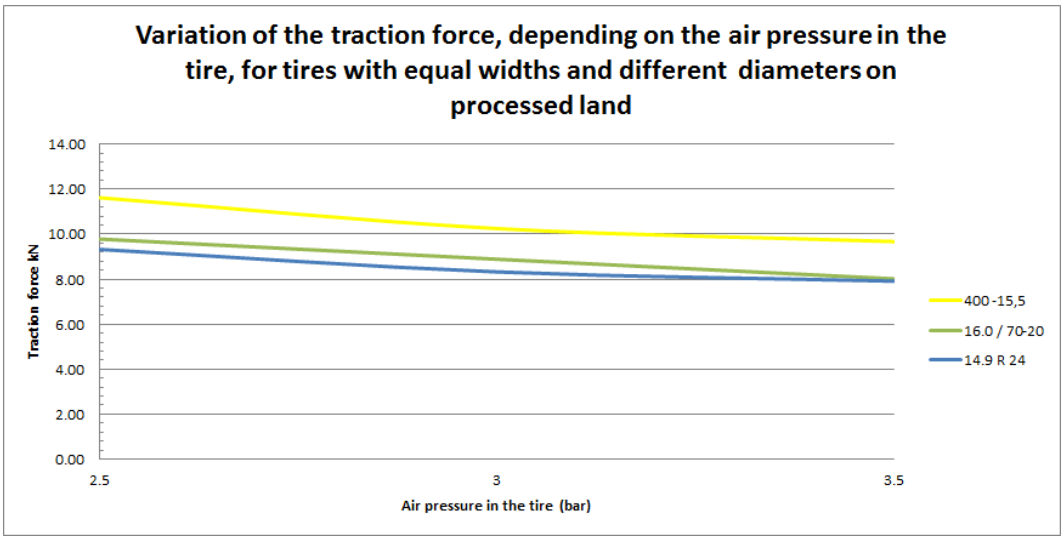


**Fig.3** – A few diagrams of traction force variation

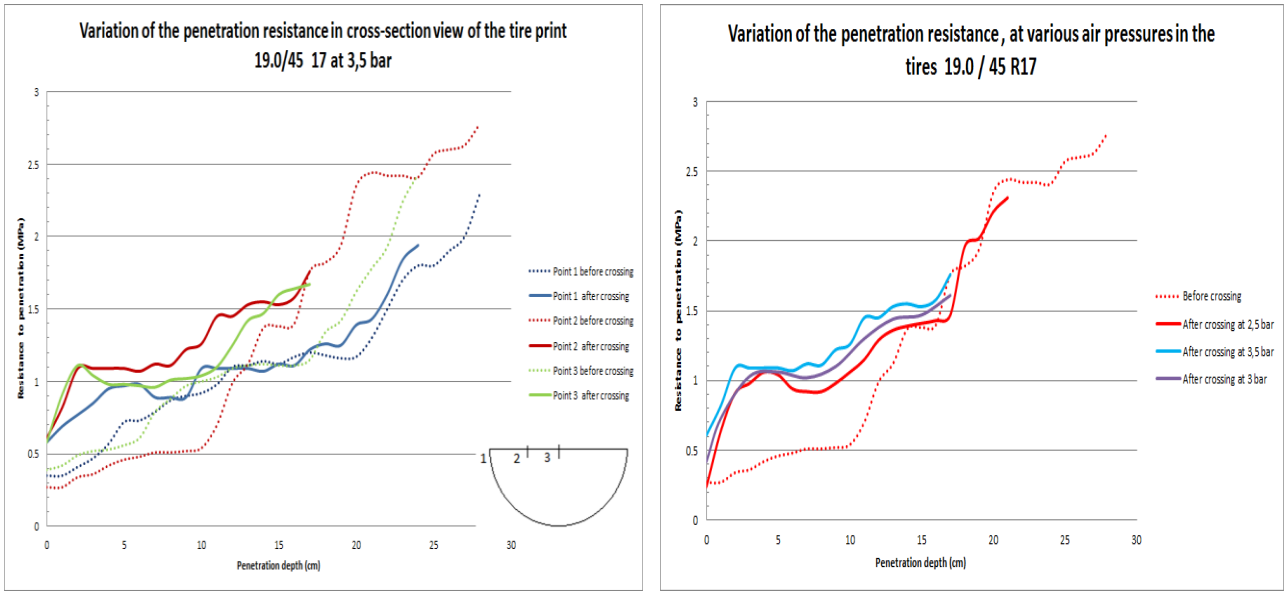


**Fig.4** – Variation of resistance to penetration of tyre 19.0/45-17

**CONCLUSIONS**

- tyre resistance to running has increased along with air pressure decrease, fig. 3;
- for tyre having the same width, resistance to running is higher at smaller diameter tyres, fig. 3;
- running resistance increases when the equipment runs in uneven field, fig. 3;
- in the cross section of the tyre track in soil, the compaction degree has increased from the exterior to interior of the track, fig. 4.
- soil compaction after tyre displacement increases along with air pressure from tyre growth, fig.4.

**REFERENCES**

[1]. Biriş S. Şt., Vladut V., Ungureanu N., Matache M., Voicea I., (2012) – *Researches on the Development of an Equation for the Contact Area Calculus for Agricultural Tires,* 40 Symposium „Actual Tasks on Agricultural Engineering", Opatja, Croatia;
[2]. Biriş S. Şt., Vladut V., Bungescu S. T., (2006) - *About the contact surface between the tire and the ground,* Scientific papers INMATEH - vol. 17, Nr. 2/2006*,pg. 113-118,* ISSN 1583 –1019.
[3]. Cardei P., Muraru V., Sfaru R., (2007) – *Interaction between vehicle wheel and soil – Estimation of soil compaction* – Scientific papers INMATEH no. 22, Vol.IV;
[4]. Dinu. L., (2010) - *Researches regarding the manufacturing of systems of pressure adjustment in tractor tyres according to field features and movement conditions,* Ph.D. thesis, UNIVERSITY *TRANSILVANIA* BRASOV, Romania;
[5]. Ionescu R., Nastasoiu S. (2007) - *Considerations Related to the Main Factors that Influence the Tractive Efficiency of Wheeled Tractors,* Scientific papers INMATEH, Vol. 21. Nr. 3/2007, pp.237-252 ISSN 1583 – 1019;
[6]. Nedelcu A., Popa L., Ciuperca R., Cojocaru I., Canpeanu A., (2006) - *Researches for the development and the means modernization of transport from agriculture and the valorification of the results*, Scientific papers, INMATEH, vol.17, Nr. 2/2006, pp.27 - 32 ISSN 1583 – 1019;
[7]. Ormenisan A. N., (2006) - *Considerations Regarding the Influence of The Driving Wheel Dimensions to the Dynamics and Energetics of the Agricultural Tractors*, Scientific papers INMATEH vol. 18, Nr. 3/2006, pp. 223 – 230, ISSN 1583 – 1019.
[8]. Popescu S., Ene T. A., Constantinescu A., (2006) - *Theoretical and experimental researches regarding the influence of tyre parameters on soil settlement and compaction*, Scientific papers INMATEH - vol.17, No. 2/2006*,* pp. 133…140*,* ISSN 1583 –1019;
[9]. Robescu V.O., Elekes C., (2008 ) - *Soil damaging as result of compaction process, a severe problem in Romania agriculture*, Scientific Papers – vol. 51(2), series Agronomy, pp. 176…182, USAMV Iasi;
[10]. Ungureanu N., Vlăduț V., Voicu Gh., Biriş S. Şt., Dincă M., Ionescu M., Cujbescu D., Persu C., Lazar G., (2015) - E*valuation of the degree of soil compaction by penetrometer tests* , ISB-INMATEH 2015, ISSN 2344 – 4118, pp. 569 – 574.

**CONCLUZII**

- rezistenta la rulare a pneului creste odată cu scăderea presiunii aerului din pneu, fig. 3;
- la pneuri cu aceeaşi lăţime, rezistenta la rulare este mai mare la pneurile cu diametru mai mic, fig. 3;
- rezistenta la rulare creste la deplasarea pe terenuri deformabile, fig. 3;
- in secţiunea transversala a urmei lăsate pe sol după trecerea pneului, gradul de compactare creste de la exteriorul spre interiorul urmei, fig. 4.
- compactarea solului in urma deplasării pneului creşte odată cu creşterea presiunii aerului din pneu, fig.4.

**BIBLIOGRAFIE**

[1]. Biriş S. Şt., Vladut V., Ungureanu N., Matache M., Voicea I., (2012) – *Cercetări privind dezvoltarea unei ecuaţii pentru calcularea zonei de contact a pneurilor agricole,* Al 40-lea Simpozion „Sarcinile actuale in ingineria agricola", Opatija, Crotia, pag.181-193;
[2]. Biriş S. Şt., Vladut V., Bungescu S.T., (2006) - *Despre suprafata de contact dintre pneu si sol,* Lucrări ştiinţifice INMATEH, vol.17, Nr. 2/2006*,* pag. 113-118*,* ISSN 1583 –1019;
[3]. Cardei P., Muraru V., Sfaru R., (2007) – *Interacţiunea dintre roata vehiculului si sol – Estimarea compactării solului* – Lucrări ştiinţifice INMATEH nr. 22, Vol.IV;
[4]. Dinu L. , (2010) - *Cercetări privind realizarea unor sisteme de reglare a presiunii în pneurile tractoarelor în concordanţă cu proprietăţile terenului şi condiţiile de deplasare*, Teza doctorat, UNIVERSITATEA *TRANSILVANIA* Brasov, Romania;
[5]. Ionescu R., Nastasoiu S., (2007) - *Consideraţii privind factorii principali care influenteza randamentul de tractiune al tractoarelor pe roti*, Lucrări ştiinţifice INMATEH, Vol. 21. Nr. 3/2007, pag. 237-252, ISSN 1583 – 1019
[6]. Nedelcu A., Popa L., Ciuperca R., Cojocaru I., Canpeanu A., (2006) - *Cercetari pentru dezvoltarea si modernizarea mijloacelor de transport din agricultura si valorificarea rezultatelor*, Lucrări ştiinţifice, INMATEH, vol. 17, Nr. 2/2006, pag. 27 - 32 ISSN 1583 – 1019;
[7]. Ormenisan A. N. (2006) - *Consideraţii privind influenta dimensiunilor rotilor de directie asupra dinamicii si energeticii tractoarelor agricole*, Lucrări ştiinţifice INMATEH vol.18, Nr. 3/2006, pag. 223 – 230, ISSN 1583 – 1019;
[8]. Popescu S., Ene T. A., - Constantinescu A. (2006), - *Cercetări teoretice si experimentale privind influenta parametrilor pneurilor maşinilor asupra proceselor de tasare si compactare a solului*, Lucrări ştiinţifice, INMATEH - vol.17, Nr. 2/2006*,* pag.133-140*,* ISSN 1583 –1019;
[9]. Robescu V.O., Elekes C., (2008) - *Degradarea solului efect al procesului de compactare. Problemă gravă în România*, Lucrări Ştiinţifice – vol. 51(2), Seria Agronomie, pag.176…182, USAMV Iasi;
[10]. Ungureanu N., Vlăduț V., Voicu Gh., Biriş S. Şt., Dincă M., Ionescu M., Cujbescu D., Persu C., Lazar G., (2015) - *Evaluarea gradului de compactare a solului prin teste de penetrometrie* , ISB-INMATEH 2015, ISSN 2344 – 4118, pag. 569 – 574.

# ANALYSIS OF THE UNSTEADY FLOW OF CENTRIFUGAL AGRICULTURAL AUTO WATER PUMPS WITH VARIABLE CURVATURES
# /
# 变曲率离心式农用汽车水泵的非定常流动分析

**Lect. Ph.D. Xue Dangqin [1], Lect. Ph.D. Ma Shibang [2*], Lect. Ph.D. Eng. Shi Huojie [3,4], Prof. Ph.D.Hou Shulin [4]**
[1] School of Mechanical ＆Automotive Engineering, Nanyang Institute of Technology, Henan / China; [2] Nangyang Normal University, Henan / China; [3]Department of Biological Systems Engineering, Washington State University, Pullman/USA; [4] College of Engineering ,China Agricultural University, Beijing / China;
*Tel: +8613782173858; Email: xqd5599@163.com*

***Abstract:*** *Existing research on agricultural auto water pumps mainly concentrate on structure optimization; nonetheless, a few works examine the characteristics of the inner flow field. The current study conducted an unsteady numerical simulation calculation of agricultural auto water pumps using an impeller model with a 0.5 mm blade tip clearance (σ) and ANSYS CFX software. The unsteady flow results were analyzed, and results indicated that the unsteady characteristics of the lift undergo significant periodic changes due to the dynamic and static interference of the cut water and the impeller. This change in frequency is in accordance with the passing frequency of the blade. The pressure fluctuation varies at different monitoring points on the same volute section. The pressure fluctuation decreases first and then increases from the bottom volute to the back volute. Additional dither components were also detected at the monitoring points on the bottom volute. The pressure fluctuation is maximized at the circumferential monitoring points proximal to the water cut. The distance between the circumferential monitoring points and the water cut increases with the circumference angle, whereas the fluctuation amplitude decreases. The results of fluid dynamics provide useful references to determine the reduction in the vibration and noise of agricultural auto water pumps.*

***Keywords:*** *Agricultural auto water pumps; Pressure fluctuation; Unsteady flow; Variable-curvature*

## INTRODUCTION

The market demand for agricultural automobiles has increased with social development. The agricultural auto water pump is a centrifugal pump that transmits medium energy based on a steady pressure difference generated under a certain flow rate. Nonetheless, unsteady flow occurs in different working conditions because of the high rotation speed of the water pump and the unsteady geometric boundaries of the rotating impeller. Furthermore, the inner fluid forms a boundary layer on the solid wall surface, which in turn causes interior backflow and interference from dynamic and static components, as well as leaking and wake flows at the blade tip. Moreover, the formation of the boundary layer results in the fluctuation of flow field pressure and the generation of an alternating acting force. In the process, resonance or fatigue damages are incurred [5,6]. For the effective operation of an agricultural auto water pump, strict requirements are proposed for its stability, although these requirements do not include the lift design requirements.

3-D unsteady numerical simulation technology is widely used because of the rapid development of computational fluid dynamics and computer technology.

***摘要:*** *目前对于农用汽车水泵的研究主要集中在结构优化上，而其内部流场特性研究较少。本文选择叶顶间隙 σ 为 0.5mm 的叶轮模型，采用 Ansys-CFX 软件对农用汽车水泵进行非定常数值模拟计算，分别研究在 Q/Qd=0.7、1 及 1.3 三种工况下的非定常压力脉动特性，并对非定常流动进行了结果分析。结果表明：由于隔舌与叶轮的动静干涉作用，扬程的非定常特性呈现明显的周期性变化，且频率和叶片通过频率一致。处于同一蜗壳断面不同位置的监测点的压力脉动幅度不同，从蜗壳底部向蜗壳背面先减小后增大，且位于蜗壳底部监测点的高频脉动成分较多。沿蜗壳周向，隔舌附近监测点压力脉动幅度最大，随着圆周角的增加，各监测点沿周向与隔舌距离变大，脉动幅值逐渐减小。从流体动力学方面对分析农用汽车水泵如何降低振动及噪声提供了有益的结果。*

***关键词:*** *变曲率; 农用汽车水泵; 压力脉动; 非定常流动*

## 引言

随着社会的发展，农用汽车市场需求旺盛。农用汽车水泵作为一种离心泵通过某一流量下产生一个稳定的压力差达到输送介质能量的目的，但由于水泵转速高，旋转叶轮的几何边界是非定常的，在任何工况下运行都存在非定常流动，且内部流体在固体壁面上会形成边界层，会导致内部回流、动静部件干涉、叶尖泄漏流动、尾流，重要的是还会引起流场压力脉动并产生交变的作用力，导致产生共振或疲劳破坏[5,6]。因而为了保持农用汽车水泵的良好运行，除了满足扬程等设计要求外，对其稳定性的要求也越来越高。

随着计算流体力学 CFD(Computational Fluid Dynamics)和计算机技术的快速发展，三维非定常数值模拟技术已广泛应用，国内外学者已经对水泵进行了试验研

Both Chinese and foreign scholars conducted research on water pumps by combining test analysis and numerical simulation calculation [4,7,12]. For example, References [2, 10, 14] described the interaction between the impeller diffuser in a pump and pump performance; these works determined that the unsteady flow at the impeller exit is the main cause of pressure fluctuation. APRE et al. of Switzerland [3] studied inner flow in a draft tube of a mixed-flow water turbine model through a steady-state analysis of six different flow points under controlled working conditions. These researchers also analyzed fluctuation amplitude and frequency characteristics in a conical draft tube as well as vortex strip frequency and pressure fluctuation at small flow points under no-steam turbid. Reference [1] conducted high-frequency pressure sensor measurement proximal to the discharge flange of the centrifugal pump. The collected data were processed with fast Fourier transform, and the results indicate that the main signal frequency is the blade passing frequency of the centrifugal pump. This signal was used to measure the rotation speed of the pump. Reference [13] summarized the pressure fluctuation testing techniques used worldwide. The researcher tested the pressure fluctuation characteristics at the different impeller exit directions of the centrifugal pump and determined the relationship between unsteady fluid flow and pressure fluctuation at the impeller exit. The results indicated that the main causes of pressure fluctuation are the fluctuation in blade frequency induced at the efflux–wake and the shaft frequency fluctuation caused by asymmetric flow in the impeller passage. The pressure fluctuation caused by the structure declines with the widening of the distance between the impeller and the volute section. Moreover, a 100–145 Hz broadband frequency between four times the shaft and the blade frequencies was discovered in the spectrum of pressure fluctuation frequency at the blade exit. Charler [8] employed large-eddy simulation to calculate the pressure fluctuations in the volute, runner, and draft tube of a mixed-flow water turbine. By contrast, a few models employed a running simulation approach that cannot set real boundary conditions at the entrance of the draft tube. Although the average inflow conditions can be selected, the calculated flow state of the draft tube remains unsteady. The pressure fluctuation test in a draft tube mainly focuses on pressure fluctuation amplitude and frequency characteristics. Internal situations are impossible to observe; therefore, pressure fluctuation amplitude must be computed and the causes of pressure fluctuation analyzed.

The current study used the RNG k-ε turbulence model and conducted an unsteady numerical simulation of the full flow path for a quadratic, variable-curvature, half-open, and centrifugal agricultural auto water pump. The unsteady pressure fluctuation characteristics in such a path were analyzed when $Q/Q_d$ = 0.7, 1.0, and 1.3. The results have strong practical significance for determining how pressure fluctuation characteristics of rotating fluid machinery are pre-estimated and how the vibration and noise of water pumps are reduced.

## MATERIAL AND METHOD

### *Unsteady numerical calculation program*

The steady calculation utilizes the standard k-ε turbulence model; by contrast, the unsteady calculation employs the RNG k-ε turbulence model because this model can handle the high strain rate and substantial flow of a significantly bending flow line while maintaining high calculation efficiency. The RNG k-ε turbulence

研究和数值模拟相结合的测试分析和数值计算研究[4,7,12]。例如：国外文献[2][10][14]研究了泵内叶轮扩散段与泵性能之间的相互影响，发现叶轮出口处的不稳定流动是造成压力脉动的主要原因。文献[3]瑞士的 APRE 等通过试验在设计工况下 6 个不同流量点进行稳态分析，对混流式水轮机模型尾水管内部流动进行了研究，分析尾水管锥管内脉动幅频特性及无汽浊情况小流量点的涡带频率和压力脉动。文献[1]对离心泵出口法兰附近进行了高频压力传感器测量，采集的数据进行了 FFT 变换，结果信号主频为离心泵叶片通过的频率，应用该信号对泵的转速进行了数据测量。文献[13]总结了国内外的压力脉动测试技术，采用试验的方法对离心泵叶轮出口各方向进行了压力脉动特性试验，获得了流体不稳定流动和叶轮出口压力脉动的关系，研究结果表明压力脉动主要成分是射流－尾迹处诱导的叶频脉动及叶轮流道内流动的不对称性诱导的轴频脉动，结构引起的压力脉动幅值随叶轮和蜗壳劈面间距的增大而逐步减弱并在叶轮出口处的压力脉动频谱中发现介于 4 倍轴频到叶频之间的 100HZ~145HZ 的宽带频率。文献[8]CHARLER 应用大涡模拟方法对混流式水轮机蜗壳、转轮和尾水管分别进行了计算，但部分模型是转轮模拟，无法在尾水管入口选择真实的边界条件。虽然选择平均入流条件，尾水管的计算流态仍很不稳定，对于尾水管压力脉动试验主要是压力脉动幅频特性，无法观测其内部，所以计算压力脉动幅值及产生压力脉动相关原因分要是十分必要的。

本文基于三维 N-S 方程，采用 RNG k-ε 湍流模型，以二次变曲率半开离心式农用汽车水泵全流道为研究对象进行非定常数值模拟，分析了在 Q/Qd=0.7、1 及 1.3 三种工况下的全流道非定常压力脉动特性。结果对于研究如何预估旋转类流体机械的压力脉动特性，对减小泵体的振动，降低水泵噪声是具有重大的现实意义。

## 材料与方法

### *非定常数值计算方案*

在定常计算中，采用的是湍流模型 Standard k-ε 模型，在非定常计算中考虑到 RNG k-ε 湍流模型可以很好地处理高应变率及流线弯曲程度较大的流动，又能够保证较高的

model was proposed by Yakhot et al. [11] in 1986 and was deduced from the mathematical method of a renormalization group. This model improves on the standard k-ε model to some extent [9]. Given an incompressible and steady flow, the RNG k-ε turbulence model is expressed as:

计算效率，选用 RNG k-ε 湍流模型。该模型是 1986 年 Yakhot 等[11]提出，它是由重化群的数学方法推导出来，针对标准 k-ε 模型做了一些改进[9]。对于不可压缩、定常流动的情况，RNG k-ε 湍流模型的表达式如下：

$$\frac{\partial(\rho u_j k)}{\partial x_j}=\frac{\partial}{\partial x_j}(\alpha_k \mu_{ef} f \frac{\partial k}{\partial x_j})+G_k-\rho\varepsilon \quad (1)$$

$$\frac{\partial(\rho u_j \varepsilon)}{\partial x_j}=\frac{\partial}{\partial x_j}(\alpha_\varepsilon \mu_{eff} \frac{\partial \varepsilon}{\partial x_j})+\frac{\varepsilon}{k}(C_1 * G_k - C_2 \rho\varepsilon) \quad (2)$$

Through a comparison between the k-ε model and the RNG k-ε model, the latter modifies $C_2$ in the ε equation of the former:

对比 k-ε 模型和 RNG k-ε 模型可以发现，RNG k-ε 模型对 k-ε 模型中 ε 方程的 $C_2$ 项进行了修正，即：

$$C^*_2=C_2+\frac{C_\mu \rho \eta^3(1-\frac{\eta}{\eta_0})}{1+\beta\eta^3} \quad (3)$$

where： $\mu_{ef}=\mu+\mu_t$； $C_\mu=0.0845$； $\alpha_k=1.39$； $C_1=1.42$； $C_2=1.68$；

式中： $\mu_{ef}=\mu+\mu_t$； $C_\mu=0.0845$； $\alpha_k=1.39$； $C_1=1.42$； $C_2=1.68$；

$$C_1^*=C_1-\frac{\eta(1-\eta/\eta_0)}{1+\beta\eta^3} \quad \eta=(2E_{IJ}.Ei_j)^{1/2}\frac{k}{\varepsilon} \quad E_{ij}=\frac{1}{2}(\frac{\partial u_i}{\partial x_j}+\frac{\partial u_j}{\partial x_i}) \quad (4)$$

where： $\eta_0=4.377$,$\beta=0.012$.

$C_2$ is modified; thus, the coefficient of the eddy viscosity of the RNG k-ε model under a low-strain rate is higher than that of the standard k-ε model but lower under the high-strain rate. The RNG k-ε model considers high-strain rate and substantial curvature flow; this model can achieve significantly higher calculation accuracy than the standard k-ε model can for rotational flow and substantial curvature. The findings are particularly applicable to the calculation of the internal flow of an impeller blade (e.g., axial flow and centrifugal pumps). The RNG k-ε model can generate higher accuracy and reliability in a more extensive flow than the standard k-ε model can because of these characteristics. Thus, the present study adopts the RNG k-ε model.

The entrance, exit, and static wall surface were similar to those for steady calculation. The interface between the inner rotor and the pump stator was set as the transient rotor stator. The steady calculation result was employed as the initial flow field for unsteady calculation.

According to the requirement of the calculation model regarding Courant number.

其中，$\eta_0=4.377$，$\beta=0.012$。

由于对 $C_2$ 进行了修正，使得在低应变率区时 RNG k-ε 模型的湍流涡粘性系数高于标准 k-ε 模型，相反，在高应变率区其湍流涡粘性系数则低于标准 k-ε 模型。由于 RNG k-ε 模型对高应变率以及大曲率过流等因素的影响进行了考虑，所以该模型在运用于旋流和大曲率情况时，能够大大的提高计算精度。对于叶轮叶片(如轴流泵、离心泵等)的内流动计算，该模型尤其适用。上述特点使得在更广泛的流动中，RNG k-ε 模型比标准 k-ε 模型具有更高的精度和可信度。因此，本文采用 RNG k-ε 方程来求解。

进出口及静止壁面设置与定常计算相同，对于泵内转子部件和定子部件之间的交界面，设置为 Transient Rotor Stator，采用定常计算的结果作为非定常计算的初始流场。

由计算模型对库朗数的要求，即:

$$C_o=\frac{|\bar{v}|\Delta t}{l}<100 \quad (5)$$

where Δt is characteristic time; v and l are the characteristic speed and characteristic scale, which were determined based on the estimated mean speed and minimum grid size in this study. The maximum length of the optional time step of this model is 5 ms. Considering the resolution requirements of pressure fluctuation in the high-speed rotating machinery, the final time step length was determined to be 1/90 of the rotation period and the rotating time was set to 4°, that is, approximately 0.11111 ms. Six full periods were calculated under every working condition; the maximum iteration steps of every time step length were set to 10 because of the effective

式中 Δt 表示特征时间，v 和 l 分别表示特征速度和特征尺度，本文分别取估算的平均速度和网格最小尺寸。本模型可选用的时间步长最大值为 5ms，同时考虑到在高速旋转机械内压力脉动的分辨率要求，最终确定的时间步长为旋转周期时间的 1/90，及 4°的旋转时间，约为 0.11111ms。每个工况均计算 6 个整周期，考虑到在定常计算中收敛性较好每个时间步长最大迭代步数设为 10。

convergence in the steady calculation.

Fig. 1 shows the variable-curvature and half-open prototyping pump and the distribution of monitoring points. P1 is the entrance pressure of the pump; P2–P9 are at the first to eighth cross sections of the volute; P10 is close to the water cut of the volute and P11 is at the downstream of the volute; and P12 is the exit pressure of the pump. Considering the positions of the actual pressure-measuring points, all the pressure-measuring points are 2 mm away from the wall surface. Fig. 2 presents the distribution of the testing points and an image of the sensor installation. Fig. 3 provides a panoramic view of the field test system.

The pressure fluctuation coefficient is defined as:

变曲率半开式原型泵及监测点设置如图 1 所示，P1 为泵入口压力，P2 到 P9 位于蜗壳第一断面到第八断面，P10 和 P11 位于蜗壳隔舌附近及下游位置，P12 则是泵出口压力。考虑到实际测压点位置，测压点位置都距离壁面位置 2mm 位置。图 2 为试验测点布置及传感器安装实物图，图 3 为现场测试系统全景图。

定义压力脉动系数为:

$$p^* = p_i - \overline{p} \tag{6}$$

where $p_i$ is the simulated transient value of the absolute pressure and $\overline{p}$ is mean pressure in the sample time.

Time coefficient is defined as:

式中 $p_i$ 为模拟绝对压力瞬态值，$\overline{p}$ 为样本时间内的压力平均值。

定义时间系数为：

$$t^* = t_i / T \tag{7}$$

where: $t_i$ is the calculated transient time and $T$ is the rotation period of the impeller, which is 0.01 s in this study.

式中 $t_i$ 为计算瞬态时间；$T$ 为叶轮旋转周期，本文中为 0.01s。

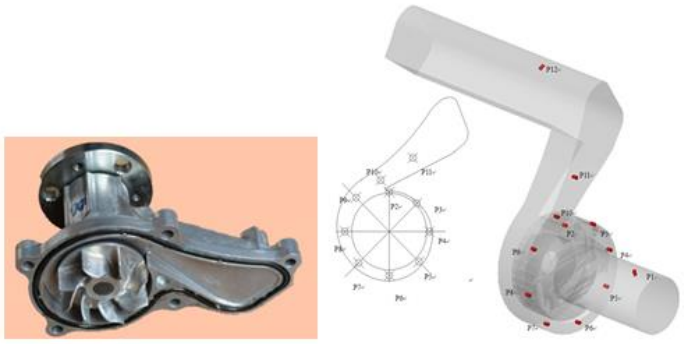

**Fig.1** - Variable-curvature and half-open prototype pump and the distribution of monitoring points for simulation analysis


**Fig.2** - Layout of test points and image of sensor installation

**Fig.3** - Panoramic view of the field test system

## RESULTS

### *Analysis of unsteady external characteristic*

Fig. 4 presents the unsteady characteristics of the lift in three periods under different working conditions. The blade positions corresponding to ABCD are marked, and the same blade is highlighted with a red frame. L1 is the start point of the period, and L2 is the end point. This figure 8 shows that:

The unsteady characteristics of a lift change periodically. This change frequency is consistent with the blade passing frequency, and this phenomenon is caused by the dynamic and static interference of the water cut and the impeller. A and B are blade phases indicating that the blade just passes through the water cut. At C and D, the blade is in the middle of the flow passage. Lift fluctuation increases gradually with flow rate. At the same time, the downward pressure fluctuation under a low flow rate exhibited the poorest law in a single period. When flow rate increases, the amplitude change within a single period stabilizes, thereby implying that a high flow rate is conducive to the stable pump operation.

## 结果

### *外特性非定常特性分析*

图 4 是各工况下在三个周期内扬程的非定常特性，其中标出 ABCD 对应的叶片位置。同一叶片采用红色线框加亮。L1 为周期的起点，L2 为周期的终点。从图中可以看出：

扬程的非定常特性呈现明显的周期性变化，且频率和叶片通过频率一致，这是由于隔舌与叶轮的动静干涉作用引起的。A、B 是叶片相位显示此时叶片恰好掠过隔舌位置，而 C、D 相位显示叶片位于流道中间位置。随着流量的增大，扬程的脉动幅值逐渐增大。同时可以发现，在小流量下的下压力脉动在单周期内的规律性最差，随着流量的增大单周期内的幅值变化逐渐平稳，表明泵的运行稳定性偏向大流量工况。

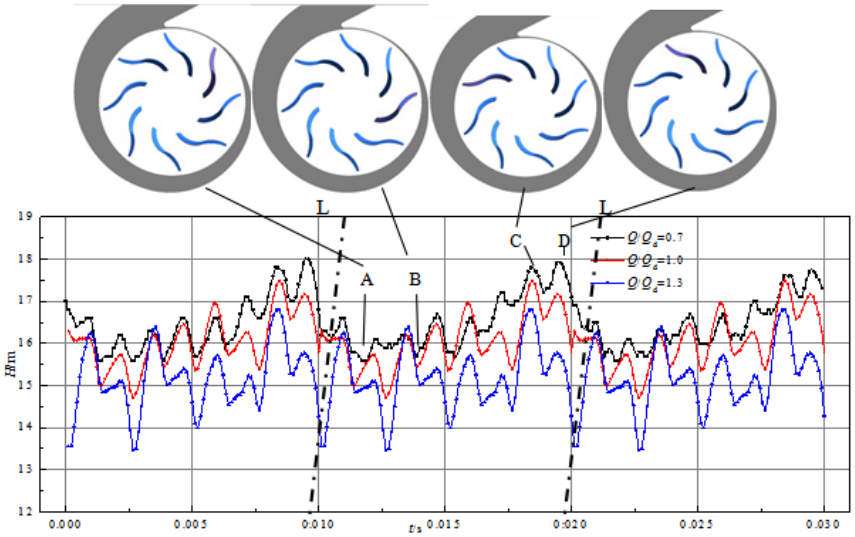


**Fig.4** - Unsteady characteristics of the lift

Fig. 5 illustrates the static pressure distribution in the middle blade section under the ABCD phases. The minimum and maximum pressures in the middle section fluctuate violently; moreover, the static pressure close to the water cut is relatively higher than that in other positions, as is the lift. A high-pressure gradient appears when the blade exit approaches the flow path of the water cut. When the blade moves to the middle of the flow path, the local high pressure area narrows but pressure increases and the entrance pressure decreases.

图 5 为叶片中间截面在相位 ABCD 下的静压分布，发现在中间截面上的压力的最值有很大的波动，且发现在隔舌附近静压值较高时，扬程出现较高值，当叶片出口边靠近隔舌时，在将要掠过隔舌的流道内出现很高的压力梯度，而当叶片运动到流道中间，局部高压区面积减小，但压力升高，而进口处压力出现降低。

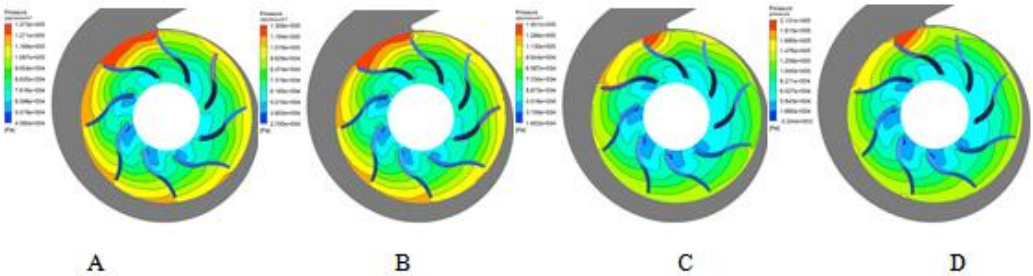


**Fig.5** - Static pressure at the middle impeller under the ABCD phases

***Entrance and exit pressure fluctuations***

Fig. 6 presents the time–domain map of pressure fluctuation at the impeller entrance under different working conditions. According to the variation of the pressure fluctuation coefficient, entrance pressure fluctuation does not vary regularly. The minimum pressure fluctuation is achieved under 1.3 Qd, and eight wave peaks occur in a single period. The maximum pressure fluctuation is observed under 1.0 Qd, and a weak correlation exists between pressure fluctuation within a single period and blade frequency. This correlation implies that the optimum working conditions of the pump are skewed to a high flow rate.

***进出口压力脉动***

图 6 为不同工况下叶轮进口的压力脉动时域图，从图中压力脉动系数的变化可知，在进口的压力脉动规律性不是很明显，在 1.3Qd 工况下压力脉动幅值最小，且在单周期内有 8 个波峰，而在 1.0Qd 工况下压力脉动幅值最大，且单周期内压力脉动与叶频相关性较弱。说明泵的最优工况出现向大流量的偏移。

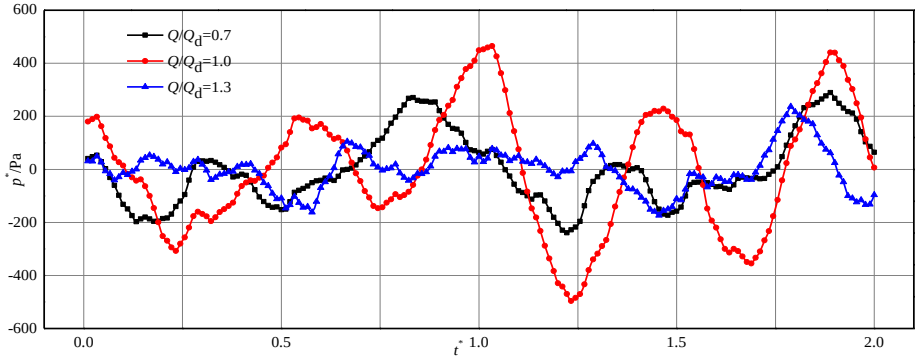


**Fig.6** - Time–domain map of pressure fluctuation at the impeller entrance under different working conditions

Fig. 7 illustrates the time–domain map of the pressure fluctuation volute exit under different working conditions. Pressure fluctuation at the volute exit is two orders of magnitude higher than that at the impeller entrance; moreover, this pressure fluctuation law is closely related to blade passing frequency. Nonetheless, pressure fluctuation amplitude changes significantly when the impeller is at different phases; the amplitude under different flow rates does not change when the impeller is at the same phase. This outcome occurs because the pressure-measuring points at the exit are downstream of the bend, and the turbulence at the bend disrupts downstream pressure monitoring.

图 7 为不同工况下蜗壳出口的压力脉动时域图，出口的幅值变化比进口高两个数量级，且脉动规律与叶片通过频率相关性较高，但叶轮在不同相位上时的压力幅值变化很明显，在不同流量下，叶轮在相同相位上的压力幅值也并不一致。这是由于出口处的测压点位置布置在弯管下游位置，弯管处的湍动对下游的压力监测产生了扰动。

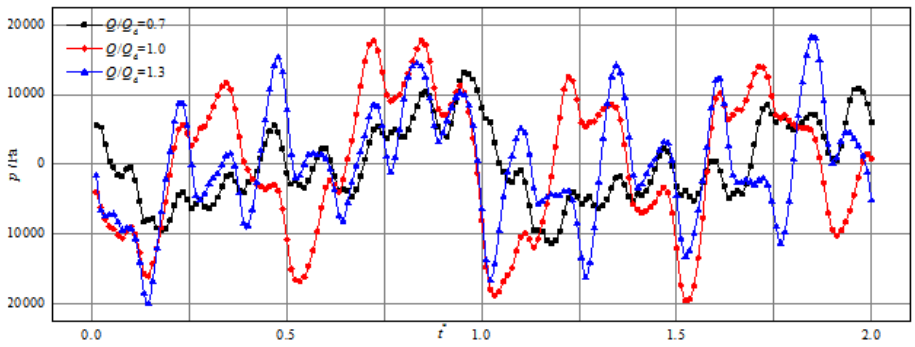


**Fig.7** - Time–domain map of pressure fluctuation at the volute exit under different working conditions

***Pressure fluctuation in volute***

Fig.8 depicts the fluctuations of P2–P9 in two periods. The water cut plays a decisive role in the pressure fluctuation caused by the interaction of the rotating impeller and the static impeller. The water cut is the main pulsation source of pressure fluctuation. In this case, pressure fluctuation amplitude decreases gradually with

***蜗壳内压力脉动***

图 8 为蜗壳内第一断面到第八断面上监测点处的绝对压力在两个周期内的压力脉动，从图中可以看出：

在旋转叶轮与静止蜗壳的相互干涉产生的压力脉动中，

an increase of flow rate. This result demonstrates that flow stabilizes and the losses caused by internal turbulence decrease with an increase in flow rate. The optimum working condition is skewed to a high flow rate.

Pressure fluctuation differs at various monitoring points on the same volute section. This fluctuation decreases first and then increases from the bottom volute to the back volute. Moreover, many dither components are detected at the monitoring points on the volute bottom. The maximum pressure amplitude along the circumference of the volute is at the monitoring points proximal to the water cut. The distance between the circumferential monitoring points and the water cut increases with the circumference angle, whereas fluctuation amplitude decreases gradually. Two wave peaks in one period are observed on the second, third, and seventh sections, thus indicating that these flow sections experience significant turbulence, which in turn covers the pulsation source of the water cut.

隔舌起着绝对作用，是产生压力脉动的主要脉动源，且本例中，随着流量的增大，压力脉动幅值逐渐减小，表明随着流量增大，流动趋于平稳，内部湍动造成的损失减小，最优工况向大流量工况偏移。

处于同一蜗壳断面不同位置的监测点的压力脉动幅度不同，从蜗壳底部向蜗壳背面先减小后增大，且位于蜗壳底部监测点的高频脉动成分较多。沿蜗壳周向，隔舌附近监测点压力脉动幅度最大，随着圆周角的增加，各监测点沿周向与隔舌距离变大，脉动幅值逐渐减小。

在第二、三及第七断面出现了在单个周期内只有两个波峰的情况，说明在这些过流断面出现了极大的湍动，覆盖了隔舌的脉动作用源。

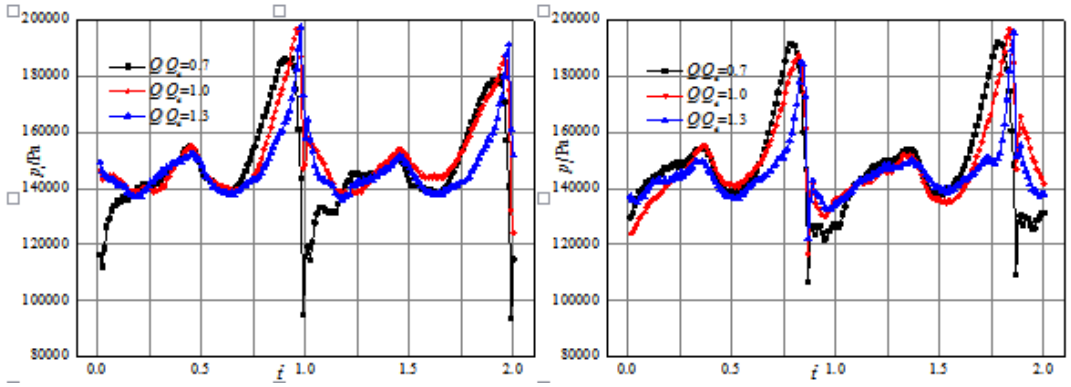


(a) Numerical calculation of the pressure fluctuation at P2 (b) Numerical calculation of the pressure fluctuation at P3

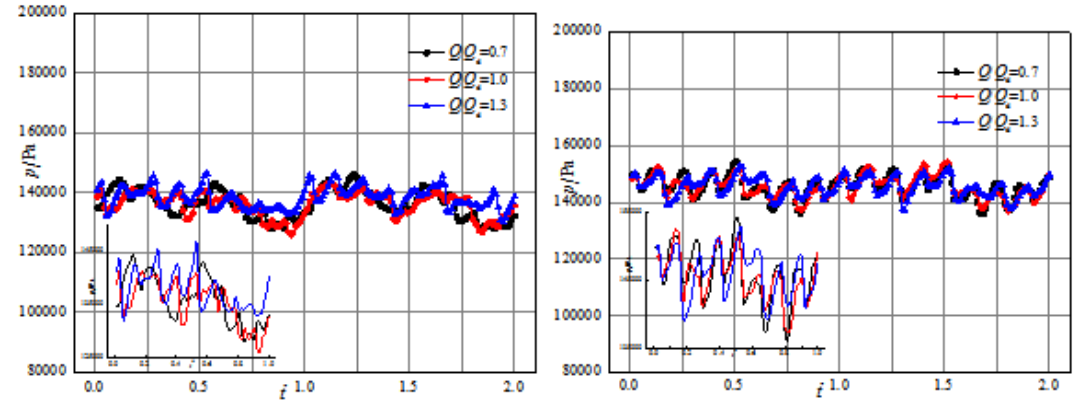


(c) Numerical calculation of the pressure fluctuation at P4 (d) Numerical calculation of the pressure fluctuation at P5

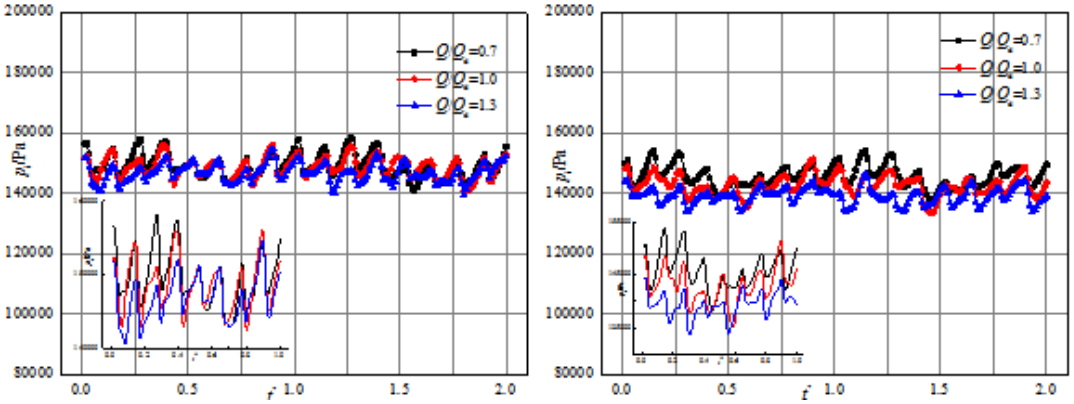


(e) Numerical calculation of the pressure fluctuation at P6 (f) Numerical calculation of the pressure fluctuation at P7

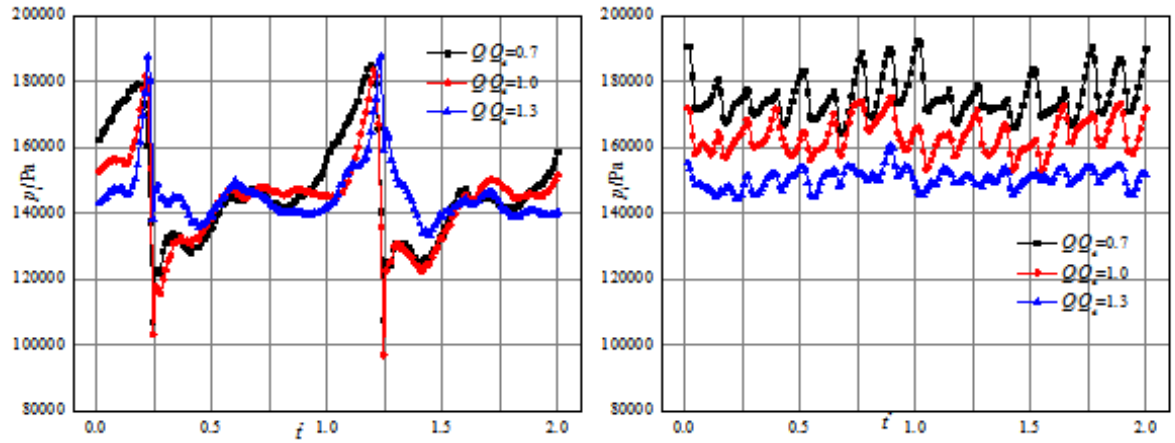


(g) Numerical calculation of the pressure fluctuation at P8 (h) Numerical calculation of the pressure fluctuation at P9

**Fig.8** - Numerical calculation of the pressure fluctuation in the volute

***Pressure fluctuation in the water cut area***

Fig. 9 displays the pressure fluctuation at the monitoring points close to the water cut. Generally, mean pressure declines with an increase in flow rate. Meanwhile, the pressure fluctuation law reflects the dynamic and static interference at the water cut. At the same time, the pressure downstream of the water cut is higher than that at a location close to the water cut. In other words, fluid pressure increases from the volute to the volute downstream. The pressure fluctuation at the water cut of the quadratic variable-curvature centrifugal pump differs from the regular pressure fluctuation of a common centrifugal pump, which is in turn positively correlated with the blade number. A significant difference is observed between the adjacent wave peaks of the pressure fluctuation in the quadratic variable-curvature centrifugal pump. Subsequently, the internal flow mechanism is analyzed further through testing.

***隔舌区域压力脉动***

图 9 是隔舌附近监测点压力脉动，整体而言压力平均值随着流量的上升而下降，而压力脉动的规律体现了隔舌处动静干涉。且隔舌下游的压力在同一时刻高于隔舌附近区域，即在流体进入蜗壳至隔舌下游仍然是增压过程。二次变曲率离心泵的隔舌处的压力脉动区别于普通离心泵的规则的与叶片数正相关的波形图，相邻波峰值之间有较大差值。这一问题需要结合试验手段进一步研究其内部流动机理。

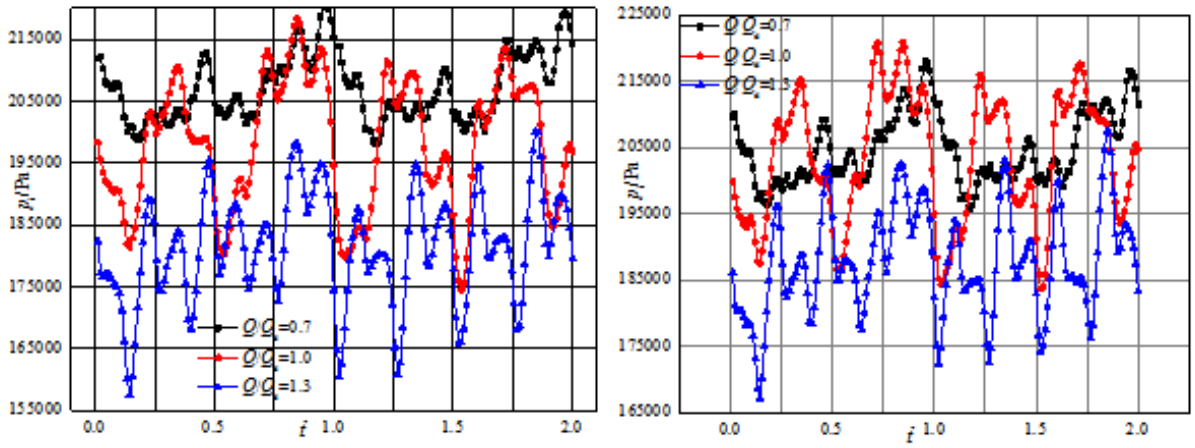


(a) Numerical calculation of the pressure fluctuation at P10 (b) Numerical calculation of the pressure fluctuation at P11

**Fig.9** - Numerical calculation of the pressure fluctuation near the water cut

***Experimental verification***

According to the distribution of the actual test points, C4–C8 pressure monitoring points are scattered on the full flow path of the volute. C7 is proximal to the water cut, and this point is the closest one to the outlet. C8 is the most proximal point to the volute exit; meanwhile, C4, C5, and C6 scattered on the volute evenly.

***试验验证***

按照试验实际测点位置布置，在蜗壳整个流道上分布着 C4~C8 压力监测点，其中 C7 在隔舌附近，离出水口最近，C8 离蜗壳出口最近，C4，C5，C6 均匀分布在蜗壳上。


**Fig.10** - Pressure fluctuation at C7 under different working conditions

Fig.10 indicates that the main frequency component at C7 under different working conditions is the blade passing frequency. Additionally, random fluctuations occur in the low-frequency area. These low-frequency random fluctuations are caused by the secondary flow in the impeller and efflux tail, as with similar to white noise. The pressure fluctuation amplitude is proportional to rotation speed and flow rate. At the same time, the pressure fluctuation under a low flow rate exhibited the poorest law in a single period. Low frequency (< twice that of blade passing frequency) can influence pressure fluctuation significantly because of the turbulence in the pump. As flow rate increases, the changes in pressure fluctuation amplitude within one period gradually stabilize and the random fluctuation declines evidently. This outcome indicates that a high flow rate is beneficial to steady pump operation. This result is consistent with the outcome of the analysis of unsteady external characteristics.

The results for C4, C5, and C6 in Fig. 11 indicate that the pressure fluctuation in the volute flow path is mainly affected by the blade passing frequency. All the monitoring points are primarily influenced by low frequency. The dominant frequency reduces continuously and is minimized at C5 from C7 to C6 and C5, which is close to the water cut. This outcome indicates that the main pressure fluctuation source is the static–dynamic coupling effect at the impeller and the water cut. Based on the results in C4 and C8, the dominant frequency amplitude at locations proximal to C8 is increased and peaks at C8. The dominant frequency is mainly influenced by twice the blade passing frequency. This outcome corresponds to the pressure fluctuation law under normal working conditions. This result is the consequence of the dynamic–static coupling effect of the water cut and the impeller as well as the influence of the right angle outlet of the auto water pump. Although the outlet is far from the pulsation source of the water cut and the dynamic–static coupling effect of fluid in volute is weak, the outlet is close to the corner and bears the direct impact. Fluid separation enhances pressure fluctuation, thus generating the same pulsation intensity at C8 and significantly higher pressure amplitude than the other monitoring points. This outcome conforms to the results of the numerical analysis.

由图 10 所知，不同工况下测点 C7 主要的频率成分为叶片通过频率。另外在低频区域出现一些随机脉动，这是由于在叶轮中有二次流及射流尾迹的影响，造成的低频随机脉动，类似于白噪声。随着转速及流量的增大，脉动幅值逐渐增大。同时可以发现，在小流量下的压力脉动在单周期内的规律性最差，由于泵内湍流，低于 1 倍叶片通过频率的低频对压力脉动有很大影响，随着流量的增大单周期内的幅值变化逐渐平稳，其随机脉动呈明显减少趋势，表明泵的运行稳定性偏向大流量工况，这与外特性的非定常结果分析一致。

由图 11 C4，C5，C6 可以看出，蜗壳流道内的压力脉动主要受叶片通过频率影响，各监测点主要是低频的影响，从 C7 点隔舌附近到 C6 点、C5 点，主频呈现递减趋势，到 C5 点处最小。这说明压力脉动源主要是叶轮与隔舌处的动静耦合。从 C4、C8 监测点可以看出，离出口 C8 点越近，主频幅值越大，到 C8 点达到最大值，主频主要是 1 倍的叶频影响较大。这与正常工况下的压力脉动规律一致，这主要都是来源于隔舌与叶轮之间的动静耦合，并且与汽车水泵的直角拐角出水口流量冲击的作用。虽然出口离隔舌脉动源较远，蜗壳内液流动静耦合影响较小，但离拐角较近，受到直角冲击，液流分流增强了压力脉动，使得 C8 点虽离隔舌脉动源较远，压力脉动强度没有出现减小，压力幅值相对其他位置有明显增大，这与数值分析结果相一致

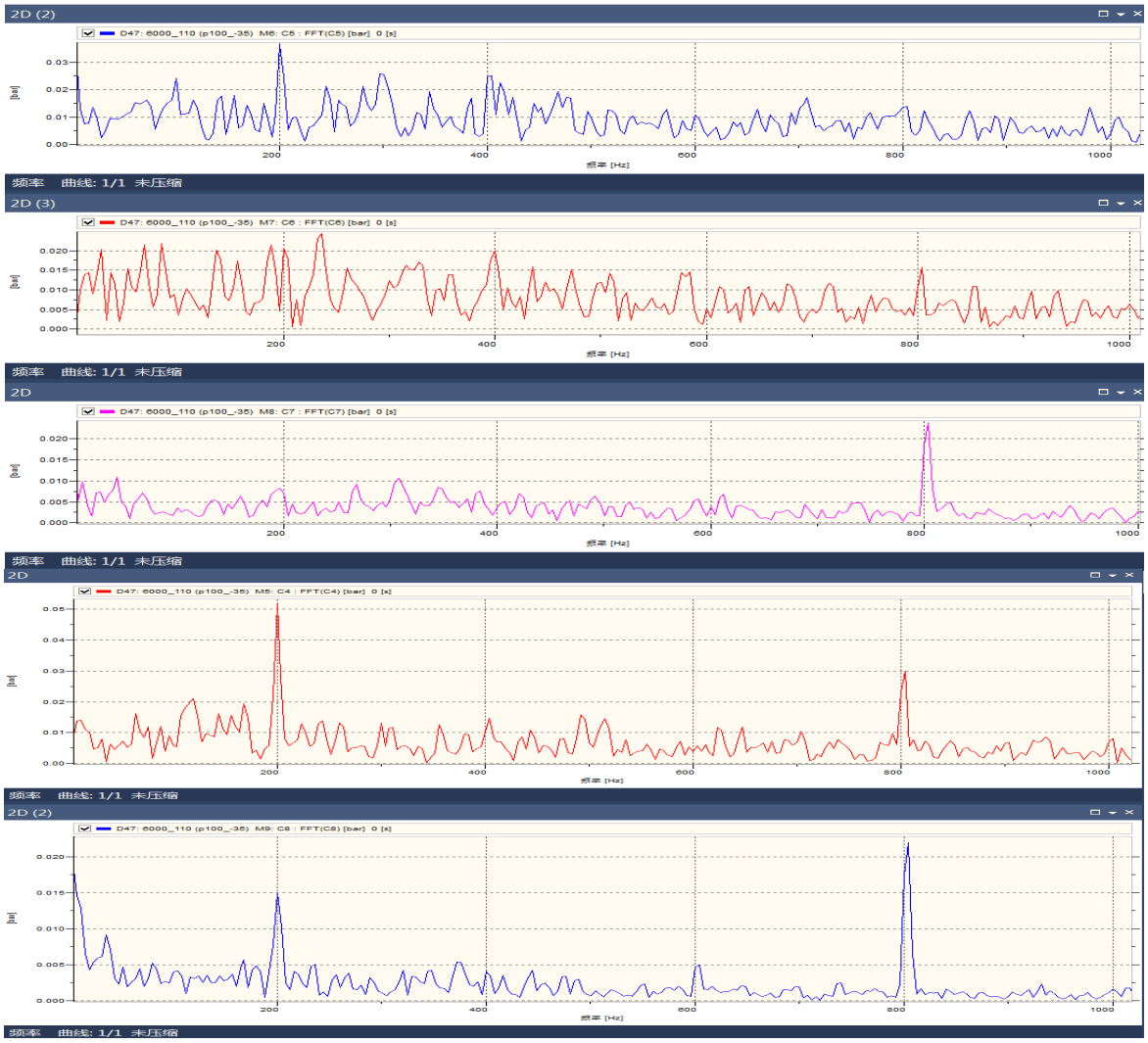


**Fig.11** - Frequency spectra of the pressure fluctuations at C4, C5, C6, C7 and C8

## CONCLUSIONS

This research conducts an unsteady numerical simulation and experimental study on quadratic variable-curvature and half-open centrifugal agricultural auto water pumps. The findings of this work are significant with respect to the application of analysis and simulation techniques in analyzing the dynamic characteristics of an agricultural auto water pump and in optimizing its structure design to improve the performance of the auto-cooling water pump, to reduce the product development period, and to lower cost. This work concludes that:

(1) The unsteady characteristics of the lift change periodically. This frequency change corresponds with the blade passing frequency, and this outcome is mainly attributed to the dynamic and static interference of the water cut and the impeller. Pressure fluctuation intensifies gradually with an increase in rotation speed and flow rate.

(2) The pressure fluctuation under a low flow rate exhibits the poorest law in a single period. The low frequency (< twice that of blade passing frequency) significantly influences pressure fluctuation because of the turbulence in the pump. As flow rate increases, the pressure fluctuation amplitude in a single period gradually stabilizes and the random fluctuation decreases significantly. This result indicates that a high flow rate is beneficial for steady pump operation.

## 结论

本文对二次变曲率半开离心式农用汽车水泵进行了非定常数值模拟及试验研究，对于分析模拟技术应用于优化设计农用汽车水泵的动态特性分析和结构设计优化上，提高汽车冷却水泵的性能，缩短产品开发周期，降低成本均具有重要的意义。得出如下结论

（1）扬程的非定常特性呈现明显的周期性变化，且频率和叶片通过频率一致，这是由于隔舌与叶轮的动静干涉作用引起的。且随着转速及流量的增大，脉动幅值逐渐增大

（2）在小流量下的压力脉动在单周期内的规律性最差，由于泵内湍流，低于 1 倍叶片通过频率的低频对压力脉动有很大影响，随着流量的增大单周期内的幅值变化逐渐平稳，其随机脉动呈明显减少趋势，表明泵的运行稳定性偏向大流量工况。

(3) Pressure fluctuation differs at the various monitoring points on the same volute section; this fluctuation decreases first and then increases from the bottom volute to the back volute. Many dither components are detected at the monitoring points at the bottom volute. The monitoring points close to the water cut along the circumference of the volute experience maximum pressure fluctuation. Moreover, the distance between the circumferential monitoring points and the water cut increases with the circumference angle, whereas the pressure fluctuation weakens gradually.

(4) The pressure fluctuation at the water cut of the quadratic variable-curvature centrifugal pump varies from the regular pressure fluctuation of a common centrifugal pump, which is in turn positively correlated with blade number. The differences between adjacent wave peaks are significant; this result conforms to the result of the experimental analysis.

**ACKNOWLEDGEMENT**

Science and Technology Research Project of Henan Province (142102210555).

**REFERENCES**

[1]. Aihua Jiang, (2011) - *Research On Vibration Of Centrifugal Pump Base Incited by Fluid Force*, Shang Hai Jiao Tong University;

[2]. Akhras A, Hajem M EI, Champagne J Y, et al., (2004) - *The Flow Rate Influence on The Interaction of a Radial Pump Impeller and The Diffuser, International Journal of Rotating Machinery*, Vol.10, no.4, pp.309-317;

[3]. Arpe J., (2003) - *Experimental Investigation of Unsteady Pressure And Velocity Field in a Draft Tube of Francis Turbine*, EPFL - Laboratory for Hydraulic Machines;

[4]. Chus, Dong R, Katz J., (1995) - *Relationship between Unsteady Flow , Pressure Fluctuation and Noise in a Centrifugal Pump-part B: Effects of Blade-tongue Interactions*, ASME J. Fluids Eng, no.117, pp.30-35;

[5]. Gonzalez J, Fernandez J, Blanco E, et al. (2002) - *Numerical Simulation of The Dynamic Effects due to Impeller-volute in a Centrifugal Pump*, ASME J. Fluids Eng,no.124, pp.348-355;

[6]. Hongjuan Ran, Xianwu Luo, Lei Zhu, et al. (2012) - *Experimental Study of the Pressure Fluctuations in a Pump Turbine at Large Partial Flow Conditions*, Chinese Journal of Mechanical Engineering, no.25, pp.1205-1209;

[7]. Jie Xu, Chuangang Gu. (2004) - *Numerical Calculation of Flow Field in Centrifugal Impeller with Splitter Blades*, Journal Of Chemical Industry and Engineering, vol.55, no.4, pp.541-544;

[8]. Jihong Yin. (1998) - *Numerical Simulation of Francis Turbine Flow by LES Model*, Abroad Large Electric Machine, no.5, pp.60-65;

[9]. Launder B E, Spalding D.B., (1972) - *Lectures in Mathematical Models of Turbulence*, London: Academic Press;

[10]. Shi F, Tsukamoto H. (2001) - *Numerical Study of Pressure Fluctuations Caused by Impeller~diffuser Interaction in a Diffuser Pump Stage*, ASME Journal of Fluids Engineering, vol.123, no.3, pp.466-474;

[11]. Yakhot V, Orszag S A. (1986) - *Renormalization Group Analysis of Turbulence*, Journal of Scientific Computing, no.1, pp.3-11;

[12]. Zhaohui Xu, Yulin Wu, Naixiang Chen. (2004) - *Unsteady Blade-Row Interaction Calculation in High Speed Pump*, Chinese Journal Of Mechanical Engineering, vol.40, no.3, pp.1-4;

（3）处于同一蜗壳断面不同位置的监测点的压力脉动幅度不同，从蜗壳底部向蜗壳背面先减小后增大，且位于蜗壳底部监测点的高频脉动成分较多。沿蜗壳周向，隔舌附近监测点压力脉动幅度最大，随着圆周角的增加，各监测点沿周向与隔舌距离变大，脉动幅值逐渐减小。

（4）二次变曲率离心泵的隔舌处的压力脉动区别于普通离心泵的规则的与叶片数正相关的波形图，相邻波峰值之间有较大差值，这与试验分析结果相一致。

**致谢**

河南省科技攻关项目资助（142102210555）。

**参考文献**

[1]. 蒋爱华. (2001) - *流体激励诱发离心泵基座振动的研究*, 上海:上海交通大学;

[2]. Akhras A, Hajem M EI, Champagne J Y, et al. (2004) -*流量对径向泵叶轮和扩散器的影响*, 国际旋转机械杂志, 第 10 卷, 第 4 期, 309-317;

[3]. Arpe J.(2003) - *混流式水轮机的非定长压和流场的实验研究*, 洛桑:洛桑联邦理工学院液压机实验室;

[4]. Chus, Dong R,Katz J. (1995) - *叶片隔舌对离心泵非定常流动、压力脉动与噪声之间的影响*, 美国机械工程师协会.流体工程, 第 117 期, 30-35;

[5]. Gonzalez J, Fernandez J, Blanco E, et al. (2002) - *离心泵叶轮与蜗壳的动力学数值模拟*, 美国机械工程师协会. 流体工程, 第 124 期, 348-355;

[6].冉红娟, 罗先武, 朱磊. (2012) - *涡轮泵局部流动的压力脉动实验研究*, 中国机械工程学报, 第 25 期, 1205 -1209.

[7]. 徐洁,谷传纲.(2004) - *长短叶片离心泵内部流动的数值计算*, 化工学报, 第 55 卷, 第 4 期, 541-544;

[8]. 尹继红.(1998) - 用 LES *法模拟混流式水轮机的水流*, 国外大电机, 第 5 期, 60-65;

[9]. Launder B E, Spalding D B.(1972) - *湍流的数学模型讲座*, 伦敦:学术出版社;

[10]. Shi F, Tsukamoto H.(2001) - *导叶泵叶轮压力脉动扩散的数值模拟研究. 美国机械工程师协会.* 流体工程杂志, 第 123 卷, 第 3 期, 466~474;

[11]. Yakhot V, Orszag S A. (1986) -*湍流的重整化群分析*, 科学计算杂志, 第 1 期, 3-11;

[12]. 徐朝晖, 吴玉林, 陈乃祥. (2004) - *高速泵内三维非定常动静干扰流动计算*, 机械工程学报, 第 40 卷, 第 3 期, 1-4;

[13]. Zhongyong Pan, Yongyan Ni, Shouqi Yuan, (2010) - *Experiment and Mechanism of Centrifugal Pumps Rotation Speed Measurement Based on Rotor-stator Interaction*, Transactions of the Chinese Society for Agricultural Machinery, vol.41, no.3, pp.81-85;
[14]. ZieglerK U, Gallus H E, Niehuis R. (2003) – *Study on Impeller~diffuser Interaction Part I: Influence On the performance*, Journal of Turbo machinery, vol.125, no.1, pp.173-182.

[13]. 潘中永, 悦永燕, 袁寿其, (2010) - *基于动静干涉的离心栗转速测量机理与实验,* 农业机械学报, 第 41 卷, 第 3 期, 81-85;
[14]. ZieglerK U, Gallus H E, Niehuis R. (2003) - *叶轮扩散器对部分零件性能的研究*, 涡轮机械杂志, 第 125 卷, 第 1 期, 173-182

# ENERGY ANALYSIS OF MANUFACTURING PROCESS OF BIODEGRADABLE AGRICULTURAL FILMS / *ANALIZA ENERGETICĂ A PROCESULUI DE FABRICAȚIE A FOLIILOR AGRICOLE BIODEGRADABILE*

**Ph.D. Eng. Deac T.[1)]., Ph.D Stud. Eng. Nagy E. M.[2)]., Eng. Coța C.[2)], Ph.D. Eng. Cioica N.[2)], Eng. Gyorgy Z.[2)]**
[1)]Technical University of Cluj-Napoca, Faculty of Mechanics / Romania;[2)]INMA Bucharest Branch of Cluj Napoca
*Tel: 0723798071; E-mail: teodora.deac@auto.utcluj.ro*

***Abstract:*** *In recent years, in the agricultural sector the amount of low density non- biodegradable polyethylene film (PV) annually used has increased considerably. Thus, worldwide the researches have intensified in order to obtain films produced from renewable agricultural sources. The paper presents the results regarding a new method for manufacturing of biodegradable agricultural film from renewable resources and energy analysis process.*

***Keywords:*** *energy analysis, agricultural film, biodegradable, renewable resources, the manufacturing process, energy consumption, extrusion lamination*

## INTRODUCTION

Worldwide, the volume of films used in agriculture has greatly increased in the last 10 years. The latest data show that agriculture and horticulture are responsible for approximately 1.500.000 t consumption of annual production of polymers in Europe. In the case of the thin films, in Europe are consumed more than 72.000 t / year as direct row covers, over 75.000 t / year films for culture in low tunnels and more than 130.000 t / year mulching films [7].

Currently, the market is still dominated by agriculture films obtained from low-density polyethylene (PE).

These films have two major disadvantages: they are manufactured from petroleum based raw materials and produce a large amount of waste that needs to be removed from the field and destroyed [6]. Non-degradable polymers accumulate on the ground creating serious problems for plastic waste management [8].

Also in their manufacturing process large amounts of energy that comes from conventional sources, are consumed.

So, besides the fact that it is an important source of waste with negative environmental impact, producing low density film is also conventional primary resource consuming [8].

An alternative solution to agricultural polyethylene film is the development and use of biodegradable plastics from renewable agricultural resources which break down completely in contact with microorganisms found in the soil [6]. In this way, we solve two problems of great importance for the environment: fossil resources are saved and emissions of greenhouse gases (GHG) are reduced [1].

At worldwide level, the research of biopolymers development has intensified. Since 1990s Germany has been financing research projects / development in the field of biodegradable thermoplastic manufacturing. The researches conducted have created a wide variety of biodegradable plastics [6].

***Rezumat:*** *În ultima perioadă în sectorul agricol cantitatea de folie din polietilenă de joasă densitate (PV), nebiodegradabilă, utilizată anual a crescut considerabil. Astfel pe plan mondial s-au intensificat cercetările de obținere a foliilor din surse agricole regenerabile. Lucrarea prezintă rezultatele obținute privind o nouă metodă de realizare de folii biodegradabile pentru agricultură din resurse regenerabile şi analiza energetică a procesului.*

***Cuvinte cheie:*** *analiză energetică, folii agricole biodegradabile, resurse regenerabile, proces de fabricație, consum energetic, extrudare, laminare*

## INTRODUCERE

Pe plan mondial, volumul foliilor pentru utilizare în agricultură a crescut foarte mult în ultimii 10 ani. Cele mai recente date arată că agricultura şi horticultura sunt responsabile pentru un consum de aproximativ 1.500.000 t din producția anuală de polimeri din Europa. În ceea ce priveşte categoria foliilor subțiri, în Europa sunt consumate peste 72.000 t/an folii pentru acoperire directă pe rânduri, peste 75.000 t/an folii pentru culturi în tunele mici şi mai mult de 130.000 t/an folii de mulcire [7].

În prezent, piața este încă dominată de foliile pentru agricultură obținute din polietilenă de joasă densitate (PE).

Aceste folii au două mari dezavantaje: sunt fabricate din materii prime pe bază de țiței şi produc o mare cantitate de deşeuri care necesită a fi înlăturate de pe câmp şi distruse [6]. Polimerii nedegradabili se acumulează pe sol creând probleme serioase de management a deşeurilor din plastic [8].

De asemenea, în procesul de fabricare a acestora se consumă cantități însemnate de energie care provine din surse convenționale.

Aşadar pe lângă faptul că este o importantă sursă de deşeuri cu impact negativ asupra mediului, producerea foliilor de joasă densitate este şi consumatoare de resurse primare convenționale [8].

O soluție alternativă viabilă la foliile agricole din polietilenă o constituie dezvoltarea şi utilizarea plasticelor biodegradabile, provenite din resurse agricole regenerabile care se descompun complet în contact cu microorganismele aflate în sol [6]. În acest fel se rezolvă două probleme de mare importanță pentru mediu: se economisesc resursele fosile şi se reduc emisiile de gaze cu efect de seră (GES) [1].

Astfel, la nivel mondial s-au intensificat cercetările în domeniul dezvoltării de biopolimeri. Încă din anii `90 Germania finanțează proiecte de cercetare/dezvoltare în domeniul producerii de termoplastic biodegradabil. În urma cercetărilor realizate au fost create o mare varietate de materiale din plastic biodegradabil [6].

However the energy consumption for producing films remains a problem because, in this case too, both in the extraction of raw materials process and in the manufacturing process the energy consumed comes also from fossil sources.

In this context, the main objective of the paper was to develop a theoretical mathematical model of analysis of energy consumption in the production process of agricultural biodegradable films and its application to determine the maximum energy consumption of the production process of agricultural biodegradable films using corn starch as raw material and the technology developed by INMA Bucharest, Branch of Cluj-Napoca. Thus, a theoretical model for analyzing energy consumption using systemic analysis method and applying mathematical model, has been developed, to determine the maximum consumed energy in the manufacturing of agricultural films from corn starch.

## MATERIAL AND METHOD

To develop the theoretical mathematical model for determining the energy consumption in the manufacturing process of biodegradable agricultural film the systemic analysis has been used. The manufacturing process was considered as a whole system (*MPF*) and the phases were considered as subsystems of the considered system (*MPF.Fi*) (Fig.1). The total energy consumed ($E_{MPF}$) in manufacturing process of films is determined by the relation (1).

Totuşi problema consumului de energie pentru producerea foliilor rămâne o problemă, deoarece şi în acest caz atât în procesul de extracție a materiei prime cât şi în procesul de fabricație energia consumată provine tot din surse de energie fosile.

În acest context, obiectivul principal a lucrării a fost de a realiza un model matematic teoretic de analiză a consumului energetic al procesului de fabricație a foliilor agricole biodegradabile şi aplicarea acestuia pentru determinarea consumului energetic maxim al procesului de producere a foliilor agricole biodegradabile utilizând ca materie primă amidon de porumb şi tehnologia dezvoltată în acest sens de către INMA Bucureşti, Sucursala Cluj-Napoca. Astfel în lucrare s-a dezvoltat un model teoretic de analiză a consumului energetic utilizând metoda analizei sistemice şi aplicarea modelului matematic pentru determinarea energiei maxime consumate în procesul de fabricație a foliilor agricole din amidon de porumb.

## MATERIAL ŞI METODĂ

Pentru dezvoltarea modelului matematic teoretic de determinare a consumurilor energetice a procesului de fabricare a foliilor agricole biodegradabile s-a utilizat analiza sistemică. Procesul de fabricatie a fost considerat ca un întreg sistem (*MPF*), iar fazele procesului au fost considerate ca subsisteme ale sistemului considerat ($MPF.F_i$). Energia totală consumată ($E_{MPF}$) în procesul de fabricație a foliilor se determină cu relația (1).

$$E_{MPF} = \sum_{i=1}^{n} E_{MPF.F_i} \quad (1)$$

$$E_{E_{MPF.F_i}} = \sum_{j=1}^{k} E_{MPF.F_{i.j}} \quad (2)$$

Where:

$E_{MPF}$ - total energy consumed in manufacturing process of biodegradable agricultural film [kWh/kg];

$E_{MPF.Fi}$ - energy consumed during *i* phase of the manufacturing process [kWh/kg];

*i = 1...n* phases of production.

By systemic analysis of the manufacturing process phases, each term of relationship (1) is divided into sub-terms of lower grade. The division of the terms in terms of lower level is performed in accordance with the phases, respectively, the activities of the technological process [7, 8] until the final relationships for determining the energy consumption (rel.2), result, which allow absolute quantification of energy consumption.

Where:

$E_{MPF.Fi,j}$ - energy consumed during the phase *i,* activity *j* of manufacturing process [kWh/kg]; *j = 1...k* activities of phase *i* of the process of production. To determine the components of relationship (2) it is necessary to analyze the technological process for manufacturing renewable agricultural film (Figure 1).

After analyzing the technological process, relation (1) became relation (3):

Unde:

$E_{MPF}$ - energia totală consumată în procesul de fabricație a foliilor agricole biodegradabile [kWh/kg];

$E_{MPF.Fi}$ – energia consumată în faza *i* a procesului de fabricație [kWh/kg];

*i=1…n* fazele procesului de fabricație.

Prin analiza sistemică a fazelor procesului de fabricație, fiecare termen a relației 1, se divide în subtermeni de grad inferior.

Divizarea termenilor în termeni de grad inferior se realizează în concordanță cu fazele respectiv activitățile procesului tehnologic [7, 8] până când rezultă relațiile finale de determinare a consumurilor energetice (rel.2), care să permită cuantificarea consumurilor energetice în valoare absolută.

Unde:

$E_{MPF.Fi,j}$ - energia consumată în faza *i*, activitatea *j* a procesului de fabricație [kWh/kg]; *j=1…k* activitățile fazei *i* a procesului de fabricatie.

Pentru determinarea componentelor relației (2) este necesară analiza procesului tehnologic de fabricație a foliilor agricole din surse regenerabile (Figura 1).

În urma analizei procesului tehnologic relația (1) devine relația (3):

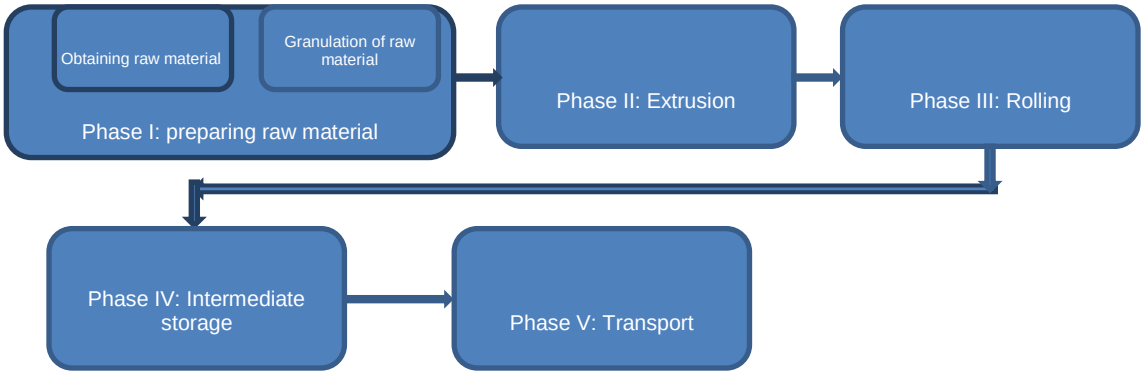


**Fig.1** – Chart of technological process for manufacturing renewable agricultural film

$$E_{MPF.F} = E_{MPF.F_1} + E_{MPF.F_2} + E_{MPF.F_3} + E_{MPF.F_4} + E_{MPF.F_5} \quad (3)$$

$$E_{MPF.F_2} = E_{MPF.F_{2.1}.} + E_{MPF.F_{2.2}} + E_{MPF.F_{2.3}} \quad (4)$$

Where:
$E_{MPF.F1}$ - energy used for preparing raw material [kWh/kg];
$E_{MPF.F2}$- energy consumed in the process of dispensing, extrusion and widening the extruded material [kWh/kg]; $E_{MPF.F3}$ - the energy consumed in the process of rolling [kWh/kg];
$E_{MPF.F4}$ - energy consumed for intermediate storage [kWh/kg];
$E_{MPF.F5}$ - energy consumed in intermediate transport phase (in manufacturing) and final transport (to the beneficiary) [kWh/kg].

The term 2 of relation (3) will further divide in terms of order 3 (relation 4).
Where:
$E_{MPF.F2.1}$ - the energy used for dosing raw materials [kWh/kg];
$E_{MPF.F2.2}$ - energy used for extrusion [kWh/kg];
$E_{MPF.F2.3}$ - the energy use by widening matrix [kWh/kg].
Energy consumption for raw material dosage can be expressed by a final relation (relation 5):

Unde:
$E_{MPF.F1}$- energia consumată pentru prepararea materiei prime [kWh/kg];
$E_{MPF.F2}$ – energia consumată în procesul de dozare, extrudare şi lățire a materialului extrudat [kWh/kg];
$E_{MPF.F3}$ - energia consumată în procesul de laminare [kWh/kg];
$E_{MPF.F4}$ – energia consumată pentru depozitare intermediară [kWh/kg];
$E_{MPF.F5}$ – energia consumată aferentă fazei de transport intermediar (în procesul de fabricație) şi final (la beneficiar) [kWh/kg].

Termenul al 2-lea al relației (3) se va divide în continuare în termeni de ordinul 3 (relația 4).
Unde:
$E_{MPF.F2.1}$- energia consumată pentru dozarea materiei prime [kWh/kg];
$E_{MPF.F2.2}$ - energia consumată pentru extrudare [kWh/kg];
$E_{MPF.F2.3}$ - energia consumată de matricea de lățire [kWh/kg].
Energia consumată pentru dozarea materiei prime poate fi exprimată printr-o relație finală (relația 5):

$$E_{MPF.F_{2.1}.} = \frac{E_d}{C_d} \quad (5)$$

$$E_{MPF.F_{2.2}.} = E_{MPF.F_{2.2.1}.} + E_{MPF.F_{2.2.2}.} + E_{MPF.F_{2.2.3}.} \quad (6)$$

$$E_{MPF.F_{2.2.1}} = \sum_{m=1}^{p} E_{MPF.F_{2.2.1.m}} \quad (7.1)$$

$$E_{MPF.F_{2.2.1.m}.} = f(C_{ma}; C_{ex}; C_{hex}) \quad (7.2)$$

$$E_{MPF.F_{2.2.1}.} = \frac{C_{hc}}{D_{hex}} \quad (7.3)$$

Where $E_d$ is hourly energy consumption of the dispenser [kWh]; $C_d$ - hourly production capacity of the dosing feeder [kg/h].
The energy consumed by the extrusion equipment will divide in terms of lower order (relation 6).

unde: $E_d$ este consumul energetic orar al dozatorului [kWh]; $C_d$ – capacitatea de producție orară a dozatorului [kg/h].
Energia consumată de echipamentul de extrudare se va divide în termeni de ordin inferior (relația 6).

Where: $E_{MPF.F2.2.1}$ is the energy used to run the extrusion screws [kWh/ kg];

$E_{MPF.F2.2.2}$ - energy consumed by heating system [kWh/kg];

$E_{MPF.F2.2.3}$ - energy consumed by cooling system [kWh / kg].

Terms from relation 6 are divided further in lower order terms (relations 7.1; 7.2, 7.3, 8, 9)

Where: $E_{MPF.F2.2.1.m}$ is energy consumed per each area of the extruder cylinder [kWh/kg]; $m = 1...p$ – identification coefficient of extruder cylinder areas [kWh/kg].

Also in relation (7.2):

$C_{ma}$ is dependence coefficient on thermo-physics characteristics of the material;

$C_{ex}$ - coefficient depending on the characteristics of the extrusion cylinder;

$C_{hex}$ - the productivity of the extruder [kg / h];

$T_{ex}$ - Extrusion temperature [C°]; $T_{ex} = f(C_{ma})$.

The relation (7.1) can be quantified by relation (7.3), where:

$C_{hc}$ – total energy consumption for driving extrusion screws [kWh];

The energy consumed by the heating system $E_{MPF.F2.2.2}$, and cooling system $E_{MPF.F2.2.3}$ is influenced by extrusion temperature and technical characteristics of the plants (relation (8.1)), and can be quantified using relations (9.1), (9.2), where:

Unde: $E_{MPF.F2.2.1}$ este energia consumată pentru acționarea melcilor de extrudare [kwh/kg];

$E_{MPF.F2.2.2}$ - energia consumată de instalația de încălzire [kwh/kg];

$E_{MPF.F2.2.3}$ - energia consumată de instalația de răcire [kwh/kg].

Termenii relației 6 se divid în continuare în termeni de ordin inferior (relațiile 7.1; 7.2, 7.3; 8, 9):

Unde: $E_{MPF.F2.2.1.m}$ este energia consumată pe fiecare zonă a cilindrilor extruderului [kwh/kg]; $m=1...p$ – coeficient de identificare a zonelor cilindrilor de extrudare [kwh/kg].

De asemenea în relația (7.2):

$C_{ma}$ este coeficent de dependență de caracteristicile termo-fizice ale materialului;

$C_{ex}$ - coeficent de dependență de caracteristicile cilindrilor de extrudare;

$C_{hex}$ – productivitatea extruderului [kg/h];

$T_{ex}$ – temperatura de extrudare [°C]; $T_{ex}$= f($C_{ma}$).

Relația (7.1) se poate cuantifica prin relația (7.3), unde:

$C_{hc}$ – consumul orar total de energie pentru antrenarea melcilor de extrudare [kwh];

Energia consumată de instația de încălzire $E_{MPF.F2.2.2}$, respectiv răcire $E_{MPF.F2.2.3}$ este influențată de temperatura de extrudare şi caracteristicile tehnice ale instalațiilor (relația (8.1)) şi se poate cuantifica utilizând relațiile (9.1), (9.2), unde:

$$E_{MPF.F_{2.2.2,3}.} = f(T_{ex}, C_i) \quad (8)$$

$$E_{MPF.F_{2.2.2}.} = \frac{C_{hi}}{D_{hex}} \quad (9.1)$$

$$E_{MPF.F_{2.2.2}.} = \frac{C_{hr}}{D_{hex}} \quad (9.2)$$

$$E_{MPF.F_{2.3}.} = \frac{C_{hml}}{D_{hml}} \quad (10)$$

$C_i$ - coefficient depending on the characteristics of the heating / cooling system;

$C_{hi}$ - hourly energy consumption of the heating system [kWh];

$C_{hr}$ - hourly energy consumption of the cooling system,[kWh].

The energy consumed by the widening area can be quantified using the relationship 10, where:

$C_{hml}$ - hourly electricity consumption for the widening matrix [kWh];

$D_{hml}$ - hourly production capacity for widening matrix [kg / h].

$C_i$ – coeficient de dependență de caracteristicile instalației de încălzire/răcire;

$C_{hi}$ – consumul de energie orar al instalației de încălzire [kwh];

$C_{hr}$ – consumul orar de energie al instalației de răcire [kwh].

Energia consumată de matricea de lățire se poate cuantifică utilizând relația 10, unde:

$C_{hml}$ este consumul orar de energie electrică a matricei de lățire [kWh];

$D_{hml}$ – capacitatea de producție orară a matricei de lățire [kg/h].

$$E_{MPF.F_{3}.} = E_{MPF.F_{3.1}.} + E_{MPF.F_{3.2}.} + E_{MPF.F_{3.3}.} \quad (11)$$

$$E_{MPF.F_{3}.} = \frac{C_{hv} + C_{hli} + C_{hlr}}{D_{hl}} \quad (12)$$

$$E_{MPF.F_4} = \frac{N_d \cdot C_d}{M_d} \quad (13)$$

$$E_{MPF.F_5.} = \frac{N_t \cdot C_{cb} \cdot H_{cb}}{M_f.} \quad (14)$$

The energy consumption of the rolling equipment $E_{MPF.F3}$ will divide in terms of lower order (relation 11), where:

$E_{MPF.F3.1}$ -is energy consumed by driving of laminating rollers [kWh];

$E_{MPF.F3.2}$ respectively $E_{MPF.F3.3}$ - the energy consumed for heating or cooling system [kWh].

The relation (11) can be quantified by the equation 12, where:

$C_{hv}$ -hourly electricity consumption for laminating rollers [kWh];

$C_{hli}$ - hourly electricity consumption of the heating system of the rolling equipment [kWh];

$C_{hl}$ - hourly electricity consumption for cooling system of the rolling equipment [kWh];

$D_{hml}$ - rolling equipment hourly production capacity [kg /h].

Energy for intermediate storage is determined by the relation (13), where:

$N_d$ - is number of storage days;

$C_d$ - energy requirement for optimal warehouse $C_d = C_{d1} + C_{d2}$ [kWh]; $C_{d1}$ - energy consumed to illuminate the deposit [kWh]; $C_{d2}$ - energy consumed for heating deposit [kWh];

$M_d$ - total amount of deposited material [kg/h]

Energy for transport is determined by the relation (14), where:

$N_t$ – is transport distance [km];

$C_{cb}$ – fuel consumption [l / km];

$H_{cb}$ - calorific value of the fuel [kW / l];

$M_f$ - the amount of material transported [kg].

Energia consumată de echipamentul de laminare $E_{MPF.F3}$ se va divide în termeni de ordin inferior (relația 11), unde:

$E_{MPF.F3.1}$ -este energia consumată cu antrenarea valțurilor de laminare [kWh];

$E_{MPF.F3.2}$ şi respectiv $E_{MPF.F3.3}$ – energia consumată de instalația de încălzire respectiv răcire [kWh].

Relația (11) poate fi cuantificată prin relația 12, unde:

$C_{hv}$ este consumul orar de energie electrică a valțurilor de laminare [kWh];

$C_{hli}$ - consumul orar de energie electrică a instalației de încălzire a laminatorului [kWh];

$C_{hl}$ - consumul orar de energie electrică a instalației de răcire a laminatorului [kWh];

$D_{hml}$ – capacitatea de producție orară a laminatorului [kh/h].

Energia consumată cu depozitarea intermediară se determină cu relația (13), unde:

$N_d$ -este numărul de zile de depozitare;

$C_d$ – energia necesară funcționării optime a depozitului $C_d = C_{d1} + C_{d2}$ [kWh]; $C_{d1}$ – energia consumată pentru iluminarea depozitului [kWh]; $C_{d2}$ – energia consumată pentru încălzirea depozitului [kWh];

$M_d$ – cantitatea totală de material depozitată [kg/h]

Energia consumată cu transportul se determină cu relația (14), unde:

$N_t$ -este distanța de transport [km];

$C_{cb}$ – consumul de carburant [l/km];

$H_{cb}$ – puterea calorică a carburantului [kW/l];

$M_f$ – cantitatea de material transportată [kg].

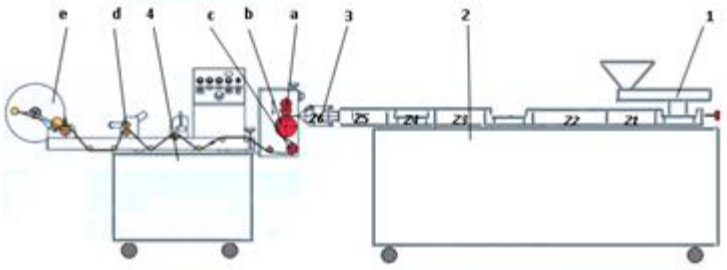


**Fig. 2** –Installation for extrusion and rolling

## RESULTS

General mathematical method developed was applied to determine the energy consumption of manufacture of biodegradable agricultural film using the system developed for this purpose by INMA Bucharest, Branch of Cluj-Napoca (fig.2). To determine the energy consumption of the process, a simplified mathematical model will be applied, taking into account only the actual two phases of the manufacturing process: extrusion and laminating respectively.

The manufacturing process of biodegradable agricultural film for which the mathematical method developed was applied, was developed under the following conditions: raw material used was a mixture of starch, glycerol and water. Corn starch used had the water content on wet basis of 10.76%, particle sizes between 2.3 and 37.3 μm, and a density of 0.561 g / $cm^3$; glycerine had a concentration of 99.5% and a density of 1.262 g / $cm^3$. The water used was from the water supply system.. Starch was introduced into the extruder by means of the dispenser and the plasticizers with a peristaltic pump. In order to use a single metering

## REZULTATE

Metoda matematică generală elaborată a fost aplicată la determinarea consumurilor energetice a procesului de fabricație a foliilor agricole biodegradabile utilizând instalația dezvoltată în acest sens de către INMA Bucureşti, Sucursala Cluj-Napoca (fig.2). Pentru determinarea consumurilor energetice a procesului, se va aplica un model matematic simplificat luându-se în calcul doar cele două faze efective ale procesului de fabricație: extrudarea şi respectiv laminarea.

Procesul de fabricație al foliilor agricole biodegradabile pentru care s-a aplicat metoda matematică dezvoltată s-a desfăşurat în următoarele condiții: materia primă utilizată a fost un amestec de amidon, glicerina şi apa. Amidonul de porumb utilizat a avut umiditatea raportată la substanta umeda de 10,76%, dimensiunile particulelor între 2,3 şi 37,3 μm şi densitatea de 0,561 g/$cm^3$; glicerina a avut o concentrație de 99,5 % şi o densitate de 1,262 g/$cm^3$. Apa utilizată a fost apa de la rețea. Amidonul a fost introdus în extruder cu ajutorul dozatorului iar plastifianții cu ajutorul pompei peristaltice. În scopul utilizării unei singure pompe dozatoare, cei doi

pump, the two plasticizers, glycerol and water, being miscible, were mixed in the proportions of the formulation and introduced into tank plasticizers. The feed rate with raw material was 12 kg / h. Temperatures in the five zones of the extruder were 30$^0$C, 50$^0$C, 100$^0$C, 130$^0$C, 150$^0$C and the temperature in the mould was 150$^0$C.

The main parts of the installation are: dispenser *1*; extruder *2*, widening matrix *3* and the rolling equipment *4*.

Extrusion equipment used was a laboratory twin-screw extruder with co-rotating intermeshing screws, with a productivity of 12 kg/h, screw diameter D=25 mm, screw length L=30xD and screw speed of 400 rpm. The extruder cylinder is modular and has five zones, each zone having independent heating and cooling. Each of the 5 zones, *Z1-Z5*, is equipped with one temperature sensor that measures temperature and controls starting or stopping of the heaters or fans to maintain the temperature set in each zone.

Dosage of powder materials in the extruder hopper was achieved using twin screw dispenser and dispensing components in the *Z2* area will be done using metering pumps.

The results obtained by applying the mathematical method developed are presented in Table 1.

plastifianți, glicerina şi apa, fiind miscibili, au fost amestecați în proporția din rețetă şi introduşi în rezervorul pentru plastifianți. Debitul de alimentare cu materie primă 12 kh/h. Temperaturile în primele cinci zone ale extruderului au fost 30$^0$C, 50$^0$C, 100$^0$C, 130$^0$C, 150$^0$C iar temperatura în zona matriței a fost de 150$^0$C.

Elementele principale ale instalatie sunt: Dozatorul *1*, Extruderul *2*, Matrița de lățire *3* şi Echipamentul de laminare *4*.

Echipamentul de extrudare folosit a fost un extruder cu doi melci modulari corotativi, cu o productivitate de 12 kg/h, diametrul melcilor: D=25 mm, lungimea melcilor: L=30xD, turația melcilor 400 rot/min. Cilindrul extruderului este modular şi are cinci zone, fiecare zona având încălzire şi răcire independenta. Fiecare dintre primele 5 zone, *Z1-Z5*, este prevazuta cu cate un senzor de temperatura care măsoară temperaturile şi comandă pornirea sau oprirea încălzitoarelor sau ventilatoarelor pentru menținerea temperaturilor reglate pe fiecare zonă.

Dozarea materialelor pulverulente ăn pâlnia extruderului s-a realizat cu ajutorul dozatorului cu doi melci iar dozarea componenților in zona *Z2* se va face cu ajutorul unor pompe dozatoare.

Rezultatele obținute în urma aplicării metodei matematice dezvoltate sunt prezentate în tabelul 1.

**Table 1**

**Energy consumption divided on biodegradable agricultural film manufacturing phases / stages**

| Parameter | Notation U.M. | Value |
|---|---|---|
| Material flow | $D_m$ [kg/h] | 12.00 |
| Energy consumption of the dispenser | $E_{MPF.F2.1}$ [kwh/kg] | 0.05 |
| Total energy consumption of extruder | $E_{MPF.F2.2}$ [kwh/kg] | 0.90 |
| Energy consumption of extrusion screws | $E_{MPF.F2.2.1}$ [kwh/kg] | 0.43 |
| Energy consumption of heating system | $E_{MPF.F2.2.2}$ [kwh/kg] | 0.37 |
| Energy consumption of cooling system | $E_{MPF.F2.2.3}$ [kwh/kg] | 0.10 |
| Energy consumption of widening matrix | $E_{MPF.F2.3}$ [kWh/kg] | 0.42 |
| Total energy consumption of rolling equipment | $E_{MPF.F3}$ [kWh/kg] | 1.20 |
| Energy consumption for driving laminating rollers | $E_{MPF.F3.1}$ [kWh/kg] | 0.03 |
| Energy consumption for heating | $E_{MPF.F3.2}$ [kWh/kg] | 0.50 |
| Energy consumption for cooling | $E_{MPF.F3.3}$ [kWh/kg] | 0.67 |
| Total energy consumption for the process | $E_{MPF}$ [kWh/kg] | 2.57 |

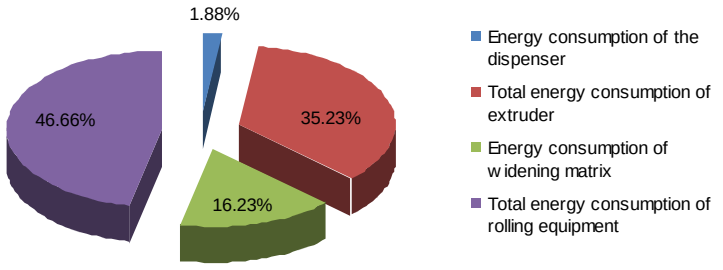


**Fig. 3** – The structure of energy consumption divided into phases of the manufacturing process of biodegradable agricultural film

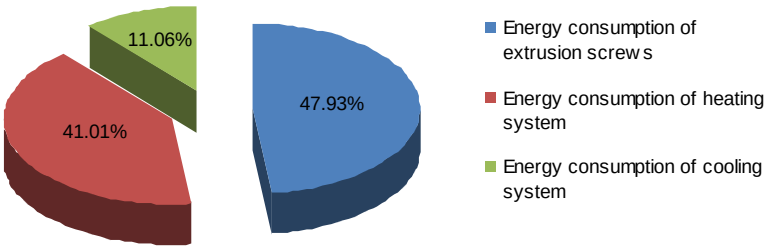


**Fig. 4** – The structure of energy consumption divided into stages of extrusion phase of biodegradable agricultural film

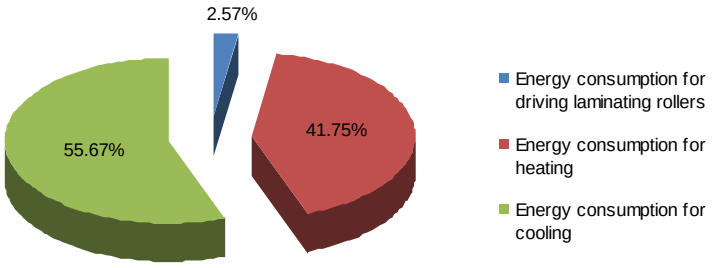


**Fig. 5** – Energy consumption structure divided into stages of rolling phase of biodegradable agricultural film

The analysis of energy consumption (Fig. 3) shows a maximum power consumption (46.66%) during the rolling, followed by energy consumption in the extrusion phase (35.23%), the phase of widening (16, 23%) and the dispenser (1.88%).

In the extrusion phase of the material (Fig. 4) The maximum power consumption is determined by the operation of the extrusion screws, followed by the heating (41.01%) and the cooling (11.06%). The energy required to drive the extrusion screws is influenced primarily by the extrusion screws speed which depends on the physical characteristics of the material and structural transformations that occur in the five phases of extrusion phase. Also, the energy consumption for the heating or cooling systems, depends on the working temperature in the 5 zones of the extruder which are determined based on the thermo-physical characteristics (glass transition temperature and the melting temperature) of the processed mixtures.

Energy-intensive stage of rolling is due to the cooling equipment (consuming about 55.67% of this total energy consumed in this phase of the process (Fig. 5), followed by heating equipment (41.75%) and driving the laminating rollers (2.57%).

The analysis of energy consumption in the manufacturing process for the respective phases of biodegradable agricultural film allows to identify equipment with high energy consumption. Thus, we can achieve energy optimization of the manufacturing process so that the energy consumed in the process to be minimized, thus ensuring a positive effect on the environment and optimum use of resources.

## CONCLUSIONS

Determining the energy consumption of the manufacturing process for biodegradable films produced from renewable sources, for agriculture is important both in terms of environmental impact and in terms of the use of energy resources needed. Such general mathematical method developed in this paper allows the determination of both total energy consumption of the manufacturing process of biodegradable agricultural film using various raw materials and to identify the main energy consumers, thus enabling optimization of the process energetically. This involves beneficial effects on the environment by saving resources, and an economic efficiency of the process.

Applying mathematical method for energetic analysis of manufacturing process for biodegradable agricultural film from renewable materials, using innovative technology developed by INMA Bucharest, Branch of Cluj-Napoca allowed assessment in terms of energy of the technology, on the one hand and on the other hand

Analiza structurii consumurilor energetice (fig.3) arată un consum maxim de energie (46,66%) în faza de laminare a materialului, urmat de consumul energetic din faza de extrudare (35,23%), a fazei de lățire (16,23%) şi respectiv al dozatorului (1,88%).

În faza de extrudare a materialului (fig.4) consumul energetic maxim se datorează acționării melcilor de extrudare, urmat de instalația de încălzire (41,01%) şi respectiv instalația de răcire (11.06%). Energia necesară pentru acționarea melcilor de extrudare este influențată în primul rând de turația melcilor de extrudare care depinde de caracteristicile fizice ale materialului şi transformările structurale care au loc pe parcursul celor 5 etape ale fazei de extrudare. De asemenea energia consumată de instalațiile de încălzire, respectiv răcire, este dependentă de temperatura de lucru pe cele 5 zone ale extruderului care se determină funcție de caracteristicile termofizice (temperatura de tranziție vitroasa şi temperatura de topire) ale amestecurilor procesate.

Consumului energetic ridicat în etapa de laminare se datorează echipamentului de răcire (acesta consumând circa 55,67% din energia totală consumată în această fază a procesului (fig.5), urmată de echipamentul de încălzire (41,75%) şi respectiv antrenarea valțurilor de laminare (2,57%).

Analiza structurii consumurilor energetice în fazele respectiv etapele procesului de fabricare a foliilor agricole biodegradabile permite identificarea echipamentelor cu consum energetic ridicat. Astfel putându-se realiza o optimizare energetică a procesului de fabricație astfel încât energia consumată în proces să fie cât mai redusă, asigurându-se astfel un efect pozitiv asupra mediului inconjurător şi o utilizare optimă a resurselor.

## CONCLUZII

Determinarea consumurilor energetice a procesului de fabricație a foliilor biodegradabile obținute din surse regenerabile, pentru agricultură este importantă atât din punct de vedere a impactului asupra mediului cât şi din punct de vedere a utilizării resurselor energetice necesare. Astfel metoda matematică generală dezvoltată în cadrul lucrării permite atât determinarea consumului energetic total al procesului de fabricație a foliilor agricole biodegradabile utilizând diverse materii prime, cât şi identificarea principalilor consumatori energetici, permițând astfel optimizarea procesului din punct de vedere energetic. Aceasta implicând efecte benefice atât asupra mediului înconjurător prin economie de resurse, cât şi o eficientizare economică a procesului.

Aplicarea metodei matematice în vederea analizei energetice a procesului de fabricare a foliilor agricole bidegradabile din surse regenerabile utilizând tehnologia inovativă dezvoltată de INMA Bucureşti, Sucursala Cluj-Napoca a permis evaluarea din punct de vedere energetic al tehnologiei pe de o parte iar pe de altă parte

the identification of rolling phase as the main consumer of energy (46,66%), followed by energy consumption in the extrusion phase (35.23%), the phase of widening (16, 23%) and the dispenser (1.88%).

Further development of the mathematical method proposed according to the specific manufacturing technology used will also allow the study of the influence of the mixtures physical-thermal characteristics from renewable material used as raw materials on the energy consumption of the phases or stages of the manufacturing process.

**Acknowledgement**

The results presented in this article were obtained under the project: New products, biodegradable, agriculture, renewable resources, Program „NUCLEU": Development System research, mechanization technologies, computerization, automation, management and technical equipment competitive for agriculture and food industry / Stimme, Contract number: 15 N / 27.02.2009 / Act ad.nr.1 / 2015.

**REFERENCES**

[1]. Briassoulis D., (2006) - *Mechanical performance and design criteria of biodegradable low-tunnel films*, Journal of Polymers and the Environment, vol.14, issue 2, ISSN 1566-2543, pg.289–307;

[2]. Briassoulis D., (2004) - *An Overview on the Mechanical Behavior of Biodegradable Agricultural Films*, Journal of Polymers and the Environment, vol.12, issue 2, ISSN 1566-2543, pg.65-81;

[3]. Briassoulis D., (2007) – *Analysis of the mechanical and degradation performances of optimized agricultural biodegradable films*, Journal of Polymer Degradation and Stability, vol.92, issue 6, pg.1115–1132;

[4]. Castillo L., Lópeza O., Lópeza C., Zaritzkyb N., Garcíab M., Barbosaa S., Villara M., (2013) - *Thermoplastic starch films reinforced with talc nanoparticles*, Carbohydrate Polymers, vol.95, issue 2, ISSN 0144-8617, pg.664– 674;

[5] Grigat, E., Koch, R., Timmermann, R. (1998) - *BAR 1095 and BAK 2195: completely biodegradable synthetic thermoplastics*, Biodegradable Polymers and Macromolecules, vol. 59, issue 1–3, pg. 223–226;

[6] Kapanen, A., · Schettini, E., Vox, G., et al. (2008) - *Performance and Environmental Impact of Biodegradable Films in Agriculture: A Field Study on Protected Cultivation*, Journal of Polymers and the Environment, vol. 16, issue 2, pp 109-122;

[7]. Kasirajan, S., Agron, M. N., (2012) - *Polyethylene and biodegradable mulches for agricultural applications: a review*, Agronomy for Sustainable Development, vol. 32, issue 2, ISSN: 1774-0746, pg.501–529;

[8]. Kyrikou I., Briassoulis D. (2007) - *Biodegradation of Agricultural Plastic Films: A Critical Review*, Journal of Polymers and the Environment, vol. 15, issue 2, ISSN: 1566-2543, pg.125–150;

[9]. López, O. V., Zaritzky, N. E., Grossmann, M., García, V.E. (2013) - *Acetylated and native corn starch blend films produced by blown extrusion*, Journal of Food Engineering, vol.116, issue 2, ISSN: 0260-8774, pg.286–297;

[10]. Rosentrater K. A., Otieno A. W., (2006) - *Considerations for manufacturing bio-based plastic products* , Journal of Polymers and the Environment, vol.14, issue 4, ISSN 1566-2543, pg.335–346.

a identificarea fazei de laminare ca fiind principalul consumator de energie (46,66%), urmat de consumul energetic din faza de extrudare (35,23%), a fazei de lățire (16,23%) şi respectiv al dozatorului (1,88%).

Dezvoltarea în continuare a metodei matematice propuse în concordanță cu specificul tehnologiilor de fabricație utilizate va permite de asemenea şi studiul influenței caracteristicilor fizico-termice ale amestecurilor din surse regenerabile utilizate ca materie primă asupra consumurilor energetice ale fazelor respectiv etapelor procesului de fabricație.

**Mulțumiri/Recunoştință**

Rezultatele prezentate în acest articol au fost obținute în cadrul proiectului : Produse noi, biodegradabile, pentru agricultura, din resurse regenerabile**,** Program NUCLEU**:** Dezvoltarea cercetarilor privind sistemele, tehnologiile de mecanizare, informatizare, automatizare, management şi echipamente tehnice competitive pentru agricultura şi industrie alimentara / STIMM, Numar contract**:** 15 N / 27.02.2009 / Act ad.nr.1/2015.

**BIBLIOGRAFIE**

[1]. Briassoulis D.. (2006) – *Performante mecanice si criterii de proiectare a foliilor biodegradabile pentru tunele joase*, Revista polimerilor si mediului, vol.14, nr.2, ISSN 1566-2543, pag.289–307;

[2]. Briassoulis D., (2004) – *O vedere de ansamblu asupra comportamentului mecanic al foliilor agricole biodegradabile*, Revista polimerilor si mediului, vol.12, nr. 2, ISSN 1566-2543**,** pag.65-81;

[3]. Briassoulis D., (2007) – *Analiza performantelor mecanice si de degradare a foliei agricole biodegradabile optimizate*, Revista Degradarea si Stabilitatea Polimerilor, vol.92, nr. 6, pag.1115–1132;

[4]. Castillo L., Lópeza O., Lópeza C., Zaritzkyb N., Garcíab M., Barbosaa S., Villara M., (2013) - *Folia din amidon termoplastic întarită cu nanoparticule de talc*, Polimeri Carbohidrați, vol. 95, nr.2, ISSN 0144-8617, pg.664– 674;

[5]. Grigat, E., Koch, R., Timmermann, R. (1998) – *Termomplasticile sintetice complet biodegradabile: BAR 1095 si BAK 2195:*, Polimeri biodegradabili şi Macromolecule, vol. 59, nr. 1–3, pag. 223–226;

[6]. Kapanen, A., Schettini, E., Vox, G., et al. (2008) – *Performanta si impactul asupra mediului a foliei biodegradabile in agricultura: Un studiu asupra cultivarii protejate*, Revista polimerilor si mediului, vol. 16, nr.2, pag 109-122;

[7]. Kasirajan, S., Agron, M. N., (2012) –P*olietilena si mulci biodegradabili pentru aplicațiile agricole*, Agronomia pentru dezvoltare sustenabilă, vol. 32, nr.2, ISSN: 1774-0746, pag.501–529;

[8]. Kyrikou I., Briassoulis D. (2007*)* – *Biodegradarea foliilor agricole din plastic: o recenzie critica*, Revista polimerilor si mediului, vol. 15, nr.2, ISSN: 1566-2543, pag.125–150;

[9]. López, O. V., Zaritzky, N. E., Grossmann, M., García, V.E. (2013) – *Folii acetilate si din amestec de amidon de porumb produse de extruziunea prin suflare*, Revista de Inginerie Alimentară, vol. 116, nr.2, ISSN: 0260-8774, pag.286–297;

[10]. Rosentrater K. A., Otieno A. W.(2006) - *Consideratii pentru realizarea produsele bio-plastice*, Revista polimerilor si mediului, vol. 14, nr.4, ISSN 1566-2543, pag.335–346.

# DETERMINATION OF THE RELAXATION TIME AT STATIC COMPRESSION OF IDARED APPLES VARIETY
# /
# *DETERMINAREA DURATEI DE RELAXARE LA SOLICITARI STATICE DE COMPRESIUNE A MERELOR DIN SOIUL IDARED*

**Ph.D.Eng. Veringă D.[1)], Ph.D.Eng. Vintilă M.[1)], Ph.D.Eng. Popa L.[2)], Ph.D.Stud.Eng.Ştefan V[2)], Ph.D.Stud.Eng.Petcu A.S. [2)]**
[1)] I.C.D.I.M.P.H. – HORTING Bucharest / Romania; [2)] INMA Bucharest / Romania
*Tel: 0745.148.071; E-mail: veringa.daniela@yahoo.com*

***Abstract:*** *Paper presents an experimental method of determining the static compression relaxation time of Idared apples variety, by preserving their integrity. Using the yield test by taking into account the viscous and elastic behaviour of the bodies described by physical rheological model of Burgers body made of elastic and viscous linear elements, the method theoretical groundwork was emphasized. A mathematical model and the suitable rheological equation describing the apples behaviour at steady static strain, has been found. Theoretical relations and experimental data are useful for evaluating (predicting) the storing time in packages which height is known.*

***Keywords:*** *apples, compression stress*

## INTRODUCTION

During the technological flow storing, the apple commercial value and quality are affected because of mechanical damage by crushing (contusion) of pulp tissue and also by apparition of deformations and deviations from characteristic shape.

Apple cellular tissue damage by contusion and remaining deformations visible through the geometrical shape modification, represent major causes of quality decrease and, consequently, of reduction of value and trading of fresh apples [7,8,12].

Value of losses represent10 – 12% out of the quantity stored [5,7], and for diminishing it, a suitable package should be chosen. Therefore, researches on finding the best solution between the package height, apple variety stored, ripening degree, time and conservation conditions, were performed.

Apple arranging height in packages has to be chosen so that any damage of fruits from lower rows do not produce, thus being detrimental to apples quality and class. Height limits depend on apple variety and ripening stage, characterized by a mechanical feature that can be a measure of rigidity (,,firmness") of fruit pulp [7,8,12].

## MATERIAL AND METHOD

### Theoretical aspects

As rheological material, fruits do not react to mechanical stress in terms of elasticity, their reaction combining an elastic component to a viscoelastic one [1,4].

When they are stored in bulk or arranged as a high pile for a longer period of time, the fruits are subject to a static load and, therefore deformation and damage may appear when pressure values are much smaller than those determined during the usual compression tests. For getting detailed data on apples deformation, a new technique allowing the automated time registering of continuous deformation under static load, has been drawn up.

***Rezumat:*** *Lucrare prezintă o metodă de determinare experimentală a duratei de relaxare la solicitări statice de compresiune a merelor din soiul Idared, cu menținerea integrității lor. Utilizând testul de fluaj prin considerarea comportării liniar vâscoelastice a corpurilor descrise de modelul fizic reologic al corpului Burgers format din elementele elastice şi vâscoase liniare s-au evidențiat bazele teoretice ale metodei. S-a găsit un model matematic şi ecuația reologica corespunzătoare care să descrie comportarea merelor la solicitări statice constante. Relațiile teoretice și datele experimentale sunt utile la evaluarea (predicția) duratei de depozitare în ambalaje de înălțime cunoscută.*

***Cuvinte cheie:*** *mere, solicitare la compresiune*

## INTRODUCERE

Pe fluxul tehnologic de depozitare de lungă durată, valoarea comercială și calitatea merelor sunt afectate datorită vătămărilor mecanice prin strivirea (contuzia) țesutului pulpei cât şi prin apariția deformațiilor şi abaterilor de la forma geometrică caracteristică.

Vătămarea prin contuzia țesutului celular la mere şi deformațiile remanente vizibile cu modificarea formei geometrice constituie cauzele majore a pierderilor de calitate şi în consecință a reducerii valorii și a gradului de comercializare în stare proaspătă a merelor [7,8,12].

Valoarea pierderilor reprezintă 10 – 12% din cantitatea depozitată [5,7], iar pentru reducerea acesteia este necesară alegerea adecvată a ambalajului utilizat. In acest sens s-au realizat cercetări privind obținerea corelației între înălțimea ambalajului, soiul de măr depozitat, gradul de coacere, durata şi condițiile de păstrare.

Înălțimea de aranjare a fructelor în ambalaje, trebuie astfel aleasă, încât să nu se producă defecte fructelor din rândurile inferioare şi să afecteze calitatea şi clasa merelor. Limitele de înălțime sunt funcție de soiul de mere şi de stadiul de coacere caracterizat printr-o proprietate mecanică ce poate fi o măsură a însuşirilor de rigiditate (fermitate ,,firmness") a pulpei fructelor [7,8,12].

## MATERIAL ŞI METODĂ

### Aspecte teoretice

Ca materiale biologice fructele nu reacționează la tensiuni mecanice, într-o manieră pur elastică, reacția lor combinând o componentă elastică şi una vâscoelastică [1,4].

La depozitarea în vrac sau în stivă înaltă pentru o durată mare de timp fructele sunt supuse unei sarcini statice și în acest caz deformarea şi vătămarea pot apare la valori ale presiunii, cu mult sub cele determinate la testele obişnuite de compresie. Pentru a obține date detaliate despre fluajul (deformarea) merelor, s-a elaborat o tehnică care permite înregistrarea automată în timp a deformației continue sub sarcină statică.

Tests on Idared variety apple behaviour during compression strain have emphasized, by deformation-time curves, the effect of time of application of deformation force and speed, demonstrating that the time effect is of practical importance in case of fruit deformation under static load. [1,4,7].
It has been tried to find out a mechanical model and its appropriate rheological equation which be suitable to experimental flow curve, similar to that from fig. 1.(through Burgers model (fig. 1a), where deformation-time curves obtained with this model are overlapping. Consequently, this curve simulates apple behaviour under static load. Following the compression tests made on whole apples located between two plane plates, the deformation-time curves have had the same profile as the curve from fig. 1 b, concluding that this curve might be described through a Burges model type, fig. 2, [2,8]. This new model type has been obtained from the classical model, by replacing: $\varepsilon \rightarrow \delta$, $\sigma \rightarrow F$, $E \rightarrow K$, $\eta \rightarrow \eta^*$, as one can see in fig.2. Appropriate experimental tests have the advantage of being performed more easily along with preserving the fruit integrity [9,11,12].

Testele privind comportarea la solicitarea de compresiune a merelor din soiul Idared au evidențiat, prin curbele forță-deformație efectul timpului de aplicare a forței şi a vitezei de deformare, dovedindu-se că efectul timpului este de importanță practică pentru cazul de fluaj al fructelor sub sarcină statică [1,4,7].
S-a încercat să se găsească un model mecanic şi ecuația reologica corespunzătoare care să se potrivească curbei de fluaj experimentală, similară celei din fig.1.(b) prin considerarea modelului Burgers (fig.1a), în care curbele deformație – timp obținute cu acest model se suprapun. In consecință, această curbă simulează comportamentul fructelor de măr sub sarcină statică.
Din testele de compresiune realizate pe merele întregi amplasate între două plăci plane s-au obținut curbe de deformație – timp cu acelaşi profil cu curba din fig. 1 b, fapt ce a permis ipoteza că se poate descrie această curbă printr-un model tip Burgers, fig. 2, [2,8]. Acest nou tip de model s-a obținut din modelul clasic prin înlocuirile: $\varepsilon \rightarrow \delta$, $\sigma \rightarrow F$, $E \rightarrow K$, $\eta \rightarrow \eta^*$, aşa cum se poate urmări în fig.2. Testele experimentale corespunzătoare au avantajul că se pot efectua mai comod, cu menținerea integrității fructului [9,11,12].

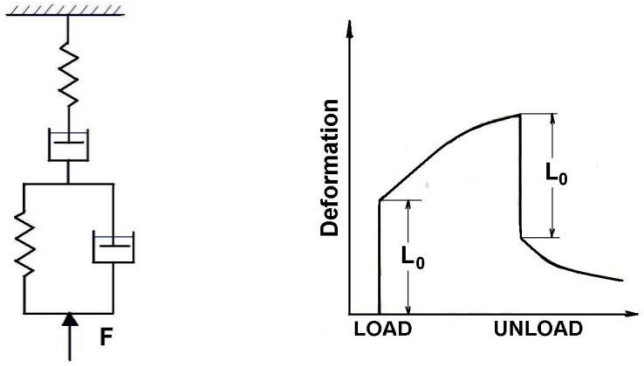


**a)** **b)**

**Fig. 1 -** Burgers physical model(a) and its deformation-time curve (b)

Establishing the rheological equation suitable to fruit behaviour at static compression was performed by taking into account the physical model of Burgers type and also the fact that equations appropriate to ideal elements state are:

- for the ideal elastic element, Hooke:

$$F = K \cdot \delta \quad (1)$$

- for ideal viscous element, Newton:

$$F = \eta^* \cdot \dot{\delta} \quad (2)$$

where
δ is deformation;
K-rigidity of elastic element [N/m];
$\eta^*$- size similar to viscosity of ideal viscous element [Ns/m].

Stabilirea ecuației reologice corespunzătoare comportării fructului la solicitarea de compresiune statică, s-a făcut ținând cont de modelul fizic tip Burgers şi s-a avut în vedere că ecuațiile de stare corespunzătoare elementelor ideale sunt:

- pentru elementul ideal elastic, Hooke:
- pentru elementul ideal vâscos, Newton:

unde
δ este deformația;
K-rigiditatea elementului elastic [N/m];
$\eta^*$- mărime similară vâscozității elementului ideal vâscos [Ns/m].

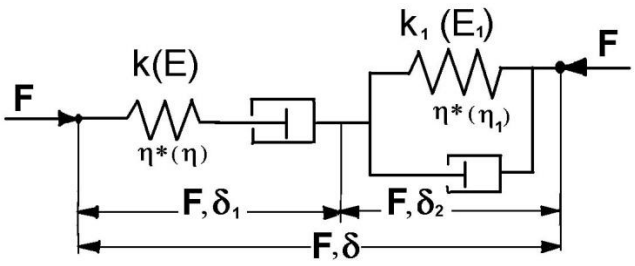


**Fig. 2** - Burgers type physical model for describing the compression behavior of the whole apple

Body represented by Burgers model, subject to a constant compression force, F = $F_0$ = const. will have a time deformation given by equation:

Corpul reprezentat prin modelul tip Burgers, supus acțiunii unei forțe de compresiune constante, F = $F_0$ = const. va avea o deformație în timp dată de ecuația:

$$\delta = \frac{F_0}{K} + \frac{F_0}{\eta^*}t + \frac{F_0}{K_1}\left(1 - e^{-\frac{t}{T_i}}\right) \quad (3)$$

**Working method**

For performing the experiments, The Idared apple variety, coming from Institute of Research-Development for Tree Growing Piteşti - Mărăcineni Argeş, was chosen, the harvesting being manually made when fruits were completely ripen.

Apple samples chosen were of different sizes, randomly selected, but though, trying to find samples with apples closer of spherical shape. Up to tests performing, apples were kept in refrigerating cells at 3-4$^0$ C temperature and 80 – 85% relative humidity.

Before performing the tests, the apples were taking out from the cells and kept in laboratory at ambient temperature during, at least 4 – 5 hours, for reaching environment temperature.

In order to perform the deformation tests for finding out the elasticity module relaxation to apple static compression strain and relaxation time, the apparatus whose scheme is shown in fig 3a), has been designed and manufactured. In fig. 3(b,c) are presented images of apparatus aimed to perform the measurements. According to testing procedure, the apple is subject to static compression by pressing down, with a steady load, either with a rigid plane plate, fig.3(c), or another half of apple fig. 3(b) and deformation is measured by means of a comparing clock, at differenttime moments, at the beginning of feeding.

**Metoda de lucru**

Pentru efectuarea experimentărilor s-a ales soiul de măr Idared, provenit de la Institutul de Cercetare – Dezvoltare pentru Pomicultură Piteşti - Mărăcineni Argeş, recoltarea s-a făcut manual când fructele s-au aflat în stadiul deplinei maturități.

Probele de mere au fost de diferite dimensiuni, selectate în mod aleatoriu, căutându-se totuşi probele cu o formă apropiată de cea sferică. Până la efectuarea experimentărilor merele au fost păstrate în celule frigorifice la o temperatură de 3-4$^0$ C şi o umiditate relativă de 80 – 85%.

Inainte de efectuarea experimentărilor, fructele au fost scoase din celule şi ținute în laborator la temperatura camerei o durată de cel puțin 4 – 5 ore pentru a avea temperatura mediului.

In scopul efectuării testelor de fluaj în vederea determinării relaxării modulului de elasticitate şi a duratei de relaxare la solicitări statice de compresiune a merelor a fost conceput, proiectat şi realizat aparatul a cărui schemă este prezentată în fig. 3a. In fig. 3(b,c) sunt prezentate vederi ale aparatului pregătit pentru efectuarea măsurătorilor. In conformitate cu procedura de testare, mărul este supus la solicitarea de compresiune statică prin apăsarea, cu o sarcină constantă, fie a unei plăci plane rigide fig.3(c) fie a unei alte jumătăți de măr fig. 3(b) iar deformația este măsurată cu ajutorul unui ceas comparator, la diferite momente de timp la începutul încărcării.

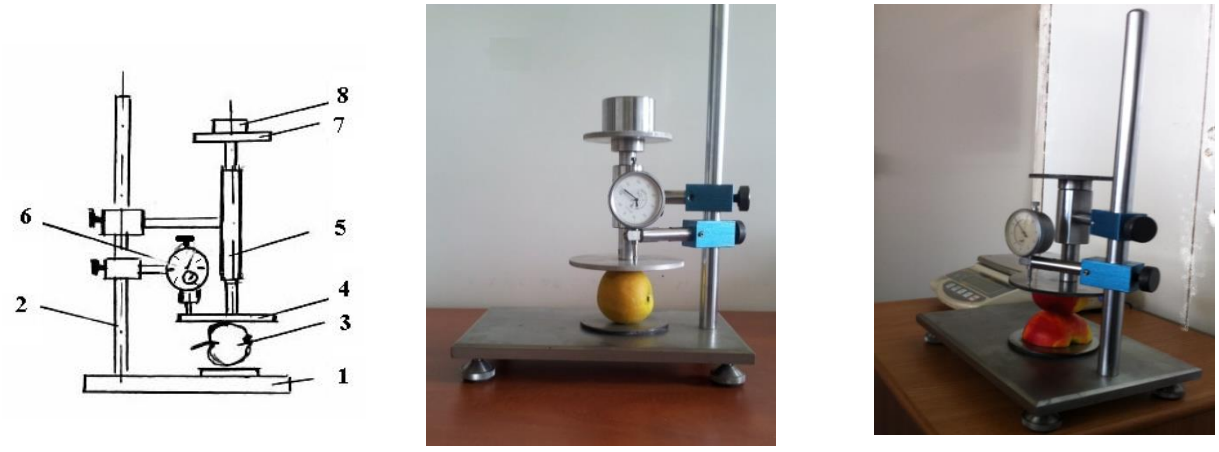


**a)** **b)** **c)**

**Fig. 3** – Scheme of apple compression deformation testing apparatus

*1- main plate; 2-support; 3-apple 4- rigid pressing plate; 5- guidance; 6- comparing clock; 7-pan 8-load*

Tests were performed in two variants, namely with the whole fruit (fig.3 b) and with halves of fruit (fig.3c). The apple was divided by a sharp knife with rigid blade and one apple half was laid on fixed surface of apparatus. The upper cup was charged with the mass appropriate to a constant pressing force F=15 N. The rigid plate was brought into contact with apple surface and cup rod was released for compression performing.

Deformation δ(t) at different moments of time was measured in seconds, starting from the beginning of strain, from 15 seconds to 15 seconds for 10 readings, from 30 seconds to 30 seconds for 5 readings, at 1

Experimentările au fost efectuate în două variante cu fructul întreg (fig.3 b) şi cu jumătăți de fruct (fig.3c). S-a secționat mărul într-un plan axial cu ajutorul unui cuțit bine ascuțit cu lama rigidă şi una din jumătăți s-a aşeazat pe suprafața fixă a aparatului. S-a încărcat platanul superior cu masa de încărcare corespunzătoare unei forțe constante de apăsare F=15 N. S-a adus placa rigidă în contact cu suprafața mărului şi s-a eliberat tija platanului pentru realizarea solicitării la compresiune.

S-a măsurat deformația δ(t) la diferite momente de timp măsurate în secunde, de la începutul solicitării din 15 în 15 secunde pentru 10 citiri, din 30 în 30 secunde

minute for 5 readings, from 5 to 5 minutes for 5 readings, from 10 minutes to 10 minutes for 5 readings and from 15 minutes to 15 minutes for 5 readings, which required a period of 2.5 hours for each experiment for which 35 values have been measured.

The elasticity module E was calculated in each point..

## RESULTS

Compression deformation experiments have been performed at pressing loads of 12.5 N; 15 N; 17.5 N for the two variants. Deformations δ for different times have been measured and values o Young elasticity modules have been calculated.

Data obtained are shown in Tab.1.

pentru 5 citiri, la 1 minut pentru 5 citiri, din 5 în 5 minute pentru 5 citiri, din 10 în 10 minute pentru 5 citiri şi din 15 în 15 minute pentru 5 citiri, ceea ce a necesitat o durată de 2,5 ore pentru fiecare experiment pentru care s-au măsurat 35 de valori.

S-a calculat în fiecare punct modulul de elasticitate E.

## REZULTATE

Experimentările de fluaj la compresiune au fost efectuate la sarcini de apăsare de 12,5 N; 15 N; 17,5 N pentru cele două variante. Au fost măsurate deformaţiile δ pentru diferiţi timpi şi calculate valorile modulelor de elasticitate Young.

Datele obţinute sunt prezentate în Tab.1.

**Table 1**

**Data of deformation test at constant force compression, deformation δ(t) at different time intervals t and elasticity longitudinal module – selective data**

| Timel [s] | F= 12,5 N | | | | F= 15 N | | | | F= 17,5 N | | | |
|---|---|---|---|---|---|---|---|---|---|---|---|---|
| | apple between plates | | apple/apple | | apple between plates | | apple/apple | | applebetween plates | | apple/apple | |
| | δ [mm] | E*10$^6$ [Pa] | δ [mm] | E*10$^6$ [Pa] | δ [mm] | E*10$^6$ [Pa] | δ [mm] | E*10$^6$ [Pa] | δ [mm] | E*10$^6$ [Pa] | δ [mm] | E*10$^6$ [Pa] |
| 15 | 0.48 | 4.07 | 0.66 | 8.62 | 0.60 | 3.81 | 0.77 | 7.82 | 0.64 | 4.12 | 0.74 | 8.61 |
| 45 | 0.51 | 3.69 | 0.73 | 7.45 | 0.66 | 3.30 | 0.83 | 6.95 | 0.66 | 3.89 | 0.83 | 7.34 |
| 75 | 0.53 | 3.51 | 0.77 | 6.91 | 0.68 | 3.14 | 0.86 | 6.56 | 0.69 | 3.68 | 0.87 | 6.84 |
| 105 | 0.54 | 3.37 | 0.79 | 6.56 | 0.70 | 3.03 | 0.88 | 6.34 | 0.71 | 3.51 | 0.89 | 6.58 |
| 135 | 0.56 | 3.25 | 0.81 | 6.39 | 0.71 | 2.95 | 0.90 | 6.15 | 0.73 | 3.39 | 0.91 | 6.35 |
| 180 | 0.57 | 3.17 | 0.83 | 6.17 | 0.74 | 2.80 | 0.92 | 5.93 | 0.75 | 3.22 | 0.93 | 6.11 |
| 240 | 0.58 | 3.06 | 0.85 | 5.97 | 0.76 | 2.65 | 0.94 | 5.75 | 0.77 | 3.14 | 0.96 | 5.88 |
| 300 | 0.59 | 2.99 | 0.86 | 5.85 | 0.78 | 2.54 | 0.96 | 5.58 | 0.78 | 3.08 | 0.98 | 5.71 |
| 420 | 0.6 | 2.89 | 0.87 | 5.68 | 0.81 | 2.40 | 0.98 | 5.41 | 0.82 | 2.90 | 1.00 | 5.52 |
| 540 | 0.61 | 2.81 | 0.89 | 5.50 | 0.84 | 2.30 | 1.00 | 5.26 | 0.83 | 2.77 | 1.02 | 5.36 |
| 900 | 0.64 | 2.64 | 0.92 | 5.28 | 0.88 | 2.15 | 1.01 | 5.16 | 0.87 | 2.60 | 1.06 | 5.07 |
| 1500 | 0.67 | 2.46 | 0.93 | 5.18 | 0.92 | 2.01 | 1.02 | 5.10 | 0.90 | 2.49 | 1.09 | 4.86 |
| 2100 | 0.69 | 2.35 | 0.94 | 5.12 | 0.94 | 1.95 | 1.03 | 5.05 | 0.92 | 2.40 | 1.11 | 4.72 |
| 3300 | 0.72 | 2.21 | 0.95 | 4.99 | 0.96 | 1.87 | 1.04 | 4.95 | 0.94 | 2.30 | 1.14 | 4.52 |
| 4500 | 0.74 | 2.12 | 0.98 | 4.80 | 0.99 | 1.80 | 1.06 | 4.81 | 0.97 | 2.21 | 1.16 | 4.42 |
| 6000 | 0.76 | 2.03 | 1.01 | 4.58 | 1.01 | 1.74 | 1.09 | 4.61 | 0.99 | 2.11 | 1.18 | 4.29 |
| 7800 | 0.79 | 1.89 | 1.05 | 4.32 | 1.03 | 1.69 | 1.10 | 4.53 | 1.04 | 2.00 | 1.20 | 4.19 |
| 9600 | 0.80 | 1.88 | 1.08 | 4.11 | 1.06 | 1.62 | 1.11 | 4.47 | 1.07 | 1.90 | 1.22 | 4.10 |

Based on the data obtained following the experiments, deformation δ depending on time (t) was represented by points, in fig.4 – fig.6 for stress scheme apple between plates and in fig.7 – fig.9 for apple/apple stress scheme..

By means of Microcal Origin program, experiments data were processed, testing the equation (4) for module relaxation through non-linear regression with experimental data and appropriate curves were represented comparing to experimental data in the same graphics – fig.4 – fig.9.

Pe baza datelor obţinute din experimente s-au reprezentat prin puncte deformaţia δ în funtie de timp (t) în fig. 4 – fig.6 pentru schema de solicitare măr între plăci şi în fig.7 – fig.9 pentru schema de solicitare măr/măr .

Cu ajutorul programului Microcal Origin s-au prelucrat datele obţinute din experimentări, testându-se ec.(4) pentru relaxarea modulului prin regresie neliniară cu datele experimentale şi curbele corespunzătoare au fost reprezentate, comparativ cu datele experimentale, pe aceleaşi grafice – fig.4 – fig.9.

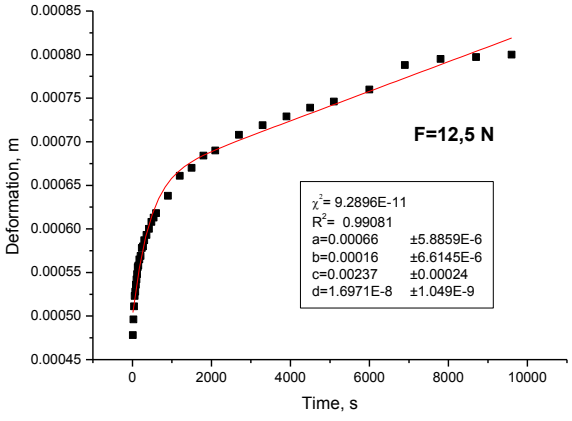


**Fig.4** – Deformation curve δ(t) depending on time, for Idared apples at F=12,5 N

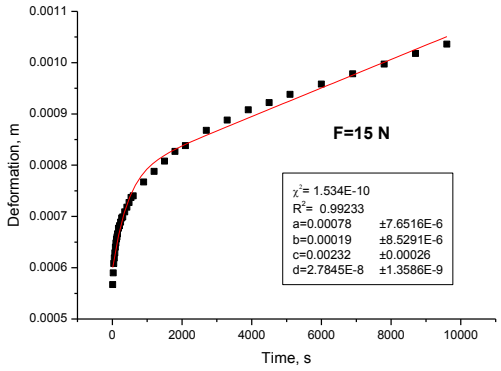


**Fig.5** - Deformation curve δ(t) depending on time, for Idared apples at F=15 N

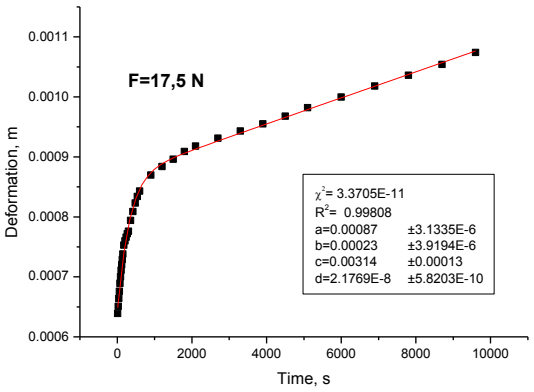


**Fig.6** - Deformation curve δ(t) depending on time, for Idared apples at F=17,5 N

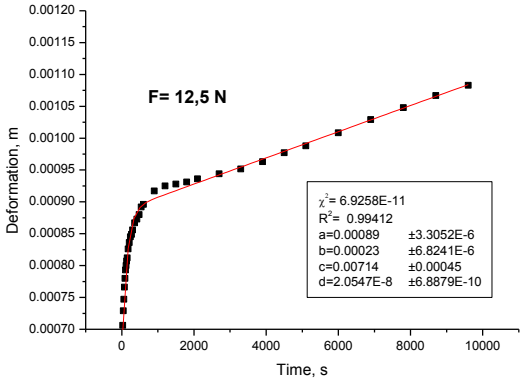


**Fig.7** – Curve of deformation δ(t) depending on time for Idared apples at F=12.5 N

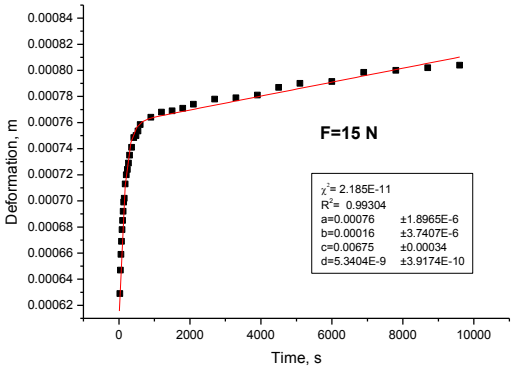


**Fig.8** - Curve of deformation δ(t) depending on time for Idared apples at F=15 N

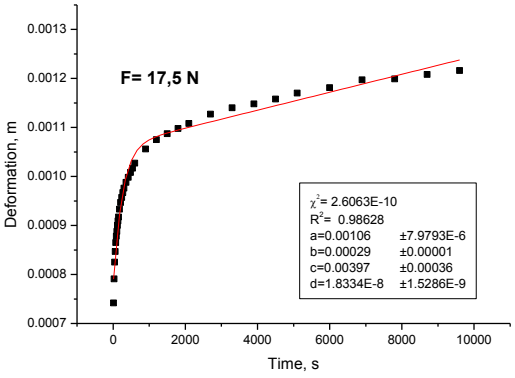


**Fig.9** - Curve of deformation δ(t) depending on time for Idared apples at F=17,5 N

## CONCLUSIONS

In technological flow, from harvesting to market, including the log time storing, operations which fruits are subject may produce mechanical damages (harvesting, sorting, storage, etc.) that affect their quality [6]. Damages are produced when strains surpass the elastic limit of fruit pulp, reaching its breaking resistance, fact manifested by crushing the fruit pulp tissue or apparition of deformations and deviations from characteristic geometrical shape.

Considering the linear viscoelastic behaviour of bodies described by physical rheological model of Burgers body,

## CONCLUZII

In lanțul tehnologic de la recoltare la comercializare, inclusiv cu păstrare de lungă durată, operațiile la care sunt supuse fructele (recoltare, sortare, depozitare, etc.) pot produce vătămări mecanice ce le afectează calitatea [6]. Vătămările se produc când tensiunile depăşesc limita elastică a pulpei fructului, atingând rezistența la rupere a acesteia, fapt manifestat prin strivirea țesutului pulpei fructului sau apariția unor deformații şi abateri de la forma geometrică caracteristică.

Considerând pentru fruct, comportarea liniar

the paper substantiates an experimental determination method of relaxation time at static compression strains. At the same time, using the deformation test, a mathematical model describing the static compression behaviour of apples is presented; it is necessary to prognosis of fruit package height, so that mechanical damages during the storing-conservation period be avoided and allow the prediction of storing time in certain packages.
A mechanical model and its appropriate rheological equation were found in order to match to experimental deformation curve, similar to that from fig.1.b, by considering the Burgers model (fig.1a), where the deformation time curves, obtained with this model are overlapped. Consequently, this curve simulates the apple behaviour subject to static load [3,10,13].

**REFERENCES**

[1]. Abbott J.A., R. Lu. (1996), *Anisotropic mechanical properties of apples*, Transactions of the ASAE, vol.39(4), pp.1451-1459;
[2]. Căsăndroiu T., Oprița N. (1994), *Experimental researches on evaluation of compression and penetration behaviour of certain apple varieties*, Scientific research report at Ctr.no.1530/25.05.1994, UPB Bucharest - ICDVPH- Bucharest);
[3]. Căsăndroiu T., Ivănescu D. (2009), *Theoretical aspects on mathematical modelling of the maximum allowable static compression received to no mechanical injury in apples*, MOCM, volume 15 (2), Alma Mater Publishing House, Bacău, pp.29-38;
[4]. Fridley R.B., Adrian P.A. (1966), *Mechanical properties of peaches, pears, apricots and apples*, Trans. Of the ASAE, volume 9(1), pp.135-138;
[5]. Gherghi A., Iordăchescu C., Burzo I. (1979), *Maintaining quality of fresh vegetables and fruits*, Tehnica Publishing House, Bucharest;
[6]. Milică C. I., Bărbat I. (1977) – *Vegetal physiology*, Didactical and Pedagogical Publishing House, Bucharest;
[7]. Mohsenin N.N. (1970), *Physical properties of plant and animal materials*, Gordon and Breach Science Publishers, N.Y.;
[8]. Nelson C.W., Mohsenin N.N. (1968), *Maximum allowable static and dynamic loads and effect of temperature for mechanical injury in apples*, J. Agric. Engng. Res., vol.13(4), pp.305-317;
[9]. Ross J.J., Isaacs G.W. (1961), *Forces acting in stacks of granular materials (part I)*, Trans. Of the ASAE, 4(1), pp.92-96;
[10]. Roudot A.C., Duprat F., Weinian C. (1991), *Modelling the response of apples to loads*, J. Agric. Eng. Res., vol.48, pp.249-259;
[11]. Rumsey T.R., Fridley R.B. (1977), *Analysis of viscoelastic contact stress in agricultural products using a finite element method*, Transactions of the ASAE, vol.20(1), pp.162-167;
[12]. Shahabasi Y., Segerlind L.J., Carroll N.J. (1995), *A simulation modal to determine the allowable depth for apples stored in bulk*, Transactions of the ASAE, vol.38(2), pp.587-591
[13]. Yang W.H. (1966), *The contact problem for viscoelastic bodies*, Applied Mechanics Journal, pp.395-401.

vâscoelastică a corpurilor descrise de modelul fizic reologic a corpului Burgers, în lucrare se fundamentează o metodă de determinare experimentală a duratei de relaxare la solicitări statice de compresiune. Totodată utilizând testul de fluaj se prezintă un model matematic pentru descrierea comportării la compresiune statică a merelor necesar la prognozarea înălțimii de aranjare a fructelor în ambalaje, astfel încât să evite apariția vătămărilor mecanice pe durate de depozitare – păstrare, şi a predicției duratei de depozitare în anumite ambalaje.
S-a găsit un model mecanic şi ecuația reologica corespunzătoare care să se potrivească curbei de fluaj experimentală, similară celei din fig.1b prin considerarea modelului Burgers (fig.1 a), în care curbele deformație – timp obținute cu acest model se suprapun. In consecință, această curbă simulează comportamentul fructelor de măr sub sarcină statică [3,10,13].

**BIBLIOGRAFIE**

[1]. Abbott J.A., R. Lu. (1996), *Proprietatile anizotropice mecanice ale merelor*, Transactions of the ASAE, vol.39(4), pag.1451-1459;
[2]. Căsăndroiu T., Oprița N. (1994), *Cercetări experimentale privind evaluarea comportării la compresiune şi la penetrare a unor soiuri de mere*, Raport şt.de cercetare, Ctr.1530/1994, UPB-ICDVPH-RA;
[3]. Căsăndroiu T., Ivănescu D. (2009), *Aspecte teoretice privind modelarea matematica a compresieimaxime statice permisibile care să nu vătămeze merele din punct de vedere mecanic*, MOCM, vol 15 (2), Ed. Alma Mater, Bacău, pag.29-38;
[4]. Fridley R.B., Adrian P.A. (1966), *Proprietatile mecanice ale piersicilor, perelor, caiselor si merelor*, Trans. Of the ASAE, vol 9(1), pag.135-138;
[5]. Gherghi A., Iordăchescu C., Burzo I. (1979), *Menținerea calității legumelor şi fructelor în stare proaspătă*, Ed. Tehnica, Bucureşti;
[6]. Milică C. I., Bărbat I. (1977) – *Fiziologia vegetală*, Ed. Didactică Pedagogică, Bucureşti;
[7]. Mohsenin N.N. (1970), *Proprietatile fizice ale materialelor provenite din plante si animale*, Editura Gordon and Breach Science Publishers, N.Y.
[8]. Nelson C.W., Mohsenin N.N. (1968), *Sarcinile statice si dinamice maxime permisibile si efectul temperaturii asupra vatamarii mecanice a merelor*, J. Agric. Engng. Res., vol.13(4), pag.305-317;
[9]. Ross J.J., Isaacs G.W. (1961), *Fortele care actioneaza asupra materialelor granulare sub forma de stiveces acting in stacks of granular materials (partea I)*, Trans. Of the ASAE, 4(1), pag.92-96;
[10]. Roudot A.C., Duprat F., Weinian C. (1991), *Modelarea raspunsului merelor asupra sarcinilor*, J. Agric. Eng. Res., vol.48, pag.249-259;
[11]. Rumsey T.R., Fridley R.B. (1977), *Analiza solicitarii de contact vasco-elastice asupra produselor agricole prin folosirea metodei elementelor finite*, Jurnalul Transactions of the ASAE, vol.20(1), pag.162-167;
[12]. Shahabasi Y., Segerlind L.J., Carroll N.J. (1995), *Un model de simulare pentru a determina adancimea permisibila pentru merele depozitate in vrac*, Jurnalul Transactions of the ASAE, vol.38(2), pag.587-591
[13]. Yang W.H. (1966), *Problema de contact pentru corpurile viscoelastice*, Revista de Mecanica Aplicata, pag.395-401.

# OPTIMIZATION DESIGN OF FRUIT PICKING END-EFFECTOR BASED ON ITS GRASPING MODEL
# /
# 基于抓取模型的水果采摘末端执行器优化设计

**Assoc. Prof. Ms. Lin Hanhui[1)], Assoc. Prof. Ph.D. Cai Ken *[2)] ,**
**Assoc. Prof. Ph.D. Chen Huazhou[3)], Eng. Zeng Zhaofeng[4)]**
[1)] Center for Educational Technology, Guangdong University of Finance and Economics, Guangzhou / China;
[2)] School of Information Science and Technology, Zhongkai University of Agriculture and Engineering, Guangzhou / China;
[3)] College of Science, Guilin University of Technology, Guilin / China;
[4)] Department of Mathematics and Computer Science, California State University, East Bay / U.S.A
** Tel: +8634172680; Email: icken@126.com*

***Abstract:*** *The development of intelligent fruit harvesting robots is important in improving agricultural production. In this paper, we initiated the R&D of a mechanical end-effector for fruit harvesting on the basis of the intelligence of agricultural robots. First, we provided a detailed description of the hardware components and software control of the mechanical end-effector, analyzed the mechanism of servo controlling and established a mathematical modelling of the mechanical end-effector junctions by analyzing the harvesting movement. Thereafter, the coordinates of the target fruits are disassembled and analyzed in the context of the mathematical model for precise locating and harvesting. Finally, a trail experiment of harvesting kiwifruit was conducted. The outcome implies that each module in the harvesting robot system functions well. The proposed mathematical modelling method and servo control can provide accurate harvesting movements to the mechanical end-effector.*

***Keywords:*** *picking, end-effector, motion optimization, models*

***摘要:*** *智能化果蔬采摘机器人的开发，对于提高农业生产力有极大的应用价值与现实意义。本论文根据农业机器人的智能化发展需要，研发了能对果实进行采摘的末端执行器。对果实采摘末端执行器的硬件构造和软件设计进行了描述，分析了舵机的控制原理，并通过对末端执行器采摘果实动作的分析，对采摘末端执行器各关节进行数学建模，然后将目标果实坐标通过数学建模进行拆解分析，使得末端执行器可以准确移动到果实的位置并进行准确采摘。最后进行了猕猴桃的采摘作业试验，试验结果表明:系统各模块运转良好，提出的建模方法与舵机控制方法可实现采摘末端执行器的精确移动和准确采摘。*

***关键词:*** *采摘；末端执行器；运动优化；模型*

## INTRODUCTION

Great efforts have been made in the past decades in the use of robots for selective harvesting, which is the most time-consuming process in agricultural operations. In natural environments, the growth of fruits depends on soil, season, and weather, which varies enormously and hinders precise locating and harvesting. Therefore, the research and development of high-end robots with accuracy and efficiency has become increasingly significant in agricultural harvesting [2,8,10,11]. Such a study has been performed for more than 40 years in many countries [16,21,18,6]. Japan, the United States, and some developed European countries have been working relentlessly on the R&D of harvesting robots. In Japan, eggplant-harvesting robots spend 64.1 s in picking one eggplant and have success rates of 62.5% [7]. Grape-harvesting robots are not only capable of harvesting but also of spraying, bagging, and clipping [1]. Kiwifruit-harvesting robots have harvesting speeds of 74.6 s for each fruit and suction attachment success rates of 95.3% [3]. Wageningen University designed cucumber-harvesting robots that utilise near-infrared visual system to identify cucumbers with success rates of approximately 70% [15]. Mushroom-harvesting robots designed in the United Kingdom can harvest one mushroom in 1.5 s with a success rate of 75% [4]. Melon-harvesting robots designed in Israel and the United States can achieve a success rate of over 85% during identification and harvesting [5]. The apple-harvesting

## 引言

过去的几十年里，人们在农业运作最为耗时的选择性采摘果实方面已经做出了巨大的努力。在自然环境中，水果的生长依赖于土壤、季节和天气，这些因素变化极大，阻碍了精确的定位和收获。因而，研究和开发有着高精度和高效率的农业采摘高端机器人的是非常重要的[2,8,10,11]。40 年前在许多国家已经进行这方面的研究[16,21,18,6]。日本、美国和一些发达国家一直致力于研发采摘机器人。日本茄子采摘机器人花费 64.1 秒采摘一个茄子，成功率达到 62.5%[7]。葡萄采摘机器人不仅能够采摘，而且可以喷药、套袋和裁剪[1]。猕猴桃采摘机器人对每个果实采摘速度达到 74.6 秒，成功率达到 95.3%[3]。瓦赫宁根大学设计的黄瓜收获机器人，利用近红外视觉系统，以确定黄瓜并成功采摘的概率约为 70%[15]。英国设计的磨菇采摘机器人采摘一个磨菇的时间是 1.5 秒，成功率达到 75% [4]。以色列和美国设计的甜瓜采摘机器人可以实现在识别和采摘，成功率达到 85%以上[5]。韩国庆北

robots developed by Kyungpook National University in South Korea can identify cucumbers from the tree crown with a success rate of 85% and harvesting speed of 5 s for each cucumber [17]. The mushroom-harvesting robots by Silsoe Research Institute in the United Kingdom can harvest at the speed of 6.7 s for each mushroom with a success rate of 75% [13]. In China, the study of harvesting robots has made significant progress in recent years. China Agricultural University has developed cucumber-harvesting robots and vegetable-grafting robots [20, 9], Nanjing Agricultural University has furthered the visual navigation system to enable automatic operations [22], and Zhejiang University has designed and optimized the visual positioning and harvesting components of robots [19]. All of these studies have accelerated the development of agricultural informatics and automation in China. In the present paper, the position coordinates of fruits were obtained from a binocular system. The necessary movement at each end-effector junction was controlled according to the 3D coordinate analytic algorithm. The revolving angle of each servo was manipulated to stretch the mechanical arm to the target fruit and for harvesting.

## MATERIAL AND METHODS

### *The Harvesting End-effector*

The system uses an end-effector (Figure 1) that is made of aluminium alloy brackets and servos. The entire end-effector is equipped with two MG995 servos and three MG996R servos. The picking tool has a highly mimicking design. In harvesting, only No.3, No.4, No.5, No.6, and No.7 servos are involved, whereas the No.2 servo is a back-up that is temporarily immovable and is vertically upward. The No.3 servo controls the base rotation, thereby controlling the movement direction of the picking robot. The No.4 and No.5 servos control the main body of the arm, which is equivalent to the hand control of humans controlling lifting and other actions. The No.6 servo, the equivalent of a human's wrist, controls the vertical movement when picking fruits. The No.7 servo controls the opening or closing of metal pincers, similar to a human's fingers. The respective location of each servo in the harvesting end-effector is shown in Figure 1(a).

国立大学研制的苹果收获机器人，在树冠上能识别 85%的黄瓜，并用 5 秒的时间采摘一个果实[17]。由英国 Silsoe 研究院研发的磨菇采摘机器人用 6.7 秒的时间采摘一个磨菇，成功率达到 75% [13]。近年来，中国在采摘机器人方面的研究取得巨大进展。中国农业大学已经研发了黄瓜采摘机器人和蔬菜嫁接机器人[20, 9]。南京农业大学在运用自动操作的可视化导航系统方面已经取得一定成就[22]。浙江大学设计并优化了机器人的视觉定位和采摘组件[19]。所有这些研究加速中国农业的自动化和信息化。在本文，从双目系统获得水果的位置坐标。在末端执行器连接处必须的移动由 3D 坐标分析算法控制。操纵每一个伺服的旋转角度，以拉伸机械臂触及采摘目标水果。

## 材料与方法

### *采摘末端执行器*

系统采用的采摘末端执行器如图 1 所示，它由铝制合金结构的支架和舵机构成，整个采摘末端执行器配置了两个 MG995 与三个 MG996R 舵机。该采摘工具高度模仿人体手臂，采摘过程只涉及末端执行器的 3、4、5、6、7 号舵机，而 2 号舵机为后备移动舵机，是暂时性固定不动竖直向上的。3 号舵机控制着末端执行器的底座转动，从而控可采摘的方向；4、5 号舵机控制着末端执行器的主要躯干，相当于人体手臂部分，控制着抬举等动作；6 号舵机控制着末端执行器采摘果实的上下移动，相当于人体手腕关节；7 号舵机则控制着采摘终端金属钳子的伸张，相当于人体手部位置。末端执行器的各舵机具体位置如图 1(a) 所示。

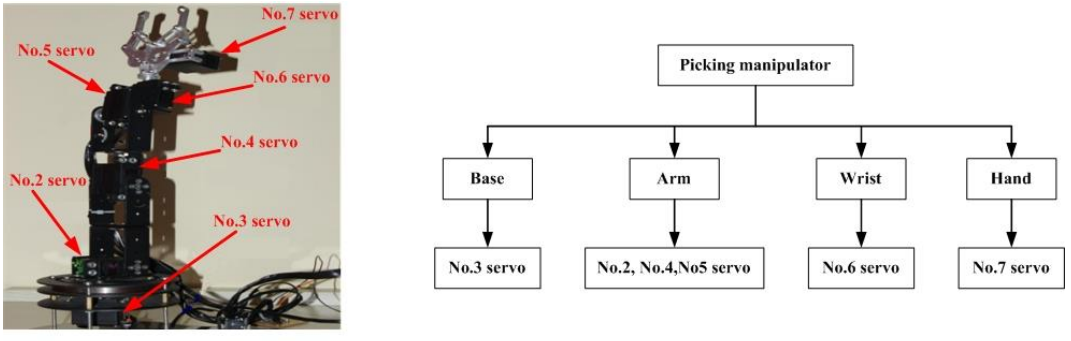


**Fig.1** - Picking robot chart. (a) The specific location of each servo. (b) Picking end-effector joint control.

### *Control of Harvesting End-effector and Motion Analysis*

### *Control of each joint*

The servo control uses a PWM signal with a unique time width between high and low levels [12]. Given that the servo system uses a digital servo type, it has a low

### *采摘末端执行器的控制及动作分析*

### *各关节控制*

本系统的舵机控制采用 PWM 进行控制。PWM 信号为脉宽调制信号[12]，其特点在于它的高电平与低电平之间

requirement for PWM signal. Furthermore, the servo system does not need to receive real-time instruction and can be auto-locked and positioned. These characteristics have outperformed the ordinary stepper motor [14]. The timing diagram of the PWM signal is shown in Figure 2.

的时间宽度。鉴于伺服系统采用数字式伺服系统，其对 PWM 信号的要求较低，不需要接收实时指令，可以自动锁定和定位。这些特性都优于普通的步进电机[14]。图 2 为 PWM 信号的时序图。

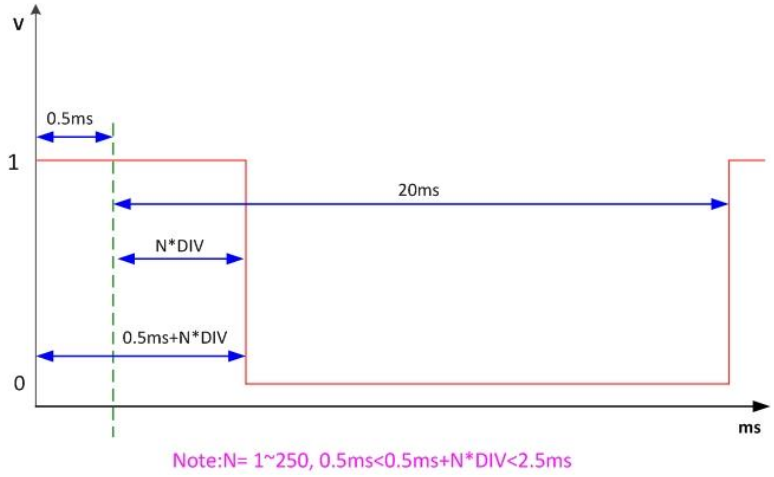


**Fig.2** - PWM timing diagram at one cycle

The servo system used for the harvesting end-effector has no requirement for low-level time, thus indicating that the use of a low time of 0.5 ms is allowable and that a cycle of the PWM waveform can be 1 ms standard square wave. The system controller uses an 8-bit micro-controller and 256 data resolution, which will be divided into 250 parts after the servo limit parameter experiment. Thereafter, when the width between 0.5 ms to 2.5 ms is 2000 μs, the width will be divided into 250 parts, thus resulting to 8 μs. The PWM control precision can be used to control the revolving and positioning of the servo at an increasing basis. Given that the servo can revolve at 185°, the servo's control precision is 0.74°. By controlling the servo's revolving angle according to PWM wave high-level duration, we obtained the data shown in Table 1 to Table 5. The 0° angle in the Tables represents the critical point in the positive and negative directions of the space coordinates. Table 1 to Table 5 shows that the revolving angle of servo has a linear relation with PWM wave high-level duration.

系统的采摘末端执行器所使用的舵机对低电平时间并没有要求，使用 0.5ms 的低电平时间也是允许的，即 PWM 波形的一个周期可以是 1ms 的标准方波。该系统控制器采用一个 8 位微控制器，其数据分辨率为 256，那么经过舵机极限参数实验，得到应该将其划分为 250 份。那么 0.5ms 到 2.5ms 的宽度为 2000us，由 2000us/250 得 PWM 的控制精度为 8us，因此可以以 8us 为单位递增控制舵机转动与定位。鉴于舵机可旋转 185 度，控制精度为 0.74 度，根据 PWM 波高电平持续时间控制舵机转动不同的角度，进而根据实际的实验测量数据得出表 1 至表 5 中的数据。表中 0 度均表示为采摘末端执行器建立的空间坐标系中正负方向的临界点。从表 1 至表 5 可清晰看出舵机转动的角度与 PWM 波高电平持续的时间成线性关系。

**Table 1**

**Relation between No.3 servo's revolving angle and PWM wave high-level duration**

| **Angle (°)** | −72 | −45 | −30 | 0 | 60 |
|---|---|---|---|---|---|
| **High-level voltage (μs)** | 2000 | 1775 | 1588 | 1380 | 1000 |

**Table 2**

**Relation between No.4 servo's revolving angle and PWM wave high-level duration**

| **Angle (°)** | −50 | −35 | 0 | 45 | 90 |
|---|---|---|---|---|---|
| **High-level voltage (μs)** | 2100 | 2000 | 1760 | 1380 | 1000 |

**Table 3**

**Relation between No.5 servo's revolving angle and PWM wave high-level duration**

| **Angle (°)** | −45 | 0 | 90 | 143 |
|---|---|---|---|---|
| **High-level voltage (μs)** | 500 | 800 | 1470 | 2100 |

Table 4

**Relation between No.6 servo's revolving angle and PWM wave high-level duration**

| Angle (°) | −14 | 0 | 90 | 173 |
|---|---|---|---|---|
| High-level voltage (us) | 500 | 620 | 1380 | 2000 |

Table 5

**Relation between No.7 servo's revolving angle and PWM wave high-level duration**

| Angle (°) | 0 | 24 | 37 | 49 |
|---|---|---|---|---|
| High-level voltage (μs) | 2100 | 1850 | 1720 | 1600 |

***Classification and coordinate composition of harvesting movement***

In harvesting, only the No.3, No.4, No.5, No.6, and No.7 servos are involved, whereas the No.2 servo is a back-up that is temporarily immovable and is vertically upward. The No.6 and No.7 servos control the picking and stabilization of the kiwifruit, respectively. Thus, the No.6 and No.7 servos do not involve the end-effector's accurate movements to the target kiwifruit. The No.3 servo controls the base rotation, thereby controlling the revolving angle according to the X and Y space coordinates of the target kiwifruit. The flow chart of the programming is shown in Figure 3.

***采摘动作的分类及其坐标分解***

在采摘过程中，只有采摘末端执行器的 3、4、5、6、7 号舵机参与工作，而 2 号舵机是后备移动舵机，暂时是固定不动竖直向上的。6、7 号舵机则分别控制猕猴桃抓取与夹稳，因此 6、7 号舵机不涉及采摘末端执行器的精确移动至目标猕猴桃的过程。3 号舵机控制着采摘末端执行器基座的旋转，可以根据目标猕猴桃空间坐标的 X、Y 数据确定 3 号舵机的转动角度。程序设计流程图如图 3 所示。

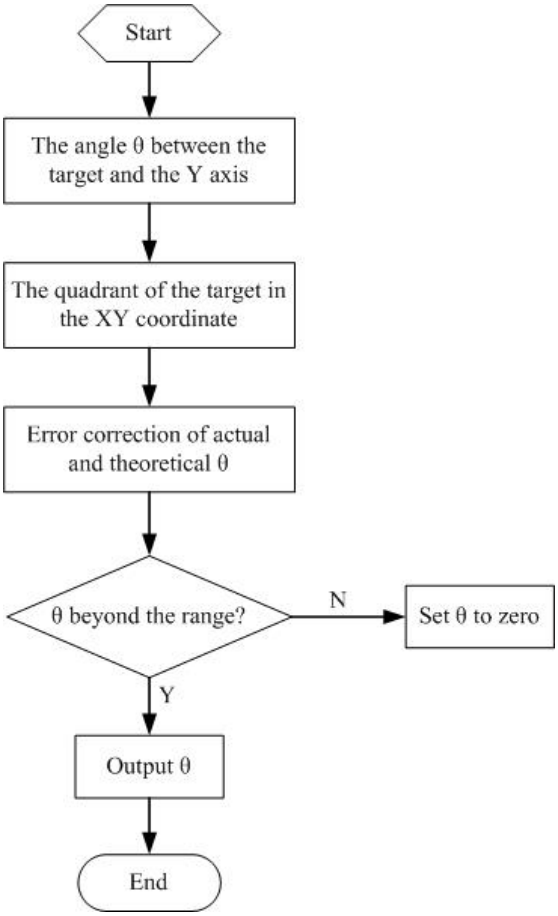


**Fig.3 -** Flow chart of No.3 servo's revolving angle

Only determining the rotational angle of the No.3 servo is insufficient to move the end-effector clamp to the target kiwifruit. This movement needs the analysis of the revolving angles of the No.4 and No.5 servos. The force manipulators that are controlled by the No.4 and No.5

仅确定 3 号舵机的转动角度还不能把采摘末端执行器采摘的钳子移动到目标猕猴桃的位置，还需要分析 4、5 号舵机转动的角度。在这里分别命名 4、5 号舵机控制的力臂为

servos are named as front arm and rear arm, respectively. As shown in Figure 4, the target kiwifruit is set as point A, the No.4 servo as one point, and the No.5 as another point. A triangle is formed by connecting the three points.

前臂与后臂，把目标猕猴桃设为 A 点，4 号舵机作为一个点，另外再把 5 号舵机设为一个点，然后把 A 点与 4、5 号舵机点相连接形成了三角形关系，如图 4 所示。

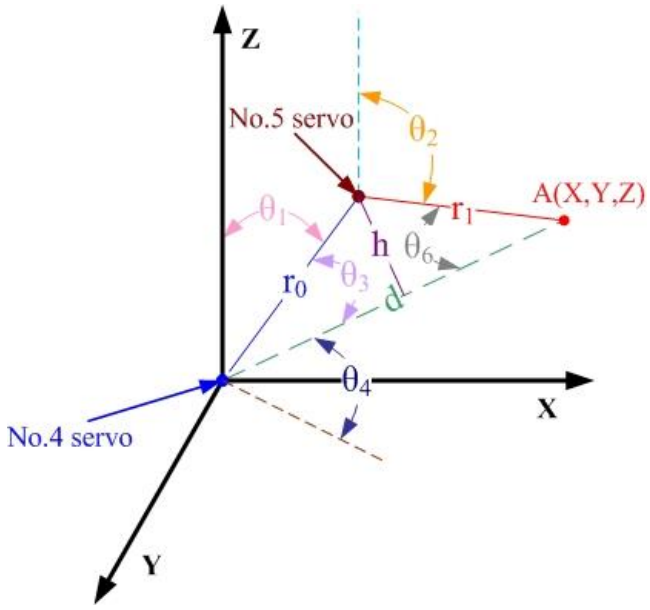


**Fig.4 -** Mathematical modelling of revolving angles of No.4 and No.5 servos

In Figure 4, $\theta_1$ and $\theta_2$ are the revolving angles of the No.4 and No.5 servos, respectively; $r_0$ and $r_1$ represent the distances from the No.4 to No.5 servos and No.5 to No.6 servos, respectively. The distance *d* from point A to original point "O" in Figure 4 can be obtained by using the XYZ coordinates transmitted by the binocular system.

在图 4 中，$\theta_1$ 与 $\theta_2$ 是 4、5 号舵机为采摘目标猕猴桃而需要转动的角度，$r_0$、$r_1$ 分别代表末端执行器 4 号与 5 号舵机间距离、5 号与 6 号舵机间的距离，通过双目系统传送过来的 XYZ 坐标即可求出 A 点到原点"O"的距离。

$$d = \sqrt{X^2 + Y^2 + Z^2} \tag{1}$$

The triangle's height *h* can be calculated by Heron's formula:

通过海伦公式可以求得该三角形的高。

$$h = \frac{2\sqrt{p(p-r_0)(p-r_1)(p-d)}}{d} \tag{2}$$

where *p* is the half perimeter defined by the following:

在这里 *p* 为半径，其定义为：

$$p = \frac{1}{2}(r_0 + r_1 + d) \tag{3}$$

By using $r_0$, $r_1$, and height *h* with anti-trigonometric function, angles $\theta_3$ and $\theta_6$ in this triangle can be acquired as follows:

利用 $r_0$, $r_1$, 和高 *h*，通过下式求他们的反三角函数可求得 $\theta_3$ 和 $\theta_6$。

$$\theta_3 = \arcsin(\frac{h}{r_0}) \tag{4}$$

$$\theta_6 = \arcsin(\frac{h}{r_1}) \tag{5}$$

By using the Z coordinates of the target kiwifruit, angle $\theta_4$ of line segment OA and the horizontal plane can be calculated as follows:

根据目标猕猴桃的坐标 Z 可得出 OA 线与水平面的夹角 $\theta_4$，如下式所示：

$$\theta_4 = \arcsin(\frac{|Z|}{d}) \quad (6)$$

Finally, according to the law of the right angle, $\theta_1$ and $\theta_2$ are given by the following:

最终根据直角取余法则求出 $\theta_1$，同理可得 $\theta_2$。

$$\theta_1 = 90^\circ - \theta_3 - \theta_4 \quad (7)$$

$$\theta_2 = 90^\circ - \theta_4 + \theta_6 \quad (8)$$

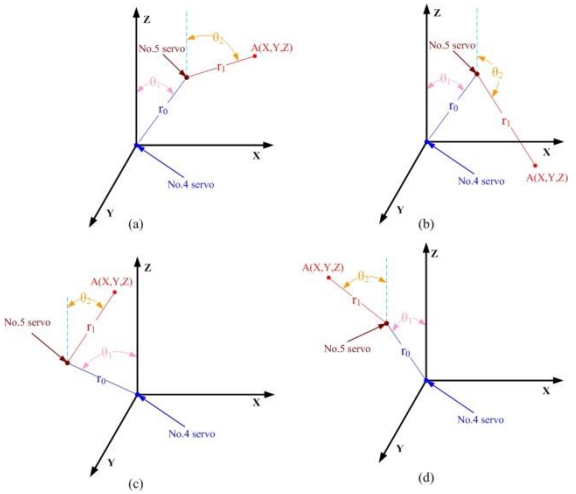


**Fig.5 -** Flow chart of receiving the coordinates by the end-effector's controller

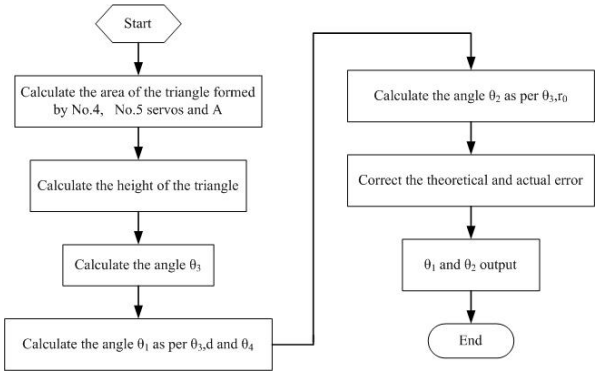


**Fig.6 -** Flow chart of picking feedback

The calculation algorithm of the steering revolving angle of the No.4 and No.5 servos is limited to the right ahead and above direction. Thus, $\theta_1$ has a positive degree value and $\theta_2$ is less than 90°. However, in actual conditions, the harvesting system is operated on the ground where complicated directions are involved such as ahead above, rear above, ahead below, and rear below. According to various experiments, the picking robot only needs four postures to achieve 360° of harvesting operation. The four postures are quite similar to a human's hand–wrist movements in all directions. As shown in Figure 5, the end-effector has four corresponding picking postures. The picking postures are distinguished on the basis of the revolving angle of over ±90°. Figure 6 shows the programming flow chart of how an end-effector controls the revolving angle of the No.4 and No.5 servos according to the space coordinates of the target fruit.

对 4、5 号舵机转动角度的计算仅限于目标猕猴桃位于采摘末端执行器三维坐标系的正前上方，即 $\theta_1$ 为正角度、$\theta_2$ 小于 90 度。然而，在实际情况下，系统的采摘过程是基于地面的，因此所有的采摘过程中猕猴桃会随机的位于末端执行器的前上方、后上方、前下方、后下方等各种情况，根据大量实验得出末端执行器只需四种采摘姿势便可采摘到 360°全方位的猕猴桃，这些姿势与人的手一样，在各个方向上都很相似，如图 5 所示，采摘末端执行器针对四种情况做出的四种采摘姿势。采摘姿势区分的依据是根据 4 号舵机和 5 号舵机转动正负角度大于 90 度而区分。采摘末端执行器根据目标果实的空间坐标控制 4 号舵机和 5 号舵机转动角度的程序设计流程图如图 6 所示。

***Communication Between the End-effector and PC***

The control system communicates with a PC through serial ports. When a PC detects a kiwifruit, it calculates the space coordinates of the target fruit. The PC will then transmit 9600 b/s baud rate of data to the control system of the robot end-effector. Given that the communication between the PC and the end-effector controller can only transmit one 8 bit binary data, a special algorithm needs to be applied to the data conversion to protect the data validity within the scope of 8 bit binary data and the data must be stored in the end-effector controller. The program of the specific data receiving the unit of the harvesting end-effector is shown in Figure 7. When the communication of serial ports is interrupted, RI is the zero setting and the flag denotes the flag bit of the data transmitted. The data transmitted from the PC is the X-axis coordinate, which is followed by Y and Z coordinates.

***末端执行器与 PC 之间的通信***

采摘末端执行器上的控制系统是通过串口与 PC 进行通信的，当 PC 检测出猕猴桃并计算出目标猕猴桃的具体空间坐标,PC 端便以 9600b/s 的波特率将数据传送到采摘末端执行器上的控制系统。由于 PC 端与采摘末端执行器上的控制器的通信一次只能传送一个 8 位的二进制数据，因此需在 PC 端通过一些特殊的数据转换算法使得数据在 8 位二进制数据的范围内以保护数据的有效性，然后在采摘末端执行器控制器中还原数据。采摘末端执行器控制器具体的数据接收程序如图 7 所示，当进入串口通信中断程序，RI 置零，flag 为数据传送个数的标记位，PC 端首先传送过来的数据是 X 轴的坐标，然后依次为 Y、Z。

When the picking end-effector completes a set of assigned actions according to the given coordinates and finally picks up the target kiwifruit, the end-effector will respond with an “OK” feedback to the PC as a signal for the picking order of the next target. The “OK” feedback procedure code is shown in Figure 8. First, ES is set to zero and “O” is placed in SBUF for data storage. Thereafter, TI is tested if it has a value of one to determine if the PC received the data. The same procedure is adopted for “K,” and ES is set to one.

当采摘末端执行器完成一组动作到达系统给定的空间坐标位置并把目标猕猴桃采摘下来后，采摘末端执行器将反馈一个“OK”给予 PC 端，从而 PC 可更有效率的传送下一个目标采摘指令。采摘末端执行器反馈“OK”的具体程序代码如图 8 所示。首先 ES 置 0，然后将数据“O”放入 SBUF 数据存储，通过检测 TI 是否为 1 即刻检测出 PC 端是否接受到数据，以同样的方法将“K”也反馈给 PC 端，最后将 ES 复位为 1。

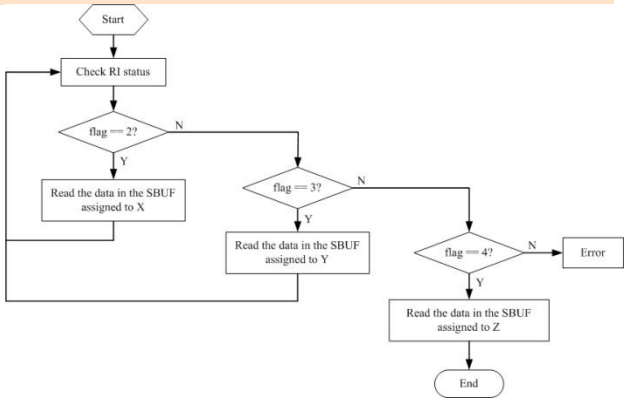


**Fig.7-** Flow chart of receiving the coordinates by the end-effector’s controller

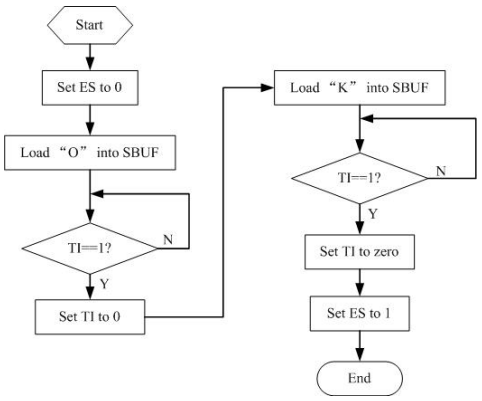


**Fig.8-** Flow chart of picking feedback

**RESULTS**

This paper selects clusters of fruits to be picked. The process is shown in Figure 9.

**结果**

本文选取一类水果进行采摘，其过程如图 9 所示。

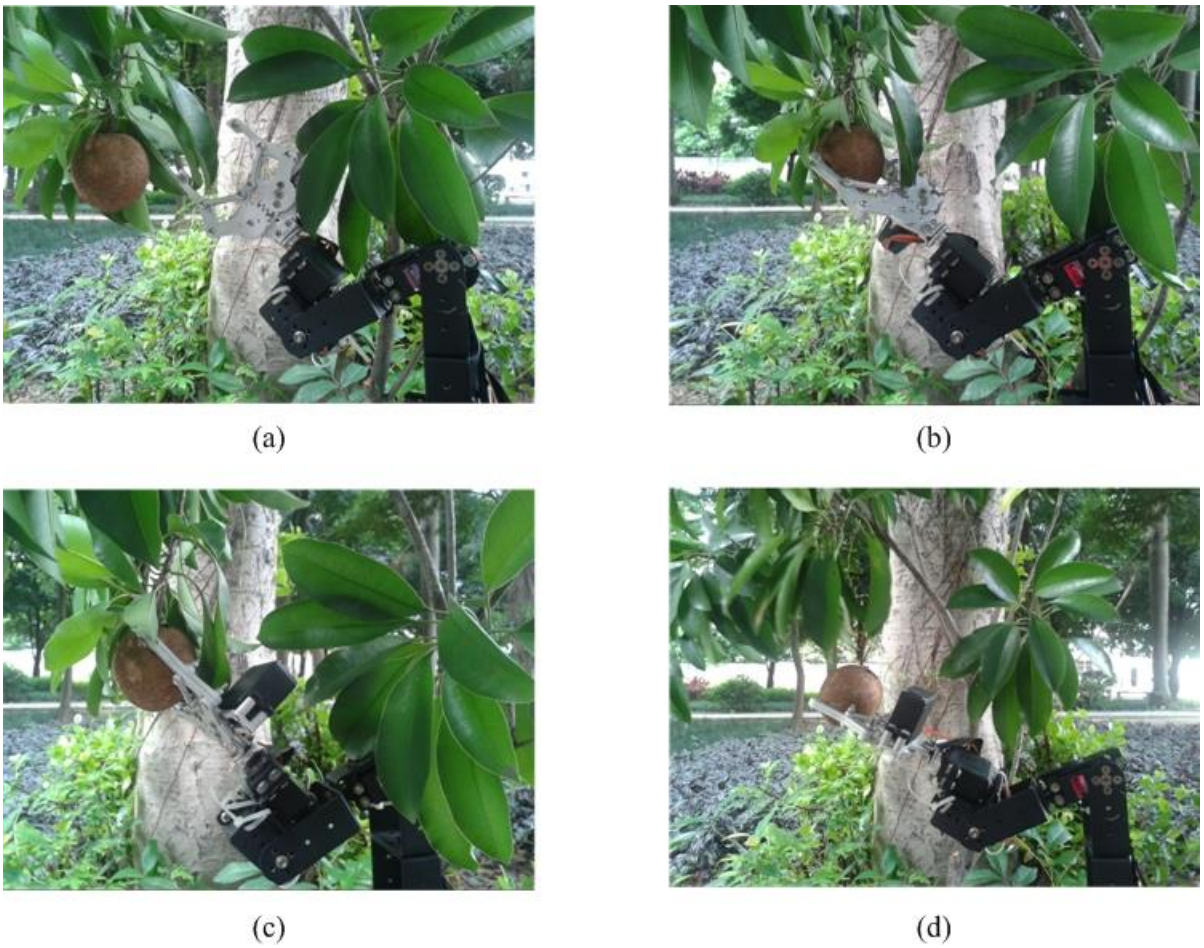


**Fig.9 -** Fruit picking process. (a) Start grabbing; (b) Finish grasping; (c) Start spinning; (d) Finish picking.

Table 6 shows how the PWM cycle affects the servo operation. When the PWM cycle is 2000 μs, the end-effector moves extremely fast, this is applicable for harvesting large fruits. When the cycle is 3000 μs, the speed is moderate, thus neither wearing off the machine because of the fast speed nor enabling harvesting because it is too slow. Therefore, the default PWM cycle utilized in this system is 3000 μs.

表 6 为 PWM 周期对舵机的影响，当 PWM 周期为 2000μs 的时候，末端执行器的运动极为快速，适用于大果实的采摘；当 PWM 波周期为 3000μs 的时候，末端执行器速度较为合适，不会因为速度太快而造成机械的磨损加剧，也不至于太慢导致无足够的力度采摘目标果实。因此本系统末端执行器的 PWM 周期默认为 3000μs。

**Table 6**

**PWM cycle and servo control**

| PWM Cycle (us) | 1500 | 2000 | 3000 | 7000 |
|---|---|---|---|---|
| How the end-effector works | No movement | Extremely fast movement, normal operation | Moderately fast movement, normal operation | Slow movement, insufficient strength |

Table 7 shows the test results of the precise movement of the end-effector to the target coordinates. This table shows that the end-effector is able to reach the space coordinates of the target transmitted by the binocular system, accurately analyze the direction of the coordinates, and determine the picking posture when harvesting. Moreover, picking robot can judge if the space coordinates are within the range of harvesting, which is in line with the system design. It means that the end-effector can determine if the target can be picked; if not, the end-effector will have no movement and give the feedback to the PC end.

表 7 为采摘末端执行器移动至目标坐标的测试情况。从该表不难观察出采摘末端执行器能准确到达双目系统传送过来的目标空间坐标，并且能准确分析给定坐标位于采摘末端执行器的哪个方位，从而判断出使用何种采摘姿势进行采摘。另一方面，采摘末端执行器对于空间坐标是否在采摘范围的判断符合本系统设计的结果，能准确地判断出目标坐标是否具备可采摘性，若不可采摘，末端执行器不做出任何采摘动作并且反馈给 PC 端。

**Table 7**

**Test results of the picking end-effector**

| Space coordinates of the target(mm) | (150, 150, 156) | (100, 200, 156) | (100, 400, 256) | (–50, 100, 160) |
|---|---|---|---|---|
| **Tested Results** | Accurate picking | Accurate picking | Target can not be picked | Accurate picking |

## CONCLUSIONS

The research on fruit picking robots is thriving in China and abroad because of its significance in the development of science and technology and human civilization. The picking end-effector is a metal structure composed of five servos that control each junction of the end-effector to adapt complicated situations. The picking end-effector is more flexible and stable than other manipulators. In this paper, the movement in harvesting fruits is discussed; and each junction of the end-effector has mathematical modelling through which the coordinates of the target fruit are disassembled and analyzed so the end-effector can reach to the target precisely. Finally, experiments have verified the validity of the end-effector and its efficiency in agricultural operation.

## 结论

果实采摘机器人是当前国内外热门研究的课题，其发展对促进科学技术的发展与人类文明发展进程有着重大的实际意义。本论文的果实采摘末端执行器的结构为金属支架，通过控制五个舵机从而控制末端执行器的各个关节，使其能适用于各种复杂的情景，比其他采摘末端执行器更灵活、更稳定。另外本论文通过分析末端执行器采摘果实的动作，对它进行数学建模，然后将目标果实坐标通过数学建模进行拆解分析，使得末端执行器可以准确移动到果实的位置。最后通过采摘试验验证了该采摘末端执行器的有效性以及作业流程的合理性。

## ACKNOWLEDGEMENT

This research was funded by the National Natural Science Foundation of China under Grant No.61505037, the National Spark Program under Grant No.2014GA780009, the State Scholarship Fund under Grant CSC No.201408440326, the Guangdong Natural Science Foundation under Grant No.S2013040014993, the Pearl River S&T Nova Program of Guangzhou under Grant No.201506010035, the University-sponsored

## 致谢

本论文得到国家自然科学基金项目资助（项目号：No. 61505037），国家星火计划项目资助（项目号：No. 2014GA780009），国家留学基金资助（项目号：CSC No.201408440326），广东省自然科学基金资助（项目号：No.S2013040014993），广州市珠江科技新星专项资助（项目号：No. 201506010035），广东财经大学校级科

Research Project of Guangdong University of Finance and Economics under Grant No.14GLL63001, the Research Project of Research Institute of Education in Guangdong Province under Grant No.GDJY-2014-C-b043, the University Scientific Research Project of Guangxi Education Office under Grant No.KY2015ZL095.

**REFERENCES**

[1]. Berenstein R., Shahar O.B., Shapiro A., Edan Yael, (2010) - *Grape clusters and foliage detection algorithms for autonomous selective vineyard sprayer*, Intelligent Service Robotics, vol. 3, no.4, pp. 233-243;
[2]. Blanes C., Ortiz C., Mellado M., Beltrán P., (2015) - *Assessment of eggplant firmness with accelerometers on a pneumatic robot gripper*, Computers and Electronics in Agriculture, vol. 113, pp. 44-50;
[3]. Chiu Yi-Chich, Yang P.Y., Chen S., (2013) - *Development of the end-effector of a picking robot for greenhouse-grown tomatoes*, Applied Engineering in Agriculture, vol. 29, no.6, pp.1001-1009;
[4]. Chua P.Y., Ilschner T., Caldwell D.G., Van Henten E.J., (2003) - *Robotic manipulation of food products - A review*, Industrial Robot, vol. 30, no.4, pp. 345-354;
[5]. Edan Yael, Rogozin Dima, Flash Tamar, Miles Gaines E. (2000) - *Robotic melon harvesting*, IEEE Transactions on Robotics and Automation, vol. 16, no.6, pp. 831-835;
[6]. Elias Lopez-Alba, Ruben Dorado-Vicente, Jose Vasco-Olmo, Francisco Alberto Diaz-Garrido. (2012) - *Design and development of a vibration clamp for agricultural purposes*, DYNA, vol. 87, no.1, pp. 114-119;
[7]. Hayashi S, Ganno K, Ishii Y, Tanaka K. (2002) - *Robotic harvesting system for eggplants*, Japan Agricultural Research Quarterly, vol. 36, no.3, pp.163-168;
[8]. Hu Zhiyong, Zhang Xuewei, Zhang Wei, Wang Lin. (2014) - *Precise control of clamping force for watermelon picking end-effector*, Transactions of the Chinese Society of Agricultural Engineering, vol. 30, no.17, pp. 43-49;
[9]. Ji Chao, Feng Qingchun, Yuan Ting, Tan Yuzhi, Li Wei. (2011) - *Development and performance analysis on cucumber harvesting robot system in greenhouse*, Robot, vol. 33, no.6, pp.726-730;
[10]. Jin Bo, Lin Longxian. (2014) - *Design and force control of an underactuated robotic hand for fruit and vegetable picking*, Journal of Mechanical Engineering, vol. 50, no.19, pp.1-8;
[11]. Lin Hanhui, Cai Ken, Zeng Zhaofeng. (2015) - *Design of a low-cost system with built-in-gps agricultural machinery*, INMATEH - Agricultural Engineering, vol. 46, no.2, pp.25-36;
[12]. M. Mustafa Ertay, Ahmet Zengin. (2014) - *Analysis of the discontinuous PWM controlled D-STATCOM for reactive power compensation applications*, Tehnicki Vjesnik, vol. 21, no.4, pp. 825-833;
[13]. Reed J.N., Miles S.J., Butler J., Baldwin M., Noble R. (2001) - *AE-automation and emerging technologies: automatic mushroom harvester development*, Journal of Agricultural Engineering Research, vol. 78, no.1, pp. 15-23;
[14]. Shen Jian-Guang, Tao Tao, Mei Xue-Song, Xu Mu-Xun, Liu Shan-Hui. (2013) - *An improved line-drawing algorithm for arbitrary fractional frequency divider/multiplier based on FPGA*, Journal of Engineering Science and Technology Review, vol. 6, no.5, pp. 90-94;

研项目资助（项目号：No. 14GLL63001），广东省教育研究院教育研究课题资助（项目号：No. GDJY-2014-C-b043），广西教育厅高校科研项目资助（项目号：No. KY2015ZL095）。

**参考文献**

[1]. Berenstein R., Shahar O.B., Shapiro A., Edan Yael. (2010) - *针对自主选择葡萄园喷雾器的葡萄簇和叶检测算法*, 智能服务机器人学报, 第 3 卷, 第 4 期, 233-243;
[2]. Blanes C., Ortiz C., Mellado M., Beltrán P.,. (2015) - *使用气动机器人夹持器上的加速度计对茄子硬度进行评价*, 计算机电子技术在农业中的应用, 第 113 卷, 44-50;
[3]. Chiu Yi-Chich, Yang P.Y., Chen S.. (2013) - *设施内西红柿采收机器人爪具之研制*, 农业应用工程, 第 29 卷, 第 6 期, 1001-1009;
[4]. Chua P.Y., Ilschner T., Caldwell D.G., Van Henten E.J. (2003) - *食物产品机器人控制综述*, 工业机器人, 第 30 卷, 第 4 期, 345-354;
[5]. Edan Yael, Rogozin Dima, Flash Tamar, Miles Gaines E. (2000) – *甜瓜采摘机器人*, IEEE 机器人学与自动化杂志, 第 16 卷, 第 6 期, 831-835;
[6]. Elias Lopez-Alba, Ruben Dorado-Vicente, Jose Vasco-Olmo, Francisco Alberto Diaz-Garrido. (2012) -*农业用途的振动夹具设计与开发*, DYNA, 第 87 卷, 第 1 期, 114-119;
[7]. Hayashi S, Ganno K, Ishii Y, Tanaka K. (2002) - *茄子机器人摘取系统*, 日本农业研究季刊, 第 36 卷, 第 3 期, 163-168;
[8]. 胡志勇, 张学炜, 张伟, 王琳. (2014) - *西瓜采摘末端执行器夹持力精确控制*, 农业工程学报, 第 30 卷, 第 17 期, 43-49;
[9]. 纪超, 冯青春, 袁挺, 谭豫之, 李伟. (2011) - *温室黄瓜采摘机器人系统研制及性能分析*, 机器人, 第 33 卷, 第 6 期, 726-730;
[10].金波, 林龙贤. (2014) - *果蔬采摘欠驱动机械手爪设计及其力控制*, 机械工程杂志, 第 50 卷, 第 19 期, 1-8;
[11]. Lin Hanhui, Cai Ken, Zeng Zhaofeng. (2015) - *一种基于嵌入式的低成本农业机械 GPS 导航定位系统设计*, 国际农业工程期刊, 第 46 卷, 第 2 期, 25-36;
[12]. M. Mustafa Ertay, Ahmet Zengin. (2014) - *针对无功补偿应用的不连续的 PWM 控制系统分析*, 技术公报, 第 21 卷, 第 4 期, 825-833;
[13]. Reed J.N., Miles S.J., Butler J., Baldwin M., Noble R. (2001) - *自动和新兴技术：自动蘑菇采摘机开发*, 农业工程研究杂志, 第 78 卷, 第 1 期, 15-23;
[14]. Shen Jian-Guang, Tao Tao, Mei Xue-Song, Xu Mu-Xun, Liu Shan-Hui. (2013) - *一种改进的基于 FPGA 的用于任意分频器/乘法器的直线绘制算法*, 工程科学与技术综

[15]. Van Willigenburg L.G., Hol C.W.J., Van Henten E.J. (2004) - *On-line near minimum-time path planning and control of an industrial robot for picking fruits*, Computers and Electronics in Agriculture, vol. 44, no.3, pp. 223-237;
[16]. Wang Xuelin, Xiao Yongfei, Bi Shuhui, Fan Xinjian, Rao Honghui. (2015) - *Design of test platform for robot flexible grasping and grasping force tracking impedance control*, Transactions of the Chinese Society of Agricultural Engineering, vol. 31, no.1, pp. 58-63;
[17]. Xiong Juntao, Ye Min, Zou Xiangjun, Peng Hongxing, Lin Guichao, Zhu Mengsi. (2013) - *System design and performance analysis on multi-type fruit harvesting robot*, Transactions of the Chinese Society for Agricultural Machinery, vol. 44, no.1, pp. 230-235;
[18]. Yan Lei, Yu Zheng, Han Ning, Liu Jinhao. (2013) - *Improved image fusion algorithm for detecting obstacles in forests*, Journal of Digital Information Management, vol. 11, no.5, pp. 378-384;
[19]. Ying Yibin, Zhang Wenying, Jiang Yiyuan, Zhao Yun, (2000) - *Application of machine vision technique in automatic harvesting and processing of agricultural products,* Transactions of the Chinese Society of Agricultural Machinery, vol. 31, no.3, pp. 112-115;
[20]. Yuan Ting, Xu Chen-Guang, Ren Yong-Xin, Feng Qing-Chun, Tan Yu-Zhi, Li Wei, (2009) - *Detecting the information of cucumber in greenhouse for picking based on NIR image*, Spectroscopy and Spectral Analysis, vol. 29, no.8, pp. 2054-2058;
[21]. Zhang Peng, Song Jian, Gong Shenglei, Jiang Bo, Muham Polar D., (2014) - *A kinematic analysis and simulation based on ADAMS for eggplant picking robot*, INMATEH - Agricultural Engineering, vol. 43, no.2, pp. 51-60;
[22]. Zhou Jun, Ji Changying, (2003) - *Multi-resolution road recognition for vision navigation*, Transactions of the Chinese Society for Agricultural Machinery, vol. 34, no.6, pp.120-123.

述, 第 6 卷, 第 5 期, 90-94;
[15]. Van Willigenburg L.G., Hol C.W.J., Van Henten E.J. (2004) - *水果采摘工业机器人的最小时间路径规划与控制*, 计算机电子技术在农业中的应用, 第 44 卷, 第 3 期, 223-237;
[16]. 王学林, 肖永飞, 毕淑慧, 范新建, 饶洪辉. (2015) - *机器人柔性抓取试验平台的设计与抓持力跟踪阻抗控制*, 农业工程学报, 第 31 卷, 第 1 期, 58-63;
[17]. 熊俊涛, 叶敏, 邹湘军, 彭红星, 林桂潮, 朱梦思. (2013) - *多类型水果采摘机器人系统设计与性能分析*, 农业机械学报, 第 44 卷, 第 1 期, 230-235;
[18]. Yan Lei, Yu Zheng, Han Ning, Liu Jinhao. (2013) - *用于森林障碍检测的图像融合改进算法*, 数字信息管理杂志, 第 11 卷, 第 5 期, 378-384;
[19]. 应义斌, 章文英, 蒋亦元, 赵匀. (2000) - *机器视觉技术在农产品收获和加工自动化中的应用*, 农业机械学报, 第 31 卷, 第 3 期, 112-115;
[20]. 袁挺, 许晨光, 任永新, 冯青春, 谭豫之, 李伟. (2009) - *基于近红外图像的温室环境下黄瓜果实信息获取*, 光谱学与光谱分析, 第 29 卷, 第 8 期, 2054-2058;
[21]. Zhang Peng, Song Jian, Gong Shenglei, Jiang Bo, Muham Polar D. (2014) - *基于 ADAMS 的茄子采摘机器人运动学分析与仿真*, 国际农业工程期刊, 第 43 卷, 第 2 期, 51-60;
[22]. 周俊, 姬长英. (2003) - *农业机器人视觉导航中多分辨率路径识别*, 农业机械学报, 第 34 卷, 第 6 期, 120-123.

# EXPERIMENTAL RESEARCH OF SOYBEAN DRYING PROCESS INTENSIFICATION
# /
# *ЕКСПЕРИМЕНТАЛЬНЕ ДОСЛІДЖЕННЯ ІНТЕНСИФІКАЦІЇ ПРОЦЕСУ СУШІННЯ СОЇ*

**Ph.D.Eng. Kirchuk R., Ph.D.Eng. Tsiz I., Ph.D. Stud. Tsiz K.**
Lutsk National Technical University (Ukraine)
*Tel: +38(0332)74-61-03; Fax: +38(0332)77-48-40; E-mail: ruslan-mail@ukr.net; katrysik00@gmail.com*

***Abstract:*** *One of the methods to intensify the process of drying soybean seeds is to increase the contact area of the drying agent with the material being dried. This result is achieved with the unit for pre-conditioning of the material to dry (patent № 87184, Ukraine). The experimental device is made in order to investigate the influence of structural parameters of this unit on seed coat deformation.*
*The aim is to study the influence of the seed area deformation coefficient k on speed of the soybean drying process.*

*The article provides two mathematical models enabling to set the time it takes to reach conditional moisture content of soybean seeds in the drying chamber with the preliminary deformation of the seed coat in the unit for pre-conditioning of the seeds before drying. These models take into account the following parameters: 1- the initial moisture content of seeds, quantity of seeds in the loading hopper and geometric parameters of the device (number of blades on the disk, the angular velocity of the disk), 2 - original material moisture content, temperature and velocity of the drying agent.*

*The calculation is made and the curves are obtained providing the following characteristics (at different initial parameters): 1- coefficient of the seed coat area deformation k while passing the material through the device to its preconditioning stage; 2 - change of soybean seeds drying speed with a certain coefficient k while drying in a drying unit. The analysis of the results showed that the coefficient k of seed coat area deformation significantly affects the rate of moisture content removal from soybean seeds and confirmed the feasibility of preconditioning of the material before drying in this way in order to intensify the process. Also, the proposed mathematical model allows establishing rational design parameters of the developed device.*

***Keywords:*** *device for preconditioning, area deformation coefficient, drying, soybeans, mathematical model, the regression equation*

## INTRODUCTION

The problem of energy saving in agriculture requires the introduction of new technologies aiming to intensify processing of agricultural products [7,11].

One of the most energy-intensive processes in soybean refining is its drying [1,3]. Thus, the study of methods of cultivation of soybean seeds that ensure fast and high quality moisture removal at minimum energy consumption, is important.

More efficient drying of agricultural materials is enabled through preconditioning. One of such drying intensification methods of the drying process is to increase the contact area of the drying agent with wet

***Резюме:*** *Одним методів інтенсифікації процесу сушіння насіння сої є збільшення площі контакту сушильного агента із матеріалом, що сушиться. Досягти такого результату дозволяє пристрій попередньої підготовки матеріалу до сушіння (Патент на корисну модель № 87184, Україна). Для дослідження впливу конструктивних параметрів даного пристрою на величину деформації оболонки насінини виготовлена експериментальна установка.*

*Метою роботи є дослідження впливу коефіцієнта зміни площі насінини k на швидкість процесу сушіння сої.*

*В статті запропоновані дві математичні моделі, які в комплексі дозволяють встановити час, необхідний для досягнення кондиційної вологості насінням сої в сушильній камері з попереднім деформуванням оболонки в пристрої для підготовки насіння до сушіння. Дані моделі враховують такі параметри: 1-початкова вологість насіння, кількість подачі насіння в завантажувальний бункер та геометричні параметри пристрою (кількість лопаток на диску, колова швидкість диска), 2- початкова вологість матеріалу, швидкість та температура сушильного агенту.*

*Проведено розрахунки і одержано графічні залежності, що характеризують (при різних вихідних параметрах): 1- коефіцієнта зміни площі насінини k при проходженні матеріалу через пристрій попередньої підготовки до сушіння; 2- зміну швидкості сушіння насіння сої з певним коефіцієнтом k при сушінні в сушильній установці. Аналіз результатів показав, що коефіцієнт зміни площі насінини k суттєво впливає на швидкість видалення вологи з насіння сої і підтвердив доцільність попередньої підготовки матеріалу до сушіння таким способом для інтенсифікації процесу. Запропонована математична модель дозволяє встановити раціональні конструктивні параметри розробленого пристрою.*

***Ключові слова:*** *пристрій для попередньої підготовки, коефіцієнт зміни площі, сушіння, соя, математична модель, рівняння регресії*

## ПЕРЕДУМОВА

Проблема енергозбереження у сільському господарстві потребує впровадження нових технологій, спрямованих на інтенсифікацію процесів переробки сільськогосподарської продукції [7,11].

Одним з найбільш енергоємних процесів у технології переробки сої є її сушіння [1,3]. Тому актуальним є дослідження методів обробітку насіння сої, які б забезпечували швидке та якісне видалення надлишкової вологи при мінімальних енерговитратах.

Забезпечити більш ефективне сушіння сільськогосподарських матеріалів дозволяє їх попередня підготовка. Одним із таких методів інтенсифікації процесу сушіння є збільшення площі контакту сушильного агента із вологим матеріалом, що, в свою чергу, дає змогу більш інтенсивно

material, which in its turn allows more intensive moisture removal due to loss of integrity of the seed coat [4,10]. The soybean treated in this way (patent № 87184, Ukraine) [5,6] can be used in oil production [2].

During development and design of the devices that would provide the necessary preconditioning of agricultural materials for drying, it is necessary to choose the rational design parameters, tooling, as well as consider the properties of the material to be processed. The studies will allow to improve the technical and economic performance of the dryers.

In order to define the regularity of the influence of structural and process parameters on the deformation area of the seed coat (coefficient k) on the drying speed, it is appropriate to apply the mathematical method of experiment planning. Development of the pattern that interconnects the preconditioning device and drying unit will justify rational mode and design parameters of the proposed mechanism.

## MATERIALS AND METHODS

To investigate the operational mode of the proposed technology, the stationary experimental unit was designed under laboratory conditions (Fig. 1).

The unit comprises a housing 4 in the form of a cylinder, with the observation window on the top. The disc 8 mounted on a shaft has blades for better distribution of the seed flow. The metal deck 7 is placed in the housing, to which the vertical knife plates are attached ensuring the necessary cut of the seed. The disk with blades is driven by the electromotor via belt transmission 2.

виводити вологу внаслідок втрати цілісності зовнішньої оболонки насінини [4,10]. Оброблена таким способом соя (Патент на корисну модель №87184, Україна) [5,6] може бути використана для виробництва олії [2].

Під час розробки і проектування пристроїв, які б забезпечували необхідну попередню підготовку сільськогосподарських матеріалів до сушіння, необхідно зробити вибір раціональних конструктивних параметрів, робочих органів, а також враховувати властивості матеріалу, з яким вони взаємодіють. Дані дослідження дозволять підвищити техніко-економічні показники роботи сушарок.

З метою встановлення закономірності впливу конструктивних та технологічних параметрів на величину деформації оболонки насінини (коефіцієнт *k*) та на швидкість сушіння доцільно застосувати математичний метод планування експерименту. Розробка моделі, що взаємопов'язує параметри пристрою підготовки насіння сої та сушильної установки дозволить обґрунтувати раціональні режимні і конструктивні параметри запропонованого механізму.

## МАТЕРІАЛИ І МЕТОДИ

Для дослідження режиму роботи запропонованої технології в лабораторних умовах була сконструйована стаціонарна експериментальна установка (фіг. 1).

Дана установка містить корпус 4 у вигляді циліндра, у верхній частині якого вмонтоване віконце для візуального спостереження. На диску 8, який закріплений на валу, встановлені лопатки, які призначені для кращого розподілу потоку насіння. За діаметром диску в корпусі розміщена металева дека 7, до якої прикріплені вертикальні ножові пластини і забезпечують необхідний надріз насінини внаслідок удару об них. Диск з лопатками приводиться в рух за допомогою електродвигун 1 через пасову передачу 2.

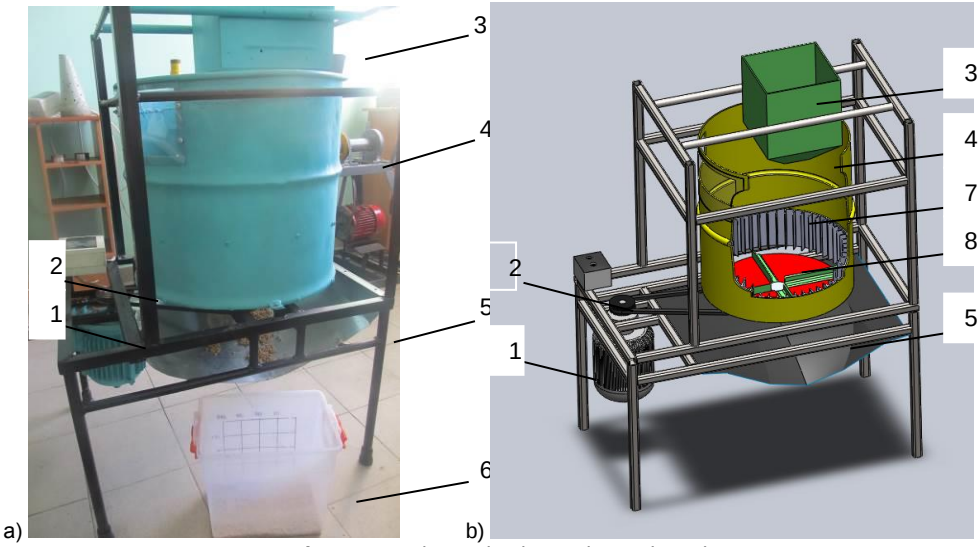


**Fig. 1** - Experimental unit: a - picture; b - scheme
*1 – electromotor ; 2 – belt transmission; 3 – loading hopper; 4 – casing; 5 – unloading tray ; 6 – seed collection container; 7 – cylindrical deck with knife plates; 3 – disk with blades*

The material is loaded to the unit through the loading hopper 3 and removed through the unloading tray 5 into the seed collection container 6.

Analysis of the literature and previous research determined the factors that have a decisive influence on the change of area deformation coefficient k, i.e. the

Подача матеріалу в установку здійснюється через завантажувальний бункер 3, а його відвід – через вивантажувальний лоток 5 у місткість для збору 6.

Аналіз літературних джерел та попередніх досліджень дозволили встановити фактори, які мають визначальний вплив на зміну коефіцієнта *k:*

initial moisture content of seeds, number of seeds in the hopper and geometric parameters of the device (number of blades on the disk, the angular velocity of the disk). On drying time $\tau$: the initial moisture content of the material, speed and temperature of the drying agent.

Thus, an experiment was conducted to define the effect of the studied factors on area deformation coefficient k (four-factor) and the soybean seeds drying time (three-factor) (Tables 1,2).

початкова вологість насіння, кількість насіння в бункері та геометричні параметри пристрою (кількість лопаток на диску, колова швидкість диска). На час сушіння $\tau$: початкова вологість матеріалу, швидкість та температура сушильного агенту.

Таким чином, проводили експеримент для визначення впливу досліджуваних факторів на коефіцієнта *k (4-факторний)* і на час сушіння насіння сої $\tau$ (*3-факторний*) (таблиці 1,2).

**Table 1**

**Factors and their levels of variation**

| Levels of variation | Factors | | | |
|---|---|---|---|---|
| | **Moisture** *W , %* | **Feed** *Q, kg/hour* | **Angular velocity** V, *m/s* | **Number of blades** *n, pcs* |
| | $x_1$ | $x_2$ | $x_3$ | $x_4$ |
| **Upper/** ***(+1)*** | 23 | 500 | 55 | 6 |
| **Basic** ***(0)*** | 19 | 350 | 40 | 4 |
| **Lower** ***(–1)*** | 15 | 200 | 25 | 2 |
| **Variability interval,** $\varepsilon$ | 4 | 150 | 15 | 2 |

**Table 2**

**Factors and their levels of variation**

| Levels of variability | Factors | | |
|---|---|---|---|
| | **Moisture,** *W , %* | **The temperature of the drying agent,** *°C* | **Velocity of the drying agent** *Vca, m/s* |
| | $x_1$ | $x_2$ | $x_3$ |
| **Upper/** ***(+1)*** | 23 | 45 | 2,2 |
| **Basic /** ***(0)*** | 19 | 40 | 1,9 |
| **Lower /** ***(–1)*** | 15 | 35 | 1,6 |
| **Variability interval,** $\varepsilon$ | 4 | 5 | 0,3 |

To reduce the number of experiments and obtain the regression equation, the mathematical method of the experiment planning based on Box-Behnken quadric plan [8,9,12] was used.

Planning stage included the following steps: factor encoding, scheduling, randomization tests, implementation plan of the experiment, testing of reproducibility of the experiments, calculation of regression coefficients, assessment of the significance of regression coefficients and adequacy of the test model.

The experiment consisted of 27 tests at threefold repetition in each of them.

In result, the seed cut was obtained at which the contact area of the material and drying agent is grown and moisture removal was intensified.

Deformation coefficient of the seed area is a factor that reflects the growth in the seed area before and after the cut. It was determined by the following formula:

Для скорочення кількості дослідів та отримання рівняння регресії було застосовано математичний метод планування експерименту за симетричним некомпозиційним планом Бокса–Бенкіна другого порядку [8,9,12].

Планування експериментальної роботи включало наступні етапи: кодування факторів, складання плану - матриці експерименту, рондомізація дослідів, реалізація плану експерименту, перевірка відтворюваності дослідів, розрахунок значень коефіцієнтів регресії, оцінка значущості коефіцієнтів регресії та перевірка адекватності отриманої математичної моделі.

Експеримент складався із 27-и дослідів за трикратної повторюваності у кожному з них.

У результаті роботи експериментальної установки був здійснений надріз насінини, що призводить до збільшення площі контакту матеріалу із сушильним агентом та інтенсивності видалення вологи під час проведення трифакторного експерименту.

Коефіцієнт зміни площі насінини - це показник, який відображає приріст площі насінини до і після надрізу. Він визначався за наступною формулою:

$$k = \frac{S_{beg} + \Delta S}{S_{beg}}, \quad (1)$$

where $S_{beg}$ - initial seed area before cut;

$\Delta S$ - area growth after the seed cut.

The samples with moisture content 15%, 19%, 23% were selected, with maximum coefficient k. These samples were used for the three factor experiment.

The method of the three factor experiment is to dry the soybean up to 12% (with different coefficient k) at speed and temperature of the drying agent determined during experiment planning. In the experiment, the time $\tau$ was recorded during which the excessive moisture was removed from the deformed soybean.

The experiment consisted of 15 tests based on the threefold repetition in each of them.

## RESULTS

Experiment results were processed using the software based on Mathcad.

1. *Four-factor experiment*. Homogeneity of variances tested was evaluated by the Cochrane criterion. Since,

$$G^{calc.}=0.187<G^{tabl.}(0.05;27;2)=0.198$$

the process is reproduced.

During the determining of confidence intervals for regression coefficients, the Student test was used, tabulated value of which at a 5 -% level of significance and the number of degrees of freedom of variance of experiment reproducibility was $f_1=2$ is = 4.3 [8,9].

The significance of regression coefficients was tested according to the established confidence intervals and covariance.

As a result, the regression equation acquired the form:

де $S_{поч}$ - початкова площа насінини до надрізу;

$\Delta S$ - приріст площі, що утворився після надрізу насінини.

У дослідах відбиралися зразки з вологістю 15%, 19%, 23%, для яких коефіцієнт *k* був максимальним. Дані зразки використовувалися для проведення трифакторного експерименту.

Методика проведення трифакторного експерименту полягала сушінні сої до 12% (з різним коефіцієнтом *k*) при визначених планом експерименту швидкості та температурі сушильного агенту. Протягом всього експерименту фіксувався час $\tau$ за який відбулося видалення надлишкової вологи з деформованого насіння сої.

Експеримент складався із 15-и дослідів за трикратної повторюваності у кожному з них.

## РЕЗУЛЬТАТИ

Обробка даних результатів експериментів здійснювалася за допомогою програми, створеної у середовищі Mathcad.

1. *Чотирифакторний експеримент*. Оцінку однорідності ряду дисперсій перевіряли за критерієм Кохрена. Оскільки,

$$G^{розр.}=0{,}187<G^{табл.}(0{,}05;27;2)=0{,}198,$$

то процес відтворюється.

Під час визначення довірчих інтервалів коефіцієнтів регресії використовували критерій Ст'юдента, табличне значення якого за 5-% рівня значущості та числі ступенів вільності дисперсії відтворюваності досліду $f_1=2$ становило $t=4.3$ [8,9].

Перевірку значущості коефіцієнтів регресії проводили за встановленими їх довірчими інтервалами та коваріаціями.

У результаті рівняння регресії набуло вигляду:

$$y=1{,}005+1{,}251\cdot10^{-3}\cdot x_1-9{,}086\cdot10^{-4}\cdot x_2+2{,}228\cdot10^{-3}\cdot x_3+6{,}292\cdot10^{-4}\cdot x_1\cdot x_3-$$
$$-5{,}267\cdot10^{-4}\cdot x_2\cdot x_3-1{,}026\cdot10^{-3}\cdot x_1^2-1{,}19\cdot10^{-4}\cdot x_3^2-5{,}178\cdot10^{-4}\cdot x_4^2 \quad (2)$$

where: $x_1$ - encoded value of moisture of soybean seeds;

$x_2$ - encoded value of amount of the fed soybean seeds;

$x_3$ - encoded value of the angular velocity of the disk;

$x_4$ – encoded value of the number of blades.

Adequacy test of hypotheses of obtained regression equation was performed by the Fisher criterion. The estimated value of this criterion in the dispersion of inadequacy $S^2_{inadeq.}$ =4,211·10$^{-7}$ and dispersion $S^2_y$ =4,869·10$^{-4}$ reproducibility of the experiment was: $F^{calc.}$ = 9,189. Tabular value of Fisher's exact test adopted by the 5 -% of significance, according to [8,9], was: $F^{tabl.}(0{,}05;f_2;f_1)=19{,}5$ where $f_2$ = 17 number of degrees of freedom variance inadequacy $f_1=2$ - the number of degrees of freedom variance reproducibility of the experiment.

Since, $F^{calc.}$ =9,189< $F^{tabl.}(0{,}05;f_2;f_1)=19{,}5$ the hypothesis by the adequacy of the regression equation is confirmed.

Final regression equation of the factors acquired the form:

де: $x_1$ – кодоване значення вологості насіння сої;

$x_2$ – кодоване значення кількості подачі матеріалу;

$x_3$ – кодоване значення колової швидкості диска;

$x_4$ – кодоване значення кількості лопаток.

Перевірку гіпотези адекватності отриманого рівняння регресії проводили за критерієм Фішера. Розрахункове значення даного критерію при дисперсії неадекватності $S^2_{неад.}$ =4,211·10$^{-7}$ і дисперсії відтворюваності досліду $S^2_y$ =4,869·10$^{-4}$ становило: $F^{розр.}$ =9,189. Табличне значення критерію Фішера за прийнятого 5-% значущості, згідно [8,9], склало: $F^{табл.}(0{,}05;f_2;f_1)=19{,}5$ де $f_2$ = 17 - число ступенів вільності дисперсії неадекватності; $f_1=2$ - число ступенів вільності дисперсії відтворюваності досліду.

Оскільки, $F^{розр.}$ =9,189< $F^{табл.}(0{,}05;f_2;f_1)=19{,}5$ то гіпотеза адекватності рівняння регресії підтверджується.

Остаточно рівняння регресії із факторами у натуральному вигляді набуло вигляду:

$$k = 0{,}0000033 \cdot Q + 0{,}000074 \cdot V + 0{,}0023 \cdot W + 0{,}00104 \cdot n - 5{,}29 \cdot V^2 - \\ - 0{,}000064 \cdot W^2 - 0{,}00013 \cdot n^2 - 2{,}341 \cdot Q \cdot V + 0{,}0000105 \cdot V \cdot W + 0{,}974 \quad (3)$$

where: *Q*- amount of the fed soybean seeds, kg/ h;
*V* - the angular velocity of the disk m/s;
*W* – moisture content, %;
*n* – number of blades on the disk.

In order to track the dynamics of the coefficient k the response surfaces (Fig. 2, a-f) were constructed.

The analysis of regression equation determined that the change in the coefficient k is mostly affected by the initial soybean moisture content W and angular velocity drive V, and, in a less degree, the amount Q of fed soybean seeds and number of blades on the disk n.

Considering the obtained response surfaces according to equation of regression and previous studies, we can conclude that the optimal values of the studied factors under which the maximum acceptable value of the coefficient k is obtained were: initial moisture content of soybean W = 17 ... 19%, the angular velocity drive V= 35…45 m/s, feeding Q = 200 ... 300 kg/h and the number of blades n = 4.

де:*Q* - подача насіння сої, кг/год;
*V* - колова швидкість диска, м/с;
*W* - вологість, %;
*n* – кількість лопаток на диску.

Для відслідковування динаміки зміни величини коефіцієнта *k* були побудовані поверхні відгуку (фіг. 2, a-f).

В результаті аналізу рівняння регресії встановлено, що на зміну величини коефіцієнта зміни площі *k* найбільший плив має початкова вологість сої *W* та колова швидкість диска *V*, і, в меншій мірі, кількість подачі *Q* насіння сої і кількість лопаток на диску *n* .

Зважаючи на одержані згідно з рівнянням регресії поверхні відгуку, а також попередні дослідження можна зробити висновок, що оптимальні значення досліджуваних факторів при яких буде отримано максимально допустиме значення коефіцієнта зміни площі *k* склали: початкова вологість сої W=17...19%, колова швидкість диска V=35…45 м/с, подача Q=200…300 кг/год та кількість лопаток n=4.

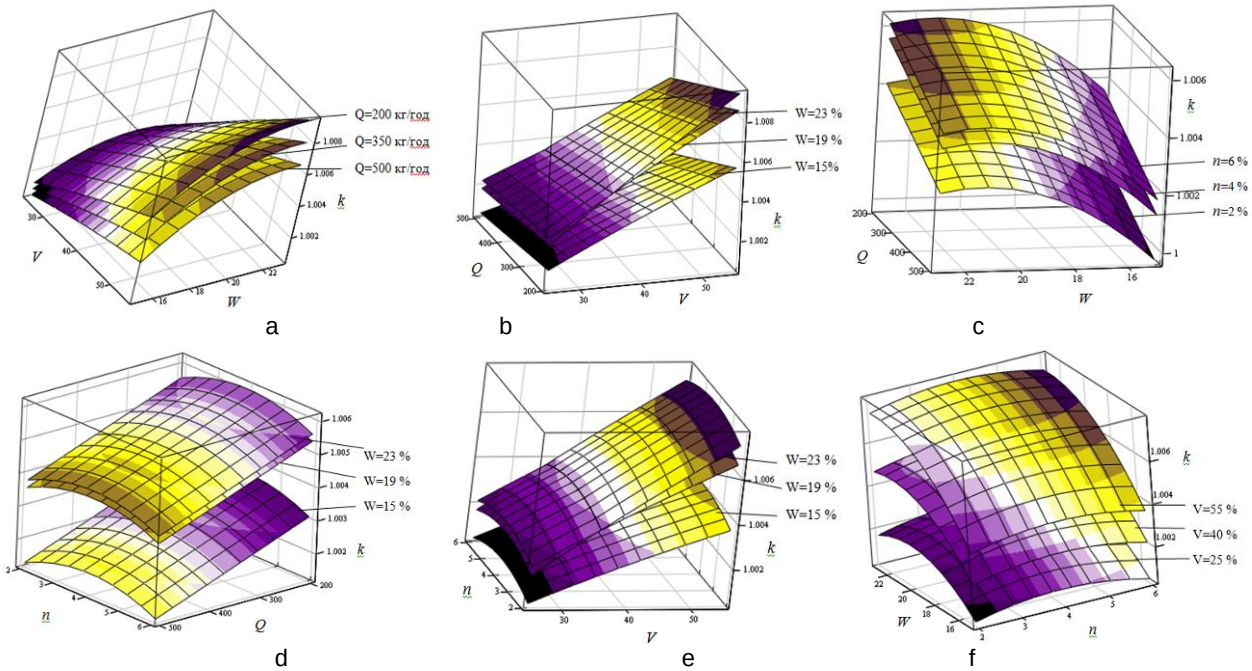


**Fig. 2 -** Response surface of the area deformation coefficient k depending on:
*a) initial soybean moisture content W , angular velocity of the disc V at feeding quantity Q=200;350 and 500 kg/hour and number of blades n=4; b) angular velocity of the disc V, feeding quantity Q at initial moisture content W=15;19 and 23 % i n=4 ; c) seed moisture content W and feeding quantity Q at the blade quantity n=2.4 and 6 and disc angular velocity V=40 m/s; d) feeding quantity Q, number of blades n at seed moisture content W=15.19 and 23% and V=40 m/s ; e) disc angular velocity V, number of blades n at moisture content W=15.19 and 23% and feeding quantity Q-350 kg/h; f) quantity of blades n, seed moisture content W at disc angular velocity V=25.40 and 55 rpm and Q=350 kg/hour.*

2. *Three-factor experiment*.

After the four-factor experiment was carried out, the samples were selected with the required W value, with maximum k coefficient: W=23% - k=1.0055; W=19% - k=1.0053; W=15% - k=1.003.

Homogeneity of variances was tested by the Cochrane criterion.

Since,
$G^{calc}$ =0.176< $G^{tabl.}(0.05;15;2)$ =0.335 the process is

2. *Трифакторний експеримент.*

Після проведення чотирифакторного експерименту були відібрані зразки з необхідними значенням *W*, максимальні значення коефіцієнта k для яких склали: W=23% - k=1,0055; W=19% - k=1,0053; W=15% - k=1,003.

Оцінку однорідності ряду дисперсій перевіряли за критерієм Кохрена.

Оскільки,
$G^{розр.}$ =0,176< $G^{табл.}(0{,}05;15;2)$ =0,335, то процес

reproduced.

During determining of confidence intervals for regression coefficients, the Student test was used, tabulated value of which at a 5 -% level of significance and the number of degrees of freedom of variance of experiment reproducibility was $f_1=2$ is $t$ = 4.3 [8,9].

Test for the significance of regression coefficients was performed according to their established confidence intervals and covariance.

As a result, the regression equation acquired form:

відтворюється.

Під час визначення довірчих інтервалів коефіцієнтів регресії використовували критерій Ст'юдента, табличне значення якого за 5-% рівня значущості та числі ступенів вільності дисперсії відтворюваності досліду $f_1$=2 становило $t$=4,3 [8,9].

Перевірку значущості коефіцієнтів регресі проводили за встановленими їх довірчими інтервалами та коваріаціями.

У результаті рівняння регресії набуло вигляду:

$$y = 12{,}222 + 3{,}292 \cdot x_1 - 4.25 \cdot x_2 - 0{,}278 \cdot x_1^2 + 1{,}306 \cdot x_2^2 + 1{,}889 \cdot x_3^2 \quad (4)$$

where: $x_1$ - encoded value of moisture of soybean seeds;

$x_2$ - encoded value of the temperature of the drying agent;

$x_3$ - encoded value of the velocity of the drying agent

Adequacy test of hypotheses of obtained regression equation was performed by the Fisher criterion. The estimated value of this criterion in the dispersion of inadequacy $S^2_{inadea.}$ =1.982 and dispersion $S^2_y$ =0.259 reproducibility of the experiment was: $F^{calc.}$ =7.645. Tabular value of Fisher's exact test adopted by the 5 -% of significance, according to [8,9], was: $F^{tabl.}(0.05; f_2; f_1) = 19.38$ where f₂=8 number of degrees of freedom variance inadequacy $f_1 = 2$ - the number of degrees of freedom variance reproducibility experiment.

Since, $F^{calc.}$ =7.645< $F^{tabl.}(0.05; f_2; f_1) = 19.38$ the hypothesis by the adequacy of the regression equation is confirmed. Final regression equation of the factors in the species acquired the form:

де: $x_1$ – кодоване значення вологості насіння сої;

$x_2$ – кодоване значення температури сушильного агенту;

$x_3$ – кодоване значення швидкості сушильного агенту.

Перевірку гіпотези адекватності отриманого рівняння регресії проводили за критерієм Фішера. Розрахункове значення даного критерію при дисперсії неадекватності $S^2_{неад.}$ =1,982 і дисперсії відтворюваності досліду $S^2_y$ =0,259 становило: $F^{розр.}$ =7,645. Табличне значення критерію Фішера за прийнятого 5-% значущості, згідно [8,9], склало: $F^{табл.}(0{,}05; f_2; f_1) = 19{,}38$ де f₂ = 8 - число ступенів вільності дисперсії неадекватності; $f_1 = 2$ - число ступенів вільності дисперсії відтворюваності досліду.

Оскільки, $F^{розр.}$ =7,645< $F^{табл.}(0{,}05; f_2; f_1) = 19{,}38$ то гіпотеза адекватності рівняння регресії підтверджується.

Остаточно рівняння регресії із факторами у натуральному вигляді набуло вигляду:

$$\tau = 1{,}48 \cdot W - 0{,}017 \cdot W^2 + 0{,}052 \cdot t^2 - 5{,}029 \cdot t + 20{,}99 \cdot V_{ca}^2 - 79{,}76 \cdot V_{ca} + 183{,}67 \quad (5)$$

where:

$t$ - temperature of drying agent, ºC;

$V_{ca}$ – velocity of drying agent, m/s;

$W$ – moisture content of soybean seeds, %.

In order to track the dynamics of the drying time, the response surfaces (Fig. 3, a-c) were constructed.

The analysis of regression equation has determined the fact that the change in the drying time $\tau$ is mostly affected by the initial soybean moisture content W, temperature of the drying agent $t_{ca}$ and, in a less degree, the feeding velocity of the drying agent $V_{ca}$.

Considering the obtained response surfaces and previous studies, we can conclude that the optimal values of the studied factors with the minimum acceptable value of the drying time were: initial moisture content of soybean W=17...19%, area deformation coefficient k=1.0053, temperature of the drying agent $t_{ca}$=42…45$^0$C and feeding velocity of the drying agent $V_{ca}$ =1.9-2.0 m/s.

де:

$t$ - температура сушильного агенту, ºC;

$V_{ca}$ – швидкість сушильного агенту, м/с;

$W$ – вологість насіння сої, %.

Для відслідковування динаміки зміни часу сушіння були побудовані поверхні відгуку (фіг. 3, а-с).

В результаті аналізу рівняння регресії встановлено, що на зміну часу сушіння $\tau$ найбільший плив має початкова вологість сої $W$, температура сушильного агенту $t_{ca}$, і, в меншій мірі, швидкість подачі сушильного агенту $V_{ca}$ .

Зважаючи на одержані поверхні відгуку, а також попередні дослідження можна зробити висновок, що оптимальні значення досліджуваних факторів при яких буде досягнуто мінімальне значення часу сушіння склали: початкова вологість сої $W$=17...19% з коефіцієнтом деформації $k$=1,0053, температура сушильного агенту $t_{ca}$=42-45$^0$C і швидкість подачі сушильного агенту $V_{ca}$ =1,9-2,0 м/с.

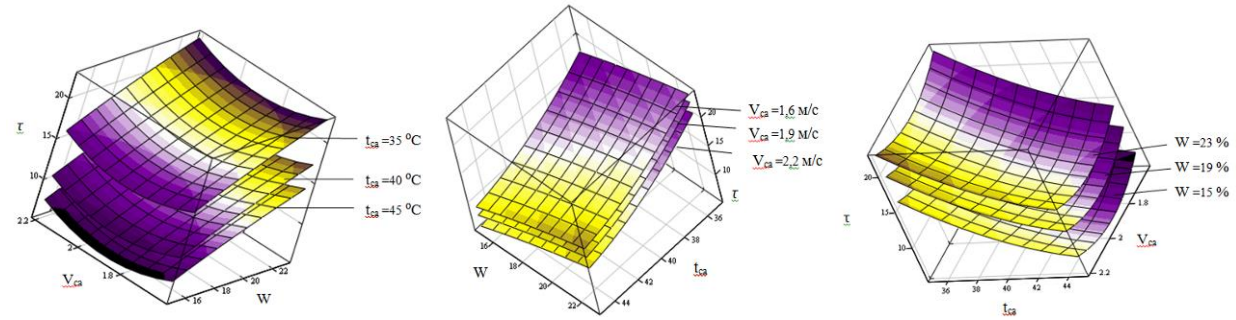


a) b) c)

**Fig. 3 -** Response surface of drying time t depending on:
*a) drying agent velocity Vca and initial moisture content of the soybean seeds W at the temperature of the drying agent tca=35;40 and 45 °C; b) initial moisture content of the soybean seeds W and the temperature of the drying agent tca at the drying agent velocity Vca=1.6;1.9 and 2,2 m/s; c) temperature of the drying agent tca and drying agent velocity Vca at the initial moisture content of the soybean seeds W=15;19 and 23 %.*

## CONCLUSION

The results of complex experimental studies allow the conclusion that all factors are significant against the area deformation coefficient of the seed and drying time.

Two proposed mathematical models resulted in determining time within 5.7...22.7 minutes, necessary to achieve moisture of the soybean seeds after previous deformation of the seed coat.

Increasing the initial moisture content of soybean seeds *W* leads to longer drying time $\tau$. The difference in drying exposure is 3…4 minutes, which is less than the difference in exposures of drying of material without pre-conditioning (8…12 min) as the coefficient k is different for various *W* values and confirms its influence on the speed of moisture removal from the seed.

Thus, considering the proposed mechanism to prepare soybean before drying, as part of the loading mechanism of the dryer, we argue it will allow reducing the energy consumption through increasing the contact area of the drying agent and material and changes in the intensity in moisture removal from the seed. Therefore, it is feasible to apply the proposed energy saving method of the soybean seed drying to produce oil. Reduction in oil yield was not observed.

## REFERENCES

[1]. Babich A.A. (1993) - *Modern production and use of soybean,* Kyiv: Urozhay, p.427;
[2]. Balakay H.T., Bezyhlova O. S., (2003) - *Soybeans: ecology, agriculture, processing,* D.: Fenuks, p.160;
[3]. Didyh V.F. (2002) - *Improving the efficiency of drying of agricultural plant materials*: monograph, Lutsk: LNTY, p.165;
[4]. Kirchuk R., Tsiz I., Tsiz K., (2014) - *Intensification of drying soybean,* The Ukrainian Farmer, Kyiv, №7(55), p.76;
[5]. Kirchuk R., Tsiz K., (2013) - *Deformation seed shell machine,* Patent №84111, Ukraine, IPC B07B, Appl. 12.04.2013; publ. 10.10.2013; Bul. № 19;
[6]. Kirchuk R., Tsiz K.E., (2014) - *Deformation seed shell machine* Patent №87184. Ukraine, IPC B07B 9/00 №u201310015, Appl.12.08.2013; publ.27.01.2014; Bul. № 2;
[7]. Kotov B.I., (1994) - *Technological and heat power bases of increase of efficiency of drying vegetable raw*

## ВИСНОВОК

Отримані результати комплексу експериментальних досліджень дозволяють зробити висновок, що всі фактори є значущими відносно коефіцієнта зміни площі насінини та часу сушіння.

Результатом запропонованих двох математичних моделей є встановлення часу, який знаходиться в межах 5,7…22,7 хв., що необхідний для досягнення кондиційної вологості насіння сої в сушильній камері з попереднім деформуванням оболонки плоду.

Підвищення початкової вологості насіння сої *W* призводить до збільшення часу сушіння $\tau$. Різниця експозицій сушіння складає 3-4 хв, що є меншою різниці експозицій сушіння попередньо непідготовленого матеріалу (8-12 хв). Це пояснюється тим, що коефіцієнт *k* є різним для досліджуваних значень вологостей *W* і підтверджує його вплив на швидкість видалення вологи з насінини.

Отже, розглядаючи запропонований механізм підготовки сої до сушіння, як складову частину завантажуючого пристрою сушарки, можна стверджувати, що це дозволить зменшити енерговитрати, шляхом збільшення площі контакту сушильного агенту і матеріалу та зміни інтенсивності видалення вологи з насінини. Тому доцільним є застосування запропонованого енергозберігаючого методу сушіння насіння сої для отримання олії. Зменшення виходу олії при цьому не спостерігалось.

## БІБЛІОГРАФІЯ

[1]. Бабич А.О.(1993) - *Сучасне виробництво і використання сої* – К. : Урожай– 427 с;
[2]. Балакай Г.Т., Безуглова О. С. (2003) - *Соя: екология, агротехніка, переработка.*- Д: Феникс.- 160 с;
[3]. Дідух В.Ф. (2002) - *Підвищення ефективності сушіння сільсько-господарських рослинних матеріалів*: монографія – Луцьк: ЛДТУ. – 165 с;
[4]. Кірчук Р., Цизь І., Цизь К.(2014) *Інтенсифікація сушіння сої*// The Ukrainian Farmer- Київ, №7(55). – С.76;
[5]. Кірчук Р., Цизь К. *Машина для деформації насіннєвих оболонок* / Патент на корисну модель №84111 Україна, МКП B07B. Заявлено 12.04.2013; Опубл. 10.10.2013; Бюл. № 19;
[6]. Кірчук Р., Цизь К. *Машина для деформації насіннєвих оболонок.* / Патент на корисну модель №87184 Україна,B07B 9/00 (Україна). – №u201310015; Заявл.12.08.2013; Опубл.27.01.2014. Бюл. №2;
[7]. Котов Б.И. (1994) - *Технологические и теплоэнергетические основы повышения эффективности*

*materials*: Hlevaha, p.440;
[8]. Melnikov S.V., (1980) - *Planning experiment of agricultural process research,* Leningrad: Kolos, p.168;
[9]. Novik F.S., Arsov I.B., (1980) - *Optimizing processes technology metals by the methods of planning experiments*. Moscow: Engineering, Sofia: Machinery, p.304;
[10]. Tsiz K.E., Kirchuk R.V., Zabrodotsjka L.Y. (2013) - *Determining the impact of soybean seed shell deformation intensity drying*, Farm Machinery: Proc. Science. Century, Vol. 25, pp.160-165;
[11]. Vashchenko V., Bondarenko O. (1999) - *Resource-saving technologies in crop production*, Agro Industrial Machines, №4, p.27-28;
[12]. Voznesensky V.A. (1981) - *Statistics methods of experiment plan of technics and economics research*. - Moscow: Finance and Statistics, p.263.

*сушки растительного сырья*: Глеваха, 440 с.
[8]. Мельников С.В. (1980) - *Планирование эксперимента в исследованиях сельскохозяйственных процессов* – Л.: Колос. Ленингр.– 168 с;
[9]. Новик Ф.С., Арсов Я.Б. (1980) - *Оптимизация процессов технологии металлов методами планирования экспериментов*. – М.: Машиностроение; София: Техника. – 304 с;
[10]. Цизь К.Є., Кірчук Р.В., Забродоцька Л.Ю. (2013) - *Визначення впливу деформації оболонки насінини сої на інтенсивність сушіння*, Сільськогосподарські машини: зб. наук. ст. - Вип. 25, с.160-165;
[11]. Ващенко В., Бондаренко О. (1999) - Ресурсозберігаючі технології у рослинництві // Техніка АПК.– №4. – С.27-28;
[12]. Вознесенский В.А. (1981) - *Статистические методы планирования эксперимента в технико-экономических исследованиях*. – 2-е изд., перераб. и доп. – М.: Финансы и статистика – 263 с.

# THE INFLUENCE OF SUSPENDING RODS ELASTICITY ON CIRCULAR MOTION OF A PLANSIFTER FOR SIFTING MILL PRODUCTS
# /
# *INFLUENȚA ELASTICITĂȚII TIJELOR DE SUSPENDARE ASUPRA MIŞCĂRII CIRCULARE A SITEI PLANE PENTRU CERNEREA PRODUSELOR DE MĂCINIŞ*

**Ph.D. Stud. Eng. Ivancu B., Prof. Ph.D. Eng. Voicu Gh., Prof. Ph.D. Eng. Filip I.**
*Polytechnic University of Bucharest, Faculty of Biotechnical Systems Engineering / Romania*
*E-mail: ivancu_bogdan@yahoo.com*

***Abstract:*** *In this paper is studied, based on the calculation model of plansifter SPP 618 A, the influence of the elastic suspending rods on the circular movement described by the plansifter. The operating regime of the plansifter must transmit to the material an adequate relative motion that should meet the requirements of a good separation. Thus, each grid point of the plansifter must describe a circle of radius equal to the eccentricity between the vertical long axis of the plansifter and the short axis of the counterweights. For usual construction of plansifters, the radius of the described circle has the value of r = 45 mm. Based on the calculation model, we determined the own pulsations, the stiffness of the suspending system and thus the radius of the circle described by the movement of the plansifter. This study was conducted in order to establish dependencies between dimensions of elastic rods and materials they are made of and the radius of the circle described by the movement of the plansifter.*

***Keywords:*** *plansifter, circular plan motion, eccentricity, suspension rods, elastic elements.*

## INTRODUCTION

The use of plansifters for sifting intermediate products, resulted in the milling process is known for over a century, during which time they have undergone many changes to improve product quality, production capacity, specific charging and reducing energy consumption. The principle of sifting was preserved regardless the type of construction of the plansifters. The plansifter assembly consists of several overlapped sieves, which are simultaneously put in motion by an oscillating mechanism, determining a circular plan motion to sieving surfaces. The plansifter offers the possibility of sorting a mixture of milled products into several fractions of the same particle size or appropriate granulations. The relative movement of the material on plansifter is ensured by transmitting to the sieve a circular motion by using a crank type mechanism. The operating regime of the plansifter must transmit to the material an adequate relative movement that should meet the requirements of a good separation [3].

The efficiency of the sifting process on sieve is ensured by a relative movement in both ways without the detachment of the material. At the same time, the material on the sieve must have a forward movement to the opposite end of feeding, to allow the discharge of the material. In order to achieve quality in sifting, the plansifter vibration parameters (amplitude and frequency) must be correlated with other parameters so as to be, simultaneously, achieved the required values for the height and the length of the material grain jumps on the sieve [2].

***Rezumat:*** *În această lucrare este studiată, pe baza modelului de calcul al sitei plane SPP 618 A, influența tijelor elastice de suspendare asupra mişcării circulare descrise de sita plană. Regimul de funcționare al sitei trebuie să asigure materialului o mişcare relativă corespunzătoare care să îndeplinească cerințele unei bune separări. Astfel, fiecare punct al sitei plane trebuie să descrie un cerc de rază egală cu excentricitatea dintre axul lung vertical al sitei plane şi axul scurt al contragreutăților. Pentru construcții uzuale de sită plană raza cercului descris are valoarea r = 45 mm. Pe baza modelului de calcul au fost determinate pulsațiile proprii, rigiditatea sistemului de suspendare şi, implicit, raza cercului descris de mişcarea plan circulară a sitei. Acest studiu a fost realizat în vederea stabilirii unei dependențe între dimensiunile şi materialele din care sunt confecționate tijele elastice şi raza cercului descris de mişcarea sitei plane.*

***Cuvinte cheie:*** *sita plană, mişcare plan circulară, excentricitate, tije de suspendare, elemente elastice.*

## INTRODUCERE

Folosirea sitelor plane pentru cernerea produselor intermediare, rezultate în procesul de măcinare este cunoscută de peste un secol, timp în care acestea au suferit numeroase modificări pentru a îmbunătăți calitatea produselor, capacitatea de producție, încărcarea specifică şi reducerea consumului de energie. Principiul de cernere a fost păstrat indiferent de tipul constructiv al sitei. Ansamblul sită plană este formată din mai multe site aşezate suprapus, care sunt acționate simultan de un mecanism liber oscilant, imprimând suprafețelor de cernere, o mişcare plan circulară. Sita plană oferă posibilitatea sortării unui amestec de produse măcinate în mai multe fracțiuni de aceeaşi granulație sau de granulații apropiate. Deplasarea relativă a materialului pe sita plană se asigură imprimând sitei o mişcare circulară cu ajutorul unui mecanism de tip bielă-manivelă (cel mai des întâlnit). Regimul de funcționare al sitei trebuie să imprime materialului o mişcare relativă corespunzătoare care să îndeplinească cerințele unei bune separări [3].

Mişcarea relativă care asigură desfăşurarea eficientă a procesului de separare pe sită este cel de deplasare relativă în ambele sensuri fără desprindere. Totodată materialul de pe sită trebuie să aibă o mişcare de înaintare către capătul opus alimentării, pentru a permite evacuarea refuzului. Pentru a realiza o cernere de calitate, trebuie ca parametrii vibrațiilor sitei (amplitudine şi frecvență) să fie corelați cu ceilalți parametri, astfel încât să se realizeze simultan valorile necesare pentru înălțimea şi lungimea saltului granulelor de material pe sită [2].

Most often, the vibration generator is composed of an electric motor with flange and a driving sheave.
The motor assembly is fitted in the interior of the central frame through a metal plate which allows the displacement of the entire system through V-belts, which ensure transmission of the motion from the drive shaft to the axis of the central mechanism for generating the rotational movement of the sieve, [1]. To achieve circular vibration and thus a circular movement, it takes only one vibration generator placed at the bottom of the plansifter.

Each grid point of the plansifter must describe a circle of radius equal to the eccentricity between the vertical long axis of the plansifter and the short axis of the counterweights in order to achieve a good separation of the product in question [5]. For usual construction of plansifters, the radius of the described circle, r = 45 mm [5]. The sieves block are suspended by a frame mounted on the ceiling by means of suspending rods that are made from different materials (e.g. elastic reed, bamboo, boiled beech, glass fiber etc.).

## MATERIAL AND METHOD

The plansifter SPP 618 A has 24 elastic suspension rods, divided by 6 in 4 attachment points that are supporting the sieves block with a weight of approximately 3935 kg and is shown in Figure 1. The suspending rods were made of fiber glass and had a length of about 1585 mm.

The plansifter SPP 618 A is equipped with a vibration generator having a mass $m_0$ = 345 kg. Its revolution speed is $n$ = 220 [rev/min] and eccentricity $e$ = 260 mm. The plansifter SPP 618 A with square frames has 6 compartments. It sums up a large number of overlapping screening surfaces (18 pcs.) that are put into motion simultaneously with a weight of $M$ = 3935 kg.

Cel mai adesea, generatorul de vibrații se compune dintr-un motor electric cu flanşă şi şaibă de antrenare. Ansamblul motor este fixat în interiorul cadrului central prin interiorul unei plăci metalice care permite deplasarea întregului sistem prin intermediul curelelor trapezoidale, ce asigură transmiterea mişcării de la arborele motor la axul mecanismului central de generare a mişcării de rotație a sitei, [1]. Pentru realizarea unor vibrații circulare şi, implicit, a unei mişcări circulare, este nevoie de un singur generator de vibrații amplasat la partea inferioară a cadrului sitei.

Fiecare punct al sitei plane trebuie să descrie un cerc de rază egală cu excentricitatea dintre axul lung vertical al sitei plane şi axul scurt al contragreutăților pentru a obține o bună separare pentru produsul în cauză, [5]. Pentru construcții uzuale de sită plană raza cercului descris, r = 45 mm, [5]. Blocul cu site este suspendat de un schelet montat pe tavan cu ajutorul tijelor de suspendare elastice care pot fi confecționate din diferite materiale (ex. trestie, bambus, fag fiert, fibra de sticlă etc.).

## MATERIAL ŞI METODĂ

Sita plană SPP 618 A prezintă 24 de tije elastice de suspendare, repartizate câte 6 în 4 puncte de prindere care susțin blocul de site cu o greutatea de aproximativ 3935 kg şi este prezentată în Figura 1. Tijele de suspendare au fost confecționate din fibră de sticlă şi au o lungime de aproximativ 1585 mm.

Sita plană SPP 618 A, este echipată cu un generator de vibrații cu o masă $m_0$ = 345 kg. Turația acestuia este de $n$ = 220 rot/min, iar ecentricitatea $e$ = 260 mm. Sita plană cu rame pătrate SPP 618 face parte din grupa sitelor plane cu 6 compartimente. Ea însumează un număr mare de suprafețe de cernere suprapuse (18 buc.) puse în mişcare simultan şi au o greutate $M$ = 3935 kg.

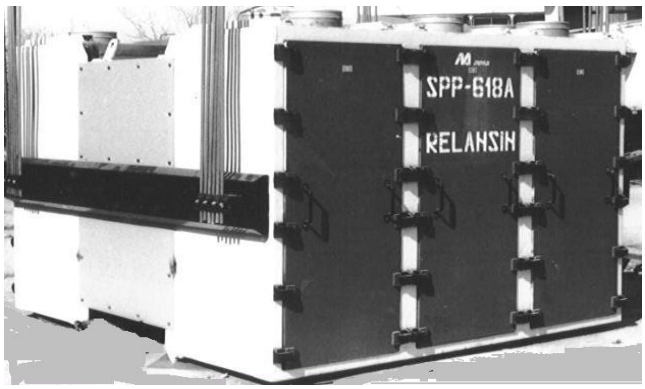


**Fig.1 -** The plansifter SPP 618 A with square frames [3]

The method used is based on the calculation model of the plansifter and graphical representation of motion described by the plansifter according to Figure 2. For the application of the calculation model (see Figure 2-b) it was based on the following considerations:

- The location of the center of mass $C_M$ of the sieves block and the center of mass $C_{m0}$ of vibration generator is symmetrical about the position of the center of mass of the whole system, $C$ (see Figure 2-a);
- The two centers of mass are moving on concentric circles centered in $C$, equilibrating the sifting system (see Figure 2-a);

Metoda utilizată are la bază modelul de calcul al sitei plane, precum şi reprezentarea grafică a mişcării descrise de sita plană în conformitate cu Figura 2. Pentru aplicarea modelului de calcul (v. Figura 2-b) s-a pornit de la următoarele considerente:

- poziția centrului de masa al blocului de site $C_M$ şi centrul de masa al generatorului de vibrații $C_{m0}$ se află în poziție simetrică cu poziția centrului de masa al întregului sistem, $C$ (v. Figura 2-a);
- cele două centre de masă se deplasează pe cercuri concentrice cu centrul în $C$, echilibrând sistemul de cernere (v. Figura 2-a);

- It is neglected the effect of elastic elements mass and their nonlinear effects;
- The amplitude of the plansifter vibrations is approximated as being the radius of the circle described by its own circular motion.

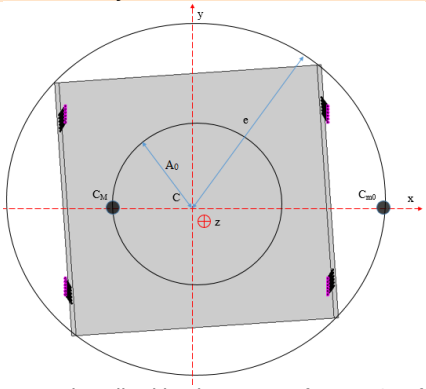


a) The trajectory described by the center of mass $C_M$ of the sieves block and the center of mass $C_{m0}$ of vibration generator

- este neglijat efectul de masă a elementelor elastice şi efectele lor neliniare;
- amplitudinea vibrațiilor sitei plane este aproximată ca fiind raza cercului descris de mişcarea circulară a sitei plane.

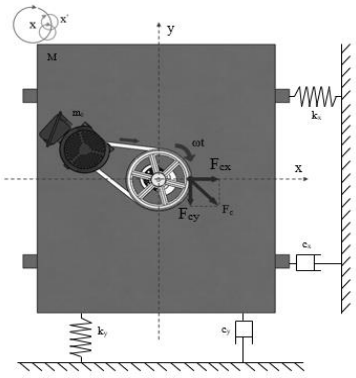


b) The calculation model of the plansifter SPP 618 A

**Fig.2 -** The 3D calculation model of the plansifter SPP 618 A [5]

The differential equations of motion for the model in Figure 2 were determined in paper [5], where was shown that each point of the plansifter describes a circle of radius equal to the amplitude of vibration $A_0$ (calculated with relation 1).

Ecuațiile diferențiale ale mişcării pentru modelul din Figura 2 au fost determinate în lucrarea [5], unde s-a demonstrat faptul că fiecare punct al sitei plane descrie un cerc de rază egală cu amplitudinea vibrațiilor $A_0$ (calculată cu relaţia 1).

$$A_0 = \frac{\frac{F_0}{k}}{\left|1-\left(\frac{\omega}{\omega_0}\right)^2\right|} \quad (1)$$

where, $F_0 = m_0 \cdot e \cdot \omega^2$ is the inertia force of the vibration generator, [N], $m_0$ is the mass of the vibration generator, [kg], $e$ eccentricity of the vibration generator, [mm], $\omega = \frac{\pi \cdot n}{30}$ is the angular velocity of the vibration generator, [rad/s], $n$ is the revolution speed of the vibration generator, [rot/min], $k = z \cdot \frac{12 \cdot E \cdot I}{l^3}$ is the stiffness of the suspending system, [N/m], $z$ is the number of the elastic suspending rods, $E$ is the elasticity modulus, [N/mm$^2$], $I = \frac{\pi \cdot d^4}{64}$ is the axial inertia moment of the rod, [mm$^4$], $d$ represent the diameter of the elastic rod, [mm], $l$ is the length of the elastic rod, [mm], $\omega_0^2 = \frac{k}{M + m_0}$ is the own pulsation of the system, [rad/s] and $M$ is the mass of the sieves block, [kg].

## RESULTS

It is noted that the stiffness of the suspending system might influence the radius of the circle described by the movement of the plansifter. To determine this influence we calculated the amplitude of vibration of SPP 618 A plansifter for elastic suspension rods made of different materials and of different sizes. The materials used in the simulation for the elastic suspension rods are shown in Table 1.

în care, $F_0 = m_0 \cdot e \cdot \omega^2$ este forța de inerție a generatorului de vibrații, [N], $m_0$ este masa generatorului de vibrații, [kg], $e$ este excentricitatea generatorului de vibrații, [mm], $\omega = \frac{\pi \cdot n}{30}$ este viteza unghiulară a generatorului de vibrații, [rad/s], $n$ este turația generatorului de vibrații [rot/min], $k = z \cdot \frac{12 \cdot E \cdot I}{l^3}$ este rigiditatea sistemului de suspendare, [N/m], $z$ este numărul de tije elastice de suspendare, $E$ este modulul de elasticitate [N/mm$^2$], $I = \frac{\pi \cdot d^4}{64}$ este momentul de inerție axial al tijei de suspendare, [mm$^4$], $d$ reprezintă diametrul tijei elastice [mm], $l$ este lungimea tijelor de suspendare, [mm], $\omega_0^2 = \frac{k}{M + m_0}$ este pulsația proprie a sistemului, [rad/s] iar $M$ este greutatea blocului de site [kg].

## REZULTATE

Se observă faptul că rigiditatea sistemului de suspendare ar putea influența raza cercului descris de mişcarea sitei plane. Pentru a determina această influență am calculat amplitudinea vibrațiilor sitei plane SPP 618 A, pentru tijele elastice de suspendare confecționate din diferite materiale şi de diferite dimensiuni. Materialele folosite în studiu, sunt prezentate în Tabelul 1.

Table 1

**Characteristics of the materials used in study**

| Material | Density [kg/m$^3$] | Poisson ratio | Elastic Modulus [MPa] | Damping |
|---|---|---|---|---|
| **Boiled beech** | 760 | 0,2...0,394 | 10000 | 0.194 |
| **Fiber glass** | 2550 | 0,21...0,23 | 80000 | 0.02 |
| **Bamboo** | 600 | 0,22...0,31 | 16170 | 0.2 |

For these, we calculated the stiffness of the suspending system, $k$ and amplitude of vibration, $A_0$ using relation (1). The results have been listed in Table 2 and Table 3.

Pentru aceasta s-a calculat rigiditatea sistemului de suspendare $k$ şi amplitudinea vibrațiilor $A_0$ cu ajutorul relației (1). Rezultatele obținute sunt prezentate in Tabelul 2 şi Tabelul 3.

Table 2

**The stiffness and the vibration amplitude for rods with Φ 12 and Φ 14 diameter**

| Material | Elastic rod length [mm] | The diameter of elastic rods [mm] | | | | | | | |
|---|---|---|---|---|---|---|---|---|---|
| | | d = 12 I = 1018 mm$^4$ | | | | d = 14 I = 1885,74 mm$^4$ | | | |
| | | Suspending stiffness k [N/m] | Own pulsation ω [rad/s] | Pulsation ratio ω/ω$_0$ | Vibration amplitude A$_0$ [mm] | Suspending stiffness k [N/m] | Own pulsation ω [rad/s] | Pulsation ratio ω/ω$_0$ | Vibration amplitude A$_0$ [mm] |
| Boiled Beech | 1285 | 1381.754 | 0.568 | 40.550 | 20.970 | 2559.558 | 0.773 | 29.794 | 20.981 |
| | 1385 | 1103.547 | 0.508 | 45.374 | 20.968 | 2044.208 | 0.691 | 33.338 | 20.977 |
| | 1485 | 895.284 | 0.457 | 50.376 | 20.966 | 1658.422 | 0.622 | 37.013 | 20.973 |
| | 1585 | 736.296 | 0.415 | 55.549 | 20.965 | 1363.912 | 0.565 | 40.814 | 20.970 |
| | 1685 | 612.831 | 0.378 | 60.888 | 20.963 | 1135.206 | 0.515 | 44.737 | 20.968 |
| | 1785 | 515.496 | 0.347 | 66.388 | 20.962 | 954.904 | 0.472 | 48.778 | 20.967 |
| | 1885 | 437.730 | 0.320 | 72.045 | 20.962 | 810.849 | 0.435 | 52.934 | 20.965 |
| | 1985 | 374.851 | 0.296 | 77.853 | 20.961 | 694.373 | 0.403 | 57.202 | 20.964 |
| Fiber glass | 1285 | 11054.036 | 1.607 | 14.337 | 21.060 | 20476.461 | 2.187 | 10.534 | 21.148 |
| | 1385 | 8828.378 | 1.436 | 16.042 | 21.039 | 16353.660 | 1.955 | 11.787 | 21.110 |
| | 1485 | 7162.273 | 1.294 | 17.811 | 21.024 | 13267.373 | 1.761 | 13.086 | 21.081 |
| | 1585 | 5890.368 | 1.173 | 19.640 | 21.012 | 10911.300 | 1.597 | 14.430 | 21.059 |
| | 1685 | 4902.646 | 1.070 | 21.527 | 21.003 | 9081.646 | 1.457 | 15.817 | 21.042 |
| | 1785 | 4123.971 | 0.982 | 23.472 | 20.996 | 7639.231 | 1.336 | 17.246 | 21.028 |
| | 1885 | 3501.839 | 0.905 | 25.472 | 20.990 | 6486.796 | 1.231 | 18.715 | 21.018 |
| | 1985 | 2998.808 | 0.837 | 27.525 | 20.985 | 5554.983 | 1.139 | 20.224 | 21.009 |
| Bamboo | 1285 | 2234.297 | 0.723 | 31.888 | 20.978 | 4138.805 | 0.983 | 23.430 | 20.996 |
| | 1385 | 1784.436 | 0.646 | 35.682 | 20.974 | 3305.484 | 0.879 | 26.217 | 20.988 |
| | 1485 | 1447.675 | 0.582 | 39.616 | 20.971 | 2681.668 | 0.792 | 29.107 | 20.982 |
| | 1585 | 1190.591 | 0.527 | 43.684 | 20.969 | 2205.446 | 0.718 | 32.096 | 20.978 |
| | 1685 | 990.947 | 0.481 | 47.883 | 20.967 | 1835.628 | 0.655 | 35.181 | 20.975 |
| | 1785 | 833.558 | 0.441 | 52.208 | 20.965 | 1544.080 | 0.601 | 38.359 | 20.972 |
| | 1885 | 707.809 | 0.407 | 56.656 | 20.964 | 1311.144 | 0.553 | 41.627 | 20.970 |
| | 1985 | 606.134 | 0.376 | 61.224 | 20.963 | 1122.801 | 0.512 | 44.983 | 20.968 |

Table 3

**The stiffness and the vibration amplitude for rods with d 16 and d 18 diameter**

| Material | Elastic rod length [mm] | The diameter of elastic rods [mm] | | | | | | | |
|---|---|---|---|---|---|---|---|---|---|
| | | d =16 I = 3217 mm$^4$ | | | | d = 18 I = 5153 mm$^4$ | | | |
| | | Suspending stiffness k [N/m] | Own pulsation ω [rad/s] | Pulsation ratio ω/ω$_0$ | Vibration amplitude A$_0$ [mm] | Suspending stiffness k [N/m] | Own pulsation ω [rad/s] | Pulsation ratio ω/ω$_0$ | Vibration amplitude A$_0$ [mm] |
| Boiled Beech | 1285 | 4366.507 | 1.010 | 22.811 | 20.998 | 6994.284 | 1.278 | 18.023 | 21.022 |
| | 1385 | 3487.339 | 0.903 | 25.525 | 20.990 | 5586.031 | 1.142 | 20.168 | 21.009 |
| | 1485 | 2829.204 | 0.813 | 28.338 | 20.984 | 4531.826 | 1.029 | 22.391 | 21.000 |

| Material | Elastic rod length [mm] | The diameter of elastic rods [mm] | | | | | | | |
|---|---|---|---|---|---|---|---|---|---|
| | | d =16 I = 3217 mm$^4$ | | | | d = 18 I = 5153 mm$^4$ | | | |
| | | Suspending stiffness k [N/m] | Own pulsation ω [rad/s] | Pulsation ratio ω/ω$_0$ | Vibration amplitude A$_0$ [mm] | Suspending stiffness k [N/m] | Own pulsation ω [rad/s] | Pulsation ratio ω/ω$_0$ | Vibration amplitude A$_0$ [mm] |
| | 1585 | 2326.782 | 0.737 | 31.248 | 20.979 | 3727.047 | 0.933 | 24.690 | 20.992 |
| | 1685 | 1936.617 | 0.673 | 34.252 | 20.976 | 3102.079 | 0.851 | 27.063 | 20.986 |
| | 1785 | 1629.029 | 0.617 | 37.346 | 20.973 | 2609.384 | 0.781 | 29.508 | 20.982 |
| | 1885 | 1383.278 | 0.569 | 40.527 | 20.970 | 2215.739 | 0.720 | 32.022 | 20.978 |
| | 1985 | 1184.574 | 0.526 | 43.795 | 20.969 | 1897.453 | 0.666 | 34.603 | 20.975 |
| Fiber glass | 1285 | 34932.056 | 2.857 | 8.065 | 21.285 | 55954.270 | 3.616 | 6.372 | 21.487 |
| | 1385 | 27898.716 | 2.553 | 9.024 | 21.218 | 44688.245 | 3.231 | 7.130 | 21.378 |
| | 1485 | 22633.628 | 2.300 | 10.019 | 21.169 | 36254.612 | 2.910 | 7.916 | 21.298 |
| | 1585 | 18614.258 | 2.085 | 11.048 | 21.131 | 29816.373 | 2.639 | 8.729 | 21.236 |
| | 1685 | 15492.939 | 1.903 | 12.110 | 21.102 | 24816.635 | 2.408 | 9.568 | 21.189 |
| | 1785 | 13032.234 | 1.745 | 13.204 | 21.079 | 20875.071 | 2.208 | 10.433 | 21.152 |
| | 1885 | 11066.224 | 1.608 | 14.329 | 21.060 | 17725.911 | 2.035 | 11.321 | 21.123 |
| | 1985 | 9476.588 | 1.488 | 15.484 | 21.046 | 15179.626 | 1.883 | 12.234 | 21.099 |
| Bamboo | 1285 | 7060.642 | 1.284 | 17.938 | 21.023 | 11309.757 | 1.626 | 14.174 | 21.063 |
| | 1385 | 5639.028 | 1.148 | 20.073 | 21.010 | 9032.611 | 1.453 | 15.860 | 21.041 |
| | 1485 | 4574.822 | 1.034 | 22.285 | 21.000 | 7327.963 | 1.308 | 17.608 | 21.026 |
| | 1585 | 3762.407 | 0.938 | 24.574 | 20.992 | 6026.634 | 1.187 | 19.416 | 21.013 |
| | 1685 | 3131.510 | 0.855 | 26.936 | 20.987 | 5016.062 | 1.083 | 21.283 | 21.004 |
| | 1785 | 2634.140 | 0.785 | 29.369 | 20.982 | 4219.374 | 0.993 | 23.205 | 20.997 |
| | 1885 | 2236.761 | 0.723 | 31.871 | 20.978 | 3582.850 | 0.915 | 25.182 | 20.991 |
| | 1985 | 1915.455 | 0.669 | 34.440 | 20.975 | 3068.182 | 0.847 | 27.212 | 20.986 |

In addition, we notice that the stiffness of the suspending system decreases proportionally with increasing length of elastic rods. In Figure 3 is represented graphically the variation of vibration amplitude with diameter of elastic rod made of boiled beech for its length values.

De asemenea, observăm că rigiditatea sistemului de suspendare scade direct proporțional cu creşterea lungimii tijelor elastice. În Figura 3 este reprezentată grafic variația amplitudinii vibrației cu diametrul tijei elastice confecționată din fag fiert pentru valorile lungimii acesteia.

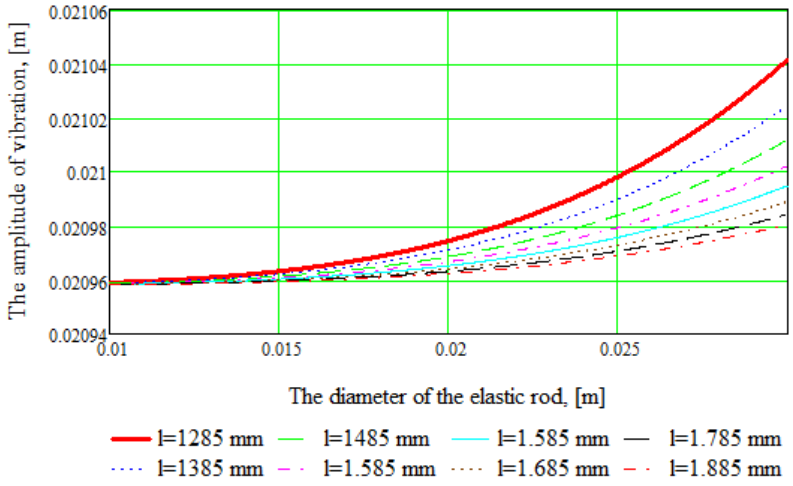


**Fig.3 -** The variation of vibration amplitude with the diameter of elastic rod made of boiled beech for its length values

The final relation that describes the amplitude dependence of the system parameters is represented by:

Relația finală care descrie dependența amplitudinii funcție de parametrii sistemului este reprezentată de:

$$A_0 = \frac{m_0 \cdot e \cdot \omega^2}{\left| \frac{12 \cdot \pi \cdot z \cdot E \cdot d^4}{64 \cdot l^3} - (M + m_0)\omega^2 \right|} \quad (2)$$

In Figure 4 is shown the variation of the amplitude of vibration with the length and the diameter of the elastic rod made of beech boiled. The step along the length of the rod is 0.1 m, the length considered: between 1 and 2 m. The step in the diameter of the rod is 0.001 m, the

În figura 4 este reprezentată variația amplitudinii sitei cu diametrul şi cu lungimea tijei confecționată din fag fiert. Pasul în lungimea tijei este de 0.1 m, lungimea considerată: între 1 şi 2 m. Pasul în diametrul tijei este 0.001 m, diametrul considerat: între 0.01 şi 0.03 m.

diameter considered: between 0.01 and 0.03 m.

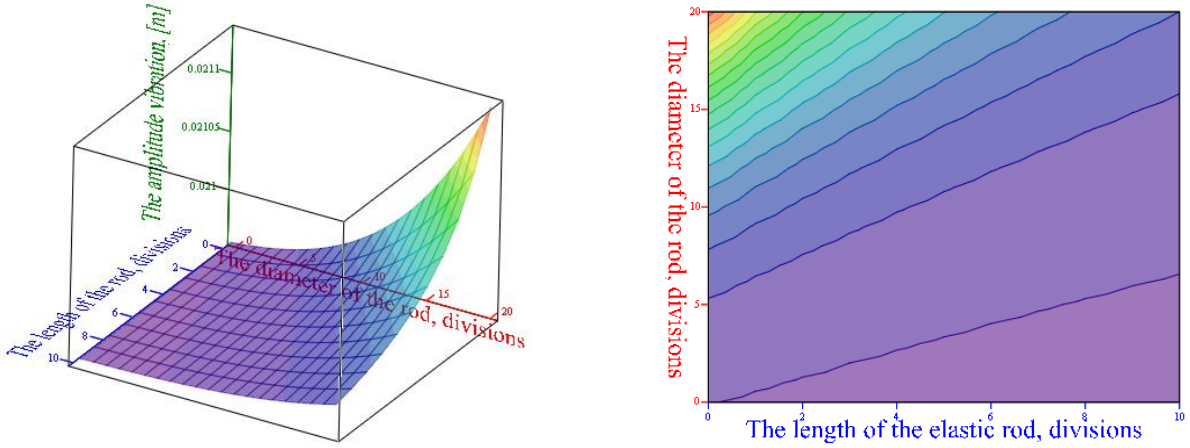


**Fig.4 -** The variation of vibration amplitude with diameter and the length of elastic rod made of boiled beech

## CONCLUSIONS

From the obtained results it is noted that the stiffness of the elastic suspending system has influenced in small amount the radius of the circle described by the movement of the plansifter.

In Figure 3 can be noted that the amplitude of vibration, has remained constant around the value of 21 mm for all cases we studied.

From Figure 4 is seen that the amplitude of the vibration increases with rod diameter increasing and decreases along with the length of the rod. For the model we studied it is observed that each grid point of the plansifter has described a circle of radius 21 mm, which is concentric with the circle described by the movement of the vibration generator radius of 260 mm.

The study establishes a dependence between the stiffness the suspending system and the circular movement described by the plansifter and provides important data on the construction of plansifter.

## REFERENCES

[1]. Constantin G. A., Moise V., Voicu Gh., Ştefan E.M., (2013) - *Structural model for an actuation mechanism of plansifters in wheat mills*, Proceedings of the 41th. International symposium on agricultural engineering, Opatija, Croatia, pp.268-278;
[2]. Ene Gh., Sima T., (2013) – *Aspects of sifting materials on vibrating screeners II, Synthesis of theoretical and applied mechanics*, vol. 4, no. 2, Bucharest;
[3]. Găgeanu P., (2001) – *Research on assimilating in manufacturing of plansifters with square frames of high-yield from medium and high capacity wheat mills*, INMA Bucharest.
[4]. Radeş M., (2008) – *Mechanical vibrations*, Printech Publisher, Bucharest;
[5]. Voicu G., Constantin G.A., Plosceanu B., Stefan E.M., Voicu P., Stoica D., (2015) – *Vibratory movement analysis of plansifters from milling plants*, Actual Tasks on Agricultural Engineering, Opatija, Croatia, pp.24-27.

## CONCLUZII

Din rezultatele obținute se observă că rigiditatea sistemului elastic de suspendare influențează în mică măsură raza cercului descris de mişcarea circulară a sitei plane.

Din Figura 3 se observă că amplitudinea vibrațiilor, rămâne constantă în jurul valorii de 21 mm pentru toate cazurile studiate.

Din Figura 4 se observă că amplitudinea vibrației creşte cu creşterea diametrului tijei şi scade odată cu creşterea lungimii tijei . Pentru modelul studiat se observă ca fiecare punct al sitei plane descrie în mişcare un cerc de rază 21 mm, cerc care este concentric cu cel descris de mişcarea generatorului de vibrații cu raza de 260 mm.

Studiul realizat stabileşte o dependență între rigiditatea sistemului de suspendare şi mişcarea circulară descrisă de sita plană şi furnizează date importante referitoare la construcția sitelor plane.

## BIBLIOGRAFIE

[1]. Constantin G. A., Moise V., Voicu Gh., Ştefan E.M., (2013) – *Model structural pentru un sistem de acționare de la sitele plane din industria morăritului*, Lucrările simpozionului internațional nr. 41, în Ingineria agricolă, Opatija, Croatia, pag. 268-278;
[2]. Ene Gh., Sima T., (2013) – *Aspecte privind cernerea materialelor pe ciururile vibratoare II,* Sinteze de Mecanica Teoretica si Aplicata, vol. 4, nr. 2, Bucureşti;
[3]. Găgeanu P., (2001) – *Cercetări privind asimilarea în fabricație a sitelor plane cu rame pătrate de mare randament din morile de grâu de medie şi mare capacitate*, INMA Bucureşti.
[4]. Radeş M., (2008) – *Vibrații mecanice*, Editura Printech, Bucuresti;
[5]. Voicu G., Constantin G.A., Plosceanu B., Ştefan E.M., Voicu P., Stoica D., (2015) – *Analiza mişcării vibratorii a sitelor plane din industria morăritului*, Activități actuale privind ingineria agricolă, Opatija, Croatia, pag.24-27.

# MATHEMATICAL MODELLING OF THE KNEADING PROCESS FOR A HORIZONTAL MIXER / *MODELAREA MATEMATICĂ A PROCESULUI DE FRĂMÂNTARE LA UN MALAXOR ORIZONTAL*

**Prof. Ph.D.Eng. Voicu Gh.[1)], Eng. Muscalu Gh. [1)], Ph.D.Eng. Stefan E.M.[1)], Ph.D.Eng. Tudor P. [1)], Ph.D.Eng. Nedelcu A.[2)]**
[1)]University Polytechnic Bucharest, Faculty of Biotechnical Systems Engineering / Romania; [2)]INMA Bucharest/Romania
*Tel: 0724715585;E-mail: ghvoicu_2005@yahoo.com*

***Abstract:*** *In the present paper it has been studied a horizontal mixer with a revolutionary kneading arm which is not treated in its domain. The purpose of this paper is to determine a mathematical model for the energetic kneading process of the studied mixer and the specific medium kneading resistance Km, for multiple types of flour mixed with different quantities of water.*

***Keywords:*** *torque, specific medium resistance to kneading, kneading arm, dough consistency, surface of the kneading arm*

## INTRODUCTION

In bread making industry, kneading is one of the key steps that determine the mechanical properties of dough, which has a direct consequence on the quality of the end product. The rheological properties of wheat flour doughs are largely governed by the contribution of starch, proteins and water.

Wheat flour dough is a very non-Newtonian viscoelastic fluid, which depends on time and strains applied. These rheological properties are related to temperature, water content and dough composition. One of the most important methods of characterizing the wheat flour quality is dough mixing. It has found that the mixing temperature greater influences the dough consistency and stability than stirring speed. It has found a powerful connection between the mixing speed and dough consistency during mixing, mixing stability, light proteins, starch jellification and amylases activity, [1]. The level of growth of the dough mostly depends on the energy input, kneading speed, as well as on deformation type (shearing vs. stretching) generated by kneading arms [2,3]. Kneading speed influences both dough consistency and its stability (the bigger the kneading speed is, the greater the dough consistency is and the smaller becomes the stability) [3]. At the same time, the paper, [4] showed that besides those mentioned above, also the mixing vat geometry influences the dough rheological characteristics (growth and stability time).

Role of a kneader is to uniformly mix particles of different dimension, humidity and density so that finally a homogenous mass should be obtained.

During kneading, a mixer must transfer sufficient energy to dough in order to stimulate the gluten production and structural development. Elastic forces of compression and shearing activated by mixer components generate the stirring energy. A part of this energy produces changes of dough composition and another part determines the dough temperature increment. Many parameters influence these forces, among which:

- form and dimensions of arms and vat;
- dough rheological characteristics (viscosity, elasticity,

***Rezumat:*** *În prezenta lucrare s-a studiat un mixer orizontal cu un braț de frământare revoluționar care nu se regăseşte în literatura acestui domeniu. Scopul lucrării este acela de a determina un model matematic pentru procesul energetic de frământare al acestuia şi rezistența specifică medie la malaxare Km, pentru mai multe tipuri de făină, la care au fost adăugate cantități de apă diferite.*

***Cuvinte cheie:*** *moment de torsiune, rezistență specifică medie la malaxare, braț de frământare, consistența aluatului, suprafața brațului de frământare*

## INTRODUCERE

În industria de panificație, frământarea este unul dintre punctele cheie care determină proprietățile mecanice ale aluatului, şi care are consecințe directe asupra calității produsului finit. Proprietățile reologice ale aluaturilor din făină de grâu sunt determinate de contribuția amidonului, a proteinelor şi a apei.

Aluatul din făină de grâu este un fluid foarte ne-newtonian, vâsco-elastic, dependent de timp şi de deformațiile aplicate. Aceste proprietăți reologice sunt foarte sensibile cu temperatura, conținutul de apă şi compoziția aluatului. Amestecare aluatului este una dintre cele mai importante căi prin care se poate caracteriza calitatea făinii de grâu. S-a constatat că temperatura de amestecare are un impact mai mare asupra consistenței şi stabilității aluatului decât de viteza de amestecare. S-a observat o legătură puternică între viteza de amestecare şi consistența aluatului în timpul amestecării, stabilitatea la malaxare, slăbirea proteinelor, gelificarea amidonului şi activitatea amilazei, [1]. Nivelul de dezvoltare (formare) a aluatului depinde în mare măsură de aportul de energie (Energy input), viteza de frământare, precum şi de tipul deformării (forfecare vs. întindere) generate de brațele de frământare [2,3]. Viteza de frământare influențează atât consistența aluatului, cât şi stabilitatea acestuia (cu creşterea vitezei de frământare creşte consistența aluatului şi scade stabilitatea) [3]. De asemenea, în lucrarea [4] a fost arătat faptul că pe lângă cele menționate mai sus, şi geometria cuvei malaxorului are influență asupra caracteristicilor reologice ale aluatului (timp de dezvoltare şi stabilitate).

Rolul unui frământător este acela de a amesteca uniform particule de dimensiuni, umidități şi densități diferite, astfel încât, în final, să se obțină o masă omogenă.

În timpul frământării, un malaxor trebuie să transfere suficientă energie aluatului pentru a stimula producerea şi dezvoltarea structurală a rețelei glutenice. Forțele elastice, de comprimare şi de forfecare activate de componentele malaxorului generează energia de malaxare. O parte din această energie produce transformări în consistența aluatului, iar o altă parte produce creşterea temperaturii aluatului. Mai mulți parametri au o influență asupra acestor forțe, dintre care:

- forma şi dimensiunile brațelor şi cuvei;
- caracteristicile reologice ale aluatului (vâscozitate,

unloading speed), which are themselves influenced by component elements (water, flour, salt, additives);
- dough reaction to external environment (friction, adhesion),
- relative quantity of dough in the mixer

Therefore, there isn't an established measuring unit for consistency, but every device used for this purpose adopts conventional measuring units.

A definition for dough consistency sounds like this: consistency is a complex rheological propriety, obtained by combining viscosity, plasticity and elasticity and which varies with humidity, temperature and time, with the proportions between dough phases (solid, liquid, gas), with flour's biochemical composition, with added materials (*Mx* – auxiliary materials) and the quantity of energy used for kneading, [5,6].

A part of the results obtained in this paper, are completely new to this area because in the analysis of the kneading arm, it was used a mathematical method of deducing the charge surface of the kneading arm, an approach which has not been tried until now.

## MATERIAL AND METHOD

For a better and explicit designing of some components, a part of the calculations were adapted taking into account those already demonstrated in specialty books and others were obtained by measuring and analyzing experimental data extracted during functioning, straight from the working machine. The kneading arm is presented in figure 1.

Due to rotary motion of the kneading arm, the material is trained in an intermittent rotary movement and a constant forward movement along the vat. The rotary movement is intermittent because, after the rotation of the material with an angle Ψ (angle at which the product falls) versus a vertical plane, it starts sliding down on the helicoidally helix under the action of its own weight and the rotary motion stops [7,8].

In the first part of the paper it is calculated the attack surface of the kneading arm.

The formula which makes it possible to establish the opposing torque at the kneading arm, is:

elasticitate, viteza de descărcare), care sunt ele însele influențate de elementele componente (apă, făină, sare, aditivi);
- reacția aluatului în ceea ce priveşte mediul său exterior (frecare, adeziune),
- cantitatea relativă de aluat în malaxor.

Din aceste considerente, nu există o unitate de măsură unică pentru consistență, ci fiecare aparat care măsoară consistența foloseşte unități de măsură convenționale. O definiție pentru consistența aluatului sună în felul următor: consistența este o proprietate de natură reologică, complexă, rezultată prin combinarea vâscozității, plasticității, elasticității, care variază cu umiditatea, temperatura şi timpul, cu proporția dintre fazele aluatului (solid, lichid, gaz), cu compoziția biochimică a făinii, cu materialele adăugate (*Mx* – materiale auxiliare) şi cu cantitatea de energie utilizată la frământare, [5,6].

O parte din rezultatele obținute în această lucrare sunt o noutate în domeniu, deoarece în analiza brațului de frământare, a fost folosită o metodă matematică de deducere a suprafeței de atac a acestuia, abordare care nu a mai fost întâlnită până acum.

## MATERIAL ŞI METODĂ

Pentru o mai bună şi explicită proiectare a unor părți componente, o parte din calcule au fost adaptate după calcule existente în cărți de specialitate şi o altă parte, au fost obținute prin măsurarea şi analizarea datelor experimentale obținute în timpul funcționării, direct de la utilaje. Brațul malaxor este prezentat în figura 1.

Datorită mişcării de rotație a brațului de frământare, materialul este antrenat într-o mişcare de rotație intermitentă şi o mişcare de înaintare uniformă în lungul cuvei. Mişcarea de rotație este intermitentă pentru că, după ce materialul s-a rotit cu unghiul Ψ (unghiul la care are loc surparea produsului) față de planul vertical, alunecă pe spira elicoidală în jos sub acțiunea propriei greutăți şi mişcarea de rotație încetează, [7,8].

În prima etapă a lucrării este calculată suprafața de atac a brațului de frământare.

Formula de calcul care face posibilă stabilirea momentului de torsiune care se opune la brațul de frământare este:

$$M_t = K_m\,(S_i\,cos\alpha \cdot cos\beta + A_{Si}) \quad (1)$$

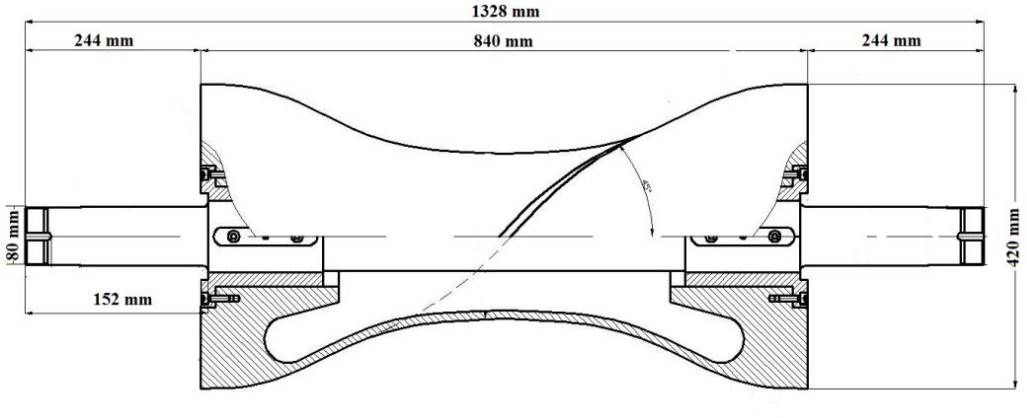


**Fig. 1 –** Horizontal kneading arm

It is taken into consideration that the surface of the kneading arm is inclined with an angle α in radial – horizontal plane and *β* angle in vertical plane.
In this situation, the attack surface will be:

Se ia în considerare faptul că suprafața brațului de frământare este înclinată cu unghiul α în planul orizontal – radial şi cu unghiul β în planul vertical.

În această situație, suprafața de atac va fi:

$$S_a = S_i \cdot cos\alpha_i \cdot cos\beta_i + A_{Si} \quad (2)$$

where:
- $S_a$ is the attack surface of the kneading arm;
- $S_i$ is the surface of one strip, expressed in cm²;
- $\alpha$ is angle made by every strip in horizontal plane, expressed in degrees;
- $\beta$ is angle in vertical plane expressed in degrees;
- $A_{si}$ is the surface for the portion between the base of the contact surface and its end, expressed in cm².

For a more accurate calculation, the surface of the arm has been divided between strips of 60 mm thickness and variable height, based on the form of the kneading arm.

In order to calculate the sum of radiuses starting from the center of the surfaces determined at the rotation axis ($r_{mi}$), it was drawn a scheme for calculus (figure 2) which ultimately helps to determine the resistant moment for a kneader with horizontal spindle.

unde:
- $S_a$ este suprafața de atac a brațului de frământare;
- $S_i$ este suprafața unei fâşii din braț, exprimată în cm²;
- $\alpha$ este unghi format de fiecare fâşie în plan orizontal, exprimat în grade;
- $\beta$ este unghi în plan vertical exprimat în grade;
- $A_{si}$ este suprafața porțiunii dintre baza suprafeței de contact şi terminația acesteia, exprimată în cm².

Pentru un calcul mai exact, suprafața brațului a fost împărțită în fâşii cu grosimea de 60 mm şi înălțime variabilă funcție de forma brațului de frământare.

Pentru a calcula suma razelor de la centrul suprafețelor determinate la axa de rotație ($r_{mi}$), a fost desenată o schemă de calcul (figura 2), ce foloseşte ulterior pentru determinarea momentului rezistent în malaxorul cu ax orizontal.

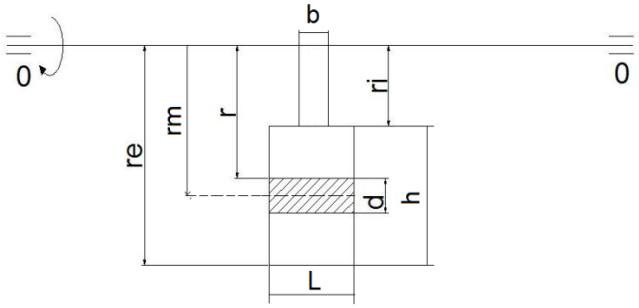


**Fig. 2** - Calculus scheme for determining the attack surface for a kneader with horizontal kneading arm [11]

The surface of an arm portion it is calculated with the formula, [15]:

Suprafața unei porțiuni din braț se calculează cu formula, [15]:

$$S_1 = h_1 \cdot L_1 \quad (3)$$

where:
- $h_1$ is the height of a palette;
- $L_1$ is the length of a palette.

The distance from the center of the contact surface ($d$) to the rotation axis, can be expressed with the following formula:

unde:
- $h_1$ este înălțimea unei palete;
- $L_1$ este lungimea unei palete.

Distanța de la centrul suprafeței de contact ($d$) la axa de rotație se poate exprima cu următoarea formulă:

$$r_{m1} = \frac{(r_e + r_i)}{2} \quad (4)$$

where:
- $r_e$ is the distance between the rotation axis and the end of a palette;
- $r_i$ is the distance between the rotation axis and the beginning of the palette.

The length of the contact surface is:

unde:
- $r_e$ este distanța de la axa de rotație la capătul paletei;
- $r_i$ este distanța de la axa de rotație la începutul paletei.

Lungimea suprafeței de contact este:

$$L_1 = r_e - r_i \quad (5)$$

The contact surface is supported by another surface, which fills into the material and is calculated with the formula:

Suprafața porțiunii suportului suprafeței de contact, care pătrunde în material se calculează astfel:

$$A_{si} = b \cdot (r_e - r_i) \quad (6)$$

where: $b$ is the width of a palette.

The spindle was divided in 14 surfaces, the equivalent for 28 blades, as shown in the figures 3, *a* and *b*, [10].

For calculating the total sum of rays at the center of the surfaces determined at the rotation axis ($\sum Ri$), table 1 is constituted.

unde: $b$ este lățimea unei palete.

Arborele a fost împărțit în 14 suprafețe, echivalent cu 28 de palete, după cum este prezentat în figura 3, *a* şi *b*, [10].

Pentru calcularea sumei totale a razelor de la centrul suprafețelor determinate la axa de rotație ($\sum Ri$), se alcătuieşte tabelul 1.

$$\sum R_i = r_{mi} \cdot (S_i \cdot cos\alpha_i \cdot cos\beta_i + A_{si}) \quad (7)$$

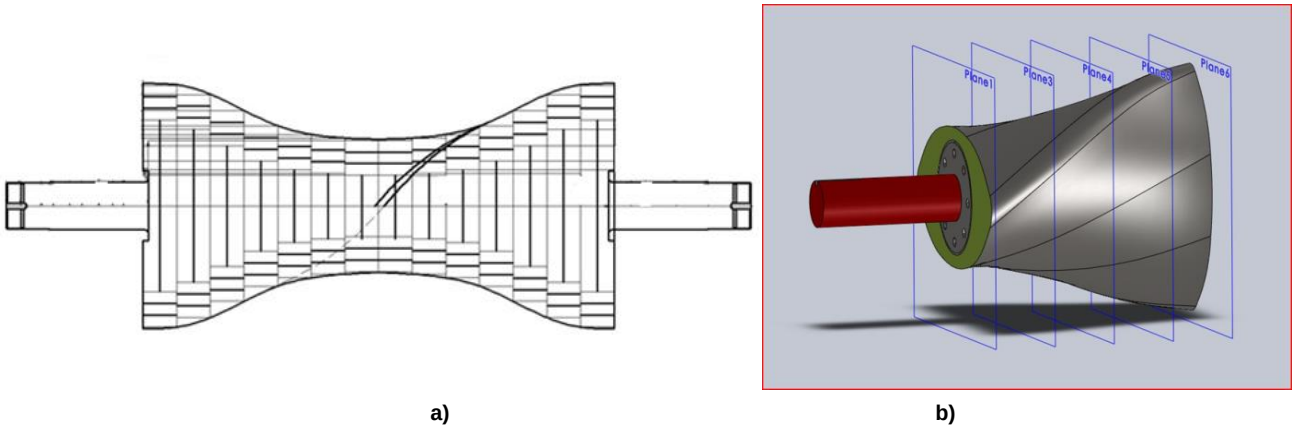


a) b)

**Fig. 3** - The spindle, divided into 28 blades: a) 2D drawing; b) 3D drawing

Because the attack surface remains constant, it is calculated just once. The variable $K_m$ and implicitly $M_t$, vary with increase and decrease of dough consistency.

The mathematical model proposes to demonstrate the correlation between torque and specific resistance at kneading, applied to the attack surface.

In the second part of the paper, it is determined the medium value for specific resistance at kneading, $K_m$.

Considering that the specific resistance, $K_i$ has a different value from one section to another, depending on tangential speed at the section's surface, it is possible to introduce in calculation, the medium value for specific resistance, $K_m$, which is valid for the entire kneader.

Întrucât suprafața de atac va rămâne constantă, ea se calculează o singură dată. Variabila $K_m$ (*rezistența specifică medie la malaxare)* şi implicit momentul de torsiune, $M_t$ variază cu creşterea sau descreşterea consistenței aluatului.

Modelul matematic îşi propune să demonstreze corelația între momentul de torsiune şi rezistența specifică la malaxare, aplicată la suprafața de atac.

În a doua etapă a lucrării, se determină valoarea rezistenței specifice medii la malaxare, $K_m$.

Având în vedere că rezistența specifică, $K_i$ în acelaşi malaxor diferă de la o secțiune la alta, depinzând direct de viteza tangențială la suprafața secțiunii, se introduce în calcule valoarea rezistenței specifice medii la malaxare $K_m$, valabilă pentru întregul malaxor.

**Table 1**

**Calculation for the attack surfaces of the kneading arm**

| Section number | $S_i$ [cm²] | cosα$_i$ | cosβ$_i$ | $A_{si}$ [cm²] | $r_{mi}$ [cm] | Σ $R_i$ [cm³] |
|---|---|---|---|---|---|---|
| I | 36 | 0.156 | 0.972 | 88.2 | 17.7 | 1657 |
| II | 36 | 0.382 | 0.972 | 78.9 | 16.1 | 1486 |
| III | 36 | 0.587 | 0.972 | 62.22 | 13.3 | 1100 |
| IIII | 36 | 0.76 | 0.972 | 46.5 | 10.7 | 783 |
| V | 36 | 0.891 | 0.972 | 37.5 | 9.2 | 632 |
| VI | 36 | 0.972 | 0.972 | 33.9 | 8.6 | 584 |
| VII | 36 | 1.000 | 0.972 | 31.5 | 8.2 | 354 |
| VIII | 36 | 1.000 | 0.972 | 31.5 | 8.2 | 354 |
| IX | 36 | 0.972 | 0.972 | 33.9 | 8.6 | 584 |
| X | 36 | 0.891 | 0.972 | 37.5 | 9.2 | 632 |
| XI | 36 | 0.76 | 0.972 | 46.5 | 10.7 | 783 |
| XII | 36 | 0.587 | 0.972 | 62.22 | 13.3 | 1100 |
| XIII | 36 | 0.382 | 0.972 | 78.9 | 16.1 | 1486 |
| XIV | 36 | 0.156 | 0,972 | 88.2 | 17.7 | 1657 |
| XV | 36 | 0.156 | 0,972 | 88.2 | 17.7 | 1657 |
| XVI | 36 | 0.382 | 0.972 | 78.9 | 16.1 | 1486 |
| XVII | 36 | 0.587 | 0.972 | 62.22 | 13.3 | 1100 |
| XVIII | 36 | 0.76 | 0.972 | 46.5 | 10.7 | 783 |
| XIX | 36 | 0.891 | 0.972 | 37.5 | 9.2 | 632 |
| XX | 36 | 0.972 | 0.972 | 33.9 | 8.6 | 584 |
| XXI | 36 | 1.000 | 0.972 | 31.5 | 8.2 | 354 |
| XXII | 36 | 1.000 | 0.972 | 31.5 | 8.2 | 354 |
| XXIII | 36 | 0.972 | 0.972 | 33.9 | 8.6 | 584 |
| XXIV | 36 | 0.891 | 0.972 | 37.5 | 9.2 | 632 |
| XXV | 36 | 0.76 | 0.972 | 46.5 | 10.7 | 783 |
| XXVI | 36 | 0.587 | 0.972 | 62.22 | 13.3 | 1100 |
| XXVII | 36 | 0.382 | 0.972 | 78.90 | 16.1 | 1486 |
| XXVIII | 36 | 0.156 | 0.972 | 88.20 | 17.7 | 1657 |
| $\sum R_i = r_{mi} \cdot (S_i \cdot cos\alpha_i \cdot cos\beta_i + A_{si})$=26384 $cm^3$ | | | | | | |

The values for medium specific resistance Km, were experimentally determined by comparing the results obtained with different sets of dough made with different types of flour and different quantities of added water, as shown in table 3. In figure 4 it can be analyzed the graph that explains the variation of specific resistance for kneading depending on dough humidity.

The physico–chemical characteristics of the flours used for the experiments are presented in table 2.

It is possible to conclude that $K_m$ values are linear functions dependent on flour quality and its capacity to absorb water and also directly dependent on medium tangential speeds inside the mixing bin, [7]. For all the tests, the tangential speed at the section surface had the same value: 2.8 m/s.

Valorile rezistențelor specifice medii la malaxare Km au fost determinate experimental de către autori prin compararea rezultatelor obținute cu diferite şarje de aluat din făinuri diferite care au necesitat hidratări diferite, aşa cum se poate observa în tabelul 3. În figura 4 se poate analiza graficul care explicitează variația rezistenței specifice la malaxare funcție de umiditatea aluatului.

Caracteristicile fizico-chimice ale făinurilor utilizate în realizarea experimentelor sunt prezentate în tabelul 2.

Se poate constata că valorile $K_m$ sunt funcții liniare de conținutul şi calitatea făinii, dar şi de capacitatea acesteia de hidratare şi depind direct de vitezele tangențiale medii în interiorul cuvei de amestecare, [7]. Toate probele au avut aceeaşi viteză tangențială la suprafața secțiunii: 2.8 m/s.

**Table 2**

**Physico – chemical characteristics of the flours used in the experiments**

| Flour type | Humidity, [%] | Wet gluten, [%] | Ash, [%] d.s. | Protein content, [%] d.s | Gluten deformation [mm] | Acidity, [degrees] | Falling number, [sec] | Gluten index |
|---|---|---|---|---|---|---|---|---|
| **FA – 650 (F1)** | 13.5 | 28 | 0.65 | 26.8 | 3.5 | 2 | 318 | 84 |
| **FN – 1350 (F2)** | 13.5 | 32.4 | 1.35 | 27.5 | 4 | 3.4 | 318 | 88 |

Analyzing the information presented above, it is possible to formulate the following observations: once with the rise of dough humidity, the effective viscosity of dough decreases, whatever the flour's quality, fermentation time and superficial tension, are [12,13,14].

An example of resistant moment $M_t$, determined for a 650 flour type which had 50% added water can be verified with the expression:

Din analiza datelor prezentate mai sus se pot formula următoarele observații: odată cu creşterea umidității aluatului, vâscozitatea efectivă a aluatului scade, indiferent de calitatea făinii, de timpul de fermentare şi de tensiunea superficială, [12,13,14].

Un exemplu de moment rezistent $M_t$, determinat pentru o făină tip 650 la care s-a adăugat apă în proporție de 50%, se verifică cu expresia:

$$M_t = K_m * \sum r_{mi}(S_i \cos\alpha_i \cdot \cos\beta_i + A_{si})$$
$$M_t = 0.088 * 26384 = 2321\ [Nm] \quad (8)$$

**Table 3**

**Experimental determinations for medium specific resistance at kneading**

| Flour type | Humidity [%] | Angular speed ω [rpm] | Efficiency of transmission | Pump flow [m³/s] | Read pressures [bar] | $K_m$ | Torque [Nm] | Difference of pressure between suction and delivery of hydraulic pump [bar] | Power [kW] |
|---|---|---|---|---|---|---|---|---|---|
| **FA - 650(F1)** | 48 | 12.56 | 0.95 | 154 | 135 | 0.091 | 2400 | 125 | 30.48 |
| **FA - 650(F1)** | 50 | 12.56 | 0.95 | 154 | 128 | 0.088 | 2321 | 118 | 28.77 |
| **FA - 650(F1)** | 52 | 12.56 | 0.95 | 154 | 120 | 0.080 | 2110 | 110 | 26.82 |
| **FA - 650(F1)** | 54 | 12.56 | 0.95 | 154 | 116 | 0.078 | 2058 | 106 | 25.85 |
| **FN - 1350(F2)** | 56 | 12.56 | 0.95 | 154 | 123 | 0.094 | 2480 | 113 | 27.55 |
| **FN - 1350(F2)** | 58 | 12.56 | 0.95 | 154 | 120 | 0.086 | 2269 | 110 | 26.82 |
| **FN - 1350(F2)** | 60 | 12.56 | 0.95 | 154 | 130 | 0.076 | 2005 | 120 | 29.26 |
| **FN - 1350(F2)** | 64 | 12.56 | 0.95 | 154 | 120 | 0.070 | 1846 | 110 | 26.82 |

Knowing the oil pressure which is introduced into the hydraulic engine, it was possible to calculate the resistant moment for the spindle of the mixing arm.

The maximum resistant moment was calculated after drawing a similar graph with the one made by a farinograph, by monitoring the pressure from 5 to 5 seconds, for 230 seconds, and which could be observed directly on the monitor screen. The dough had in its composition, 650 flour type (ash content 0.65%). The obtained graph can be observed in figure 5.

The necessary power for the hydraulic engine ($P_{ab}$)

Cunoscând presiunea de ulei introdusă în motorul hidraulic a fost posibilă calcularea momentului rezistent la arborele brațului de malaxare.

Momentul rezistent maxim a fost calculat după realizarea unui grafic asemănător cu cel trasat de un farinograf prin monitorizarea presiunii din 5 în 5 secunde, timp de 230 s, care se poate citi direct de pe ecranul monitorului. Aluatul avea în componență făină tip 650 (conținut de cenuşă 0,65%). Graficul poate fi observat în figura 5.

Puterea necesară motorului hidraulic ($P_{ab}$) se

can be calculated by knowing the difference between aspiration pressure and plenum pressure ($p\Delta_p$), the introduced flow into the hydraulic engine ($Q_m$) and the transmission's efficiency, ($\eta_{tm}$ = 0.95), [8].

calculează cunoscând diferența de presiune între aspirație şi refulare ($p\Delta_p$), debitul introdus în motorul hidraulic ($Q_m$) şi randamentul transmisiei ($\eta_{tm}$ = 0.95), [8].

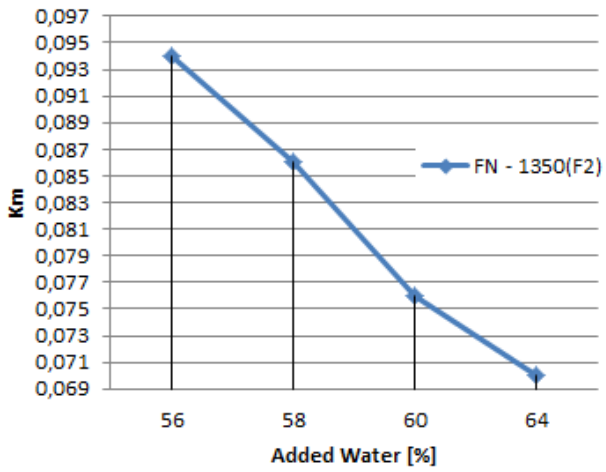


a) $K_m$ variation for 1350 flour type

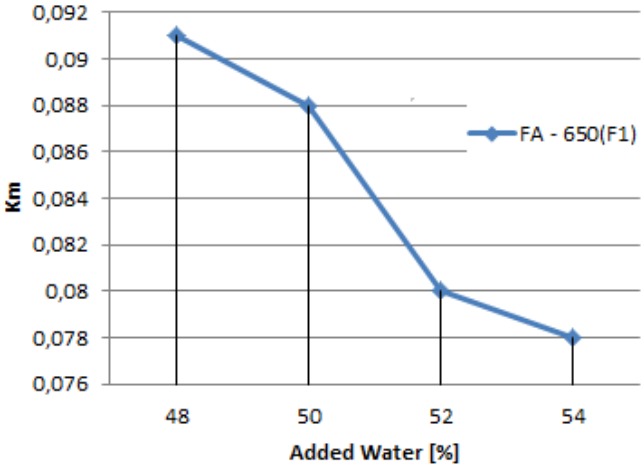


b) $K_m$ variation for 650 flour type

**Fig.4 -** Graph which explains the variation for Km, depending on dough humidity and type of flour

$$P_{ab} = \frac{p\Delta_{p*}Q_m*\eta_{tm}}{600} \quad (9)$$

The necessary torque for driving the kneading arm, after overcoming the resistant moment if the power and angular speed $\omega_m$ are known, can be calculated with the following formula, [9]:

Momentul învârtitor necesar antrenării brațului de frământare după învingerea momentului rezistent dacă se cunoaşte puterea şi viteza unghiulară $\omega_m$ a brațului de frământare se calculează cu formula, [9]:

$$M = \frac{P_m}{\omega_m} \quad (10)$$

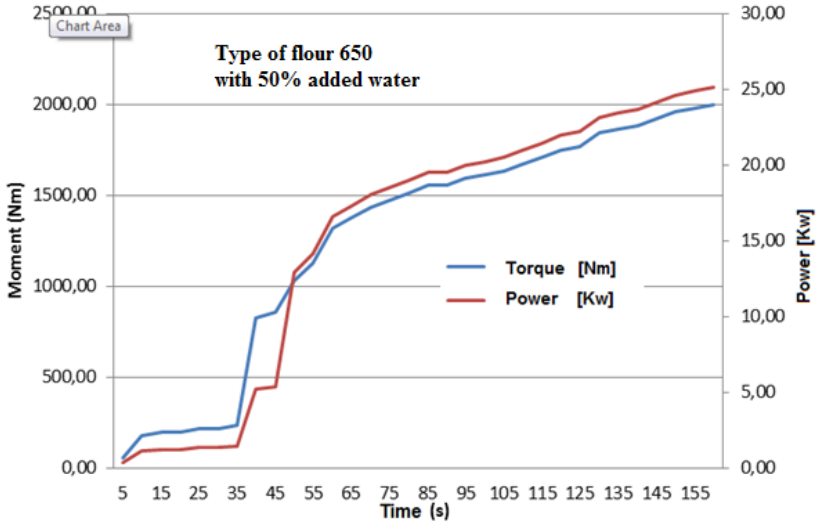


**Fig. 5 -** Graph which explains the variation for the resistant moment depending on time of kneading

The maximum value registered on the diagram for the torque, is:

Valoarea maximă înregistrată pe diagrama pentru momentul de torsiune este:

$$M_t = 2252\ [Nm] \quad (11)$$

Following the analysis of graphic shown in figure 5, it has found that during the first seconds of mixing process (about 30 seconds) the moment of torsion of kneader's arm is almost steady, as well as the driving power. This is possible, because the arm moves only in flour, without

Din analiza graficului prezentat în figura 5, se observă că în primele secunde ale procesului de malaxare (circa 30 secunde) momentul de torsiune la brațul frământătorului este aproximativ constant. La fel şi puterea necesară acționării. Acest lucru este posibil

water supplement. When one begins to add water into kneader's vat, the torque (and power) of kneader's arm start to increase, at the beginning almost suddenly (during 5-10 seconds), then more slowly up to reaching the maximum moment. What cannot be noticed in the graphic is reaching this moment and also the maintenance of dough formed at this value. The moment is neither noticed at the beginning of consistency decreasing, namely in the dipping phase. This could be determined by prolonging the duration of data acquisition (respectively of power consumed by kneader's arm). In graphic shown, the acquisition duration was of only 160 seconds and this moment could not be noticed. Both values shown in the graphic have approximately the same variation, taking into account the mathematical relation between the two values.

## CONCLUSIONS

The correlation between the mathematical model and the conducted experiment is quite accurate for determining the resistant moment for a kneading arm, depending on dough consistency and the type of flour used.

Intensive and fast kneading, known also as mechanical development for dough, represents much more active dough kneading, which is achieved at higher speed for kneading arms and in smaller time compared to classical mixers.

The kneading process at high speed for kneading arms determines a more pronounced loosening of globular proteins, along with surface exposure for a bigger number of reactive groupings, capable of reacting with those of neighbor molecules in order to form a bigger number of intermolecular connections.

Besides flour quality, the optimal quantity of energy which must be introduced in the kneading process depends also on its humidity and temperature, the quality of raw material used in the process, the type and speed of the kneading arm.

Beside the amount of energy introduced, it is of very high consequence the speed with which the energy is transmitted, respectively, the kneading time. When increasing speed at the kneading arm, the kneading time reduces. From this point of view, there is an optimal speed for introducing the necessary energy into dough.

The importance of designing and analyzing the shape of the kneading arm becomes determinant in the way of transmitting the energy, as well as the speed with which the energy is transferred to the dough in order to obtain a dough with superior quality.

The understanding of the kneading process for this kind of machine is useful in industrial bread making process because it helps the technological engineer to find solutions for quality problems which can appear because of defective forming of dough in the vat or caused by flour's physical and chemical characteristics like weak flours which necessitate slow kneading, flours with increased hydration capacity, at which it can be determined the optimal quantity of added water by controlling the value for maximum consistency, or the optimization of the entire kneading process by adapting the speed of the kneading arm (setting the hydraulic pressure into the radial engine with axial pistons for four configurable speeds) for the type of dough wished to be obtained.

deoarece brațul se mişcă numai în făină simplă, fără adaos de apă. În momentul începerii adăugării apei în cuva frământătorului, momentul (la fel şi puterea) la brațul frământătorului începe să crească, la început aproape brusc (pe o durată de 5-10 secunde), apoi mai lent până la atingerea momentului maxim. Ceea ce nu se observă pe grafic este atingerea acestui moment şi cât timp se menține la valoarea acestuia aluatul format. Nu se observă nici începutul scăderii consistenței, adică faza de înmuiere. Aceasta ar putea fi determinată prin prelungirea duratei de achiziție a datelor (respectiv a puterii consumate de brațul frământătorului). În graficul prezentat, durata de achiziție a fost de numai 160 secunde, iar acest moment nu a putut fi semnalat. Ambele mărimi prezentate pe grafic au aproximativ aceeaşi variație având în vedere relația matematică dintre acestea.

## CONCLUZII

Corelația între modelul matematic şi experimentul efectuat este una destul de exactă pentru a putea determina momentul rezistent la brațul de frământare funcție de consistența aluatului şi tipul de făină utilizat.

Frământarea intensivă şi rapidă, cunoscută şi ca dezvoltarea mecanică a aluatului, constă într-o frământare mult mai energică a aluatului, care se realizează la turații mai mari ale brațelor de frământare şi într-un timp mai scurt față de frământătoarele clasice.

Frământarea la turații mari ale brațelor de frământare determină desfacerea mai pronunțată a proteinelor globulare, însoțită de expunerea la suprafață a unui număr mai mare de grupări reactive, capabile să reacționeze cu cele ale moleculelor vecine şi să formeze un număr mai mare de legături intermoleculare.

În afară de calitatea făinii, cantitatea optimă de energie ce trebuie transmisă la frământarea aluatului mai depinde de umiditatea şi temperatura acestuia, de starea materiilor prime folosite în proces, de felul şi turația brațului de frământare.

În afara cantității de energie, foarte importantă este viteza cu care este transmisă energia, respectiv timpul de frământare. La mărirea turației brațului de frământare, timpul de frământare se reduce. Din acest punct de vedere, există o viteză optimă de transmitere a energiei aluatului.

Importanța proiectării şi analizei formei brațului de frământare devine determinantă în modul cum este transmisă energia, precum şi viteza cu care aceasta este cedată aluatului pentru a obține o calitate superioară a acestuia.

Înțelegerea procesului de frământare la acest tip de utilaj este utilă în procesul de producție deoarece ajută inginerul tehnolog să găsească soluții la probleme de calitate care pot apărea din cauza formării defectuoase a aluatului în cuva malaxorului sau care au la bază caracteristicile fizico-chimice ale făinii, cum sunt făinuri mai slabe care necesită o frământare mai lentă, făinuri cu o capacitate de hidratare mare la care se poate determina cantitatea optimă de apă adăugată la făină, prin controlul valorii consistenței maxime, optimizarea întregului proces de frământare prin adaptarea turației brațului de frământare (setarea presiunii hidraulice în motorul radial cu pistoane axiale pentru cele 4 viteze configurabile) la tipul de aluat care se doreşte a fi obținut.

**REFERENCES**
[1]. Pastukhov A., Dogan H., (2014) – Studying of mixing speed and temperature impacts on rheological properties of wheat flour dough using Mixolab, Agronomy Research 12(3), 779–786;
[2]. Campos D.T., Steffe J.F., Ng P.K.W.(1997) – *Rheological behavior of undeveloped and developed wheat dough,* Cereal Chem. 74(4):489-494;
[3]. Muchova Z., Zitny B. (2010) – *New approach to the study of dough mixing process*, Czech J. Food Sci., vol28, no.2:94-107;
[4]. Hwang CH., Gunasekaran (2001) – *Determining wheat dough mixing characteristics from power consumption profile of a conventional mixer,* Cereal Chemistry 78(1):88-92;
[5]. Leonte M. (2011) – *The study of the factors which influence rheological properties of bread dough,* Rompan Magazine 1, pg5, Bucharest;
[6]. Giurca V. (1980) - *Technology and equipment for bakery industry,* vol. I and II, Danubius university, Galati;
[7]. Haraszia R., Larroque O.R., Butow B.J., Gale K.R., Bekes F. (2008) - *Differential mixing action effects on functional properties and polymeric protein size distribution of wheat dough,* Journal of Cereal Science 47, pg. 41–51;
[8]. Babiciu P., Scripnic V., Fratila Al. (1984) – *Hidraulic systems for tractors and machines for agriculture*, CERES Publishing house, Bucharest;
[9]. Voicu Gh. (1999) – *Processes and equipment for bakery*, Bren Publishing house, Bucharest;
[10]. Talaba D. (2000) – *CAD bases - Computer -aided design*, Transilvania University of Brasov, Publishing house;
[11]. Jiscanu V. (1972) – *Operations and equipment in food industry, vol.1-2*, University of Galati;
[12]. Zeng H., Morgenstern M.P., Companella O.H., Larsen N.G. (2000) - *Rheological properties of dough during mechanical dough development*, Journal of Cereal Science, 32, pg. 293-306;
[13]. Kilborn R.H., Tipples K.H. (1972) - *Factors affecting mechanical dough development. I. Effect of mixing intensity and work input.* Cereal Chemistry 49: pg.34-47;
[14]. Wang M., Tweed A. R., Carson G. (2010) - *How Dough Mixing Properties Affect Bread-Making Performance,* Canadian International Grains Institute, Winnipeg, MB Canada;
[15]. Sarbu L. (2003) – *Equipment and technological processes in industry of construction materials – Elements calculus technological design,* vol 2 Millenium Publishing House.

**BIBLIOGRAFIE**
[1]. Pastukhov A., Dogan H., Studiul impactului vitezei şi temperaturii de amestecare asupra proprietăților reologice ale aluatului din făină de grâu folosind Mixolab, Agronomy Research 12(3), 779–786, 2014.
[2]. Campos D.T., Steffe J.F., Ng P.K.W. (1997) – *Comportarea reologică a aluatului de grâu nedezvoltat şi dezvoltat,* Cereal Chem. 74(4):489-494.
[3]. Muchova Z., Zitny B. (2010) – *Nouă abordare a studiului procesului de frământare a aluatului,* Czech J. Food Sci., vol28, no.2:94-107.
[4]. Hwang CH., Gunasekaran (2001) – *Determinarea caracteristicilor de frământare ale aluatului din făină de grâu plecând de la profilul consumului de energie al unui mixer convențional,* Cereal Chemistry, 78(1):88-92.
[5]. Leonte M. (2011) - *Studiul factorilor care influențează proprietățile reologice ale aluatului pentru panificație*, Revista Rompan 1, pag 5, Bucureşti;
[6]. Giurcă V. (1980) - *Tehnologia şi utilajul industriei de panificație ,* vol. I şi II, Univ. "Dunărea de Jos" Galați;
[7]. Haraszia R., Larroque O.R., Butow B.J., Gale K.R., Bekes F. (2008) – *Efectele acțiunii de amestecare diferențială asupra proprietăților funcționale si distribuției de mărime a proteinei polimerice a aluatului de grâu,* Journal of Cereal Science 47, pag. 41–51;
[8]. Babiciu P., Scripnic V., Frățilă Al. (1984) - *Sisteme hidraulice ale tractoarelor si maşinilor agricole*, Editura CERES, Bucureşti;
[9]. Voicu Gh. (1999) - *Procese şi utilaje pentru panificație,* Editura BREN, Bucureşti;
[10]. Talabă D.(2000) – *Bazele CAD –Proiectare asistată de calculator*, Editura Universității Transilvania Braşov;
[11]. Jişcanu V. (1972) – *Operații şi utilaje în industria alimentară*, vol.1-2, Universitatea Galați;
[12]. Zeng H., Morgenstern M.P., Companella O.H., Larsen N.G .(2000) – *Proprietățile reologice ale aluatului in timpul creşterii mecanice a acestuia,*, Journal of Cereal Science, 32, pag. 293-306;
[13]. Kilborn R.H., Tipples K.H. (1972) – *Factori care afectează dezvoltarea mecanica a aluatului. I. Efectul intensității de amestecare si a inputului de lucru,* Cereal Chemistry 49: pag.34-47;
[14]. Wang M., Tweed A. R., Carson G.(2010) – *Felul in care proprietățile de amestecare a aluatului afectează performanta de formare a pâinii,* Canadian International Grains Institute, Winnipeg, MB Canada;
[15]. Sârbu L. (2003) - *Utilaje şi procese tehnologice din industria materialelor de construcții - Elemente calcul proiectare tehnologică,* vol 2. Editura Milenium.

# STUDY ON THE SHAPE DETECTION METHOD FOR THE PRECIOUS SEAFOODS BASED ON COMPUTER VISION
/
# 基于计算机视觉的海珍品体形检测方法研究

**Assoc. Prof. Huihui Wang[1,2)], Master.stud. Shiyuan Xing[1,2)], Master.stud. YuansongZheng[1,2)], Master.stud. Weiwei Gu[1,2)], Lect. Master. Yan Lv[1,2)], Prof. Ph.D. Jixin Yang[1,2)]**
[1)]School of Mechanical Engineering and Automation, Dalian Polytechnic University, Dalian Liaoning 116034;
[2)]National Engineering Research Center of Seafood, Dalian Liaoning 116034
*Phone:(+86)0411-86323682；E-mail:15040537906@126.com*

***Abstract**: The precious sea foods are rich in nutrients and have fairly high commercial values. The appearance quality is an important criterion for assessing their commercial values. Currently, the assessment of the precious sea food appearance quality mainly depends on manual detections on its body size and colour, with great labour intensity and strong subjectivity. In this article, using the sea cucumber and abalone, two typical precious sea foods, as the research objects, a vision detection system was established. Because of the big differences between sea cucumber and abalone, according to typical body size characteristics, the targeted non-destructive testing methods based on computer vision technology were proposed. In the previous studies, the detection accuracy using the enclosing rectangle method was not high and the thorns on sea cucumbers imposed severe effects on the detection results. To solve these problems, the neighbourhood comparison method was proposed, so that an accurate and non-contact measurement of the long-axis and short-axis sizes of the sea cucumber body except thorns can be achieved. With the actually measured values as the standards, the average detection errors of long-axis and short-axis sizes are +2.10 and +1.61mm, respectively. According to the habits in manual detection for abalones, the area and perimeter of the Region of Interest (ROI) in the abalone image were adopted as the detection characteristics, and thus the rapid abalone shape detection can be realized. By contrast with the clustering results using the estimated values, it can be concluded that the proposed detection method can be applicable to the practical production, detection and grading of abalone, algorithm detection rate can be up to 14 abalones per second.*

***Keywords:** computer vision; sea cucumber; abalone; shape detection*

***摘要：**海珍品营养丰富、商业价值高，外观品质的好坏是决定其商业价值高低的重要标准。目前海珍品外观品质主要依靠人工进行体形、体色等特征的检测，劳动强度大、主观性强。本文以海参、鲍鱼为研究对象，建立视觉检测系统，进行了基于计算机视觉技术的海珍品体形检测方法研究。针对海参前期研究使用的外接矩形法检测精度不高、肉刺影响严重的问题，提出邻域比较法，实现了无肉刺参体长轴和短轴尺寸精确、无接触检测，以实际测量值为标准，长轴平均误差为+2.10mm，短轴为+1.61mm。依照人工检测习惯，选择鲍鱼图像感兴趣区域面积和周长作为检测特征，实现了鲍鱼体形的快速检测，与实际测量值的聚类分析比较结果表明，该方法可以用于鲍鱼实际生产检测分级，算法检测速率可达 14 个/s。*

***关键词：**计算机视觉；海参；鲍鱼；体形检测*

## INTRODUCTION

China has a vast maritime territory and boasts a coastline of 18 thousand kilometres. The sea areas along the continental margins are rich in nutrients and therefore favourable for the reproduction and growth of marine organisms. As the sea foods occupy a significantly increasing ratio in human diets, the consumers set increasingly high demands for their appearance quality. In particular, for some precious sea foods with relatively high prices such as sea cucumber and abalone, their commercial values largely depend on their appearance quality grades mainly including body size and colour. With the advancement of the deep processing industrialization, manual detection has become a major factor hampering its development. Using the computer vision technique, the sample shape can be described in a non-destructive, non-contact and visual way. Owing to these strengths, the shape tracking of crops and foods based on computer vision and image processing technology now has become a subject of intense interest,

## 引言

中国海域辽阔，海岸线长约 1.8 万千米，大陆边缘内海域，营养丰富，有利于各种海洋生物的繁殖和生长。随着海产品在居民膳食结构中的比重显著增加，消费者对于海产品的外观品质要求越来越高。特别是价格相对较高的海珍品，如海参、鲍鱼，体形、体色等外观品质的等级在很大程度上决定了其商业价值。随着海珍品深度产业化加工的进程，人工检测成为了制约其发展的重要因素之一。计算机视觉技术可以无损、非接触、直观的表达被测物形态，因此利用计算机视觉和图像处理技术跟踪农作物、食

and a lot of favourable detection results were achieved [1],[2],[5-8]. Yang *et al*. extracted the morphological characteristics from the crop pest images and constructed the score function for effectively distinguishing the pests [15]. By extracting some image characteristics such as the morphological structural parameters, Yang *et al*. proposed an effective identification scheme for the rice types based on sparse presentation [11].In view of the diversity and complexity of the precious sea foods, there are few reports on the automatic shape detection by means of computer vision technique. In this article, the sea cucumber and abalone from the Bohai Gulf were adopted as the detection objects. In consideration of the thorns on the sea cucumber, the long-axis and short-axis sizes can be detected using the proposed neighbourhood comparison method. According to the habits in manual detection for abalones, the area and perimeter of Region of Interest (ROI) were adopted as the characteristic parameters for rapid abalone shape detections.

## MATERIALS AND METHODS

### *Materials*

The ready-to-eat sea cucumbers and the fresh and alive abalones purchased from Changxing seafood market, Dalian, were adopted as the experimental materials, which were then placed in the preservation boxes and transported to the laboratory for image acquisition.

### *Visual Detection System*

The detection system mainly consists of a computer, a dome diffuse-reflection light source and an industrial camera (MV-1300C, Microvision, China). As shown in Fig. 1, the white light was produced and the samples were placed in the dome diffuse-reflection light source so that the stability of collecting environment could be guaranteed. The control system based on Windows operation system was programmed with Visual C++, in which the images were collected by the industrial camera via software triggering. Moreover, using the control system, the collected images could be automatically displayed, processed and stored. All the collected images were the 24-bit colour images in the format of BMP, with image resolution of 640*512.

品等形态的研究已成为热点，同时取得了较好的检测效果[1][2][5-8]。杨炎等提取作物害虫图像形态特征，建立判别评分函数，从而有效区分害虫[15]；杨蜀秦等通过提取图像的形态结构参数等特征，利用稀疏表示法提出了大米品种识别的有效方案[11]。由于海珍品的多样性和复杂性状，利用计算机视觉技术进行其体形自动检测的相关报道较少。本文以渤海湾刺参和鲍鱼为检测对象，针对刺参存在肉刺的特殊性状实现无肉刺影响的体壁长轴、短轴检测；根据人工检测习惯，提取鲍鱼图像感兴趣区域（ROI）面积和周长作为检测特征，实现了鲍鱼体形的快速检测。

## 试验材料与方法

### *试验材料*

试验材料选用购置于大连长兴海产市场的即时海参和鲜活鲍鱼，由保鲜盒快速运送至实验室进行图像采集。

### *视觉检测系统*

检测系统主要由计算机、漫反射圆顶光源、MV-1300UC 工业相机（维视，中国）组成。如图 1 所示，光源为白光，检测样本置于漫反射圆顶光源内，可保证采集环境的稳定性。使用 Visual C++开发工具，设计开发基于 windows 平台的控制系统，可通过软触发控制工业相机采集图像，并自动实施显示、处理、存储动作。所采集图像为 24 位 BMP 彩色图像，图像分辨率为 640×512。

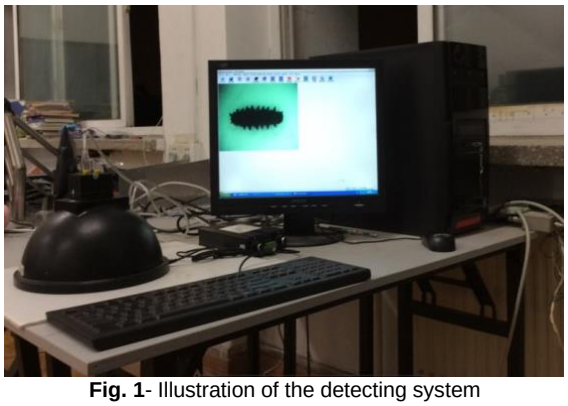

**Fig. 1**- Illustration of the detecting system

## Precious Seafood Shape Detection Method Based on Computer Vision

### *Data Pre-processing*

As described above, the sample images were collected and displayed via the control system. In order to improve the shape information precision in the images, the image backgrounds were removed using the maximum class square error method [12], [14] and then ROI was extracted. A

## 海珍品体形计算机视觉检测方法

### *预处理*

利用控制系统采集并显示样本图像，为提高体形的图像信息精度，首先使用最大类间方差法将图像背景去除

denotes the ratio of the ROI pixel numbers to the pixel numbers of the whole image, with the average grey degree of $G_1$, and B denotes the ratio of the pixel numbers of image backgrounds to the pixel numbers of the whole image, with the average grey degree of $G_2$, the overall average grey value of the sample image can be calculated by:

[12][14]，提取 ROI， ROI 像素数占整副图像的比例为 A，平均灰度为 $G_1$；图像背景像素数占整副图像的比例为 B，平均灰度为 $G_2$，计算得样本图像的总平均灰度值，如式 1 所示，

$$G_{SUM} = A \times G_1 + B \times G_2 \quad (1)$$

in which $G_{SUM}$ denotes the overall average grey value of the sample image.
The variance (VAR) of the ROI and the image backgrounds can then be calculated by:

式中，$G_{SUM}$ 为样本图像的总平均灰度值。
根据式 1，计算 ROI 与图像背景的方差 VAR，结果如式 2 所示，

$$VAR = A(G_1 - G_{SUM})^2 + B(G_2 - G_{SUM})^2 \quad (2)$$

Bring Equation (1) into Equation (2), VAR:

把 1 式带入 2 式，VAR 得：

$$VAR = A \times B \times (G_1 - G_2) \quad (3)$$

The calculation was conducted by traversing the image. When VAR is maximal, it is supposed that the great difference exists between ROI and image backgrounds, i.e., VAR can be regarded as the segmentation threshold between ROI and backgrounds. Considering that only the shape information was extracted in the present study, we then performed binary conversion and filtering processing on the images after segmentation for improving the detection speed. Fig. 2(a) and Fig. 3(a) display the original images of samples, while Fig. 2(b) and Fig. 3(b) display the images after segmentation, binary conversion and filtering.

遍历图像并进行计算，当 VAR 最大时，可认为 ROI 与样本图像背景间存在最大差异，即为 ROI 与背景的分割阈值。由于只进行体形信息的提取，为提高检测速度，将分割后图像进行二值及滤波处理，样本图像原图如图 2(a)、3(a)所示，分割后二值滤波图像如图 2(b)、3(b)所示。

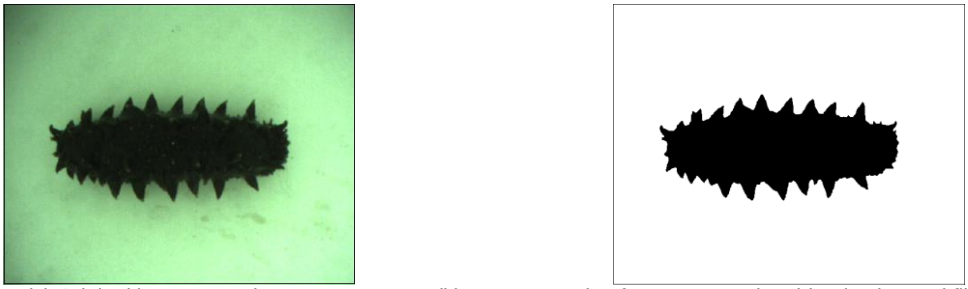

(a) Original image sample (b) Image sample after segmentation, binarization and filtering

**Fig. 2 -** Image of sea cucumber

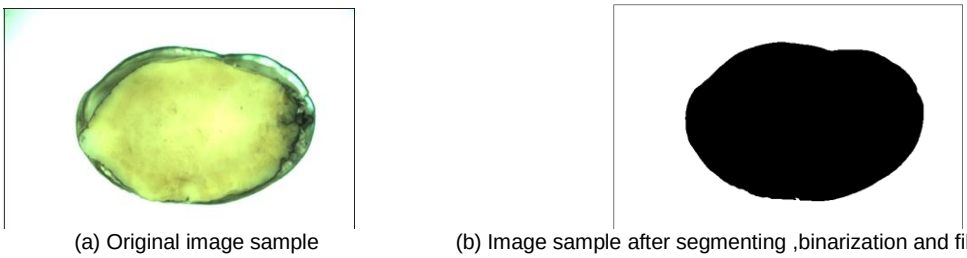

(a) Original image sample (b) Image sample after segmenting ,binarization and filtering

**Fig.3 -** Image of abalone

***Shape Detection of Sea Cucumber***

According to the manual detection habits, the body core size not including the thorns was adopted as the primary index for the appearance quality detection of the sea cucumber. In the previous studies, the minimum enclosing rectangle (MER) was determined using the rotation comparison method [4],[10]. Then the long-axis and short-axis sizes of the sea cucumber were acquired by calculating the length and width of the enclosing rectangle. Fig.4 displays the minimum enclosing rectangle of the sea cucumber, from which we can

***海参体形检测***

依据人工检测习惯进行海参外观品质检测，主要指标为不包含肉刺的参体尺寸。在前期研究中通过旋转比较法[4][10]确定了海参图像的最小外接矩形，如图 4 所示。通过计算外接矩形的长、宽，获得海参长轴、短轴尺

observe that the acquired long-axis and short-axis sizes are only the estimated values due to the existence of thorns. The researches have conducted the detection on 30 sea cucumber samples, and the results indicate that the average detection errors of the long-axis and short-axis sizes were +2.15 and +8.97mm, respectively. The primary reason of the great errors is that the effect induced by the thorns was not eliminated in calculating the body core size.

寸。由于肉刺的影响，所得长轴、短轴尺寸仅为估算值，对 30 份海参样本进行检测，长轴平均检测误差可达+2.15mm，短轴为+8.97mm。未消除肉刺的影响是造成上述误差的最主要原因。

**Fig.4**- Minimum enclosing rectangle of the sea cucumber

Based on the above-described studies, by taking the special structures of the sea cucumber (including thorns and body) into account, the marking of the body core and the fitting of the body core outer contour were implemented with the use of neighbourhood comparison, i.e., the auto-detection of the sea cucumber body core size can be achieved. The proposed algorithm consists of two steps, firstly, the overall contour tracing and then the body contour identification. In this article, the eight neighbourhood boundary tracking method was adopted for contour tracing. On the basis of the contour tracing results, the coordinate sequences of the sea cucumber boundary were denoted as $P(x_k,y_k),k=1,2,...,N$, in which N denotes the number of the boundary coordinate points. In other words, $x_k$ and $y_k$ denote the coordinates of the sea cucumber boundary points in the image.
Then the centre coordinate of the sea cucumber image was determined using the minimum enclosing rectangle, denoted as $O(x_0,y_0)$.Generally, a sea cucumber except the thorns is elliptical. Assuming that $Ny_0$ denotes the centre line of the horizontal axis, the distance between the boundary point and the centre line of the horizontal axis, denoted as $r_k$, can be calculated by:

基于上述研究和海参肉刺、体壁的特殊结构，本文通过邻域比较法完成了无肉刺体壁的标记和体壁外部轮廓拟合，实现了海参体壁尺寸的自动检测。算法需首先进行整体轮廓的跟踪，再实现体壁轮廓的识别。本文采用八邻域边界跟踪法进行轮廓跟踪，基于轮廓跟踪结果，记海参边界坐标点序列为 $P(x_k,y_k)$，其中 $k=1,2,...,N$，N 为边界坐标点个数，$x_k$ 和 $y_k$ 即为海参边界点在图像中的坐标值。

通过最小外接矩形确定海参图像中心坐标，记为 $O(x_0,y_0)$，设横轴中心线为 $Ny_0$，由于除肉刺外参体呈椭圆状，利用 4 式求出海参边界点坐标到横轴中心线 $Ny_0$ 的距离，记为 $r_k$，

$$r_k=|y_k-y_0| \tag{4}$$

The distance between each pixel point and the centre line of the horizontal axis $Ny_0$, was calculated by traversing the contour tracing image, and then compared with the neighbouring points according to the comparison flow as shown in Fig. 5.

遍历轮廓跟踪图像，计算每个像素点到横轴中心线 $Ny_0$ 的距离 $r_k$，并对相邻若干点进行比较，比较流程如图 5 所示。

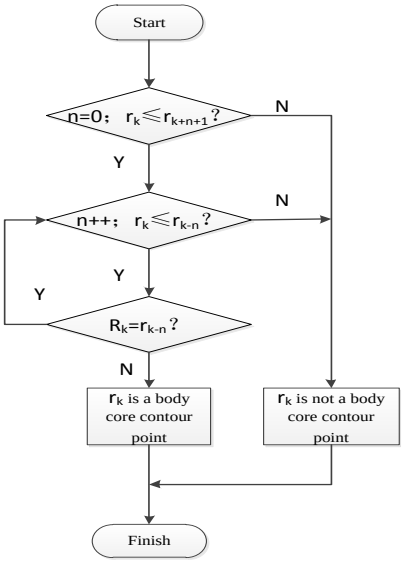


**Fig. 5** - Flow chart of the comparison

Then an array R was constructed. The point whose coordinate can meet the body core contour requirements was added into R, and the body core coordinate sequence was acquired, as shown in Fig. 6(b). According to the parabolic spline principle [3],[13], using the interpolations of coordinate sequence to obtain the closed curve, the outer contour of the body core was fit, as shown in Fig. 6(c). Therefore, the body size of the sea cucumber, i.e., the body size not including the thorns, can be calculated.

建立数组 R，当满足体壁轮廓要求时，将该点坐标赋于 R，获得体壁坐标序列，如图 6(b)所示。根据抛物线样条原理[3][13]，利用上述坐标序列插值，使其呈闭合曲线，实现海参体壁外部轮廓拟合，结果如图 6(c)所示。由此可计算体壁尺寸，即得去除肉刺后参体大小。

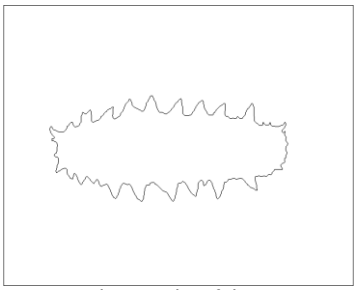

(a) Contour tracing results of the sea cucumber

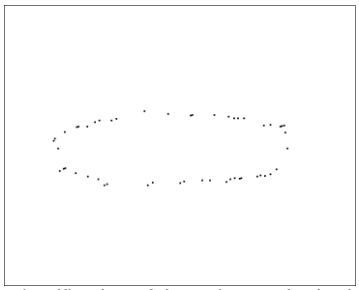

(b) Identification of the points at the body core

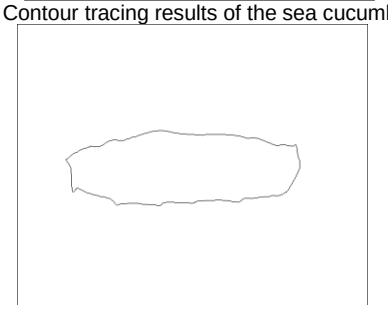

(c) Fitting image of the body core

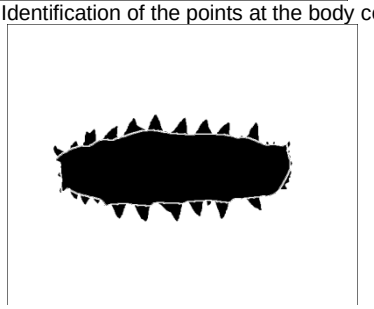

(d) Edge detection

**Fig.6**-The image processing and feature extraction

***Shape Detection of Abalone***

The abalones have much simpler shapes and contours than the sea cucumbers. It's no need to deal with abalone images in accordance with aforesaid methods. The size of the abalone is generally adopted as the index for manually detecting its appearance quality. According to the habits in manual detection, the area and perimeter of the ROI in an abalone image were used as the shape characteristics for detecting the appearance quality.

The abalone contour was traced using the method proposed in aforementioned content, with the tracing results presented in Fig. 7. The calculations of area and perimeter were conducted by traversing the binary contour tracing image. Assuming that the pixel point in the image is denoted as $f(x,y)$, the perimeter can be calculated by the following Eq.(5) and Eq.(6). Using the extracted binary ROI after filtering, the area was calculated by the following Eq.(5) and Eq.(7). The algorithm detection rate can be up to 14 abalones per second.

***鲍鱼体形检测***

与海参的体形轮廓比较，鲍鱼体形简单，无需完全按照前述方法进行处理。人类鉴评鲍鱼外观品质指标主要为获取其尺寸信息，根据人类的检测习惯，应提取鲍鱼图像 ROI 面积、周长作为鉴评鲍鱼体形特征，进行外观品质鉴评。通过前述方法跟踪鲍鱼轮廓，跟踪结果如图 7 所示，遍历二值化轮廓跟踪图像，设图像像素点 $f(x,y)$，根据式 5、6 计算周长 C。按式 5、7 方法，利用 ROI 提取后的二值滤波图进行面积 S 的计算。鲍鱼体形算法检测速率可达 14 个/s。

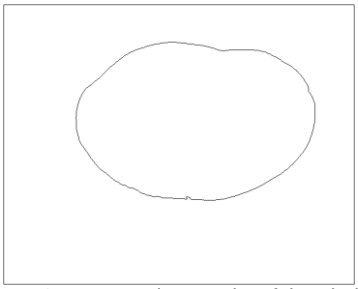

**Fig. 7** - Contour tracing results of the abalone

$$Q(x,y)=\begin{cases}1, f(x,y)=0\\0, f(x,y)=255\end{cases} \quad (5)$$

$$C=\sum Q(x,y) \quad (6)$$

$$S=\sum Q(x,y) \quad (7)$$

## RESULTS

### *Detection Results of Sea Cucumber*

Using the aforesaid method, the body cores of the sea cucumbers were identified. By effectively eliminating the effects of the thorns on the detected sizes, this method can significantly enhance the detection precision. With the adoption of the actual body core sizes as the standard, using neighbourhood comparison method, 30 sea cucumbers were used to verify the detection performances. The results demonstrate that the average detection errors of long-axis and short-axis sizes are +2.10 and +1.61mm, respectively.

### *Detection Results of Abalone*

According to the habits in manual detection, the area and perimeter of abalone were used as detection indexes. Quick and non-destructive detection for abalone was realized utilizing computer vision technology. Since the abalones are generally irregular ellipses, the actually measured long-axis and short-axis lengths were used to estimate the areas and perimeters according to calculation formula for ellipse. Then, using the ROI and estimated areas and perimeters as the samples values, the cluster analysis was conducted by within-group linkage method in hierarchical clustering. Fig. 8 displays when the number of clusters is less than 6, grading results based on the vision characteristic parameters and the estimated values are consistent. The results indicate that the proposed method can be applicable to the quality assessment of abalones.

## 检测结果分析

### *海参检测结果*

使用前述方法进行海参体壁的识别，能够有效规避肉刺在图像上对于测量尺寸的影响，与通过外接矩形获得的海参尺寸相比，该方法大幅提高了检测精度，以实际体壁尺寸为标准，进行邻域比较法验证，通过 30 个海参样本计算得，长轴平均误差为+2.10mm，短轴为+1.61mm。

### *鲍鱼检测结果*

根据人工检测习惯，将面积和周长作为鲍鱼主要检测指标，利用计算机视觉技术实现鲍鱼体形快速无损检测。由于鲍鱼为不规则椭圆状，因此通过实际测量的长轴、短轴长度，按椭圆面积、周长计算公式进行估算。选择系统聚类的组内联结法，对 ROI 和估算所得面积 S 和周长 C 分别进行聚类分析，聚类图谱如图 8 所示，当聚类数小于 6 时，基于计算机视觉检测的样品分类与基于估算值的分类一致，因此该方法可用于鲍鱼的快速分级。

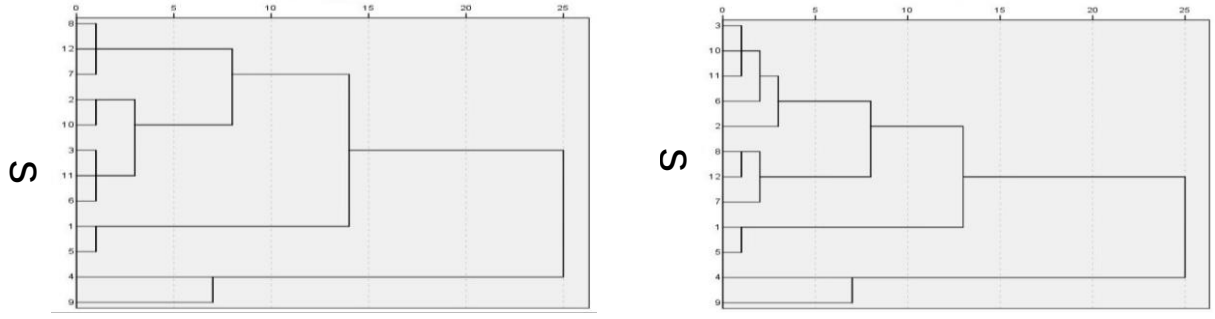


(a) Clustering chart based on the visual sample values (b) Clustering chart based on estimated sample values

**Fig. 8** - Clustering charts

## CONCLUSIONS

(1) Using the neighbourhood comparison method, the identification of the body core coordinates of the sea cucumbers and the fitting of body core can be achieved in this article. By effectively avoiding the effects of thorns on the detection results, the non-contact detection of the long-axis and short-axis sizes of the sea cucumbers can be realized. The results demonstrate that, using the proposed method, the errors of the long-axis and short-axis errors are + 2.10 and +1.61 mm, respectively.

(2) According to the habits in abalone manual detection, the area and perimeter of the ROI in the image were adopted as the characteristic parameters for rapid detection. By comparing with the clustering results using the estimated values, the effectiveness and accuracy of

## 结论

(1)利用邻域比较法实现了去除肉刺后海参体壁坐标的识别和体壁的拟合，从而有效规避了海参肉刺影响，实现去除肉刺参体长轴、短轴尺寸的无接触检测，长轴平均误差为+2.10mm，短轴为+1.61mm。

(2)依据人工检测鲍鱼的习惯，选择鲍鱼图像 ROI 面积和周长作为特征实现了快速检测，与估算值聚类分析结果比

the proposed method were proved, i.e., the proposed method can be applied to abalone detection, the algorithm detection rate can be up to 14 abalones per second.

**ACKNOWLEDGEMENT**
This study is funded Public Science and Technology Research Funds Projects of Ocean (201505029) and National Engineering Research Centre of Seafood (2012FU125X03).

**REFERENCES**

[1]. Baohua Zhang, Wenqian Huang, Liang Gong, Jiangbo Li, Chunjiang Zhao, Chengliang Liu, Danfeng Huang, (2015) - *Computer vision detection of defective apples using automatic lightness correction and weighted RVM classifier*, Journal of Food Engineering, Volume 146, pp.143–151;
[2]. Chandraratnea M.R., Kulasirib D., Samarasingheb S., (2007) - *Classification of lamb carcass using machine vision: Comparison of statistical and neural network analyses*, Journal of Food Engineering, Volume 82, Issue 1, pp. 26–34;
[3]. Chenglong Wang, Xiaoyu Li, Wei Wang, Yaoze Feng, Zhu Zhou, Hui Zhan, (2011) - *Recognition of worm-eaten chestnuts based on machine vision*, Mathematical and Computer Modelling, Volume 54, Issues 3–4, pp. 888–894;
[4]. Chi-Chang Wang, (2010) - *Applying the differential equation maximum principle with cubic spline method to determine the error bounds of forced convection problems*, International Communications in Heat and Mass Transfer, Volume 37, Issue 2, pp. 147–155;
[5]. Eunju Kwak, Ayman Habib (2014) - Automatic representation and reconstruction of DBM from LiDAR data using Recursive Minimum Bounding Rectangle, ISPRS Journal of Photo grammetry and Remote Sensing,Volume 93, pp. 171–191;
[6]. Hanmei Hong, Xiaoling Yang, Zhaohong You, Fang Cheng.(2014) - *Visual quality detection of aquatic products using machine vision*, Aquacultural Engineering, Volume 63, pp. 62–71;
[7]. Kurtulmuşa F., Kavdir İ., (2014) - *Detecting corn tassels using computer vision and support vector machines*, Expert Systems with Applications, Volume 41, Issue 16, pp. 7390–7397;
[8]. Kurtulmuş F., Ünal H., (2015) - Discriminating rapeseed varieties using computer vision and machine learning, Expert Systems with Applications, Volume 42, Issue 4, pp. 1880–1891;
[9]. Muhammad Makky, Peeyush Soni., (2013) - *Development of an automatic grading machine for oil palm fresh fruits bunches (FFBs) based on machine vision*, Computers and Electronics in Agriculture, Volume 93, pp. 129–139;
[10]. Ni Jiang, Wanneng Yang, Lingfeng Duan, Xiaochun Xu, Chenglong Huang, Qian Liu, (2012) – *Acceleration of CT reconstruction for wheat tiller inspection based on adaptive minimum enclosing rectangle*, Computers and Electronics in Agriculture Volume 85, pp. 123–133;
[11]. Shuqin Yang, Jifeng Ning, Dongjian He, (2011) - *Identification of varieties of rice based on sparse representation*, Transactions of the CSAE, Volume 27, pp. 191－195;
[12]. Weiya Guo, Xiaofei Wang, Xuezhi Xia. (2014) - *Two-dimensional Otsu's threshold segmentation method based on grid box filter*, Optik - International Journal for Light and Electron Optics, Volume 125, Issue 18, pp. 5234–5240;

较，说明根据此方法可对鲍鱼体形大小进行有效、准确分级，算法分级速率可达 14 个/s。

**基金支持：**
海洋公益性行业科研专项经费资助（201505029），国家海洋食品工程技术中心资助（2012FU125X03）。

**参考文献**

[1]. Baohua Zhang，Wenqian Huang，Liang Gong，Jiangbo Li，Chunjiang Zhao，Chengliang Liu, Danfeng Huang.计算机视觉检测有缺陷的苹果使用自动亮度校正和加权 RVM 分类器[J].食品工程学报,2015(146):143-151;
[2]. Chandraratnea M.R., Kulasirib D., Samarasingheb S. 基于机器视觉的羔羊胴体分类：统计与神经网络分析比较[J].食品工程学报, 2007,82(1): 26–34;
[3]. Chenglong Wang，Xiaoyu Li, Wei Wang, Yaoze Feng, Zhu Zhou, Hui Zhan.基于机器视觉的虫蛀栗子的识别[J].数学和计算机建模, 2011,54(3-4):888-894;
[4]. Chi-Chang Wang.运用微分方程最大值原理与三次样条方法来确定强制对流的问题误差范围[J]. 热与传质的国际交流, 2010,37(2):147-155;
[5].Eunju Kwak, Ayman Habib.自动代表性和使用递归最小边界矩形 LiDAR 数据重建的 DBM[J]. 摄影测量学与遥感学报, 2014(93):171-191;
[6].Hanmei Hong, Xiaoling Yang, Zhaohong You, Fang Cheng.利用机器视觉检测水产品的视觉质量[J]. 水产养殖工程, 2014(63): 62–71;
[7]. Kurtulmuşa F., Kavdir i.检测基于计算机视觉的玉米穗和支持向量机[J]. 应用专家系统，2014,41(16): 7390–7397;
[8].Kurtulmuş F.,Ünal H.利用计算机视觉和机器学习鉴别油菜品种[J]. 应用专家系统,2015,42(4): .1880–1891;
[9].Muhammad Makky, PeeyushSoni.基于机器视觉的油棕鲜果的自动分选机的开发[J].农业电子计算机，2013(93:) 129–139;
[10]. Ni Jiang, Wanneng Yang, Lingfeng Duan, Xiaochun Xu, Chenglong Huang, Qian Liu.基于自适应最小外接矩形的小麦分蘖 CT 重建[J]. 农业电子计算机,2012(85): 123–133;
[11].杨蜀秦，宁纪锋，何东健. 基于稀疏表示的大米品种识别[J]. 农业工程学报,2011(27): 191－195;
[12].Weiya Guo，Xiaofei Wang，Xuezhi Xia.基于网格框过滤器的维大津的阈值分割方法[J].光学和电子光学国际学报，2014，125(18): 5234–5240;
[13].Xiaofeng Xue, Xingwu Zhang, Bing Li, Baijie

[13]. Xiaofeng Xue, Xingwu Zhang, Bing Li, Baijie Qiao, Xuefeng Chen (2014) - *Modified Hermitian cubic spline wavelet on interval finite element for wave propagation and load identification*, Finite Elements in Analysis and Design, Volume 91, pp. 48–58;
[14]. Xiaolu Yang, Xuanjing Shen, Jianwu Long, Haipeng Chen (2012) - *An Improved Median-based Otsu Image Threshold Algorithm*, AASRI Procedia, Volume 3, pp. 468–473;
[15]. Yan Yang, Sa Liu, Shibin Lian, Xiaodong Zhu. (2013) - *Analysis of fruit tree pests morphological characteristics based on computer vision*, Journal of Jilin University (Engineering and Technology Edition), Volume 43,Sup, pp. 235-236.

Qiao, Xuefeng Chen.改进的 Hermite 三次样条小波区间有限元波动和负载识别[J].有限元分析与设计, 2014(91): 48–58;
[14].Xiaolu Yang, Xuanjing Shen, Jianwu Long, Haipeng Chen.一种改进的基于中值的 Otsu 图像阈值分割算法[J].AASRIProcedia, 2012(3): 468–473;
[15]. 杨 焱,刘 飒,廉世彬,朱晓冬.基于计算机视觉的果树害虫的形态特征分析[J]. 吉林大学学报(工学版), 2013,43(Suppl): 235-236.

# STUDY OF THE VIBRATIONS OF A PLOW BLADE
# /
# *STUDIUL VIBRAȚIILOR UNEI LAME DE PLUG*

**Lecturer PhD. Eng. Orăşanu N., Assoc. Professor PhD. Eng. Dragomirescu C.**
University "Politehnica" of Bucharest, Department of Mechanics
*Tel: 021-4029503; E-mail: norasanu62@yahoo.com*

***Abstract:*** *The paper analyses the bending vibrations of a plow blade, modeled as a variable cross-section beam, clamped at one end and free at the other. The study is performed by using the discretization method, while the differential equations of the free vibrations are deduced by means of the influence coefficients method.*

***Keywords:*** *bending vibrations, variable cross-section, discretization, influence coefficient*

## INTRODUCTION

Vibration study is of considerable importance in agricultural machinery design, due to two reasons: first, the interaction between soil and tillage tools generates oscillatory phenomena that can affect the functionality and the service life of such tools and, second, certain oscillations induced to active organs of agricultural units can increase the quality and efficiency of the process they carry out.

For this reason, a large number of scientific works were dedicated to the subject. Thus, in paper [11], the influence of the oscillation frequency was studied, upon the tillage and upon the energy consumption. Reference [1] presents the results of some experiments performed on decompaction plows, which determine the frequency bands specific to actuators. A study model of the vibrations of a tillage tool, based on the finite element method, is proposed in paper [17]. In reference [2], spectral domains of the oscillations due to the soil irregularities and to the quasi-periodical variations of the resistant forces are presented. The energetic efficiency of the tillage processes with vibratory devices is analyzed in papers such as [10, 13].

Part of this framework, the present paper is dedicated to the study of the vibrations of a plow blade. Knowing the eigenfrequencies of such a device as early as in the design stage allows it to determine the optimal work parameters of actuators.

## MATERIAL AND METHOD

In order to study the vibrations of an arbitrary blade with variable section, the model of a rectangular cross-section beam is adopted, with variable width. The beam is clamped at one end and free at the other (Fig.1a). The beam performs bending vibrations, in the longitudinal plane (vertical in the figure).

**Rezumat:** *Lucrarea analizează vibrațiile de încovoiere ale unei lame de plug, modelată ca o bara de secțiune variabilă, încastrată la un capăt şi liberă la celălalt. Studiul vibrațiilor se efectuează prin metoda discretizării, iar ecuațiile diferențiale ale vibrațiilor se deduc cu ajutorul metodei coeficienților de influență*

**Cuvinte cheie:** *vibrații de încovoiere, secțiune variabilă, discretizare, coeficient de influență*

## INTRODUCERE

Studiul vibrațiilor prezintă o importanță deosebită în proiectarea maşinilor agricole din două motive: în primul rând, interacțiunea dintre sol şi uneltele de prelucrare a solului generează fenomene oscilatorii care pot afecta funcționalitatea şi durata de viață a uneltelor, iar în al doilea rând, anumite oscilații induse unor organe active ale agregatelor agricole pot creşte calitatea şi eficiența procesului pe care acestea îl îndeplinesc.

Din acest motiv, un mare număr de lucrări au fost dedicate acestui obiect. Astfel, în lucrarea [11] au fost studiate vibrațiile active ale cuțitelor şi influența frecvenței de oscilație asupra prelucrării solurilor şi a consumurilor energetice. Referința [1] prezintă rezultate ale unor experimente efectuate pe pluguri de decompactare, care determină benzile de frecvență specifice mecanismelor de acționare. Un model de studiu al vibrațiilor unei unelte de prelucrare a solului, bazat pe metoda elementului finit, este propus în lucrarea [17]. În referința [2] sunt prezentate domeniile spectrale ale oscilațiilor datorate neregularităților solurilor şi variațiilor cvasiperiodice ale forțelor de rezistență la înaintare. Eficiența energetică a unor procese de prelucrare a solului cu organe de lucru vibratoare este analizată în lucrări precum [10, 13].

Lucrarea de față se înscrie în acest cadru, fiind dedicată studiului vibrațiilor unui cuțit de plug. Cunoaşterea din stadiul de proiectare a frecvențelor proprii ale unui astfel de organ permite stabilirea parametrilor optimi de lucru pentru mecanismele de acționare.

## MATERIAL ŞI METODĂ

Pentru studiul vibrațiilor unui cuțit oarecare, cu secțiune variabilă, în lucrarea de față se adoptă modelul unei bare de secțiune dreptunghiulară, de lățime variabilă, încastrată la una dintre extremități şi liberă la cealaltă (fig.1a).

Bara efectuează oscilații de încovoiere în plan longitudinal (vertical pe figură).

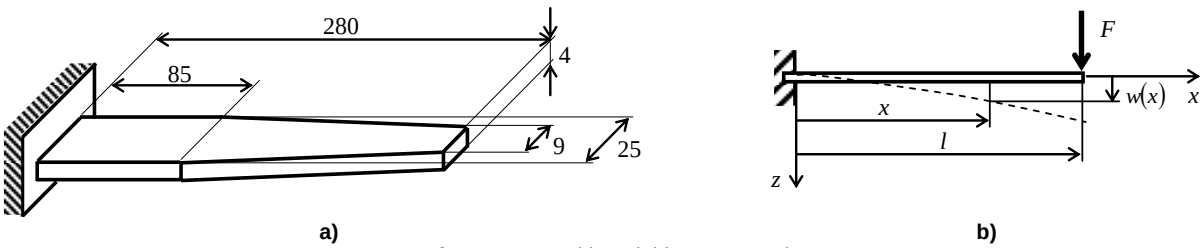


a) b)

**Fig. 1** - Beam with variable cross-section

The width of the beam varies with abscissa $x$ according to the law

Lățimea barei variază cu abscisa $x$ după legea

$$b(x)=\begin{cases}0.025\text{m} & \text{if} \quad 0\le x\le 0.085\text{m}\\ 0.03197436-0.08205x & \text{if} \quad 0.085\text{m}<x\le 0.280\text{m}\end{cases} \tag{1}$$

It is known from the strength of materials [16] that the deflection $w$ of the neutral fiber of the beam acted by a force $F$ in static regime (Fig. 1 b) results from the equation

Se cunoaşte din rezistența materialelor [16] că deplasarea pe direcție transversală, $w$, a fibrei medii a barei acționate în regim static de o forță $F$ (fig. 1 b) rezultă din ecuația

$$w''(x)=-\frac{M_z(x)}{EI_y(x)} \tag{2}$$

where

în care

$$M_z(x)=-F(l-x) \tag{3}$$

is the bending moment produced by the force in the section defined by abscissa $x$,

este momentul încovoietor produs de forță în secțiunea definită de abscisa $x$,

$$I_y(x)=\frac{b(x)h^3}{12} \tag{4}$$

is the geometrical moment of inertia of the section, while $E$ is the Young's modulus of the material of the beam.

By integrating two times equality (2), the equation of the neutral fiber in static regime is obtained:

este momentul de inerție geometric al secțiunii, iar $E$ este modulul lui Young al materialului barei.

Integrând de două ori egalitatea (2), rezultă ecuația fibrei medii deformate, în regim static:

$$w(x)=\int_0^x\left(\int_0^x\frac{M_z(x)}{EI_y(x)}\,\mathrm{d}x\right)\mathrm{d}x=\frac{12F}{Eh^3}\int_0^x\left(\int_0^x\frac{l-x}{b(x)}\,\mathrm{d}x\right)\mathrm{d}x \tag{5}$$

It is known from the literature [8, 9, 12, 14, 15] that the bending vibrations of the beam are governed by the partial derivative differential equation

Se cunoaşte din literatură [8, 9, 12, 14, 15] că vibrațiile de încovoiere ale barei sunt guvernate de ecuația diferențială cu derivate parțiale

$$\frac{\partial^2}{\partial x^2}\left[EI_y(x)\frac{\partial^2 w}{\partial x^2}\right]=-\rho A(x)\frac{\partial^2 w}{\partial t^2} \tag{6}$$

where $A(x)$ is the area of the cross-section of the beam, while $\rho$ is the density of the material of the beam.

However, the differential equation (6) cannot be integrated analytically in the general case, i.e. for arbitrary functions $I_y(x)$ and $A(x)$, respectively. Therefore, in the present paper, the study is performed numerically, by means of the discretization method, which was presented and successfully used in papers [3, 4, 5, 6, 7], for the study of the free and forced bending oscillations, respectively, of homogeneous beams with or without a number of attached concentrated masses.

The method consists in replacing the distributed mass system by a discrete one, made of a relatively high number $n$ of material points, of masses:

unde $A(x)$ este aria secțiunii barei, iar $\rho$ este densitatea materialului barei.

Ecuația diferențială (6) este, însă, imposibil de integrat analitic în cazul general, adică în cazul unor funcții oarecare $I_y(x)$, respectiv $A(x)$.

Ca urmare, în lucrarea de față, studiul este efectuat numeric, cu ajutorul metodei discretizării, prezentată şi utilizată cu succes în lucrările [3, 4, 5, 6, 7], pentru studiul oscilațiilor de încovoiere libere şi forțate, ale unor bare omogene, unele dintre acestea având ataşate un număr de mase concentrate.

Metoda constă în înlocuirea sistemului continuu printr-unul discret, alcătuit dintr-un număr $n$, relativ mare, de puncte materiale, de mase:

$$m_i=\rho b(x_i)h\cdot(x_i-x_{i-1}) \quad (i=1,2,\ldots,n) \tag{7}$$

which are attached to a beam with negligible mass (fig. 2).

ataşate unei bare de masă neglijabilă (fig. 2).

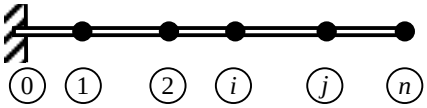


**Fig.2** - Discretized beam

The differential equations of the free small oscillations can be obtained by means of the method of the influence coefficients [8, 10]. The influence coefficient $\delta_{ij}$ represents

Ecuațiile diferențiale ale micilor oscilații libere se pot obține cu ajutorul metodei coeficienților de influență [8, 10]. Coeficientul de influență $\delta_{ij}$ reprezintă deplasarea

the deflection of the neutral fiber in section $i$, produced by a unit force, applied statically in section $j$ (fig. 2).

For the analyzed beam

fibrei medii în secțiunea $i$, produsă de o forță egală cu unitatea, aplicată static în secțiunea $j$ (fig. 2).

În cazul barei analizate

$$\delta_{ij} = \delta_{ji} = \frac{12}{Eh^3}\int_0^{x_i}\left(\int_0^{x}\frac{x_j - x}{b(x)}\,\mathrm{d}x\right)\mathrm{d}x \quad (i,j = 1,2,\ldots,n) \quad \text{if} \quad x_i \le x_j\,. \tag{8}$$

In the present paper, integrals in formula (8) were computed numerically.

By defining the matrix of the influence coefficients, the mass matrix and the dynamic matrix, respectively,

In lucrarea de față, integralele din formula (8) au fost calculate numeric.

Construind matricea coeficienților de influență, matricea maselor, respectiv matricea dinamică,

$$[\delta] = [\delta_{ij}], \quad [m] = [m_{ij}], \quad [D] = [\delta][m], \tag{9}$$

it is shown in references [3, 4, 5, 6, 7] that the circular eigenfrequencies are

se arată în referințele [3, 4, 5, 6, 7] că pulsațiile proprii ale sistemului sunt

$$\omega_i = \frac{1}{\sqrt{\lambda_i}} \quad (i = 1,2,\ldots,n)\,, \tag{10}$$

where $\lambda_i$ represent the eigenvalues of matrix $[D]$, while the eigenmodes are equal with the corresponding eigenvectors of the same matrix.

în care $\lambda_i$ reprezintă valorile proprii ale matricei $[D]$, iar modurile proprii sunt egale cu vectorii proprii corespunzători ai aceleiaşi matrice.

**RESULTS**

The numerical study of the vibrations of the beam in Figure 1 a was performed based of the following values:

**REZULTATE**

Studiul numeric al vibrațiilor barei din figura 1 a s-a efectuat considerând următoarele valori:

$$E = 210\,\mathrm{x}\,10^9\ \mathrm{N/m^2}, \qquad \rho = 7850\ \mathrm{kg/m^3}, \qquad n = 40\,.$$

The first 10 circular eigenfrequencies and the corresponding eigenfrequencies are presented in Table **1**.

Primele 10 pulsații proprii obținute şi frecvențele proprii corespunzătoare sunt prezentate in tabelul 1.

**Table 1**

**Values of the first 10 circular eigenfrequencies and the corresponding eigenfrequencies**

| $i$ | 1 | 2 | 3 | 4 | 5 | 6 | 7 | 8 | 9 | 10 |
|---|---|---|---|---|---|---|---|---|---|---|
| $\omega_i\,[\mathrm{s}^{-1}]$ | 263.41 | 1534.18 | 4409.33 | 8921.36 | 15035.13 | 22669.89 | 31656.21 | 41724.28 | 52766.81 | 65273.29 |
| $f_i\,[\mathrm{Hz}]$ | 41.92 | 244.17 | 701.77 | 1419.88 | 2392.92 | 3608.03 | 5038.24 | 6640.63 | 8398.1 | 10388.57 |

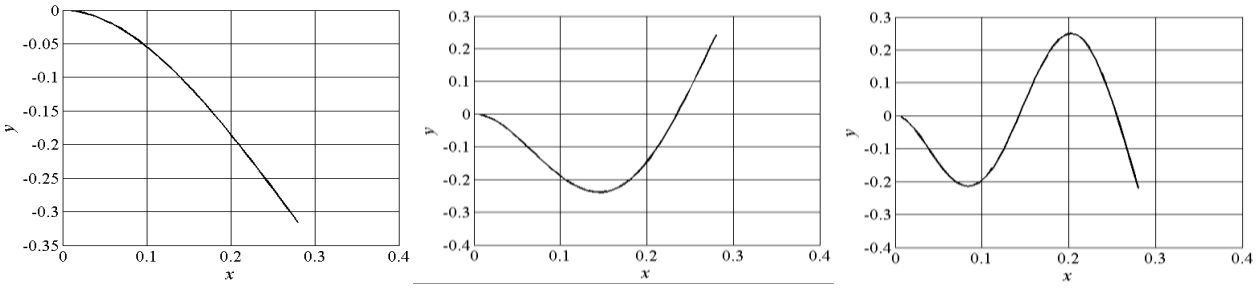


**Fig.3** - First three eigenshapes

The first three vibration eigenshapes are illustrated in Figure 3.

The experimental study of the system was performed on the measuring stand shown in Figures 4-6.

Primele trei forme proprii de vibrație sunt ilustrate în figura 3.

Studiul experimental al sistemului s-a efectuat cu ajutorul bancului de probă prezentat în figurile 4-6.

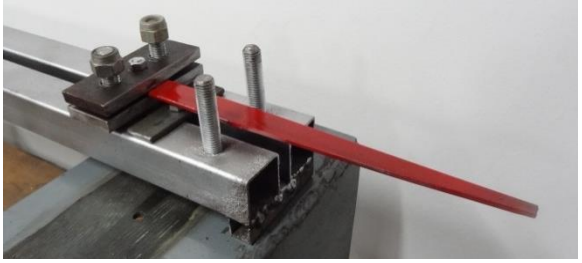

**Fig. 4** - Measuring Stand

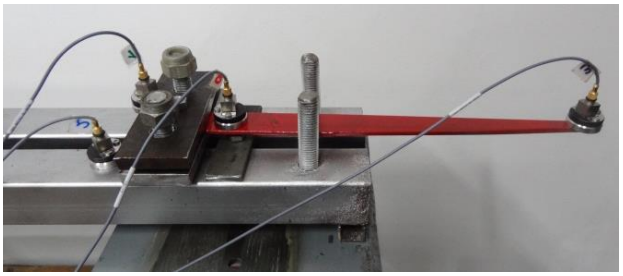

**Fig.5** - Accelerometer layout

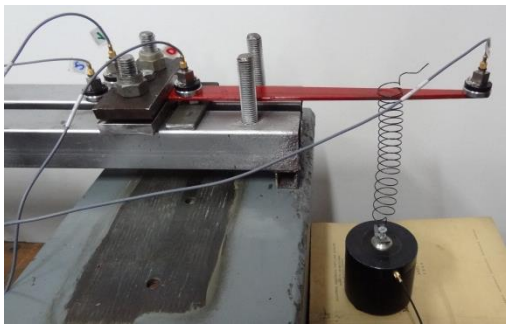

**Fig.6** - Excitation system

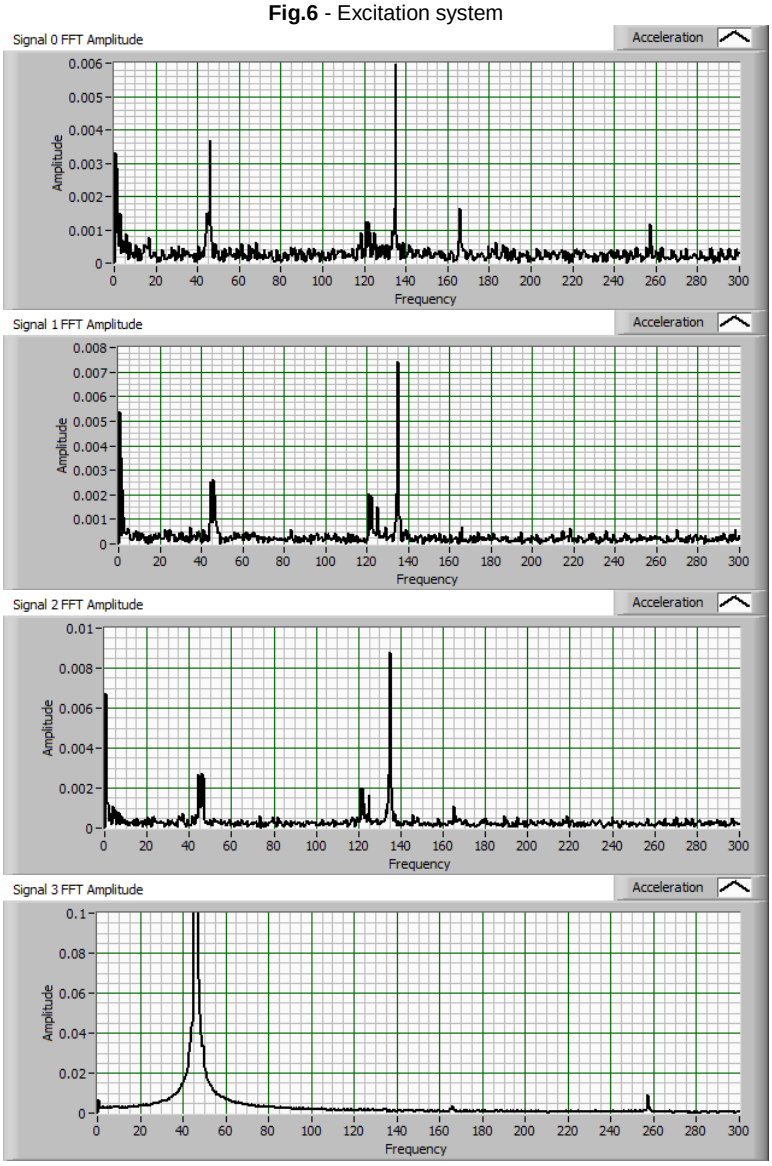


**Fig.7** - Free vibrations spectra

A measuring chain was used, with four accelerometers, counted from 0 to 3. Accelerometer 3 was positioned at the free end of the beam, while accelerometer 0 on the beam, near the fixing system. Accelerometers 1 and 2 were placed on the fixing system.

Similar to references [3. 4], free vibrations produced by applying percussions on the beam were studied, as well as forced vibrations, produced by the excitation system in Figure 6, with white signal.

The obtained date were processed with LabVIEW program, resulting the spectra in Figures 7-8.

S-a utilizat un lanț de măsură cu patru accelerometre, numerotate de la 0 la 3. Accelerometrul 3 a fost amplasat în capul liber al barei, iar accelerometru 0 pe bară, lângă încastrare. Accelerometrele 1 şi 2 au fost plasate pe sistemul de prindere.

Ca şi în referințele [3, 4], s-au studiat vibrații libere, produse prin aplicare unor percuții pe bară, precum şi vibrațiile forțate, produse de sistemul de excitație din figura 6, cu semnal alb.

Datele au fost prelucrate cu ajutorul programului LabVIEW, obținându-se spectrele din figurile 7-8.

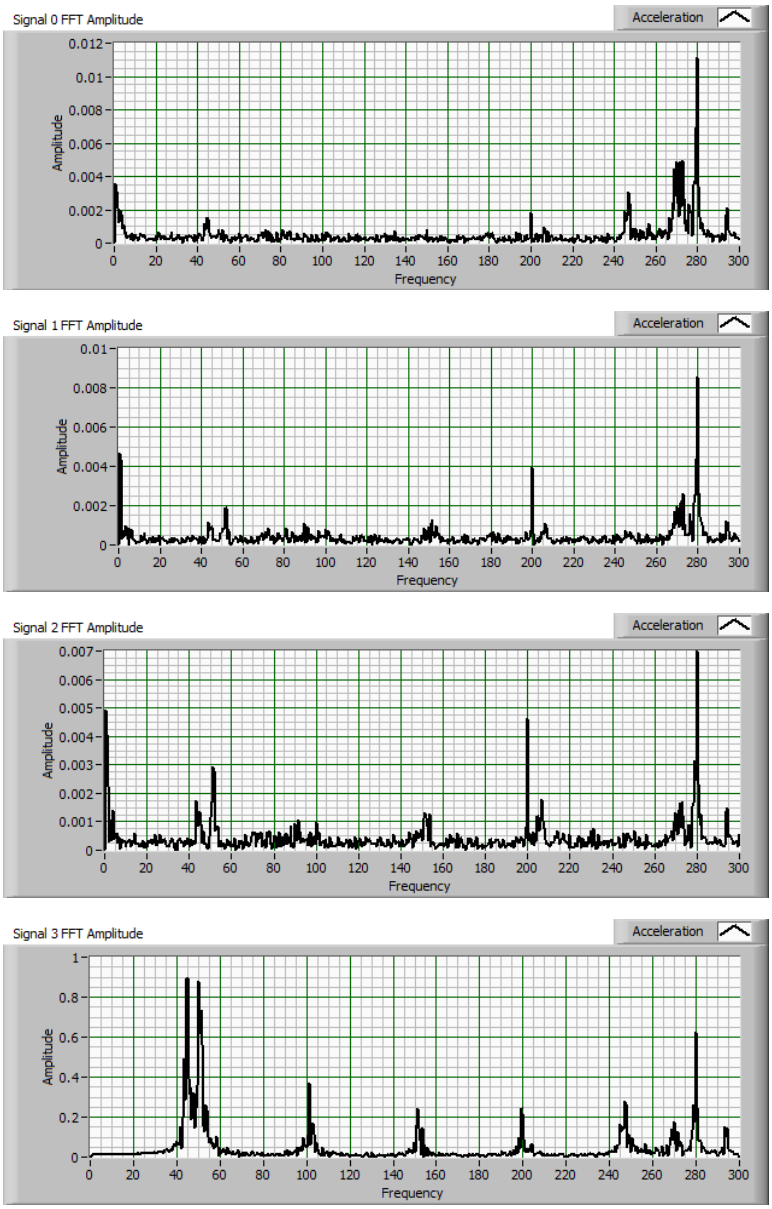


**Fig. 8** - Forced vibrations spectra - white signal

## CONCLUSIONS

Based on a simple model, the paper analyzed the vibrations of an arbitrary blade with variable section, which can represent a plow coulter.

The spectra obtained by processing the experimental data in the case of free vibrations present a pronounced peak at a frequency close to the first computed eigenfrequency. The spectrum of the signal measured by accelerometer 3, placed at the free end of the beam, shows a lower peak close to the second computed eigenfrequency. The first three accelerometers, situated close to the fixing system and on the fixing system, respectively, exhibit supplementary peaks, due to the stand vibrations.

The spectra obtained in the case of forced vibrations confirm the presence of the first two components, but the signal captured by accelerometer 3 presents also some components multiple of 50 Hz, due to the excitation system which is placed close to this accelerometer.

The numerical method used in the paper provided results in agreement with the experiments. The method allows it to determine the eigenfrequencies and, consequently, the resonance domains of the active

## CONCLUZII

Lucrarea a analizat pe baza unui model simplu vibrațiile unei lame oarecare de secțiune variabilă, ce poate reprezenta un cuțit lung de plug.

Spectrele obținute prin prelucrarea datelor experimentale în cazul vibrațiilor libere prezintă un vârf accentuat la o frecvență apropiată de prima frecvență proprie calculată. Spectrul semnalului măsurat de accelerometrul 3, plasat în capătul liber al barei, prezintă un vârf mai redus în apropierea celei de a doua frecvențe proprii calculate. Primele trei accelerometre, aflate în apropierea sistemului de prindere, respectiv pe acesta, prezintă vârfuri suplimentare, datorate vibrațiilor bancului.

Spectrele obținute în cazul vibrațiilor forțate confirmă prezența primelor două componente, dar semnalul captat de accelerometrul 3 prezintă, de asemenea, componente în apropierea unor frecvențe multiplu de 50 Hz, datorate sistemului de excitație, plasat lângă acest accelerometru.

Metoda numerică utilizată a condus la rezultate în acord cu experimentele. Metoda permite determinarea frecvențelor proprii şi, în consecință, identificarea domeniilor de rezonanță ale organelor de lucru active.

organ. The resonance phenomenon presents a double importance in agricultural machine design, since the displacement amplification it implies can cause damage of the organ, but, in certain circumstances, it can be exploited in order to increase the efficiency of the device.

**REFERENCES**

[1]. Badalan E.P., Salokhe V.M., Gupta C.P., (1999) – *Performance of an oscillating subsolier in breaking a hardpan*, Journal of Terramechanics, Vol.36, pp.117-125;
[2]. Chung S.O., Sudduth K.A., Tan J., (2008) – *Spectral Analysis of On-the-go Soil Strength Sensor Data*, Journal of Biosystems Eng. Vol. 33, pp. 355-361;
[3]. Craifaleanu A., Orăşanu N., (2011) – *Theoretical and experimental analysis of the vibrations of an elastic beam with four concentrated mass*, Proceedings of the Annual Symposium of the Institute of Solid Mechanics, SISOM 2011, Bucharest, May 25-26, 2011, pp.471-480;
[4]. Craifaleanu A., Orăşanu N., (2012) – *Experimental study of the forced vibrations of a system with distributed mass and four concentrated masses*, Proceedings of the Annual Symposium of the Institute of Solid Mechanics, SISOM 2012, Bucharest, May 30-31, 2012, pp.200-205;
[5]. Craifaleanu A., Orăşanu N., Dragomirescu C., (2013) – *Theoretical and Experimental Studies on Magnetic Dampers*, Applied Mechanics and Materials, Vol.430, pp.351-355, Trans Tech Publications, Switzerland;
[6]. Craifaleanu A., Dragomirescu C., Craifaleanu I.G., (2014) – *Animated graphic simulator for the study of bending vibrations of homogeneous rectilinear bars*, ICERI 2014 Proceedings, 7th International Conference on Education Research and Innovation, November 17th-19th, 2014, Edited by IATED Academy, Sevilla, Spain, 2014, pp.1738-1744;
[7]. Craifaleanu A., Orăşanu N., Dragomirescu C., (2015) – *Bending vibrations of a viscoelastic Euler-Bernoulli beam – two methods and comparison*, Applied Mechanics and Materials, Vol.762, pp.47-54, Trans Tech Publications, Switzerland;
[8]. Den Hartog J. P., (1947) – *Mechanical Vibrations*, McGraw-Hill Book Company, Inc;
[9]. Dimarogonas, A.D., Haddad S., (1992) – *Vibrations for Engineers*, Prentice Hall, Englewood Cliffs;
[10]. Fenyvesi L., Hudoba Z., (2009) – *Vibrated Tillage Tools for Energy Saving*, Journal of Agricultural Machinery Science, Vol. 5, Nr. 4, pp.445-449;
[11]. Johnson C.E., Buchele W.F., (1967) – *Energy in clod-size reduction of vibratory tillage.* Transactions of the ASAE, 12(3), pp.371-374;
[12]. Meirovitch L., (2001) – *Fundamentals of Vibrations*, McGraw-Hill;
[13]. Niyamapa T.A, Salokhe V.M., *Soil disturbance and force mechanics of vibrating tillage tool*, Journal of Terramechanics, Vol. 37, pp.151-166,2000;
[14]. Rao S., (2011) – *Mechanical Vibrations*, Prentice Hall;
[15]. Silaş Gh., (1968) – *Mechanics. Mechanical Vibrations* (in Romanian), Ed. Didactică şi Pedagogică, Bucureşti;
[16]. Timoshenko S., (1948) – *Strength of Materials. Part I. Elementary Theory and Problems*, D. van Nostrand Company, Inc.;
[17]. Zang J., Kushawaha R.L., (1998) – *Dynamic analysis of a tillage tool: Part I - Finite element method*, Canadian Agricultural Engineering, Vol.40, Nr.4, pp.287-292.

Fenomenul de rezonanță prezintă o dublă importanță în proiectarea maşinilor agricole, deoarece amplificarea deplasărilor pe care o implică poate conduce la distrugerea organului respectiv, dar, în anumite condiții, poate fi exploatată în vederea creşterii eficienței agregatului.

**BIBLIOGRAFIE**

[1]. Bandalan E.P., Salokhe V.M., Gupta C.P., Niyamapa T., (1999) – *Perfomanța unui plug vibratoriu de decompactare*, Revista Mecanicii Solului, Vol.36, p.117-125;
[2]. Chung S.O., Sudduth K.A., Tan J., (2008) – *Analiza spectrală a datelor furnizate de un senzor al rezistenței solului*, Revista Ingineria Biosistemelor. Vol.33, pg.355-361;
[3]. Craifaleanu A., Orăşanu N., (2011) – *Analiză teoretică şi experimentală a vibrațiilor unei bare elastice cu patru mase concentrate*, Lucrarile simpozionului anual al Institutului de Mecanica Solidelor, SISOM 2011, Bucharest, May 25-26, 2011, pag.471-480;
[4]. Craifaleanu A., Orăşanu N., (2012) – *Studiu experimental al vibrațiilor forțate ale unui sistem cu masă distribuită şi patru mase concentrate*, Proceedings of the Annual Symposium of the Institute of Solid Mechanics, SISOM 2012, Bucharest, May 30-31, 2012, pag.200-205;
[5]. Craifaleanu A., Orăşanu N., Dragomirescu C., (2013) – *Studii teoretice şi experimentale asupra amortizorilor magnetici*, Lucrarile simpozionului anual al Institutului de Mecanica Solidelor, Vol.430, pag. 351-355, Trans Tech Publications, Switzerland;
[6]. Craifaleanu A., Dragomirescu C., Craifaleanu I.G., (2014) – *Simulator grafic animat pentru studiul vibrațiilor de încovoiere ale unei bare drepte omogene*, ICERI 2014 Lucrările celei de-a 7-a Conferinta Internationala de Educație, Cercetare şi Inovare, 17-19 Nov.2014, Editată de Academia IATED, Sevilla, Spania, pag.1738-1744;
[7]. Craifaleanu A., Orăşanu N., Dragomirescu C., (2015) – *Vibrații de încovoiere ale unei bare Euler-Bernoulli viscoelastice – două metode şi comparație*, Mecanici Aplicate şi Materiale, Vol.762, pag.47-54, Trans Tech Publications, Switzerland;
[8]. Den Hartog J. P., (1947) – *Vibrații mecanice*, McGraw-Hill Book Company, Inc.;
[9]. Dimarogonas, A.-D., Haddad, S., (1992) – *Vibrații pentru ingineri*, Prentice Hall, Englewood Cliffs;
[10]. Fenyvesi L., Hudoba Z., (2009) – *Economisirea energiei prin utilizarea unor unelte vibratoare pentru prelucrat solului*, Revista de Maşini Agricole, Vol. 5, Nr. 4, pag.445-449;
[11]. Johnson C.E., Buchele W.F., (1967) – Aspecte e*nergetice privind reducerea dimensiunii bulgărilor prin utilizarea uneltelor vibratoare.* Lucrările ASAE 12(3), pag. 371-374;
[12]. Meirovitch L., (2001) – *Bazele vibrațiilor*, McGraw-Hill;
[13]. Niyamapa T.A, Salokhe V.M., (2000) – *Dislocarea solului şi mecanica forțelor la uneltele vibratoare*, Revista Mecanicii Solului, Vol. 37, pag. 151-166;
[14]. Rao S., (2011) – *Vibrații mecanice*, Prentice Hall;
[15]. Silaş Gh., (1968) – *Mecanică. Vibrații mecanice*, Ed. Didactică şi Pedagogică, Bucureşti;
[16]. Timoshenko S., (1948) – *Rezistența materialelor. Partea I. Teoria elementară şi Probleme*, D. van Nostrand Company, Inc.;
Zang J., Kushawaha R.L., (1998) – *Analiza dinamică a unei unelte de lucrat solul: Partea I – Metoda elementului finit*, Canadian Agricultural Engineering, Vol. 40, Nr. 4, pag.287-292.

# NUMERICAL AND EXPERIMENTAL VIBRATION ANALYSIS OF THE SUSPENSION SYSTEM OF AN AGRICULTURAL MACHINE
# /
# *ANALIZĂ NUMERICĂ ŞI EXPERIMENTALĂ A VIBRAȚIILOR SISTEMULUI DE SUSPENSIE AL UNEI MAŞINI AGRICOLE*

**Assoc. Prof. PhD. Eng. Craifaleanu A., Assoc. Prof. PhD. Dragomirescu C.**
University "Politehnica" of Bucharest, Department of Mechanics / Romania
*Tel: (004)021.402.92.50; E-mail: ycraif@yahoo.com*

***Abstract:*** *The paper analyses the bending vibrations of leaf springs, devices that are largely used in agricultural machinery. The studied type of spring is modeled as a system of straight superposed bars, consisting of three bars of different lengths, fixed at one end and free at the other. The paper presents, in its first part, a theoretical study, by the discretization method, of the free vibrations of the studied model, with the determination of the eigenfrequencies of the system. The cases in which the bars are clamped with strong and weak tightening, respectively, are analyzed. For the case of weak tightening, two modalities are proposed for the computation of the influence coefficients matrix, necessary for determining the differential equations of the vibration. In the second part of the paper, the eigenfrequencies of the system are determined experimentally for the two cases and a comparative study of the analytical and numerical results is performed.*

***Keywords:*** *bending vibrations, leaf spring, eigenfrequencies, discretization, influence coefficient.*

## INTRODUCTION

Leaf springs are frequently used in agricultural machinery for the damping of vibrations; thus, the development of methods for their efficient modeling and computation are of a particular practical interest. In the paper, the bending vibrations of a leaf spring, modeled as a system of superposed bars, are analyzed. The system consists of three bars with different lengths, fixed at one end and free at the other. A theoretical study of the free vibrations of the studied model is first performed, by the discretization method, with the computation of the eigenfrequencies of the system. The cases in which the bars are clamped with weak and strong tightening, respectively, are analyzed. For the case of weak tightening, two modalities are proposed for the computation of the influence coefficient matrix, necessary for the determination of the differential equations of vibration. Next, an experimental study for the determination, for the two cases, of the eigenfrequencies of the system is presented. The paper is concluded with a comparative study of analytical and numerical results.

The paper continues previous studies of the authors, in which the discretization method and the influence coefficients method were applied for the study of the free and forced vibrations of other types of mechanical systems, demonstrating the efficiency of the mentioned method in the assessment of vibration characteristics [1, 2, 3, 4].

## MATERIAL AND METHOD

For the study of the vibrations of a leaf spring, used as a main element of the suspension system in many agricultural machinery (Fig. 1), a system of three superposed bars, with rectangular, constant and identical cross-sections, made from the same material, fixed at one end and free at the other, is adopted as a study model (Fig. 2).

***Rezumat:*** *Articolul analizează vibrațiile de încovoiere ale arcurilor lamelare, dispozitive de largă utilizare la maşinile agricole. Tipul de arc studiat este modelat ca un sistem de bare drepte suprapuse, fiind format din trei bare de dimensiuni diferite, încastrate la un capăt şi libere la celălalt. Articolul prezintă, în prima sa parte, un studiu teoretic al vibrațiilor libere pentru modelul studiat, prin metoda discretizării, cu determinarea frecvențelor proprii ale sistemului. Se analizează cazurile în care barele sunt prinse cu strângere slabă, respectiv puternică. În cazul strângerii slabe, sunt propuse două modalități de calcul a matricei coeficienților de influență, necesară pentru determinarea ecuațiilor diferențiale ale vibrațiilor. În partea a doua a articolului, sunt determinate pe cale experimentală, în cele două cazuri, frecvențele proprii ale sistemului şi este efectuată o analiză comparativă a rezultatelor obținute analitic şi numeric.*

***Cuvinte cheie:*** *vibrații de încovoiere, arc lamelar, frecvențe proprii, discretizare, coeficient de influență.*

## INTRODUCERE

Arcurile lamelare sunt frecvent utilizate la maşinile agricole pentru amortizarea vibrațiilor, motiv pentru care dezvoltarea unor metode eficiente de modelare şi calcul al lor este de un deosebit interes practic. În articol se analizează vibrațiile de încovoiere ale unui arc lamelar, modelat ca un sistem de bare drepte suprapuse. Sistemul este format din trei bare de lungimi diferite, încastrate la un capăt şi libere la celălalt. Este realizat mai întâi un studiu teoretic al vibrațiilor libere pentru modelul studiat, prin metoda discretizării, cu determinarea frecvențelor proprii ale sistemului. Se analizează cazurile în care barele sunt prinse cu strângere slabă, repectiv puternică. În cazul strângerii slabe, sunt propuse două modalități de calcul a matricei coeficienților de influență, necesari pentru determinarea ecuațiilor diferențiale ale vibrațiilor. În continuare, este prezentat un studiu experimental de determinare în cele două cazuri a frecvențelor proprii ale sistemului. Articolul se încheie cu o analiză comparativă a rezultatelor obținute analitic şi numeric.

Articolul continuă studii anterioare ale autorilor, în care metoda discretizării şi metoda coeficienților de influență au fost aplicate pentru studiul vibrațiilor libere şi forțate ale unor alte tipuri de sisteme mecanice, demonstrându-se eficiența metodelor respective în estimarea caracteristicilor vibrațiilor [1, 2, 3, 4].

## MATERIAL ŞI METODĂ

Pentru studiul vibrațiilor unui arc lamelar, utilizat ca element principal al sistemului de suspensie la multe maşini agricole (fig. 1), se adoptă ca model de studiu un sistem de trei bare suprapuse, cu secțiuni dreptunghiulare constante şi identice, de lungimi diferite, realizate din acelaşi material, încastrate la un capăt şi libere la celălalt (fig. 10).

The bar system performs bending vibrations in the *Oxz* plane.

Sistemul de bare efectuează oscilații de încovoiere în planul *Oxz*.

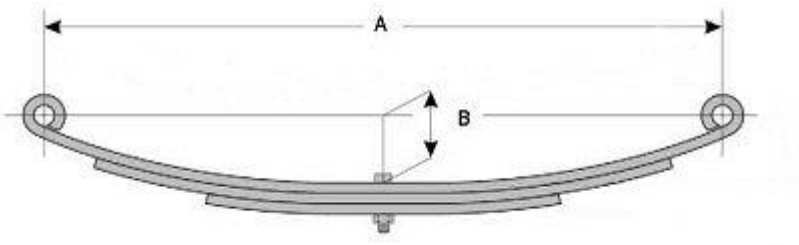


**Fig. 9** – The suspension system

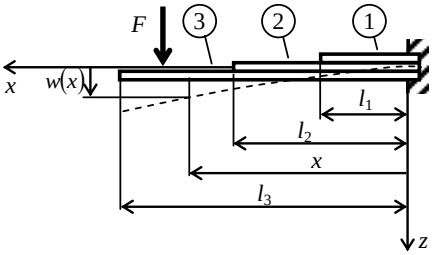


**Fig. 10** – Leaf spring model

The bars are kept in permanent contact by the use of tightening clamps, such that the deflections of all bars are equal in the same transverse section. If the tightening of these bars is weak, the bars slide on one another during the bending, forming a system of elastic bodies mounted in parallel. If the tightening is strong, the bars do not slide and the system behaves like a single bar with variable section, equal to the sum of the component sections. The paper analyzes both situations, the first of them by using two theoretical methods. Three analysis cases result, all of them based on the modeling by the discretization method and on the study of vibrations by the influence coefficients method.

As known from the literature, the approximate study of the vibrations of continuous bodies can be performed by the discretization method, which consists in the approximation of the system by a number *n* of material points, connected by elastic elements of negligible mass [16]. For the studied system, the model in Figure 3 results.

The mass in section $i$ is

Barele sunt ținute în contact permanent cu ajutorul unor cleme de fixare, astfel încât deplasările tuturor barelor în aceeaşi secțiune transversală sunt egale. Dacă strângerea acestor cleme este redusă, barele alunecă una peste alta în timpul încovoierii, alcătuind un sistem de corpuri elastice montate în paralel. Dacă strângerea este puternică, barele nu alunecă, sistemul comportându-se ca o singură bară, de secțiune variabilă, egală cu suma secțiunilor componente. Lucrarea analizează ambele situații, prima dintre ele cu ajutorul a două metode teoretice. Rezultă trei cazuri de calcul, toate bazate pe modelare prin metoda discretizării şi pe studiul vibrațiilor prin metoda coeficienților de influență.

Aşa cum se cunoaşte din literatura de specialitate, studiul aproximativ al vibrațiilor corpurilor continue se poate face cu ajutorul metodei discretizării, ce constă în aproximarea sistemului printr-un număr *n* de puncte materiale, conectate prin elemente elastice de masă neglijabilă [6]. În cazul sistemului studiat rezultă modelul din figura 2.

Masa din secțiunea $i$ este

$$m_i = \rho b h(x) \Delta x_i \quad (i = 1,2,...,n) \tag{11}$$

where $\rho$ is the density of the bar material, $b$ is the width of the bar section,

unde $\rho$ este densitatea materialului barei, $b$ este lățimea secțiunii barelor,

$$h(x) = \begin{cases} h_1 = 2h_0 & \text{if / } dacă \quad 0 < x \le l_1 \\ h_2 = 2h_0 & \text{if / } dacă \quad l_1 < x \le l_2 \\ h_3 = 3h_0 & \text{if / } dacă \quad l_2 \le x \le l_3 \end{cases} \tag{12}$$

represents the height of the cross-section of the bar package, $h_0$ is the height of the section of a bar and

reprezintă înălțimea secțiunii pachetului de bare, $h_0$ este înălțimea secțiunii unei bare, iar

$$\Delta x_i = x_i - x_{i-1} \quad (i = 1,2,...,n) \tag{13}$$

is the distance between sections $i-1$ and $i$.

este distanța dintre secțiunile $i-1$ şi $i$.

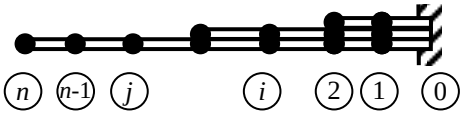


**Fig. 11** - Discretized system of beams

The vibrations of the discrete system can be studied with the methods specific to the systems with a finite number of degrees of freedom [6, 7, 8, 9]. One of these is the influence coefficients method [6, 9].

As known from the literature, the influence coefficient $\delta_{ij}$ is defined as the transverse displacement

Vibrațiile sistemului discret rezultat pot fi studiate cu metodele specifice sistemelor cu un număr finit de grade de libertate [6, 7, 8, 9]. Una dintre acestea este metoda coeficienților de influență [6, 9].

Aşa cum se cunoaşte din literatură, coeficientul de influență $\delta_{ij}$ este definit ca deplasarea transversală

$$w_i = w(x_i) \tag{14}$$

undergone by section $i$, when the bar is submitted to a force equal to unity, applied perpendicularly in the section $j$.

In the case of a homogeneous bar fixed at one end and free at the other [6, 9],

suferită de secțiunea $i$, atunci când bare este acționată de o forță egală cu unitatea, aplicată perpendicular în secțiunea $j$.

În cazul unei bare omogene încastrate la un capăt şi liberă la celălalt [6, 9],

$$\delta_{ij} = \delta_{ji} = \frac{x_i^2}{2EI_y}\left(x_j - \frac{x_i}{3}\right) \quad \text{if} \quad x_i < x_j, \tag{15}$$

where $E$ is the Young's modulus of the bar material and $I_y$ is the moment of inertia of the cross-section.

In the general case of a bar with variable section, in which the moment of inertia varies with the $x$ abscissa, the deformation in section $i$ produced by a force applied in section $j$ takes the form [10]

unde $E$ este modulul lui Young al materialului barei, iar $I_y$ este momentul de inerție al secțiunii transversale.

În cazul general, al unei bare de secțiune variabilă, în care momentul de inerție variază cu abscisa $x$, deformația din secțiunea $i$ produsă de o forță aplicată în secțiunea $j$ ia forma [10]

$$w(x_i) = \int_0^{x_i}\left(\int_0^{x}\frac{F(x_j - x)}{EI_y(x)}\mathrm{d}x\right)\mathrm{d}x \quad \text{if} \quad x_i < x_j. \tag{16}$$

The influence coefficients result from this relation:

Rezultă de aici coeficienții de influență:

$$\delta_{ij} = \int_0^{x_i}\left(\int_0^{x}\frac{x_j - x}{EI_y(x)}\mathrm{d}x\right)\mathrm{d}x \quad \text{if} \quad x_i < x_j. \tag{17}$$

It is shown that the differential equations of the free vibrations take the form [6, 9]

Se arată că ecuațiile diferențiale ale vibrațiilor libere iau forma [6, 9]

$$[D]\{\ddot{w}\} + \{w\} = \{0\} \tag{18}$$

where the following were introduced:
- dynamic matrix

unde s-au introdus:
- matricea dinamică

$$[D] = \begin{bmatrix} \delta_{11} & \delta_{12} & \cdots & \delta_{1n} \\ \delta_{21} & \delta_{22} & \cdots & \delta_{2n} \\ \cdots & \cdots & \cdots & \cdots \\ \delta_{n1} & \delta_{n2} & \cdots & \delta_{nn} \end{bmatrix} \cdot \begin{bmatrix} m_1 & 0 & \cdots & 0 \\ 0 & m_2 & \cdots & 0 \\ \cdots & \cdots & \cdots & \cdots \\ 0 & 0 & \cdots & m_n \end{bmatrix} \tag{19}$$

- state vector

- vectorul de stare

$$\{w\} = (w_1 \quad w_2 \quad \ldots \quad w_n)^T, \tag{20}$$

- null vector

- vectorul nul

$$\{0\} = (0 \quad 0 \quad \ldots \quad 0)^T. \tag{21}$$

Under these conditions, denoting by $\alpha_i \ (i = 1,2,\ldots,n)$ the eigenvalues of the matrix (19) and $\{a\}_i$ the corresponding eigenvectors, the circular eigenfrequencies of the system result,

În aceste condiții, notând cu $\alpha_i \ (i = 1,2,\ldots,n)$ valorile proprii ale matricei (19) şi $\{a\}_i$ vectorii proprii corespunzători, rezultă pulsațiile proprii ale sistemului,

$$\omega_i = \left(\sqrt{\alpha_i}\right)^{-1}, \tag{22}$$

as well as the eigenmodes

precum şi modurile proprii de vibrație,

$$\{w\}_i = \{a\}_i \cos(\omega_i t - \varphi_i). \tag{23}$$

**The case of weak tightening – first mehod**

In the case of weak tightening, the influence coefficients of the bar package can be determined with formula (17), in which

**Cazul strângerii slabe – prima metodă**

În cazul strângerii slabe, coeficienții de influență ai pachetului de bare se pot determina cu formula (17), în care

$$I(x)=\begin{cases} I_1 = 2I_0 & \text{if / dacă} \quad 0 < x \le l_1 \\ I_2 = 2I_0 & \text{if / dacă} \quad l_1 < x \le l_2 \\ I_3 = 3I_0 & \text{if / dacă} \quad l_2 \le x \le l_3 \end{cases} \tag{24}$$

where the moment of inertia of a bar in the package was introduced,

unde s-a introdus momentul de inerție al unei bare din pachet,

$$I_0 = \frac{b\,h_0^3}{12}. \tag{25}$$

**The case of weak tightening – second method**

A more general method for the study of the bar package is based on the observation that the elasticity matrix $[K]$ of a system of elastic bodies mounted in parallel can be obtained by adding the elastic matrices corresponding to each body.

The elasticity matrix of the bar $k\ (k=1,2,3)$ is linked to the influence coefficients matrix of the same bar by the relation

**Cazul strângerii slabe – a doua metodă**

O metodă mai generală de studiu al pachetului de bare, se bazează pe observația că matricea de elasticitate $[K]$ a unui sistem de copuri elastice montate în paralel se obține adunând matricele elastice corespunzătoare fiecărui corp component.

Matricea de elasticitate a barei $k\ (k=1,2,3)$ este legată de matricea coeficienților de influență a aceleiaşi bare prin relația

$$[K]_k = [\delta]_k^{-1} \tag{26}$$

It should be noted that, since the lengths of the bars are not equal, the number of sections of discretization differs from one bar to another and, therefore, the dimensions of matrices $[K]_k\ (k=1,2,3)$ are also not equal. Consequently, in the assemblage of matrix $[K]$ of the system, modified matrices $[K']_k$ will be used, obtained by completing the matrices $[K]_k$ with null lines and columns, corresponding to the sections that are not covered by the concerned bars.

Finally, the matrix of the influence coefficients of the system is determined.

Este de remarcat că, deoarece lungimile barelor sunt diferite, numărul de secțiuni de discretizare diferă de la o bară la alta şi, în consecință, dimensiunile matricelor $[K]_k\ (k=1,2,3)$ sunt, la rândul lor, diferite. Ca urmare, în compunerea matricei $[K]$ a sistemului se vor utiliza matricele modificate $[K']_k$ prin completarea matricelor $[K]_k$ cu linii şi coloane nule, corespunzătoare secțiunilor neacoperite de barele respective.

În final, se determină matricea coeficienților de influență a sistemului,

$$[\delta] = [K]^{-1}. \tag{27}$$

**The case of strong tightening**

In the case of strong tightening, the influence coefficients of the system can be determined with relation (17), in which

**Cazul strângerii puternice**

În cazul strângerii puternice, coeficienții de influență ai sistemului se pot determina cu formula (17), în care

$$I(x) = \frac{b\,h^3(x)}{12}, \tag{28}$$

where
$h(x)$ is given by formulas (12).

unde
$h(x)$ este dat de formulele (12).

**RESULTS**

The numerical and experimental study of the vibrations of the system was performed based on a model defined by the following values:

**REZULTATE**

Studiul numeric şi experimental al vibrațiilor sistemului s-a efectuat cu ajutorul unui model definit de următoarele valori:

$$l_1 = 0.260\,\text{m}, \quad l_1 = 0.537\,\text{m}, \quad l_3 = 0.865\,\text{m},$$

$$E = 210\,\text{x}\,10^9\ \text{N/m}^2, \quad \rho = 7850\ \text{kg/m}^3, \quad b = 0.025\text{m}, \quad h_0 = 0.008\text{m}, \quad n = 157$$

The first 10 circular eigenfrequencies and the corresponding eigenfrequencies in the three analysis

Primele 10 pulsații proprii obținute şi frecvențele proprii corespunzătoare in cele trei cazuri de calcul sunt

cases are presented in Table 1.

prezentate in tabelul 1.

**Table 2**

**Values of the first 10 circular eigenfrequencies and the corresponding eigenfrequencies**

| | Weak tightening – first method | | Weak tightening – second method | | Strong tightening | |
|---|---|---|---|---|---|---|
| $i$ | $\omega_i$ [s$^{-1}$] | $f_i$ [Hz] | $\omega_i$ [s$^{-1}$] | $f_i$ [Hz] | $\omega_i$ [s$^{-1}$] | $f_i$ [Hz] |
| 1 | 81.97 | 13.05 | 82.19 | 13.08 | 190.83 | 30.37 |
| 2 | 359.36 | 57.19 | 360.21 | 57.33 | 594.58 | 94.63 |
| 3 | 931.44 | 148.24 | 933.19 | 148.52 | 1617.09 | 257.37 |
| 4 | 1867.93 | 297.29 | 1870.05 | 297.63 | 2864.48 | 455.90 |
| 5 | 3021.86 | 480.94 | 3021.56 | 480.90 | 5253.97 | 836.20 |
| 6 | 4585.05 | 729.73 | 4584.61 | 729.66 | 7379.12 | 1174.42 |
| 7 | 6384.88 | 1016.18 | 6369.45 | 1013.73 | 10653.4 | 1695.55 |
| 8 | 8528.96 | 1357.43 | 8512.19 | 1354.76 | 13627.3 | 2168.85 |
| 9 | 11087.80 | 1764.68 | 11061.70 | 1760.52 | 18383.6 | 2925.84 |
| 10 | 13583.60 | 2161.89 | 13505.80 | 2149.52 | 22522.1 | 3584.50 |

The experimental study of the system was performed on the measuring stand shown in Figures 4-13.

Studiul experimental al sistemului s-a efectuat cu ajutorul bancului de probă prezentat în figurile 4-13.

**Fig. 12** - Measuring Stand

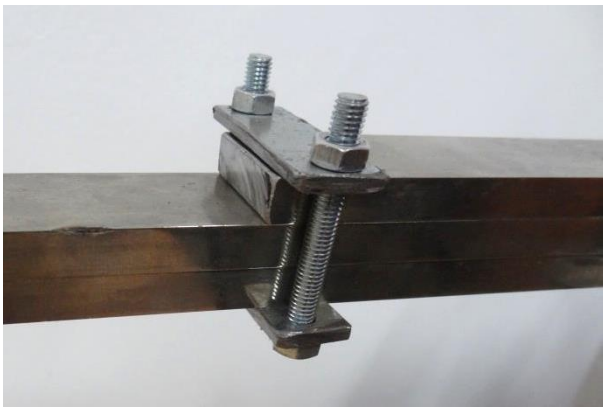

**Fig. 13** – Tightening system

A measuring chain with four Bruel&Kjær accelerometers, type 4508 B004, was used, numbered from 0 to 3, an acquisition board NI9233 and a laptop.

Accelerometer 3 was placed at the free end of the bar 3, while accelerometer 0 was placed on bar 1, near the fixing system. Accelerometers 1 and 2 were placed on bars 2 and 3, respectively.

Free vibrations produced by applying percussions on the bar were studied.

The obtained data were processed with LabVIEW[1] program, resulting in the spectra of Figures 7 -7.

The vibrations produced in a free elastic system reveal the eigenfrequencies of the system, that can be

S-a utilizat un lanț de măsură cu patru accelerometre, Bruel&Kjær, tip 4508 B004, numerotate de la 0 la 3, o placă de achiziție NI9233 şi un laptop.

Accelerometrul 3 a fost amplasat în capul liber al barei 3, iar accelerometrul 0 pe bara 1, lângă încastrare. Accelerometrele 1 şi 2 au fost plasate pe barele 2, respectiv 3.

S-au studiat vibrațiile libere, produse prin aplicare unor percuții pe bară.

Datele au fost prelucrate cu ajutorul programului LabVIEW[1], obținându-se spectrele din figura 7 -7.

Vibrațiile produse într-un sistem elastic liber scot în evidență frecvențele proprii ale sistemului, care pot fi

[1] Product of National Instruments Corporation, 11500 Mopac Expwy, Austin, TX 78759-3504, USA, (512) 683-0100.

identified by the analysis in the frequency domain of the acceleration signals measured in time and recorded.

identificate prin analiza în frecvență a semnalelor de accelerație măsurate în timp şi înregistrate.

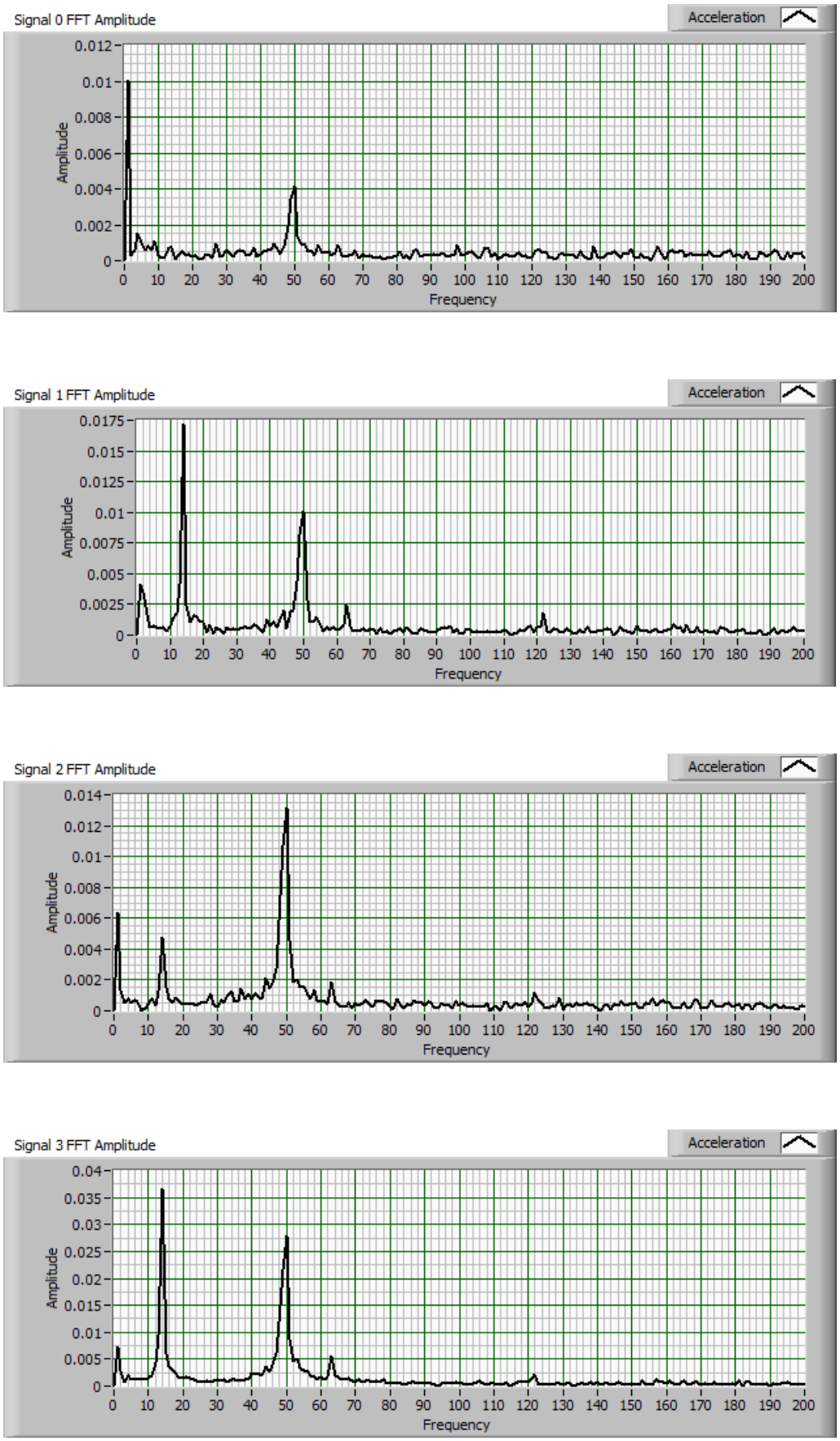


**Fig. 14** - Free vibrations spectra – weak tightening tightening (Frequency - in Hz; Amplitude – in m/s$^2$)

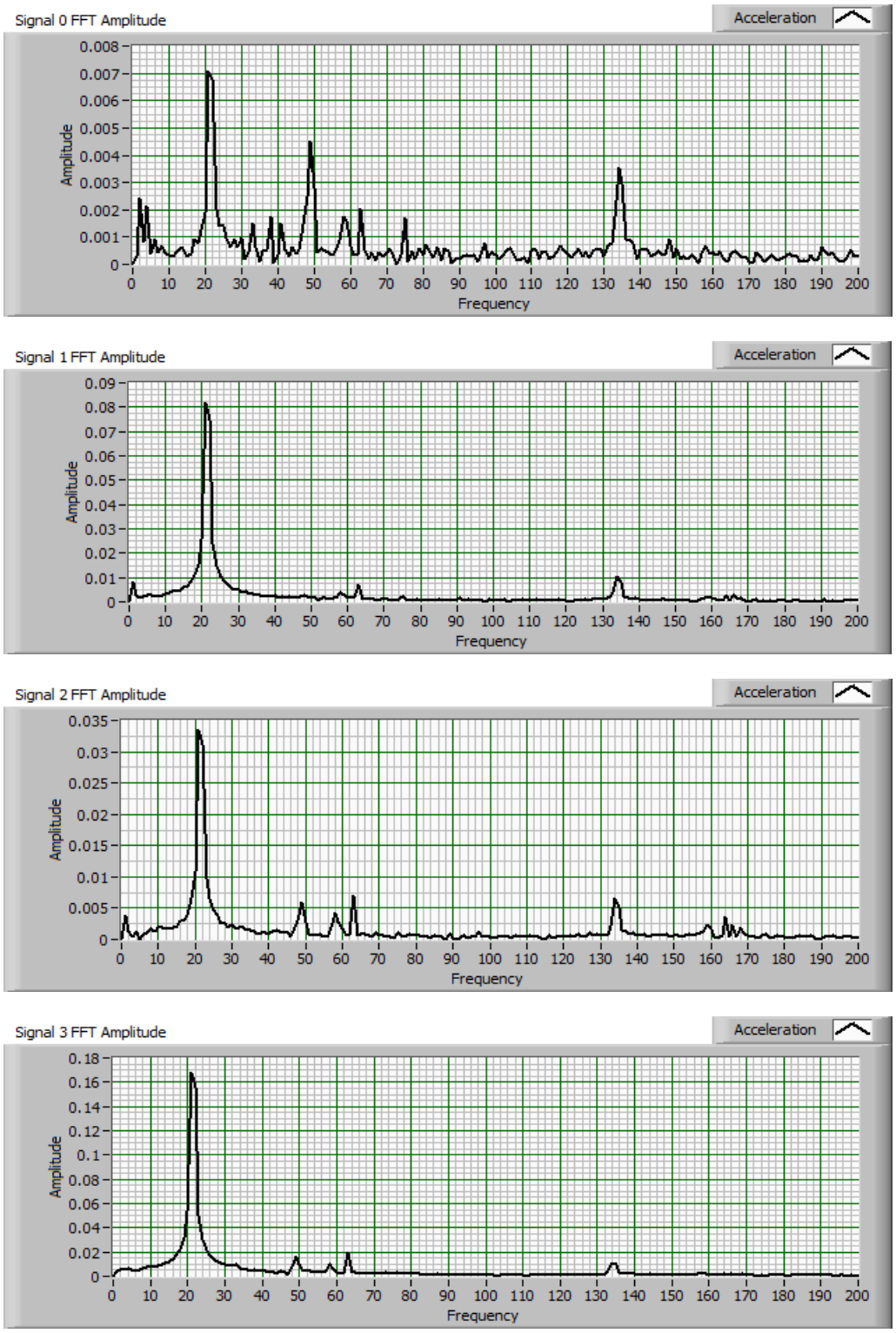


**Fig. 15** - Free vibrations spectra – strong tightening (Frequency - in Hz; Amplitude – in m/s$^2$)

**CONCLUSIONS**

The paper analyzed the vibrations of a system of superposed bars, used as a model for a leaf spring.

The eigenfrequencies of the bar system were computed numerically for two cases: the case in which the bars can slide on one another and the case in which the system is rigid. In the first case two modalities were proposed for the computation of the influence coefficients, the modalities providing very close results.

The eigenfrequencies of the bar system were identified also by spectral analysis of the signal measured on an

**CONCLUZII**

Articolul a analizat vibrațiile unui sistem de bare suprapuse, utilizat ca model pentru un arc lamelar.

Au fost calculate numeric frecvențele proprii ale sistemului de bare în două cazuri: cel în care barele pot aluneca între ele, respectiv cel în care sistemul este rigid. În primul caz au fost propuse două modalități de determinare a coeficienților de influență, modalitățile furnizând rezultate foarte apropiate.

Frecvențele proprii ale sistemului de bare au fost determinate şi prin analiza spectrală a semnalului măsurat

experimental model, for the two above mentioned cases: weak and strong tightening, respectively.

The peaks detected by accelerometers 1-3, in the case of the weak tightening, close to the 14 Hz frequency (Fig. 7), correspond to the fundamental eigenfrequency calculated by the two methods (13.05 Hz and 13.08 Hz, respectively – Table 1). Accelerometer 0 did not detect any peak close to this frequency, since it was placed near the fixing system, where the motion takes place with a reduced amplitude. In the case of the weak tightening a good agreement was obtained between the numerical and the experimental results.

In the case the strong tightening, all four accelerometers detected a peak close to the 20 Hz frequency. This value is higher than the one in the previous case, which was expected, the system being more rigid, but it is far from the calculated one, of 30.37Hz. This discrepancy is due to the imperfections of the tightening system, which allowed a certain relative sliding of the three bars.

The measurements validate the proposed model, for the fundamental eigenfrequency, and show that this frequency is situated in the neighborhood of the numerically determined value, translated with a larger amount as the rigidity of the leaf spring is greater. The fundamental eigenfrequency is of a particular interest, as it can lead to the resonance phenomenon, undesirable for transportation means.

It can be concluded that the eigenfrequencies of a leaf spring depend essentially on the way in which the strips can slide on one another, thus on their state of wear, as well as on their tightening system.

**REFERENCES**

[1]. Craifaleanu A., Orăşanu N., (2011) – *Theoretical and experimental analysis of the vibrations of an elastic beam with four concentrated masses*, Proceedings of the Annual Symposium of the Institute of Solid Mechanics, SISOM 2011, Bucharest, May 25-26, 2011, pp.471-480;
[2]. Craifaleanu A., Orăşanu N., (2012) – *Experimental study of the forced vibrations of a system with distributed mass and four concentrated masses*, Proceedings of the Annual Symposium of the Institute of Solid Mechanics, SISOM 2012, Bucharest, May 30-31, 2012, pp.200-205;
[3]. Craifaleanu A., Orăşanu N., Dragomirescu C., (2013) – *Theoretical and Experimental Studies on Magnetic Dampers*, Applied Mechanics and Materials, Vol. 430, pp 351-355, Trans Tech Publications, Switzerland;
[4]. Craifaleanu A., Orăşanu N., Dragomirescu C., (2015) – *Bending vibrations of a viscoelastic Euler-Bernoulli beam – two methods and comparison*, Applied Mechanics and Materials, Vol. 762, pp 47-54, Trans Tech Publications, Switzerland;
[5]. Trailer Parts Superstore, (2015), http://www. easternmarine.com/Double-Eye-Trailer-Leaf-Springs;
[6]. Meirovitch, L., (2001) – *Fundamentals of Vibrations*, McGraw-Hill Book Company, New York;
[7]. Rao S. (2011) – *Mechanical Vibrations*, Prentice Hall Publishing House, University of Miami;
[8]. Rădoi M., Deciu E., Voiculescu D., (1973) – *Elements of mechanical vibrations* (in Romanian), Tehnical Publishing House, Bucharest;
[9]. Silaş Gh., (1968) – *Mechanics. Mechanical* Bucharest;
[10]. Timoshenko S., (1948) – *Strength of Materials. Part I. Elementary Theory and Problems*, D. van Nostrand Company, Inc.

pe un model experimental, în cele două cazuri menționate: strângere slabă şi puternică.

Vârfurile detectate de accelerometrele 1-3 în cazul strângerii slabe, în apropierea frecvenței de 14 Hz (fig. 7), corespund frecvenței proprii fundamentale calculate prin cele două metode (13,05 Hz, respectiv 13,08 Hz – tabelul 1). Accelerometrul 0 nu a detectat un vârf în apropierea acestei frecvențe, fiind amplasat în imediata apropiere a sistemului de prindere, unde mişcarea are loc cu amplitudine redusă. În cazul strângerii slabe rezultă o bună concordanță între rezultatele numerice şi cele experimentale.

În cazul strângerii puternice, toate cele patru accelerometre au detectat un vârf în apropierea frecvenței de 20 Hz. Această valoare este mai ridicată decât cea din cazul anterior, ceea ce este de aşteptat, sistemul fiind mai rigid, dar ea se află la mare distanță de frecvența fundamentală calculată, de 30,37Hz. Această discrepanță se explică prin imperfecțiunile sistemului de strângere, ce au permis anumite alunecări relative ale celor trei bare.

Măsurătorile validează modelul propus pentru frecvența fundamentală şi arată că această frecvență este situată în vecinătatea valorii determinate numeric, deplasată cu atât mai mult cu cât rigiditatea arcului lamelar este mai mare. Frecvența proprie fundamentală prezintă un interes deosebit, deoarece poate conduce la fenomenul de rezonanță, nedorit pentru mijloace de transport.

Se poate concluziona că frecvențele proprii ale unui arc lamelar depind în mod esențial de felul în care pot aluneca relativ între ele foile arcului, deci de starea lor de uzură, precum şi de sistemul de strângere.

**BIBLIOGRAFIE**

[1]. Craifaleanu A., Orăşanu N., (2011) – *Analiză teoretică şi experimentală a vibrațiilor unei bare elastice cu patru mase concentrate*, Proceedings of the Annual Symposium of the Institute of Solid Mechanics, SISOM 2011, Bucharest, May 25-26, 2011, pag.471-480;
[2]. Craifaleanu A., Orăşanu N., (2012) – *Studiu experimental al vibrațiilor forțate ale unui sistem cu masă distribuită şi patru mase concentrate*, Proceedings of the Annual Symposium of the Institute of Solid Mechanics, SISOM 2012, Bucharest, May 30-31, 2012, pp.200-205;
[3]. Craifaleanu A., Orăşanu N., Dragomirescu C., (2013) – *Studii teoretice şi experimentale asupra amortizorilor magnetici*, Applied Mechanics and Materials, Vol. 430, pag. 351-355, Trans Tec Publications, Switzerland;
[4]. Craifaleanu A., Orăşanu N., Dragomirescu C., (2015) – *Vibrații de încovoiere ale unei bare Euler-Bernoulli viscoelastice – două metode şi comparație*, Applied Mechanics and Materials, Vol. 762, pag. 47-54, Trans Tech Publications, Switzerland;
[5]. Trailer Parts Superstore, (2015), http://www. easternmarine.com/Double-Eye-Trailer-Leaf-Springs;
[6]. Meirovitch, L. (2001) – *Bazele vibrațiilor*, Editura McGraw-Hill, New York;
[7]. Rao S. (2011) – *Vibrații mecanice*, Editura Prentice Hall, Universitatea din Miami;
[8]. Rădoi M., Deciu E.,Voiculescu D., (1973) – *Elemente de vibrații mecanice*, Ed. Tehnică, Bucureşti.
[9]. Silaş Gh., (1968) – *Mecanică. Vibrații mecanice*, Ed. Didactică şi Pedagogică, Bucureşti.
[10]. Timoshenko S., (1948) – *Rezistența materialelor. Partea I. Teoria elementară şi Probleme*, D. van Nostrand Company, Inc.

# STUDY ON FIELD WATER-SALT BALANCE SIMULATION USING SWAP MODEL: A CASE STUDY OF FARMLAND IN THE CENTRAL SHAANXI PLAIN
# /
# 基于SWAP 的田间水盐平衡模拟研究——以关中农田为例

**M.S. Liang Dong[1)], Ph.D. Quan Quan[1)], Prof. Ph.D. Bing Shen[1)], Prof. Ph.D. Wan Luo [2)], Ph.D. Qinger Jung [3)]**
[1)] State Key Laboratory Base of Eco-hydraulic Engineering in Arid Area, Xi'an University of Technology, Xi'an / China;
[2)] Yangzhou University, Yangzhou / China
[3)] Technological Center of Modern Agricultural Production in SEIR Co.Ltd., Oviedo, Spain
*Tel: +8613772431776; Email: qq@xaut.edu.cn*

***Abstract:*** *To study the variation law of key components for water-salt balance of typical farmland in the central Shaanxi Plain, this paper calibrated and verified the SWAP model based on a field trial of summer maize growing season from 2013 to 2014. Variations of different components during different summer maize growth stages were analyzed and discussed according to the calculated results of water-salt balance by the verified SWAP model. Results showed that the calibrated and verified SWAP model could well simulate dynamic variation laws of water-salt content of different soil layers in the study area. Within the study period, transpiration of maize in 2013 and 2014 was restricted by water content in the surface layer. The accumulative actual transpiration accounted for 57.6% and 64.9% of potential transpiration, respectively. Soil water supply from underground water was mainly in the vigorous growth of maize. The accumulative underground water supplies in 2013 and 2014 were 10.3cm and 7.4cm, respectively. Water flux at bottom soil was highly sensitive to rainfall and irrigation, presenting the obvious deep leakage. The soil salinity changes at 0~120cm layer in 2013 and 2014 were -72.87 mg/cm$^2$ and -81.32mg/cm$^2$, respectively. Great desalination was observed in the rainy season of maize growth.*

***Keywords:*** *Soil moisture; Salinity; SWAP model; Water balance; Salt balance*

***摘要:*** *为了研究关中平原典型农田水盐平衡关键组分的变化规律，本文基于 2013～2014 年夏玉米生长季的田间试验，对 SWAP 模型进行了率定和验证，并根据验证后模型的水盐平衡计算结果，对其各分量在夏玉米不同生长阶段的变化过程进行了分析与讨论。研究结果表明：经过率定和验证后的 SWAP 模型较好地模拟了研究区田间土壤各层水盐含量的动态变化规律。模拟期内，2013 与 2014 年季玉米的蒸腾量受到了表层含水量的制约，累积实际蒸腾量占潜在蒸腾量的比值分别为 57.6%和 64.9%；地下水对于土壤水的上升补给主要出现在玉米生长的旺盛阶段，累积地下水上升补给量分别为 10.3cm 和 7.4cm；土壤底部水分通量变化对降雨和灌溉的响应强烈，并表现为明显的深层渗漏。2013 与 2014 年季田间 0～120cm 土壤盐分变化量分别为-72.87 mg/cm$^2$ 和-81.32mg/cm$^2$，主要在玉米生长的雨季脱盐明显。*

***关键词:*** *土壤水分; 盐分; SWAP 模型; 水量平衡; 盐分平衡*

## INTRODUCTION

Salinization is a universal soil character in arid and semi-arid regions in China [8]. Soil salinization and soil secondary salinization caused by irrigation are main constraints against local agricultural development and the main influencing factors of local ecological environmental stability [2]. The Lubotan at the junction of Pucheng County and Fuping County lies in the central Shaanxi Plain where it has the richest agriculture in arid and semi-arid regions. The local groove terrain of low-in-middle but high-in-surroundings, diversion irrigation in the Luoxi irrigation area and common flood irrigation implemented in Lubotan have caused drainage silting, groundwater level rise and intensifying salinization of soil, thus influencing local food production and sustainable agricultural development significantly[5]. Through a series of farmland ameliorative measures like perfecting the irrigation and drainage system, no large-scale salinization of soil has occurred and crop output has recovered to the normal level. However, local crop growth is still influenced by different degrees of salt stress.

The SWAP (Soil-Water-Atmosphere-Plant) model developed by Wageningen University (Netherlands) calculates water movement and solute transport in soils by using the one-dimensional Richards equation and the convection-dispersion equation. With consideration to

## 引言

盐渍化是我国干旱、半干旱地区土壤的一个普遍特征[8]。土壤的盐渍化和灌溉引起的土壤次生盐渍化问题是制约该地区农业发展的主要障碍，也是影响该区生态环境稳定的重要因素[2]。陕西省富平县与蒲城县交界的卤泊滩地区位于干旱、半干旱区农业最富庶的“关中平原”地带，滩区四周高中间低的槽形地势特点，加之洛西灌区引水灌溉及当地常年实施的漫灌方式，造成滩区内排水沟道淤积，地下水位上升，土壤盐碱化逐渐加剧，严重影响了当地的粮食生产及农业的可持续发展[5]。通过一系列健全灌排系统等土地改良措施，滩区内整治后的地块没有再发生大面积的盐渍化，且作物产量接近正常，但当地农作物的生长，仍会受到不同程度上的盐分胁迫影响。

由荷兰 Wageningen 大学研制的 SWAP（Soil-Water-Atmosphere-Plant）模型，利用一维 Richards 方程和对流-弥散方程分别计算土壤的水分运动以及溶质运移过程，同时考虑了水盐等逆境胁迫对于作物生长的影响[7]，使得该

effect of adversity stresses like water and salt on crop growth [7], the SWAP model is more applicable to simulation study on water-salt movement and balance in salinization farmland soils. The SWAP model has been widely used in both China and foreign countries for its perfect physical mechanism. However, few researches on its applicability in the central Shaanxi Plain have been reported yet. Based on field trial data of summer maize in 2013 and 2014, the SWAP model was calibrated. It was confirmed feasible to describe component variation law of water-salt balance in the study area. Dynamic changes of different components of water-salt balance at different summer maize growth stages were analyzed and discussed, aiming to provide theoretical basis for soil secondary salinization control in the agricultural irrigation area in the central Shaanxi Plain.

## MATERIAL AND METHOD

### *Field test*

One improved typical salinization farmland in the midwest of Lubotan was chosen as the study area. It belongs to semi-arid continental climate, with extremely uneven precipitation distribution in one year. Most precipitations are received from July to September, accounting for 49% precipitation of the whole year. It is dry in rest time of the year. The groundwater depth is about 2m throughout the year. There're distinct dry and wet seasons. The dry season is longer than the wet season. Particularly, it is windy but has less rainfall in spring, accompanied with great evaporation. The annual sunshine duration is 2349.5~2472.0 h. The 0 ℃ accumulated temperature is 4906.5～5022℃ and the ≥10℃ accumulated temperature is 4276.3～4477.3℃, basically satisfying growth demands of wheat, maize and cotton . Physical and chemical parameters of soil in the study area are listed in Table 1 .

The State Key Laboratory of Ecohydraulic Engineering for Northwest Arid Regions, Xi'an University of Technology established a field observation station in the study area in 2013 in order to observe the water cycle elements and water-salt dynamics of typical farmlands in the Lubotan. Instruments in this station are mainly for conventional meteorological observation, soil water-salt observation and groundwater level observation. The observation items of conventional meteorological elements could be used to calculate evapotranspiration of reference crops. Soil water-salt observation is mainly accomplished by multiparameter sensors (Campbell-CS655) which are buried 2m deep in test pits. There are four small shafts surrounding the test pit, where water level sensors (Campbell-CS450) are buried in to observe groundwater level. Crop rotation of wheat in winter and maize in summer is adopted for farmlands surrounding the soil water-salt observation profile. The summer maize uses "Zhengdan 958" which is generally sowed in early June and harvested in middle October. According to farming habit of local peasants, since there are plentiful precipitation after the elongation stage of summer maize (July~September), two flood irrigation with subsiding water from the Yellow River will be implemented at trefoil stage and elongation stage of maize. To observe dynamic growth of maize in the observation stage, the 101m×105m study area was divided into 25 20m (L)×20m (W) blocks. Plant height, root depth, leaf area index and aboveground biomass were observed manually through regular uniform sampling of each block. The field test design and instrument layout in the observation station are displayed in Fig.1.

模型更可能适用于盐渍化农田土壤水盐运动及其平衡过程的模拟研究。SWAP 模型以其较为完善的物理机制在国内外各地区得到了广泛应用。但在关中平原地区的相关适用性研究还相对较少。本文利用 2013～2014 年两季夏玉米的田间试验观测资料，率定并验证了 SWAP 模型对于描述研究区田间水盐平衡分量变化规律的适用性，并对模型计算的两季夏玉米各生长阶段的水盐平衡各组分动态进行了分析与讨论，旨在为关中农灌区土壤次生盐渍化的防治提供理论基础。

## 材料与方法

### *田间观测实验*

选取卤泊滩中西部(109°22′E、34°48′N)一处改良过后的典型盐渍化农田作为研究区域。研究区属半干旱大陆性气候，降雨年内分布极不均匀，多集中在 7 到 9 月份，占全年降雨量的 49%，其他季节较为干旱，常年地下水埋深约 2m 左右。干湿季节分明，干季长于湿季。尤其是春季多风少雨，蒸发量大。年日照时数 2349.5~2472.0h，0℃积温 4906.5～5022℃，≥10℃积温 4276.3～4477.3℃，基本上满足小麦、玉米、棉花等作物的生长需求。研究区土壤理化特性指标如表 1 所示。

西安理工大学西北旱区生态水利工程国家重点实验室于 2013 年在研究区建立了田间观测站，目的是为了对卤泊滩地区典型田间的水循环要素及水盐动态进行观测。站内布设的仪器主要用于常规气象观测、土壤水盐观测以及地下水位观测等。常规气象要素的观测项目可以满足参考作物腾发量的计算需要；土壤水盐观测主要由埋深 2m 的测坑当中所布设的多参数传感器（Campbell-CS655）完成；测坑附近打有 4 口小型竖井并分别埋设了水位传感器（Campbell-CS450）用于地下水位的观测。环绕土壤水盐观测剖面的农田，种植模式为冬小麦-夏玉米轮作。其中，夏玉米品种为“郑单 958”，大致在每年 6 月初播种至同年 10 月中旬收获。按照当地农民的耕作习惯，由于每年夏玉米拔节期后（7 月～9 月）的降水充沛，故基本在玉米的三叶期和拔节期前后进行两次淡水灌溉，方式为大水漫灌，所用灌溉淡水为黄河退水。为了对观测期内的玉米生长动态进行观测，将 101m×105m 的研究区域均匀划分为长宽约 20m×20m 的样方，共计 25 个。通过定期在每个样方当中进行的均匀采样来完成作物株高、根深、叶面积指数以及地上部生物量的人工观测。田间观测试验设计和站内仪器的布设概况如图 1 所示。

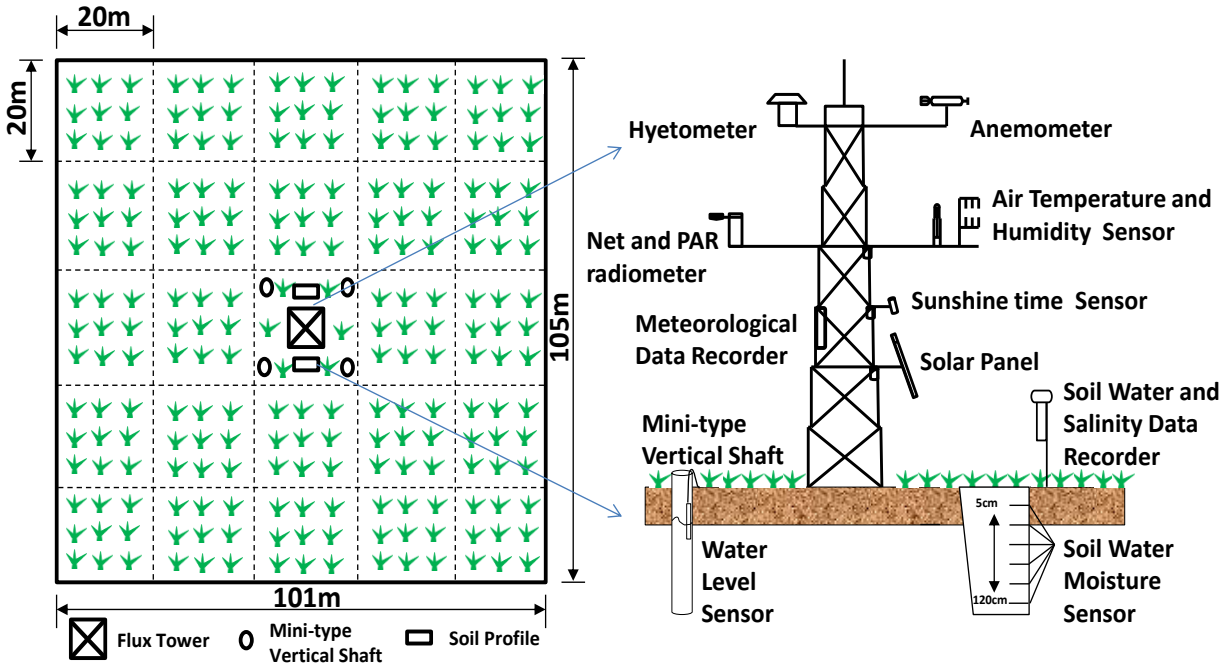


**Fig. 1 -** Schematic representation of the experimental design and instruments layout

**Table 1**

**Physical and chemical properties in the soil profile of 0–100 cm**

| Depth (cm) | Soil particle size distribution (%) | | | Bulk density (g/cm$^3$) | pH ($H_2O$) | Organic C (%) |
|---|---|---|---|---|---|---|
| | Sand (>0.05mm) | Silt (0.002-0.05mm) | Clay (<0.002mm) | | | |
| 0-20 | 44.1 | 52.7 | 3.2 | 1.48 | 8.3 | 1.15 |
| 20-40 | 43.2 | 54.0 | 2.8 | 1.46 | 8.4 | 1.03 |
| 40-70 | 44.1 | 53.4 | 2.5 | 1.45 | 8.6 | 0.82 |
| 70-100 | 42.5 | 53.8 | 3.7 | 1.45 | 8.6 | 0.76 |

***SWAP model***

SWAP model is an open-source simulation model applicable for field macro quantitative analysis. It is developed by Wageningen University (Netherlands) on the basis of new research fruits concerning water dynamics and soil water movement of the current SPAC (Soil-Plant-Atmosphere Continuum) system. It is mainly used for simulation analysis on field soil water movement, solute transport and crop growth under different irrigation levels, and also could solve research and practice problems involving agriculture, water resources management and environmental protection . The SWAP model could be divided into three main parts: meteorology part, crop part and soil part. Each part could be further divided into several sub-modules (which are realized by different functions). It simplifies soil heat and water movement as well as solute transport into vertical one-dimensional movement and solves the partial differential equation by finite different method. Soil water movement is described by Richards equation and soil solute transport is described by traditional convection-dispersion equation. It reflects effect of water and salt stress on crop growth through water absorption rate of crop roots under different water potentials.

Considering practical soil texture in the study area and active layer depth of summer maize roots, the simulated soil depth in this paper was 0～120cm, which was divided into three layers: 0～30cm, 30～60cm and

***模型介绍***

SWAP 模型是荷兰 Wageningen 大学在充分吸取了当前 SPAC（Soil-Plant-Atmosphere Continuum） 系统水分动态以及非饱和土壤水分运动最新研究成果的基础上，研制开发的适用于田间宏观量化分析的开源模拟模型，主要用于田间尺度不同灌溉水平下的土壤水分运动、溶质运移及作物生长等过程的模拟分析，并能够解决农业、水资源管理和环境保护等几个领域的研究与实践问题 。模型分为 3 个主要部分，即气象部分、作物部分、土壤部分，每个部分又分为若干个子模块（由各个函数实现）。模型将土壤水热运动和溶质运移简化为垂向一维运动，并采用有限差分法求解偏微分方程。土壤水分运动利用 Richards 方程描述，土壤溶质运移过程采用传统的对流-弥散方程描述。模型通过分析作物根系吸水速率在不同水势下的削减情况来体现水盐胁迫对于作物生长的影响。

根据研究区土壤质地的实际情况以及夏玉米根系活动层深度，本文选择模拟的土层深度为 0～120cm，并将土柱划分为 0～30cm、30～60cm、60～120cm 三个层次。模

60～120cm. When simulating water and salt contents in different layers of the soil profile, each soil layer shall be further divided into several units. In this simulation, the soil depth 0～120cm was divided into 32 units. To simulate water dynamics in the upper soil layers precisely, units close to the earth surface were set at 0.5~1cm thick and those of the lower layer were set at 5~10cm thick. The upper boundary inputs of the model were parameters that determine water flux in surface soil layer, such as irrigation, rainfall and surface evaporation. Due to the shallow water table in the study area, variation of groundwater level with time was taken as the lower boundary condition of the model. Initial condition setting includes initial salinity of soil layer and pressure head which could be gained from observation data of instruments in the station.

## RESULTS AND DISCUSSIONS

### *Model calibration and verification*

Measured data of meteorology and soil water and salt content from 2013 to 2014 in the observation station were collected for model parameter calibration and verification. Field observation data in 2013 were used to calibrate model parameters and those in 2014 were used to verify the model. In this paper, international universal root-mean-square error (RMSE) and mean relative error (MRE) were used as the evaluation indexes of model simulation effect.

拟土壤剖面各层次的水盐含量时，要求将每个土层再细分为若干单元。本次模拟将 0～120cm 土柱共划分为 32 个单元。为了能精确模拟土柱上层的水分动态，将接近土表的单元格设定为 0.5～1 cm 厚度，下层设为 5～10 cm 厚度。模型上边界条件输入为灌溉、降雨以及土面蒸发等决定土壤表层水分通量状况的有关参数。考虑到研究区地下水位常年为浅埋深状态，故以地下水位随时间的变化过程作为模型的下边界条件。初始条件设定包括各土层初始时刻的含盐量及压力水头等，均可从站内仪器的观测资料当中获得。

## 结果与分析

### *模型率定与验证*

收集并整理观测站 2013～2014 年的气象和土壤水盐含量等实测数据作为模型参数率定与验证的数据资料。其中，2013 年的田间观测数据用来率定模型参数，2014 年的数据用于模型验证。本文采用国际上较为通用的均方根误差（RMSE）和平均相对误差（MRE）作为模型模拟效果的评价指标。

$$\mathrm{RMSE} = \sqrt{\frac{1}{N}\sum_{i=1}^{N}\left(P_i - O_i\right)^2} \quad (1)$$

$$\mathrm{MRE} = \frac{1}{N}\sum_{i=1}^{N}\left|\frac{P_i - O_i}{O_i}\right| \times 100\% \quad (2)$$

Where N is number of measured data, $O_i$ is the $i^{th}$ measured data and $P_i$ is the corresponding simulated value.

To simulate soil water content, hydraulic characteristic parameters of soil layers have to be determined. Soil samples of different layers were collected from the test pit profile in the study area, which were then carried back to the laboratory to get the soil water characteristic curve through “tensiometer weighing method”. Later, related test data were fitted using the RETC (retention curve program for unsaturated soils) software developed by USSL (US Salinity Laboratory) [4], thus getting the initial values of hydraulic characteristic parameters of soils. With reference to measured soil water of summer maize during the calibration period (2013), meteorological and irrigation system of the study area as well as initial values of soil hydraulic characteristic parameters gained from laboratory test were input into the SWAP model together until getting the optimum fitting result between the simulated results and measured results. In this way, calibration results of VG (Van Genuchten) model parameters of soil layers in the study area were gained (Table 2).

Limited by test conditions, this paper has not set parameters of solute adsorption and decomposition rate in the soil solute transport module of the model when simulating soil salinity. Dispersity and molecular diffusion coefficient are the main calibrating parameters in soil salinity simulation. The multi-parameter sensor CS655 in

上式中的 $N$ 为实测值的个数，$O_i$ 表示第 $i$ 个实测值，$P_i$ 表示对应的模拟值。

对于土壤含水量的模拟，需要确定土柱各层次的土壤水力特性参数。具体是通过在研究区测坑剖面各层采集土样并带回室内进行“张力计称重法”得到其对应的土壤水分特征曲线后，利用 USSL（美国盐改中心）开发的 RETC（retention curve program for unsaturated soils）软件对相关试验数据进行拟合[4]，从而得到土壤水力特性参数的初值。参考 2013 年率定期夏玉米整季的土壤含水量实测资料，并将研究区气象、灌溉制度以及室内试验得到的土壤水力特性参数初值一并输入 SWAP，以模拟值与实测值拟合度达到最优为止，从而得到了研究区土壤各层 VG（Van Genuchten）模型参数的率定结果，如表 2 所示。

针对土壤含盐量的模拟，鉴于试验条件的限制，本文省略了模型土壤溶质运移模块里的溶质吸附及其分解速率等细节问题的参数设定。因此，进行含盐量模拟时率定的参数主要是弥散度和分子扩散系数。站内的多参数传感器

the station couldn't output soil salinity directly. Laboratory "conductometry" is needed to further determine the transformational relation between soil bulk electrical conductivity ($EC_b$, dS/m) measured by the multi-parameter sensor in the station and the salinity (S, g/kg). The goal is to get the optimum fitting between measured salinity and simulated result. The calibration results of dispersity and molecular diffusion coefficient are 13cm and 0.4cm$^2$/d, respectively.

Maize growth dynamics in the study area within the observation period were simulated by the simple crop module in the SWAP model. Based on regular manual observation of maize growth in the study area, plant height, leaf area index and root depth of different stages that have to be input in the module, could be determined. Additionally, initial values of parameters difficult to be measured, such as extinction coefficient of canopy, critical pressure head that causes water stress and critical soil conductivity that causes salt stress, are all determined through literature review [1,9]. Calibration results of main input parameters of this module are shown in Table 3.

CS655 并不能直接输出土壤的含盐量结果，需要借助室内“电导法”试验来进一步确定站内多参数传感器测量的土壤电导率值 $EC_b$（bulk electrical conductivity , dS/m）与全盐量 S（salinity，g/kg）之间的转换关系。以含盐量实测值与模型模拟值的吻合度达到最优为目的，弥散度和分子扩散系数的率定结果分别为 13cm 和 0.4cm$^2$/d。

对于观测期内研究区玉米生长动态的模拟，本文采用了 SWAP 模型当中的简单作物模块。基于对研究区玉米生长定期的人工观测，能够确定该模块所需要输入的各阶段株高、叶面积指数以及根系深度三方面的生长动态。另外，冠层消光系数、引起水分胁迫的临界压力水头值和引起盐分胁迫的土壤临界电导率值等不易测量的参数，均是通过查阅相关文献来确定其初始值[1,9]。经过反复调参，该模块的主要输入参数率定值如表 3 所示。

**Table 2**

**VG model parameters calibrated values of soil moisture characteristic curve**

| Soil Depth (cm) | Saturated water content $\theta_s$ (cm$^3$/cm$^3$) | Residual water content $\theta_r$ (cm$^3$/cm$^3$) | Saturated hydraulic conductivity Ks (cm/d) | Shape factor | | |
|---|---|---|---|---|---|---|
| | | | | α | n | $\lambda$ |
| 0～30 | 0.37 | 0.0885 | 11.4 | 0.017 | 1.26 | 0.5 |
| 30～60 | 0.41 | 0.0936 | 10.7 | 0.011 | 1.48 | 0.5 |
| 60～120 | 0.40 | 0.1031 | 10.2 | 0.010 | 1.66 | 0.5 |

**Table 3**

**Calibrated values of primary crop biological parameters in simple crop growth module**

| Parameters | Selected values (summer maize) |
|---|---|
| Extinction coefficient for diffuse visible light (-) | 0.53 |
| Extinction coefficient for direct visible light (-) | 0.75 |
| Press head (cm) below which roots: h1, h2, $h3_{high}$, $h3_{low}$, h4 # | -15, -30, -325, -600, -15000 |
| ECsat level below which no salt stress (dS/m) | 1.5 |
| Decline root water uptake above this level (%/dS/m) | 8.5 |
| Minimum canopy resistance (s/m) | 70.0 |
| Precipitation interception coefficient (-) | 0.25 |

Note: #. Parameters of water stress response function adjusted as per value suggested by Veenhof and McBride (1994).

***Analysis on simulation results of soil water and salt contents***

Calibrated parameters for simulating soil water content (SWC) were input into the SWAP model to simulate SWC of summer maize in 2013 and 2014. Results are shown in Fig.2. Meanwhile, a statistical test on the fitting degree between measured and simulated SWC was made (Table 3). Overall, RMSE of soil layers during the calibration period and verification period was smaller than 0.03cm$^3$/cm$^3$, and MRE was lower than 10%, indicating that calibrated and verified SWAP model could well simulate SWC dynamics in the study area. However, water content in the surface layer (0～30cm) fluctuates more violently than that in deeper layers (>30cm). Moreover, the simulation precision of surface soil volumetric moisture content is lower than that of deep soil layer. This is mainly because organic content, macro

***土壤水盐含量模拟结果分析***

将用于土壤含水量模拟的相关参数率定值输入到模型当中，并分别对 2013 与 2014 年两季夏玉米田间土壤各层的含水量（SWC）状况进行了模拟，结果如图 2 所示。同时，对土壤含水量各层实测与模拟结果的吻合程度进行了统计检验，如表 3 所示。总体来看，率定期与验证期各层的 RMSE 值不超过 0.03cm$^3$/cm$^3$，且各层的 MRE 值均低于 10%，说明经过率定和验证后的 SWAP 模型能够较好地模拟研究区土壤剖面各层的水分动态。然而，表层 0～30cm 含水量的波动要明显高于埋深 30cm 以下土层，且表层土壤体积含水量的模拟精度要低于深层的模拟精度，这主要是由于有机质含量、大孔隙和其它土壤属性通常在

pores and other soil properties often have high spatial temporal variability in upper layer, thus making surface SWC dynamics more complicated than deeper layers [3]. When simulating SWC dynamics under crop influence by uploading crop files, some parameters, especially those related with water absorption of roots, were set as theoretical values provided by associated references. This will bring great error in describing transpiration of crop root zone in the study area.

Soil salt content (SSC) of summer maize in 2013 and 2014 were simulated based on calibrated relative parameters. Results are shown in Fig.2. A statistical test on measured and simulated SSC was made (Table 3). RMSE during the calibration period and verification period was smaller than 1.5mg/cm$^3$, and MRE was lower than 15%, indicating that the calibrated and verified SWAP model could reflect general variation law of SSC in the study area within the observation period. However, the statistical test reported that the SSC simulation of the SWAP model is poorer than the SWC simulation. It has great simulation errors to surface soil layer (0~30cm). This is mainly because when adjusting parameters of the solute transport module, no targeted laboratory soil column test was conducted except for neglecting solute adsorption and decomposition rate. Therefore, the limited parameter calibration results are inadequate to describe dynamic changes of SSC in the crop root zone in the study area. Meanwhile, SSC in surface layer (0～30cm) changes more violently than that in deeper layers (>30cm) and surface SSC simulation precision is lower than the deeper layer. This is similar with SWC simulation results, indicating that SWC simulation influences SSC simulation precision significantly.

上层具有较高的时空变异性，使得表层土壤水分的动态比深层土壤复杂得多[3]；而且通过加载作物文件来模拟作物影响下的土壤水分动态时，个别参数的设置主要来源于相关文献提供的理论值，尤其是与根系吸水有关的参数设置，这在一定程度上会对研究区作物根系层蒸腾耗水过程的描述带来较大偏差。

基于率定后的相关参数分别对 2013 与 2014 年两季夏玉米田间土壤各层含盐量（SSC）状况进行了模拟，结果如图 2 所示。对各层含盐量的实测和模拟值进行了统计校验，见表 3。率定期和验证期的 RMSE 值不超过 1.5mg/cm$^3$，且各层的 MRE 值均低于 15%，说明经过率定和验证后的 SWAP 模型较好地反映了观测期内研究区土壤剖面各层含盐量的大致变化趋势。但从统计校验结果来看，模型对于土壤含盐量的模拟效果并没有土壤含水量的模拟效果好，尤其是表层 0～30cm 含盐量的模拟偏差较大。这主要是因为在对溶质运移模块进行调参的过程当中，除了未考虑溶质吸附及其分解速率等细节问题以外，未开展针对性较强的室内土柱试验，使得有限的参数率定值不足以描述研究区作物根系层土壤盐分的动态变化。同时，表层 0～30cm 含盐量变化较 30cm 以下土层剧烈，且表层含盐量的模拟精度要低于深层，这与含水量的模拟结果类似，说明对于土壤含水量的模拟在很大程度上影响了土壤含盐量的模拟精度。

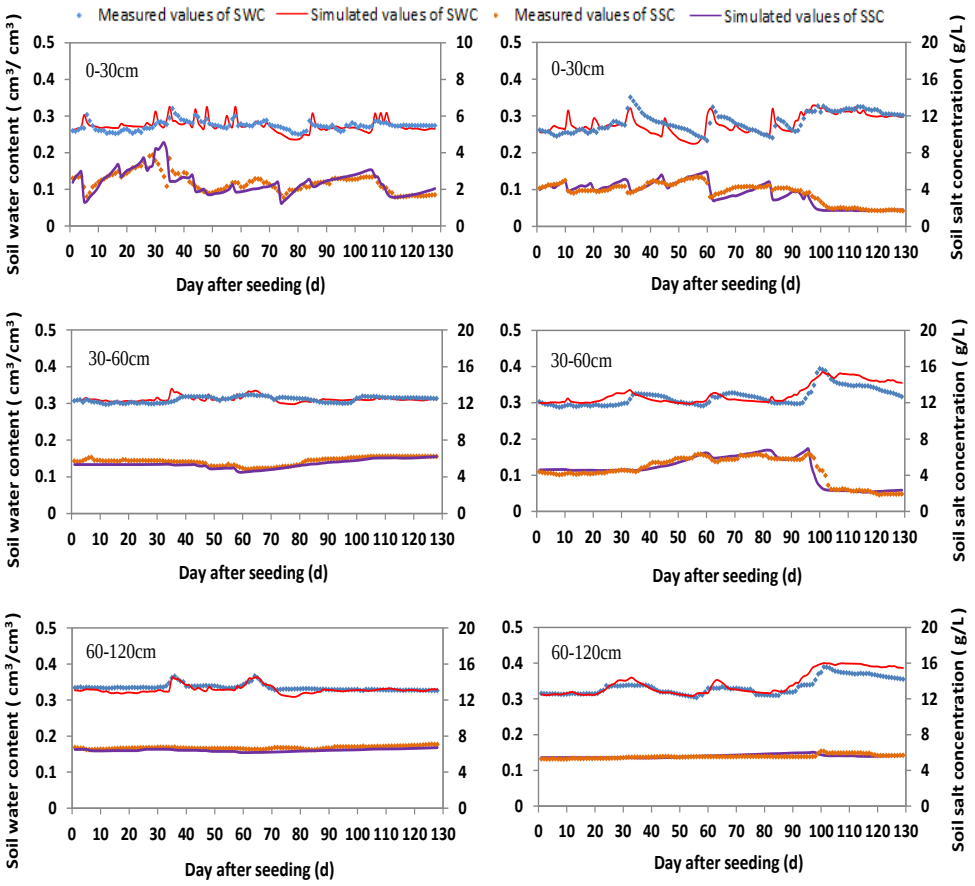


**Fig.2**- Simulated versus measured water and salt content of the soil solution in different soil layers during model calibration (left) and verification (right)

Table 4

**Goodness-of-fit test indicators relative to SWAP model calibration and verification**

| Growing season | Soil depth（cm） | Soil water content（$cm^3/cm^3$） | | Soil salt content（$mg/cm^3$） | |
|---|---|---|---|---|---|
| | | RMSE（$cm^3/cm^3$） | MRE（%） | RMSE（$mg/cm^3$） | MRE（%） |
| Calibration (2013) | 0-30 | 0.014 | 4.2 | 1.392 | 13.8 |
| | 30-60 | 0.008 | 2.2 | 0.827 | 8.2 |
| | 60-120 | 0.009 | 2.0 | 0.490 | 4.1 |
| Verification (2014) | 0-30 | 0.022 | 5.9 | 1.268 | 11.1 |
| | 30-60 | 0.018 | 3.8 | 0.922 | 9.3 |
| | 60-120 | 0.016 | 3.4 | 0.424 | 3.2 |

***Analysis on calculated results of water-salt balance***

The calibrated and verified SWAP model maintains high simulation precision of SWC, implying that this model could simulate soil water movement and solute transport in the study area and the simulated results of field water-salt balance components are reliable.

***Calculated results of water balance***

Daily results of precipitation, irrigation (IRR) and groundwater level (GWL) during the summer maize growth period from 2013~2014 as well as main water balance components output by the model are exhibited in Fig.3. Main water balance components include crop transpiration, surface evaporation, bottom water flux (QBOT) and water storage changes in 0～120cm soil layers (DSTOR). No independent observation data of surface evaporation and crop transpiration were available in the station. However, it can be seen from Fig.3 that simulated results of the SWAP model basically conform to different forms of evapotranspiration change features of maize in different growth stages and under different surface coverage. In the study area, field evapotranspiration during seedling stage of summer maize (about 30d from emergence stage to seven leaves stage) is dominated by surface evaporation because of the slow growth of aboveground parts and low field coverage. The summer maize achieves the most vigorous growth of nutritive organs like leaves and stems during the heading stage (about 50d from the elongation stage to tasseling stage). During this stage, leaf area index and crop transpiration increase significantly compared to the early period, but surface evaporation reduces because of the high canopy density. Reproductive growth takes the dominant role during the anthesis maturity period (about 45d from milk-ripe stage to maturity stage), while vegetative growth stops basically. With the gradually aging of nutritive organs, crop transpiration declines. In the model output results, the accumulative actual transpiration in 2013 and 2014 accounted for 57.6% and 64.9% of potential transpiration, respectively. This symbolizes crop transpiration in the simulation period is influenced by surface soil water content to a certain extent.

Viewed from dynamic changes of water flux on the soil water-groundwater interface during maize growth period in 2013 and 2014, groundwater level in the study area was mainly influenced by precipitation and irrigation. The simulated soil water storage changes are consistent with observed groundwater level changes. The bottom flux changes were less influenced by crop factors, and made strong responses to only rainfall and irrigation. The accumulative soil water supplies from groundwater in 2013 and 2014 were 10.3cm and 7.4cm, respectively.

***水盐平衡计算结果分析***

经过率定和验证后的 SWAP 模型对土壤水盐含量的模拟保证了较高的精度，说明该模型能够进行研究区土壤水分运动及溶质运移的模拟，且模拟得到的田间水盐平衡分量的计算结果是可靠的。

***水量平衡计算结果分析***

图 3 所示为 2013～2014 年两季夏玉米生长期内降雨、灌溉（IRR）、观测地下水位（GWL）以及模型输出的田间水量平衡主要分量的逐日计算结果，包括作物蒸腾量、土面蒸发量、底部水分通量（QBOT）和 0～120cm 土壤储水变化量（DSTOR）。试验站缺乏对土面蒸发和作物蒸腾的分别观测，但由图 3 可以看出，模型对于两个分量的模拟，基本符合玉米在各生育期内不同形态及地表覆被情境下的蒸散变化特征。其中，研究区夏玉米由于苗期（出苗期至七叶期，约 30 天左右）地上部茎叶生长缓慢，农田覆被率较低，因而田间蒸散发以土面蒸发为主。穗期阶段（拔节期至抽穗期，约 50 天左右），玉米叶片及茎节等营养器官的生长是整个生育期内最为旺盛的阶段，所以叶面积指数及作物蒸腾量相比初期显著增加，但此时较高的冠层郁闭度使得土面蒸发呈现低值。夏玉米到了花粒期（乳熟期至成熟期，约 45 天左右），生殖生长占据主导，而营养生长已基本停止，伴随着营养器官的逐渐老化，作物蒸腾量亦呈现衰减趋势。模型输出的计算结果当中，2013～2014 年两季玉米生育期内累积实际蒸腾量占潜在蒸腾量的比值分别为 57.6%和 64.9%，说明模拟期内的作物蒸腾量在一定程度上受到了表层土壤含水量的影响。

从两季玉米各生育期土壤水-地下水界面水分通量的动态变化来看，研究区地下水位主要受降雨和灌溉的影响，且模拟得到的土壤储水变化量与观测地下水位的波动较为一致。两季的底部通量变化受作物因素影响较小，仅在降雨和灌溉时响应强烈。2013 年与 2014 年两季玉米田间的地下水累积入渗补给量分别为 10.3cm 和 7.4cm，0～120cm

The water storage in 0~120cm layers reduced by 5.52cm in 2013 and increased by 1.58cm in 2014. Specifically, the negative soil water supply from groundwater mainly occurred after the elongation stage when maize grows vigorously. With the growth of leaves, field evapotranspiration intensified gradually, so that soil water in saturated zone flows to the unsaturated zone through capillary action, thus resulting in the positive bottom flux and upward supply. Increase of soil water storage and deep leakage of soil water mainly occurred after irrigation and heavy rainfall. For example, twice irrigation at the 30th day and 58th day after summer maize sowing in 2013 as well as the twice irrigation at the 28th day and 59th day after summer maize sowing in 2014 accumulated 6.7cm and 7.2cm deep leakage, respectively. The highest accumulative deep leakage was in the lasting heavy rainfall at late maize growth period in 2014, reaching 4.86cm. Deep leakage of soil water is a kind of waste of farmland water resources. In particular, plentiful deep leakage after irrigation lowers utilization of irrigation water. It is strongly suggested to adopt corresponding measures to relieve deep leakage of irrigation water [6].

土壤储水变化量分别为-5.52cm 和 1.58cm。具体来看，地下水给予土壤水方向向上的负补给主要出现在拔节期以后，该阶段玉米生长发育旺盛，随着叶片的增大增多，田间蒸散日趋强烈，使得饱和带土壤水经由毛细作用补给至非饱和带，底部通量为正值，方向向上。土壤储水量的增大及土壤水的深层渗漏主要发生在灌溉和强降雨过后。例如，2013 年夏玉米播种后第 30 天和第 58 天的两次灌溉，2014 年夏玉米播种后第 28 天和第 58 天的两次灌溉，分别累计产生了 6.9cm、7.2cm 的深层渗漏量；2014 年夏玉米生长后期发生的长历时强降雨期间产生的累计深层渗漏量最高达 4.86cm。土壤水的深层入渗属于农田水资源的无效损耗，尤其是灌溉后的大量深层入渗降低了灌溉水的利用效率，应采取相应的措施用以缓解灌水所造成的深层入渗[6]。

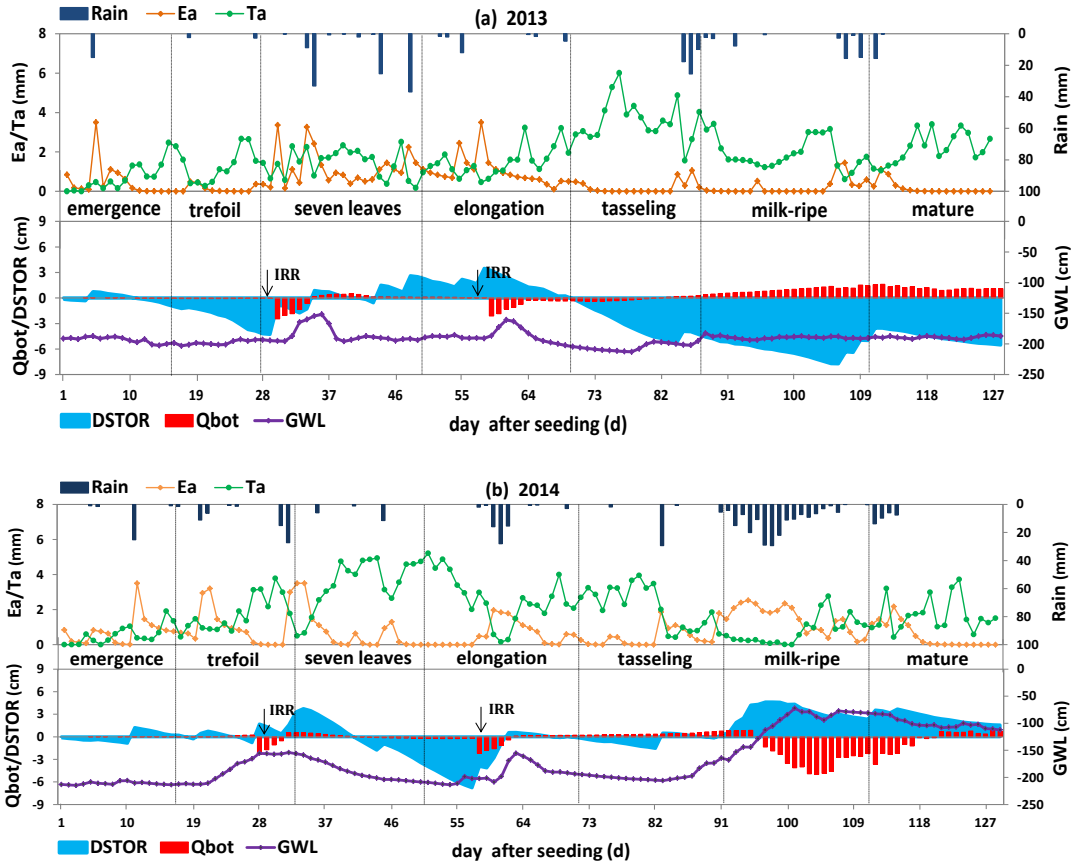


**Fig.3**- Actual evaporation (Ea), actual transpiration (Ta), vertical bottom flux (Qbot) and change water storage (DSTOR) at 120 cm soil profile versus rainfall (Rain), irrigation (IRR) and groundwater level (GWL) changes during summer maize's growth seasons of 2013 (a) and 2014 (b).

***Calculated results of salt balance***

Fig.4 shows simulated results of salt balance components at different maize growth stages from 2013~2014, including solute flux at soil surface (SQTOP), solute flux at soil bottom (SQBOT) and solute storage of 0~120cm soil layers (SAMPRO). In Fig.4, SAMPRO at maize harvest in 2013 and 2014 decreased by 72.87 mg/cm$^2$ and 81.32mg/ cm$^2$ compared to that at early

***盐分平衡计算结果分析***

图 4 所示为 2013～2014 两季夏玉米各生长阶段田间盐分平衡组分的模拟结果，包括土壤表层盐分通量（SQTOP）、底部盐分通量（SQBOT）和 0～120cm 土壤盐分储量（SAMPRO）。由图 4 可以看出，两季玉米收获时的土壤盐分储量相比初期均有不同程度上的削减，表明每经过一季玉米种植后，0～120cm 土壤将处于脱盐状

period, indicating the desalinization of 0~120cm soil layers after maize plant. The most distinct desalinization was in the mid and late growth periods of summer maize. SQBOT presented evident downward leaching states at the same periods. Due to the lasting heavy rainfall during the milk-ripe stage of maize in 2014, both salt reduction and downward SQBOT reached the maximum of the simulation period. This is mainly caused by the frequent heavy rainfalls in the study area if neglecting lateral drainage. However, this paper set few parameters for the solute transport module and neglected salt storage in macro pores and absorbed salt by root system . Therefore, the simulated salt balance result is still one-sided and needs further deep researches.

态。2013 与 2014 年季的盐分储量分别减少了 72.87 mg/cm$^2$ 和 81.32mg/ cm$^2$，主要是在夏玉米生长的中后期脱盐明显，而且两季的底部盐分通量变化，亦在该时段表现为明显的向下淋洗状态，尤其是发生在 2014 年玉米乳熟期的长历时强降雨事件，使得盐分削减量与向下的底部盐分通量均达到了模拟期内的最大值。究其原因主要是该生长时段正值当地的雨季，本研究在不考虑侧向排水的情况下，该阶段频繁发生的强降雨事件是导致研究区土壤盐分向下淋洗的主要因素。然而，本文针对溶质运移模块所设定的参数较少，未考虑到大孔隙盐分储量和根系吸盐量等盐分平衡输出项，因此模型计算得到的盐分平衡结果仍较为片面，有待后续对此进行深入研究。

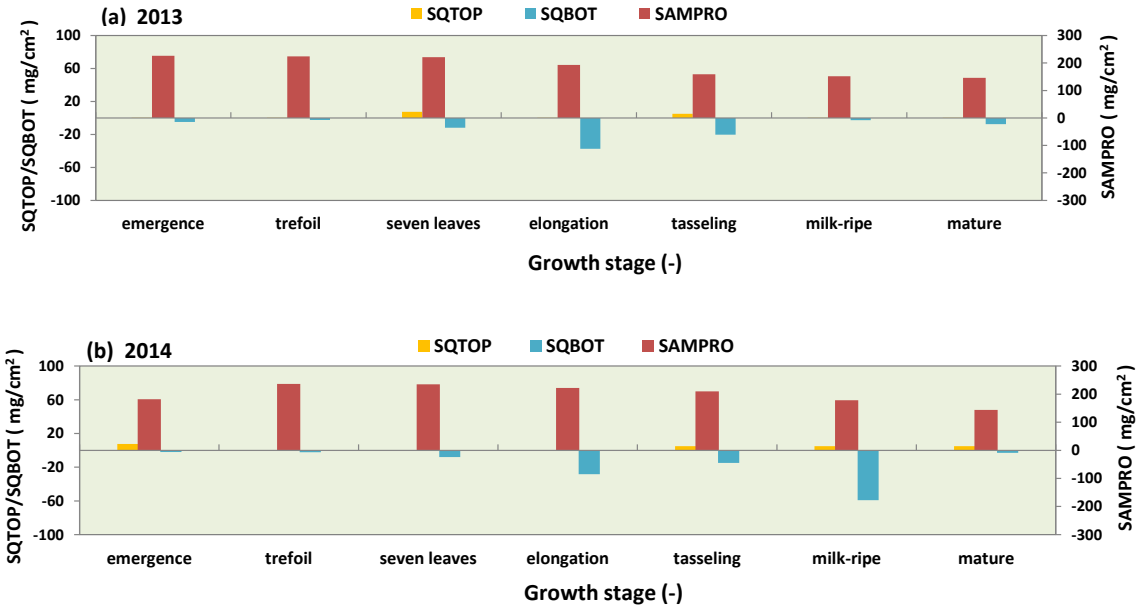


**Fig.4**- Solute flux at soil surface (SQTOP), solute flux at soil bottom (SQBOT) and solute amount at 120cm soil profile (SAMPRO) in different summer maize's growth stages during seasons of 2013 (up) and 2014 (down)

## CONCLUSIONS

Field applicability of SWAP model is tested by the observation data during summer maize growth period from 2013~2014 in typical farmland in the irrigation area of the central Shaanxi Plain. Meanwhile, water-salt balance results simulated by the verified SWAP model are analyzed and discussed. It concludes that:

(1) During model calibration and verification, simulated soil water and salt contents reflect the general variation trend of measured values. During the calibration (2013) and verification (2014), RMSE of SWC is smaller than 0.03cm3/cm3 and MRE is lower than 10%. RMSE of SSC is smaller than 1.5mg/cm3 and MRE is lower than 15%. This means that the calibrated and verified SWAP model is applicable for simulation study on water-salt dynamic changes of the soil profile in the study area. The simulated water-salt balance components are reliable.

(2) According to SWAP results on field water balance components during summer maize growth periods in 2013 and 2014, the accumulative actual transpiration accounts for 57.6% and 64.9% of potential transpiration, indicating that crop transpiration is restricted by surface soil water content. DSTOR reduced by 5.52cm in 2013 and increased by 1.58cm in 2014. Soil water supply from groundwater mainly is mainly achieved in vigorous growth of maize. The accumulative soil water supply from

## 结论

本文利用关中灌区典型农田 2013～2014 年夏玉米生长季的观测数据，对 SWAP 模型进行了田间适用性检验。同时，对验证后的模型所模拟的水盐平衡结果进行了分析与讨论。得到主要结论如下：

（1）模型率定和验证的过程中，土壤水盐含量的模拟值均较好的反映了实测值的大致变化趋势。其中，率定期与验证期各层含水量的 RMSE 值不超过 0.03cm$^3$/cm$^3$，且各层的 MRE 值均低于 10%；率定期和验证期各层含盐量的 RMSE 值不超过 1.5mg/cm$^3$，且各层的 MRE 值均低于 15%，说明经过率定和验证后的 SWAP 模型适用于模拟研究区土壤剖面各层的水盐动态变化，且模拟得到的水盐平衡分量结果是可靠的。

（2）根据 SWAP 对研究区两季夏玉米田间水量平衡各分量的计算结果：2013 与 2014 年季夏玉米生育期内累积实际蒸腾量占潜在蒸腾量的比值分别为 57.6%和 64.9%，说明作物蒸腾受到了表层土壤含水量的制约。2013 与 2014 年季 0～120cm 土壤储水变化量分别为-5.52cm 和 1.58cm，地下水给予土壤水的上升补给主要出现在作物生

groundwater in 2013 and 2014 was 10.3cm and 7.4cm, respectively. In the study area, QBOT is highly sensitive to rainfall and irrigation, mainly manifested by great deep leakage. The accumulative deep leakages after irrigation in 2013 and 2014 reached 6.9cm and 7.2cm.

(3) According to SWAP results on field salt balance components during summer maize growth periods in 2013 and 2014, SAMPRO at the harvest reduced by 72.87 mg/cm2 and 81.32mg/ cm2 compared to that at early stage, indicating the desalinization of 0~120cm soil layers after maize plant. The most distinct desalinization is observed in the mid and late growth periods of summer maize. Neglecting lateral drainage, heavy rainfalls are the main cause of overall desalinization of 0～120cm soil layers in the study area.

**ACKNOWLEDGEMENT**

This work was supported by National Natural Science Foundation of China (Grant No.51509202), China Postdoctoral Science Foundation Funded Project (Grant No.2014M562438), Open Foundation of State Key Laboratory of Hydrology-Water Resources and Hydraulic Engineering (Grant No. 2013490511), the Hydraulic Science and Technology Plan Foundation of Shaanxi Province (Grant No. 2013slkj-08) and Natural Science Foundation of Shaanxi Province (Grant No. 2014JQ5188).

**REFERENCES**

[1]. Haverkamp R, Vauclin M. (1977) - *Comparison of numerical simulation models for one-dimensional infiltration*, Soil Sci Soc Am J, 41, pg.285-294;

[2]. Hongyu Zhu, Shaoshao Du. (2013) - *Analysis of the Characteristics of Soil Salinization in Eastern Guanzhong Basin*, Water Sciences and Engineering Technology, no.9, pg.43-45;

[3]. Hu C S, Saseendran S A, Green T R, et al. (2006) - *Evaluating nitrogen and water management in a double-cropping system using RZWQM*, Vadose Zone Jounal, 5, pg.493-505;

[4]. J Yang, D J Greenwood, D L Rowell, et al. (2000) - *Statistical methods for evaluating a crop nitrogen simulation model*, N_ABLE, Agricultural Systems, 64, pg.37-53;

[5]. Lizhi Wu, Yan Di. (2005) - *Demonstrational study on the land consolidation and rehabilitation (LCR) project of saline-alkali soil in arid areas: a case study of Lubotan LCR project in Pucheng county, Shaanxi Province*, Transactions of the CSAE, vol.21, no.z1, pg.179-182;

[6]. Peng Wang, Xianfang Song, Ruiqiang Yuan, et al. (2011) - *Water flux estimation in SPAC system of farmland using Hydrus-1d model: A case of Dongcun Farm in Yuncheng City, Shanxi Province*, Geographical Research, vol.30, no.4, pg.622-634;

[7]. Quan Quan, Bing Shen, Runxun Jin, et al.(2014) - *Simulation of salinity stress on growth of winter wheat by soil water atmosphere plant model in loess plateau*, INMATEH–Agricultural engineering, vol.44, no.3, pg.51-58;

[8]. Quan Quan, Jiancang Xie, Bing Shen, et al. (2010) - *Soil sampling method based on field measurements and remote sensing images*, Transactions of the CSAE, vol.26, no.12, pg.237-241;

[9]. R.A. Feddes, P.A.C. Raats. (2004) - *Parameterizing the soil – water – plant root system*, Symposium on Unsaturated Zone Modeling, NETHERLANDS: Wageningen, pg.95-141.

长旺盛阶段，地下水累积上升补给量分别为 10.3cm 和 7.4cm；研究区土壤底部水分通量变化对降雨和灌溉的响应强烈，主要表现为明显的深层渗漏，2013 与 2014 年季灌水后的累计深层入渗量分别为 6.9cm 和 7.2cm。

（3）根据 SWAP 对研究区两季夏玉米田间盐分平衡各分量的计算结果：2013 与 2014 年季玉米收获时的土壤盐分储量相比初期的盐分储量分别减少了 72.87 mg/cm$^2$ 和 81.32mg/ cm$^2$，表明经过一季的玉米种植后，研究区 0～120cm 土壤处于脱盐状态，并且两季玉米普遍在生长的中后期脱盐明显。在不考虑侧向排水的条件下，强降雨事件是造成研究区 0～120cm 土层整体脱盐的主要因素。

**致谢**

本课题受到国家自然科学基金项目的资助（项目号：51509202），博士后面上基金项目的资助（项目号：2014M562438），水文水资源与水利工程科学国家重点实验室开放基金的资助（项目号：2013490511），陕西省水利厅科技项目的资助（项目号：2013slkj-08）， 陕西省科技厅科技项目资助（项目号：2014JQ5188）。

**参考文献**

[1]. Haverkamp R, Vauclin M. (1977) – *一维入渗数值模拟模型的对比研究*, 美国土壤学会志, 41, 285-294;

[2]. 朱红玉, 杜少少. (2013) - *关中盆地东部土壤盐渍化特征分析*, 水科学与工程技术, 第 9 期, 43-45;

[3]. Hu C S, Saseendran S A, Green T R, et al. (2006) – *利用 RZWQM 模型评价轮作体系下的农田水氮管理*, 包气带杂志, 5, 493-505;

[4]. J Yang, D J Greenwood, D L Rowell, et al. (2000) – *评价作物氮利用的统计模型, N_ABLE*, 农业系统, 64, 37-53;

[5]. 五黎芝, 底艳. (2005) - *干旱区盐碱化土地整理工程实证研究-以陕西蒲城县卤泊滩土地整理项目为例*, 农业工程学报, 第21卷, 第z1期, 179-182;

[6]. 王鹏, 宋献芳, 袁瑞强, 等. (2011) - *基于 Hydrus-1d 模型的农田 SPAC 系统水分通量估算-以山西省运城市董村农场为例*, 地理研究, 第 30 卷, 第 4 期, 622-634;

[7]. Quan Quan, Bing Shen, Runxun Jin, et al. (2014) - *用 SWAP 模拟盐分胁迫对黄土高原冬小麦生长的影响*, INMATEH - 农业工程, 第 44 卷, 第 3 期, 51-58;

[8]. 权全, 解建仓, 沈冰, 等. (2010) - *基于实测数据及遥感图片的土壤采样方法*, 农业工程学报, 第 26 卷, 第 12 期, 237-241;

[9]. R.A. Feddes, P.A.C. Raats. (2004) – *土壤-水-作物根系系统的参数化*, 非饱和带的模拟与探讨, 荷兰瓦郝尼罕, 95-141.

# STABILITY ANALYSIS OF THE AGRICULTURAL ARTICULATED VEHICLE BASED ON INTERVAL METHOD
# /
# 基于区间数学法的农业铰接车的稳定性分析

**Ph.D. Wei Kou [1, 2)], Prof. Xinhui Liu [1, 2)], Ph.D. Wei Chen [1, 2)]**
[1)] College of Mechanical Science and Engineering, Jilin University, Jilin/China;
[2)] China State Key Laboratory of Automobile Simulation and Control, Jilin University, Jilin/China
*Tel:+86013654376173; E-mail: rudong1415@163.com*

***Abstract:*** *The agricultural mechanization operation is highly efficient, but many types of agricultural mechanical equipment are difficult to move or to operate on hilly terrain and mountains. Thus, these machines play a limited role. This study designs an agricultural articulated vehicle whose front and rear bodies exhibit relative yawing and a rolling degree of freedom; this vehicle can perform agricultural construction operations on different terrains. The agricultural articulated vehicle may roll over during operations such as digging; therefore, its stability should be determined. This research builds a dynamic model of the vehicle during digging through homogeneous coordinate transformation and with the use of the multi-body dynamics method. The interval method is applied to the stability analysis for such operations and describes the uncertain parameters that affect stability as a bounded interval. The stabilities of the front and the rear bodies are analyzed as follows: first, the influence of tire deformation on the rear body stability of the vehicle is determined. The critical rollover angle of the vehicle decreases with an increase in tire deformation. Second, the influence of different digging material weights on the front body stability of the vehicle is measured. Finally, the results obtained with the interval analysis method indicate that the vehicle remains stable while digging if the values of yaw angle $\varphi$ and roll angle $\theta$ are located in the minimum envelope zone of [−42°, 42°] and [−28°, 28°]. The analysis results can guide structural improvement, provide an early warning for rollover during digging, and extend the application range of the proposed vehicle in agricultural construction.*

***Keywords:*** *Agricultural articulated vehicle; Multi-body dynamics; Interval analysis; Stability*

## INTRODUCTION

Wheeled construction machineries have been applied to various aspects of agricultural production, such as grapery ditching, soil loosening and preparation in upland fields, the exploitation of low-lying and easily waterlogged wasteland, water supply, and dredging work in paddy fields, given that these processes are difficult to perform manually. Moreover, efficiency is low and the operational hazard is high. In north China, the construction machineries should also be used for farmland water conservancy in the winter because of the frozen surface layer. The use of construction machineries has effectively economized on manpower, shortened product time, and saved cost. Nonetheless, many types of agricultural mechanical equipment are difficult to move and control on hilly terrains and mountains; thus, these machines play a limited role. In this study, we design a vehicle whose front and rear bodies are joined by a universal hinge; this vehicle displays relative yawing and a rolling degree of freedom. Therefore, the wheels can make

***摘要：****农业机械化生产虽然效率高，但是在地形复杂的丘陵地带和山区，很多农用机械设备移动和操作困难，难以发挥作用。设计了一种农业铰接车，它的前后车体相对有横摆和扭转自由度，可以在不同的地形下进行农业工程作业。农业铰接车在农业作业，例如挖掘过程中容易产生倾翻，需要研究挖掘作业过程中的稳定性，本文采用齐次坐标变换和多刚体动力学方法，建立了农业铰接车挖掘作业时的动力学方模型。在挖掘作业稳定性分析中，应用区间数学法，把影响稳定性的不确定参数作为一个数学区间，然后结合车辆的稳定性判据，分别对农业铰接车前后车体的稳定性进行了分析，首先，分析了轮胎变形对后车体倾翻稳定性的影响；其次，分析了挖掘物质量的不同对前车体倾翻稳定性的影响。最后，通过仿真分析，在挖掘作业过程中，保证车辆不产生倾翻，前后车体的横摆角$\varphi$和侧偏角$\theta$落在[-42°，42°]和[-28°，28°]的包络区域内。分析结果可以为 农业铰接车结构设计的改进和挖掘稳定性预警提供设计方法和参考，拓展它在农业工程中的应用范围。*

***关键词:*** *农业铰接车；多刚体动力学；区间分析法；稳定性*

## 引言

轮式工程机械已经用到农业生产的各个方面，如葡萄园挖沟作业；旱田的松土、整地；地势低洼、易涝的荒地开发；水田给水清淤工程，人工作业相当困难，而且效率低，作业危险性大；在北方冬季里进行农田水利施工，地表冻层，只有采用工程机械可以施工。工程机械应用在农业生产上，节约了大量劳动力，又缩短了生产时间，节省成本。但是在地形复杂的丘陵地带和山区，由于很多农用机械设备移动和操作困难，难以发挥作用。因此我们设计了一种农业铰接车，它的前车体和后车体采用铰链关节连接，前后车体相对有横摆和扭转自由度，在复杂的农田地形下车轮充分和地面接触，增加了车辆的运动和作业的稳定性，能更好的适应不同农业生产的地形环境，它的结构

sufficient contact with the complex farmland terrain, and vehicle stability improves for operating and digging operations. The vehicle can adapt to different terrain environments for agricultural production, is low-cost, possesses a simple structure, is convenient to operate, and is widely applicable. Nonetheless, the stability of agricultural construction vehicle operation on hills, mountains, and paddy fields containing silt must be determined; at present, studies on agricultural mountain vehicles mainly concentrate on static and dynamic stabilities to overcome obstacles [1, 2, 3, 8] and to warn against rollover in advance [7, 9, 12]. According to statistics, more than 90% of rollover accidents related to agricultural mountain vehicles occurred in operation [5, 11] rather than in running. Few studies have been conducted on vehicle rollover in agricultural construction operations although the complex operation environment and uncertain factors, such as vehicle position and pose, tire deformation, and digging state, influence the stability of agricultural construction vehicles. Furthermore, traditional stability analysis methods are applied only in specific states [4, 10]. The current study applies the interval method to an analysis of stability during digging, describes all factors that affect stability as a bounded interval, and derives a dynamic equation. The effect of all uncertain factors on vehicle stability is determined with the stability criterion in combination with the interval method. Researching vehicle stability in agricultural construction operation generates a reference for structure design improvement as well as for follow-up rollover protection and early warning system design. Thus, the safety and convenience of vehicle implementation in the agricultural construction operation are improved.

## MATERIALS AND METHODS

### Dynamic Model for an Agricultural Articulated Vehicle

The backhoe device of the agricultural articulated vehicle is driven by a hydraulic system, and the revolving mechanism is driven by two lever-type cylinders, as shown in Figure 1. This vehicle can excavate soil and rock at different heights, angles and distances, as depicted in Figure 2. Furthermore, the operating range of the agricultural articulated vehicle is presented in Table 1.

简单，操作方便，成本也低廉，应用更广泛。农业工程车辆在丘陵、山区或者淤泥的水田工作，需要研究它工作过程中的稳定性。目前国内外对于山地农业工程车辆的稳定性研究，主要集中在车辆静态稳定性研究和越障行驶中的动态稳定性研究[1,2,3,8]以及车辆侧翻预警研究[7,9,12]等。根据文献资料统计山地农业工程车辆的倾翻 90%以上都是在作业过程中发生的[5,11]，而工程车行驶过程中的倾翻较少。对于工程车在农业工程作业过程的倾翻研究，国内外相关文献资料极少；山地农业工程车挖掘作业环境复杂，车体位姿，轮胎变形，挖掘工作状态等不确定性因素多，常用的求解稳定性的数学方法，只能求解特定状态下的车体稳定性[4,10]。本文利用区间数学的方法，分析农业铰接车在工作过程中的稳定，把影响农业铰接车稳定性的任一不确定因素当成一个数学区间，建立动力学方程，结合铰接式车辆倾翻的稳定性判据，求解农业铰接车的动力学方程，得到在不确定因素影响下，农业铰接车前后车体姿态的范围。通过研究农业铰接车在农业工程作业中的稳定性研究，可以为农业铰接车的结构设计改进和后期防倾翻预警系统设计提供参考依据，能够使车辆更安全方便的应用于农业工程生产建设。

## 材料与方法

### 农业铰接车动力学模型

农业铰接车的挖掘装置通过液压系统驱动，挖掘臂回转系统采用杠杆式双液压缸驱动方式，如图 1 所示，可以实现农业铰接车在不同角度、不同高度、不同距离的挖掘作业，如图 2 所示，农业铰接车的作业装置作业范围如表 1 所示。

**Fig.1** -Wasteland development operation of the vehicle

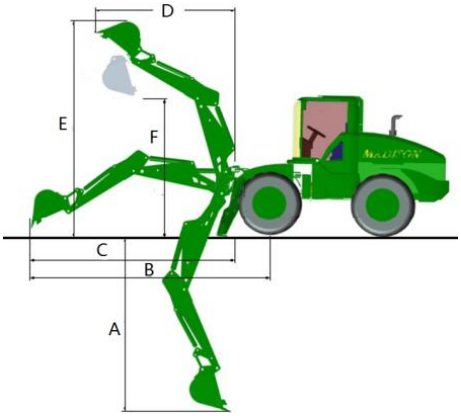


**Fig.2** - Sketch of the vehicle operating range

Table 1

**Parameters of the vehicle operating device**

| Definition of the parameter | Parameter values |
|---|---|
| A. Maximum digging depth | 3.03 m |
| B. The horizontal distance between the bucket and the center of the front wheel | 5.31 m |
| C. The horizontal distance between the bucket and the rotating center | 4.11 m |
| D. The horizontal distance between the bucket on top and the rotating center | 2.64 m |
| E. Maximum digging height | 3.40 m |
| F. Maximum unloading height | 2.85 m |

Many uncertain factors are observed in this scenario, such as the velocity of the backhoe device, its angular velocity, and the attitude displayed during the operation process. The interval method is applied to solve the problem of stability given uncertain factors. The vehicle and the backhoe device are simplified as a rigid body, and the vehicle coordinate system is built through the multi-body dynamics method, as illustrated in Figure 3.

工作过程中，挖掘装置的速度、角速度及在工作区域位姿等影响农业铰接车稳定性的不确定参数众多，采用区间分析方法，能有效解决包含不定参数的系统分析问题。农业铰接车和其挖掘装置简化成刚体，通过多刚体动力学方法建模。建立农业铰接车坐标系，如图 3 所示。

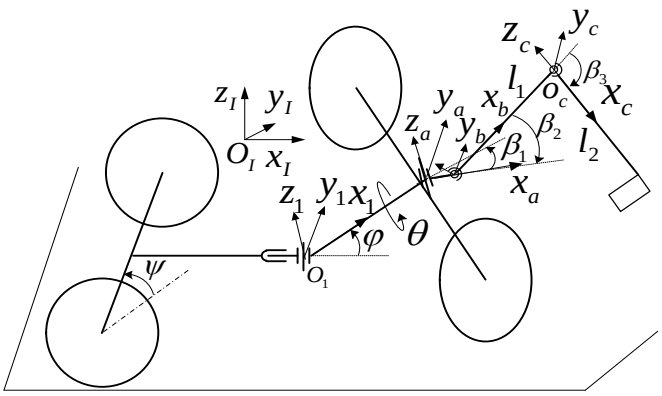


**Fig.3** -Schematic for the vehicle coordinate system

where the origin of the inertial coordinate system $O_I x_I y_I z_I$ is the rear body centroid $M_r$ and axle $x_I$ is detected along the drive shaft of the rear body. Axle $z_I$ is the vertical axis, and the front and rear bodies are joined by a universal hinge. The front body coordinate system $O_1 x_1 y_1 z_1$ originates at the yaw hinge, and the roll angle of the rear body is represented by $\psi$. The roll and yaw angles of the front body are denoted by $\theta$ and $\varphi$, respectively. The backhoe device and the front body are also connected through a universal hinge. The yaw angle between the backhoe device and the front body is represented by $\beta_1$, the pitching angle is denoted by $\beta_2$, and the angle between the boom and the bucket rod corresponds to $\beta_3$.

The position vector of a generic point $P$ on the vehicle in a generic coordinate system $B$ is ${}^B\vec{p}$, which transforms a generic coordinate system $A$ into ${}^A\vec{p}$. This vector is described in the form of homogeneous coordinates:

其中惯性系 $O_I x_I y_I z_I$ 原点在后车体质心 $M_r$，$x_I$ 轴沿后车体传动轴方向。$z_I$ 轴铅垂向上。前后车体之间为万向铰连接，前车体本体坐标系为 $O_1 x_1 y_1 z_1$，原点在横摆铰接点处。后车体的侧偏角为 $\psi$，前车体的侧偏角为 $\theta$，横摆角为 $\varphi$。挖掘装置和前车体通过万向铰连接，挖掘装置和前车体传动轴之间的横摆角为 $\beta_1$，俯仰角为 $\beta_2$，动臂和斗杆之间角度为 $\beta_3$。

车辆上任一点 $P$，在某参考坐标系 $B$ 中位置矢量为 ${}^B\vec{p}$，则变换到某参考坐标系 $A$ 中位置矢量采用齐次坐标可表示为：

$$\begin{bmatrix} {}^A\vec{p} \\ 1 \end{bmatrix} = \begin{bmatrix} {}^A R_B & {}^A p_{Bo} \\ 0 & 1 \end{bmatrix} \begin{bmatrix} {}^B\vec{p} \\ 1 \end{bmatrix} = {}^A T_B \begin{bmatrix} {}^B\vec{p} \\ 1 \end{bmatrix} \quad (1)$$

where ${}^{A}T_{B}$ is the matrix of position and orientation transformation from the $B$ coordinate system to the $A$ coordinate system, ${}^{A}R_{B}$ is the attitude matrix from the $B$ coordinate system to the $A$ coordinate system, and ${}^{A}\vec{p}_{Bo}$ is the position vector that indicates the origin of coordinate system $B$ in coordinate system $A$.

其中 ${}^{A}T_{B}$ 为坐标系 $B$ 系到 $A$ 系的位姿变换，${}^{A}R_{B}$ 为 $B$ 系到 $A$ 系的姿态变换矩阵，${}^{A}\vec{p}_{Bo}$ 为 $B$ 系的原点在 $A$ 系中的位置矢量。

When the vehicle excavates soil and rock, the body vehicles remain motionless, and the backhoe device alone moves. The boom and the bucket rod can be simplified as rods with lengths that are denoted by $l_1$ and $l_2$. The centroids of both the boom and the bucket rod are positioned at the middle points; moreover, the bucket and the digging mixture are simplified as the centralization mass of $m_3$. The driving moment of the backhoe device is represented by $M_1$, $M_2$, $M_3$, and the force of the backhoe device during digging is illustrated in Figure 4.

农业铰接车在挖掘作业时，车体行进到工作位置固定，只有工作装置进行一系列的挖掘作业。工作装置的动臂和斗杆可简化成杆长度为 $l_1$，$l_2$ 的杆，动臂和斗杆的质心在均在杆的中点，铲斗和挖掘物可看作 $m_3$ 的集中质量点。挖掘装置的转动关节力矩为 $M_1$，$M_2$，$M_3$，则工作中，挖掘装置的受力如图 4 所示。

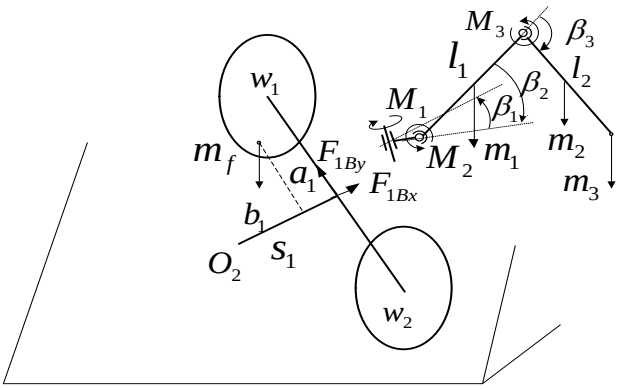


**Fig.4 -** Forces exerted on the front body during digging

In the inertial coordinate system, the position vector of centroid $m_1$ of the boom, centroid $m_2$ of the bucket rod, and centroid $m_3$ of the digging mixture are written as

在惯性坐标系下，动臂质心 $m_1$，斗杆质心 $m_2$，挖掘物质心 $m_3$ 的位置矢量为：

$$\begin{bmatrix} {}^{O}\vec{p}_{m1} \\ 1 \end{bmatrix} = {}^{O}T_{1}\,{}^{1}T_{a}\,{}^{a}T_{b}\begin{bmatrix} {}^{b}\vec{p}_{m1} \\ 1 \end{bmatrix} \tag{2}$$

$$\begin{bmatrix} {}^{O}\vec{p}_{m2} \\ 1 \end{bmatrix} = {}^{O}T_{1}\,{}^{1}T_{a}\,{}^{a}T_{b}\,{}^{b}T_{c}\begin{bmatrix} {}^{c}\vec{p}_{m2} \\ 1 \end{bmatrix} \tag{3}$$

$$\begin{bmatrix} {}^{O}\vec{p}_{m3} \\ 1 \end{bmatrix} = {}^{O}T_{1}\,{}^{1}T_{a}\,{}^{a}T_{b}\,{}^{b}T_{c}\begin{bmatrix} {}^{c}\vec{p}_{m3} \\ 1 \end{bmatrix} \tag{4}$$

The angle velocity of the boom $l_1$ and the bucket rod $l_2$ in the inertial coordinate system can be described as

动臂 $l_1$ 和斗杆 $l_2$ 在惯性系中的角速度可以表示为：

$${}^{O}\vec{\omega}_{m1} = {}^{O}R_{1}\,{}^{1}R_{a}\dot{\vec{\beta}}_{1} + {}^{O}R_{1}\,{}^{1}R_{a}\,{}^{a}R_{b}\dot{\vec{\beta}}_{2} \tag{5}$$

$${}^{O}\vec{\omega}_{m2} = {}^{O}R_{1}\,{}^{1}R_{a}\dot{\vec{\beta}}_{1} + {}^{O}R_{1}\,{}^{1}R_{a}\,{}^{a}R_{b}\dot{\vec{\beta}}_{2} + {}^{O}R_{1}\,{}^{1}R_{a}\,{}^{a}R_{b}\,{}^{b}R_{c}\dot{\vec{\beta}}_{3} \tag{6}$$

The velocity and the acceleration of $m_1$, $m_2$, $m_3$ can be written as

质心 $m_1$，$m_2$，$m_3$ 的在惯性系下的速度和加速度可表述为：

$${}^{O}\vec{v}_{mi} = {}^{O}\vec{\omega}_{mi} \times {}^{O}\vec{p}_{mi} \tag{7}$$

$${}^{O}\vec{a}_{mi} = {}^{O}\vec{\varepsilon}_{mi} \times {}^{O}\vec{p}_{mi} + {}^{O}\vec{\omega}_{mi} \times {}^{O}\vec{v}_{mi} \tag{8}$$

where $i=1,2,3$ , ${}^{O}\vec{\omega}_{m2}={}^{O}\vec{\omega}_{m3}$ , ${}^{O}\vec{\varepsilon}_{m2}={}^{O}\vec{\varepsilon}_{m3}$ , and $\vec{\varepsilon}=d\vec{\omega}/dt$ is angular acceleration.

We define $\beta_1$ , $\beta_2$ , $\beta_3$ as generalized coordinates. The driving moment $M_1$ , $M_2$ , $M_3$ is calculated by solving the Lagrange equation. When the vehicle performs a digging task under the assumption that the acceleration of the boom and of the bucket rod is represented by $\vec{\varepsilon}=0$ , the kinetic energy of the boom and bucket rod system is written as

其中 $i=1,2,3$ ， ${}^{O}\vec{\omega}_{m2}={}^{O}\vec{\omega}_{m3}$ ， ${}^{O}\vec{\varepsilon}_{m2}={}^{O}\vec{\varepsilon}_{m3}$ ， $\vec{\varepsilon}=d\vec{\omega}/dt$ 为角加速度。

设 $\beta_1$、$\beta_2$、$\beta_3$ 为广义坐标，采用拉格朗日方程求解驱动力矩 $M_1$、$M_2$、$M_3$，农业铰接车在挖掘工作时，假设动臂斗杆的加速度 $\vec{\varepsilon}=0$，则 农业铰接车动臂斗杆系统的动能可写为：

$$T=\frac{1}{2}\sum_{i=1}^{3}m_i\,{}^{O}\vec{v}_{mi}^{T}\,{}^{O}\vec{v}_{mi}+\frac{1}{2}\sum_{i=1}^{2}{}^{O}\vec{\omega}_{mi}^{T}\vec{J}_{mi}\,{}^{O}\vec{\omega}_{mi} \tag{9}$$

The potential energy in the system is written as

系统势能可写为：

$$V=\sum_{i=1}^{3}m_i\,{}^{O}\vec{p}_{mi}{}^{T}\vec{g} \tag{10}$$

The driving moment is calculated as

求得驱动力矩为：

$$M_i=\frac{d}{dt}\left(\frac{\partial L}{\partial\dot{\beta}_i}\right)-\frac{\partial L}{\partial\beta_i} \tag{11}$$

where $L=T-V$ is the Lagrange function.

When D'Alembert's principle is applied, the force and the moment of the front body as induced by the backhoe device can be computed as

其中 $L=T-V$ 为拉格朗日函数。

根据达郎贝尔原理可求得挖掘装置对前车体的作用力和作用力矩为：

$$\vec{F}_{1B}={}^{1}R_{O}\sum_{i=1}^{3}m_i\,{}^{O}\vec{a}_{mi} \tag{12}$$

$$\vec{M}_{1B}=-({}^{1}R_a\vec{M}_1+{}^{1}R_a\,{}^{a}R_b\vec{M}_2+{}^{1}R_a\,{}^{a}R_b\,{}^{b}R_c\vec{M}_3) \tag{13}$$

The vehicle consists of two parts. During digging, the front body may be influenced by the boom and bucket rod motion. When the force on wheels $w_1$ and $w_3$ is zero, the front and rear bodies tip over at approximately $O_2W_2$ and $O_2W_4$ , respectively, as shown in Figure 5.

由于农业铰接车分为前后两部分，挖掘作业时，由于动臂斗杆的影响，前车体最容易发生倾翻。此时有轮 $w_1$、$w_3$ 受力为零，前车体绕 $O_2W_2$ 轴倾翻，后车体绕 $O_2W_4$ 轴倾翻，如图 5 所示。

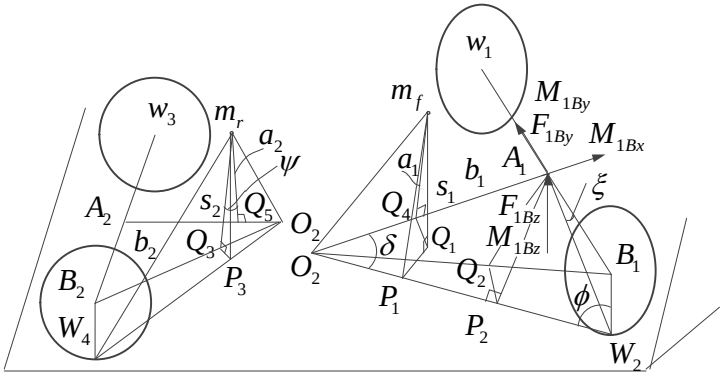


**Fig.5 -** Schematic of vehicle stability

The front and rear bodies of the vehicle are stationary during digging; this problem is one of static stability.

When the rear body remains stable, its centroid $m_r$ should be located in plane $\Delta A_2B_2O_2$ . Thus, the centroid can be calculated as

设农业铰接车的前后车体在挖掘作业过程中静止不动，前后车体属于静态稳定性问题。

当后车体保持稳定时，后车体质心 $m_r$ 应落到平面 $\Delta A_2B_2O_2$ 内，可得：

$$Q_3P_3>0 \tag{14}$$

The roll angle of the rear body in stable state can be computed by using the geometric relation presented in Figure 5.

通过图 5 中几何关系，可得后车体保持稳定时的侧偏角为：

$$\psi < \arctan\left(\frac{s_2 d(s_2-b_2)\sqrt{d^2+s_2^2}}{d^2 s_2 a_2 - 2d^2 b_2 r + s_2^3 r + s_2^3 a_2 - s_2^2 b_2 r} - \frac{\delta}{2d}\frac{s_2}{\sqrt{d^2+s_2^2}}\right) \tag{15}$$

where $s_2$ is the length of the rear vehicle, $d$ is half of wheel track, $a_2$ is the length between centroid $m_r$ and point $Q_5$ which is the centroid $m_r$ projection onto the rear drive shaft, $b_2$ is the length between point $A_2$ and point $Q_5$, $r$ is the wheel radius, $\delta$ is the static deformation of the tire when the vehicle is unstable. In the experiment, the measured value of the tire radius is [0.736 m, 0.775 m].

When the front body is in stable state, the moment of mass center $m_f$, which is relative to axle $O_2W_3$, is greater than the other moments that are also relative to this axle. Therefore, we can obtain

其中 $s_2$ 是后车体长度，$d$ 是车轮距的一半，$a_2$ 是质心 $m_r$ 与点 $Q_5$ 的长度，其中 $Q_5$ 是质心 $m_r$ 在后驱动轴上的投影，$b_2$ 是点 $A_2$ 和点 $Q_5$ 之间的长度，$r$ 是车轮半径，$\delta$ 为失稳时轮胎的静变形量。通过测量，轮胎滚动半径变化量为 [0.736m, 0.775m]。

前车体保持稳定时，前车体质心 $m_f$ 绕轴 $O_2W_3$ 的力矩大于其它外力绕轴此轴的力矩。因此，通过计算可得：

$$\overrightarrow{\sqrt{\frac{(s_1-b_1)^2(\delta^2+d^2)}{(s_1^2+d^2)\cos^2\varphi}+\frac{s_1^2 a_1^2\sin^2\theta}{s_1^2+d^2+r^2}}\times m_f\vec{g}} > \overrightarrow{\sqrt{\frac{(s_1^2+d^2)(r^2+d^2)}{s_1^2+d^2+r^2}}\times\vec{F}_{1Bz}-\vec{r}\times\vec{F}_{1By}+\vec{M}_{1Bx}-\vec{M}_{1By}-\vec{M}_{1Bz}} \tag{16}$$

where $s_1$ is the length of the front vehicle, $a_1$ is the length between centroid $m_f$ and point $Q_4$ which is the centroid $m_f$ projection onto the front drive shaft, $b_1$ is the length between point $A_1$ and point $Q_4$.

When the vehicle is performing a digging task, the uncertain interval parameters are the angles $\beta_1$, $\beta_2$, $\beta_3$ among the boom, the bucket rod, and the rotational velocity $\dot{\beta}_1$, $\dot{\beta}_2$, $\dot{\beta}_3$, the mass of the digging material $m_t$, and the deformation of the tire $\delta$. To obtain acceptable stability in the digging operation, the allowable range of roll angle $\theta$ and yaw angle $\varphi$ should be determined with the interval method.

其中 $s_1$ 是前车体长度，$a_1$ 是质心 $m_f$ 与点 $Q_4$ 的长度，其中 $Q_4$ 是质心 $m_f$ 在前驱动轴上的投影，$b_1$ 是点 $A_1$ 和点 $Q_4$ 之间的长度。

对于农业铰接车来说，当在进行挖掘作业时，动臂斗杆间夹角 $\beta_1$、$\beta_2$、$\beta_3$，以及转动角速度 $\dot{\beta}_1$、$\dot{\beta}_2$、$\dot{\beta}_3$，$m_t$，轮胎变形量 $\delta$ 分别为不确定的区间参数，要保证挖掘作业过程中前车体的稳定性，需要求解在不确定区间参数中，农业铰接车的前车体侧偏角 $\theta$ 和横摆角 $\varphi$ 的允许范围。

**Analysis of Stability in Digging Operations based on the Interval Method**

Interval analysis theory has been applied to many project fields [6, 13]. The closed interval of a real number can be described as

**区间法分析农业铰接车挖掘作业稳定性**

目前区间分析理论已经应用于很多工程领域[6,13]。实的闭区间可表示为：

$$X^I = [\underline{X}, \overline{X}] = \left\{X \in R \mid \underline{X} \le X \le \overline{X}\right\} \tag{17}$$

where $\underline{X}$ and $\overline{X}$ are the interval endpoints.

When the center interval method is applied, Eq. (17) is rewritten as

其中 $\underline{X}$，$\overline{X}$ 分别称为区间的下端点和上端点。

采用中心区间法，式（17）可以表示为：

$$X^I = X^C + \Delta X\, e_\Delta \tag{18}$$

where $X^C$ is defined as the middle point of the interval, $\Delta X$ is defined as the interval radius, and the range of $e_\Delta$ is [-1, 1].

The vehicle parameters can be written in the interval form

其中 $X^C$ 称为区间中点，$\Delta X$ 称为区间半径，$e_\Delta$ 的范围为 [-1, 1]。

农业铰接车的设计参数, 可以用区间法表示为：

$$\begin{cases} \beta_1 = \dfrac{\pi}{2} e_\Delta \\ \beta_2 = \dfrac{\pi}{6} + \dfrac{\pi}{6} e_\Delta \\ \beta_3 = 0.39\pi + 0.39\pi e_\Delta \\ \dot{\beta}_1 = \dfrac{\pi}{3} e_\Delta \\ \dot{\beta}_2 = 0.055\pi + 0.055\pi e_\Delta \\ \dot{\beta}_3 = 0.055\pi + 0.055\pi e_\Delta \\ m_t = 300 + 300 e_\Delta \\ \delta = 0.7555 + 0.0195 e_\Delta \end{cases} \quad (19)$$

Eq. (19) is substituted into Eq. (16) to yield

把式（19）代入式（16），可得到如下函数：

$$F(\theta, \varphi, e_\Delta) > 0 \quad (20)$$

When the agricultural articulated vehicle is performing a digging task, the values of the parameters that maintain front body stability must satisfy the boundary conditions of Eq. (20). The vehicle parameters are $l_1$ = 2.4 m, $l_2$ = 2 m, $m_1$ = 600 kg, $m_2$ = 450 kg, $m_f$ = 7000 kg, and $m_r$ = 5900 kg. The track value is $2d$ = 1.6 m, and the wheel radius value is $r$ = 0.75 m, $S_1$ = 0.72 m, $S_2$ = 2.2 m, $a_1$ = 0.65 m, $a_2$ = 0.65 m, $b_1$ = 0.2 m, and $b_2$ = 1.4 m. The range of the roll angle $\theta$ is [−40°, 40°], and the range of the yaw angle $\varphi$ is [−42°, 42°].

当农业铰接车挖掘时，保证前车体稳定性，车体相关参数的取值需要满足式（20）。农业铰接车设计参数为：$l_1$ =2.4m，$l_2$ =2m，$m_1$ =600kg，$m_2$ =450kg，$m_f$ =7000kg，$m_r$ =5900kg，轮距 $2d$ =1.6m，车轮半径 $r$ =0.75m，$S_1$ =0.72m，$S_2$ =2.2m，$a_1$ =0.65m，$a_2$ =0.65m，$b_1$ =0.52m，$b_2$ =1.4m，侧偏角 $\theta$ 的设计范围为[-40°，40°]，横摆角 $\varphi$ 的设计范围为[-42°，42°]。

## RESULTS

### Influence of Tire Deformation on Rear Body Stability

When the roll angle of the rear body vehicle increases, tire deformation changes. As a result, the actual rollover angle shifts as well. The relationship between the rollover angle of the rear body and tire deformation is calculated with Eq. (15); the result is shown in Figure 6.

The rollover angle of the rear body decreases when tire deformation increases in Figure 6. Thus, this deformation should be considered in the analysis of vehicle stability during agricultural construction to enhance the accuracy of the calculated rollover angle. If tire deformation is disregarded, then the calculated rollover angle is large; when this angle is used in the design of a vehicle rollover warning system, rollover accidents occur easily.

## 结果

### 轮胎变形量对后车体稳定性的影响

农业铰接车的后车体的侧偏角的增大，后车体左边和右边轮胎上的受力产生变化，轮胎的变形量就随着改变，造成后车体实际失稳的侧偏角也会不同。根据后车体侧偏的稳定性公式（15），可得后车体保持稳定的侧偏角随轮胎变形量的变化关系如图 6 所示。

由图 6 可知，轮胎变形量的增大，后车体失稳时的侧偏角会变小。所以在挖掘作业稳定性分析时，必须要考虑轮胎才能使计算的保持稳定性的侧偏角更准确，如果不考虑轮胎变形，会使计算的稳定侧偏角偏大，按照此计算结果进行倾翻预警设计，容易造成车辆翻车事故。

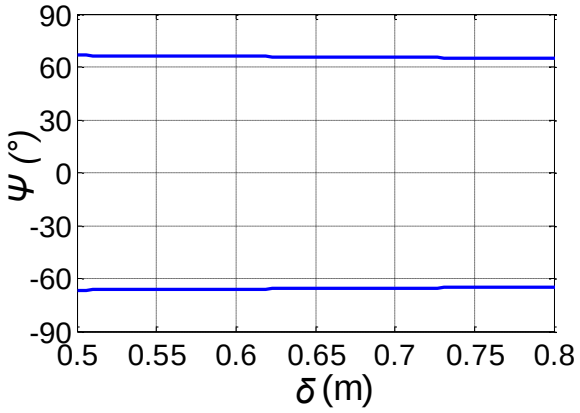


**Fig.6 -** Variation in the rollover angle of the rear body with tire deformation

**Influence of Digging Material Weight on Front Body Stability**

When the agricultural articulated vehicle is working, the digging material weight in the bucket strongly affects front body stability. If $\varphi = 0$, then the boom and bucket rod of the digging device are motionless, $\beta_2 = 0.12\pi$, $\beta_3 = 0.3\pi$, the rotation angular velocity around the $Z_a$ axis is denoted by $\dot{\beta}_1$, and $\dot{\beta}_1 = 0.3\pi / s$. When the digging material weight is $m_t$=0 kg and $m_t$=300 kg, the stability curves of the front body are as depicted in Figure 7.

**挖掘物质量对前车体稳定性的影响**

当农业铰接车进行作业时，抓斗中挖掘物质量对前车体的倾翻稳定性有很大的影响，若给定 $\varphi = 0$，挖掘装置的动臂和斗杆相对不动，$\beta_2 = 0.12\pi$，$\beta_3 = 0.3\pi$ 只有绕 $Z_a$ 轴的转动角速度 $\dot{\beta}_1$，设 $\dot{\beta}_1 = 0.3\pi / s$，当铲斗中的挖掘物质量 $m_t$=0 kg 和 $m_t$=300 kg 时，可以分别求的前车体保持倾翻稳定性的曲线，如图 7 所示。

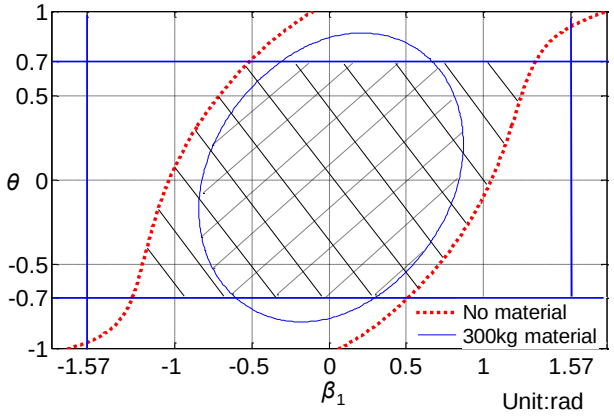


**Fig.7 -** Stability region of the front body under different digging material weights

According to the stability analysis results, the front body is stable when $m_t$=0 kg and if the roll angle of the front body $\theta$ and the rotation angle of the digging device $\beta_1$ are located in the elliptic region surrounded by a solid line. The same is true when $m_t$=300 kg, if $\theta$ and $\beta_1$ are located in the region surrounded by the dotted line. The range of $\theta$ is [−40°, 40°], and the range of $\beta_1$ is [−90°, 90°]; therefore, the stability region of the front body is the intersection of the same parameters under different conditions. This region is denoted by the areas marked with solid and dotted slashes in Figure 7.

根据稳定性分析结果，可知当 $m_t$=0 kg 时，前车体倾角 $\theta$ 和挖掘装置转角 $\beta_1$ 在曲线围成的椭圆区域内，前车体是稳定的；当 $m_t$=300 kg 时，前车体倾角 $\theta$ 和挖掘装置转角 $\beta_1$ 在曲线围成的区域内，前车体是稳定的；由于 $\theta$ 的范围为[-40°，40°]，$\beta_1$ 的范围为[-90°，90°]，所以实际的前车体挖掘中的稳定性应该是同一参数不同取值范围的交集，为图 7 中的斜实线和斜虚线区域。

**Influence of All the Parameters on Front Body Stability**

As per an analysis of the influence of all the parameters on front body stability based on Eq. (19) and (20), the values of $\varphi$ and $\theta$ should be located in the minimum envelope zone of $F(\theta, \varphi, e_\Delta) > 0$ when $e_\Delta \in [-1,1]$. The simulation result is presented in Figure 8.

The maximum value of roll angle $\theta$, which maintains the stability of the front body, is ± 28°, as indicated in Figure 8, when the vehicle is performing a digging task and if the value of yaw angle $\varphi$ is zero. The roll angle decreases with an increase in yaw angle. Thus, the value of the roll angle cannot reach the extreme point ±40°. When the value of the yaw angle reaches such points (lines 1 and 2 are displayed in Figure 8), roll angle value is ±18.7°. Therefore, the front body is stable when the values of roll angle $\theta$ and of yaw angle $\varphi$ are located in the region shown in Figure8; otherwise, the front body faces the risk of tipping over.

**前车体稳定性的所有参数综合影响分析**

根据公式（19）和公式（20）分析所有参数对农业铰接车前车体稳定性影响，则 $\varphi$，$\theta$ 取值为：对于任意给定的 $e_\Delta \in [-1,1]$，$\varphi$，$\theta$ 应在函数 $F(\theta, \varphi, e_\Delta) > 0$ 的最小包络区域内，计算结果如图 8 所示。

由图 8 分析结果可知，在农业铰接车在挖掘作业时，当横摆角 $\varphi$ 为 0 时，前车体保持稳定的最大侧偏角 $\theta$ 约为±28°，随着横摆角 $\varphi$ 的增大，侧偏角 $\theta$ 减小，无法达到车体设计的侧偏角极限范围±40°。当横摆角 $\varphi$ 增大到车体设计的极限位置时（图 8 中直线 1 和直线 2），侧偏角 $\theta$ 约为±18.7°。前车体侧偏角 $\theta$、横摆角 $\varphi$ 的值落在图中区域内时，前车体能保证挖掘时的稳定性，不会有倾翻风险，当落在区域外时，可能会有倾翻的风险。

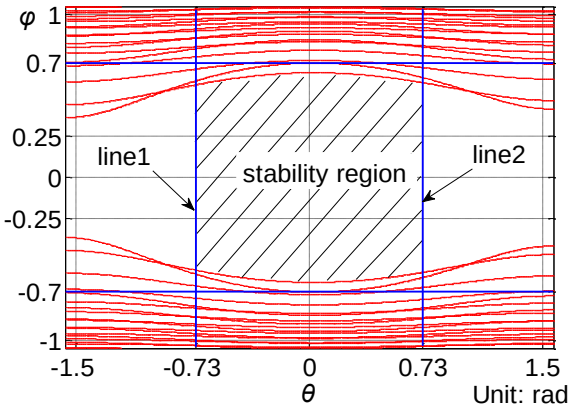


**Fig.8 -** Stable region of the front body during digging

## CONCLUSION

Agricultural articulated vehicles can adapt well to different terrains; thus, such vehicles can be used on the rough terrains of upland fields, paddy fields, and mountainous and hilly areas during agricultural production. To protect the safety of the operator, the stability of this vehicle must be determined during agricultural production. We analyze the stabilities of the front and rear bodies when the vehicle performs a digging task. The factors that affect stability during digging operations are defined as the mathematical interval. Moreover, we build a stability analysis model in combination with multi-body dynamics, the interval method, and the stability criterion to analyze vehicle stability. The region of the roll and yaw angles is determined based on the simulation result and the yaw angle keeps the front body stable. Therefore, the simulation results can be fed back to a designer to optimize vehicle design and to provide data for early rollover warning design in agricultural production.

## ACKNOWLEDGEMENT

This work was supported by the National Natural Science Foundation of China (Grant No. 51405187).

## REFERENCES

[1]. Ahmadi. (2011) - *Dynamics of tractor lateral overturn on slopes under the influence of position disturbances*. Journal of Terramechanics, Vol.48, pp.339-346;
[2]. Batista M., Perkovic M., (2014) - *A simple static analysis of moving road vehicle under crosswind*, Journal of Wind Engineering and Industrial Aerodynamics, Vol. 128, pp.105-113;
[3]. Cheng S.Y., Tsubokura M., Okada Y., Nouzawa T., Nakashima T., Doh D.H., (2013) - *Aerodynamic stability of road vehicles in dynamic pitching motion*, Journal of Wind Engineering and Industrial Aerodynamics, Vol.122, pp.146-156;
[4]. Franceschetti B., Lenain R., Rondelli V., (2014) - *Comparison between a rollover tractor dynamic model and actual lateral tests*. Biosystems Engineering, Vol.127, pp.79-91;
[5]. Frechede B., Mcintosh A., Grzebieta R., (2011) - *Characteristics of single vehicle rollover fatalities in three Australian states*, Accident Analysis & Prevention, Vol.43, No.3, pp.804-812;

## 结论

农业铰接车因为地形适应能力强，在农业工程作业中可以应用在旱地、水田、山地等地形环境恶劣的地方，但是为了保证操作者的人身安全，研究农业铰接车在农业工程作业时的稳定性是十分重要的。本文对前车体和后车体在挖掘作业过程中的稳定性进行了单独分析。在建立静态稳定性分析模型时，把影响挖掘过程中稳定性的因素设为数学区间，结合多体动力学、区间数学方法和稳定性判据，来分析挖掘过程中的车体稳定性。通过仿真计算分析得到前车体在挖掘过程中不发生倾翻的侧偏角和横摆角区域范围。通过分析挖掘过程中的稳定性计算结果，可以反馈给设计人员改进和提高农业铰接车的结构设计，同时也可以为农业工程作业中车辆的倾翻预警装置研发提供参考。

## 致谢

本工作得到中国国家自然科学基金的支持（基金号：51405187）。

## 参考文献

[1]. Ahmadi. (2011) -拖拉机在位置扰动的影响下的斜坡倾翻动力学. 地面力学, 第48卷, 339-346;
[2]. Batista M., Perkovic M., (2014) – 公路车辆在侧风下运动时的简单分析, 风力工程和工业空气动力学, 第128卷, 105-113;
[3]. Cheng S.Y., Tsubokura M., Okada Y., Nouzawa T., Nakashima T., Doh D.H., (2013) -公路车辆的动态俯仰运动中气动稳定性, 风力工程和工业空气动力学, 第122卷, 146-156;
[4]. Franceschetti B., Lenain R., Rondelli V., (2014) -一种拖拉机倾翻动态模型与实际模型的横向试验比较. 生物系统工程, 第127卷, 79-91;
[5]. Frechede B., Mcintosh A., Grzebieta R., (2011) -澳大利亚三个州的车辆倾翻死亡事故特征, 事故分析和避免, 第43卷, 第3期, 804-812;

[6]. Hesham E.S., Robert P.B., (1993) - *Using interval mathematics in cost-benefit analysis of distribution automation*. Electric Power Systems Research, Vol.27, No.2, pp.145-152;
[7]. Huang H.H., Yedavalli R.K., Guenther D.A., (2012) - *Active roll control for rollover prevention of heavy articulated vehicles with multiple-rollover-index minimization*, Vehicle System Dynamic, Vol.50, No.3, pp.471-493;
[8]. Liu B., Bulent A.K., (2013) - *Safe Driving: A mobile application for tractor rollover detection and emergency reporting.* Computers and Electronics in Agriculture, Vol. 98, pp.117-120;
[9]. Liu Z.H., (2007) - *Characterization of optimal human driver model and stability of a tractor-semitrailer vehicle system with time delay*, Mechanical Systems and Signal Processing, Vol. 21, No.5, pp. 2080-2098.
[10]. Malviya V., Mishra R., (2014) - *Development of an analytical multi-variable steady-state vehicle stability model for heavy road vehicles*. Applied Mathematical Modeling, Vol.38, No.19, pp.4756-4777;
[11]. Mccann M., (2006) - *Heavy equipment and truck-related deaths on excavation work sites*, Journal of Safety Research, Vol.37, No.5, pp.511-517;
[12]. Yoon J.Y., Cho W.K., Kang J.Y., Koo B.Y., Yi K.S., (2010) - *Design and evaluation of a unified chassis control system for rollover prevention and vehicle stability improvement on a virtual test track*. Control Engineering Practice, Vol.18, No.6, pp.585-597;
[13]. Zhang W., Liu J., Cho C., Han X., (2015) - *A hybrid parameter identification method based on Bayesian approach and interval analysis for uncertain structures*, Mechanical Systems and Signal Processing, Vol.61, pp.853-865.

[6]. Hesham E.S., Robert P.B., (1993) -区间数学法在配电自动化成本效益分析中的应用. 电力系统研究, 第127卷, 第2期, 145-152;
[7]. Huang H.H., Yedavalli R.K., Guenther D.A., (2012) –具有综合倾翻系数最小的重型铰接车倾翻主动控制, 车辆系统动力学,第50卷, 第3期, 471-493;
[8]. Liu B., Bulent A.K., (2013) -安全驾驶:移动通讯技术在拖拉机倾翻检测和意外事故报告中应用. 农业中的计算机和电子技术, 第98卷, 117-120;
[9]. Liu Z.H., (2007) –最优驾驶员模型和半挂汽车稳定性的时滞特性, 机械系统和信号处理, 第21卷, 第5期, 2080-2098;
[10]. Malviya V., Mishra R., (2014) –多变量稳态分析法分析公路卡车的车辆稳定性. 应用数学建模, 第38卷, 第19期, 4756-4777;
[11]. Mccann M., (2006) –重型设备和卡车工作中的事故死亡, 安全研究, 第37卷, 第5期, 511-517;
[12]. Yoon J.Y., Cho W.K., Kang J.Y., Koo B.Y., Yi K.S., (2010) -防倾和车辆稳定性改进的底盘综合控制系统的虚拟测试的设计和评价. 控制工程实践, 第18卷, 第6期, 585-597;
[13]. Zhang W., Liu J., Cho C., Han X., (2015) -一种基于贝叶斯方法和区间分析的不确定结构混合参数识别方法, 机械系统和信号处理, 第61卷, 853-865.

# THE STUDY OF BULK MATERIAL KINEMATICS IN A SCREW CONVEYOR-MIXER
/
# *ДОСЛІДЖЕННЯ КІНЕМАТИКИ СИПКОГО МАТЕРІАЛУ В ГВИНТОВОМУ КОНВЕЄРІ-ЗМІШУВАЧІ*

**Hewko B.M., Popovich P.V., Diachun A.Y., Lyashuk O.L., Liubachivskyi R.O.**
Ternopil Ivan Pul'uj National Technical University, Ruska str., 56, Ternopil, Ukraine
*E-mail: Oleg-lashyk@rambler.ru*

***Abstract:*** *Based on the equation of motion in a screw conveyor-mixer, the kinematics of bulk material is researched. The motion of bulk material in medium speed operation mode of screw conveyor-mixer is analyzed in details. The technique of determining the nature of loading the screw conveyor elements is developed. The analytical dependences for determining the speed change of the given bulk material volume in relation to a casing in medium speed mode of conveyor while mixing the bulk material are developed. This technique can be widely used for designing the screw transport and technological systems*

***Key words:*** screw working body, screw conveyor, auger, bulk material.

## INTRODUCTION

Nowadays screw conveyors are widely used for technological transporting and mixing the bulk materials. These conveyors are characterized by simplicity of their design. They are highly reliable, easy to use and easy to adapt when used in automated systems, and they are ecologically friendly as well [7,8,9]. To cut down power consumption and to increase the quality of mixing the bulk materials, a number of screw mixers' original designs are developed. The use of the working body depends on the peculiarities of bulk material loading the auger as well as on the peculiarities of the nature of bulk material motion, and the practicability of using the auger working body.

The advantages of using such augers include the increase of load coefficient in the area of transporting the bulk material from a tanker into auger that leads to the increase of conveyor's productivity.

*Analysis of recent research and publications*

The works of Grygoryev A.M. [2], Hewko B.M., Rohatynskyi R.M. [4, 5, 6], Hewko I.B. [3, 6] and others are dedicated to the issue of transporting and mixing different materials.

However, taking into account the diversity of technological processes and structural designs of screw transport and technological mechanisms (STTM), this issue requires further research and refinement of various parameters of theoretical and practical importance.

The objective is to develop engineering methods of computing the screw conveyor-mixer operation mode with a choice of kinematic and dynamic parameters that minimize their power consumption.

***Резюме:*** *Приведено дослідження кінематики сипкого матеріалу на основі рівнянь руху у гвинтовому конвеєрі-змішувачі. Проведено детальний аналіз руху сипкого матеріалу у середньошвидкісному режимі гвинтовому конвеєрі-змішувачі і розроблено методику встановлення характеру навантаження на елементи гвинтового конвеєра, виведено аналітичні залежності для визначення зміни швидкості руху виділеного об'єму сипкого матеріалу відносно кожуха у середньошвидкісному режимі конвеєра під час змішування сипкого матеріалу, що можна широко використовувати при проектуванні гвинтових транспортно-технологічних систем.*

***Ключові слова:*** *гвинтовий робочий орган, гвинтовий конвеєр, шнек, сипкий матеріал.*

## ПЕРЕДМОВА

Для технологічних операцій переміщення і змішування сипких матеріалів велике розповсюдження набули гвинтові конвеєри, які характеризуються простотою конструкції та, відповідно, високою надійністю, прості в користуванні та легкістю адаптування при використанні в автоматизованих системах, екологічністю використання [7,8,9]. Для зменшення енергетичних витрат і підвищення якості змішування сипких матеріалів розроблено ряд оригінальних конструкцій гвинтових змішувачів. Застосування таких шнеків потребує вирішення питань, пов'язаних з особливостями визначення навантажень на робочий орган та характеру руху сипкого матеріалу, а також доцільності їх використання.

До переваг застосування таких шнеків можна віднести збільшення коефіцієнта завантаження у зоні переміщення сипкого матеріалу із бункера на шнек, що призводить до зростання його продуктивності.

*Аналіз останніх досліджень і публікацій*

Питанням транспортування і змішування різних матеріалів присвячені праці Григор'єва А.М. [2], Гевко Б.М., Рогатинського Р.М. [4, 5, 6], Гевко І.Б. [3, 6] та інших.

Однак, враховуючи різноманітність технологічних процесів і конструктивного виконання гвинтових транспортно-технологічних механізмів (ГТТМ), потребує подальших досліджень та уточнень різних параметрів теоретичного й практичного значення.

Мета роботи є розроблення інженерної методики розрахунку середньошвидкісному режимі гвинтового конвеєра-змішувачіа з вибором кінематичних та динамічних параметрів, які мінімізують їх енергоємність.

## MATERIAL AND METHOD

To mix the bulk material effectively, the conveyor should work in the medium speed mode, this is the characteristic feature of screw conveyor-mixers (fig.1).

Based on experimental research it is proved that the material in the cross section of conveyor casing is lifted to the upper point and falls on the inner surface of the cylindrical casing under the force of gravity, repeating the cycle by the cycle.

The motion trajectories of the given bulk material volume in the cross section of conveyor casing in the fast- and medium speed modes are compared in fig. 2.

The angular parameter $\theta$ is determined by the nature of bulk material motion during the screw conveyor operation.

To determine the nature of bulk material transportation, the motion of the given bulk material volume along the coordinates xyz (fig.1) should be considered.

## МАТЕРІАЛ І МЕТОДИКА

Особливістю гвинтових конвеєрів-змішувачів (рис. 1.) є те, що для ефективного змішування сипкого матеріалу конвеєр повинен працювати у середньошвидкісному режимі.

При цьому на основі експериментальних досліджень встановлено, що матеріал у поперечному перерізі кожуха конвеєра піднімається до верхньої точки і під дією сили ваги падає на внутрішню циліндричну поверхню кожуха, повторюючи наступний цикл.

Порівняння траєкторій руху виділеного об'єму сипкого матеріалу у поперечному перерізі кожуха конвеєра при швидкісному та середньошвидкісному режимах представлено на рис. 2.

Під час роботи гвинтового конвеєра кутовий параметр $\theta$ визначається особливостями руху сипкого матеріалу.

Для встановлення характеру переміщення сипкого матеріалу розглянемо рух виділеного об'єму сипкого матеріалу в координатах xyz (рис. 1).

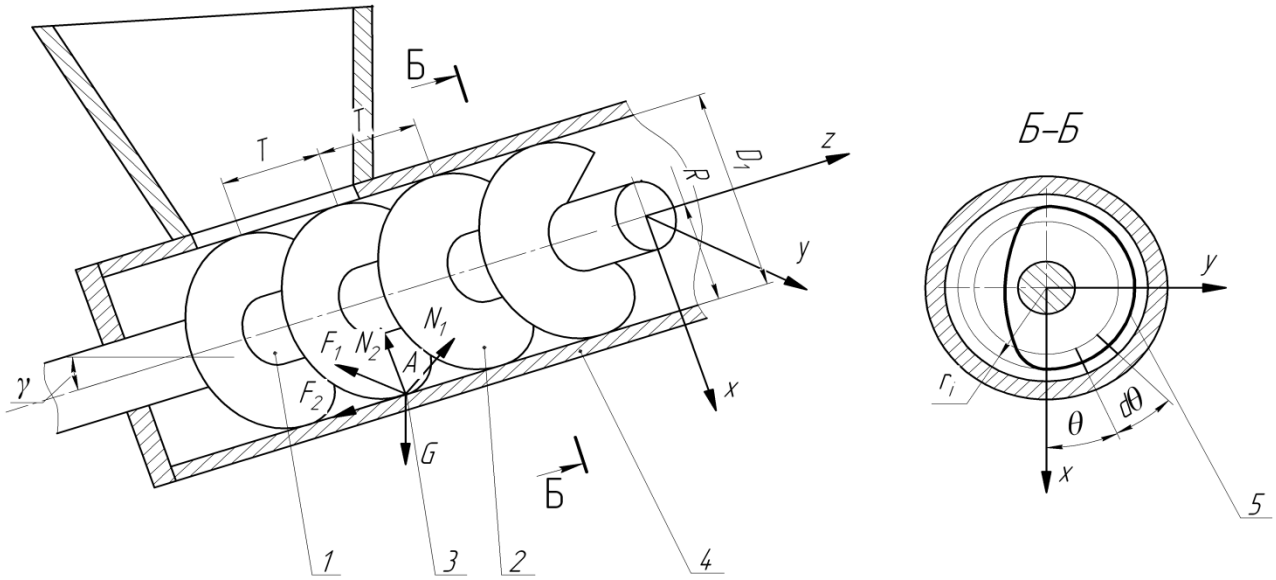


**Fig. 1.** - Computation scheme of transporting the given bulk material volume in the inclined screw conveyor:

*1 - drive shaft; 2 – screw working body; 3 – given bulk material volume; 4 – casing; 5 – trajectory of bulk material motion in the medium speed mode (mode of transporting and mixing)*

When the conveyor operates in the medium speed mode, the bulk material is mixed and transported simultaneously.

Taking into account the contact of the given bulk material volume *A* with the auger's screw surface and the cylindrical surface of the casing, the placement is determined by the radial parameter *R* and the angular parameter *θ*.

Розглянемо середньошвидкісний режим роботи конвеєра, при якому відбувається одночасне змішування та транспортування сипкого матеріалу.

Із умови контакту виділеного об'єму сипкого матеріалу *A* з гвинтовою поверхнею шнека та циліндричною поверхнею кожуха, її розміщення визначається радіальним параметром *R* і кутовим параметром *θ*.

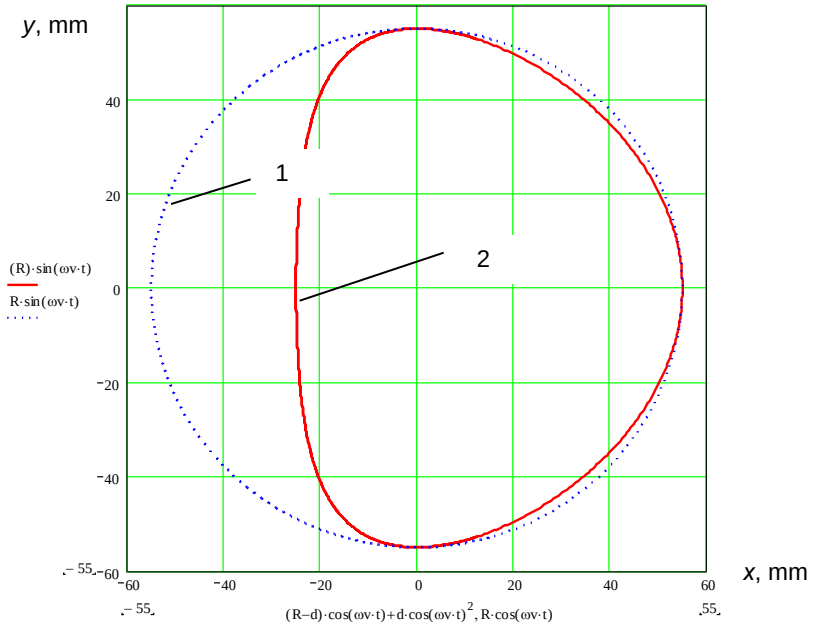


**Fig. 2.** - Motion trajectories of the given bulk material volume in cross section of casing in the fast speed 1 and medium speed 2 modes as compared

In parametric form, with sufficient approximation, the coordinates of the given bulk material volume *A* are determined by the dependences:

В параметричному вигляді, з достатньою апроксимацією, координати виділеного об'єму сипкого матеріалу *A* визначаються такими залежностями:

$$\begin{cases} x_A = (R-d)\cdot\cos\theta + d\cos^2\theta; \\ y_A = R\cdot\sin\theta; \\ z_A = \dfrac{T_0(\omega t-\theta)}{2\pi}. \end{cases} \quad (1)$$

Where:

$x_A$, $y_A$, $z_A$, – coordinates of the given bulk material volume, m; R – radial parameter of the given bulk material volume, m; $\theta$ – angular parameter of the given bulk material volume, rad; ω – angular speed of working body rotation, rad/s; t – time, s; d – parameter that determines the displacement of motion trajectory of the given bulk material volume in medium speed mode as compared with the fast speed mode, $T_0$ - step, mm.

Parameter *d* is the function of angular speed of working body rotation, the inner radius of casing, and the transported material properties. The angular speed of working body rotation increases, the parameter d decreases. The inner radius of casing increases, the parameter d increases as well. In fast speed mode d=0, this parameter can be determined with the use of parametrical dependences based on experimental research.

Motion speeds of the given bulk material volume related to the auger along the axes x, y, z:

Де:

$x_A$, $y_A$, $z_A$, – координати виділеного об'єму сипкого матеріалу, м; R – радіальний параметр виділеного об'єму сипкого матеріалу, м; θ – кутовий параметр виділеного об'єму сипкого матеріалу, рад; ω – кутова швидкість обертання шнека, рад/с; t – час, с; d – параметр, що визначає зміщення траєкторії руху виділеного об'єму сипкого матеріалу при середньошвидкісному режимі від швидкісного режиму, мм; $T_0$ - крок витків, мм.

Параметр *d* є функцією кутової швидкості обертання шнека, внутрішнього радіуса кожуха та властивостей транспортованого матеріалу, при чому із збільшенням кутової швидкості обертання шнека цей параметр зменшується, а при збільшенні внутрішнього радіуса кожуха – збільшується. При швидкохідному режимі d=0. Цей параметр можна визначити за емпіричними залежностями на основі експериментальних досліджень.

Швидкості руху виділеного об'єму сипкого матеріалу відносно шнека в напрямку осей x, y, z:

$$\begin{cases} \dot{x}_1 = \dot{x}_A - \dot{x}_{1u}; \\ \dot{y}_1 = \dot{y}_A - \dot{y}_{1u}; \\ \dot{z}_1 = \dot{z}_A - \dot{z}_{1u}, \end{cases} \quad (2)$$

where $\dot{x}_A, \dot{y}_A, \dot{z}_A,$ - projections of motion speed of the given bulk material volume on the axes of coordinates xyz, m/s.
$\dot{x}_{1u}, \dot{y}_{1u}, \dot{z}_{1u}$ – projections of motion speed of the working body on the axes of coordinates xyz, m/s.
As the casing is motionless, the motion speeds of the given bulk material volume related to the casing along the axes x, y, z equal:

де $\dot{x}_A, \dot{y}_A, \dot{z}_A,$ - проекції швидкості руху виділеного об'єму сипкого матеріалу на осі координат xyz, м/с;
$\dot{x}_{1u}, \dot{y}_{1u}, \dot{z}_{1u}$ – проекції швидкості руху шнека на осі координат xyz, м/с.
Оскільки кожух нерухомий, то швидкості руху виділеного об'єму сипкого матеріалу відносно кожуха в напрямку осей x, y, z, дорівнюють:

$$\begin{cases} \dot{x}_2 = \dot{x}_A; \\ \dot{y}_2 = \dot{y}_A; \\ \dot{z}_2 = \dot{z}_A. \end{cases} \quad (3)$$

The projections of motion speed of the given bulk material volume are defined by differentiating the equation (1) for the general case, when $R \neq const$ :

Проекції швидкості руху виділеного об'єму сипкого матеріалу знаходимо, диференціюючи рівняння (1) для загального випадку, коли $R \neq const$ :

$$\begin{cases} \dot{x}_A = \dfrac{d(R-d)}{dt}\cos\theta - (R-d)\cdot\sin\theta\cdot\dfrac{d\theta}{dt} + \dfrac{d(d)}{dt}\cos^2\theta - 2d\cos\theta\sin\theta\dfrac{d\theta}{dt}; \\ \dot{y}_A = \dfrac{dR}{dt}\sin\theta + R\cdot\cos\theta\cdot\dfrac{d\theta}{dt}; \\ \dot{z}_A = \dfrac{T}{2\pi}\left(\omega - \dfrac{d\theta}{dt}\right). \end{cases} \quad (4)$$

Motion speed of screw working body is determined by dependences:

Швидкість руху гвинтового робочого органу визначаємо за залежностями:

$$\begin{cases} \dot{x}_{1u} = R\cdot\omega\sin\theta; \\ \dot{y}_{1u} = R\cdot\omega\cos\theta; \\ \dot{z}_{1u} = 0. \end{cases} \quad (5)$$

According to (2) and taking into account the dependences (4) and (5), we develop the formulas:

Згідно з (2), враховуючи залежності (4) і (5), знаходимо:

$$\begin{cases} \dot{x}_1 = \dfrac{d(R-d)}{dt}\cos\theta + R\cdot\sin\theta\cdot\left(\omega - \dfrac{d\theta}{dt}\right) + d\sin\theta\dfrac{d\theta}{dt} + \dfrac{d(d)}{dt}\cos^2\theta - 2d\cos\theta\sin\theta\dfrac{d\theta}{dt}; \\ \dot{y}_1 = \dfrac{dR}{dt}\sin\theta - R\cdot\cos\theta\cdot\left(\omega - \dfrac{d\theta}{dt}\right); \\ \dot{z}_1 = \dfrac{T_0}{2\pi}\left(\omega - \dfrac{d\theta}{dt}\right). \end{cases} \quad (6)$$

The modules of motion speed of the given bulk material volume are determined by formulas:

Модулі швидкості руху виділеного об'єму сипкого матеріалу визначаємо за формулами:

$$\left|\dot{s}_1\right| = \sqrt{\dot{x}_1^2 + \dot{y}_1^2 + \dot{z}_1^2} \tag{7}$$

$$\left|\dot{s}_2\right| = \sqrt{\dot{x}_A^2 + \dot{y}_A^2 + \dot{z}_A^2}\ . \tag{8}$$

Inserting the equations (4) and (6) into (7) and (8), and hypothesizing that the casing has a cylindrical shape with R = const, d = const, after the cuts, we get the formulas:

Підставляючи рівняння (4) і (6) у (7) і (8), приймаючи допущення, що жолоб має циліндричну форму, при цьому R=const, d=const, після скорочень, отримаємо:

$$\left|\dot{s}_1\right| = \sqrt{\left(R^2 + \frac{T_0^2}{4\pi^2}\right)\left(\omega - \frac{d\theta}{dt}\right)^2 + 2Rd\sin^2\theta\left(\omega - \frac{d\theta}{dt}\right)\frac{d\theta}{dt}(1-2\cos\theta) + d^2\sin^2\theta\left(\frac{d\theta}{dt}\right)^2(1-2\cos\theta)^2} \tag{9}$$

$$\left|\dot{s}_2\right| = \sqrt{R^2\left(\frac{d\theta}{dt}\right)^2 + \frac{T_0^2}{4\pi^2}\left(\omega - \frac{d\theta}{dt}\right)^2 + 2Rd\sin^2\theta\left(\frac{d\theta}{dt}\right)^2(1-2\cos\theta) + d^2\sin^2\theta\left(\frac{d\theta}{dt}\right)^2(1-2\cos\theta)^2} \tag{10}$$

The acceleration of the given bulk material volume is determined by differentiating the equation (6) when R=const; d=const.

Прискорення виділеного об'єму сипкого матеріалу визначаємо, диференціюючи рівняння (6) при R=const; d=const.

$$\begin{cases} \ddot{x} = R\cos\theta\dfrac{d\theta}{dt}\left(\omega - \dfrac{d\theta}{dt}\right) - R\sin\theta\dfrac{d^2\theta}{dt^2} + d\cos\theta\dfrac{d^2\theta}{dt^2} + d\sin\theta\dfrac{d^2\theta}{dt^2} + \\ +2d\left(\sin^2(\theta)\dfrac{d^2\theta}{dt^2} - \cos^2(\theta)\dfrac{d^2\theta}{dt^2} - 2\cos\theta\sin\theta\dfrac{d^2\theta}{dt^2}\right); \\ \ddot{y} = R\sin\theta\dfrac{d\theta}{dt}\left(\omega - \dfrac{d\theta}{dt}\right) + R\cos\theta\dfrac{d^2\theta}{dt^2}; \\ \ddot{z} = -\dfrac{T_0}{2\pi}\dfrac{d^2\theta}{dt^2}. \end{cases} \tag{11}$$

**RESULTS**

The numerical and experimental research as well as the research presented in the work [8] prove that the stable mode of transportation is set regardless of the initial conditions of transportation after the passage of transitional mode zone.

The stable mode of transportation in medium speed mode of conveyor (fig.3) should be considered, In this mode the bulk material is transported along the complex

**РЕЗУЛЬТАТИ**

Результати числових та експериментальних досліджень, а також досліджень, представлених в роботі [8] свідчать, що незалежно від початкових умов транспортування після проходження зони перехідного режиму встановлюється стабільний режим транспортування.

Розглянемо стабільний режим транспортування у середньошвидкісному конвеєрі (рис. 3), в якому сипкий матеріал рухається по складній гвинтовій

screw trajectory; and when the bulk material is lifted to the upper point, the following conditions are actual: $\frac{d\theta}{dt} = const = \omega_в$ , $\frac{d^2\theta}{dt^2} = 0$ , $\frac{dR}{dt} = 0$ , $R = const$ , $\frac{d(d)}{dt} = 0$ , $d = const$ , where $\omega_в$ - angular speed of working body rotation, rad/s.

траєкторії і для якого при підніманні вантажу до верхньої точки дійсні умови: $\frac{d\theta}{dt} = const = \omega_в$ , $\frac{d^2\theta}{dt^2} = 0$ , $\frac{dR}{dt} = 0$ , $R = const$ , $\frac{d(d)}{dt} = 0$ , $d = const$ , де $\omega_в$ - кутова швидкість обертання сипкого матеріалу, рад/с.

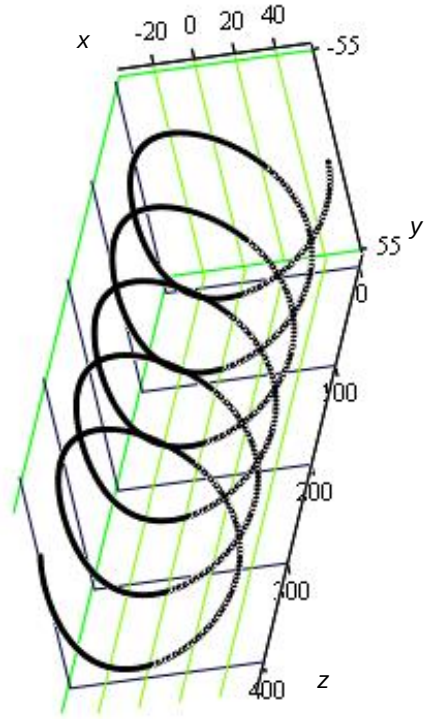


**Fig. 3.** - Motion trajectory of the given bulk material volume in medium speed mode of conveyor R=55 mm, ω=15 rad/s.

Under the acceptable conditions from (6), the projections of motion speed of the given bulk material volume related to the auger on the axis of coordinate system xyz can be developed

При прийнятих умовах з (6) знайдемо проекції швидкості руху виділеного об'єму сипкого матеріалу відносно шнека на осі системи координат xyz

$$\begin{cases} \dot{x}_1 = R \cdot \sin(\omega_в t) \cdot (\omega - \omega_в) + d \sin(\omega_в t)\omega_в - 2d \cos(\omega_в t)\sin(\omega_в t)\omega_в; \\ \dot{y}_1 = -R \cdot \cos(\omega_в t) \cdot (\omega - \omega_в); \\ \dot{z}_1 = \frac{T_0}{2\pi}(\omega - \omega_в). \end{cases} \quad (12)$$

Projections of motion speed of the given bulk material volume related to the casing on the axis of coordinate system xyz:

Проекції швидкості руху виділеного об'єму сипкого матеріалу відносно кожуха на осі системи координат xyz:

$$\begin{cases} \dot{x}_2 = (R - d) \cdot \sin(\omega_в t) \cdot \omega_в - 2d \cos(\omega_в t)\sin(\omega_в t)\omega_в; \\ \dot{y}_2 = R \cdot \cos(\omega_в t) \cdot \omega_в; \\ \dot{z}_2 = \frac{T}{2\pi}(\omega - \omega_в). \end{cases} \quad (13)$$

Modules of motion speed of the given bulk material volume are determined by formulas:

Модулі швидкості руху виділеного об'єму сипкого матеріалу визначаємо за виразами:

$$\left|\dot{s}_1\right| = \sqrt{\left(R^2 + \frac{T_0^2}{4\pi^2}\right)\left(\omega - \omega_в\right)^2 + 2Rd\sin^2(\omega_в)\left(\omega - \omega_в\right)\omega_в(1-2\cos(\omega_в)) + d^2\sin^2(\omega_в)\left(\omega_в\right)^2(1-2\cos(\omega_в))^2} \quad (14)$$

$$\left|\dot{s}_2\right| = \sqrt{R^2\left(\omega_в\right)^2 + \frac{T_0^2}{4\pi^2}\left(\omega - \omega_в\right)^2 + 2Rd\sin^2\left(\omega_в\right)\left(\omega_в\right)^2(1-2\cos\left(\omega_в\right)) + d^2\sin^2\left(\omega_в\right)\left(\omega_в\right)^2(1-2\cos\left(\omega_в\right))^2} \quad (15)$$

Based on the formula (15), the graphics of changing the motion speed of the given bulk material volume in time related to the casing in medium speed mode of conveyor (fig. 4) are developed:

На основі формули (15) будовані графіки зміни швидкості руху виділеного об'єму сипкого матеріалу відносно кожуха у сердньошвидкісному режимі конвеєра в часі (рис. 4)

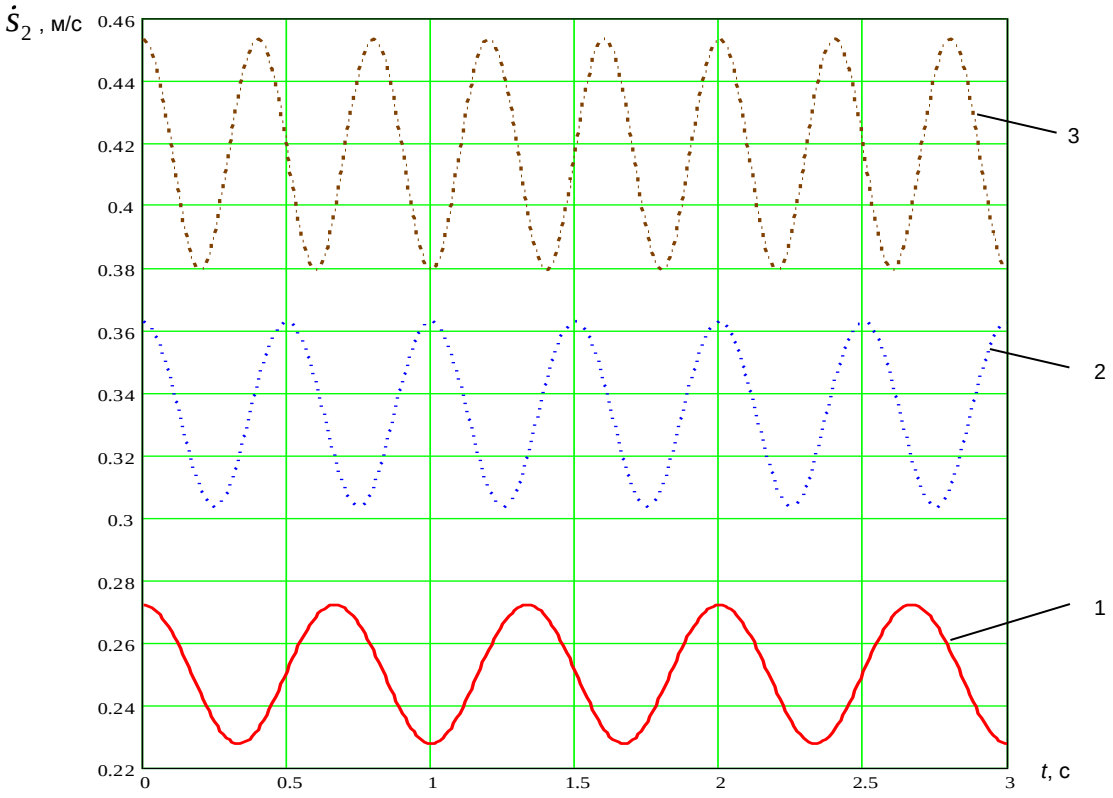


**Fig. 4**. - Graphics of changing the motion speed of the given bulk material volume in time related to the casing in medium speed mode of conveyor *R*=0,055m, T0=0,11m: 1 - n=90rpm; 2 - n=120rpm; 3 - n=150rpm

Acceleration of the given bulk material volume is determined by equations:

Прискорення виділеного об'єму сипкого матеріалу визначаємо за рівняннями:

$$\begin{cases} \ddot{x} = R\omega_в\cos\left(\omega_в t\right)\left(\omega - \omega_в\right); \\ \ddot{y} = R\omega_в\sin\left(\omega_в t\right)\left(\omega - \omega_в\right); \\ \ddot{z} = 0. \end{cases} \quad (16)$$

Based on the graphics in Fig. 4 we conclude that the speeds of bulk material transportation periodically change when the screw conveyor in medium speed mode are used. This fact intensifies the process of mixing.

**CONCLUSIONS**

1. The engineering technique of determining the nature of loading on the elements in medium speed mode of screw conveyor, on the casing and the screw working body in particular is developed. The speeds of bulk material transportation periodically change when the augers with axis motion are used. This fact improves the process of mixing the bulk materials.
2. The analytical dependences to determine the parameters during transportation of the given bulk material are developed. These dependences can be widely used in designing the screw transport and technological systems.

**REFERENCES**

[1]. Aleksandrov M. P., (1974) – *Lifting and transport machines/ Mechanical engineering*, – 503 p., Moscow;
[2]. Grigoryev A.M., (1972) – *Screw conveyers. Mechanical engineering* – p.286, Moscow;
[3]. Hewko I. (2011) – *Model of loading on the screw working bodies*, Bulletin TNTU. –V.16, № 1. – pp.69-77., Ternopil;
[4]. Hewko B. M., (1989) – *Screw falling mechanisms of agricultural machinery,* Higher school,– p.176, Lviv;
[5]. Rohatynskyi R. M., (1997) – *Mechanical and technological backgrounds of interaction of screw working bodies with agricultural raw materials: the thesis of Doctor of Sciences (Engineering) 05.20.01, 05.05.05* / Rohatynskyi Roman Mykhailovych. – p.502, Kyiv;
[6]. Rohatynskyi P.M., Hewko I.B., Diachun A.Y., (2014) - *Scientific and applied backgrounds of creating the screw transport and technological mechanisms* –TNTU– p.278, Ternopil;
[7]. Volkov R .A., Gnutov A. N., Diachkov V. K. et al - (1984), *Conveyors: Guide – under the editionship of Y.A. Perten.* – Mechanical engineering– p.367, Leningrad;
[8]. *** All Union State Standards, (1980) - Screw conveyors for feedstuff. Main parameters– AUSS 23976 – 80 – M.: Standards publisher p.19. - (National standards of Ukraine);
[9]. *** All Union State Standards Augers for agricultural machinery (1973) – AUSS 2705 - 73. – Standards publisher p.16 - (National standards of Ukraine).

На основі графіків рис. 4 можна зробити висновки, що при застосуванні гвинтових конвеєрів на середньошвидкісних режимах відбувається періодична зміна швидкості переміщення сипкого матеріалу, що сприяє інтенсифікації процесу змішування.

**ВИСНОВОК**

1. Розроблено інженерну методику встановлення характеру навантаження на елементи на середньошвидкісному режимі гвинтовому конвеєрі: на кожух та на гвинтовий робочий орган. Встановлено, що при застосуванні шнеків з осьовим рухом відбувається коливання швидкості транспортування, що покращує умови змішування сипких матеріалів.
2. Виведено аналітичні залежності для визначення параметрів під час переміщення виділеного об'єму сипкого матеріалу, що можна широко використовувати при проектуванні гвинтових транспортно-технологічних систем.

**БІБЛІОГРАФІЯ**

[1]. Александров М. П., (1974) – *Подъемно-транспортные машины*. Машиностроение,– 503 с., Москва;
[2]. Григорьев А. М. (1972) – *Винтовые конвейеры.* Машиностроение, – 184 с., Москва;
[3]. Гевко І. (2011) – *Моделювання характеру навантаження на гвинтові робочі органи. Вісник ТНТУ*– Т. 16, № 1. – С. 69-77., Тернопіль;
[4]. Гевко Б.М., Рогатынский Р.М. (1989) - *Винтовые подающие механизмы сельскохозяйственных машин.* Выща школа, – 175 с., Львов;
[5]. Рогатинський Р. М. (1997) – *Механіко-технологічні основи взаємодії шнекових робочих органів з сировиною сільськогосподарського виробництва : дис. докт. техн. наук* : 05.20.01, 05.05.05 / Рогатинський Роман Михайлович. – 502с., Київ.;
[6]. Рогатинський Р.М., Гевко І.Б., Дячун А.Є. (2014) *Науково-прикладні основи створення гвинтових транспортно-технологічних механізмів* –ТНТУ імені Івана Пулюя,– 278 с., Тернопіль;
[7]. Волков Р .А., Гнутов А. Н., Дьячков В .К. и др. - (1984); *Конвейеры: Справочник–под общ. ред. Ю.А. Пертена*. Машиностроение,– 367 с., Ленінград.
[8]. ГОСТ *Конвейеры винтовые для кормов*, (1980) – ГОСТ 23976-80 – М.: Изд-во стандартов 19 с. - (Національні стандарти України);
[9]. ГОСТ Шнеки для сельскохозяйственных машин (1973) – ГОСТ 2705 - 73. Изд-во стандартов 16с. - (Національні стандарти України).

# STUDY ON RESISTANCE AND STRUCTURE OPTIMIZATION OF TREE TRUNK INJECTOR'S NEEDLE HEAD
# /
# 注干机针头的进针阻力和结构优化研究

**Assoc. Prof. Shang Qingqing[1)], Stud. Jiang Tiantian[1)], Prof. Ph.D. Yin Tongming[2)]**
[1)]College of Electronic and Mechanical Engineering, Nanjing Forestry University
[2)] College of Forestry, Nanjing Forestry University
*Tel: +8613813990580; Email: qqshnfu@126.com*

***Abstract:*** *The paper optimizes the design for the needle head by mechanical analysis, the experiments of the needle head, structural improvements. The purpose is to design the best structure of the needle head, reduce the trunk fibre squeezed by the outer surface of the needle head. Extrusion capacity just is the thickness of the needle head's wall, which decreases splitting of wood fibres, thus ensuring the sealing effect and improving the injection efficiency of the trunk injector. According to the theory and experiments, it is obtained the range of the needle head's best size: the outer diameter is 6-8 mm, the thickness of the wall is 0.5-1mm. There are some relationships between the resistance and sizes of the needle heads. If the head needle's outer diameter is same, the larger the needle head's aperture is, the smaller the resistance of the needle head entering the trunk is. If the thickness of the wall is the same, the larger the needle head's outer diameter is, the larger the needle head's aperture is, the larger the resistance of the needle head entering the trunk is. Comparing the new needle head with the old needle head, the resistance of the needle head has been reduced. It can enhance strength and avoid fracture. It makes the wood core exist in the grooves of both sides without squeezing trunks and has good sealing effect.*

***Keywords:*** *Tree trunk injector; Needle head; Resistance; Structure optimization*

***摘要：****通过力学分析、进针实验、结构改进，对针头进行优化设计，设计出最优的针头结构形式，减少针头外表面对树干纤维的挤压，挤压量仅为针头壁厚，减小了木材纤维胀裂，从而保证了密封效果，提高注干机注射效率。理论和实验得出最佳针头尺寸大小范围：直径6-8mm,孔的壁厚0.5-1mm。其进针阻力与尺寸的关系为：外径相同时，针头孔径越大，进针阻力越小；当壁厚相同时，针头外径越大，则孔径也越大，进针阻力越大。优化的新针头同旧针头相比，进针阻力有所减小，强度增强，不易断裂。使木芯能够存在两侧槽中，不会挤压树干，密封效果好。*

***关键词：****注干机；针头；进针阻力；结构优化*

## INTRODUCTION

Tree trunk injection is a new method of preventing and controlling fruit tree disease and eliminate pests [1]. It is one of the best ways to control the trees insect. It plays an active role in reducing pollution of the environment [3], maintaining ecological balance, and increasing forest coverage. Now the research of tree trunk injector is becoming more and more widely.

And needle head is one of the most critical parts of tree trunk injector, whether the type of manual or mechanical power tree trunk injector is, the performance of needle head directly affecting the efficiency of the injection [4]. So the study of needle head has a vital significance.

This paper main research content includes: first, doing mechanical analysis for the needle head; Second, measuring the resistance of the needle head by the experiment for determining the range of the size of the needle head that has a smaller resistance; Third, optimizing the design of the structure of the needle head [2]; Fourth, doing experimental verification of the needle head. The purpose is to select the optimal size and design the best structure of needle head in order to improve the efficiency of tree trunk injector [5].

## 引言

树木注射施药技术是一种新型的林木果树病虫害防治技术 [1]，其作为防治树木生虫的最佳方法之一，在减少环境污染、保持生态平衡、提高森林覆盖率方面起着积极的作用 [3]。目前，对于注干机的研究也越来越广泛，而针头作为注干机最为关键的部件之一，无论是人力手动型还是机械动力型的注干机，针头的性能都将直接影响注射效率 [4]。因此，对注干机针头进行研究具有重要的意义。

本文主要研究的内容有：一是对针头进行力学分析；二是通过实验测出进退针阻力，确定进针阻力较小的针头尺寸范围；三是对针头结构进行优化设计 [2]；四是进行实验验证。目的是选择最优的针头尺寸大小和合理的结构形式，以提高针头强度和密封效果，提高树干注射机的注射效率[5]。

## MATERIALS AND METHOD

### *Characteristics of A New Type 0f Needle Head*

The paper introduces a new type of needle head we studied, as show in Fig.1. Its structure is a hollow cylinder [6]. The forepart of the needle head is ring-shaped knife, a slot is in the middle, the slot is used for medicine and scrape outlet, pontes which connects to the needle head seat is at the back, equipped with O-ring seal, a little wider cylinder lie between the pontes and cylinder-shaped seal. During the progress of entering the trunk, the needle head is pushed by external force, the ring-shaped knife with a hole cuts off the wood fibre and keeps it in the hole and slot(to be pushed out by new wooden meal in the next injection). When the needle head enter the trunk and it forms a good seal with trunk, we stop pressing needle head and start to inject drugs, then the drugs through the medicine hole inflow into the trunk. When injecting drugs is over, the needle head will be pulled out by external forces, then a drug infusion process is over. Due to using this structure of needle head, amount of extrusion is very small, can't result in cracks, it has a good performance of sealing and increase the injection volume [7].

## 材料和方法

### *注干施药和针头概况*

此次我们研究的注干机针头结构如图 1 所示，其结构为中空圆柱形 [6]。针头的前部为圆环形刀刃，中前部侧面开槽，槽的作用为出药孔和出屑孔，中部结构为圆柱形密封部分，中后部直径较大部分为二次密封的圆柱面，后部为与针头座连接部分，设有 O 形圈密封槽。进退针过程是由外力将针头压入树干，针头在压入树干的过程中，由前面的中孔环形刀刃将木材纤维切断，并保留在中间孔内(由下次注射时新的木芯将其顶出)，当针头中后部直径较大部分挤入树干中与树干形成较好的密封时，停止挤压针头，开始注药，则药液通过出药孔流入树干里。注药结束，由外力将针头往拉出，则一次注药过程结束。由于采用这种结构的针头进针是由针头外表面挤压树干，挤压量为针头壁厚，因此大大地缩小了挤压量，不容易引起木材纤维胀裂，从而保证了密封效果，提高注药量 [7]。

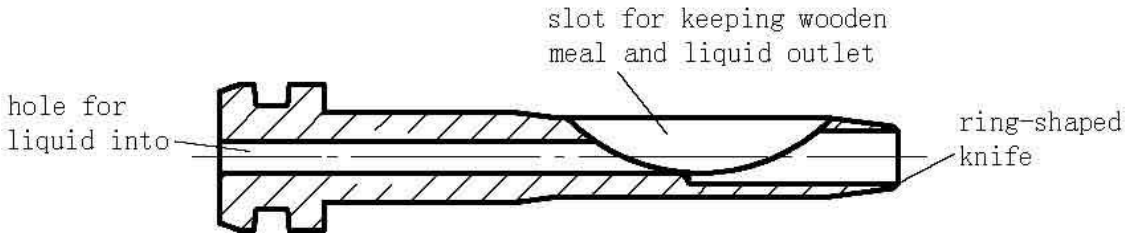


**Fig.1 –** The needle head of trunk injector

### *Stress Analysis of the New Type of Needle Head*

As show in Fig.2, the force of the needle head can be divided into two parts: the process of the needle head entering the trunk and the needle head exiting from the trunk.

### *针头受力分析*

针头的受力情况可以分为两部分：进针过程和退针过程，如图 2 所示：

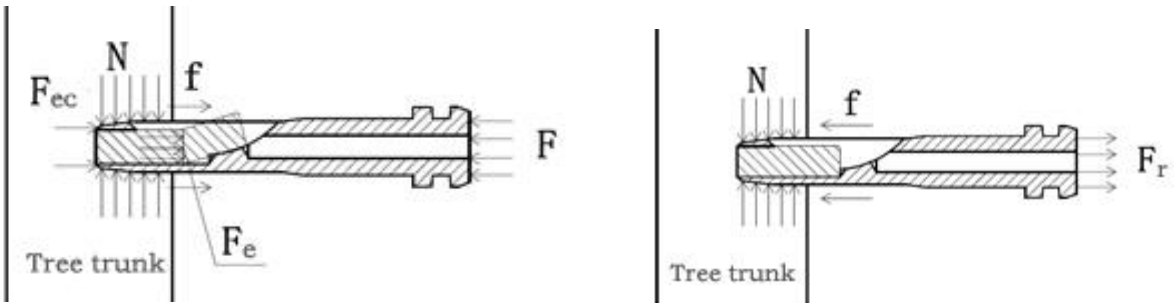


(a) (b)

**Fig.2** - Stress analysis for the process of the needle head
(a) the needle head entering the trunk (b) the needle head exiting from the trunk

### *A. The Process of Needle Head into the Trunk*

The needle head squeezes the trunk by external forces. Due to the forepart of the needle head which is ring-shaped knife, the needle head is by cutting wood fibre into the trunk and not by brute force. This force by the needle head cutting wood fibre is named extrusion and cutting force, called Fec. The wood fibre will be left

### *A.进针过程*

针头在外力的作用下开始挤入树干中，由于针头头部为圆形刀刃，因此针头是靠切断木材纤维进入树干而不是靠蛮力挤压，这种由针头切断木材纤维所需的力称

in the hole and it will be squeezed out by the new wood fibre next time. At the same time, because the trunk can produces positive pressure to the needle head's surface, and with the needle head sliding constantly, it produces sliding friction force between the needle head and the trunk. The force is called f. This is the first time that the needle head enters the trunk.
The second, third time, the needle head bears the force except for extrusion and cutting force and sliding friction force. Because there is no cleaning the wood fibre remains in the needle head's hole（referred to as wood core）, Then it will produce the extrusion with the new wood core to the old wood core, and it is named extrusion force, expressed in Fe.

***B. The Process of Needle Head Exiting from the Trunk***

When needle head exits from the trunk by the action of external force the only remaining force is sliding friction force f between the needle head and the trunk. Therefore, the resistance of the needle head exiting from the trunk is only related to sliding friction force.

Above all, the resistance of the needle head entering the trunk and exiting from the trunk should be considered in two different conditions, respectively for the first time the needle head entering the trunk (excluding wood cores) and the second, third…time the needle head entering the trunk (including wood cores). That is to say:

The resistance into the trunk excluding wood cores is: *F1=f+Fec*

The resistance into the trunk including wood cores is: *F2=f+Fec+Fe*

The resistance exiting from the trunk is: *Fr1=Fr2=f*

***C .Experiment For Measuring The Resistance***

The purpose of this experiment is to measure the resistance data of the needle head entering the trunk and determine the appropriate range of the needle head's size by comparing the data [8]. The specifications of the needle head list in table 1, putting the 8 kinds of size of the needle heads code as 1, 2, 3... 8. Then we connect the experimental equipment and install the needle head in the tree trunk injector. At the same time, we put the tree trunk injector clamping on the poplar and intensify it, process power and begin to do experiments for the needle head entering the trunk.

We take the eight kinds of the needle heads to do experiments for the needle head entering the trunk for four objects, each object performing a group of experiments, being a total of four groups of experiments and each group having eight kinds of the needle heads; each needle head performs experiments for five times. We do image processing for the data collected by using Matlab. In this way, we can intuitively observe the difference between the resistances of two needle heads.

为挤切力，用 Fec 表示。被切断的木材纤维会遗留在针头孔内，由下次进针时新的木芯将其顶出。当针头挤入树干时，因树干会对针头表面产生正压力，并随着针头不断前进产生了针头与木材之间的滑动摩擦力，用 f 表示。这是针头第一次进针。

第二、三…次进针时，针头除了受到挤切力和滑动摩擦力外，由于没有清除遗留在针头孔内的木材纤维（简称木芯），进针产生的新木芯会对旧木芯的挤压，即新木芯将前一个木芯顶出的挤压力，用 Fe 表示。

***B.退针过程***

针头在退针时，针头在外力的作用下逐渐退出树干，只剩下针头与木材之间的滑动摩擦力 f。因此，退针阻力只与滑动摩擦力 f 有关。

综上所述，针头进退针阻力分两种情况考虑，分别为第一次进退针受力（不含木芯）情况和第二、三…次进退针（含木芯）时受力情况，即：

不含木芯的进针阻力:F1=f+Fec

含木芯的进针阻力 : F2=f+Fec+Fe

退针阻力 : Fr1=Fr2=f

***C.测进退针头阻力实验***

本次实验的目的是测出进针阻力的数值，并通过数据对比确定合适的针头尺寸范围 [8]。针头规格如表 1 所示，将这 8 种规格尺寸的针头，依次编号为 1、2、3…8。

将实验器材进行连接，并将 1 号针头安装在注干机上，同时将注干机装夹在杨树上并加紧,接通电源，则开始进针实验。

将 8 种针头一一进行进针实验，4 个对象，每一个对象进行 1 组实验，我们共进行了 4 组实验，每组 8 种针头，每种针头进行 5 次进退针实验。将实验采集的数据通过用 Matlab 对其进行做图处理，可以直观清楚地观察出两两针头之间进针阻力的差异。

**Table 1**

**The 8 kinds of the needle heads' main dimensions**

| Code | The outside diameter (mm) | The aperture (mm) | The outside diameter of sealing surface (mm) |
|---|---|---|---|
| 1 | 7.8 | 6.0 | 8.6 |
| 2 | 7.8 | 5.0 | 8.6 |
| 3 | 7.8 | 4.0 | 8.6 |
| 4 | 6.8 | 4.5 | 7.6 |
| 5 | 6.8 | 4.0 | 7.6 |
| 6 | 6.8 | 3.0 | 7.6 |
| 7 | 5.8 | 3.5 | 6.6 |
| 8 | 5.8 | 3.0 | 6.6 |

Analyzing and comparing the four groups of experiment graphics, because the conclusions are consistent, now we choose one group to analyze, here the choice being the fourth group.

## RESULTS AND ANALYSIS

### *A. The Comparison For Two States of the Same Needle Heads*

The two states of the same needle heads refer to excluding wood cores and including wood cores. The first time that the needle head enters the trunk it expresses the state of the excluding wood cores and the second, third…time that including wood cores. As shown in figure 3, each graph with A - A expressed, the first number A expresses No. X needle head, the second number A expresses the time the needle head entering the trunk. The curves show the resistance of the first time that the needle head enters the trunk is the least of the three curves. This result is in accordance with the result concluded by theoretical analysis. When X is in the range of 0 to 32 mm, any point on the X axis in the three curves is corresponding to the value of Y which expresses the resistance of the needle head in this depth of the needle head entering the trunk. And the value between the curve of the first time and the second, third…time expresses the extrusion force. In addition, the resistance of the needle head exiting from the trunk is less than the resistance of the needle head entering the trunk, namely below 0 line. It also conforms to the theoretical analysis.

分析比较 4 组实验，由于 4 组实验图形得出的结论基本一致，现选其中一组进行分析说明，这里选择的是第四组实验。

## 结果和分析

### *A.同种针头两种状态的比较*

同种针头两种状态指的是：不含木芯与含木芯两种状态。第一次进退针表示不含木芯的状态，第二、三次进退针表示含木芯的状态。如图 3 所示，每一个曲线图用 A-A 表示，前一个数字 A 表示 X 号针头，后一个数字 A 表示第几次进退针。曲线图中显示第一次进针阻力是三个曲线中最小的，这个结果是符合理论分析中得出的结论的。X 在 0-32mm 区间时，X 轴上任意一点分别在三条曲线上对应的 Y 值为此进针深度下的进针阻力，且第一次进针曲线分别与第二、三次进针曲线 Y 值差表示就是挤压力 F 挤。另外，0 线以下的退针阻力与进针阻力相比明显较小，这同样符合理论分析的结论。

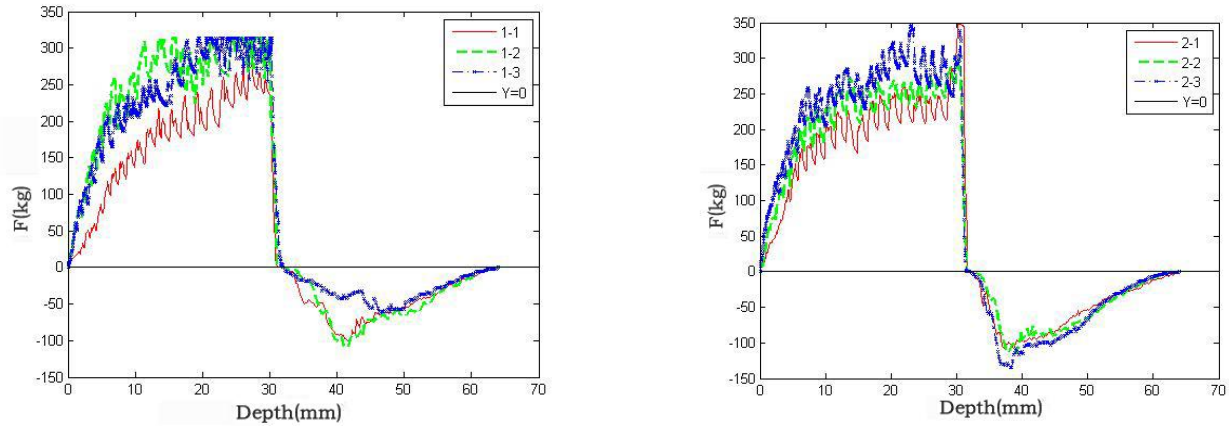


（a） （b）

**Fig. 3-** The comparison chart for No.1 and No.2 the needle head of the fourth group of experiments

### *B. The Comparison For the Resistance of the Different Needle Heads*

#### *(1) The Comparison of the Same Outer Diameter*

There are three groups of the same outer diameter, respectively for outer diameter of No.1, No.2 and No.3 needle heads are 7.8 mm, the outer diameter of No.4, No.5 and No.6 needle heads are 6.8mm, the outer diameter of No.7 and No. 8 needle heads are 5.8mm. As shown in figure 4, comparing the resistance of the three groups of the needle heads respectively, we get the conclusion for *F1<F2<F3, F4<F5<F6, F7<F8* (F1 expresses the resistance of No.1 needle head entering the trunk). Namely when the outer diameter is the same, the larger the aperture is, the thinner the thickness of the wall is, the smaller the resistance of the needle head entering the trunk is. This is because under the condition of remaining the outer diameter unchanged

### *B.不同种针头的进针阻力比较*

#### *（1）相同外径比较*

相同外径的针头有三组，分别是外径为 7.8mm 的 1、2、3 号针头，外径为 6.8mm 的 4、5、6 号针头，外径为 5.8mm 的 7、8 号针头。如图 4 所示，分别对这三组针头的进针阻力比较，结论为 F1〈F2〈F3，F4〈F5〈F6，F7〈F8〈F1 表示 1 号针头的进退针阻力）。即当外径相同时，针头孔径越大，则壁越薄，进针阻力越小。这是因为在针头外径不变、孔径变大的情况下，摩

and the aperture get larger, though the friction force remains unchanged, the extrusion force increases, the impact is not obvious. And the extrusion and cutting force decrease with the cross-sectional area decreasing, so the resistance of the needle head entering the trunk is decreasing.

擦力大小不变，挤压力虽然有所增大，但影响不大，而挤切力因针头横截面减小而减小，故进针阻力减小。

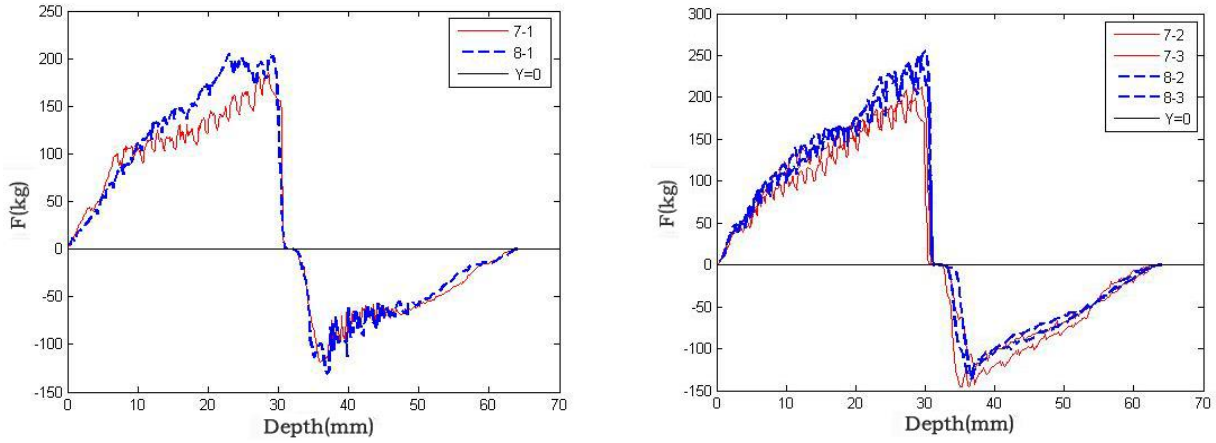


（a） （b）

**Fig. 4** -The comparison of the same outer diameter

***(2)The Comparison of the Same Thickness of the Wall***

There are three groups of the same thickness of the needle heads' wall, respectively for the thickness of the wall of No.2, No.5 and No.8 needle heads is 1.4mm, the thickness of the wall of No.3 and No.6 needle heads is 1.9mm, the thickness of the wall of No. 4 and No.7 needle heads is 1.15mm. As shown in figure 5, comparing the resistance of the three groups of the needle heads respectively, we get the conclusion for *F8<F5<F2, F6<F3, F7<F4*. Namely when the thickness of the wall is the same, the larger the outer diameter is, the larger the aperture is, the larger the resistance of the needle head entering the trunk is. Also, the differences of the needle heads' size are greater and the resistance is greater and more obvious.

***（2）相同壁厚比较***

相同壁厚的针头有三组，分别是壁厚为 1.4mm 的 2、5、8 号针头，壁厚为 1.9mm 的 3、6 号针头，壁厚为 1.15mm 的 4、7 号针头。如图 5 所示，分别对这三组针头的进针阻力比较，结论为 F8〈F5〈F2，F6〈F3，F7〈F4。即当壁厚相同时，针头外径越大，则孔径也越大，进针阻力越大。同样，针头尺寸差异越大，则进针阻力差距越大，越明显。

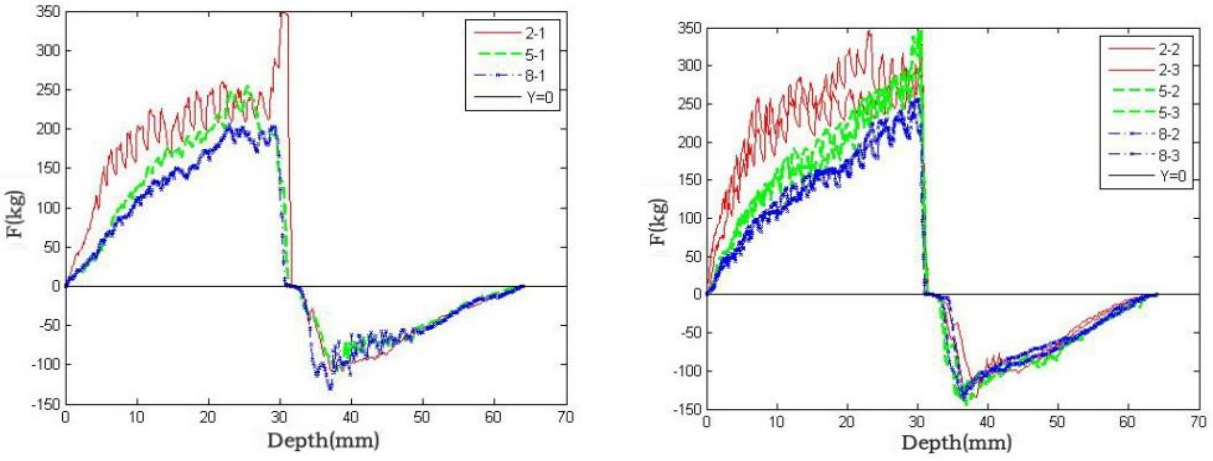


a) b)

**Fig. 5** - The comparison of the same thickness of the wall

***(3) The suitable size of needle head***

Combined with the experience of the tests and the result of the data analysis, we finally choose the suitable size for:

***（3）针头的尺寸范围***

结合现场的实验体会和数据分析的结果，最终选择的合适的尺寸规格为：

The outer diameter is 7.8 mm, the aperture is 4.5-5.0 mm.
The outer diameter is 6.8 mm, the aperture is 4.0-4.5 mm.
The outer diameter is 5.8 mm, the aperture is 3.0-3.5 mm.

***C．The Optimization Structure of the Needle Head***

The purpose of the optimization design for the needle head is to decrease the resistance, guarantee the strength of the needle and improve the efficiency of the injection [9]. Because the tests in the above paragraph have determined the size range of the needle heads, here the design is mainly to optimize the structure of the needle head. The design is shown as figure 6. The new needle head turns the original circular part into the structure that the cross-sectional area of the structure's middle part is an I-shaped sharp edge and both sides are grooves. And it leaves a short length for the structure that is a top and bottom hole, which can easily make the sharp edge cutting the wood core into two pieces and the wood core easy falls off from grooves. This structure can guarantee the strength of the needle, and can improve the extruding way of the wood core. It is as much as possible to reduce the extrusion pressure, improve the effect of sealing and the pesticide penetration.

当外径为 7.8mm 时，孔径为 4.5~5.0mm；
当外径为 6.8mm 时，孔径为 4.0~4.5mm；
当外径为 5.8mm 时，孔径为 3.0~3.5mm。

***C．针头优化结果***

针头优化设计的目的是为了减小进针阻力，保证针头强度，提高注射效率[9]。由于上述实验已经确定了合理的针头尺寸范围，故此处的优化设计主要是对针头结构进行优化。设计方案如图 6 所示，将针头原来圆弧部分改成中间横截面为工字型的尖刃、两侧为槽的结构，并留一小段长度为上下通孔，方便尖刃将被挤出的木芯切成两块，使之容易从两侧凹槽处掉落。这种结构既能保证针头强度，又能改善木芯的挤出方式，尽可能地减少的挤压力，提高密封和药液渗透效果。

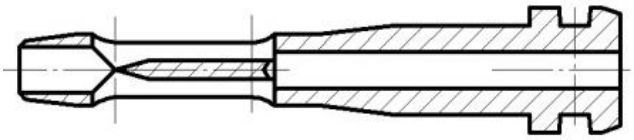

**Fig. 6**-The structure of the new needle head

***Result of Experiment for new structure***

The purpose of the experiments is to validate the resistance of the new needle head entering the trunk whether or not reduced. Here we choose two kinds of the new needle heads, specifications for that the outer diameter is 7.8 mm and the aperture is 4.5 mm, the outer diameter is 7.8 mm and the aperture is 5.0 mm. We choose an old needle head, specifications for that the outer diameter is 7.8 mm and the aperture is 5.0 mm. As shown in figure 7, we can know that in the case of excluding wood cores, the relationship between the resistance of the three needle heads is *F2 < F1< F3 (F1, F2, F3* respectively it expresses the resistance of No.1, No.2 and No.3 needle heads).

The formula *F2<F1* verifies that when the outer diameter is the same and the aperture is different, the thickness of the wall is thinner, the resistance of the needle head entering the trunk is smaller. The formula F2 < F3 clarifies that when the structure and the size of the needle heads are the same, the resistance of the new needle head entering the trunk is smaller.

Comparing the new needle head to the old needle head, the resistance of the new needle head is decreasing. But the effect is not obvious, it needs to be improved. However, the handling method of wood core for the new needle head is better. The wood cores cut into two pieces can exist on the grooves of both sides. The wood cores don't squeeze the trunk and have good sealing. What's more, the strength of the new needle head is better.

***新针头实验结果***

实验目的是验证新针头进针阻力是否有所减小。这里选择 2 种新针头，规格为外径 7.8mm、孔径 4.5mm，外径 7.8mm、孔径 5.0mm；1 种旧针头，规格为外径 7.8mm、孔径 5.0mm，分别用 1、2、3 表示。如图 7 所示，在不含木芯的情况下，这 3 种针头的进针阻力大小关系为 F2<F1<F3（F1、F2、F3 分别表示 1、2、3 号针头的进针阻力）。

F2<F1 验证了相同外径，不同孔径，壁越薄，针头进针阻力越小；

F2<F3 说明在针头外形尺寸相同的情况下，新针头进针阻力小。

新针头同旧针头相比，进针阻力有所减小，但是效果不是很明显，说明已达到进针力最低要求，但是它对木芯的处理效果则比较好，切成两段的木芯能够存在两侧槽中，不会挤压树干，密封性好，且新针头的强度也比较好。

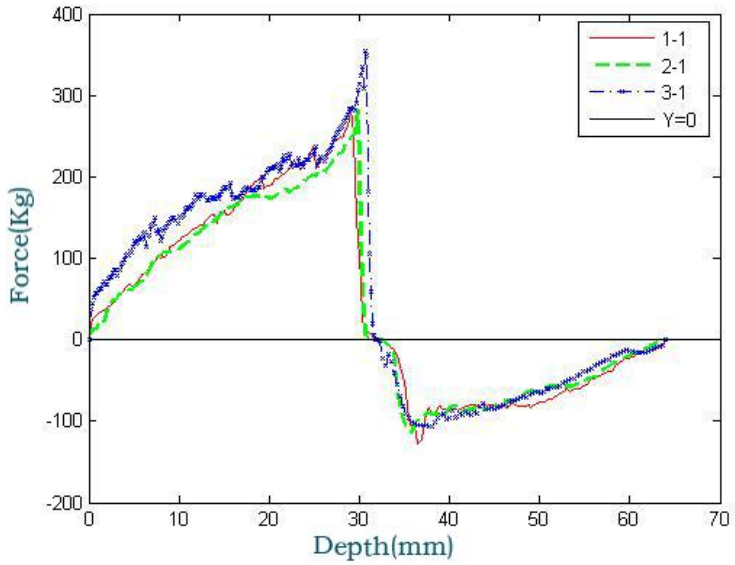


**Fig. 7-** The comparison of the three needle heads

## CONCLUSIONS

The paper optimizes the design for the needle head by mechanical analysis, experiments of the needle head, structural improvements. The purpose is to design the best structure of the needle head. It is obtained the range of the needle head's best size: the outer diameter is 6-8 mm, the thickness of the wall is 0.5-1mm. Comparing the new needle head with the old needle head, the resistance of the needle head has been reduced. But the new structure can enhance strength and avoid fracture. It makes the wood core exist in the grooves of both sides without squeezing trunks. It has good sealing effect and improves the injection efficiency of the trunk injector.

**Acknowledgement**

The work has been funded by the Special Fund for Forest Scientific Research in the Public Welfare by the state forestry administration (201304102).

## REFERENCES

[1]. Caspari HW, Green SR, Edwards WRN, (1993) - *Transpiration of well－watered and water－stressed Asian pear trees as determined by lysimeter, heatpulse and the Penm - a monteith model.* Agri and For Meter, Volume 67, pp.13-27;

[2]. De Filippis Stefano, Košel Vladimír, Dibra Donald, Decker Stefan, Köck Helmut, Irace Andrea, (2011)-*ANSYS based 3D electro-thermal simulations for the evaluation of power MOSFETs robustness.* Microelectronics Reliability, Volume 51, Issue 9-11, pp.1954-1958;

[3]. Guo Shun, Chen Jian, Li Wuyun, Guo Xiaofeng, Gao Guohua, (2011)-*The Progress and Development Trend for the Research of Tree Trunk Injection Machine.* Agricultural Mechanization Research, Volume 9, pp.245-248;

[4]. Liu Jingyuan, He Jinyi, Qi Fei. (2011)- *A Comparative Study of Pesticide Injection Devices Intended for Trees.* Forestry Machinery and Woodworking Equipment, Volume 39, Issue 1, pp.12-15;

## 结论

本文通过力学分析、进针实验、结构改进，对针头进行优化设计。目的是设计出最优的针头结构形式，并得出最佳针头尺寸大小范围：直径 6-8mm,孔的壁厚 0.5-1mm。优化的新针头同旧针头相比，进针阻力有所减小，但新结构使针头强度增强，不易断裂。使木芯能够存在两侧槽中，不会挤压树干， 密封效果好，提高注干机注射效率。

**致谢**

本文受到国家林业局林业公益性行业科研专项基金项目(201304102)资助。

## 参考文献

[1]. Caspari HW, Green SR, Edwards WRN, (1993)-*Trans－piration of well－watered and water－stressed Asian pear trees as determined by lysimeter, heatpulse and the Penm - an monteith model*. Agri and For Meter,1993,67:13-27;

[2]. De Filippis Stefano, Košel Vladimír, Dibra Donald, Decker Stefan, Köck Helmut, Irace Andrea, (2011)-*ANSYS based 3D electro-thermal simulations for the evaluation of power MOSFETs robustness.* Microelectronics Reliability, 51(9-11): 1954-1958;

[3]. 郭顺,陈建,李云伍,郭小峰,高国华. (2011)-树干注射施药机械研究进展及发展趋势[J].农机化研究,(9):245~248;

[4]. 刘景元,何树川,李瑾义,秦飞. (2011)-树木注射施药装置的比较研究[J].林业机械与木工设备, 39(1):12~15;

[5]. Otho. S, Gary. E. (2010)-*Tree Injector System:* United States Patent 5,355,619[P]. [2010－10－10].

[5]. Otho. S, Gary. E., (2010) -*Tree Injector System:* United States Patent 5,355,619 [P] [2010-10-10];
[6]. Shang Qingqing, Zhao Boguang, Zhang Yiquan, (2009)-*Study on a High Pressure and Large Capacity Tree Trunk Injector*.Journal of Nanjing Forestry University, Volume 9, Issue 5, pp. 101-104;
[7]. Shang Qingqing, Liao Kai, Liu Huan, Zhao Boguang, (2011)- *Study on Structure of Needle Head and Seal Mechanism of Tree Trunk Injection*. Proceedings 2011 International Conference on Transportation, Mechanical, and Electrical Engineering, TMEE 2011. December 16-18, Changchun, pp.813-816;
[8]. Zamora M. A. S., Escobar R.F.(2000)-*Injector size and the time of application affects uptake of tree trunk-injected solutions,* Scientia Horticulturae, Volume 84, Issue 1, pp.163-177;
[9]. Ye Lin, Wei Min Cui,Bi Feng Song.( 2012)-*Reliability Optimization Design of Spacecraft Valve Spring.* Advanced Materials Research, pp.851-857.

[6]. 商庆清,赵博光,张沂泉.(2009)-高压大容量树木注干机的研制[J].南京林业大学学报,9(5):101~104.
[7]. Shang Qingqing, Liao Kai, Liu Huan, Zhao Boguang, (2011)- *Study on Structure of Needle Head and Seal Mechanism of Tree Trunk Injection.* Proceedings 2011 International Conference on Transportation, Mechanical, and Electrical Engineering, TMEE 2011. December 16-18, Changchun, 813-816;
[8]. Zamora M. A. S., Escobar R.F., (2000)- *Injector size and the time of application affects uptake of tree trunk-injected solutions*, Scientia Horticulturae, 2000,84(1):163~177;
[9]. Ye Lin,Wei Min Cui, Bi Feng Song,( 2012)-*Reliability Optimization Design of Spacecraft Valve Spring*. Advanced Materials Research, pp.851~857.

## WRITING NORMS / *NORME DE REDACTARE*

### Article Types

Three types of manuscripts may be submitted:

**1. Regular articles:** These should describe new and carefully confirmed findings, and experimental procedures should be given in sufficient detail for others to verify the work. The length of a full paper should be the minimum required to describe and interpret the work clearly (max. 8 pages);

**2. Short Communications:** A Short Communication is suitable for recording the results of complete small investigations or giving details of new models or hypotheses, innovative methods, techniques or apparatus. The style of main sections has not necessarily to be in accordance with that of full-length papers (max. 6 pages);

**3. Reviews:** Submissions of reviews and perspectives covering topics of current interest are welcome and encouraged (max. 8 pages).

### Review Process

All manuscripts are reviewed by the 2 members of the Scientifically Review. Decisions will be made as rapidly as possible, and the journal strives to return reviewers' comments to authors in approx. 3 weeks. The editorial board will re-review manuscripts that are accepted pending revision.

**NOTE:** Submission of a manuscript implies: that the work described has not been published before (excepting as an abstract or as part of a published lecture, or thesis) that it is not under consideration for publication elsewhere.

### 1. REGULAR ARTICLES

- All portions of the manuscript must be typed *single-spaced, A4***,** top and bottom: 2 cm; left: 2 cm; right: 2 cm, font: **Arial,** size 9 pt, except the title which will be 11 pt. and explicit figures, which will be 8 pt.
- Text paper will be written in two equal columns of 8.3 cm, 0.4 cm space between them, except the title, authors and their affiliations, tables, figures, graphs and equations to be entered once.
- Text will be written in English in the left column, respectively in native language in the right column.
- The chapter titles are written Uppercase (eg: INTRODUCTION, MATERIAL AND METHODS), between chapters is left a space for 9 pt. At the beginning of each paragraph to leave a tab of 0.5 cm.
- The paper will be written in Word, "Justify" alignment;
- The paper should be transmitted by E-mail.
- There are allowed 2 papers by each first author.

**Title** should be a brief phrase describing the contents of the paper. PAPER'S TITLE will be uppercase, Bold (the title in English language) and *Bold italic (the title in native language),* center, 11 pt. Under the paper's title, after an space (enter) 9 pt., write *authors' names* (eg: Vasilescu G.). (font: 9 pt., bold) and *affiliations*, the *name of the corresponding author* (next row), (9 pt., regular). Also be passed: the phone, fax and E-mail information, for the first author of paper's (font: 8 pt., italic).
Title should be short, specific and informative. Avoid long titles; a running title of no more than 100 characters is encouraged (without spaces).

***Abstract*** should be informative and completely self-explanatory, briefly present the topic, state the scope of the experiments, indicate significant data, and point out major findings and conclusions. The Abstract should be 100 to 300 words in length. Complete sentences, active verbs, and the third person should be used, and the

### Tipuri de Articole

Trei tipuri de manuscris pot fi trimise:

**1. Articole obişnuite (normale):** acestea trebuie să descrie cercetări noi şi confirmate, iar procedurile experimentale să fie descrise pentru a putea fi verificate in detaliu, fără a leza dreptul de proprietate intelectuală. Mărimea unei lucrări trebuie să cuprindă minimul necesar pentru a descrie şi interpreta în mod clar conținutul (max.8 pagini);

**2. Comunicări scurte:** o comunicare scurtă este folosită pentru înregistrarea rezultatelor din investigații complete de dimensiuni reduse sau pentru a oferi detalii despre modele noi de ipoteze, metode inovative, tehnici sau infrastructuri. Tipul secțiunilor (capitolelor) principale nu trebuie să fie neapărat în concordanță cu articolele normale (max. 6 pagini);

**3. Sintezele:** Prezentarea unor comentarii şi perspective acoperind subiecte de interes actual sunt binevenite şi încurajate (maxim 8 pagini).

### Procesul de evaluare (recenzie)

Toate manuscrisele sunt evaluate de către 2 membri ai Comitetului Ştiințific. Deciziile vor fi luate cât mai rapid posibil şi revista va returna comentariile evaluărilor înapoi la autori în aproximativ 3 săptămâni. Conducerea editorială va reevalua manuscrisele care sunt acceptate în vederea publicării în revistă.

**Notă:** Sunt acceptate numai lucrările care nu au mai fost publicate anterior. În cazul în care autorii trimit spre publicare lucrări ce conțin date, informații, capitole, etc., din alte lucrări publicate anterior şi nu se fac referiri la acestea în text, răspunderea aparține acestora.

### 1. ARTICOLE OBIŞNUITE

- Toate capitolele manuscrisului trebuie să fie scrise *single-spaced, A4***,** sus şi jos: 2 cm; stânga: 2 cm; dreapta: 2 cm, font: **Arial,** mărime 9 pt, cu excepția titlului care se scrie cu 11 pt. şi figurile explicite, care se scriu cu 8 pt.
- Textul lucrării va fi scris în două coloane egale de 8,3 cm, 0,4 cm spațiul dintre ele, exceptând titlul, autorii şi afilierea acestora; tabelele, figurile şi ecuațiile care nu se scriu pe coloane ci pe toată pagina (vezi modelul ataşat);
- Textul se va scrie în limba engleză în coloana din stânga, respectiv în limba maternă - coloana din dreapta.
- Titlurile capitolelor sunt scrise cu majuscule (ex: INTRODUCERE, MATERIAL ŞI METODE), între capitole se lasă un spațiu de 9 pt. La începutul fiecărui paragraf se lasă un "tab" de 0.5 cm;
- Lucrarea va fi scrisă în Word, aliniere "Justify".
- Lucrarea trebuie trimisă prin e-mail.
- Sunt permise max. 2 lucrări ca prim autor.

**Titlul** trebuie să fie o frază scurtă care să descrie conținutul lucrării. Acesta *va fi scris cu majuscule, centrat*, mărime: 11 pt., bolduit, (titlul in engleză) şi *bolduit italic (titlul în limba maternă)*. Sub titlul lucrării după un spațiu de 9 pt., se scriu numele autorilor (ex: Vasilescu G.) (9 pt., bold), imediat sub numele autorilor se scrie: afilierea autorilor (9 pt., normal) iar pe următorul rând: telefonul, faxul, e-mailul corespunzător celui care a trimis lucrarea - primului autor (8 pt., italic).
Titlul trebuie să fie scurt, specific şi informativ. Evitați titlurile lungi, un titlu de sub 100 caractere este recomandat (fără spații).

***Rezumatul*** trebuie să fie informativ şi uşor de înțeles; prezentați pe scurt topica, stadiul experimentelor, date semnificative, şi evidențiați descoperirile majore şi concluziile. Rezumatul trebuie să cuprindă între 100 şi 300 cuvinte. Propozițiile complete, verbele active, şi persoana

abstract should be written in the past tense. Standard nomenclature should be used and abbreviations should be avoided. No literature should be cited (font: 9 pt., the title - *bold italic*; the text of abstract: *italic*).

Following the abstract, about 3 to 10 ***Keywords*** that will provide indexing references should be listed (font: 9, bold italic - the title and 9 pt., *italic* - the text).

A list of non-standard **Abbreviations** should be added. In general, non-standard abbreviations should be used only when the full term is very long and used often. Each abbreviation should be spelled out and introduced in parentheses the first time it is used in the text. Only recommended SI units should be used. Authors should use the Solidus presentation (mg/ml). Standard abbreviations (such as ATP and DNA) need not to be defined.

**INTRODUCTION** should provide a clear statement of the problem, the relevant literature on the subject, and the proposed approach or solution. It should be understandable to colleagues from a broad range of scientific subjects.

**MATERIALS AND METHODS** should be complete enough to allow experiments to be reproduced. However, only truly new procedures should be described in detail; previously published procedures should be cited, and important modifications of published procedures should be mentioned briefly. Capitalize trade names and include the manufacturer's name and address. Subheadings should be used. Methods in general use need not be described in detail.

**RESULTS** should be presented with clarity and precision. The results should be written in the past tense when describing findings in the authors' experiments. Results should be explained, but largely without referring to the literature. Discussion, speculation and detailed interpretation of data should not be included in the Results but should be put into the Conclusions section. Subheadings should be used.

**CONCLUSIONS** should interpret the findings in terms of the results obtained in this and in past studies on this topic. State the conclusions in a few sentences at the end of the paper. The Results and Discussion sections can include subheadings, and when appropriate, both sections can be combined.

**Acknowledgments** of people, grants, funds, etc. should be brief (if necessarily).

**Tables** should be kept to a minimum and be designed to be as simple as possible. Tables are to be typed single-spaced throughout, including headings and footnotes. Each table must be written on the entire width of the page, into the text where reference is made, the columns are broken - one column (see attached sample). Tables should be self-explanatory without reference to the text. The details of the methods used in the experiments should preferably be described in the legend instead of in the text. The same data should not be presented in both table and graph form or repeated in the text. Table's title will be centered bold (in English) and bold italic native language then separated by a slash. In the table, each row will be written in English (Arial, regular, size: 9 pt.) / *native language* (Arial, italic, 9 pt.). The table and its number is written right justified, bold - in English and bold italic - native language, separated by a slash (/).
**Figure legends** should be typed in numerical order.

a III-a trebuiesc folosite (rezumatul să fie scris la timpul trecut). Se va utiliza nomenclatura standard iar abrevierile trebuiesc evitate. Nu se vor utiliza citări de lucrări în "rezumat" (font: 9 pt., titlu - *bold italic*; textul rezumatului - *italic*).

***Cuvinte cheie***: ca urmare a rezumatului, între 3 şi 10 cuvinte cheie trebuiesc listate, aceste oferind referinţe de indexare (font: 9 pt., **bold italic** – titlul şi 9 pt., *italic* - textul).

Trebuie adăugată o listă de abrevieri specifice. În general, aceste abrevieri se folosesc atunci când termenul folosit este foarte lung şi des întâlnit în lucrare. Fiecare abreviere ar trebui introdusă în paranteză pentru prima dată când este folosită în text. Doar unităţi din SI trebuiesc folosite. Autorii trebuie să folosească prezentarea Solidus (mg/ml). Abrevierile standard (ca ATP sau ADN) nu trebuiesc definite.

**INTRODUCEREA** trebuie să ofere o expunere clară a problemei, esenţa relevantă a subiectului şi abordarea propusă sau soluţia. Aceasta trebuie să poată fi înţeleasă de către colegi din diferite domenii ştiinţifice.

**MATERIALE ŞI METODE:** trebuie să fie suficient de complete pentru a permite experimentelor să fie reproduse. Totuşi, numai metodele cu adevărat noi trebuie descrise în detaliu; metodele publicate anterior trebuie citate; modificările importante ale metodelor publicate trebuie menţionate pe scurt. Scrieţi cu majuscule denumirile comerciale şi includeţi numele şi adresa producătorilor. Subcapitolele trebuie utilizate. Metodele utilizate în general, nu trebuie descrise în detaliu.

**REZULTATELE** trebuie prezentate cu claritate şi precizie. Acestea trebuie scrise la timpul trecut, atunci când descriu constatările în experimentele autorilor. Rezultatele trebuie să fie explicite, dar în mare măsură, fără a se face referire la literatura de specialitate. Discuţiile, speculaţiile şi interpretarea detaliată a datelor nu trebuie să fie incluse în rezultate, ci trebuie incluse în capitolul Concluzii. Subcapitolele trebuie utilizate.

**CONCLUZIILE** trebuie să interpreteze constatările în ceea ce priveşte rezultatele obţinute în această lucrare şi în studiile anterioare pe această temă. Concluziile generale vor fi prezentate în câteva fraze la sfârşitul lucrării. Rezultatele şi discuţiile pot include subpoziţii, şi atunci când este cazul, ambele secţiuni pot fi combinate.

**Mulţumirile** către oameni, cei care au acordat burse, fonduri, etc., trebuie să fie scurte (dacă este necesar).

**Tabelele** trebuie menţinute la un nivel minim şi să fie proiectate pentru a fi cât mai simple posibil. Tabelele vor fi scrise la un rând, inclusiv titlurile şi notele de subsol. Fiecare tabel trebuie scris pe întreaga lăţime a paginii, între textul în care se face trimitere; coloanele sunt eliminate - o singură coloană (vezi ataşat modelul). Tabelele trebuie să fie auto-explicative, fără referire la text. Detaliile cu privire la metodele utilizate în experimente trebuie să fie, de preferinţă, descrise în legendă şi nu în text. Aceleaşi date nu trebuie prezentate atât în tabel cât şi sub formă grafică (decât dacă este absolut necesar) sau repetate în text. Titlul tabelului va fi scris centrat, bold (în engleză) şi bold italic (în limba maternă), separate de un slash (/). În tabel, fiecare rând va fi scris în limba engleză (9 pt., normal) / limba maternă (9 pt., italic). Tabelul şi numărul acestuia se scrie aliniat la dreapta, bold - în limba engleză şi bold italic în limba maternă, despărţite de un slash (/).

Graphics should be prepared using applications capable of generating high resolution JPEG before to introducing in the Microsoft Word manuscript file (Insert - From File - ...jpeg). Use Arabic numerals to designate figures and upper case letters for their parts (Figure 1). Begin each legend with a title and include sufficient description so that the figure is understandable without reading the text of the manuscript. Information given in legends should not be repeated in the text. Each figure must be inserted on the entire width of the page, into the text where reference is made, single columns (see attached sample). Leave a space between the figure and the text of figure, size: 3 pt., figure number is written in **Arial bold**, size: 8 pt., followed by what represent the figure or graph, written with Arial, regular, 8 pt. Left to write in English (regular), followed by a separating slash (/) and text in native language (*Arial italic*). Eg:

**Fig 1** - Test stand / *Stand de testare* (size: 8 pt.)

The figures should be "*In line with text*" - Center, not "*Square*"; "*Tight*"; "*Behind text*" or "*In front of text*" (from "*Format picture*" - right mouse button on picture and then "*Layout*".

**Mathematics**

Authors must provide instructions on how symbols and equations should be set. Equations should be numbered sequentially in the right-hand side and in parenthesis. They should be referred to in the text as Equation (4) or Eg. (4). Each equation must be written on the entire width of the page, into the text where reference is made, the columns are broken (see attached sample).

**REFERENCES:** are made in the text; a reference identified by [1], [2], ... [n] is written in the order that was placed at the end of the work - alphabetically.

Example:

[1], [2], [3], ..., [n]

References should be listed at the end of the paper in alphabetical order. Articles in preparation or articles submitted for publication, unpublished observations, personal communications etc. should not be included in the reference list but should only be mentioned in the article text (e.g., A. Danciu, University of Bucharest, Romania, personal communication). Authors are fully responsible for the accuracy of the references.

Examples:

**Journal / Magazine:**

[1]. Nicolescu M.A., (2007) - *Relevant characteristics of alternative liquid fuels aimed at Diesel engines exploitation in polycarburation duty*. INMATEH - Agricultural Engineering, vol. 27, no. 1/2009, ISSN 1583-1019, pp. 50-55;

[2]. Pirna I, Nicolescu M., Marin M., Voicea I., (2009) - *Alternative supply of agricultural tractors with raw oils*. INMATEH - Agricultural Engineering, vol. 29, no. 3/2009, ISSN 1583-1019, pp.89-92.

**Conference / Symposium:**

[1]. Bungescu S, Stahli W, Biriş S, Vlăduț V, Imbrea F, Petroman C., (2009) - *Cosmos programm used for the strength calculus of the nozzles from the sprayers,* Proceedings of the 35 International Symposium on Agricultural Engineering *"Actual Tasks on Agricultural Engineering",* Opatija - Croația, ISSN 1333-2651, pg. 177÷184.

**Book:**

[1]. Vlăduț V., (2009) - *Studiul procesului de treier în aparatul cu flux axial*, Editura "Terra Nostra", ISBN 973-1888-26-8, Iasi - Romania.

**Figurile** trebuie scrise în ordine numerică. Grafica trebuie realizată utilizând aplicații capabile să genereze JPEG de înaltă rezoluție, înainte de a introduce în dosarul manuscris Microsoft Word (Insert - From File - ... JPEG). Folosiți cifre arabe, pentru a desemna cifre şi litere majuscule pentru părțile lor (Figura 1). Începeți fiecare legendă cu un titlu care să includă o descriere suficientă, astfel încât figura să poată fi înțeleasă, fără citirea textului din manuscris. Informațiile furnizate în legende, nu trebuie repetate în text. Fiecare figură trebuie introdusă pe întreaga lățime a paginii, în text, acolo unde se face referire, o singură coloană (vezi ataşat eşantion), centrat. Lăsați un spațiu între figură şi textul figurii, mărimea: 3 pt.; numărul figurii va fi scris cu bold, 8 pct., centrat, urmat de ceea ce reprezintă figura sau graficul, scris cu 8 pt., normal. Prima dată se scrie textul în limba engleză (normal), urmat de un slash (/) apoi textul în limba maternă (italic).

Exemplu:

**Fig. 1** - Test stand / *Stand de testare* (mărimea: 8 pt.)

Figurile introduse trebuie să fie "*In line with text*" - Center, nu "*Square*"; "*Tight*"; "*Behind text*" or "*In front of text*" (din "*Format picture*" - butonul dreapta mouse pe figură şi apoi "*Layout*").

**Formulele matematice, ecuațiile**: autorii trebuie să furnizeze instrucțiuni privind modul de simbolizare şi de ecuații stabilite şi utilizate. Ecuațiile trebuie numerotate secvențial, în partea dreaptă şi în paranteze. Ele trebuie menționate în text ca ecuația (4) sau Ex. (4). Fiecare ecuație trebuie scrisă pe întreaga lățime a paginii, în text, acolo unde se face referire, o singură coloană (vezi ataşat model).

**REFERINȚELE**: se fac în text; o referință identificată prin intermediul [1], [2], ...[n], se scrie în ordinea în care a fost trecută la sfârşitul lucrării - ordine alfabetică.

Exemplu:

[1], [2], [3], ..., [n]

Referințele trebuie prezentate la sfârşitul lucrării în ordine alfabetică. Articole în curs de pregătire sau articole trimise spre publicare, observațiile nepublicate, comunicările cu caracter personal, etc, nu trebuie incluse în lista de referință, dar pot fi menționate în textul lucrării (exemplu, A. Danciu, Universitatea din Bucureşti, România, comunicare personală). Autorii sunt pe deplin responsabil pentru exactitatea referințelor.

Exemple:

**Jurnal / Revistă**

[1]. Nicolescu M.A., (2007) - *Proprietățile relevante ale combustibililor lichizi alternativi vizați pentru exploatarea motoarelor Diesel în regim policarburat*, INMATEH - Inginerie Agricolă, vol. 27, nr. 1 / 2009, ISSN 1583-1019, pag. 50-55;

[2]. Pirna I, Nicolescu M., Marin M., Voicea I., (2009) - *Alimentarea alternativă a tractoarelor agricole cu uleiuri vegetale crude,* INMATEH - Inginerie Agricolă, vol. 29, nr. 3 / 2009, ISSN 1583-1019, pag.89-92.

**Conferință / Simpozion**

[1]. Bungescu S, Stahli W, Biriş S, Vlăduț V, Imbrea F, Petroman C., (2009) - *Cosmos programm used for the strength calculus of the nozzles from the sprayers,* Proceedings of the 35 International Symposium on Agricultural Engineering *"Actual Tasks on Agricultural Engineering",* Opatija - Croația, ISSN 1333-2651, pag. 177÷184.

**Carte**

[1]. Vlăduț V., (2009) - *Studiul procesului de treier în aparatul cu flux axial*, Editura "Terra Nostra", ISBN 973-1888-26-8, Iaşi - România.

**Book Chapter:**
[1]. Vlăduț V., (2009) - Considerații şi ipoteze privind modelarea unui proces de treier şi separare. In: *Studiul procesului de treier în aparatul cu flux axial*, Editura "Terra Nostra", ISBN 973-1888-26-8, pg. 61-69, Iasi - Romania.

**Dissertation / Thesis:**
[1]. Constantinescu A., (2010) - *Optimizarea agregatelor formate din tractoare de putere mare cu maşini agricole pentru pregătirea terenului în vederea însămânțării*. PhD dissertation, University of Transylvania Braşov, Romania.

**Units, Abbreviations, Acronyms**

- Units should be metric, generally SI, and expressed in standard abbreviated form.
- Acronyms may be acceptable, but must be defined at first usage.

## 2. SHORT COMMUNICATIONS

Short Communications are limited to a maximum of two figures and one table. They should present a complete study that is more limited in scope than is found in full-length papers. The items of manuscript preparation listed above apply to Short Communications with the following differences: (1) Abstracts are limited to 100 words; (2) instead of a separate Materials and Methods section, experimental procedures may be incorporated into Figure Legends and Table footnotes; (3) Results and Conclusions should be combined into a single section.

## 3. REVIEWS

Summaries, reviews and perspectives covering topics of current interest in the field, are encouraged and accepted for publication. Reviews should be concise (max. 8 pages). All the other conditions are similar with regular articles.

**Capitol din carte**
[1]. Vlăduț V., (2009) - Considerații şi ipoteze privind modelarea unui proces de treier şi separare. În: *Studiul procesului de treier în aparatul cu flux axial*, Editura "Terra Nostra", ISBN 973-1888-26-8, pg. 61-69, Iaşi - România.

**Disertații / Teze de doctorat**
[1]. Constantinescu A., (2010) - *Optimizarea agregatelor formate din tractoare de putere mare cu maşini agricole pentru pregătirea terenului în vederea însămânțării*. Teză de doctorat, Universitatea Transilvania Braşov, România.

**Unități, Abrevieri, Acronime**

- unitățile metrice trebuie să fie, în general, SI, şi exprimate în formă prescurtată standard;
- acronimele pot fi acceptate, dar trebuie să fie definite la prima utilizare.

## 2. COMUNICĂRILE SCURTE

Comunicările scurte sunt limitate la maxim 2 figuri şi un tabel. Acestea trebuie să prezinte un studiu complet, care este mai limitat decât în cazul articolelor normale (de dimensiuni mai mari). Elementele de pregătire a articolelor normale (manuscriselor) enumerate mai sus se aplică şi la comunicările scurte, cu următoarele diferențe: (1) Rezumatul este limitat la 100 cuvinte; (2) capitolele Materiale şi Metode, Procedurile experimentale pot fi scrise împreună, încorporând figurile şi tabelele; (3) Rezultatele şi Concluziile pot fi combinate într-o singură secțiune.

## 3. SINTEZELE

Sintezele, comentariile şi perspectivele acoperind subiecte de interes din domeniu sunt încurajate şi acceptate spre publicare. Sintezele trebuie să fie concise şi nu mai mari 8 pagini. Toate celelalte condiții sunt similare cu cele de la articolele normale (obişnuite), enumerate mai sus.

**Edited by: INMA Bucharest**
6 Ion Ionescu de la Brad Blvd., sect. 1, Bucharest, ROMANIA
Tel: +4021.269.32.60; Fax: +4021.269.32.73
http://www.inmateh.eu